Regional Geology Reviews

Akif A. Alizadeh
Ibrahim S. Guliyev
Fakhraddin A. Kadirov
Lev V. Eppelbaum

Geosciences of Azerbaijan

Volume II: Economic Geology and Applied Geophysics

Springer

Regional Geology Reviews

More information about this series at http://www.springer.com/series/8643

Akif A. Alizadeh · Ibrahim S. Guliyev
Fakhraddin A. Kadirov
Lev V. Eppelbaum

Geosciences of Azerbaijan

Volume II: Economic Geology and Applied Geophysics

Springer

Akif A. Alizadeh
Institute of Geology and Geophysics Sciences
Azerbaijan National Academy of Sciences
Baku
Azerbaijan

Fakhraddin A. Kadirov
Institute of Geology and Geophysics Sciences
Azerbaijan National Academy of Sciences
Baku
Azerbaijan

Ibrahim S. Guliyev
Institute of Geology and Geophysics Sciences
Azerbaijan National Academy of Sciences
Baku
Azerbaijan

Lev V. Eppelbaum
Faculty of Exact Sciences, Department of Earth Sciences
Tel Aviv University
Tel Aviv
Israel

ISSN 2364-6438 ISSN 2364-6446 (electronic)
Regional Geology Reviews
ISBN 978-3-319-40492-9 ISBN 978-3-319-40493-6 (eBook)
DOI 10.1007/978-3-319-40493-6

Library of Congress Control Number: 2016936973

Printed on acid-free paper

This Springer imprint is published by Springer Nature
The registered company is Springer International Publishing AG Switzerland

To the 70th Anniversary of the Azerbaijan National Academy of Sciences foundation

Contents

Groundwater Generation and Distribution Regularities

1

1.1 Hydrogeological Zonation

Geological and structural conditions within Azerbaijan permit to isolate the Greater and the Lesser Caucasus mountain zones and the Kur-Araz Lowland that separates them, though the Talysh Mountains is separated from the Lesser Caucasus by the Araz River in the southeast. Three regions are isolated as geostructural regions (first-order tectonic structures): A—the Greater Caucasus fold-mountain zone, B—the Lesser Caucasus fold-mountain zone, and C—the Kur-Araz Lowland (Alekperov et al. 2008).

Geological and hydrogeological conditions encouraged the fact that non-artesian and pressure fault, fracture-vein, and fissure-stratal waters were mostly developed in the Meso-Cenozoic and more ancient bed rocks. Artesian porous-edge waters are generated in the local development areas of low-thickness alluvial, proluvial, and fluvioglacial deposits (in the mountain river floodplains and small depressions).

All piedmont plains are basically composed of continental boulder–gravel–cobble, sandy and clay deposits of merged river debris cones and contain pore-edge groundwaters.

The so-called Neogene piedmonts of Jeiranchel, Ajunohur as well as the Shamakhy-Gobustan zone and the western Absheron are mostly composed of the Paleogene–Neogene age argillaceous deposits, less frequently, of arenaceous and detrimental deposits of continental and marine genesis. The Republic lowlands are composed of the mass of the Upper Pliocene–Quaternary age argillaceous–arenaceous deposits of continental and marine genesis. Artesian and pressure pore-edge waters are developed in all piedmont plains and lowlands.

Uniformity of hydrogeological conditions, similar formation mode for groundwater resources and reserves, as well as distribution regularities of its hydrodynamic and hydrochemical parameters permit to isolate 18 hydrogeological basins of pore-fissure, pore-stratal, and fissure waters within their boundaries (Table 1.1).

1.2 Groundwater Formation and Distribution Regularities in the Fold-Mountain Zones

According to hydrogeological zoning (Alekperov et al. 2008), the Greater Caucasus fold-mountain zone includes the Greater Caucasus porous-fissured water basins and the Shamakhy-Gobustan porous-edge and fault water basins, and the Lesser Caucasus fold-mountain zone includes the Lesser Caucasus, Nakhchivan, and Talysh porous-fissured water basins. Due to the severalty of the Talysh fold-mountain zone, it is viewed separately (Lange 1961; Babayev 1974; Israfilov et al. 1994; Aliyev et al. 1996; Alekperov et al. 2008).

1.2.1 The Greater Caucasus Fold-Mountain Zone

Azerbaijan section of the Greater Caucasus fold-mountain zone covers the area from the Tinovroso Mt. in the west to the Pirsaat River head in the east; in the south, it adjoins the Ganykh-Airichay valley, and in the north, its border passes along the Lateral Ridge foot. This area is characterized by variegated lithological composition of rocks, their weathering in the upper zone and splintering by numerous tectonic faults, the topography sharp compartmentalization with hydrographic network incision down to 1500–1800 m depth, increased quantity of atmospheric precipitation, presence of many talus deposits along steep slopes, and sporadically developed low-thickness soil covering. All these features predetermine accumulation and distribution of fault waters in the weathering zone, and of fracture-vein waters confined to the abyssal tectonic fractures.

The Quaternary deposit aquifer system. Quaternary deposits are mainly represented by eluvial–deluvial formations and are of limited development. They occur most widely in the Greater Caucasus southeastern plunge.

A.A. Alizadeh et al., *Geosciences of Azerbaijan*,
Regional Geology Reviews, DOI 10.1007/978-3-319-40493-6_1

Table 1.1 Taxonomic hydrogeological zoning units in Azerbaijan territory

Indices of geostructural regions	Geostructural regions	Indices of hydrogeological basins	*Hydrogeological basins*
A	The Greater Caucasus fold-mountain zone	I	The Greater Caucasus porous-fissured water basin
		II	The Shamakhy-Gobustan porous-fissured and fault water basin
		III	The Absheron Peninsular porous-edge water basin
		IV	The Samur-Gusarchay porous-edge water basin
B	The Lesser Caucasus fold-mountain zone	I	The Lesser Caucasus porous-fissured water basin
		II	The Nakhchivan porous-fissured water basin
		III	The Talysh porous-fissured water basin
C	The Kur-Araz Lowland	I	The Ganykh-Airichay porous-edge water basin
		II	The Ganja-Gazakh porous-edge water basin
		III	The Garabagh porous-edge water basin
		IV	The Mil porous-edge water basin
		V	The Jebrail porous-edge water basin
		VI	The Nakhchivan porous-edge water basin
		VII	The Shirvan porous-edge water basin
		VIII	The Mughan-Salyan porous-edge water basin
		IX	The Lenkaran porous-edge water basin
		X	The Jeiranchel Neogene piedmont porous-edge water basin
		XI	The Ajunohur porous-edge water basin

Glacial deposits are found in the area of Bazardyuzyu, Shakhdagh, etc., pinnacles. Permanently operating water table springs with 1–30 l/sec output are confined to them. Water mineralization is 0.2–0.4 g/l, chemical composition—hydrocarbonate calcium, with temperature of 3–5 °C.

Alluvial deposits occurring in the valley flattened areas contain underflow conduits of local importance. In the Shamakhy-Gobustan basin of porous-edge and fault waters, the Quaternary rocks are represented by deluvial loams, developed at the slopes of gulches, ravines, mountains, and hills, and by alluvial boulder–gravel and gravel–cobble deposits with arenaceous, sandy loam, and loam aggregates, developed in the Pirsaat, Gozluchay, and other riverbeds. Numerous springs and wells of outputs from second decimal places to 1–2 l/sec (strongly dependent of the amount of precipitates) are confined to them.

The Pirsaat River underflow conduits have been studied at the site located 6.0 km southeastward of the city of Shamakhy. The river valley within this area is composed of the Quaternary alluvial deposits represented by boulder–cobble and gravel–cobble deposits with argillo-arenaceous aggregate. Deposit thickness in the area equals to 4–50 m and sometimes reaches 65–68 m. Underflow conduit rate is 6.4 l/sec. Outputs of wells drilled in the area amounted to 0.5–7.7 l/sec, with specific capacities of 2.3–2.5 l/sec·m. Permeability code for water-containing rocks varies within 1.7–14.2 m/day, and transmissivity is 2.2–373.5 m^3/day. The underflow waters are basically sweet, with 0.5–1.0 g/l mineralization, of hydrocarbonate calcium–sodium, sulfate–chloride–hydrocarbonate sodium–calcium composition. Weakly brackish waters with mineralization value of 1.3–1.4 g/l and chloride–sulfate sodium composition are also met and are confined to the areas bordering the river valley sides. Based on the surveys conducted in the region, the National Reserves Commission calculated and approved commercial reserves of fresh groundwaters of A + B categories as 8670 m^3/day, and of A + B + C_1 categories, as 13,030 m^3/day.

The Chigilchay River underflow waters were investigated at Shikhlar village area. Thickness of alluvial deposits represented by boulder–cobble and gravel–cobble deposits with arenaceous and sandy loam aggregates is about 30 m. Depth of underflow water level is 0.7–0.9 m. Permeability codes are 3–4 m/day. Well yields are 1.9–2.6 l/sec., and specific yields are 0.4–0.6 l/sec·m. The water is fresh, with 0.4–0.6 g/l mineralization, of hydrocarbonate–sulfate sodium–calcium–magnesium composition.

To study the underflow waters of the Guba-Gusar zone rivers (Samur, Gusarchay, Gudialchay, Velvelchay, etc.), 42 wells of 40–45 m depth were drilled. In all wells, water-containing rocks are represented by boulder–gravel–cobble deposits with arenaceous and argillo-arenaceous

aggregates and sands. Thickness of water-containing rocks varies from 12.5 to 37.8 m, prospect hole yields vary from 3.3 to 8.5 l/sec, with specific yields of 0.35–0.86 l/sec·m. Permeability codes of water-containing rocks vary within 1.63–9.04 m/day, water transmissibility is 129–597 m^3/day. Chemical composition of underflow waters is hydrocarbonate calcium and hydrocarbonate sodium, their mineralization does not exceed 0.8 g/l.

In places, where limestone outcrops are covered by impervious rocks, pressure waters are generated. Here, the drilled well exposed pressure waters at the depth of 74.9 m, well yield by spouting is 1.0 l/sec, and the established level is +0.8 m. The water is weakly mineralized, dissolved solids constitute 2.7 g/l, it is sulfate–chloride sodium. Limestone water-bearing hilltops have limited distribution area, are not water-bearing in all places, and do not contain sufficient reserves.

Prospect holes drilled along the Lengebiz Ridge southwestern slope exposed the Absheron Age water-bearing rocks within the depth interval of 15–95 to 184–254 m that are lithologically represented by sands and pack sands. The deposit efficient thicknesses vary within considerable range from 36 to 91.5 m. Water statistical levels are 4.3–8.7 m, well yield varies from 0.87 to 5.55 l/sec, with specific yields of 0.29–0.6 l/sec·m. Permeability codes are insignificant, from 0.69 to 2.86 m/day. Chemical composition of groundwaters is hydrocarbonate calcium–magnesium, hydrocarbonate–sulfate sodium–magnesium, and chloride–sulfate sodium, with mineralization value from 0.3–0.5 to 1.7–3.1 g/l.

The Paleogene–Neogene deposit aquifer system. Groundwaters of the Akchagyl regional stage (the Upper Pliocene) are exposed by boreholes within the Greater Caucasus proper porous-fissured water basin, near Yukhary Leger village. Overlying bed is found at the 92.5–151 m depth, statistical level is at 68.7–115.0 m depth. Hole yields vary within 2.1–9.5 l/sec, with specific yields of 0.13–0.94 l/sec·m. Permeability codes of water-containing rocks vary within considerable range from 0.71 to 5.75 m/day. Groundwaters are fresh, with 0.4–0.9 g/l mineralization and chemical composition of sulfate–hydrocarbonate sodium–calcium, hydrocarbonate calcium–magnesium.

Groundwaters of productive strata deposits (Lower Pliocene). The productive strata stretch as a narrow strip north of the Gusarchay River and are represented by the mass of gravel–cobble deposits with sandy aggregate, unconformly lying on the Pontian to the Jurassic age clays. The productive strata deposits in the Shamakhy region are outcropped within the Jeirankechmez depression and in the Lengebiz Ridge area and are represented by interstratified clays, aleurites, sands, sandstone with subordinate development of gravels and conglomerates. Here, the productive strata edge waters are generally pressure waters, sometimes hyperpiestic. Well yields vary from 0.01 to 2.3 l/sec. Aquiferous properties of the productive strata deposits within the area under investigation, except individual springs and wells, have been essentially found from the prospect holes. The aquifer system gross interval varies within 37–258 m, efficient thickness is 25.5–109.0 m, static level is 3.1–8.3 m, well yields are 3.85–4.29 l/sec with specific yield of 0.41–1.1 l/sec·m. Permeability code is about 2.0 m/day. The waters are chloride–hydrocarbonate–sulfate sodium–calcium.

Groundwater of Pontian regional level (Upper Miocene). Pontian bassets have wide occurrence within the Sundi-Marazy plateau and at minor areas of the Shamakhy region central and southern parts. Lithologically, the Pontian regional-level deposits are represented by clays, sandstone, limestone, and marls. The limestone and sandstone waters are basically fissure-stratal and porous-edge waters. Catchment area of the Pontian regional-level water-bearing deposits coincides with their development area. Waters are discharged as springs. Spring yields vary within 0.1–60 l/sec and are highly dependent on their location. The springs located at the mountain foot have higher yield than those situated higher on the slope. Spring water has hydrocarbonate–sulfate sodium–magnesium and sulfate–hydrocarbonate–chloride calcium–magnesium–sodium composition with dry residue from 0.4 to 2 g/l. In the springs that are confined to limestone, hydrocarbonate ions and magnesium ions are predominant, while in those confined to sandstone and sandy limestone, hydrocarbonate, and calcium ions predominate.

Groundwater of diatom deposits (Middle–Lower Miocene). In most cases, the structures with confined diatomic deposits are brachyanticlines, complicated by fractures and thrusts. Water ingress is rarely met there and is confined to the fissured limestone and sandstone development areas. The borehole that was drilled in the Gurudere camping ground has outcropped fine-grained sands and dolomitic marls within the depth interval of 58.0–63.5 m that contained pressure water. Hydraulic gradient is 3.3 m below the well mouth. Well yield by testing is 0.003 l/sec. The water is bitter salty with 32.6 g/l mineralization, of sulfate–chloride composition. In the well drilled at the Syundu area to the depth of 78 m, water overflow was observed with 1.0–1.5 l/sec yield and with 34–46 g/l mineralization.

The well drilled southeastward of Shikhzairli village exposed diatom-age water-bearing rocks within the 28–77.5-m-depth interval that were represented by fine-grained argillaceous sands. The effective thickness of horizon is 49.5 m. Standing water level is 6.0 m below the surface. Well yield is 0.85 l/sec. Specific yield is 0.27 l/sec·m. The water is subsaline with 1.7 g/l mineralization.

Groundwater of the Maykop suite (Oligocene–Lower Miocene). The wells drilled in the Shamakhy-Gobustan zone northern part exposed the Maykop suite water-bearing

rocks represented by interbeds of fine-grained sandstone and sands of up to 3–5 m thickness with the system effective output from 11 to 24.5 m. The waters confined to these deposits are basically fresh with up to 1.0 g/l mineralization, of hydrocarbonate–sulfate calcium–magnesium composition. Well yields by testing were 1.43–4.8 l/sec, with specific yields of 0.1–0.4 l/sec·m. The water-bearing system efficient thickness moderately increases in its southern part and reaches (with rare exceptions) 14–46 m. Groundwaters are both fresh with up to 1 g/l mineralization and weakly saline (1.72 g/l, and their chemical composition varies from chloride–hydrocarbonate–sulfate sodium–calcium composition to hydrocarbonate–sulfate calcium–sodium one. Hydraulic gradients are 3.25–5.95 m. Well yields by testing are 1.2–5.0 l/sec, and specific yields are 0.1–0.6 l/sec·m. Permeability codes of water-containing rocks vary from 0.48 to 3.71 m/day.

Groundwater of the Koun suite (Lower–Middle Eocene). The well drilled in Chukhuryurt village exposed Koun deposits within 3.0–83.0 m range. Lithologically, the deposits are represented by yellow–brown or greenish-brown clays with thin interbeds (0.2–0.3 m) of poorly cemented fine-grained sand and grey, fissured pack sand. It is a pressurized, fissure-stratal, sulfur water. Hydraulic gradient is +0.75 m. Well yield by discharge is 0.06 l/sec. The water is fresh, with dissolved solids of 0.5–0.7 g/l, hydrocarbonate sodium water. Yield of a nearby spring is very low. The territory major part, particularly the Shamakhy region eastern part, where the Koun suite deposits are developed at large areas, shows that they are mostly expressed as argillaceous facies and are of no interest with regard to their water-bearing properties.

The Cretaceous deposit aquifer system. The Upper Cretaceous deposits are abundant in the southern and southeastern areas of the Azerbaijan part of the Greater Caucasus. The water-bearing layer is the terrigenic flysch represented by alternating marls, clays, sandstone, limestone, clay marls, and to a lesser degree, by argillites and oil shales.

Water table springs are generally confined to weathering joints, while non-gravity springs are confined to tectonic dislocation lines; many springs have mineral waters. Thus, a series of parallel faults is found at the Central High northern edge, and these faults are associated with hydrogen sulfide seepages. The Zykhir hot spring as well as the Gyulekh, Sadykh-Kayam, and Uchakh cold hydrogen sulfide mineral springs, related to the Upper Cretaceous rocks, gravitate to the most southern of these faults, coinciding with the Kazma-Kryz thrust and with the Garabulagh thrust that substitutes it in the east. The Budug springs that have both cold-water and thermal springs of 46.2–48.1 °C temperature are associated with the same rocks. Thermal spring yields are about 0.012 l/sec; they contain H_2S of up to 4.7 mg/l. The Budug cold spring temperature is 7 °C, its yield is 0.013 l/sec, and hydrogen sulfide content is 4.7 mg/l. The water is hydrocarbonate–sulfate, sodium–calcium.

In the Chukhuryurd anticline area (Chukhuryurd and Kalaiburugt villages) groundwaters, in addition to natural outputs, are stripped by boreholes. An aquifer with up to 3-m well mouth head was exposed at 5–6 km depth in Sabunlu Yarghan area, 5–6 km southwestward of Chukhuryurd village. The well's specific yields are 0.01–1.6 l/sec·m. At Kalaibugurt area, the overlying bed was stripped at 5–14 m depths. Water level was established above the mouth by 0.3–0.5 m, the well's specific yields are 0.14–0.9 l/sec·m. In the fracture zone that passes westward of Chukhuryurd village, mineral hydrogen sulfide waters were revealed at 10–12 m depth, water head was 2.8–3.0 m above the earth surface, the well's specific yield was 0.09–0.2 l/sec·m, and permeability code for water-containing rocks was 0.6 m/day. Dissolved solids of hydrogen sulfide waters amounted to 0.3–1.3 g/l. Water is hydrocarbonate sodium or calcium with 12–16 °C temperature; total hardness is 4.6 mg-equiv/l.

The Jurassic deposit aquifer system. The Upper Jurassic fissured limestone abundant in the Shakhdag-Sudur zone is also water-bearing. The well drilled in Sudur village area stripped Jurassic sandstone at 151–228 m depth. The water-static level is 57.5 m. Well yield by testing is 2.2 l/sec, permeability code is 0.76 m/day. The water is fresh, with 0.9 g/l mineralization level and sulfate–chloride sodium–calcium composition.

The Jurassic deposit thermal waters are sodium hydrocarbonate, hydrogen sulfide, with 0.9–1.7 g/l mineralization and 34.4–47.8 °C temperature. In the Gabala district, the waters are sodium hydrocarbonate with 1.08–1.24 g/l mineralization and 23–39.4 °C temperature, the yields of two major seepages are about 0.57 l/sec. In the Guba district mountainous area, mineral hydrogen sulfide springs with water temperature of 26 °C are found.

1.2.2 The Lesser Caucasus Fold-Mountain Zone

At the Lesser Caucasus, groundwaters do not have definite stratigraphic confinedness and occur in various deposits, from contemporary to Paleozoic ones (Alekperov et al. 2008). However, water-cut level differs in various rocks and depends on their composition, fracture intensity, and area drainage. Highly fissured limestone, and sometimes karst limestone, is the most water-abundant, and volcanogenic rocks are less water encroached, and intrusive formations are extremely poor in water.

Spring runoff distribution manner demonstrates radial direction of subsoil runoff, from the mountain zone center to its peripheries, and is completely similar to the prechannel flow.

The Quaternary deposit aquifer system. The Quaternary deposits are represented by alluvial, residual-and-talus, and lava formations.

Groundwater of residual-and-talus deposits is distributed sporadically at ridge slopes and in river valleys. Its occurrence depth decreases down the slope, and spring boils are observed at slope bases and in backlands. The springs are rather numerous, with the yield of 0.1–1.0, occasionally of 2–3, and in certain cases, even 10 l/sec. Here, underflow recharge by the core deposit pressure waters is observed. Water temperature changes from 4 to 13 °C, depending on the spring hypsometric level. Temperature variation amplitude rises with the area decrease. The water is of calcium hydrocarbonate composition, usually of 0.3–0.6 g/l mineralization. In the points, where it is recharged by the core deposit waters, mineralization rises to 1 g/l, and increased content of sulfate ions and ion–ion–sodium is noted (for instance, Dashkesan and Gedabey districts).

Underflow conduits generated owing to rivers are confined to the river valley alluvial deposits. In submountain regions, alluvial deposits stretch as continuous belt at a distance of several kilometers, they are represented by boulder–cobble and cobble formations with sand–loam or sand–gravel aggregates (depending on the lithological composition of the river basin-composing rocks). Hydrogeological study results, aimed at determining stream estimation for underflow conduit of the rivers descending from the Lesser Caucasus northern and northeastern slopes, permit to judge the underflow conduit significant resources (Table 1.2).

In certain structures, the Quaternary deposits have lateral extension. The Upper Quaternary deposit groundwaters in Gedabey district are distributed within the Gedabey syncline and the Shamkir High around Zakhmetkend, Maarif, Slavyanka, etc., villages, in Gubatly district, within the Kafan High and the Gochassy trough. Water-containing rocks are represented by boulder–gravels and pebble-gravels with sandy or argillo-arenaceous aggregate. Depths of occurrence of groundwater levels generally decrease from piedmonts to plains, from 29.8 to 3.30 m. Horizon-effective depth varies within 25.9–36.60 m; prospect hole yields vary from 3.0 to 8.4 l/sec; specific yields vary from 0.18 to 0.40 l/sec·m. Permeability code of water-containing rocks equals to 1.2–3.0 m/day, coefficients of transmissibility vary from 35 to 105 m^2/day. The Upper Quaternary deposit groundwaters within the district under study are fresh. Their total mineralization does not exceed 0.7 g/l. According to their chemical composition, they are hydrocarbonate–sulfate calcium–sodium, and hydrocarbonate–sulfate sodium–magnesium at certain sites.

The Middle Quaternary deposit water-bearing stratum (aquifer) is distributed within the Bazarchay River left bank along the entire river length. The results of conducted prospecting showed that the Gerusin suite at the Bazarchay River left-bank edge is represented by boulder–gravels with sandy or argillo-arenaceous aggregate and confined groundwaters manifested by a number of springs. The spring yields vary from 0.6 to 2.2 l/sec. Water-static levels are established at 15–18 m depth, well yields are 5–7 l/sec, specific yields are up to 0.6 l/sec·m. Permeability code of water-containing rocks is 1.7 m/day, transmissibility coefficient is 20–50 m^2/day. Chemical composition of the Gerusin suite is hydrocarbonate–sulfate calcium–sodium, and water mineralization equals to 0.4 g/l. In the Yazy Plateau area, the Gerusin suite deposits have no practical importance due to their poor water inflow.

The Lower Pleistocene deposits cover the Khojavend district northeastern and eastern parts. Here, their thickness varies within 62–160 m. Depths of occurrence of groundwater levels

Table 1.2 Characteristics of underflow conduits for the rivers descending from the Lesser Caucasus northern and northeastern slopes

River name and cross-sectional place	Aquifer thickness, in m	Permeability code, in m/day	Seepage flow slope	Seepage flow width, in km	Stream flow, in l/sec
Gasanlu, Gojaly village	42–65	8.8–14.3	0.016	1.7	140.7
Tauzchay, Gazykuly village	43–59	18.3–45	0.017	1.8	264.4
Asrikchay, Ashagy-Kushchu village	41–48	38.4–54.5	0.026	0.32	82
Dzegamchay, Ibrahim-Gojaly village	50–63	12.4–25.6	0.015	3.2	251.8
Jagirchay, Morul village	26–36	27.8–38	0.029	1.0	163.5
Shamkirchay, Seifali village	33–53	13–22	0.02	2.0	101.2
Koshkarchay, Ballyja village	9.7–70	22–69.9	0.02	1.3	481.6
Ganjachay, Zurnabad village	14–32	15.4–43	0.026	0.6	273.8
Kyurakchay, Khoilu village	34–46	5.4–39.0	0.019	1.0	194.5
Injachay, Borsunlu village	52–56	31.7–46.8	0.015	1.5	285.4
Terterchay, Chayly village	72–106	56–96	0.014	2.5	724.3
Khachinchay, Kyzylkengerly village	35–96	8.1–50.6	0.016	1.5	384.3
Karkarchay, Askeran village	60–69	17.6–41.9	0.012	1.5	323.5

generally decrease from the mountainous part to the plain and vary from 44.5 to 1.5 m. Water-containing rocks are represented by boulder–gravels and pebble–gravels with sandy or argillo-arenaceous aggregate, by sands. The effective thickness of aquifer varies within 21–175 m. Their mineralization values do not exceed 1.0 g/l.

In the Lesser Caucasus southeastern part, mainly within the Gybadly, Fizuli, Jebrail districts, the Akera suite is prominent (the Pliocene–Quaternary aquifer system) represented by boulder–gravel and gravel–cobble deposits with sandy aggregate, conglomerates, tuff conglomerates, clays with gravel, sands. It is most widely distributed within the Gubadly district and contains ground and pressure subsoil waters. The springs confined to the Akera suite have 0.1–3.5 l/sec yields. Yields of these springs vary during the year. Some of them dry up during arid years, which complicate the issue of their utilization for water supply to populated localities. The spring waters are fresh (up to 1.0 g/l) or weakly mineralized (up to 1.17 g/l), hydrocarbonate calcium–sodium, sulfate–hydrocarbonate–chloride sodium. The Akera suite groundwaters are stripped by boreholes at the depths of 8–102 m. The effective thickness of water-containing rocks changes from 17.5 to 122 m. Water-static level is established at 0.5–52.5 m depth. Well yields are from 1.2 to 12.0 l/sec, with specific debits from 0.10 to 1.10 l/sec·m. Permeability codes of water-containing rocks vary within 0.10–3.80 m/day, and coefficients of transmissibility are 16.2–111.0 m^2/day. Chemical composition and mineralization level of the Akera suite groundwaters are very diversified. In Makhmudly-Giyasly and Dondorly-Giyasly village areas, mineralized water was tapped (3.8–11.3 g/l) with predominant chloride ions, while in the other districts freshwater of hydrocarbonate type is abundant (up to 1.0 g/l).

The lava formation aquifer system. Volcanogenic formations represented by highly fractured trachyandesites, quartz latites, trachyandesibasalts, latites, trachydolerites, and subalkaline basic basalts are mostly water-abundant at the sites where the poor water-abundant rocks underlie them. Thickness of lava formations depends on the topography they cover and varies from 3–5 to 120 m. High porosity and fracturing of these formations promote infiltration of heavy (up to 700 mm) atmospheric precipitations and meltwaters, resulting in powerful groundwater flows. Water-bearing horizons pinch out to the surface as numerous springs, often linearly arranged. Spring yields vary from 1 to 2 l/sec, enhancing at the sites of old topography depressions. The largest springs are known in Minkend village area, in the Terter and Akera valleys. The water is ultrafresh, with dissolved solids of 0.05 g/l, hydrocarbonate calcium, with hardness of up to 1–1.5 mg-equiv/l. Tuffaceous deposits of the Bazarchay-Akerachay interfluve are poorly inundated, the fact being explained by insignificant quantity of occurring atmospheric precipitation. The springs are just a few, their yields do not exceed 1 l/sec with average value of 0.3–0.4 l/sec. The water is fresh, with dissolved solids of 0.1–0.5 g/l, hydrocarbonate calcium, soft (total hardness of 0.4–1.0 mg-equiv/l).

The Eocene deposit aquifer system. This system is distributed predominantly within the Nakhchivan basin of porous-fissured waters, and subsoil and pressure waters are associated with it. Subsoil waters occur sporadically in the Upper Eocene deposits, and they are confined to the weathering zones and are manifested by scarce springs in ravines, at mountain and highland feet (Ilandagh, Nagajir, Khanaga Mts., etc.). Spring yields are 0.2–1, sometimes 3 l/sec. Water temperature is 11–14 °C, and it is fresh. In the northwestern part of these highlands, where the waters are confined to the sedimentary rock series, they have hydrocarbonate–sulfate sodium composition, while in the southeastern part of the district, where volcanogenic-sedimentary series rocks are developed, the waters are hydrocarbonate magnesium–calcium.

The Middle Eocene tuffaceous sandstone, sandstone, tuff aleurites, and tuff conglomerates are distributed in the basin heads of the Nakhchivanchay, Alinjachay Rivers, in the middle and lower basins of the Gilyanchay and eastern Arpachay rivers. The Lower Eocene deposits are exposed at water partings of the area highland part and stretch as stripes southward of the Gilyanchay River origins. They are composed of porphyrites, tuff sandstone, and tuff conglomerates. Groundwaters saturate the weathering zone of said rocks and are exposed as numerous springs on ridge slopes and in river valleys at their feet. In the north and northeast of said area, the spring yields are from 1 to 4 l/sec; in the south and southeast, they drop down to 0.1–0.5 l/sec. Water temperature is 7–1 °C, it is fresh with 0.17–0.5 g/l mineralization, hydrocarbonate calcium, less frequently hydrocarbonate–sulfate calcium. Groundwater movement trend is southward and southwestward. Their recharge is supplied by atmospheric precipitation and meltwaters. Pressure waters are associated with zones of crush and tectonic dislocations and, as a rule, are deed-circulating mineral waters.

The Eocene deposits, represented by metacherts, tuffaceous conglomerates, liparites, and andesite–dacites, are widely developed in the southern and southeastern parts of Gedabey district. The spring yields vary within 0.2–3.0 l/sec scope, with mineralization of up to 1 g/l, they have hydrocarbonate calcium–sodium composition. In the Eocene calcareous tuffaceous sandstone, groundwaters are stripped at 46.40 m depth, with 8.0 l/sec yield, and specific yield of 0.4 l/sec·m. Thickness of the stripped mass-fissured part is 70 m. Permeability code of water-containing tuffaceous sandstone is 2.2 m/day, transmissibility coefficient is 156.0 m^2/day with 0.39 g/l mineralization. The water chemical composition is hydrocarbonate calcium–magnesium.

The Cretaceous deposit aquifer system. Cretaceous deposits within the Lesser Caucasus have wide but at the

same time non-uniform occurrence. It should be noted that the springs associated with Cretaceous deposits are ascending and descending in the Gedabey district and, as a rule, crop out as concentrated jets. Spring yields vary within 10–100 l/sec. The most water-abundant rocks are the Upper Cretaceous fissured limestone developed at the Mrovdagh Ridge slope, in the Terter and Khachinchay River middle stream, in the Akera and Bazarchay basins, and in Aterk village area. Numerous springs with yields varying from 0.005 to 7.5 l/sec are confined to the Cretaceous volcanogenic formations, with predominant yields of 1.5–2 l/sec. In the southeastward of the Kyapaz Mt., the springs of the Cenomanian porphyry thickness have yields of 0.04–0.7 l/sec. Tuffaceous deposits are water-abundant in the Injacha-Khachinchay and the Karkachay-Kozluchay interfluves. The first of these districts hosts numerous springs of 0.1–2, less frequently 2.5 l/sec yields, with predominant yields of 0.5–0.6 l/sec. Along the tectonic fracture lines, one can see the springs with up to 10–15 l/sec yield; tuffaceous deposits of Khankendi display prevailing springs of up to 1.5 l/sec yield.

Groundwaters of volcanogenic deposits are fresh with dissolved solids of 0.1–0.6 g/l, hydrocarbonate calcium, with 0.4–1.1 m-equiv. hardness. The sedimentary complex waters show certain mineralization increase, with dissolved solids of 0.4–1 g/l, and hydrocarbonate calcium composition (in Dashkesan and Khanlar districts) or sulfate calcium. Water hardness is 2.5 mg-equiv./l.

Clayey composition of the Cretaceous deposits in the Nakhchivan Autonomic Republic (AR) mountainous zone combined with small quality of atmospheric precipitation determines their poor water abundance. In most springs, their yields do not achieve 1 l/sec, and the water is hydrocarbonate sodium or calcium.

Numerous mineral and thermal springs, associated with abyssal tectonic dislocations that are described separately, are confined to the Cretaceous deposits.

The results of prospecting well data permit to characterize water content in the Upper and Lower Cretaceous deposits that the non-artesian and artesian waters lying at the depth of down to 200–300 m are confined to. The Upper Cretaceous deposits stripped by wells at 9.4–298.0 m depth are distinguished everywhere by their elevated water content. The Upper Cretaceous age is mainly represented by the Maastrichtian, Campanian, Santonian, Cognac, and Cenomanian stages. The effective thickness of water-containing rocks changes from 27.0 to 175.0 m. Static level is established at the 5.0–43.0 m depths. Well yields are 0.5–12.0 l/sec, and specific yield is 0.01–1.03 l/sec·m. Permeability code of water-containing rocks is 0.03–5.5 m/day, and transmissibility coefficient is 3.0–746.0 m^2/day. According to the prospecting well data, chemical composition of groundwaters in the Upper Cretaceous deposits varies with the area. At its largest part the hydrocarbonate-sulfate sodium–calcium, hydrocarbonate–sulfate calcium–magnesium waters are found. At certain sites, increased content of sulfate ion is noted in groundwaters. Groundwater mineralization level is 0.2–1.3 g/l, and it is fresh and suits for agricultural needs.

The Lower Cretaceous deposits represented by the rocks of Albian, Aptian, Barremian, and Valanginian stages are stripped at the depths of 3–250 m. The effective thickness of water-containing rocks changes from 13.0 to 70.0 m. Static level is established at 2.30–40.0 m depths. Well yields vary from 1.8 to 11.5 l/sec, and specific yields are 0.10–0.26 l/sec·m. Permeability codes of water-containing rocks are 0.8–2.3 m/day, and transmissibility coefficients are 13.6–87.0 m^2/day. At this area largest parts of the Lower Cretaceous groundwaters contain essentially hydrocarbonate–sulfate calcium–sodium–magnesium. At certain sites, groundwaters display increased content of sulfate ion. Groundwater mineralization level is 0.3–0.9 g/l. These deposit waters are fresh and suit for agricultural water supply.

The Jurassic deposit aquifer system. According to their water abundancy, the Jurassic deposits are subdivided into volcanogenic–tuffaceous and carbonate ones (limestone). The former ones occur in the middle mountainous zone of Gedabey, Dashkesan and Agderi districts, where the largest number of springs with 0.4–0.5 l/sec yield is met. Along the Mrovdagh Ridge southern slope, groundwaters crop out along the thrust line that is not covered with talus. The spring yields are from one to tens liters per second, with prevailing yields of 10 l/sec. Tuffaceous formations compose vast areas in the Lesser Caucasus northern part, in the Dzegamchay-Koshkarchay interfluve. Along with high fracturing, a dense network of tectonic dislocations is observed here, and it is associated with the variability of outcropping springs. In the weathering zone, the spring yields are 0.1–2.0, occasionally 2–5 l/sec (0.5–0.6 l/sec on the average). Along the tectonic fracture line (2–3 km northeastward of Zaglik village), dense outcrop of water aquifers is observed and high-yield springs (9–32 l/sec) are confined to them. Limestone is characterized by elevated water abundance, and the confined springs have average yields of 5–8 l/sec.

In the Nakhchivan porous-fissured water basin, the Jurassic deposits occupy scarce areas. They are actually arid. In the weathering zone freshwaters with dissolved solids of 0.3–0.7 g/l are met, they are hydrocarbonate calcium and soft (total hardness is 3–7 mg-equiv/l).

In the area of iron ore (Dashkesan) and iron pyrite (Chiragidzor) deposits, sulfate ion content rises to 400–500 mg/l and more, and waters become sulfate–hydrocarbonate calcium and even sulfate calcium.

The Upper Jurassic deposits are stripped by the wells drilled in Novo-Ivanovka and Kichik-Karamurad villages in the Dzegamchay River upstream flow, in Gedabey district,

in Khojavend district, and in the town of Shusha. Water aquifer lying depth varies within 3.5–298.0 m. The effective thickness of water-containing rocks is 22.0–151.0 m. Static level is established at 3.50–47.0 m depth. The well yields vary from 5.3 to 7.3 l/sec, and specific yields are within 0.35–0.4 l/sec·m. Permeability code of water-containing rocks is 2.71 m/day. Transmissibility coefficient varies within 72.0–143.6 m^2/day. Groundwater chemical composition is hydrocarbonate calcium–magnesium. According to their chemical and physical properties, groundwaters have good drinking qualities and may be used for agricultural water supply.

The Middle Jurassic deposits are represented by the varieties of tuffaceous formations, by andesite porphyrites, quartz porphyrites, agglomerate lavas, lava breccia, and sandstone of the Bajocian and Bathonian stages. They are stripped by the wells drilled at the Shamkir High, the Khojavend trough, near the town of Shusha (Dashalty village). Water aquifer lying depth varies within 50–250 m. The effective thickness of water-containing rocks is 71.0–108.0 m. Static level is established at 50–70 m depth. The yields of the wells that stripped the Middle Jurassic deposits vary from 3.0 to 10.0 5.3 l/sec, and specific yields vary within 0.33–0.55 l/sec·m. Permeability code of water-containing rocks is 0.6–2.1 m/day. Transmissibility coefficient varies within 162–316.0 m^2/day. At the majority of the area, the Middle Jurassic groundwater chemical composition is hydrocarbonate calcium–sodium. Mineralization values vary within 0.26–0.45 g/l. The groundwaters are fresh, suitable for drinking and water supply for distant pastures.

Pressure waters of deep-seated circulation are, as a rule, mineral waters, and their seepages are concentrated in the Kyalbajar, Shusha, Gedabey, and Dashkesan districts.

The Triassic and Permian deposit aquifer system. The Triassic deposit complex is most widely spread in the Nakhchivan AR northwestern part and is sufficiently water-abundant. Its fissured and partly karst limestone and dolomites are water-bearing. A minor number of springs with yield of about 0.5 l/sec are confined to the Triassic deposits. A group of springs with overall yield of about 3.5 l/sec comes out of limestone. The waters are hydrocarbonate calcium, water temperature varies from 10 to 14 °C.

Water aquifer of the Permian deposits is developed at minor areas in the Nakhchivan AR northwestern part, where it is mainly represented by poorly watered marlstones. The amount of springs is very insignificant, their yields do not exceed 2 l/sec. In the Eastern Arpachay River valley, the spring yield reaches 35 l/sec. The water is fresh with dissolved solids of up to 1 g/l, hydrocarbonate calcium.

The Carboniferous and Devon deposit aquifer system. The Carboniferous deposits are mostly found in the Nakhchivan AR northwestern part. Here, they are represented by massive poorly fissured crystalline limestone and clay slates, with confined small number of low-yield springs. The water is fresh, hydrocarbonate calcium.

Water aquifer of the Devonian deposits is found sporadically, specifically, on Dashburun Mountain southern slope (Sadarak village). Overall yield is about 150 l/sec. The water is fresh (0.5 g/l), hydrocarbonate calcium, with temperature of 18–19 °C.

The intrusive formation aquifer system. Intrusive formations are investigated in Gedabey district and in certain areas of Khojavend district. The aquifer is confined to massive crystalline bodies, poorly exposed to fissuring and weathering. The intrusive formations are represented by acidic (granodiorites and granites), basic (gabbro, gabbro–diorites, pegmatites), and subvolcanic (dacites, andesite–dacites) differences. By their age, the rocks refer to the period of pre- and post-formation of the Cretaceous and Jurassic deposits. At their distribution area, some actually waterless rocks are met along with water-abundant ones. The springs confined to subvolcanic and intrusive rocks are represented by fissured dacites and granodiorites. They have a yield of up to 1.0 l/sec, and general water mineralization of up to 0.5 g/l. Springwater is used for drinking. It is hydrocarbonate calcium by its chemical composition.

Intrusive formations are stripped by the wells drilled at the northeastern part of the Lesser Caucasus, between the towns of Gedabey and Shamkir (Kharkhar, Slavyanka villages, etc.). Here, water-containing rocks are fissured gabbro–diorites, secondary quartzites, liparite–dacites, diorite–porphyrites. The groundwater lying interval varies within 12.5–45.0 m. Well yields are 5.0–6.5 l/sec, permeability code of water-containing rocks is 0.7–2.4 m/day, and transmissibility coefficient is 42.0–144.0 m^2/day. Water has hydrocarbonate calcium chemical composition.

1.2.3 The Talysh Fold-Mountain Zone

High rugged topography, intense drainage, limited formation areas, and scarcity of groundwater supply sources are responsible for the complexity of the Mountainous Talysh hydrogeological conditions. Within the region, some isolated structures are found that look like small-sized, isolated from one another groundwater basins, where the entire cycle of groundwater formation takes place: their supply, transit, outcropping, or discharge. In this aspect, the Yardymly artesian basin of the same-name depression is specifically distinguished as it consists of a series of small lower-order basins, confined to synclines and erosion cavity of lower tectonic order.

Groundwaters are associated **with the Quaternary period deposits** such as river valley alluvial formations, with proluvial and deluvial (talus) formations of the pediment

stripe and with upper weathered zone of basic rocks. Water supply areas for the ground rocks are mountain piedmonts and slopes within the weathering and distribution zone of deluvial formations represented by rudaceous non-bonded rock clusters that provide easy penetration of surface water into the soil and its further movement along the stratum dip direction or along topographic drift. In addition, the waters met in the river valley alluvial sediments are fed from surface water infiltration. At the deluvial deposit thinning border, groundwaters outcrop to the surface as ascending springs. Their yields do not exceed 0.6 l/sec.

Subsoil waters confined to alluvial sediments and to fissured main bottoms are stripped by wells drilled during prospecting. In the mountain zone, subsoil waters are met as separate flows confined to mountain slopes and confluent as a single flow at the topography flat plain. Local flows mainly correspond to the terrain inclination, while general, regional flows correspond to the river valley orientation. Occurrence depth of subsoil water bottom within the area under study varies from 42 to 80 m, sometimes even more. Their level depends on the area terrain and varies from fractions of a meter to 72 m. Yields of the wells that stripped subsoil waters by testing vary from 0.3 l/sec to 6.0 l/sec, their specific yields do not exceed 0.6 l/sec·m. Permeability codes of water-containing rocks vary from fractions of a meter to 4.5 m/day. Subsoil water mineralization values vary according to the investigation districts: In the northeastern part of Yardymly district, they are from 0.3 to 0.5 g/l; in the Vilyashchay River middle stream, they vary from 0.5 to 0.9 g/l, and in the northwestern area of the district, they vary from 0.3 to 0.5 g/l. Mineralization value rises up to 2 g/l. Increased mineralization water is essentially met in the Yardymly zone and is confined to the Maykop age deposits and to their debris that form the Quaternary age deluvial, proluvial, and alluvial formations.

Chemical composition of groundwaters is hydrocarbonate sodium and, sometimes, hydrocarbonate calcium.

Natural outcrops of groundwaters are confined to the Miocene–Oligocene and Eocene deposit water aquifers. Here, the wells discovered pressure waters, as well.

The Middle and Upper Miocene water aquifer is widely developed in the northwestern and northeastern zones of Talysh, where it is confined to the strata of broken sandstone and marls, lying among gray and brownish-grey clays. The aquifer is poorly watered. The yields of ascending spring do not reach 0.1–0.2 l/sec, water temperature reaches 11–16.5 °C. In the Talysh foothills, the water is at 10–13 m depth. It is fresh or weakly saline, with dissolved solids from 0.5 to 1.6 g/l, hydrocarbonate calcium–sodium–magnesium or hydrocarbonate–sulfate and hydrocarbonate–chloride calcium–magnesium.

The Maykop suite water aquifer is distributed in the Lilyushchay River middle stream. It is represented by interlayers of fissured argillites, sandstone, aleurolites, and their alternations. Here, the ascending springs are met with the yield of up to 3 l/sec, water temperature varies from 10–11 to 15–16 °C, water mineralization is 0.2–1.5 g/l, its contents are hydrocarbonate–sulfate calcium–magnesium.

Water aquifers of porous-edge-type water are sometimes confined to sandstone, tuff sandstone, they are stripped by the wells drilled at the Yardymly depression area. Stripped aquifer thicknesses vary from 33 to 95 m. Normal water pressure levels vary from +16 to −58 m. Well yields by spouting are 12–25 l/sec. Yields of the wells drilled in the terrain elevated parts are considerable lower, from 0.3 to 6.66 l/sec. Specific debits usually do not exceed 0.4 l/sec·m. Permeability codes of water-containing rocks vary from fractions of a meter to 2.4 m/day. Groundwater chemical content is hydrocarbonate sodium, with mineralization value from 0.4 to 2.0 g/l.

In the Yardymly depression central part pressure waters are found confined to the Maykop age sandstones. The aquifer depth of occurrence is 42–156 m. Well yield is 12 l/sec, specific yield is 1.05 l/sec·m, and permeability code is 1.1 m/day. The water contains hydrogen sulfide and hydrocarbonate sodium, with mineralization value of 0.4 g/l.

The Eocene water aquifer is confined to the fissured thickness of tuffaceous–sedimentary rocks that compose the highest sections of Talysh Mts. Numerous ascending springs are observed on the mountain slopes with yields from thousands of fractions to 2–2.5 l/sec and more. Water temperature is 8–16 °C. Mineralization reaches 0.1–0.5, occasionally, 0.7–0.9 g/l; the water contains hydrocarbonate calcium and calcium–sodium, sometimes hydrocarbonate–sulfate calcium. Water-level depth of occurrence varies from 16 to 37 m. Aquifer thickness is 83–125 m. The deposits that contain pressure waters are characterized by the code of permeability value of about 0.1–2.4 m/day. Well yields by pumping vary from 2.4 to 2.6 l/sec. Specific yields vary from 0.01 to 0.1 l/sec·m. The water is fresh, with dissolved solids of 0.3–0.4 g/l, hydrocarbonate calcium.

Within the Lerik syncline, the Eocene deposits are represented by tuff sandstones, sandstones, and argillites. Pressure waters confined to these deposits lie at the depth of 48–150 m, depths of occurrence of well water levels vary from 4.6 to 33 m. Yields by pumping do not exceed 2–6 l/sec, and specific yields vary from 0.2 to 0.4 l/sec·m. Permeability codes of water-containing rocks rise up to 1 m/day. It is a freshwater with dissolved solids of 0.4–0.5 g/l and has hydrocarbonate calcium chemical composition.

The Paleocene deposit aquifer system is found in the Tangerud, Istisu, and Astarachay River upper streams. According to lithological composition of its water-containing rocks, the aquifer is subdivided into three horizons (from the bottom upward): the aleurite–tuffite, the aleurolite, and the tuff sandstone. Water abundance of these deposits is defined

from their fracturing degree and manner. The springs are nearly all ascending, their yields are 0.5–0.7 l/sec, occasionally 1–1.2 l/sec. Water temperature rises to 8–16.5 °C, overall mineralization is 0.1–0.4 g/l. The composition is usually hydrocarbonate one, less frequently—hydrocarbonate–sulfate calcium–sodium.

1.3 Groundwater Formation and Distribution Regularities in the Piedmont and Intermountain Zones

Piedmont and intermountain plains (the Ganja-Gazakh, Ganykh-Airichay, Shirvan, Garabagh-Mil, Jebrail, Gusar, Lenkaran, and Nakhchivan) are distinguished by high yield of fresh and poorly brackish porous-edge waters. They consist of confluent river fans and are represented by the Upper Pliocene–Quaternary alluvial, alluvio-proluvial and alluvio-deluvial sediments, frequently of considerable thickness (up to 300–500, less frequently to 150–2000 m) and are composed of boulders, gravels, pebbles, sand, and clay loams. During its formation, the continental mass removed from the mountain area was deposited within piedmonts with perfectly traceable regularity. In the near-to-top sections of river fans, the lithological cross section consists of well-graded and washed coarse-grained material such as boulders and gravels, which further up the flow are replaced by gravel–pebbles, sands, clay loams, and clays. River fan periphery has predominant fine-dispersed clay loam–clay deposits (Israfilov 1972; Askerbeyli et al. 1974, 1977; Israfilov 1978; Listengarten 1983, 1987; Alekperov 1986; Alimov 2002; Alekperov et al. 2008).

Groundwater in the near-to-top sections of river fans creates a single unconfined aquifer, whereas in central and peripheral parts, following emergence of clays or clayey fillers, a single water aquifer is subdivided into the proper unconfined aquifer and a number of pressure water aquifers. Actually, unconfined and several pressure water aquifers occur in each of said pore-edge water basins. Thus, river fan deposits of the Ganja-Gazakh piedmont plain demonstrate one unconfined and four pressure aquifers down to the investigated depth: Those of the Gusar, Garabagh, and Mil have one unconfined and five pressure aquifers; the Ganykh-Airichay deposit has one unconfined and one poorly defined pressure horizon; the Lenkaran deposit has one unconfined and five pressure horizons; the Jebrail and Nakhchivan deposits have one unconfined and one pressure water-bearing horizons.

In the near-to-top section, intense absorption of precipitations and surface runoff takes place. Moving further along the plain, already like isolated unconfined and pressure aquifers, groundwater, owing to comb-type structure of the Upper Pliocene–Quaternary and Quaternary coarse deposits, tends to the regional discharge zone. The central parts of the river fan serves as a groundwater transit zone and as runoff redistribution zone between individual water-bearing horizons. The unconfined aquifer, having maximal thickness in its formation zone, sweepingly loses it, and thins out approaching the discharge zone, while the pressure aquifers obtain thickness downstream, in the transit zone. In the discharge zone, thickness of pressure aquifers decreases.

The Kur River is the discharge zone for the Ganja-Gazakh, Garabag-Mil, and Shirvan plains groundwater, and the Araz River is the discharge zone for the Nakhchivan and Jebrail plains. Alternative situation is observed at the Ganykh-Airichay plain. Distinguishing feature of the plain hydrogeological conditions is the fact that groundwater flow that originates from the Greater Caucasus foothills, abuts in its lower part, along the Neogene foothill borders, a powerful layer of essentially watertight deposits. Due to the absence of a distinctly pronounced discharge drainage (such as the Kur and Araz rivers), groundwater flow acquires high head that is also spread backward, to the Greater Caucasus foothills.

1.3.1 Groundwater Hydrochemical Characteristics and Their Zoning

Groundwater of all plains contains fluorine, nitrates, iron, copper, zinc, stable strontium, molybdenum, uranium, arsenic, selenium, and lead, and only at some of the plains, it also contains beryllium and manganese. Average content of beryllium, manganese, iron, selenium, molybdenum, and radioactive elements is close to the sensitivity of their determination technique (Table 1.3).

1.3.2 Groundwater Formation and Distribution Regularities in the Piedmont Neogene Deposits

Let us take a look at groundwater formation and distribution regularities in the Neogene deposits of Jeiranchol and Ajinour plateaus of Azerbaijan (Lange 1961; Alekperov et al. 2008).

The Jeiranchol Plateau is composed of the rocks from the Sarmatian to the Quaternary age, and the Ajinour Plateau rocks are from the Lower Pliocene (productive strata) to the Quaternary age. The Ajinour basins are filled with thick mass of continental Quaternary formations. All these precipitations are dislocated so that the most intense dislocation is within the elevations. The deposits are represented by all lithological differences of sedimentary rocks (from coarse conglomerates to clays).

Arid climate, poor rock permeability, area drainage conditions owing to ravine and gulch network and the presence

Table 1.3 Distribution of trace elements in poorly mineralized groundwaters of Azerbaijan piedmont and intermountain plains

Parameters of water chemical composition	Maximum admissible concentration according to state standard for agricultural and drinking consumption	PLAIN S								
		Gusar	Ganykh-Airichay	Shirvan	Ganja-Gazakh	Garabagh	Mil	Jebrail	Lenkaran	Nakhchivan
1	2	3	4	5	6	7	8	9	10	11
Beryllium, μg/l	0.2	0.04–0.2	N\det	Traces	no	Traces	N\det	N\det	N\det	no
Fluorine, μg/l	1500	257–1500	123–680	373–750	470–1520	221–800	429–1500	183–1080	186–600	362–1200
Manganese, μg/l	100	no	6.2–30	no	Traces	4.6–90	Traces	Traces	N\det	Traces
Iron, μg/l	300	7.2–30	3.3–10	15.1–50	15.8–125	4.7–70	17.7–130	10.5–100	N\det	6.3–25
Copper, μg/l	1000	83–750	21.3–60	75–500	12–200	43–200	1.7–35	4.1–34	3.6–15	4.6–100
Zinc, μg/l	5000	90–4000	13.2–50	1.3–12	13.2–400	23.9–400	4.6–42	57.5–160	8.0–45	318–4200
Arsenic, μg/l	50	2.4–40	6.1–30	no	9.9–44	7.0–45	13.9–50	11.5–30	16.4–40	12.1–50
Selenium, μg/l	1	0.4–1	N\det	0.42–1	No	0.33–0.9	N\det	N\det	N\det	0.37–1
Strontium stable, μg/l	2000	545–1400	656 300–1700	641 250–1300	670–2000	419– 1950	433–1800	548 85–2000	895 350–2100	684–2000
Molybdenum, μg/l	500	3.0–70	Traces	1.6–4	5.5–20	2.8–10	1.0–10	31.9–100	0.9–3	1.9–50
Lead, μg/l	100	27–100	no	40–80	37–90	22–80	2.3–50	2.8–20	no	9.1–40
Uranium, μg/l	1700	1.5–7	0.34–0.6	0.74–1.9	Traces	1.94– 15.5	N\det	N\det	N\det	Traces
Radium-226, Ku/l	1.2×10^{-10}	5.1×10^{-13}– $2.7 \times 1\ 0^{-12}$	N\det.	Traces	10.5×10^{-13} to 1.6×10^{-12}	Traces	N\det	N\det N \det	N\det	9.4×10^{-13} to 3.7×10^{-12}
Strontium-90, Ku/l	4×10^{-10}	2.8×10^{-13}– 1.2×10^{-12}	N\det	5×10^{-13}	3.5×10^{-13} to 6.2×10^{-13}	N\det	N\det		N\det	2.3×10^{-13} to 3×10^{-13}
pH	no	7.7 6.9–8.2	7.7 6.7–8.2	7.6 7.5–7.7	7.7 6.5–8.2	7.8 7.4–8.4	7.7 7.1–8.3	7.6 7.0–8.1	7.5 6.6–8.2	7.8 6.6–8.3

Notes In parameter columns for various plains, the numerator is the average content and the denominator contains limited values of the parameters

of deeply incised valleys of transit rivers (Ajinour), of numerous thrusts and faults (Jeiranchol) that isolate separate blocks, do not promote the formation of large groundwater reserves here—either as groundwater basins or as consistent aquifers. In Ajinour, potential groundwater basins are the steppes filled by thick (up to 600 m) mass of coarse deposits. Mountain ridges that separate the steppes are composed essentially of clays, and for this reason, their role in groundwater recharge is not significant.

Non-artesian waters, confined to the Quaternary deposits, are found in the western part of the Jeiranchol Plateau, and as infrabed water in the Aljiganchay, Turianchay, Geichay, and Girdymanchay River valleys of the Ajinour Plateau, as well as within the Aresh Trough and the Ivanovka Plateau.

Thickness of water-containing rocks in river values varies from 27.9 (the Girdymanchay River) to 91 m (the Aljiganchay River). Depth of occurrence of infrabed waters varies from 0.0 (the Aljiganchay River valley) to 17.1 m (the Girdymanchay River). Well yield varies from 6.25 (the Girdymanchay River) to 12.2 l/sec (the Aljiganchay River). Specific yields are from 0.28 (the Aljiganchay River) to 1.04 l/sec·m (the Turianchay River). Permeability codes of water-containing rocks, represented by coarse boulder–gravel–pebble deposits with sandy filler, vary from 1.04 (Aljiganchay River) to 5.28 m/day (the Turianchay River). Rock water transmissibility is from 75 (Girdymanchay River) to 350 m^2/day (the Aljiganchay River). The infrabed waters are fresh everywhere, with mineralization varying from 0.35 to 1.0 g/l, water chemical composition varies from hydrocarbonate calcium to sulfate sodium. General hardness is 3.39–6.95 mg-equiv/l.

Non-artesian waters of the Quaternary deposits occur within the Aresh trough and the Ivanovka Plateau at the depth of 12.0–26.6 m. The effective thickness of water-containing rocks represented by boulder–gravel–pebble deposits with sandy filler varies from 20.5 to 37.0 m. Well yields vary from 2.3 to 9.1 l/sec, and specific yields are 0.1–1.0 l/sec·m. Permeability codes of water-containing rocks vary from 0.42 to 4.34 m/day, and water transmissibility varies from 0 to 180 m^2/day. Water is fresh and sometimes low-mineralized. Water mineralization varies from 0.4 to 1.9 g/l, and its chemical content varies from hydrocarbonate calcium to sulfate sodium. Chloride sodium waters are also met.

In Jeiranchol, the Quaternary deposits water out periodically, resulting in the emergence (after rains) of springs with 0.07–0.1 l/sec yield. The water is low mineralized and drinkable. In Ajinour, the largest number of springs is confined to the northern ridge coarse rocks, and they frequently outcrop in ravine and gulch lower parts, along the contact lines of watertight and Pleistocene rocks.

In Ajinohur Lake area, subsoil waters are met sporadically. The bottom of water-saturated thickness is stripped at 16.1 m depth. Water level is established at 2 m below well mouth. The water contains dissolved solids of 88.6 g/l, of chloride sodium composition, with 273.5 mg-equiv/l hardness. Total yield of the right-bank springs is about 30 l/sec, the dissolved solids in spring water amount to 1.55 g/l, total hardness is 11 mg-equiv/l. Total yield of the left-bank springs is 4-5 l/sec, hardness equals to 13 mg-equiv/l.

Pressure waters. The Quaternary deposit aquifer in Jeiranchol is confined to thin sand bands in clay thickness. It is a thin aquifer of highly mineralized pressure waters stripped by wells at 150 m depth.

At Ajinour area, overlying bed of pressure waters is stripped at 67.0–79.0 m depth. Normal pressure surface level varies within −(15.5–66.0) m. Water strikes are confined to gravel–pebble deposits with sandy filler and to sands. Thickness of water-containing rocks varies from 51.0 to 266.5 m. Permeability codes are 0.24–4.85 m/day, and transmissibility coefficients are 50–250 m^2/day. Well yields vary from 3.3 to 10.5 m/sec, and specific yields vary from 0.15 to 1.0 l/sec·m. Water strikes of Quaternary deposits are fresh; their mineralization does not exceed 1.0 g/l, and their chemical composition varies from hydrocarbonate calcium–sodium to chloride–sulfate sodium–calcium, and water hardness is 5.20–12.36 mg-equiv/l.

The well, drilled south of the Ajinohur Lake, has encountered a water strike aquifer in the Quaternary deposits, at 108–123 m depth. The water pressure surface level was established at 8.1 m higher that the well mouth. Well yield by spouting was 0.8 l/sec, specific yield was 0.1 l/sec·m, and permeability codes of water-containing rocks amounted to 0.8 m/day. The water is low mineralized with dissolved solids of 3.4 g/l, hydrocarbonate–chloride sodium–magnesium.

In the Ajinour Lake area, groundwater is mineralized (68.23 g/l) and very hardly mineralized (331.5 mg-equiv/l).

Pressure waters confined to the Upper Pliocene deposits are stripped at 60–300 m depth. Groundwater pressure surface level was established at 15.5–81.4 m depth. Well yields vary from 2.8 to 10.5 l/sec, and specific yields are from 0.06 to 1.0 l/sec·m. Permeability codes of water-containing rocks amount to 0.13–4.85 m/day, and transmissibility coefficients are 10–190 m^2/day. The water is fresh and low mineralized. Mineralization value varies from 0.3 to 2.5 g/l, and hardness is 5.50–6.10 mg-equiv/l. chemical composition varies from calcium hydrocarbonate to sodium chloride.

Water aquifer of the Miocene deposits is represented by sandstone bands, sands, and conglomerates, confined to clays. All of them, except the Sarmatian stage deposits, are virtually waterless. Several ascending springs confined to the Tortonian stage sandstones are recorded in a gulch north of

Bandygel Lake, at the southern slope of Yaylajik Ridge, and in Udabno Mountain area. Spring yields are small, with 40 g/l mineralization, sodium sulfate.

1.4 Groundwater Formation and Distribution Regularities in Lowlands

The republic lowlands include the southeastern part of Shirvan porous-edge water basin and the Mughan-Salyany porous-edge water basin. The lowland area is composed of the Upper Pliocene–Quaternary age marine and continental deposits. Continental deposits, represented by alluvium of the Kur, Araz, and Bolgarchay rivers, are subordinate and do not play significant role in the formation of hydrogeological conditions (Lange 1961; Israfilov 1972; Listengarten 1983; Alekperov et al. 2008).

1.4.1 Groundwater Formation and Distribution Regularities in Azerbaijan Lowlands

One ground and two pressure aquifers are confined to the Upper Pliocene–Quaternary deposits. Ground aquifer is found everywhere.

In southeastern part of the Shirvan porous-edge water basin, the water table aquifer lies essentially at the depths from 0.1–1.0 m to 3–5 m. Within Kyursengya, Babazanan, Durovdagh, and Geitepe anticline highs, as well as within the buried Pirsaat River fan, depth of occurrence of water table aquifer exceeds 5–10 m. The distinguishing property of the southeastern part of the Shirvan porous-edge water basin is that the groundwater flow is directed to the basin center with 0.001–0.002 inclination. The thickness of groundwater aquifer varies within 10–20 m, prospecting well yields by testing are 1.1–4.5 l/sec, permeability code of water-containing rocks is 1.5–10.0 m/day, and transmissibility value is from 22 to 165 m^2/day.

Within the Mughan-Salyany plain, the water table aquifer lies at the depths from 1–3 to 10–15 m, and at the area predominant part, it approaches the daylight surface. Direction of the groundwater flow is west-to-east, and within the northern Mughan area, it is directed southeastward. The groundwater discharge areas are the Kur River and the Caspian Sea. Sloping water table is 0.01–0.001 and less.

Confined aquifers are stripped by prospect boreholes everywhere in the Khvalyn-Khazar deposits (the Middle–Upper Pleistocene) and in the Baku horizon (the Lower Pleistocene), at the depths from 20 to 200 m and lower, except the foothill stripe. At the Araz River fan, the overlying bed lies at the depth of 15–120 m. Water-containing rocks are represented by gravel–cobble deposits with sandy filler and sands. The aquifer thickness reaches up to 20 m. Piezometric levels are established both higher (up to +10 m) and lower (down to 20 m) of the earth surface, and groundwater flow slope is within 0.0007–0.0004. Prospect well yields by testing reach up to 0.1–3.1 l/sec, by spouting, they reach 1–2 l/sec. Permeability codes of water-containing rocks are 0.31–6.32 m/day.

At lowland sites contacting the near-Talysh zone, water aquifer of alluvial–proluvial deposits is exposed by well at the depth of 15–35 m. Lithological composition of water-containing rocks, represented by gravel–cobble deposits in the west, is in the east replaced by sands and sandy loam. Deposit thickness is less than 10 m, occasionally even more. Piezometric levels are established from 20 m lower to 15 m higher than the earth surface and rise toward the sea. Groundwater flow slope is within 0.001–0.0001.

Approaching the Kur River delta, the overlying bed is exposed at 22.5–38.0 m depth. Water-containing rocks are represented by sands of up to 25 m thickness. Permeability codes of water-containing rocks vary within 0.55–0.96 m/day, and rarely reach 4.86 m/day. Piezometric levels are established either higher (up to +0.09–0.86 m) or lower (down to −0.5–−1.6 m) than the earth surface.

At the Bolgarchay River cone delta, the overlying bed is exposed at up to 150 m depth. Water-containing rocks are also represented by sands of up to 35 m thickness. Well yields by testing are 3–5 l/sec. Permeability codes of water-containing rocks amount to 0.65 m/day. Piezometric levels are established at 3 m above the earth surface.

In the Kur River delta, the aquifer is exposed at 130–150 m depth. Thickness of water-bearing sands varies within 5–10 m, permeability codes amount to 1 m/day. Piezometric levels are established at 0.09–0.9 m below at the southern part of the area, and at 1–2 m higher than the earth surface at the northern part of the area.

On the Kur River alluvial plain, the aquifer overlying bed is exposed at 150–200 m depth. Water-containing rocks are represented by fine-grained loam sands. Their thickness is 8–12 m and more, their permeability codes reach up to 0.54–1.05 m/day. Piezometric levels are set up to 2 m above the earth surface.

Level of knowledge of pressure waters in the southeastern part of the Shirvan porous-edge water basin is insufficient for providing their complete hydrogeological behavior. Pressure waters are exposed here in the Quaternary deposits, at 35–116 m depths. Thickness of the aquifer represented by sands with clay veins varies within 5–74 m. Yields of prospecting wells by testing amount to 0.3–2.2 l/sec. Permeability codes of water-containing rocks are from 0.01 to 1.3 m/day, and aquifer transmissibility amounts to 28 m^2/day.

Fresh and low-mineralized groundwater is distributed within the Mughan-Salyany porous-edge water basin only in confined areas such as the Araz and Bolgarchay River fans.

Mineralization values of these waters are from 0.8–1.0 g/l to 2.0–2.6 g/l, chemical composition is hydrocarbonate and hydrocarbonate–sulfate calcium. Toward the Caspian Sea, groundwater mineralization value rises up to 50–60 g/l, its chemical composition turns into sodium chloride. Useful groundwater resources of the Bolgarchay River fan are estimated and approved as 23.4 thousand m^3/day.

Mineralization values of both groundwater and pressure water in the southeastern part of the Shirvan porous-edge water basin are rather high and vary from 3–5 g/l to 100–150 g/l, its chemical composition is sulfate–chlorite and sodium chloride.

1.4.2 Groundwater Formation and Distribution Regularities in the Absheron Peninsula

The Absheron Peninsula is characterized by rather complicated hydrogeological conditions. Due to combining separate hydrogeological elements of piedmont plains, sea coasts, steppes, resulting from peculiar physical geographical, geological, and geomorphological features, the Peninsular hydrogeological conditions cannot be finally classified in accordance with generally accepted hydrogeological classifications of geological structures (Listengarten 1983; Israfilov 1999; Alekperov 2005; Alekperov et al. 2008).

Non-artesian and artesian waters are abundant within the Absheron Peninsula and are confined to limestone, sandstone, sands, and sandy loams from the Quaternary age to productive strata. Hydrogeological conditions of the eastern and western Absheron show considerable difference. The stratigraphic border between the Upper Pliocene and the Eopleostocene serves as the boundary between these two hydrogeological regions. It passes southeastward along the eastern suburbs of Goradil, Fatmai, Mamedli, Zabrat, Surakhany settlements, and, acquiring a strictly southern direction, reaches the Govsan Cape. This border is traced on actually all geological and hydrogeological maps.

As it was already remarked, in natural conditions, the region was a sporadically watered zone, with absent regionally distributed aquifer. As the territory was being developed, as artificial water supply sources emerged, the area of sporadic groundwater distribution decreased consistently. The process was particularly accelerated after commissioning of the Jeiranbatan storage reservoir and the Samur-Absheron channel (SAC) in 1956. At present, groundwater is consistently developed at the largest part of the western Absheron. Of high importance is the fact that upper part of cross section of all stratigraphic units participates in the generation of a single non-artesian aquifer. Under current conditions, the western and eastern Absheron non-artesian waters are hydrogeologically linked and constitute a unified hydrodynamic system.

Non-artesian water. The non-artesian water flow is directed from the western Absheron toward the eastern one (Alekperov et al. 2008). Within the eastern Absheron, some areas of sporadic groundwater distribution are isolated as islets. They pass in the shape of chain through the Novkhany, Fatmai, and Kirmaki anticlines. Non-artesian groundwater is also sporadically distributed at the vast area between the Jeiranbatan storage reservoir and Masazyr Lake.

On the western Absheron, non-artesian water levels at the areal extent sites are found at 0 to 13.4 m depths. Depth of non-artesian water occurrence within the western Absheron has a rather complicate nature. The smallest depth of occurrence is found at the areas in the Peninsula NE part, between the town of Sumgayit and the Jeiranbatan storage reservoir.

Groundwater of the Greater Baku that was generated at the area of about 200 km^2 is forced to leak in the city central part, at the lowest marks, and discharge into the Caspian Sea as 15 km front through thin and low-permeable rocks. Geological and structural conditions of the Baku trough region predetermined generation of the groundwater basin over its entire area so that all flows are confluent in the city central seaside section. In the Baku trough area, despite the fact that non-artesian water is met at various levels, the depth of 5–10 m is the predominant one. The lowest depth of occurrence of non-artesian water is found at the western, northwestern, eastern, and northeastern edges of the trough. In the west, it occurs at 14–58 m depths, and in the east, at 27–52 m depths.

In the eastern Absheron, depths of occurrence of non-artesian water vary within very broad limits, from 0 to 30 m and more. The central part of the peninsula, located west of the boundary between the western and eastern Absheron, virtually along the entire boundary length is characterized by minimal values of water occurrence depths. This area includes Zabrat settlement area, and the territory where Baku Airport is located. Groundwater occupies the entire lowland around these areas and has depth of 1–2 m occurrence. Westward of this zone, depth of occurrence promptly increases with the terrain rise. The entire said raised part of eastern Absheron, from Nardaran village to Zire village, is characterized by 10–20 m depths of occurrence of non-artesian water. On the Nardaran-Buzovna plateau, from Bilgya settlement to Buzovna settlement, and in the Shuvelyany water intake area, groundwater occurs at maximal depths.

Rock water abundance in the western Absheron is low. In its NE part, at the area between the town of Sumgayit and Novkhany summer cottages, the yields of 0.3–3.0 l/sec were obtained by well testing. The largest yields were in this part

obtained from the wells of 30–50 m depths, drilled at the site of Novkhany summer cottages. It seems that the Absheron principal channel also shows its impact. In Jeiranbatan settlement area, well yields are 0.4–0.9 l/sec, and specific yields in the NW are from 0.05 to 0.31, essentially, 0.06–0.09 l/sec·m. Permeability codes of water-containing rocks vary here from 0.3 to 3.6 m/day. At the site located among Mirzaladi, Masazyr, and Beyuk-Shor Lakes, specific yields are 0.06–0.12 l/sec·m, and the permeability code for water-containing rocks is from 0.9 to 2.1 m/day. The well drilled in the town of Khyrdalan yielded 0.6 l/sec, with specific yields of 0.05 l/sec·m. Rock permeability code is 0.7 m/day. It should be noted that not the entire area of the town of Khurdalan is water-abundant, groundwater of practical importance is found mainly in the town SW section. At the area, NW adjoining Khoja Gasan lake, well yields amount to 0.2 l/sec, specific yields are 0.02–0.05 l/sec·m, and rock permeability code varies from 0.1 to 0.7 l/sec; the well located SW of the lake yielded 0.5 l/sec, with specific yield of 0.06 l/sec·m. Rock permeability codes are large (3.1 m/day).

In the southwest part of the peninsula, well yields increase seaward (Lokbatan settlement—0.7 l/sec, sea shore—3.5 l/sec). Specific yields also rise in this direction, from 0.01–0.09 to 0.15–0.23 l/sec·m. Permeability codes of water-containing rocks are 0.03–1.0 m/day.

Within the Baku trough, non-artesian aquifer is characterized by good water intake. In the trough peripheral zone, where construction is under way, the aquifer thickness is highly variable and varies with the development rate. By water pumping from wells, yields from 0.2 to 5.9 l/sec were obtained. Peak yields were obtained near Yasamal village. Specific yields vary from 0.02 to 0.36 l/sec·m. Permeability code of water-containing rocks varies from 0.1 to 25.9 m/day. Permeability codes of water-containing rocks in the Baku trough central part vary from 0.2 to 9.2 m/day. Their highest values are observed in the seaside stripe, in the new market area, in the territory eastern part. During pumping, water yields from 0.2 to 5.0 l/sec were produced, with predominant yields of 0.4–0.8 l/sec. Specific yields vary from 0.02 to 0.30 l/sec·m.

In the eastern Absheron, wells yielded up to 9.8 l/sec of water from unconfined aquifer. The Nardaran-Zagulba plateau displayed the best hydrogeological parameters, where well yields by testing amounted to 2.0–10.0 l/sec. Permeability codes of water-containing rocks are 1.1–5.2 m/day. Aquifer thickness amounts to 60–70 m. It should be noted that such thickness is actually typical for the entire eastern Absheron.

Water strikes. The data on water strikes given below relate to the upper 200–300 m thickness of geological cross section.

In the western part of the peninsula, the water strike aquifer is confined to the productive strata deposits. The aquifer overlying bed is NW exposed at 49–70 m depth, and SW exposed at 30–54 m depth. The depths under investigation are 200–250 and 100 m, respectively. In the Peninsula NW, at the site between the town of Sumgayit in the west, Geradil village in the east, and Masazyr Lake in the south, pressure water levels are established at the depths from 3.4 to 18.7 m. By water pumping from wells, the yields of 1.0–7.0 l/sec were produced. The highest yields (7.0 l/sec) were produced in Geradil village area. Well's specific yields are 0.07–0.80 l/sec·m. Permeability codes of water-containing rocks vary from 0.2 to 1.9 m/day, with peak value in Geradil village area. In the SW, at Garadag-Puta site, piezometric levels are established at 1–2 m depth from the earth surface. By water pumping, 0.3–0.9 l/sec yields were produced, with specific debits of 0.03–0.11 l/sec·m. Rock permeability code is 0.07–0.14 m/day.

Pressure waters are distributed within the Gyuzdek Trough, in the Middle Absheron limestone, at 13–35 m depths. Prospect well yields are from fractions to 7.7 l/sec (up to 2.0 l/sec by spouting), and specific yields are up to 2.2 l/sec·m. Permeability code of water-containing thickness is from 0.17 to 13.8 m/day.

Within the Baku trough, pressure waters are mainly distributed in Baku central part. The unconfined aquifer system, composed of a number of aquifers and layers, is confined to the Lower Quaternary system and is represented by sands, sandstones, limestone. General trend of groundwater flow is radial, toward the Caspian Sea, and it correlates with the region geological and tectonic structure and geomorphological features and is identical to the non-artesian water flow. The relation between artesian and non-artesian water within the basin is very intricate. Judging from the relationship between the absolute values of non-artesian water table and piezometric surface of artesian water, complex hydrodynamic processes take place in the city central part: pressure flow discharges both into the unconfined aquifer and into the Caspian Sea. Overlying bed of artesian aquifer lies at the depth from 20 to 105 m. Its least depth is in the seaside stripe, where artesian waters are stripped within the trough narrow seaside stripe. The largest depth of occurrence of artesian aquifer overlying bed (from 92 to 105 m) is observed in the Nasimi neighborhood upland part and in Bakikhanov township. Pressure water piezometric levels are established at the depths from −40 to +0.8 m. At the areas located below initial level, the wells blow out. Well yields by pumping vary from 0.1 to 3.8 l/sec. Permeability code of water-containing thickness varies within 0.1–1.2 m/day.

At the eastern Absheron, artesian waters are stripped by wells in all places, except the Gala uplift. They are confined to the Pleistocene sands, sandstone, limestone (the Baku, Gyurcya, Khazar aquifers), and to the Eopleistocene middle and upper parts. Distribution areas of the Akchagyl regional stage and the Lower Eopleistocene deposits are mostly

waterless. In vertical section, these deposits, particularly the Akchagyl ones, separate hydrodynamic systems of the Quaternary deposit pressure water from those of the productive thickness. In view of the fact that the Quaternary complex bottom lies at the depths of below 700–800 m, while the relatively investigated depth does not exceed 200–250 m, we find it impossible to provide comprehensive hydrogeological characteristic of the system. Confining overlying bed of the Lower Eopleistocene aquifer at the north part of the peninsula is exposed by wells at 63–88 m depth, and its bottom, at 144–235 m depth. Piezometric levels at these sites are established at 7.4–12.9 m depths. By water pumping from the wells, the yields from 0.6 to 2.6 l/sec were produced, with specific yields from 0.5 to 0.21 l/sec·m. Permeability code of water-containing rocks is 0.3–1.9 m/day.

Within the Bina-Govsan trough, two artesian aquifers are well stripped. The upper aquifer roof, confined to the Lower Pleistocene limestone and fine-grained sands (the Baku horizon), lies at the depths of 30–46 m, and its bottom is at the depths of 35–72 m. Piezometric level is established at the depths from 4.0 to 16.0 m, and in the south, in Govsan Settlement area, at +0.5 m mark. Well yields by pumping vary from 1.0 to 5.0 l/sec, specific debits are 0.9–4.5 l/sec·m. Permeability codes of water-containing rocks vary from 0.04 to 3.0 m/day. The southern part of the trough is characterized by peak water abundancy, where rock permeability codes amount to 10 m/day, and water transmissibility is up to 400–500 m^2/day.

The second pressure aquifer of the Bina-Govsan trough, confined to the Eopleistocene deposits (the Absheron regional stage) is stripped within 19–69 m range at the area adjacent to the Gala uplift. Piezometric level is established at the earth surface, water pumping showed the yield of 1.0 l/sec and specific yield of 0.15 l/sec·m. The thickness permeability code is 0.32 m/day.

An artesian aquifer confined to the Lower Pleistocene and Eopleistocene fine-grained sands is distributed in the area located southeastward of the Gala uplift and including the Zire Trough and the Shakh foreland. The aquifer roof is stripped by wells at the depths of 27–62 m, and its bottom is at 40–68 m depths. The efficient thickness of the aquifer is rather small, from 4 to 6 m. Piezometric level is established at the depths of 17–23 m. Well yields by pumping are 0.7–1.0 l/sec, and specific yields are 0.02–0.04 l/sec·m. Permeability code of water-containing rocks amounts to 1.0 m/day.

Rather high variability in mineralization value and in non-artesian water chemical composition in vertical and horizontal sections hinders the detection of certain regularities in their variations.

At western Absheron, mineralization value of non-artesian water varies within a broad range. Here, water with mineralization value from 0.5–0.7 to 100 g/l and more can be met. The largest part of this area is occupied by non-artesian water with mineralization value of above 20 g/l. Groundwater originating in the west, in Pre-Pliocene deposits of sporadic distribution, is as a rule, highly mineralized.

Predominant chemical composition of the western Absheron non-artesian water is chloride–sulfate sodium–magnesium. At some areas, basically at the region southwest, chloride sodium water is met.

The area of Gala uplift stands out against the general background of the eastern Absheron low-mineralized water by its highly mineralized (up to 20–25 g/l) non-artesian waters of chloride sodium–magnesium and chloride–sulfate sodium–magnesium composition. The entire Shakh foreland is occupied by water of sodium chloride composition with mineralization value of 55–60 g/l.

At the large part of eastern Absheron virtually freshwater is distributed, with mineralization value of 1.0–1.5 g/l and of mixed chemical composition. Such areas are observed on the Nardaran-Bilgya plateau, near Mardakyan, Shuvelyan, Zire, Dyubendi villages, in the Bina-Govsan Trough. Lithological composition of constituent rocks plays essential role in the formation of relatively favorable hydrochemical situation in the eastern Absheron, in addition to all other factors.

1.5 Resources and Reserves of Fresh Groundwater

Estimation of groundwater commercial reserves in Azerbaijan was made, basing on porous-edge water basins at piedmont plains, and was used for the substantiation of master plans of multipurpose utilization and protection of water resources (regional estimate) and at local sites, for water supply to cities, towns, rural populated areas, individual industrial and agricultural facilities (Aliyev et al. 1971; Israfilov and Krasilschikov 1973; Askerbeyli et al. 1974, 1977; Babayev 1974; Israfilov 1978, Israfilov et al. 1979; Krasilschikov et al. 1978; Israfilov et al. 1979; Listengarten 1983, 1987; Israfilov 1983; Aliyev 1996; Alimov 2001, 2002; Israfilov 2001; Alekperov et al. 2008).

1.5.1 Formation Conditions of Fresh Groundwater Resources and Reserves

Formation, transit, and discharge conditions for groundwater in fold-mountain zones and in piedmont plains differ greatly, and it is basically caused by man-made factors, extensively developed in the piedmont plains and poorly apprehensible in the mountain regions. In this connection, groundwater reserves and resources in fold-mountain zones are closer to the natural ones. At the same time, extensive water

development activities on the Republic lowlands resulted in changes in natural supply sources and in emergence of additional artificial sources that create groundwater reserves and resources.

A portion of natural subsoil runoff in fracture-vein rocks of fold-mountain zones in the active water exchange or free circulation zones (the zone thickness is determined by the depth of hydrographic incision, amounting to 1500–1800 m) is vigorously drained by hydrographic network and comprises the underground constituent of overall river runoff from the mountain regions. For this reason, subsoil flow of fracture-vein waters in active water exchange zone, contacting with the piedmont plain deposits, is quite insignificant. Another portion of groundwater that has been generated here is the deep circulation runoff for fracture-vein waters subjacent to the cross section of active water exchange zone.

Israfilov (1999) research indicates that it is at the contact between the ridge-tops of piedmont plain river fans and fracture-vein waters in deep circulation zones that the

Table 1.4 Commercial reserves of fresh (up to 1 g/l) and low-mineralized (1–3 g/l) groundwater of Azerbaijan Republic

Code	Name of hydrogeological region or of the first-order groundwater basin (GWB-I) and second-order GWB-II (according to state water cadastre)	*Hydrogeology of the USSR*, vol. **XII** (Azerbaijan), 1969, Moscow (p. 51)	Regional commercial reserves, thou. m^3/day					Registered in water consumption inventory, the numerator means regional reserves and the denominator means tested and approved reserves
			Approved			Approved by the SCR	Non-approved by the SCR	
			State committee on reserves (SCR) of the former USSR	Areal committee on reserves of the former Azerbaijan SSR	Total			
1	2	3	4	5	6	7	8	9
I	The Greater Caucasus folded system	241.92	–	10.1	10.1	–	241.62	$\frac{251.72}{10.1}$
I_1	including: Mountain zone	–	–	–	–	–	–	–
I_2	The Absheron Peninsula	241.92	–	0.3	0.3	–	241.62	$\frac{241.92}{0.3}$
I_3	The Greater Caucasus southeastern plunging (Gobustan)	–	–	9.8	9.8	–	–	$\frac{9.8}{9.8}$
II	The Eastern near-Caucasian artesian basin	3481.92	1664.2	33.1	1697.3	–	1784.62	$\frac{3481.92}{1697.3}$
II_1	Including: Mountain zone	–	–	–	–	–	–	–
II_2	The Gusar-Devechi piedmont plain	3481.92	1664.2	33.1	1697.3	–	–	$\frac{1697.3}{1697.3}$
III	The Kur Depression	5875.2	2953.9	327.8	3281.7	5806.0	–	$\frac{9087.7}{3281.7}$
III_1	Including: the Alazan-Ayrichay valley	1503.36	2000.0	–	2000.0	–	–	$\frac{2000.0}{2000.0}$
III_2	The Ganja-Gasakh piedmont plain	1650.24	433.6	18.8	452.4	3772.2	–	$\frac{4224.6}{452.4}$
III_3	The Shirvan plain	639.36	–	158.7	158.7	359.0	–	$\frac{517.7}{158.7}$
III_4	The Garabag-Mil piedmont plain	2082.24	444.3	150.3	594.6	1674.8	–	$\frac{2269.4}{594.6}$
III_5	The Mughan-Salyany plain	–	76.0	–	76.0	–	–	$\frac{76.0}{76.0}$
IV	The Lesser Caucasus folded system	1140.48	1193.5	53.6	1247.1	–	–	$\frac{1247.1}{1247.1}$
IV_1	Including: Mountain zone	–	24.3	–	24.3	–	–	$\frac{24.3}{24.3}$
IV_2	The Jebrail piedmont plain	216.0	181.0	53.6	234.6	–	–	$\frac{234.6}{234.6}$
IV_3	The Nakhchivan piedmont plain	120.96	902.2	–	90.2	–	–	$\frac{902.2}{902.2}$
IV_4	The Lenkaran lowland	803.52	86.0	–	86.0	–	–	$\frac{86.0}{86.0}$
Total in Azerbaijan Republic		10739.52	5811.6	424.6	6236.2	5806.0	2026.24	$\frac{14068.44}{6236.2}$

Note the table does not list the data (with the "–" sign) for BPV-II, where groundwater reserves are not assessed

intensive subsoil flow is noted. It explains low water abundancy of actually all river fan ridge-top parts in active water exchange areas contacting with mountain regions, and drastically increasing water abundance in water-saturated thickness of the piedmont plain central parts.

Fresh groundwater is distributed everywhere and its natural resources are formed at the expense of diversified supply sources over the entire development area. Hence, in this case, areal parameter is the function of subsoil flow, i.e., the subsoil flow increases with the increase in area, respectively.

1.5.2 Commercial Reserves of Fresh Groundwater Reserves

Peculiarities of formation of fresh groundwater commercial reserves cited above have determined the methods of its qualitative assessment.

Table 1.4 lists approved and tested commercial reserves of fresh (up to 1 g/l) and low saline (up to 3.0 g/l) groundwater at Azerbaijan piedmont and intermountain plains.

1.6 Generation and Accumulation Conditions and Resources of Mineral, Thermal, and Industrial Water

The overwhelming portion of Azerbaijan Republic mineral and thermal waters is generated in mountain region fissured systems, in deep tectonic fractures, and in folded mountain structures. At that, all of them are confined to the fault and fracture-vein rocks of various ages. By their hydrodynamic conditions such as water exchange intensity, two levels are isolated in hydrogeological section of mountain structures. The upper stage (the zone of water shallow circulation) is characterized by high drainage level and, as a consequence, by intensive water exchange. Its thickness is determined by the depth of incision of the region ravine-and-gully and hydrographic networks. Lower in the succession, the deep circulation zone (decelerated water exchange) is located, whose thickness is determined by the region-specific geological and tectonic structure (Askerov 1954; Kashkay 1955; Babayev 2000; Tagiyev et al. 2001; Alekperov et al. 2008).

Water deposits are classified in conformity with spatial distribution of geological zones with similar hydrochemical processes, generating mineral and thermal waters with close qualitative parameters. Basing on tectonic zoning of the Republic, mineral and thermal water deposits are given as the following geostructural units (Tagiyev et al. 2001):

I. The Greater Caucasus mountain area,
II. The Lesser Caucasus mountain area,
III. The Talysh Mountain area,
IV. The Kur Trough.

I. Within the Greater Caucasus mountain area, structural zones of the Greater Caucasus southwestern and northeastern slopes and of the Absheron Peninsula are isolated where 69 major springs of pool mineral and thermal water deposits were discovered (Tagiyev et al. 2001).

Generation sources for mineral and thermal waters of the Greater Caucasus southwestern slope are infiltration waters arriving to the Mesozoic fracture-vein rocks down to the depth of about 2.5–3 km. All discharges of hot and cold mineral waters are concentrated along tectonic fractures of general Caucasian direction. According to their chemical compositions, they are related to hydrocarbonate, hydrocarbonate–sulfate, hydrocarbonate–chloride, chloride, and chloride–sulfate types with variegated cation composition and nitrogen–hydrosulfuric, methane–hydrosulfuric, and methane–nitrogen–hydrosulfuric content. Nitrogen, methane, methane–nitrogen mineral, and thermal waters are saturated by sulfurous gas as a result of mixing of deep circulation zone mineral waters that contain sulfate-reducing microflora, with freshwater of the upper shallow circulation (intensive water exchange) zone that is enriched by organic substances.

Mineralization of mineral and thermal waters varies within 0.6–1.9 g/l. A drop in general mineralization and rise in hydrocarbonate and sulfate ions take place with the temperature increase. Broad scope of changes in their saline and gas compositions as well as changes in temperature of mineral and thermal waters indicates their generation at various depths with differing lithological and thermodynamic conditions that alter with movement from the generation region to the discharge region.

Mineral and thermal waters of the Greater Caucasus northeastern slope are confined to the Malkamud-Khaltan-Germi regional fault and are generated in the Mesozoic rocks at the depths of about 1.3–1.5 km. This fault is characterized by a ramified system of fissures, whose intersections create favorable hydrodynamic conditions for transportation of mineral and thermal waters. Well-developed fracturing of water-containing rocks in their discharge zone, i.e., at the sites of natural outcrops, promoted the development of numerous gryphons here.

Vigorous participation of infiltration waters in generation of mineral and thermal waters, high fissuring level of water-bearing thickness, and good hydraulic gravels explain their low mineralization, varying within 0.8–1.4 g/l. Chemical composition of thermal waters shows high predominance of hydrocarbonate anions as compared to sulfate ion. Sodium ions are isolated from

cations, and low calcium and magnesium content here can be explained by poor solubility of their silicates.

Thermal water gas composition is essentially composed of air nitrogen, its content varying within 80–90 % with general gas saturation of up to 52 ml/l. Low quantity of hydrogen sulfide (11.2–27.8 mg/l) is explained by the fact of its chemical production. Methane is present only as 5.7–12.9 %, and this low quantity is explained by weak biochemical processes.

Unlike thermal waters, mineral waters lie closer to the surface, mostly in the active water exchange zone. Their chemical composition is formed by leaching of saline components in water-containing rocks. Water types are hydrocarbonate, hydrocarbonate–sulfate, sulfate–hydrocarbonate, chloride–sulfate, and chloride–hydrocarbonate, with mineralization of about 0.4–7.2 g/l.

As far as they penetrate the decelerated water exchange zone, chemical composition transforms from hydrocarbonate into sulfate and chloride water. Thus, within the Yalama-Khachmaz and Chadagar-Zorat areas, sedimentary deposits of the Paleogene, Jurassic, and Cretaceous ages display wide distribution of sodium–chloride waters with mineralization that occasionally reaches 94 g/l, of apparently sedimentation genesis, because Cl/Br, rNa/rCl, Cl/B, rSO_4/rCl relations are close to the marine water parameters. At the same time, in certain springs with chloride water, the indexes of $\frac{rNa}{rCl}$; $\frac{Cl}{Br}$ relations are 0.9 and 283.9, thus indicating mixing of ancient infiltration waters and metamorphosed sedimentation waters.

Organic substances in the Paleogene, Cretaceous, and Jurassic sedimentary rocks are supply sources for the methane-generating microorganisms that created mineral water gas composition, predominantly due to the methane presence.

Absheron Peninsula that occupies the Greater Caucasus southeastern peripheral part and by its geological–hydrological and physical–geographical conditions is subdivided into the western and the eastern subzones. The western subzone is characterized by active mud volcanism manifestations, confined to tectonic dislocation lines. Mineral edge water, productive strata oil-bearing capacity, and mud volcanism are closely interrelated here. The eastern Absheron mineralized water is associated with oil deposit tectonic structures and confined to porous-edge water aquifers. Stratigraphically, it relates to sands and limestone of the Pontian regional stage, Lower Pliocene (productive thickness), Eopleistocene, as well as to the Quaternary system Pleistocene formations. In most cases, the water outcrops in economic oil wells, rarely as springs. It is a sedimentation water with high mineralization level and high iodine and bromine content.

II. The Lesser Caucasus mountain zone, by its specific features of mineral and thermal water development, is subdivided into three areas: the Lok-Garabagh, the Goycha-Hakeri, and the Nakhchivan, where more than 100 major springs have been revealed and investigated.

The Lok-Garabagh folded area is situated at the Lesser Caucasus eastern slope and is prominent for abundance and diversity of hydromineral resources. Various rocks participate in the regional geological structure, starting from the Paleozoic and to the Quaternary ages. Outcrops of cold and hot springs are mainly concentrated on the Gazakh-Tovuz hydrogeological massif and the Dashkesan-Gedabey folded structure, which are characterized by near-latitudinal or general Caucasian orientation. In the Gazakh-Tovuz massif, spring overall yield is above 120,000 l/day, carbon dioxide content is 0.5–1.4 g/l, mineralization is 1.1–6.6 g/l, and water temperature is 7–50 °C. In the Dashkesan-Gedabey structure, carbonate mineral water relates to the hydrocarbonate, hydrocarbonate–sulfate, and hydrocarbonate–chloride types with diversified cation content. Water general mineralization varies within 0.9–4.44 g/l, and its temperature consists of 6–18.5 °C. The water gas composition is carbonate, and free carbon dioxide volume is determined as 0.7–1.1 g/l.

The Lok-Garabagh folded area mineral water is altogether characterized by the diversity of ion-saline composition, mineralization level, content of pharmacologically active trace elements and micro components (silver, nickel, copper, strontium, barium, etc.).

The Goycha-Hakeri folded area is located in the Lesser Caucasus central part and is essentially composed of the Quaternary lavas, and of the effusive and intrusive magmatic rocks. Structurally, the region represents the northwestward syncline and includes the Istisu-Kyalbajar, Turshsu-Shirvan, and Minkend-Akhmedly provinces.

Tectonically, the Istisu-Kyalbajar province forms a part of the Kyalbajar Trough, where numerous springs of carbonate mineral water of various temperatures have been studied. Here, thermal water occurs in deep fractures, whereas cold mineral water is found in shallow tectonic dislocations with variegated circulation conditions. The processes of regional and intrusive metamorphism and post-magmatic hydrothermal activity result in carbon acid entry to the section upper horizons. Volatile components created in this process (H_2S and CO_2), having high temperature and pressure, penetrate

the Earth crust upper section. This field is characterized by areal development and is classified as geostructural type of intrusion-dislocated hydrogeological massifs and folded structures. The water chemical composition is identical to the springs of Karlovy Vary (Czech Rep.), Zheleznovodsk (Russia), and Vichy (France).

The fields of carbonate mineral water of the Turshsu-Shirvan Province are situated in the Gargarchay and Khalifalichay river valleys, 18–20 km away from the town of Shusha, and are confined to the Lesser Caucasus thrust line. The thrust of the Middle Jurassic volcanogenic thickness onto the Lower Cretaceous shale–sandy thickness took place along the ultrabasic rock massif, which promoted their considerable fissuring and brokenness.

Here, the source of mineral water is infiltration meteoric water that reaches the zone of contact of the Jurassic and Lower Cretaceous fissured rocks and the ultrabasic rocks that serve as major mineral water catch basins. Under the impact of elevated hydrostatic pressure and carbon dioxide, the upper zone mineral water is diluted by fresh infiltration water and discharged by means of ascending springs.

Water chemical composition is hydrocarbonate magnesium–calcium, with mineralization of about 1.1–2.7 g/l. Water temperatures vary within 8.5–9.5 °C. Gas content is basically comprised of free carbon dioxide (99.2–99.9 %), genetically related to carbonate rocks, particularly, to limestone.

Water is saturated by ferrous oxide (up to 16 mg/l), and hydrogen ion concentration (pH) is within neutral limits. Content of free carbon dioxide is 1–2.7 g/l. Free gas yield is usually 4–5-fold higher that the dissolved gas yield.

The Minkend-Akhmedly province is situated 2 km south of Minkend village, in the Lachin district. The Paleogene, Neogene, and Quaternary horizon volcanogenic deposits are water-bearing materials. Here, cold (9–15 °C) and warm (21.0–36.5 °C) carbonate mineral water is developed. Carbon dioxide content in cold water is 2.4 g/l, in warm water it is 1.2 g/l, free gas contains about 91.7–98.3 % of carbon acid. Chemical composition of mineral water is essentially hydrocarbonate–chloride sodium–magnesium–calcium type.

The Nakhchivan folded area forms the Ordubad syncline southwestern part, characterized by overlapping of linear folds of later elevations and troughs, and by the development of rupture dislocations.

Generation of mineral water occurs in fracture abyssal zones, in the Middle Eocene and Upper Cretaceous terrigenic carbonate rocks. Infiltration water that entered these zones (2000–2500 m) after cation exchange and carbon acid effect under elevated temperatures is transformed in flysch-like rocks into mineral pressure water and outcrops to the surface by fractured dislocations. Mineral water discharge is essentially noted at anticline fold bends.

Major mineral water deposits are located along the deep occurrence faults: carbonate Darydagh, Nagajir, Sirab, Vaikhir, Badamly, Gyzylveng deposits and others, as well as hydrosulfuric Karavansarai, and Shakhtakhly deposits. All of them drastically differ in their chemical composition, mineralization, and temperature. For instance, at the Darydagh deposit, mineralization, chlorine, and sodium content decrease northwestward of the fracture, while hydrocarbonate, sulfate, calcium, and magnesium contents increase. At the Badamly deposit, the springs with highest mineralization and chlorine and sodium content are found closer to the regional fracture, and decrease in all hydrochemical parameters is observed with distance. The Sirab deposit is characterized by increased general mineralization and sodium content, and by decreased calcium and chlorine content from east to south. At the Vaikhir deposit, increased chlorine and calcium concentration is also noted, and it is associated with the arrival of highly mineralized water from the depth. As a consequence, general mineralization of the entire upper zone water rises from 4.5 to 7.5 g/l. The Gakhab and Daralik deposits are characterized by hydrocarbonate prevalence among anions, and sodium prevalence among cations, and their mineralization is 3.4–4.7 g/l.

The Ordubad syncline as a whole demonstrates regional mineralization increase from 1.2 g/l (Badamly) to 21 g/l (Darydag), tending from central part to the margins. Basic mineral water type also transforms in this direction: from carbonate hydrocarbonate sodium–calcium type to chloride–hydrocarbonate sodium one. The content of trace elements (lithium, strontium, boron, arsenic, etc.) varies with changes in water chemical content. Free carbon acid content is 97.5–99.9 % and is related to young volcanism processes.

III. The Talysh mountain zone (with the Lenkaran lowland) is separated from the Lesser Caucasus structures by the transversal Lower Araz depression. Here, the Astara and the Buroval Highs that are essentially composed of the Eocene volcanogenic complexes. The Lerik, Yardymly, and Jalilabad depressions composed of the Oligocene–Miocene complexes, and the South Mughan buried high are distinguished tectonically. This mountain zone is rich in mineral and thermal water, confined to various tectonic fractures and faults. The water temperatures vary within broad range: cold water varies within 12.4–18 °C range, while hot water varies within 47.3–66.1 °C range. Overall yield of more than 180 springs is about 21.0 million liters/day of mineral and thermal water.

IV. The Kur trough separates the Greater and the Lesser Caucasus folded systems and is characterized by specific composition of its mineral water and brines. Natural thinning of mineral and thermal water occurs here very rarely. The Kyasamy mineral water deposit is confined to a rupture fissure at the Neogene formation anticline fold. The Geranboi district iodine brines (up to 35 g/l) are also associated with this structure. Cold and hot sulfur springs are also known in Salyan district (Babazanan) and are confined to the thrust-type tectonic fracture lines or the tension areas at the Pliocene brachyanticline fold domes. The trough mineral water is distinguished by its high iodine (117 mg/l) and bromine (139 mg/l) content.

Mineral water with temperatures from 20–50 °C to 100 °C and more is stripped by wells in the Quaternary Neogene–Paleogene and Mesozoic deposits, in porous-edge and fissure-stratal waters at the depth of below 300 m.

In the Absheron and Akchagyl deposits, the wells strip piestic pressure water at below 500 m depths. Its piezometric levels exceed daylight surface and its mineralization varies within 10–35 to 100 g/l and more. Water chemical content is essentially sodium chloride or sodium–magnesium with small content of iodine and bromine. In the trough eastern part, oil-sunk wells expose in the productive thickness some pressure aquifers with thermal waters. Depending on the depth of occurrence, the water is weekly thermal or weakly overheated.

Thermal and highly thermal water is also stripped in the Maykop deposits of the Ganja oil- and gas-bearing region, with temperatures from 28–30 °C to 60–70 °C. The water is also artesian one with piezometric level of 2–3 m above the daylight surface. Water mineralization level varies from 7 to 35 g/l.

Physical parameters and gas composition of thermal and mineral water determine its curative properties and possibilities of commercial utilization in therapeutic resort-and-spa industry, in chemical production, as a source of treatment drinking water and thermal energy. Nine major balneological groups of mineral and thermal water of various destinations are found in the Republic (Tagiyev et al. 2001):

I. Water without specific components and properties, whose therapeutic significance is determined by its basic ionic composition and mineralization value (the sum of all water-dissolved substances without gases);
II. Acidulous water, containing CO_2 in potable mineral water at least as 0.5 g/l, in external use water, at least as 1.4 g/l (in highly mineral water with temperature exceeding 40–50 °C, freely releasing CO_2 that can be transformed into soluble state by water cooling, should also be taken into account);
III. Sulfide water, containing $H_2S + HS^-$ at least as 10 mg/l. Depending on water pH value, sulfides can reside in the water only as H_2S (hydrogen sulfide water, with pH < 6.5 H_2S constitutes above 70 % of all sulfides) or as HS^- (hydrosulfide water with pH > 7.5 HS^- constitutes approximately above 60 % of all sulfides) or jointly (and it is most frequently), as $H_2S + HS^-$ (hydrosulfide–hydrogen sulfide water with pH 6.5–7.0 $H_2S > HS^-$), or hydrogen sulfide–hydrosulfide water with pH 7.0–7.5 $HS^- > H_2S$;
IV. Ferriginous, arsenous, and polymetallic water: a—ferriginous water, containing at least 10 mg/l Fe; b—arsenous water (rarely, arsenic), containing As below 0.7 mg/l; c—polymetal water, containing increased contents of a number of metals simultaneously (Fe, Al, As, Mn, Cu, etc.);
V. Bromine, iodine–bromine, bromine water: a—bromine water, containing at least 25 mg/l Br; b—iodine–bromine water, containing at least 25 mg/l Bromine and at least 5 mg/l I; c—iodine water, containing at least 5 mg/l I;
VI. Radioactive (radon) water: a—nitric water; b—carbonic acid water, containing at least 5 nKu/l Rn;
VII. Siliceous thermal water (siliceous therms): a—nitric water; b—carbonic acid water, containing at least 35 mg/l $H_2SiO_3 + HSiO_3^-$;
VIII. Water with high organic matter content—C_{org} is at least 5 mg/l (with water mineralization of no more than 2 g/l);
IX. Thermal water, of low mineralization (less than 2 mg/l) that does not contain increased quantities of any specific biologically active components.

Therapeutic properties of mineral water by its external and internal use are as a rule made up of its ionic, micro-component, and gas compositions, mineralization level, and temperature. According to the classification (Tagiyev et al. 2001), acidulous, iodine–bromine, hydrocarbonic, radon, ferruginous, arsenous, siliceous therapeutic and table waters are distributed in Azerbaijan.

The most widely developed are acidulous mineral springs of Darydag, Sirab, Nagajir, Badamly, Jakhar, Gemyur, Gakhab, Zerin-Gala, Vaikhir, etc., that are used at balneological resorts in industrial bottling. They have vast hydromineral resources (about 30 million liters and 30 tons per day of carbon dioxide).

Mineral water of Absheron, Neftchala, Altyagach, Bozdag, etc., contains large amount of iodine and bromine that influence the functional state of nervous system, thyroid

Table 1.5 Averaged estimation of thermal water energy capacity of Azerbaijan hydrogeological areas

Hydrogeological areas	Water temperature, °C	Water flow rate, m^3/day	Energy potential, MW
Absheron Peninsula	20–90	20,000	up to 5.04×10^2
Kur Depression	22–95	172,500	up to 4.7×10^4
Greater Caucasus	30–50	2000	up to 1.68×10^2
Lesser Caucasus	30–74	4170	up to 7.71×10^2
Gusar foothills lowland	30–97	21,650	up to 6.09×10^2
Nakhchivan	40–53	3000	$(1.26–2.90) \times 10^2$
Talysh	31–64	14,400	$(6.05–7.78) \times 10^2$
Lenkaran	42–84	7900	$(4–11.3) \times 10^2$
Total	–	≅ 245,600	up to 5.1×10^4

gland, metabolism, etc., Iodine and bromine contribution to defense industry, nuclear engineering, manufacturing of dyes, agricultural fertilizers, etc., also increased significantly.

In the areas of mud volcanism development, as well as in Arkevan, Gotursu, Shikhov, Babazanan, Puta springs, methane evolves in large quantities but has not been utilized so far.

Sulfide hydrogen sulfide mineral water with free hydrogen sulfide presence in water is confined to Karvansarai, Shakhtakhty, Yerfi, Khudat, Kesh, etc., springs.

Across the Republic, qualitative and quantitative parameters of investigated hydromineral resources permit to set up the industrial production of iodine, bromine, arsenic, liquid carbon dioxide, soda, and naphthenic acids.

Azerbaijan Republic is rich in thermal water, as well. Various natural springs (Istisu, Alasha, Arkevan, Gotursu, Donuzoten, Ter-Ter, Gazanbulagh, Shikhov, etc.) erupt about 50 million liters per day of warm (up to 20–50 °C), hot thermal (50–75 °C), and overheated highly thermal water (75–100 °C) to the earth surface. Thermal water peak temperature in Azerbaijan achieve, as a rule, 75 °C, and its overall energy intensity equals to combustion of about 200,000 tons of coal (Babayev 2000). In prospect, this potential can be used in various economy branches.

Total energy capacity of thermal waters of hydrogeological areas estimated on the basis of their commercial reserves is presented in Table 1.5 (after Tagiyev et al. 2001; Mukhtarov and Hammedov 2003; Mukhtarov et al. 2015).

Several examples illustrating application of different geophysical methods for solving hydrogeological problems are presented in Chap. 9 of this volume.

References

Alekperov, A.B., 1986. Forming chemical composition of underground waters under influence of anthropogenic factors. In: *Underground Waters and Evolution of Lithosphere*, Vol. **II**. Nauka, Moscow, 352-353 (in Russian).

Alekperov, A.B., 2005. Regularities of hydrogeological processes in natural-technogenic systems and application of artificial intellect methodology for their prognosis and management (on example of Absheron agglomeration). *D.Sci Thesis*, Baku (in Russian).

Alekperov, A.B., Aliyev, F.Sh., Israfilov, P.O., Mamedov, V.A., Panakhov, A.M., Shabanov, A.I. and Shaksuvarov, A.S. (Ak.A. Alizadeh, Ed.), 2008. *Azerbaijan Geology*, Vol. **VIII**: Hydrogeology and Engineering Geology, Nafta-Press, Baku (in Russian).

Aliyev, F.Sh., Anton'eva, N.L. and Listengarten, V.A., 1971. Main regularities of forming chemical composition of underground waters (on example of some deposits of fresh and industrial waters of Azerbaijan Republic). In: *Problems of Theory and Regional Hydrochemistry* (Materials of the All-Union Conf.), Nauka, Moscow (in Russian).

Aliyev, F.Sh., Ismailov, T.A. and Tagiyev, I.I., 1996. Underground waters of Azerbaijan Republic, their resources, utilization and problems of protection from contamination and depletion. In.: "*Problems of Surrounding Medium and Natural Resources*". Review, No. 6, Moscow, 28-65 (in Russian).

Alimov, A.K., 2001. *Hydrogeological Processes and Quantitative Estimations of Regulation Sources of Water-Saline Balance of Underground Waters for Substantiation of Hydrogeological-Melioration Prognoses*. Elm, Baku (in Russian).

Alimov, A.K., 2002. *Modern Condition of Determination of Elements of Thermal, Water-Saline Regime of Rocks and Underground Waters as Basis for Ecological Prognoses*. Elm, Baku (in Russian).

Askerbeyli, E.K., Popov, A.P., Bulatov, R.V. and Kyazimov, S.M., 1974. *Underground Waters of North-Eastern part of Azerbaijan and Perspectives of Their Utilization for Water-Supplying*. Stroitekhizdat, Moscow (in Russian).

Askerbeyli, E.K. et al., 1977. Underground waters of south-western slope of the Greater Caucasus and perspectives of their using for water-supplying. *Trans. of the Baku Branch of the VNII VODGEO*, Vol. **XIV**, Baku, 31-36 (in Russian).

Askerov, A.G., 1954. *Mineral Springs of Azerbaijan*. Baku (in Russian).

Babayev, A.H., 1974. Estimation of regional exploitation reserves of underground waters by balance method. *Prospecting and Protection of Entrails*, No. 5, 35-41 (in Russian).

Babayev, A.M., 2000. *Mineral Waters of the Mountain-Fold Regions of Azerbaijan*. Chashygogly, Baku (in Russian).

Israfilov, G.Yu., 1972. *Subterranean Waters of the Kur-Araz Plain*. Maarif, Baku (in Russian).

Israfilov, G.Yu. and Krasilschikov, L.A., 1973. Exploitation reserves of underground waters of submontane plains and steppes of north-eastern and eastern slopes of the Lesser Caucasus. *Scient. Notes of the Azerb. State Univ.*, 25-32 (in Russian).

Israfilov, G.Yu., Tagiyev, I.I., Listengarten, V.A. and Aliyev, F.Sh., 1979. Exploitation of fresh underground waters in Azerbaijan and problems of their protection. *Scient. Notes of Azerb. State Univ*., Ser.: Geol-Geogr, No. 6 (in Russian).

Israfilov, G.Yu., 1978. Resources of fresh underground waters of continental deposits of the south-eastern slope of the Lesser Caucasus and perspectives of their utilization (Jebrail submontane trough). *PhD Thesis*, Baku (in Russian).

Israfilov, R.G. and Israfilov, G.Yu., 1994. Condition and perspectives of rational using fresh underground waters of Azerbaijan Republic. In: *Trans. of **VIII** Conf. of Islam Assoc. "Water in Islam World – Oncoming Crisis"*. Khartoum, 449-452.

Israfilov, R.G., 1999. Forming hydrodynamic regime of underground waters of urbanized areas of Azerbaijan (on examples of Baku, Ganja and Sumgayit cities). *D.Sci Thesis*, Tbilisi (in Russian).

Israfilov, G.Yu., 1983. Main directions of hydrogeological investigations with the aim to optimize exploitation and utilization of underground waters of Azerbaijan. *Trans. of AzNII*, Baku, 38-49 (in Russian).

Israfilov, G.Yu., 2001. On the problem of transport of part of reserves of the Alazan-Agrichay underground water deposit to other region. *Trans. of Scient. Confer. "Perspectives of evolution of melioration and water Industry of Azerbaijan"*. Baku, 143-146 (in Azerbaijanian).

Kashkay, M.A., 1955. *Mineral Springs of Azerbaijan*. Baku (in Russian).

Krasilschikov, L.A., Melnikova, I.N. and Listengarten, V.A., 1978. Perspectives of integrated using resources of fresh underground waters of plain areas of the Kur River basin (within territory of Azerbaijan). *Water Resources*, No. 5 (in Russian).

Lange, O.K. (Ed.), 1961. *Geology of Azerbaijan*. Vol. **VII**: Hydrogeology. Azerb. Acad. Sci., Baku (in Russian).

Listengarten, V.A., 1983. *Regularities of Forming and Peculiarities of Resources Estimation and Perspectives of Using Low-Mineralized Mineral Waters of Azerbaijan's Plains*. Elm, Baku (in Russian).

Listengarten, V.A., 1987. *Forming Resources of Underground Waters of Alluvial-Proluvial Plains*. Elm, Baku (in Russian).

Mukhtarov, A.Sh., Hammedov, A.M., 2003. Geothermal resources of Azerbaijan. *In*: *Problems of Geothermal Energy Development in Countries of the Former Soviet Union and Activity of International GeoFund*. Materials of Intern. Symp., Moscow (in Russian).

Mukhtarov, A.Sh., Nadirov, R.S., Mammadova, A.V. and Mammadov, V.A., 2015. Geological conditions and business opportunities for geothermal energy development in Azerbaijan. *Izvestiya* (*Proceedings*), *Acad. Sci. Azerb*., No. 3, 54-59.

Tagiyev, I.I., Ibragimova, I.Sh. and Babayev, A.M., 2001. *Resources of Mineral and Thermal Waters of Azerbaijan*. Chashyoglu, Baku (in Russian).

Economic Minerals of Azerbaijan

2

Azerbaijan is very well endowed with mineral deposits. More than one billion tons of crude oil has been produced in the Absheron Peninsula and Azerbaijan sector of the Caspian Sea over last 100 years. Large reserves of oil and gas have been concentrated in producing horizons of the Lower Pliocene. Oil and gas fields have been also discovered in the Miocene, Oligocene, and Eocene horizons of the Shamakhy-Gobustan, Evlakh-Agjabedi, and Ganja regions and in the watershed of Kur and Gabyrry rivers. Nearly 350 mineral deposits of metallic (e.g., gold, silver, lead, copper, zinc, iron, cobalt, molybdenum, etc.) and non-metallic minerals, construction materials, and drilling brines with mineable reserves have been explored in the country (Azizbekov et al. 1976).

This chapter is subdivided into two parts: Sect. 2.1—'Oil and Gas' (land and sea) and Sect. 2.2—'Hard useful minerals' (land).

2.1 Oil and Gas

2.1.1 Lithological and Facial Characteristics, Porosity, and Permeability of Meso-Cenozoic Deposits

Reliable information on rock qualities in oil- and gas-bearing reservoirs is of high scientific and practical importance. Therefore, many geologists (Gubkin 1934; Aliyev 1949; Avdusin 1952; Abramovich 1955; Aliyev and Daidbekova 1955; Akhmedov 1957; Aliyev and Akhmedov 1958; Alizadeh et al. 1966, 1972, a. o.) dedicated their researches to the study of reservoir rocks in the Meso-Cenozoic deposits of Azerbaijan major oil- and gas-bearing regions. Azerbaijan Meso-Cenozoic deposits host detrital, carbonate, volcanogenic-sedimentary, volcanogenic, and clayey reservoirs.

Detrital collectors are subdivided into *coarsely clastic* (psefitic) and *fine detrital* (sandy–aleuritic) rocks.

Coarsely clastic rocks (debris sizes of above 1 mm) are of limited distribution and are found as small interlayers of gravelites and conglomerates in the Mesozoic and Paleogene deposits. These rocks consist of the debris of effusive, metamorphic, sedimentary rocks and are consolidated by sandy–aleuritic and carbonate materials. Consolidation type is basal and mixed. Quartz, feldspars, pyroxenes, and grains of other minerals are found in the rock compositions. By their structural signs, they are subdivided into conglomerates (in the Ganja oil- and gas-bearing region—OGBR) and gravelites (the Kur and Gabyrry interfluve, the Muradkhanly and Lower Kur OGBRs). Their formation is associated with continental facies accumulation in the basin coastal zone.

Fine detrital rocks are represented by sandy–aleuritic formations. They are widely distributed in the near-Caspian-Guba region Mesozoic deposits, in the Yevlakh-Agjabedi trough Cretaceous, Eocene, Pliocene deposits, in the Lower Kur-Gabyrry interfluve, Upper Eocene and Oligocene deposits, etc. Their thickness varies from several cm to 50 m.

These rocks are extensively distributed in the Lower Pliocene deposits, i.e., the Azerbaijan productive series (PS) and are represented alternating with clay materials.

Reservoirs of carbonate composition are most widely distributed in the Upper Cretaceous (Upper Santonian–Campanian–Maastrichtian age) deposits of Western Azerbaijan, and they are relatively limited in the Kur-Gabyrry

A.A. Alizadeh et al., *Geosciences of Azerbaijan*,
Regional Geology Reviews, DOI 10.1007/978-3-319-40493-6_2

interfluve (the Lower Eocene), in the Yevlakh-Agjabedi trough, and in the near-Caspian-Guba regions (the Upper Cretaceous).

Reservoirs of volcanogenic-sedimentary composition are distributed rather widely in the Lower Santonian and Middle Eocene deposits of Western Azerbaijan, in the upper part of the Muradkhanly PS (Jarly, Sor-Sor, Muradkhanly) where the presence of commercial accumulations has been established.

Reservoirs of volcanogenic composition are distributed in the Upper Cretaceous effusives (the Turanian–Lower Santonian). Oil- and gas-bearing properties of these reservoirs were determined for the Turonian and Maastrichtian deposits of Muradkhanly area.

Clayey reservoirs are met in the Cretaceous deposits of the Kur-Gabyrry interfluve, in the Ganja and Muradkhanly OGBRs, and in the near-Kur-Guba region Jurassic deposits. Lithological and petrographic peculiarities of reservoir rocks in the Azerbaijan Meso-Cenozoic deposits, their petrophysical properties, and other rock parameters that influence their porosity and permeability properties are given below according to individual stratigraphic units.

The Absheron and Akchagyl stages. The Absheron stage sandy–aleuritic rocks show oil- and gas occurrence signs at separate areas of Absheron Peninsula, of Gobustan southwestern part, the Lower Kur OGBR, and the Baku archipelago.

Commercial oil- and gas occurrence of the *Akchagyl deposits* is found in the near-Kur region and is associated with granular (sandy–aleuritic) reservoirs, alternating with thick clay members.

2.1.2 Productive Series (PS) and Its Lithofacial Types

Productive series (PS) and red-bed series (RBS), its analog at the South Caspian Basin (SCB), are the most significant commercial oil- and gas-bearing reservoirs of the South Caspian Basin (SCB) and are, thus, examined in more detail.

PS-RBS is a rhythmic alteration of argillo-arenaceous deposits that are 7 km thick at the basin most deeply plunged section. Vigorous orogenic movements of SCB-adjacent folded areas and plunging of its central parts in the Late Pontian–Early Pliocene ages resulted in dramatic drop of the Paleo-Caspian level that, according to some estimates, was from 600 to 1500 m. The Lower Pliocene sedimentation took place in closed basin conditions (in the South Caspian region) that finally separated from the Eastern Paratethys about 5.5 Ma.

PS deposits accumulated here in various geotectonic environments (Aliyev et al. 2005): plunging anticline (the Absheron Peninsula), intermountain trough (the near-Kur lowland), fore troughs (fore-Talysh-Elburs trough, near-Caspian region, Jeirankechmez depression), as well as in platform conditions. These are latter represented by the facies of river canyons and valleys, mainly of the Paleo Volga, that laid its course in the platform region of the so-called Middle Caspian dryland.

Peculiarity of the South Caspian paleogeographic conditions in the Early Pliocene, avalanche sedimentation rate that amounted to 3 mm per year resulted in formation of the powerful complex, unique in its facial image and serving as storage of huge hydrocarbon clusters in the region.

PS has large distribution area within the SCB western margin and encompasses the areas of Absheron Peninsula, Absheron, and Baku archipelagos, Jeirankechmez depression, Alyat ridge, and near-Caspian-Guba region. Several types of PS lithofacial deposits are distinguished: Absheron, Gobustan, Lower Kur, near-Caspian, South Caspian types (Fig. 2.1) (Azizbekov et al. 1972; Akhmedov et al., 1973; Azizbekov et al. 1976; Ismailzadeh et al. 2008).

The Absheron type

This type was selected by V.P. Baturin in 1931 under the name of "disthene–ilmenite province." It occupies nearly all area of the Absheron Peninsula and Absheron archipelago, as well as the Baku archipelago northern part, and is essentially composed of the sediments that the Paleo Volga has brought from the Russian Platform.

It is proved by the presence of large amount of quartz light fraction that occasionally achieves up to 95 % of its mineralogical composition. Feldspars (up to 20 %) and rock debris (up to 10 %) are also found.

Along with the Russian Platform as the northern distributive province, alternative source areas existed as well but are of subordinate importance that is confirmed by the presence of Paleozoic gravels in the Absheron-type sediments (that were evidently brought from the Middle Caspian dryland), as well as by the Cretaceous and Quaternary fauna from the Greater Caucasus.

Southern distribution boundary of the Absheron-type sediments differed considerably at the separate stages of PS accumulation, depending on the Paleo Volga delta location. The extreme northern boundary passes in the Amiya Cape area, and the western one is in the Perekyushkyul area.

Thickness of units of rhythmical alternating of sands, aleurites, and clays varies widely from several meters to several hundreds and thousands of meters. The PS Absheron

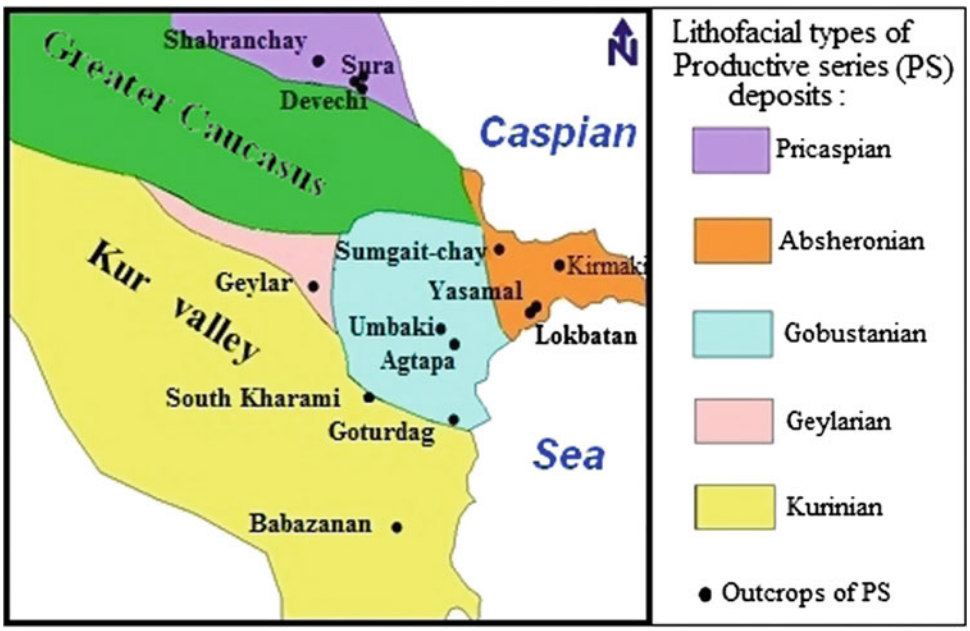

Fig. 2.1 Lithofacial types of PS deposits

facies achieves its greatest thickness of 5000 m in the South Absheron depression.

Increased sandiness of the PS Absheron facies sediments as compared to the other lithofacial types, their peculiar organization in thick terrigenic masses are conditioned by specific genesis of the Absheron-type sediments, and we will deal with it below.

The Absheron lithofacial type of the PS sediments consists of nine oil- and gas-bearing suites (from bottom to top): Kalin, sub-Kirmakin, Kirmakin, supra-Kirmakin sandy, supra-Kirmakin clayey, break, Balakhan, Sabunchi, and Surakhan—which are characterized by successive northwestward thinning out of lower suites.

The PS lower division combines the first five suites.

The Kalin suite (KaS) is exposed at the Chilov (Zhiloi) Island surface and has limited distribution in the Absheron Peninsula southern and southeastern parts. Kalin suite is absent at the substantial part of the Absheron Peninsula. It is composed of clays, thick units of sands, and aleurites. Certain difference between coarse and fine rock fractions is observed in mineralogical composition. The suite peak thickness is 430 m.

The sub-Kirmakin (SK) suite deposits occupy the Absheron Peninsula central part and thin out in its western part. It is basically represented by medium- and large-grained quartz sands. Quartz composition achieves 95 %. Small black angular gravels that are generally poorly sorted are observed in the section lower half sands. Upsection, a decrease in sand fraction grains, is observed. Suite thickness achieves 150 m.

The Kirmakin suite (KS) is distributed along the entire Absheron Peninsula, thinning out in its southwestern part. It is represented by the alternation of clayey, sandy, aleuritic beds that interchangeably dominate in various section parts. The suite thickness is about 300 m. West of the Absheron Peninsula, in a meridional strip bordering between Absheron and Gobustan, the Kirmakin suite also drops out of the section, and PS begins from the supra-Kirmakinsand suite.

The supra-Kirmakin sandy (SKS) and the supra-Kirmakin clayey (SKC) suites are called so basing on the predominance of sandy or clayey material in them. The SKS suite sands and sandstone are medium- and coarse-grained, and poorly sorted, and they occasionally contain small black gravel. Quartz is predominant in the light fraction up to 85 %, while heavy fraction contains ilmenite, magnetite, disthene, staurolite, stable minerals, and pyrite. Significant admixture of sand material is found in clay composition. Large amount of clay loam and sandy loam is also observed. In the peninsular southwestern part, the SKC section is nearly totally composed of clays. Overall thickness of two suites, the SKS and the SKC, is 250–280 m.

Upper division starts from *the break suite* (BS) 90 % composed by coarse- and medium-grained sands. A conglomerate bed, achieving 4.3 m thickness in the Kirmakin valley, occurs at the bottom. Upsection the break suite, sands become more medium-grained. Quartz prevails in the light fraction, constituting up to 90 %. Magnetite and ilmenite prevail in the heavy fraction. The break suite clays are highly arenaceous and frequently look like clay balls resulting from the river flow activity that outwashes and redeposits the PS clays. The suite thickness is about 100 m.

The Balakhan suite consists of six production sand horizons, from V to X, characterized by alternating predominance of sandy or clayey material. Sand and sandstone

are essentially composed of fine- and medium-grained differences. The suite thickness growth from the Absheron Peninsula toward the Absheron and Baku archipelagos, where it achieves 900 m, is observed.

Similarly to the other PS suites, quartz predominates in the light fraction and then follows the percentage composition of feldspars (up to 35–40 %) and rock debris. Minor content of rock glass and analcime is also typical for the Balakhan suite.

Aleurite porosity varies from 10 to 26 %, and permeability varies from 12 to 94 × 10^{-15} m^2. In sandstone, it is 7–28 % and (6–82) × 10^{-15} m^2 (respectively, in clay loam, it is 13–16 % and (4–30) × 10^{-15} m^2, and in clays, it is 10–18 %, and the permeability is very poor).

Sorting coefficient is 1.2–2.1, in clay loams, 1.4–2.2, in aleurolites, and 1.2–2.0, in sandstone. Cementation type is essentially contact one and, less frequently, porous and basal (Suleimanova and Atayeva 2002).

The Sabunchi suite consists of poorly sorted aleurites, aleurite clays, fine-grained clayey sand, but the suite composition varies in different Absheron Peninsula parts. In the peninsula central part, sand and clay contents are approximately equal and elongated sand units of up to 50–60 m thickness and similar, thick, predominantly clayey interlayers are observed. The presence of large amounts of brown loam and gypsum is noted. In the western part of the peninsula, clay content grows, whereas in the eastern part, three oil-bearing sand layers are isolated.

Like in all other PS suites, quartz predominance is typical. In addition, large amount of rock debris takes place in aleurite and clay compositions. Rock glass is found in small quantities. Heavy fraction contains ore minerals in large quantities. Rock cement is calciferous. The suite thickness is 450 m.

The Surakhan suite has the largest thickness in the PS cross section, of up to 1680 m maximally. It is represented by alternation of silty clays, sandy clays, clayey silts, and sands. Upsection clay content grows, where the thickness of sandy interbeds does not exceed 2–10 m. In the suite lower part, thickness of sandy units is 30–35 m.

The Gobustan type

It is also called the "zircon–epidote province" due to the prevalence of these two minerals in the sediments. Two subtypes, the Donguzdyk and the West Gobustan ones, are isolated within the Gobustan type of PS deposits.

The Donguzdyk series is developed in Central Gobustan, along the Jeirankechmez depression northeastern part, and bears the name of Donguzdyk camping ground, where the most typical cross section has been described. The zone area is 4–5 km, and its length is 25–30 km. It is subdivided into two divisions, where the lower one is represented by the alteration of calciferous, arenaceous, argillaceous interbeds with gravel-containing coarse-grained sands, while the upper one displays the alternation of brown loams with conglomerates and gravels. Gravel is of Miocene age. The Donguzdyk series thickness is from 200 to 400 m.

More southward, the Donguzdyk series gradually passes into the *East Gobustan subtype* of sediments with decreasing grain sizes and increasing level of deposit sorting, and more eastward, into the Absheron type. The sediments of this type occupy the Jeirankechmez depression itself and the Alyat-Pirsaat zone, where typical cross sections are being developed. These deposits also participate in the formation of marine structures, located in Gobustan proximity. The sediments are poorly sorted and weakly differentiated. Urely sandy or clayey units are absent, and mixed rock types predominate. Thickness of sandy interbeds sometimes achieves 20 m, and overall thickness is up to 2200–2500 m. It is subdivided into six suites (from top to down).

The Solakhai suite is represented by clays with interbeds of aleurite, sands, and sandstone. Its thickness is 500–550 m. The *Duvany suite* deposits, lithologically expressed in sandstone and aleurolites, conformably overlap this suite. Its thickness is 225–275 m.

The clayey suite is essentially composed of fine-grained differences, which is evident from the series name. Its thickness is 150–170 m.

The Miajik suite is expressed by alternation of sands, sandstone, sandy clays, and aleurolites. Its thickness is 420–430 m.

The argillo-arenaceous suite is composed of gray clays with thin interbeds of fine-grained sands and sandstone. Its thickness is 170–180 m.

The sandy–argillaceous suite, as it follows from its title, is distinguished by the predominance of more coarse differences in its cross section. Its thickness is 550–700 m.

Mineralogical composition is noted for significant drop in quartz content as compared to the Absheron type and predominance of feldspars and sedimentary rock debris, in the light fraction, and of epidote, zircon, and garnet tourmaline, in the heavy fraction. Such mineral composition is identical to the composition of the Greater Caucasus southern slope sediments, thus testifying to the major role of this distributive province in the formation of the Gobustan-type deposits.

The Lower Kur type

This type of sediments is accumulated in the Lower Kur Depression. The boundary between the Lower Kur and the Gobustan-type deposits passes along the Lengebiz-Alyat range.

Overall thickness of the Lower Kur lithofacial type sediments is 3500–4000 m. Detrital material was basically brought to the basin by the largest river, i.e., the Paleo Kur and by the Paleo Araz that bore the Kur lowland, the Greater and the Lesser Caucasus, and the Talysh erosion products. The cross section is represented by the alternation of aleuritic, clayey, sandy rocks. It is characterized by significant clay alteration in comparison with the Absheron type, low content of quartz, and growth in the amount of feldspars, pyroxene, and hornblende, which witnesses the predominance of erupted rocks in the washout area. Thickness of the sandy units reaches 20 m.

Along the Lengebiz ridge, the northern border of this lithofacial zone, the *Lengebiz* subtype of sediments that represents the combination of the Donguzdyk and the East Gobustan lithofacial types is found. Here, along with predominant fine-grained differences, inequigranular sands and sandstone are met, as well as interstratified beds of conglomerates. Its thickness is about 1000 m.

The near-Caspian type

This type is developed along the Greater Caucasus northeastern slope. Lithologically, it is represented by aleurite–sandy, gravel and conglomerate formations. Stratigraphically, the deposits are analogous to the Surakhan suite of the Absheron lithofacial type.

Clear-cut distribution zoning is found for two types of sedimentary material: the argillo-arenaceous type in the southeast (the Gyzylburun type) and the gravel type in the northwest (the Guba type).

The argillo-arenaceous *Guzulburun* complex is essentially composed of fine-grained sediments; sands and sandstone are adminicular and are basically represented by fine-grained differences. The Gyzylburun complex largest thickness is 2000 m. In total, gradual thickness reduction of these deposits is noted from the southeast to the northwest, where the Gyzylburun-type transforms into the Guba one. In its mineralogical composition, feldspars (up to 70 %), quartz (up to 32 %), and rock debris (up to 68 %) prevail in the light fraction and brown iron ore (up to 98 %), muskovite (up to 14 %), magnetite, and ilmenite (up to 10 %) prevail in the heavy fraction.

The Guba lithofacial type is represented by intercalation of poorly sorted coarse sands, sandstone, gravels, and conglomerates. Light fraction is mainly represented by feldspars and rock debris.

Analysis conducted on some areas of the SCB western margin showed in general the similarity of the PS facial composition, whose sedimentation is related to the encroachment of two large river systems, the Paleo Volga, and the Paleo Kur, to the Paleo-Caspian basin. It resulted in the formation of a network of laterally connected sandy units that can be traced to the far south up to the Atashkyakh structure. This fact permits to treat the PS as fluid conducting one within the basin. At the same time, PS reservoirs are characterized by inhomogeneity of their structure through the section, which is caused by numerous changes of facial conditions. Quite thick clay masses that can be regionally traced within the VII and V horizons can be considered as regional seals for underlying argillo-aleurite reservoirs of fluvial genesis.

The Miocene sediments

Detrital rocks have wide occurrence in the Miocene deposits and serve as principal oil and gas containers.

Reservoir properties of deposit rocks of the ***Chokrak horizon*** have been studied at Shirinkum and Muradkhanly areas. Porosity of these areas is 11.4 and 15.4 %, respectively. All investigated rocks were actually impermeable, which is principally associated with their high carbonate content.

The ***Sarmatian*** stage sandy–aleuritic rocks that have been investigated at Muradkhanly, Eldaroyugi, Kangly, Chabandag, Alajigi, Akhtakhtatepe, Damirtepe-Udabno, Papantekyan, etc., areas differ from the above-described Chokrak rocks in their better porosity and permeability properties.

Average porosity, permeability, and carbonate content values for the Sarmatian stage rocks are listed in Table 2.1.

The Meotian stage in Azerbaijan is essentially represented by clayey lithofacies and reservoir rocks are absent in its cross section.

Reservoir rocks that deserve attention from the viewpoint of commercial oil- and gas-bearing capacity are absent in the **Pontian** stage deposits.

The Oligocene sediments

Sandy–aleuritic rocks in the Oligocene deposits are widely distributed in Azerbaijan. These deposits bear oil and gas in some of the Republic regions.

Sandy–aleuritic rocks of the ***Khadum*** horizon in the Ganja region are related to polymictic and tuffaceous differences. Their thickness varies from fractions of cm to 8 m. In the Shamakhy-Gobustan region, only rare interlayers of aleurites in the Khadum horizon section are met. In the Absheron region, the Khadum horizon does not contain sandy–aleuritic formations.

In the ***Maykop series*** (the Oligocene and Miocene ages), sandy–aleuritic formations are predominantly found at Meshrif-Zeifa, Tengialty, Zagly, Amirkhanly, Saadan, and Siazan-Nardaran areas of the near-Caspian-Guba region. The cross section is represented by alternation of aleurolites,

Table 2.1 Reservoir properties of the Sarmatian stage sandy–aleurite rocks

Area	$CaCO_3$ content, %		Porosity, %		Permeability, 10^{-15} m^2	
	Average value	Number of measurements	Average value	Number of measurements	Average value	Number of measurements
Muradkhanly	21.6	2	21.0	2	5.6	1
Eldaroyugi	_	_	13.6	48	–	–
Kangly			10.5	25	–	–
Chobandag			14.5	29	–	–
Alajigi			11.9	14	–	–
Akhtakhtatepe	–	–	12.0	20	–	–
Damirtepe-Udabno	2.6	2	20.9	2	115.3	2
Large Palantekyan	–	–	16.3	16	36.0	6

Table 2.2 Reservoir properties of the Maykop suite rocks, the near-Caspian-Guba region

Subsuites, horizons	Area	Carbonate content, %	Porosity, %	Permeability, 10^{-15} m^2
		Average value (number of tests)		
Upper Maykop	Siazan	6.2(35)	15.0(30)	18.4(4)
	Saadan	4.2(4)	15.8(32)	12.6(3)
	Amirkhanly	5.0(5)	16.3(57)	99.0(4)
Lower Maykop	Siazan	3.5(18)	18.2(8)	32.5(5)
	Amirkhanly	16.0(12)	21.1(10)	18.5(11)
	Zagly	9.6(4)	18.6(8)	16.0(2)
	Tengialty		16.4(7)	32.0(6)

sands, sandstone, and solid clays with breccia interlayers. Thickness of sandstone interlayers varies from 10 to 30 cm. The Lower Maykop sandy–aleuritic rocks are sorted worse than the same rocks in the Upper Maykop and are related to the group of clayey silts. Quartz content is 40–43 %, and feldspar content is 40–55 %.

Table 2.2 lists reservoir properties of sandy–aleuritic rocks of the near-Caspian-Guba oil and gas field (OGF).

In the Shamakhy-Gobustan region, the sandy–aleuritic rocks are distributed non-uniformly. In the northern part region, these rocks either are found like separate interlayers of 0.1–0.2 m thickness or are nearly absent. In the northern part region, they are widely distributed and in some places (Ajiveli, Cheildere, etc.) have significant thickness. Quartz differences with well-rounded grains (Cheildag, Ajiveli, Sundi, etc.) are frequently met among these rocks. Certain parameters of sandy–aleuritic rocks are given in Table 2.3.

In *Ganja region*, sandy–aleuritic rocks are distributed along the entire Maykop suite section, both in the shape of thin millimeter-sized interlayers and as up to 5 m and more thick strata. The thickest strata are found in Dalmamedly, Gazanbulagh, Naftalan, Ajudere, and Gedakboz sections.

Peak values of sand fraction contents are confined to the Maykop suite lower division sections at Kharkhanput, Karachinar, and Agjakend areas. It is nearly absent at Ajidere, Gazanbulagh, Aliushagi, Dalmamedly, Naftalan, Borsunlu, Zeiva, Injachay, and Mirbashir areas and is replaced by the aleuritic fraction. Further southeastward, the aleuritic fraction content does not exceed 55 %.

Average parameter values of sandy–aleuritic rocks are given in Table 2.4.

In *Lenkaran region*, sandy–aleuritic rocks constitute the considerable part of the Maykop suite section. At Kenjibaryu, Lerik, and Shovli areas, these rocks occupy 60–79 % of the section.

The Gabyrry-Ajinour and the Yevlakh-Agjabedi troughs. In the Maykop suite sections of these troughs, detrital rocks are distributed throughout and are major oil and gas reservoirs. Average values of their petrochemical characteristics are listed in Table 2.5.

The Eocene sediments

Terrigenic, carbonate, and volcanic-sedimentary reservoirs are abundant in the Eocene sediments. Reservoirs of sandy–aleuritic composition are developed in the Upper Eocene sections, less frequently, in the Middle and Lower Eocene, in the Yevlakh-Agjabedi trough, in the Lower and Upper

Table 2.3 Reservoir properties of the Oligocene rocks, the Gobustan region

Subsuites, horizons	Area	Carbonate content, %	Porosity, %	Permeability, 10^{-15} m^2
		Average value (number of tests)		
Zuramakend horizon	Umbaki	3.5	1.8(12)	68.0(3)
	Ajiveli	7.5(46)	2.2(17)	32.0(9)
	Cheildag	9.0(27)	4.2(8)	170.0(7)
	Sundi	10.7(4)	1.0(2)	157.0(3)
	Nardaran-Suleiman	4.2(2)	1.5(12)	41.0(11)
	Gijaki-akhtarma	10(12)	2.7(12)	163(11)
	Sheitanud	–	3.4(8)	179(7)
	Kyrkishlak		1.0(5)	13.0(2)
Riki 2	Umbaki	4.7(4)	1.0(3)	46.0(3)
	Ajiveli	2.0(10)	4.2(19)	136.0(28)
	Cheildag	9.5(12)	2.5(9)	101.0(9)
	Sundi	21.0(21)	3.1(21)	214.0(16)
	Nardaran-Suleiman	19.6(2)	3.2(33)	224(23)
Riki 1	Umbaki	5.2(4)	1.7(22)	56.0(28)
	Ajiveli	5.8(7)	4.8(47)	251.0(34)
	Cheildag	25.8(12)	3.7(19)	172.0(13)
	Ilkhichi	2.4(1)		
	Sundi	21.1(21)	2.1(22)	165.0(15)
	Gijaki-akhtarma	30.3(21)	3.1(21)	345.0(14)
Lower Maykop	Umbaki	6.9(6)	2.1(11)	22.0(4)
	Cheildagh	8.0(5)	3.4(24)	72.0(16)

Table 2.4 Certain parameters of the Oligocene sandy–aleuritic rocks in Ganja region

Area	$CaCO_3$, %	Porosity, %	Permeability, 10^{-15} m^2
	Average value (number of specimens)		
Gazanbulagh	7.0(140)	16.6(51)	15.6(37)
	9.8(2)	6.4(2)	0.2(1)
Gedakboz	25.9(22)	15.0(19)	50.8(16)
Sariyaldyg	28.6(15)	15.2(6)	6.0(6)
Naftalan	5.7(515)	17.1(440)	44.0(265)
Mirbashir	44.1(56)	15.7(122)	8.3(49)
Shirvanly	–	5.0(4)	<0.001(6)
ShirinkumShirinkum	0.8(1)	15.5(1)	<0.001(1)
Karachinar	7.2(65)	19.3(91)	108.6(66)
Kharkhaput	30.9(30)	15.8(32)	23.4(34)
Zeiva	15.1(60)	15.1(69)	113.8(68)

Eocene of the Kur–Gabyrry interfluve. Their commercial oil- and gas-bearing capacity is determined only for the Upper Eocene.

Generalized results of porosity and permeability determinations are given in Table 2.6.

Table 2.7 lists generalized research results of reservoir properties in carbonate rocks. A numerator gives measurement limits and a denominator, a number of determinations.

The reservoirs of volcanogenic-sedimentary composition (of porous-fractured type) are mainly developed in the

Table 2.5 Certain parameters of the Oligocene reservoir rocks

Area	$CaCO_3$ content, %	Porosity, %	Permeability, 10^{-15} m^2
	Average value (number of specimens)		
The Kur–Gabyrry interfluve			
Damirtepe-Udobno	8.2(3)	15.8(3)	1.86(3)
Sazhdag	12.3(11)	15.0(11)	1.77(4)
Gyrakhkeseman	5.6(17)	27.3(17)	353.2(16)
Gaflandere	15.7(11)	22.1(11)	79.9(10)
Borzundag	19.4(3)	4.8(3)	<0.001(3)
Tarsdallyar	0.4(2)	20.3(2)	2.0(2)
The Muradkhanly OGF			
Amirarkh	0.1(1)	16.8(1)	0.03(1)
Zardab	3.7(1)	14.4(1)	2.9(1)
Muradkhanly	20.3(1)	8.0(35)	0.22(7)
Shikhbagi	1.0(1)	18.1(1)	0.3(1)
Mil	17.6(1)	14.2(1)	130(4)

Table 2.6 Porosity and permeability of the Eocene sediments

Region	Stratigraphic frameworks		Porosity, %	Permeability, 10^{-15} m^2
			Measurement limits (number of determinations)	
The Yevlakh-Agjabedi trough	Eocene	Upper	2.8–22.8(38)	<0.001–2.9(32)
		Lower	4.6–15.5(9)	<0.001–0.1(9)
		Middle	2.2–7.4(3)	<0.001–0.8(3)
The Kur–Gabyrry interfluve	Eocene	Upper	2.4–34.8(26)	<0.001–368(15)
		Lower	6.0–23.3(3)	<0.001–0.4 (3)
		Middle	4.0–27.4(20)	<0.001–5.5(20)

Table 2.7 Reservoir properties of the Eocene carbonate rocks

Region	Porosity, %	Permeability, 10^{-15} m^2	Specific density of cracks, m^{-1}
The Yevlakh-Agjabedi trough	(0.2–17.0)/46	(<0.001–10.4)/40	(<0.001–147.0)/33
The Kur–Gabyrry interfluve	(3.6–16.7)/70	(<0.001–0.01)/12	(<0.001–0.74)/32

Table 2.8 Reservoir properties of the Middle Eocene volcanogenic–sedimentary rocks

Region	Porosity, %	Permeability, 10^{-15} m^2	Specific density of cracks, m^{-1}
	Measurement limits (number of specimens)		
The Yevlakh-Agjabedi trough	(1.0–22.8)/54	(<0.001–27.8)/50	(<0.001–48.0)/22
The Kur–Gabyrry interfluve	(5.0–26.6)/61	(<0.001–0.3)/18	(<0.001–89.0)/31

Middle Eocene cross sections in the Western Azerbaijan, with confined oil and gas fields. Storage capacities of volcanogenic-sedimentary rocks are associated with pores and fractures, and their filtration properties are essentially related to macro- and microfractures of tectonic and lithogenetic origin. The pore sizes in these rocks vary from deciles of micrometer to several micrometers.

Table 2.8 lists generalized research results of reservoir properties in the Eocene volcanogenic-sedimentary rocks.

The Paleocene sediments

The Paleocene sediments are distributed in nearly all oil- and gas-bearing fields and are predominantly represented by clay rocks that in most cases constitute above 90 % of the section. Detrital rocks are found rarely as thin intercalations (0.5–10 cm) in the Lower Paleocene deposits of the near-Caspian-Guba OGF. The rocks are polymictic, graywacke–feldspar–quartz, poorly sorted ones. Sandy fraction content is 4.0–46.8 %.

In Absheron OGF, the Paleocene sandy–aleuritic rocks constitute only 3 % of the section. Thin intercalations (10–20 cm) are also found in Lenkaran district. They are oligomictic and tuffaceous.

In Shamakhy-Gobustan region, as well as in other OGF, sandy–aleuritic rocks have limited distribution in the Paleocene section.

The Azerbaijan Paleocene sediments as a whole are essentially represented by clayey lithofacies in many regions. And only in certain instances, the interbeds of sandy–aleuritic formations are found that in most cases are packed due to high clay content and, in some cases, due to increased carbonate content and are not thus characterized by high capacity and filtration properties. Therefore, one should not expect commercial-scale accumulation of hydrocarbons in these deposits.

The Cretaceous sediments

Terrigenic, carbonate, volcanogenic-sedimentary, volcanogenic, and clayey reservoirs are distributed in the Cretaceous sediments.

The Lower Cretaceous sediments have been essentially investigated in the near-Caspian-Guba region, partly in Northern Gobustan and in the Muradkhanly OGF. Cross section of these sediments is represented by alternating intercalations of clays and sandy–aleuritic formations. Reservoir properties of these latter are generally good (particularly in the Albian sediments).

The Lower Cretaceous carbonate rocks are characterized by low reservoir properties (Table 2.9).

The Lower Cretaceous sediments of the Muradkhanly OGF are represented by fractured argillites that have undergone the mesocatagenesis stage and might have acted as reservoirs.

The Upper Cretaceous deposits are widely distributed over Azerbaijan territory and bear oil and gas fields in many regions.

In the near-Caspian-Guba region, these sediments are represented by the argillo-arenaceous lithofacies with intercalations of fissured limestone.

Relatively promising perspectives are associated with fissured carbonate rocks in the Shamakhy region southern part as well as with central and southern Gobustan that frequently show oil saturation. Similar fissured carbonate reservoirs take place in sedimentary cross-section of Absheron region and the SCB.

Thus, the presence of conditions favorable for the formation of hydrocarbon clusters, i.e., the presence of reasonably good fissured carbonate reservoirs, overlapped by impermeable seal rocks such as the Paleocene plastic clays gives grounds to assign the Upper Cretaceous sediments of Shamakhy region, central, and southern Gobustan, Absheron region, and the SCB to promising oil- and gas-bearing deposits (Table 2.10).

Table 2.9 Reservoir properties of the Lower Cretaceous carbonate rocks in the near-Caspian-Guba region

Stage	Porosity, %	Permeability, 10^{-15} m^2	Specific density of cracks, m^{-1}
Aptian	0.1–10.7	0.17–2.04	41–114
Barremian	0.5–6.1	0.01–1.49	10–110
Hauterivian	2.8–8.0	0.001–2.27	25–113
Valanginian	0.2–6.0	0.001–0.19	28–120

Table 2.10 Reservoir properties of the Upper Cretaceous carbonate rocks

Region	Rock type	Porosity, %	Permeability, 10^{-15} m^2	Specific density of cracks, m^{-1}
		Measurement limits (number of specimens)		
The Yevlakh-Agjabedi trough	Limestone	(1.5–19)/298	(2.1–42.2)/250	(1.7–233)/300
	Marls	(1.2–21.3)/85	(1.1–13.2)/86	(1.2–230)/97
	Dolomite	(0.2–27.4)/436		
The Kur–Gabyrry interfluve	Limestone	(0.2–27.4)/436	(0.001–12.0)/451	(1.2–230.0)/490
	Marls	(0.6–27.4)/178	(0.001–40.5)/195	(1.5–210.0)/200

Table 2.11 Reservoir properties of the Upper Cretaceous volcanogenic rocks

Field	Porosity, %	Permeability, 10^{-15} m^2	Specific density of cracks, m^{-1}
	Measurement limits (number of specimens)		
Muradkhanly	0.6–28.2 (210)	<0.001–527(185)	1.1–126.0(140)
Duzdag, Mirbashir, Gedakboz, Mil, Zardab, Karajaly, Sor-sor, Jarly	0.6–21.9(41)	<0.001–15.2(30)	1.2–98.0(25)
Mamedtepe, Tovuz-Gazakh	3.5–23.5(31)	<0.001–22.0(32)	1.0–80.0(33)

Hydrocarbon-bearing prospects are also associated with the Santonian-Maastrichtian age carbonate rocks of the Muradkhanly and Ganja OGFs and with pre-Lesser Caucasian Depression. Oil- and gas-bearing capacity is found for the Muradkhanly (Muradkhanly, Zardab) and Ganja OGFs.

The Upper Cretaceous deposits of above 1000 m thickness are widely developed within the pre-Lesser Caucasus Depression and are exposed by the wells of deep-hole prospect at Sovetlyar, Beilagan, Agjabedi, Borsunly, etc. areas. They are represented by fissured carbonate rocks and are characterized by good reservoir properties. Therefore, it is not by chance that significant oil and gas manifestations of commercial importance were discovered in many boreholes of Sovetlyar and Borsunly areas. It serves as the evidence of high prospects for oil- and gas-bearing capacity in the deposits.

Commercial oil and gas inflows were not found in the Upper Cretaceous sandy–aleuritic formations of the Yevlakh-Agjabedi trough and the Kur-Gabyrry interfluve despite the fact that they are characterized by porosity and permeability similar to those of carbonate rocks.

In 1971, commercial oil fields were discovered in the Upper Cretaceous volcanogenic rocks of Muradkhanly area. These Turonian-Santonian age reservoirs were occasionally even more productive than normal sedimentary ones, the fact being explained by their rather good reservoir properties (Table 2.11).

The Upper Cretaceous fissured argillites of Jarly, Sor-Sor, and Muradkhanly areas can also serve as reservoirs, as their porosity varies within 1.1–28.0 %, and they have rather high permeability.

According to D.M. Javadov estimates, the Upper Cretaceous argillite from the Ganja OGF (well 18, interval 350–355 m, Dallyar area) is also characterized by good capacity (18.2 %) and high permeability (366×10^{-15}m^2).

Of particular interest is the reservoir discovered within 4007–4020 m depths at the cross section of borehole 9, Tarsdallyar area (Upper Cretaceous) (Table 2.12).

Riff formations that are widely distributed in the Mesozoic sediments can also become the potential promising oil- and gas-bearing features.

The Jurassic sediments

The section of investigated Middle Jurassic deposits is represented by the alternation of sandy–aleuritic and clay (argillites and shales) rocks with thin limestone intercalations. Carbonate formations are predominant in the Upper Jurassic age.

The Jurassic sediments are uncovered by deep-hole prospect drilling principally in the near-Caspian-Kur region (at Yalama, Khudat, Khachmaz, Agzybirchala, Talabi, Begimdag, Keshchay areas, and Siyazan monocline) with maximally exposed thickness of about 3000 m at Khachmaz area and in the Jarly-Saatly zone (Ismailzadeh et al. 2008).

Sandy–aleuritic rocks are widely distributed along the entire Jurassic cross section at the Greater Caucasus area. Sandstone are represented by fine-, median-, and (rarely) coarse-grained closely cemented, frequently foliated, and generally well-sorted differences. Aleurites are poorly sorted and latter contain a clayey impurity.

Reservoir rocks of the Jurassic deposits are thoroughly studies in the near-Caspian-Guba OGF. These rocks have totally undergone the metacatagenesis stage, in some places, even apocatagenesis stage, which resulted in their severe packing and consolidation. Despite that, the rocks are met

Table 2.12 Certain parameters of oil-bearing tephroites of Trasdallyar area (borehole 9)

Interval, *m*	Carbonate content, %	Porosity, %	Permeability, 10^{-15} m^2	Oil and water saturation, %	
				Oil	Water
4007–4012	2.0	30.0	385.0	33.2	66.8
4012–4020	1.3	29.1	192.0	30.5	10.1

Table 2.13 Average values of some parameters for sandy–aleuritic rocks in the near-Caspian-Guba region [the data were taken from Aliyev and Akhmedov (1958)]

Stage	Granulometric content, % (mm)			Carbonate content, %	Porosity, %		Permeability, 10^{-15} m^2
	>0.1	0.1–0.01	<0.01		General	Effective	
Tithonian	21.3	31.6	47.1	18.8	8.9	–	1.3
Bajocian	27.3	35.4	39.3	15.6	8.3	–	1.3
Aalenian	19.9	44.7	37.4	12.8	6.5	1.1	1.3
Toarcian	32.3	34.6	36.1	4.1	613.8	1.8	6.9

here (Yalama, Khudat, Afurja, Atachay, Keshchay, Tekchay-Begimdagh areas) that possess satisfactory filtration and capacity properties (Table 2.13). So, a gas fountain of 15,300 m^3/day gas yield and 70–80 m^3/day water yield was discovered at Tekchay area (well 1). Out of the Middle Jurassic deposits, high water inflow (250 m^3/day) with oil film was found at Afurja area.

The majority of 1000–1300-m-thick tested features in the Middle Jurassic deposits at Yalama and Khudat areas turned out to be dry that might be related to low porosity and permeability values of sandy–aleuritic formations.

Also, potential oil and gas reservoirs in the Azerbaijan part of the Greater Caucasus are fissured carbonate rocks of the Tithonian stage. These rocks are characterized by fissured porosity of 1 %, specific density of cracks of 96–300 × 10^{-1} m, and permeability of 80–85 × 10^{-15} m^2. Fissured limestone of this stage that stretches as a range along the Tengi-Beshbarmag anticline and are widely distributed in the Lesser Caucasus northeastern submountain regions (Fizuli, Jebrail, etc.) can also be thought as potential hydrocarbon receptacles.

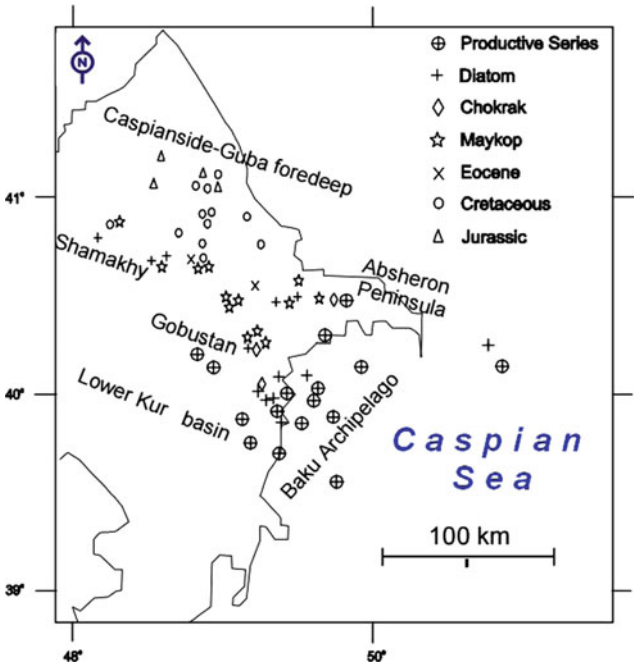

Fig. 2.2 Distribution of sample collection localities (outcrops, oil fields, and mud volcanoes)

2.1.3 Geochemistry of Organic Matter and Hydrocarbon Fluids and Simulation of Oil and Gas Formation Processes

2.1.3.1 Geochemical Characteristic of Organic Matter in the Meso-Cenozoic Sediments

Study of organic matter (OM) geochemistry and assessment of oil and gas generation potential in the South Caspian basin (SCB) sedimentary rocks are based on pyrolytic analysis data of more than 600 rock samples selected from above 50 areas, including outcrops, mud volcanoes (ejected rocks), and boreholes (Fig. 2.2).

It is vital to take into account that due to weathering processes, OM of outcropped rocks is characterized by relatively lower values of all examined geochemical parameters as compared to the OM of drill-hole cores.

Stratigraphic range of examined deposits embraces the range from the Middle Jurassic to the Lower Pliocene ages. Geochemical investigation of OM in the Lower Pliocene deposits (net oil and gas thickness—PS) was basically conducted using core samples collected from marine oil fields. The research results were set forth in a number of publications (e.g., Korchagina et al. 1988; Guliyev et al. 1991; Bailey et al. 1996; Guliyev and Feyzullaev 1996; Abrams and Narimanov 1997; Inan et al. 1997; Lerche et al. 1997a, b; Tagiyev et al. 1997; Katz et al. 2000; Feyzullayev et al. 2001; Gurgey 2003; Huseynov et al. 2004; Feyzullayev et al. 2008; Ismailzadeh et al. 2008).

The results of pyrolytic studies are graphically represented in Fig. 2.3.

Horizons with favorable HC potential for both qualitative (S_1 + S_2) and quantitative factors (hydrogen index—HI) are

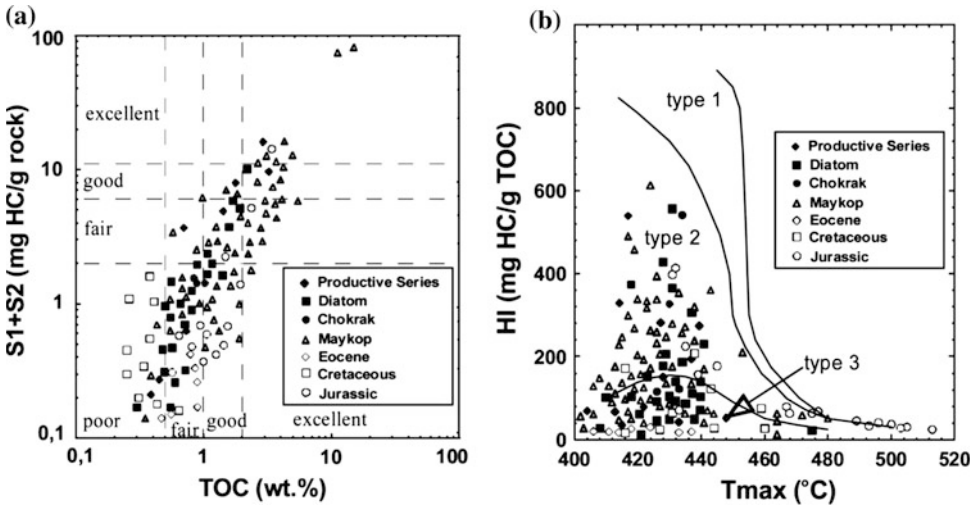

Fig. 2.3 Annotate graphs based on pyrolysis parameters: **a** oil and gas source potential of deposits according to Peters et al. (1986) classification; **b** OM qualitative behavior

most commonly encountered in the section Oligocene–Miocene interval.

Below is a brief description of geochemical special features of the Azerbaijan Meso-Cenozoic deposits.

The Jurassic deposits. The sections from the Aalenian to the Callovian age have been studied. Oil and gas source rocks of good quality were found in the Late Bathonian and Early Callovian ages. Paleogeographic data show that basin closing took place at that period, and depositional environment changed due to increase in water salinity. Pr/Ph ratio is 0.39–1.41. Organic matter is mixed and consists of amorphous algae, woody, and higher vegetation, thus corresponding to types 2 and 3. Organic carbon content averages to 0.76, varying within a rather wide range, from 0.05 to 3.41 %. Oil generation potential of the Jurassic deposits is rather low, and HI averages to 87. The Jurassic rocks are predominantly gas producing.

The Cretaceous deposits. The samples from Hauterivian, Albian–Cenomanian, and Maastrichtian stages have been studied. The cretaceous deposits in whole are characterized by low content of C_{org}, which varies from 0.05 to 1.84 % (with average value of 0.22 %). Low value of HI equal to 83 testifies to gas-producing capacity of the sediments under study.

The Paleocene deposits. There are the poorest C_{org} content rocks of the Meso-Cenozoic section. OM content varies within 0.01–0.08, averaging to 0.03 %.

The Eocene deposits are characterized by low C_{org} content and OM quality. OM consists of inertinite and wood residues. OM average value is 0.46 %, and HI does not exceed 29.

The Oligocene–Lower Miocene deposits (the Maykop series). The Maykop series sediments are distinguished by high C_{org} content, achieving 15.1 %, with average content of 1.86 %. HI varies from 11 to 612 with an average value of 146. OM quality and content in the Maykop deposits improve eastward to the Caspian Sea.

The Middle Miocene deposits (the Chokrak horizon) are characterized by C_{org} content within 0.09–2.44 % and by hydrogen index values of 73–541, thus indicating the OM satisfactory quality and potential generation of liquid and gaseous hydrocarbons by these sediments.

The diatom suite is considered as one of the principal oil-generating complexes in the SCB. In the basin northern part, the suite is characterized by median content of C_{org} equaling to 0.63 %, with HI variation from 12 to 427 mg HC/g of rock (average value is 105 mg HC/g of rock). OM content and quantity in the diatom suite deposits concerning liquid HC generation improve with depth and with deposit regional subsidence. It is witnessed by the characteristics of ejected rocks of the Shamakhy-Gobustan zone mud volcanoes and by the Baku archipelago drill-hole cores (Fig. 2.4).

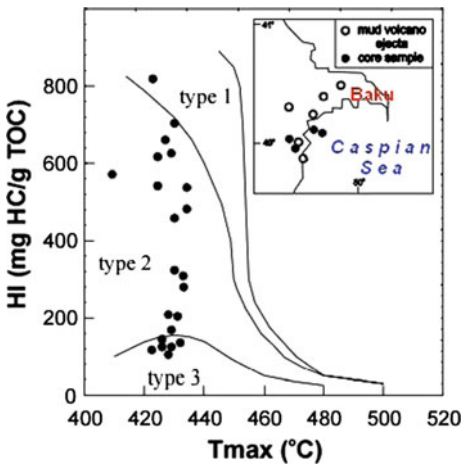

Fig. 2.4 Annotated diagram, indicating improvement of organic matter source quality in the diatom sediments toward the basin deeps

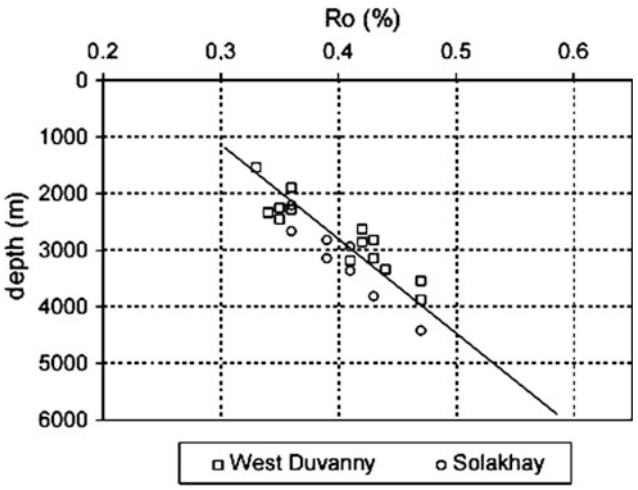

Fig. 2.5 Changes in vitrinite reflectivity with depth in the range of the Miocene deposits exposed at Zapadny Duvanny and Solakhai fields

Kerogen of these formations in most cases corresponds to the 2nd type (see Fig. 2.4). High C_{org} content (0.09–7.8 %, average value of 1.03 %) and HI (107–708, average value of 308 mg HC/g of rock) display good oil generation potential of the diatom suite in the basin deep-sunk part.

The Lower Pliocene deposits (PS). The Lower Pliocene deposits, being generated in the deltaic and shore marine conditions, are characterized by low OM quality, which in most cases belongs to the 3 type and consists of resedimented remnants of woody vegetation with insignificant admixture of amorphous and algal OM. C_{opr} content is 0.02–2.71 % (average value of 0.47 %). Hydrogen index varies from 15 to 334 mg HC/g of rock (average value of 147 mg HC/g of rock).

Thermal maturation of the Miocene rock OM was assessed from the data of vitrinite reflectivity (Ro, %). These parameter values in drill-hole cores from Zapadny Duvanny and Solakhai areas (down to 4500 m depth) do not exceed 0.48 % (Fig. 2.5). Similar investigations of the drill-hole cores from the Baku archipelago areas down to 5300 m depth give Ro (%) values, not exceeding 0.6 that testifies to low OM maturation and much deeper occurrence of the "oil window."

2.1.3.2 Geochemistry of Azerbaijan Oils

Oils of differing properties and compositions occur in Azerbaijan. Qualitative variety of oils manifests itself not only between the oil- and gas-bearing fields (OGF) but also within separate OGFs and deposits, both in various stratigraphic frameworks and in coeval horizons.

Composition of Azerbaijan oils, inherited from the oil source OM, undergoes significant transformations at all stages of their generation and migration.

Oils of the Azerbaijan Meso-Cenozoic sediments are characterized by considerable qualitative changes, reflecting facial–geochemical environments in paleo-basins and compound effect of aggregate factors of migration, catagenic metamorphism, and hypergenesis. It is evident that at shallow depths of occurrence (according to the available estimates, down to about 2 km), oils are essentially exposed to the impact of supergene factors, while at great depths only the thermocatalytic factors prevail.

The effect of supergene factors is most pronounced within the Absheron OGF, where highly cyclic oils, basically of naphthene base, with large content of resinous components, are observed at certain fields in the PS section.

Thermocatalytic transformation process affects first the changes in group hydrocarbon composition of the light fraction, i.e., the fraction that distillated at 200 °C. These processes result in the increase in methane and aromatic HC content—as a consequence of destruction of complex high-boiling molecules, the number of naphthene HCs decreases.

Qualitative variety inherent in Azerbaijan oils is particularly manifested in the PS. The *Absheron OGF* can serve as an example: There, we meet both light and heavy oils, and low and high resinous, with various content of asphaltenes and solid paraffin, with methane and naphthene base, with various degrees of cyclicity and maturation.

This region is characterized by the absence of stringent stratigraphic orientation of changes in oil physical–chemical properties and compositions within the field stratigraphy, specifically "inversion" pattern of density variations, tending to increase with stratigraphic depth. Such "anomalies" are noted by relatively shallow occurrence of petroliferous beds (1000–2500 m) in highly dislocated structures, where supergene processes are acting.

On the other hand, rather definite regularities in oil content changes are observed regionally in the PS like-named horizons, as a function of the basin paleogeographic conditions and hypsometric depth of occurrence.

Heavy tarry oils containing complex high molecular cyclic compounds are found in upraised parts of anticlinal structures, developing in the PS basin shore zones with alternating redox conditions and predominantly humus source organic matter.

Light methane-base oils are abundant in the paleo-basin distant parts, where sapropel-type autochthonous organics was accumulated and stable reducing environment was created. By the subsidence of productive horizons to 3000–5000 m depths, the processes of oil catagenic alterations become primary importance.

Oils of the *Gobustan OGF* deposits are less diversified in their physical–chemical characteristics as compared to the oils of any other field. Their density values permit to classify them as middle and heavy oils (890–910 kg/m^3), so that

these values increase with oil occurrence depths. Density value reaches the least-for-the-field value of 870 kg/m^3 only at much deeper fields (4697–4714 m), in the VII horizon oil of the PS, at Kyanizdagh area.

The field oils are tarry and highly resinous, and tar content is 6.5–14.0 %. Nitrogen content fits in 0.11–0.19 % range, sulfur, in 0.11–0.17 %, and so that sulfur content slightly drops with subsidence of coeval beds. In this process, larger quantity of nitrogen and sulfur finds correspondence in larger quantity of silicagel resins, thus permitting to state the existence of genetic bond between sulfur and nitrogen and tarry agents.

Blend composition of oils shows more distinct differences and demonstrates the impact of the depth of occurrence on oil reduction level that is evidenced by oil fraction presence in petroleum compositions, the fraction gradually increasing with depth from 70.6 to 82.4 %, and by the decreased ratio of alcohol–benzene tars to benzene tars.

In the Maykop and Chokrak deposit fields, the oils are heavy, and their density varies from 887 to 957 kg/m^3.

The *Lower Kur OGF* oils have relatively deep occurrence and are mostly confined to regionally immersed structures; for this reason, they bear the principal feature of catagenic transformation. The oils are predominantly of middle density, occasionally light ones and less frequently heavy ones, and are characterized by methane base of top (petroleum naphtha) and high-boiling fractions. The pools confined to the structure plunged parts or sealed by tectonic dislocation have more favorable conditions for preservation of light hydrocarbons than the upraised blocks, particularly when these latter connect the pool with daylight surface. Degree of transformation in these oils, with relatively homogeneous hydrogeological, lithofacial, and alternative conditions, directly depends on the depth of occurrence.

The influence of stratigraphic depth on catagenic change degree in the Lower Kur OGF oils is exhibited only when productive horizons have considerable thickness. Then, hypsometric depth markedly grows with increase in horizon ages. Such regularity is most prominently seen at Kyursangya and Garabagly fields, where in the PS I and V–VI horizons depth of occurrence of oils increases by 700–800 m and reservoir temperature increases by 12–15°C.

Blend composition of the *Baku archipelago* oils shows oil fraction within 44.0–76.4 %, while the quantity of benzene and alcohol–benzene tars varies within a small range, as 3.8–4.7 and 3.8–5.1 %, respectively. At Duvanny field, oil content consistently increases with depth, from 59 to 82.9 %.

Predominance of methane HC in the group composition of light and high-boiling fractions is common for all Baku archipelago oils. At Sangachal-deniz field, the content of methane HC decreases downdip from 66.8 to 52.7 %, and the content of naphthene HC and light aromatics rises from 12.2 to 21.5 %, respectively. At Duvanny-deniz field, the content of methane HC rises with hypsometric depth from 48.4 to 64.3 %, while the content of naphthene HC, on the opposite, decreases from 33.6 to 15.9 %. High-boiling oil fractions are characterized by similar values of common cyclicity, varying within 1.7–1.9. The content of aromatic HC in the investigated oils varies from 8.71 to 15.3 %.

Within the *Siazan monocline*, oil- and gas-bearing capacity is confined to the section range from the Upper Cretaceous to the Middle Miocene Chokrak horizon. Here, from Chokrak to Maykop, and deeper in, in the Paleogene and Upper Cretaceous stages, oils become lighter and lose nitrogen and sulfur. In the light fraction, content of alkanes and aromatics increases, and their aliphaticity degree rises.

The oils of the Siazan monocline southeastern part, where seal integrity is violated by tectonic dislocations, differ from Zeiva area oils by their higher density, resin content, lesser reduction, and maturation.

Heterochronous oils of the *Yevlakh-Agjabedi trough* fields are characterized both by similar features and by noted differences in properties and contents.

Identity of contents in oils of various stratigraphic level reduces principally to three relatively similar density values within 860–880 kg/m^3 range, to low sulfur content, increased content of tarry components, predominantly methane composition, and elevated oil paraffinicity (3.12–6.35 %).

With that, the Chokrak deposit oils differ in their properties from the Maykop, Eocene, and Upper Cretaceous oils. They are characterized by comparatively high density (887 kg/m^3), content of sulfur (0.32 %), total resins (44 %), boiling point (135 °C), and methanization. These parameters decrease from the Chokrak horizon petroleum to the Maykop, Eocene, and Cretaceous petroleum, while the content of oil, low molecular aromatics, petroleum ether resins, asphaltenes grows (from 3.4 to 6.8 %). Total light fraction content in the Chokrak oil is considerably less (11.65 %) than in more ancient oils (16.9–22.8 %).

Thus, the reduction and methanization degree, and consequently the catagenic transformation, build up by transfer from the Chokrak to more ancient oils, achieving its peak in the Upper Cretaceous volcanogenic thickness.

Oils of the *Kur-Gabyrry interfluve* (Tarsdallayar and Gyurzundagh areas) differ between them even within each one of the areas under study. As the depth of occurrence increases, density, initial boiling point, oil viscosities, and content of silicagel resins in them decrease. Brend composition shows predominance of petroleum oils and other neutral compounds.

Regional catagenic oil changes within the entire Azerbaijan territory are manifested as general tendency to the

transformation depth increase from the SCB margins to depression zones, specifically from Absheron Peninsula and Gobustan to Baku archipelago and Lower Kur Depression. Facilitation, methanization, and oil decycling are observed in this direction under relevant changes in the maturation index-averaged values.

Typical feature of Azerbaijan oils is permanent predominance of nickel ash over vanadium in their composition, as well as iron over nickel predominance in most fields. Another typical feature is low content of some heavy metal ashes in their composition. Thus, for instance, the sum of CuO + NiO + V_2O_5 oxides does not exceed 3.5 %, whereas in oil ashes of certain world fields, they amount to above 50 % of ash.

Confinement of oil deposits to the reservoirs of broad age range—from the Upper Cretaceous to the Upper Pliocene–Anthropogen—as well as extremely high, one-of-a-kind, thickness of its sedimentary filling, is characterized by the presence of several oil-generating systems. These systems present great difficulties by identification of actual contribution of each of components into the formation of hydrocarbon clusters in the principal oil-bearing facility, i.e., the net oil and gas pay thickness (PS and Lower Pliocene). One group of researches believes that oil in the PS is primary, i.e., it was produced by organic matter of the PS per se (or by its lower division), and then laterally, laterally stepwise, and vertically migrated to the accumulation point from various generation regions located in the South Caspian Mega Depression (SCMD) deeply subsided parts (Weber 1947; Alizadeh et al. 1975, 1985; Bagirzadeh et al. 1987, etc.).

Another group of researchers develops the idea of oil secondariness and its migration to the PS reservoir rocks from the lower lying Paleogene–Miocene and more ancient deposits by fissures and cracks (Gorin 1934, 1958; Mekhtiyev 1956; Mekhtiyev et al. 1971; Abrams and Narimanov 1997, etc.).

Investigation results for stable isotopes of total carbon of oils and for the carbon of their alkane and aromatic fractions are given from 152 samples from 38 oil fields of Absheron, Yevlakh-Agjabedi, Shamakhy-Gobustan, and Lower Kur OGFs, from the Baku and Absheron archipelagos, and from the Kur-Gabyrry interfluve, taken from oil reservoirs, starting from the Upper Cretaceous to the Upper Absheron inclusively (67 investigated samples are crude oils, and 85 are alkane and aromatic fractions, in separate). The values of carbon isotopic ratios, $\delta^{13}C$, in Azerbaijan oils vary within the broad range from −28.0 to −24.34 ‰ for overall carbon and from −29.1 to −24.8 ‰ for oil alkane fraction. In this process, Azerbaijan oils are grouped into two classes: (1) isotopic light, with $\delta^{13}C$ values of −28.0 ‰ to −27.0 ‰ by total carbon, and −29.1 ‰ to −27.0 ‰, by alkane fraction carbon, and (2) isotopic weighted as −26.5 ‰ to −24.0 ‰ and −26.5 ‰ to −24.5 ‰, respectively, by total carbon and alkane fraction carbon.

The second group oils constitute the overwhelming bulk of Azerbaijan oils. Their share is from 57.6 to 68.6 % of analyzed samples, whereas the isotopic light ones constitute 31.3–42.3 %. The circumstance of major importance is the clearly pronounced regular variation in isotopic ratios in stratigraphic cross section.

So, the most isotopic light oils are typical for the Upper Cretaceous reservoirs (−28.15 ‰; −28.0 ‰) (here and further, the first figure corresponds to $\delta^{13}C$ in alkane fraction, and the second one corresponds to oil total carbon), which successively replace the oils from the Eocene (−8.32 ‰; −27.86 ‰), Maykop (−28.05 ‰; −27.64 ‰), and Chokrak system reservoirs (−27.95 ‰; −27.5 ‰). Dramatic isotope weighting of oils takes place by transfer to the oils from diatom suite reservoirs (−26.45 ‰; −26.13 ‰). The most isotopic weighted oils are confined to the Lower and Upper Pliocene age reservoirs (−26.35 ‰; −25.75 ‰). Spread in values between the upper and the lower limits of $\delta^{13}C$ increases simultaneously.

General peculiarities of Azerbaijan oils are high concentrations of normal alkanes *n*-C_{15}, *n*-C_{17}, and *n*-C_{19} with incomparably low *n*-C_{27}, *n*-C_{29}, *n*-C_{31}, as well as low values of pristane-phytane ratio and sulfur content that in rare cases can reach 1.4 and 0.4 %, respectively, that according to (Sofer 1984; Peters et al. 1986; Chung et al. 2000; Collister and Wavrek 1996) is typical for the oils generated in marine delta conditions.

The importance of this conclusion for the Pliocene reservoir oils should be particularly emphasized because it essentially indicates their epigeneticity to a given age system of deposits, because, according to paleogeographic factors, formation of these latter took place in a closed desalinated basin, where continental organics was vigorously fed along with terrigenic clastic material. This fact had to be reflected in carbon isotopic signature of generated oils. The outlined theory is also confirmed by biomarker parameters of the Pliocene reservoir oils in all OGFs.

It is necessary to stress the observed pronounced differentiation between OGFs based on $\delta^{13}C$ values of alkane fraction from the Pliocene reservoir oils. Taking into account average weighting values of this parameter, the OGFs are arranged in the following sequence: the Lower Kur field (−26.8 ‰), the Absheron field (−26.29 ‰), the Shamakhy-Gobustan field (−26.1 ‰), the Baku archipelago (−26.04 ‰), and the Absheron archipelago (−25.87 ‰).

Different oil-generating intervals of the Paleogene–Lower Miocene and diatom systems play approximately similar role in the formation of oil deposits at the Absheron Peninsula Pliocene reservoir fields. It is typical for the Pliocene reservoirs of both southeastern Gobustan and Baku archipelago, though certain advantage of diatom complex can be

observed here. About 3/4 of oils of the Lower Kur OGF have been developed in the Paleogene–Lower Miocene sediments, whereas diatom deposits played the leading part in generation of the Absheron archipelago PS and account for 2/3 of oils.

In general, the tendency for oil isotope weighting can be noted in dryland-to-sea direction that can be explained by the involvement of younger deposits in "oil window." It is quite expected because apparent increase in thickness of young Pliocene–Quaternary deposits in sediments is noted in this direction, and they subside at deep depths.

The mud volcano oils basically have naphthene–aromatic and methane composition; they are highly oxidized and biodegradable. Carbon isotopic signature in saturated oil fraction varies from −28.5 to −25.4 ‰.

2.1.3.3 Maturation Degree of Oils from Heterochronous Reservoirs of the South Caspian Mega Depression

Oil maturation degree is the most essential parameter that, combined with other geological and geochemical indexes, permits to obtain sufficient data concerning depth of oil and gas generation zone, stratigraphic confinement of oil source rocks, migration tendency, and conditions of hydrocarbon fluids and finally to assess the oil- and gas-bearing basin potential. Investigations of oil maturation degree are of extrinsic value for oil- and gas-bearing basins (OGBB), where a number of systems are involved in hydrocarbon generation processes. The vigorously developing South Caspian Mega Depression (SCMD) can serve as an example because several fluid-generating systems are distinguished in its Cenozoic section such as the Eocene, the Oligocene–Lower Miocene (the Maykop), the Middle Miocene (Chokrak horizon), and the Middle–Upper Miocene (diatom) systems (Alizadeh et al. 1975).

Tectonically, the South Caspian area of regional downwarping, being conjugated to the principal geostructural elements of Caucasus, Kopetdagh, and Elburs of differing geodynamical conditions, happened to be broken into a series of depression structures that were the integrity of intermountain depressions and downwarps differing in their geological and tectonic configuration (Aliyev et al. 2005). Geological and tectonic configuration of the SCMD downwarps finds its reflection on geochemical image of oils condensed therein.

The mega basin most essential feature is high qualitative geochemical diversity of oils from the Pliocene reservoir, where from different in composition oils are produced: both light and heavy, both low sulfur and high resinous, both methane and naphthenic oils, etc.

Another SCMD feature is low maturity level of oils from the Upper Cretaceous, Oligocene–Lower Miocene (Maykop), and Miocene reservoirs of the Shamakhy-Gobustan OGR, as compared to the oils from the Pliocene age reservoirs of adjacent OGFs. It is known that oil maturity is the function of temperature conditions in the Earth depths and of duration of stay of oil-generating deposits in the oil generation zone. It is directly interrelated with the age of oil-generating thicknesses.

The third, utterly surprising circumstance is the extremely low oil maturity in known oil and gas condensate fields, which does not fit into existing concepts of oil and gas formation vertical zoning, where under the condensates are the products of organic matter highly catagenetic destruction.

High-tech methods (widely used in organic geochemistry) of organic matter and oil research at the level of molecular fossils (biomarkers) permitted to conduct oil–oil, oil–oil source rock correlations, to determine oil stratigraphic age, and, what is most vital, to define catagenetic transformation level for kerogene and maturity level for oil derivatives. To this objective, such parameters as hopane and sterane isomerization degree, sterane aromatization, and relationships between aromatic sterandes and steroids, have been used.

Research results for the deposits in all OGFs of the SCMD showed that, basing on sterane isomerization, oil maturity varies from 0.155 to 0.49. The most mature oils are grouped within the Middle Kur Basin OGF, where in 50 % of facilities, oils have maturity value, basing on sterane isomerization, Req. = 0.68–0.73 %, and in 40 % cases, they are 0.4–0.5 or Req. = 0.63–0.68 %, i.e., the investigated oils in general show low-level and median kerogene transformation in oil source rocks.

In the Lower Kur, Shamakhy-Gobustan, Absheron troughs, and Baku and Absheron archipelago Pliocene deposits, oil maturity level varies within Req. = 0.45–0.67 %. The facilities with middle values of this parameter, lying in the Req. = 0.53–0.63 % range, constitute the main body (81.6 %) of the SCMD Pliocene deposits (the reservoir age is meant here), thus evidencing to OM low transformation level in oil source rocks. The least transformation degree is found in the Absheron Peninsula and the Shamakhy-Gobustan trough oils (Ro = 0.43–0.56 %). Increased maturity is typical for the Lower Kur Depression (LKD) oils and for the Baku and Absheron archipelago fields (Req. = 0.62 %).

It is important to note sharp isotope weighting of oils southeastward against the general lightweight isotope background of the LKD oils, with isolation of anomalies, having typical diatom mark, in the oils of the most distant southeastward Neftchala field. Particularly notable is that this field features the most mature oils, both within the LKD and in the SCMD central part.

Thus, on the whole, rather low-level maturity has been found for the SCMD oils, not exceeding Req. = 0.73 % (Middle Kur Depression) that significantly raises the prospects for discovering of more mature stage oils.

Table 2.14 Hydrocarbon composition of gases from various stratigraphic frameworks (average values)

Age of enclosing rocks	Methane + ethane	Propane	Butane	Pentane	Propane + high	Carbon dioxide	Methane heavy
Absheron stage	95.28	1.57	0.8	0.37	2.74	0.8	35
Productive strata	90.92	0.64	0.60	0.60	1.84	6.2	49
Chokrak horizon	94.50	1.58	1.25	0.77	3.60	1.6	26
Maykop suite	88.66	3.90	2.65	1.63	8.18	3.1	10
Foraminiferal layers	84.61	5.50	6.22	2.96	14.68	0.7	5

Table 2.15 Change in *n*-butane\isobutane and *n*-pentane \isopentane relationship with stratigraphic depth

Age of enclosing rocks	Number of tests	*n*-butane isobutane	n-pentane Isopentane
Absheron stage	25	0.31	0.20
Productive strata	62	0.67	0.58
Chokrak horizon	9	1.10	0.87
Maykop suite	28	2.01	1.06
Foraminiferal layers	1	3.24	1.58
Cretaceous age	1	4.2	2.0

Isotope weighting of the PS oils with simultaneous increase in their maturity level toward the SCMD deeper area is the consequence of diatome deposit involvement in oil generation zone as they produce the isotope-heavy oils.

2.1.3.4 Geochemistry of Hydrocarbon Gases

Azerbaijan, that through many centuries is being called "the Land of Flames," together with adjacent Caspian Sea area, is characterized by extensive development of natural surface manifestations of gas.

Many dry gas discharges are being developed at Azerbaijan territory, with 10 burning, above 300 gas manifestations associated with mud volcanoes, about 150 manifestations related to mineral springs, as well as gas manifestations as gas hydrates at the Caspian Sea bottom. Numerous gas manifestations were noted by drilling of exploratory wildcat wells.

Azerbaijan area and the Caspian Sea offshore area are characterized not only by focused gas flows but also by their macro manifestations, related to the Earth regional gas breath.

Azerbaijan natural gases are characterized by diversified chemical composition. Assays of above 500 gas samples showed that natural gas basic constituents are methane, carbon dioxide, and nitrogen. Alternative components such as ethane, propane, butane, and argon are admixtures, with their content not exceeding units of percentage, and such substances as hydrogen sulfide, helium, and neon are contained in micro concentrations.

Methane gases are most widely abundant and are essentially confined to the South Caspian and Kur Depressions, as well as to the Greater Caucasus and the near-Caspian-Guba superimposed trough. Carbon dioxides occupy the Lesser Caucasus area and the Talysh western part. Nitrogen gases are present as small-area zones in the Greater Caucasus, in Talysh, and in the northeast of near-Caspian-Guba superimposed trough.

Hydrocarbon Gases of Oil and Gas Fields

Chemical composition of hydrocarbon gases at the Azerbaijan oil, gas condensate, and gas fields is represented by the following components and their composition limits:

1. hydrocarbon components: methane—from 51.0 to 99.0 %, ethane—from 0.14 to 11.0 %, propane—from 0.04 to 4.4 %, butane—from 0.04 to 3.8 %, and pentane —from 0.04 to 3.3 %.
2. incombustible gases: carbon dioxide—from 0 to 46.0 %, nitrogen—from 0.01 to 9.0 %, argon—from 0.001 to 0.04 %.
3. trace substances: helium—from 0.0002 to 0.03 %; hydrogen sulfide from 0 to 0.5 %.

In some samples, unsaturated hydrocarbons and hydrogen were present. Content of various gaseous components varies in broad range.

We failed to establish a unified trend in methane content changes in the PS section.

Table 2.16 Isotope composition of deposit gases (average values)

Stratigraphy	Number of tests	$\delta^{13}C_{CH4}$ (−) ‰	δDC_{CH4}, (−) ‰	$\delta^{13}C_{C2H6}$, (−) ‰	$\delta^{13}C_{CO2}$	$\delta^{18}O_{CO2}$
PS upper division	22	43.7	202	28.5	+0.6	−4.9
PS lower division	16	43.9	211	27.4	+8.6	−2.3
PS in a whole	38	43.8	206	28.0	+4.5	−3.5
PS-underlying deposits	7	51.7	207	33.9	+2.1	1.7

Regular decrease in methane content with stratigraphic depth was noted from the data of Umbaki, Siazan, and Gazanbulagh fields (Table 2.14).

Interesting results were obtained from the data of normal butane-to-isobutene ratio and normal pentane-to-isopentane ratio for the gases of some Absheron Peninsula, Gobustan SE, and the near-Caspian-Guba region oil fields. The values of these ratios regularly increase from top downward through the Tertiary and Mesozoic deposit section vertically (Table 2.15).

Carbon and Hydrogen Isotope Composition in Azerbaijan Gases

Within the recent decade, the study of isotope composition of elements constituting the investigated facilities has been widely used in geochemical research. Oil and gas geology investigates carbon isotopes of methane and its homologs, carbon dioxide, hydrogen, and oxygen isotopes of carbon dioxide. The works that had been conducted earlier (e.g., Dadashev et al. 1986) studied carbon isotopes of methane. Isotope analysis of 60 samples from 15 Azerbaijan oil fields was conducted at VNIIGeoinformsistem (Moscow).

Later on, Geological Institute, in collaboration with *British Petroleum*, conducted some studies of carbon isotopes not only in methane but also in its homologs as well. Gas specimens were sampled from boreholes into special metal vessels with preserved gas specimen pressure conforming to wellhead pressure. Forty-five specimens of free gas from various PS horizons and suites (38 samples) and from the PS-underlying deposits (7 samples) (Chokrak, Maykop) were taken to containers from 27 oil, gas condensate, and gas fields of Azerbaijan in order to study gas isotope composition. In addition, AMOK Company has studied 9 gas specimens from the Lower Kur OGF deposits.

According to the analysis results, carbon isotope composition of methane ($\delta C^{13}CH_4$) varies from −37.2 to −60.3 ‰ (averagely, −45.0 ‰), ethane carbon—from −21.0 to −40.3 ‰ (averagely, −28.9 ‰), propane—from −10.5 to −33.7 ‰ (averagely, −23.7 ‰), isobutane—from −21.5 to −35.8 ‰ (averagely, −27.0 ‰), normal butane—from −14.8 to −30.8 ‰ (averagely, −23.5 ‰), butane—from −18.0 to −32.6 ‰ (averagely, −25.3 ‰), and hydrogen isotope composition of methane, δDCH_4, from −101.0 to −277 ‰ (averagely, −207 ‰).

Carbon dioxide accompanies hydrocarbon gases. In sampled gases, carbon dioxide δC^{13} varies from −13.2 to +21.5 ‰, average value being +3.6. Oxygen isotope composition in carbon dioxide also varies in broad range, from +2.5 to −12.5 ‰, averagely, −2.9 ‰. Wider range of changes in carbon dioxide isotopes as compared to carbon isotopes of hydrocarbons adequately corresponds to diversified CO_2 sources, their origins, and fractionation. Results of study of gas isotope composition permit to compare the distribution of gas isotope composition in oil and gas deposits, basing on cross section, depth, and deposit types.

We did not succeed in finding a clear-cut regularity of changing carbon isotopes in HC gases and carbon dioxide, as well as changes of hydrogen isotope in methane and oxygen isotope in carbon dioxide according to the PS individual horizons and suites. Comparison of gas isotope compositions in the PS upper and lower divisions (Table 2.16) shows that they are close to each other by their absolute values. Thus, no changes are found for carbon isotope composition in methane, and only moderate weighting is noted for hydrogen isotopes in methane and carbon isotopes in ethane and propane. More remarkable weighting is found in carbon dioxide isotope composition. $\delta C^{13}CO_2$ weighs from +0.5 to +8.6 ‰ on the average, and $\delta O^{18}CO_2$ weighs from −5.4 to −1.6 ‰.

A tendency to carbon isotope composition lightening in HC gases, carbon dioxide, as well as hydrogen and oxygen lightening is observed at interval from the PS to underlying deposits.

Comparison of isotope average values in HC gases and carbon dioxide from various types of deposits demonstrates that carbon isotope composition is enriched by heavy isotope in all HC and carbon dioxide components by passing from oil fields to gas fields, that hydrogen isotope composition of methane is lightened, and that oxygen in carbon dioxide does not change. The gases of gas condensate fields occupy an intermediate position. Carbon and hydrogen in methane, both from oil fields and by transfer from gas to gas condensate fields, are enriched by a heavy isotope. Carbon isotope composition in ethane, propane, iso- and normal butane, carbon dioxide, and carbon dioxide oxygen is lightened.

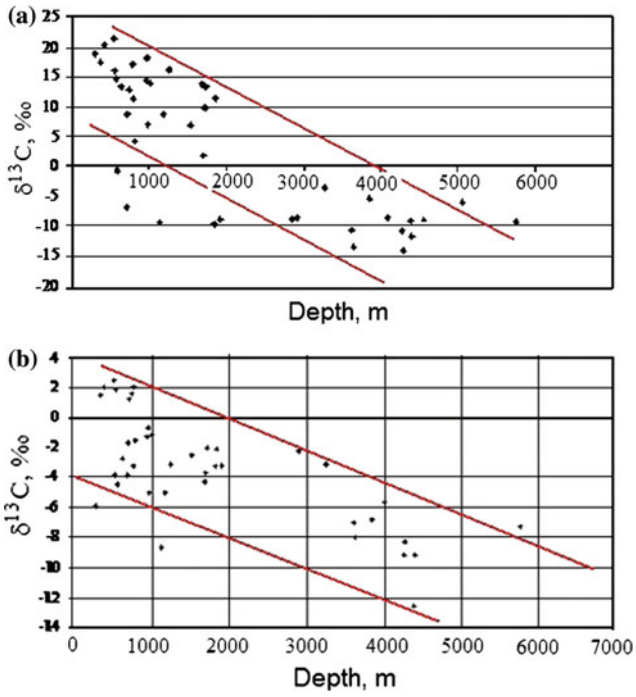

Fig. 2.6 Changes in $\delta^{13}Cco_2$ (**a**) and $\delta O^{18}co_2$ and (**b**) values with depth

The investigated samples encompass the depths from 230 to 5754 m; therefore, an attempt was made to trace the changes in gas isotope composition with depth as well. Carbon isotope composition both in methane and in carbon dioxide experiences the tendency to lightening with depth increase (Fig. 2.6).

Carbon isotope composition in the fields' methane shows that two principal zones are found here. The first zone that embraces the fields of the Lower Kur region and the Baku archipelago southern part is characterized by reduced-weight methane isotope, varying within −(57.3 to 46.2)‰. The second zone embraces the Absheron Peninsula, the Absheron archipelago, and the Baku archipelago northern part and Gobustan and is distinguished by its heavier carbon isotope of methane within −(37.2 ÷ 46.0) ‰.

Two zones are also found in the distribution of hydrogen isotopes of methane. The first one, with −(277 to 194) ‰ values, covers the Absheron Peninsula, the Absheron archipelago, Gobustan, and the Lower Kur region. The second zone, with hydrogen isotope values of −(194 to 101) ‰ in methane, is isolated within the central, southwestern Absheron and within the Baku archipelago.

Two zones are also prominent in areal distribution of carbon isotope composition and other HC gases (ethane, propane, butane), as well as distribution of oxygen and carbon isotopes in carbon dioxide.

On the whole, lightening of carbon isotopes in HC gases and in carbon dioxide and weighting of oxygen isotope in carbon dioxide are observed in downwarping trend of the PS rocks.

According to the dependence graph between $\delta^{13}Cc_{H_4}$ and $\delta^{13}Cc_{2H_6}$, the conclusion was made that all mud volcano gases are thermogenic, whereas field gases are represented both by thermogenic and biogenic gases and by their mixture.

Thus, isotope analysis that was conducted permits to point to the diversity of gas genesis and sources in the PS and in underlying deposits. Main scope of the PS gases was generated concertedly with liquid HC generation, i.e., as associated gases. Lesser gas scopes were generated at the expense of OM late transformation stage and oil cracking.

Basin Modeling

Qualitative estimate of oil and gas potential realization was given, and density charts for generated HCs were plotted for

Table 2.17 The scope of oil and gas generation in the South Caspian trough Meso-Cenozoic deposits (from kinetic simulation results)

Stratigraphic framework	Overall quantity			Average-specific quantity (per 1 km^2 of basin area)		
	Liquid HC[a] × 10^9 t		Gas[b] × 10^{12} m^3	Liquid HC × 10^6 t		Gas × 10^9 m^3
	Aggregated generation	Preserved after cracking		Aggregated generation	Preserved after cracking	
Upper Pliocene	58.4	58.4	9.0	0.344	0.344	0.053
Middle Pliocene	159	159	54.3	0.938	0.938	0.32
Miocene–lower Pliocene	534	465	305	3.15	2.74	1.8
Paleogene	1247	732	1240	7.35	4.32	7.34
Mesozoic age	811	233	1170	4.78	1.37	6.88
The whole sedimentary thickness	2815	1670	2780	16.56	9.71	16.39

Notes
[a]Liquid HCs that preexist in kerogene structure are included in this quantity
[b]Gaseous HCs that generated both from kerogene and from the cracking of high molecular HCs

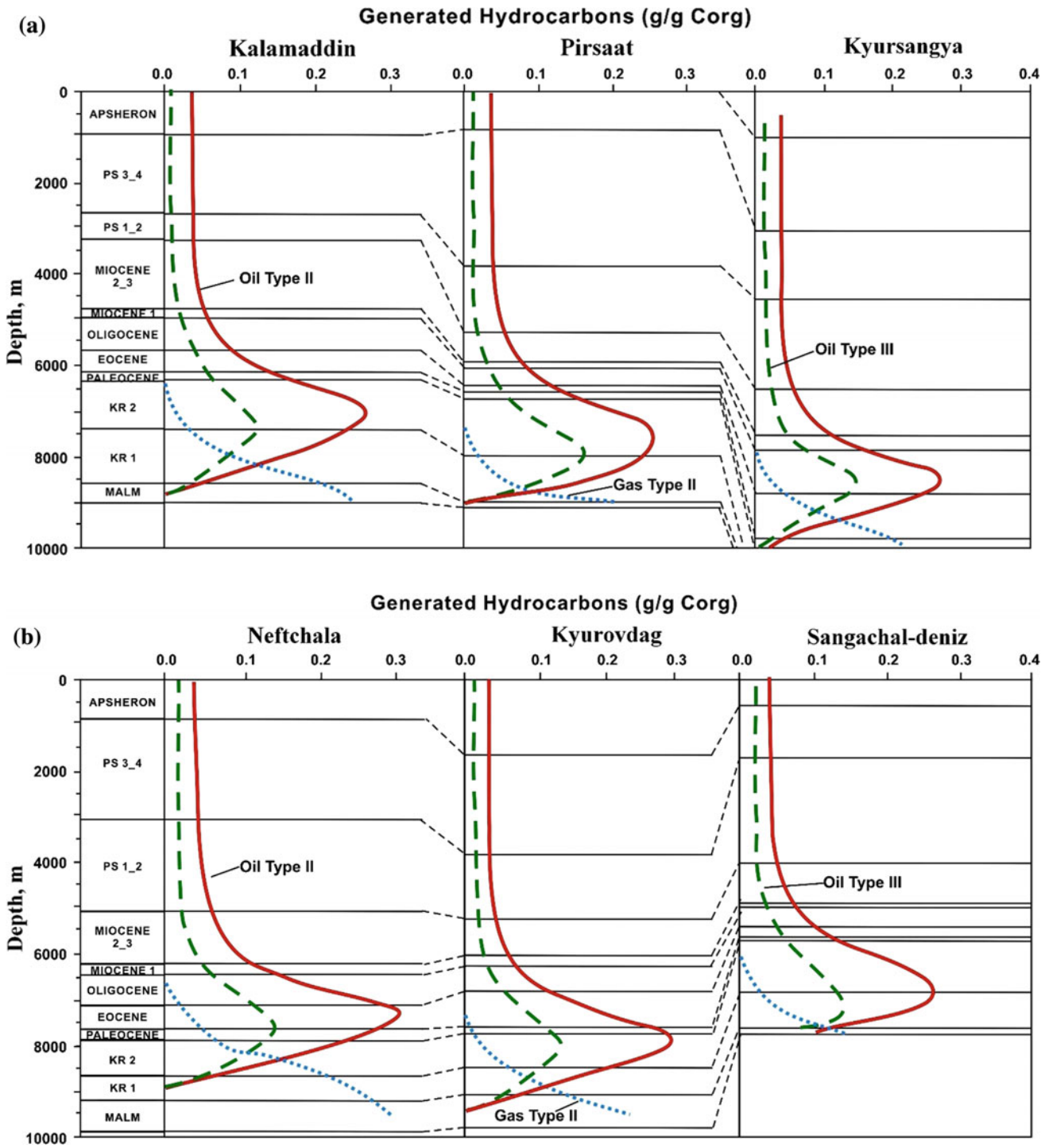

Fig. 2.7 Changes in oil window positions along Kalamaddin-Pirsaat-Kyursangya (**a**) and Neftchala-Kyurovdagh-Sangachal-deniz (**b**) sections. The depth of oil and gas generation start increases toward the depression depocenter

various South Caspian Basin (SCB) systems using basin modeling (Table 2.17). In addition, the depth intervals in the SCB section with the highest methane concentrations were predicted by plotting the integrated model of gas generation and following migration.

Modeling of oil and gas formation process in the Lower Kur trough sedimentary thickness (Inan et al. 1997) permitted to establish that oil window in the Lower Kur Depression cross section embraces the Paleogene stratigraphic interval. According to this model, oil generation started in the Late

Pliocene and has been continuing at present at 6–12 km depths (Fig. 2.7). The SCB basin modeling was also made, using the SIGMA-2D software, developed at the Engineering Research Center of the Japan National Oil Company. A broad spectrum of geological, geothermal, and geochemical data was used by model plotting.

According to the modeling results, liquid HCs that had been generated in the Oligocene–Miocene deposits and migrated there from in the Late Miocene–Early Pliocene period migrated northward and were accumulated in the Absheron-near-Balkhan threshold structure. Shakhdeniz, Bulla deniz, Bakhar, etc., structures situated in the basin deeper area were not yet generated at that period. Later, by the moment when these structures started to generate, the source deposits were already located at the condensate and gas generation zone. Accordingly, the late generation products, predominantly gaseous HCs, were already arriving there (Fig. 2.8). Implementation of the South Caspian hydrocarbon system key elements (petroleum systems) during the basin geological history is illustrated by special annotated diagram with two areas as an example (Fig. 2.9).

For the organic matter of marine origin (type 2), it corresponded to the initial stage of oil generation. In the diagram built for the specified area, there are two basic phases of hydrocarbon generation—the first one is 6 Ma, and the next one is 2 Ma ago. These two generation impulses were the result of submersion, subsequent rise, and repeated submersion. In Bakhar area, there is only one phase of hydrocarbon generation. Here, according to the vitrinite reflectance equivalent, the Late Oligocene sediments are on the same level of organic matter maturation as it was forecast for Pirsaat area (Fig. 2.10).

Abrams and Narimanov (1997) used BasinMod, the basin modeling package, to assess OM maturity degree and temperature in the SCB Oligocene deposits lying at the depths not exposed by drilling. Thus, OM maximal transformation degree in the Upper Oligocene deposits at Pirsaat area, expressed in the vitrinite reflectivity equivalent, is equal to 0.75 %.

For the marine-origin OM (type 2), it corresponds to the primary oil generation stage. The diagram plotted for the area displays two principal stages of HC generation: The first one was 6 million years ago, and the second one was 2 million years ago. These two generation impulses are the consequence of deposit subsidence, subsequent rising, and repeated subsidence. Only one generation stage was noted at Bakhar area. Here, the Upper Oligocene deposits (according to the vitrinite reflectivity equivalent) are at the same OM maturity level that was predicted for Pirsaat.

According to the data of modeling made by Klosterman et al. (1997), vigorous oil generation in the Yevlakh-Agjabedi trough embraced the depths of 4–6 km and started 3 million years ago. Only minor portion of potential source rocks was plunged to the depths requisite for thermal maturity, and consequently, small volumes of oil were generated in the sedimentary thickness.

For qualitative description of contemporary and paleotemperature conditions and the ensuing oil and gas generation features, modeling on separate areas was conducted in the near-Caspian-Guba region. These models were based on permanent and time-dependent thermal flow calculated from the well temperature data, with due consideration for rock geothermal properties. Plotted thermal models were compared with the data on vitrinite reflectivity (Ro). Thus, it was established that oil and gas formation processes in the near-Caspian-Guba region encompass the stratigraphic interval from the Jurassic up to and including the Early Pliocene.

Figure 2.11 gives as an example of the OM transformation dynamics superimposed on deposit submersion history at Yalama area. According to the calculation results, oil generation in the Lower Jurassic deposits reached its peak already at the boundary between the Jurassic and Cretaceous periods (Ro 0.7–1.0 %). The Cretaceous bottoms enter the oil window zone only in the Miocene period.

Analyzing the results of basin modeling in Azerbaijan, we can conclude that oil formation processes here embrace a broad stratigraphic interval (from the Jurassic up to and including the Early Pliocene) and are characterized by spatial variability.

Judging by modeling results, while oil formation process in the SCB central, most plunged marine part, involves mostly the Miocene deposits, then in the dryland, within the Lower Kur Depression, the Paleogene deposits are predominant.

At the same time, in the near-Caspian Guba marginal trough, where these processes were significantly weakened during the Cenozoic age and had superimposed character, and where Mesozoic rocks have shallow occurrence or are even exposed on the surface (at the Greater Caucasus eastern edge northern outskirts), oil-intensive generation interval is, as a rule, confined to the Cretaceous and Jurassic rocks.

It should be noted in conclusion that peculiar features of HC formation and migration resulting from the modeling are of great importance for the understanding of field formation mechanisms, for the assessment of oil- and gas-bearing prospects, and for planning of oil and gas exploration.

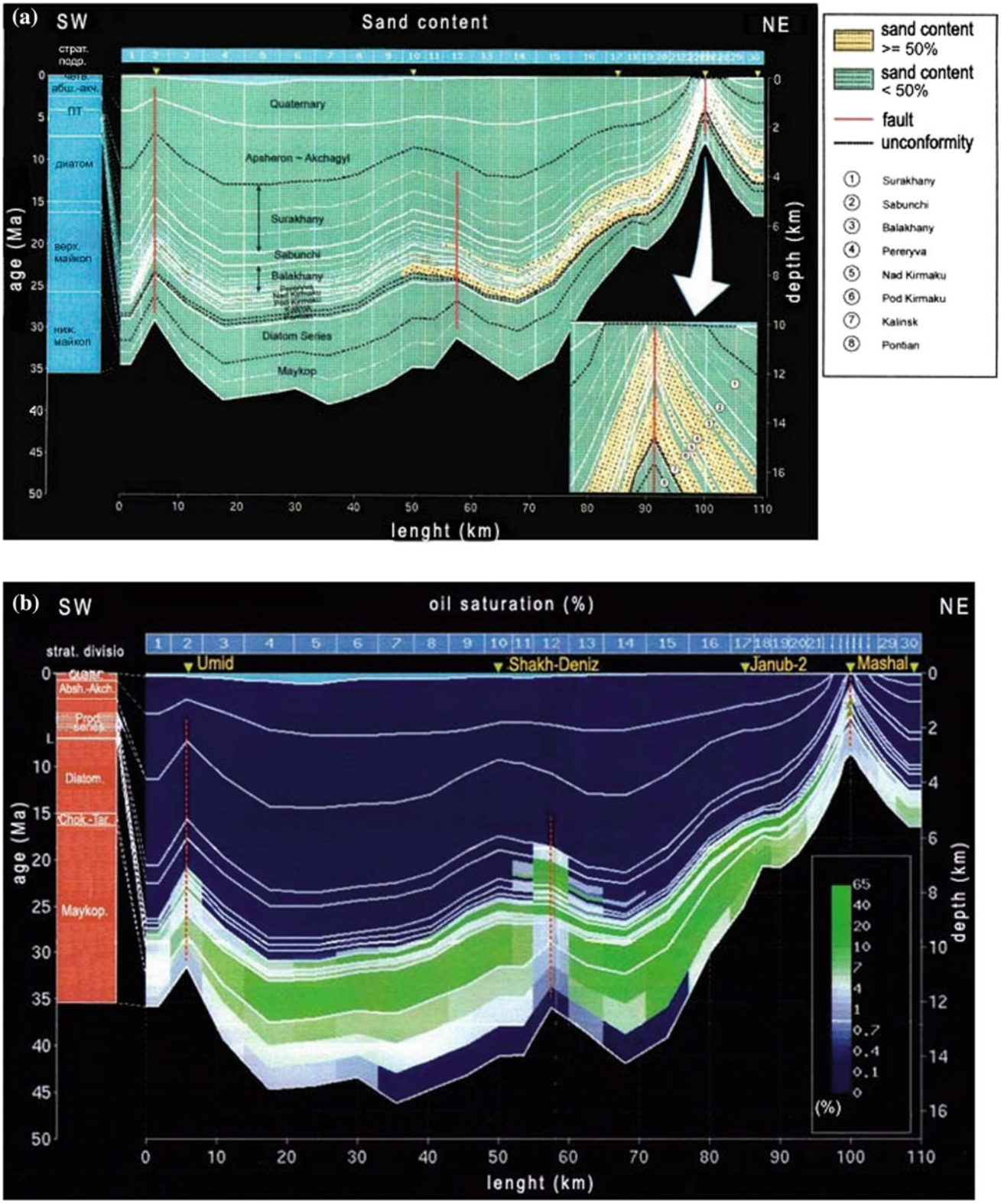

Fig. 2.8 Model of generation, migration, and accumulation of HC, built using the SIGMA-2D software package. In the South Caspian Basin, the presence, location, and extension of the permeable horizons in the section (**a**) are the key factors for HC migration and accumulation (**b**)

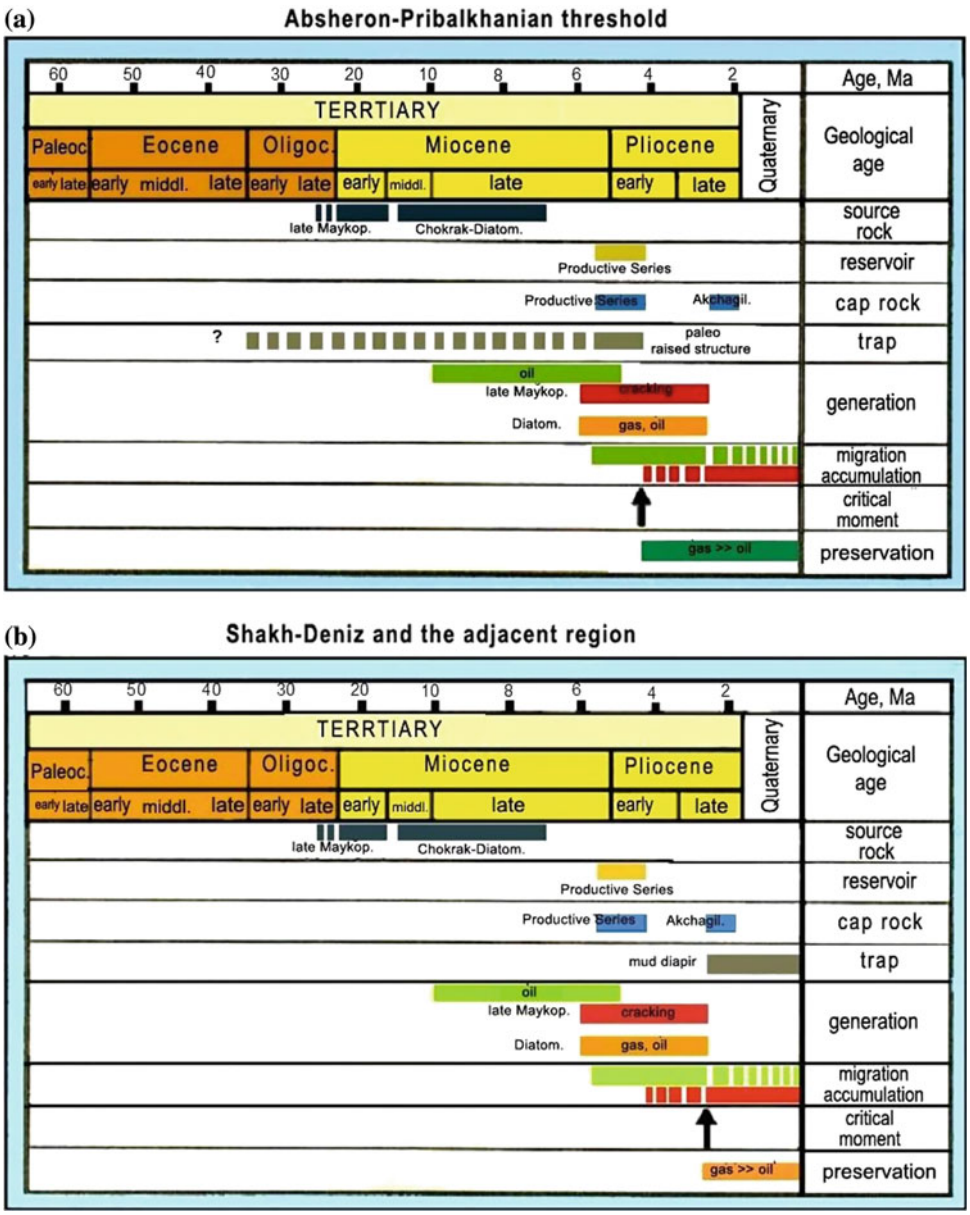

Fig. 2.9 Annotated diagrams of element realization of the South Caspian hydrocarbon system in the course of the basin geological history for **a** Absheron-near-Balklhan threshold and **b** Shakh deniz field

2.1.4 Thermobaric Conditions and Hydrochemical Characteristics of Oil- and Gas-Bearing Complexes

2.1.4.1 Baric Conditions

The SCB is one of the outstanding instances, where extremely favorable conditions for the formation of anomalous high pressures existed due to the peculiarities of development history and contemporary geological structure. Here, avalanche-type (up to 3 km/million years) sedimentation was observed in the Pliocene–Quaternary period and thick (up to 25 km) sedimentary system was formed, where plastic terrigenic rocks are prevailing. Clay rocks constitute 80–90 % in the SCB Cenozoic section. The SCB is characterized by abnormally low-temperature gradient that varies within 1.5–1.8 °C/100 m in its central, most submersed part. As a result, porous pressures here exceed hydrostatic pressure by 1.5–2.0-fold. Thus, for instance, porous pressure at Zafar-Mashal structure in the SCB deeper area measured at 6475 m depth amounted to 132 MPa, which more than 20-fold exceeds hydrostatic pressure and constitutes about

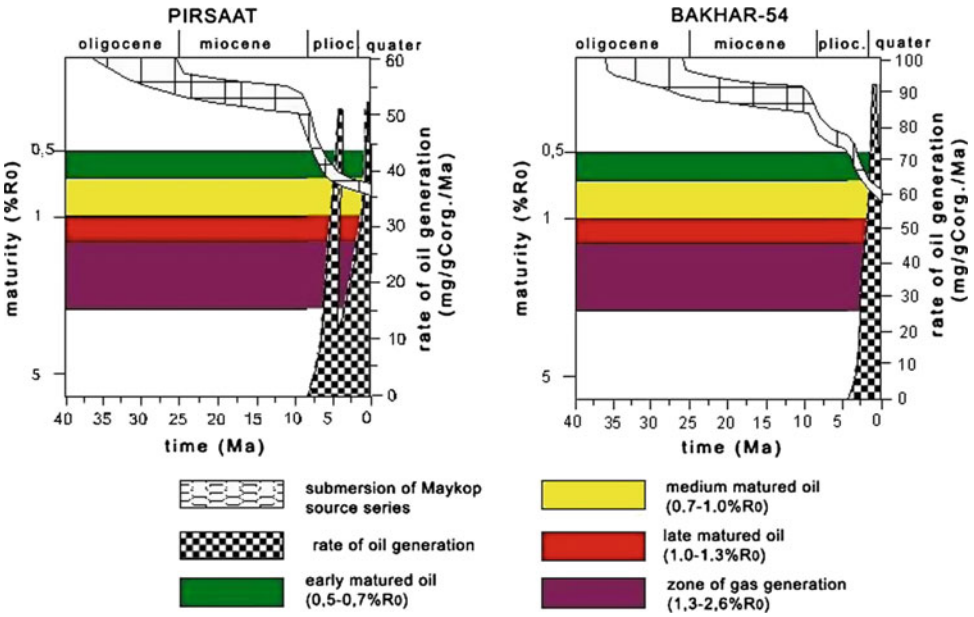

Fig. 2.10 Rate of hydrocarbon generation (mg oil/g organic matter/Ma) in the Oligocene deposits over the fields: *left panel* Pirsaat and *right panel* Bakhar. Vertically on the *left*, the maturity scale by vitrinite reflectance (% Ro)

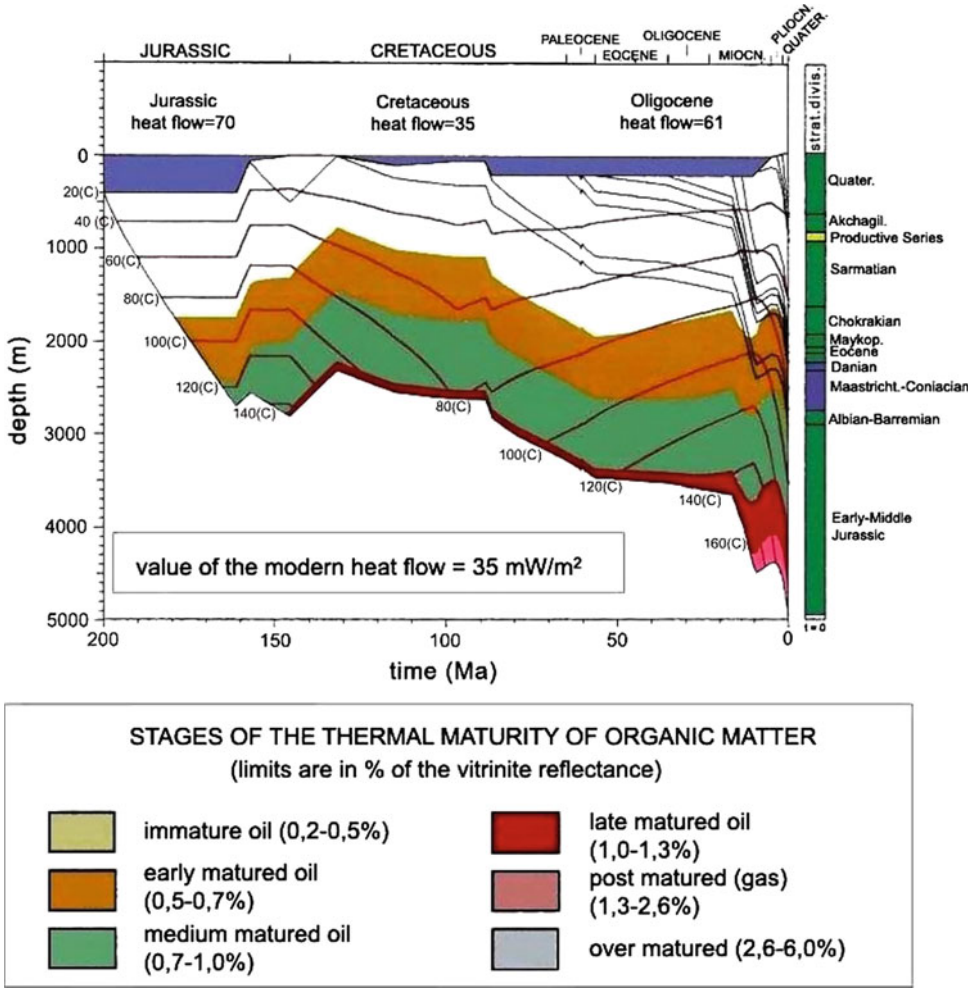

Fig. 2.11 Thermal transformation of organic matter versus submersion of sediments in Yalama area of the near-Caspian-Guba region

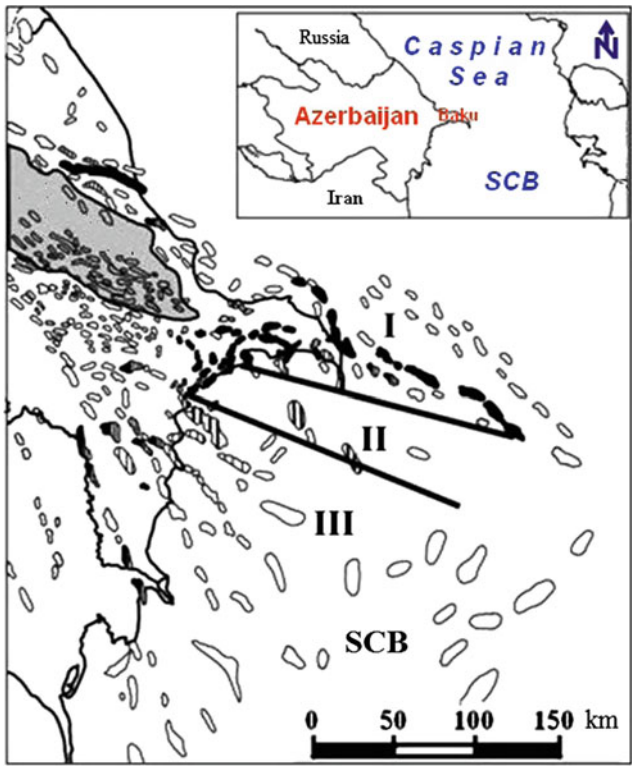

Fig. 2.12 Zoning of formation pressure distributions in the SCB: *I* Absheron Peninsula and Absheron archipelago; *II* South Absheron water area; *III* Baku archipelago

Table 2.18 The SCB: spatial changes in clay mass thicknesses and pressure gradients

Zones	Average values of clay mass thicknesses at various depth intervals, km				Average values of pressure gradients, MPa/km
	1–2	2–3	3–4	4–5	
I—Absheron Peninsula and Absheron archipelago	50	40	30	20	13.5
II—South Absheron water area	750	235	185	150	16.3
III—Baku archipelago	900	725	460	350	18.0

90 % of lithostatic pressure. It is, therefore, not accidental that the SCB structures are as a rule of diapir nature and that mud volcanism is widely developed here.

Analysis of the data on formation pressures and their gradients in the SCB permitted to reveal their inhomogeneous spatial variation. Their intensity grows southward and southwestward in clear-cut correlation with the changes in

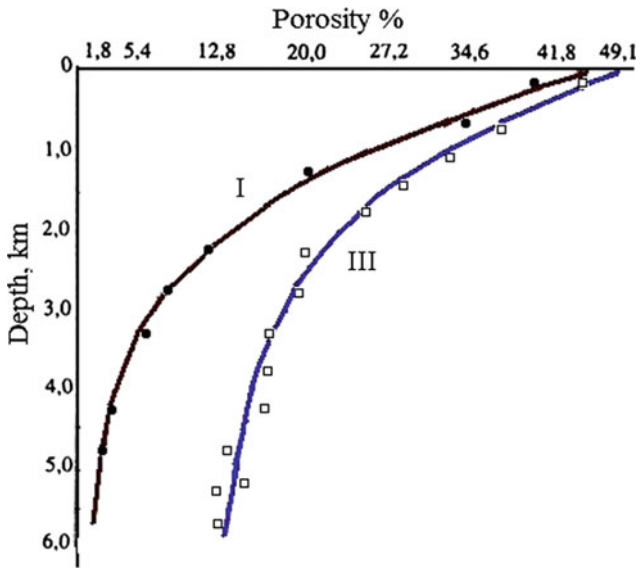

Fig. 2.13 Rock porosity changes with depth in the SCB OGF: Absheron archipelago (zone I in Fig. 2.12) and Baku archipelago (zone III in Fig. 2.12)

rock clay content and in clay mass thicknesses in the same direction (Buryakovsky et al. 1986) (Fig. 2.12; Table 2.18).

The highest geofluid pressures are found within the Baku archipelago (zone III), where pressure gradient average value is 18.0 MPa/km (see Table 2.18). It is reflected in the process of rock compaction. The anomalous high pressures decelerate the process of rock compaction within the Baku archipelago that is vividly seen from the manner of rock porosity changes with depth in the Baku archipelago, as compared to the Absheron archipelago with its relatively moderate geofluid pressures (pressure gradient average value is close to 13.5 MPa/km) (Fig. 2.13).

Investigations of changes in clay porous pressure gradients with depth conducted at Bulla deniz area and calculated from log information and from drilling fluid-specific weight established that independently of drill-hole sites at the structure, upper limit of anomalous pressures is confined to the depth interval of 600–1230 m. Stratigraphically, it embraces the bottoms of Pliocene deposits (ancient Caspian and Absheron), Akchagyl (the Pliocene tops), and, in some boreholes, the PS roof areas (PS, the Lower Pliocene) (Yusufzade et al. 1976; Khalilov and Imanov 1980). In said interval, porous pressure gradients reach 23 MPa/km.

The second jump in changes through the section vertically in the SCB was found below 5 km depths (Khalilov and Imanov 1980; Buryakovsky et al. 1986) (Fig. 2.14). It is the most contrasting zone, where the abnormally high reservoir pressure (AHRP) values become comparable with geostatic pressure.

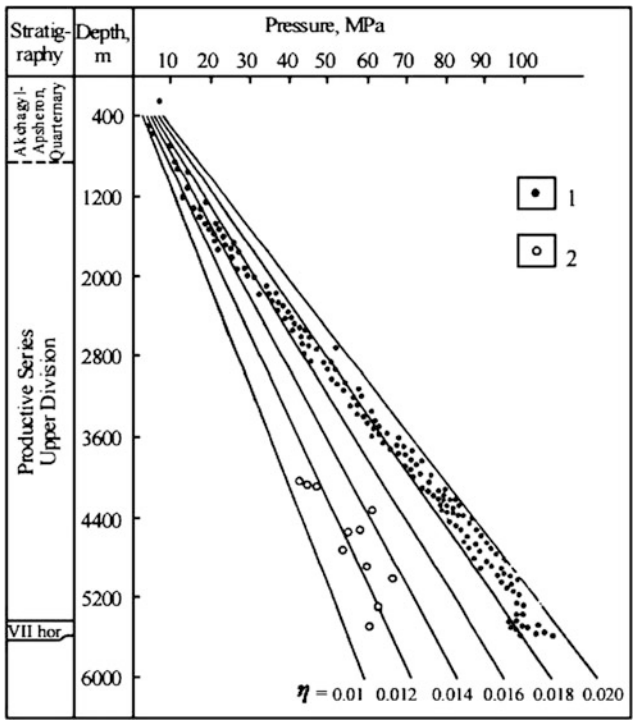

Fig. 2.14 Changes in porous pressure in the clays (*1*) and formation pressure in the reservoir sands (*2*) with depth in the Baku archipelago oil fields (η is the pressure gradient, MPa/m)

Generalization of results of all previously made investigations of distribution regularities of geofluid pressures in the SCB—both from geophysical well logging (GWL) and from well actual measurements down to 7 km depths—gives grounds to isolate two major AHRP zones that are most contrasting in the Baku archipelago, in this area. Depending on the section lithofacial characteristics, the roof of the AHRP first zone is within 600–1200 m range. Lower, approximately 4 km depth, pressure gradients, though still remaining high, are sufficiently stable. Starting from approximately 5 km depth, a new, more intense AHRP zone finds its commencement (Feyzullayev and Lerche 2009).

The formation reason for the first, higher AHRP zone is most probably related to the rock non-equilibrium compaction (undercompaction) caused by high sedimentation rates (Guliyev et al. 1989). This zone is easily predictable and, as a rule, does not create problems by borehole making (Shykhaliyev et al. 2010).

The AHRP lower zone presents the highest risk as its intensity level is hardly predictable that hinders correct selection of drilling mud-specific weight by drilling in this section range. Length of this zone at deeper depths that have not yet been exposed by drilling is unclear.

The highest pressure gradients and enhancement of risk level by well drilling should be associated with the depths below 9 km, where vigorous gas formation processes start out. It is also confirmed by the predictions based on 2D basin modeling of the SCB (Fig. 2.15).

2.1.4.2 Geothermal Conditions

As is well known, temperature affects the degree of OM catagenetic transformation, controls the processes of oil primary migration, its maturity and deposit accumulation, HC phase conditions, their vertical distribution and areal zoning.

Mekhtiyev et al. (1960), Aliyev (1982, 2002), Buryakovsky et al. (1986), Kerimov and Pilchin (1986), Mukhtarov (2011), Eppelbaum et al. (2014), and others dealt with thermal research of the Azerbaijan oil- and gas-bearing regions.

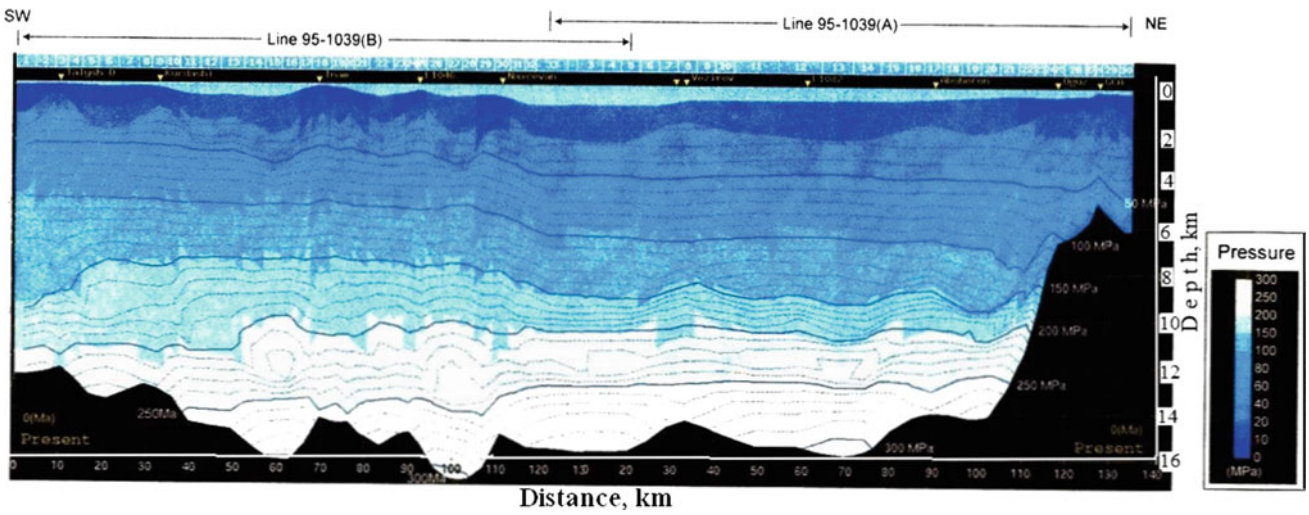

Fig. 2.15 Distribution of geofluid pressures in the South Caspian Basin deep part from the data of 2D modeling

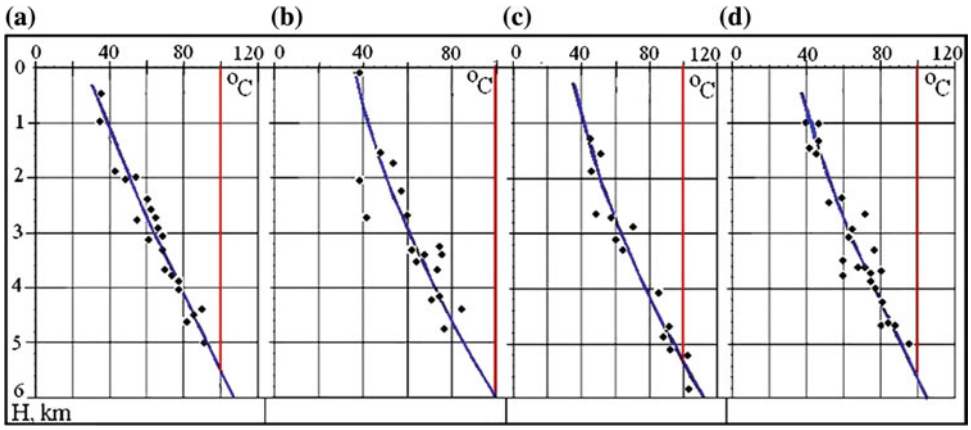

Fig. 2.16 Changes in reservoir temperatures with depth at some SCB marine sites: **a** Aran-deniz; **b** Hamamdagh-deniz; **c** Karasu; **d** Sengi-MughanSengi-Mughan

Above 10,000 measurements were taken in more than 150-m-deep nonoperating wells within 100–6000 m depth range in Azerbaijan oil and gas fields (OGF). Geothermal parameters were determined for more than 3000 rock samples from the Azerbaijan and Western Turkmenistan Meso-Cenozoic complexes.

Typical feature of the thermal conditions of the SCB is low warming of the Pliocene–Anthropogenic deposits. Their temperature at 5000 m depth does not exceed 100 °C in marginal zones, which is explained both by high sedimentation rate and by significant depth of occurrence of crystalline foundation (Fig. 2.16).

Decreased thermal behavior of the trough Pliocene and Anthropogenic deposits is to a great degree also determined by lithological composition of the underlying Paleogene–Miocene rocks, a thick 3–5-km clay strata with reduced thermal conductivity.

Conductive and convective components of abyssal thermal flow play important role in the formation of local elevation temperature fields. It is witnessed by 3–7 °C elevated (and more) temperature values at the same hypsometric marks in the area of mud volcano and tectonic dislocations that contribute to the transfer of formation fluids and heat from the Earth crust abyssal zones. Thus, at Balakhan-Sabunchi-Ramany, Lokbatan, Zykh, and Gum Island fields, in the area of mud volcanoes, temperature is 3–5 °C higher than that in alternative parts of the structure. Positive temperature anomaly within the Neft Dashlary, Pirallakhi Island, and other fields is associated with the area of large rupture dislocations that intersect the fold.

Thermal activity of structures that do not contain oil and gas deposits is essentially lower than that of the productive ones. Thermal activity of structures holding gas and gas condensate accumulations (Garadagh, Ziryam Janub, Galmaz, etc.) is much lower than that of the oil-saturated structures.

Generalization and temperature analysis testify to significant differences in geothermal conditions of separate OGFs. Below, a brief description of geothermal conditions in separate Azerbaijan OGFs is given.

The Absheron OGF. Twenty-three structures of 3 anticlinal zones were included into geothermal research. Within the region, the temperature field was found with background values at 3000- and 4000-m sections equal to 74 and 88 °C, respectively. Thermal flow values vary within broad limits, from 20 to 90 mW/m^2.

The Lower Kur OGF. Ten structures in 2 anticlinal zones have been studied. The plotted map of temperature cross sections for 3000 and 4000 m depths has background temperature of 64.5 and 76.4 °C, respectively. The region is characterized by thermal flow values of about 20–50 mW/m^2.

The Baku archipelago region. The research included 15 structures of 3 anticlinal zones. Within the archipelago, background temperature value at 3000- and 4000-m-deep sections was equal to 62.6 and 75.4 °C, respectively. Average thermal flow value for the region is 30–50 mW/m^2.

The Shamakhy-Gobustan OGF relates to the geothermally poorly studied regions. It is characterized by small amount of temperature, thermal conductivity, and, correspondingly, thermal flow measurements. The region larger part is characterized by thermal flow values within 70–90 mW/m^2 with its southeastward decrease.

The Yevlakh-Agjabedi OGF. Geothermal research included 8 structures that served as the basis for cross-sectional maps of 3000 and 4000 m depths, where background values equaled 75 and 95 °C, respectively. Thermal flow values vary within 20–50 mW/m^2.

The Ganja OGF. Eight structures were investigated, and their section background values for 3000 and 4000 m depths are 99.5 and 129 °C, respectively.

The Mil-Mughan promising OGF. The research encompassed three structures. In two Orta-Mughan wells, the

investigated depth reached 4910 m, with a depth temperature of 95 °C. At Novogolovka area, at 4910 m depth, temperature was equal to 39.8 °C. At Shorsulu area, at 4500 m depth, temperature was 89 °C.

The Nakhchivan potentially promising OGF. It is one of the poorly investigated regions. The studies were conducted at two prospect wells. At 3500 m depth, temperature was 98 °C. Thermal flow density was about 20 mW/m^2.

2.1.5 Oil- and Gas-Bearing Capacity of Azerbaijan Sedimentary Sequences

Commercial development of Azerbaijan onshore and offshore areas includes 65 oil and gas fields, where above 405 producing horizons were found, including 45 fields and 320 horizons onshore and 20 fields and 85 horizons offshore. Above 30,000 wells were drilled onshore, and 5000 wells were drilled offshore so that operating well stock preserved about 8200 and 1500 wells, respectively, with average oil yield of 0.9 and 1.4 t/day, respectively.

The largest of onshore developed fields is Balakhan-Sabunchi-Ramany one that is situated in the Absheron Peninsula central part, within the Fatmai-Bakhar tectonic belt. But this field is the mature production field. At present, the largest field is the offshore Gyuneshli-Chirag-Azeri field confined to a large mega structure within the Absheron-near-Balkhan threshold (field map).

The Mesozoic, Paleogene–Miocene, and Pliocene deposit systems are regionally oil- and gas-bearing within Azerbaijan boundaries. Oil- and gas-bearing capacity of these systems varies considerably, both as a function of paleogeographic accumulation conditions in their separate stratigraphic units and as a function of regional tectonic process directions. Study of paleotectonic and paleogeographic factors shows that organic matter accumulation and burial took place in more intensively sinked basin parts at a definite geological period.

The Aalenian and the Bajocian oil- and gas-bearing suites are prominent in the sequence of the near-Caspian-Guba OGF ***Middle Jurassic deposits***. Surface indications of oil and gas presence, associated with the Aalenian stage deposits, are noted at Afurja, Ugakh, Atachay, and Keshchay areas. In addition, moderate light oil inflows were obtained by testing sandy–aleurolite interlayers in stratigraphic test wells of Afurja area. At Keshchay area, gas flow to surface was produced by testing a sandy horizon, with initial yield of about 75,000 m^3/day and with small condensate volume.

In the ***Cretaceous deposits***, first commercial gas flow of up to 67.9 thou. m^3/day and oil of 19 m^3/day was produced from the Valanginian rocks in well 3, drilled at the crestal position of SE pericline of Tekchay anticline. In said fold area, the Valanginian deposits were also commercially oil-bearing in wells 20, 21.

In the Siazan monocline region, oil flows of 3–4 to 20–30 t/day were produced from the Upper Cretaceous deposits.

Oil and gas content of the Lower Cretaceous system within the *Shamakhy-Gobustan OGF* is associated with the Barremian, Aptian, and Albian stage deposits. Natural oil and gas indications, such as moderate outflow of thick black oil near Astrakhanka village, as well as intense gas and light oil discharge from the Barremian stage clastic rocks that was observed at Novo-Astrakhanka area, might witness the favorable conditions for oil and gas accumulation in said regions (Akhmedov 1957).

An oil pool is being developed at the Yevlakh-Agjabedi depression northeastern margin, in the Muradkhanly elevation crestal part. It is confined to the weathering crust and is represented by andesites and porphyrites.

There are specific data on oil-bearing content of the *Paleocene* deposits. For instance, at Zagly area, well 665 on the Paleocene deposit Sumgayit suite was put into operation with yield of up to 30 t/day, and well flowed at a primary rate of 70–80 t/day of clean oil. Intense oil and gas shows from the *Eocene* deposits were observed at all Siazan monocline areas. Testing of a number of prospect wells gave oil yield from 8.0 to 40 t/day. During joint operation of the Eocene and Upper Cretaceous deposits, yields of some wells rose by 5–10 t/day (Salayev et al. 1964).

Oil and gas shows were observed by drilling and testing of the Eocene deposits in Ganja region, at Dalmamedly, Gazanbulagh, Gyzylgajali, Naftalan, Sovetlyar, and Beilagan areas. At Dalmamedly area, by testing from the Eocene sequence middle part, light oil with primary yield of up to 5–7 t/day was produced. The III Gazanbulagh oil-bearing horizon is prominent at Gazanbulagh area, in the Eocene deposit upper part. Primary oil yields of individual wells of this horizon were rather high, but they rapidly dropped to 0.2–0.5 t/day. At Ter-Ter area, testing of well 153 gave well flow of up to 0.5 t/day. At Beilagan area, testing of well 22 produced oil with primary yield of up to 18 m^3/day, and well 20 produced a short-term oil and water free flow from the Eocene deposits (Alizadeh et al. 1966).

At the Yevlakh-Agjabedi trough northeastern margin, the HC pools are found in the Eocene deposits at Muradkhanly and Jafarly areas. Here, in the Eocene sequence, the Middle Eocene loamy–tuffaceous unit is the major oil-bearing facility.

At Zardab area, use of drill stem tester for well 3 gave 350–400 t/day oil yield from the Eocene deposits. The Middle Eocene deposits are also oil-bearing at Amirakh area, where use of drill stem tester on well 2 yielded commercial oil inflow (up to 20 t/day).

The Oligocene–Miocene subcomplex is widely developed within Azerbaijan oil- and gas-bearing regions and consists

of the deposits of Maykop suite, Chokrak, Kong-Karagan horizons, the Sarmatian, and Meotian stages. The *Maykop suite* deposits are noted for the highest oil-bearing capacity. The suite is commercially oil-bearing within Siazan monocline, western Absheron, southwestern Gobustan, and northeastern part of the Lesser Caucasus piedmont. In all these regions, Maykop deposits are represented by argillo-arenaceous lithofacies, and their oil-bearing capacity is in most cases associated with the Lower Maykop sandy horizons. The Upper Maykop deposits turned out to be oil-bearing at the southwestern Gobustan and western Absheron areas.

The Maykop Suite is the principal oil- and gas-bearing facility of Siazan monocline. Commercial agglomerations are mainly related to the section lower sandy part. Primary yields of some wells amounted to 30–50 t/day. The Upper Maykop sandy horizons rank much below the Lower Maykop ones.

At western Absheron area, the Upper Maykop deposits are oil-bearing at Gezdek, Garaeibat, Damlamaja, Shorbulag, etc., areas where quite thick (5–15 m) layers of sands, sandstone, and aleurolites are found in the sequence.

In southwestern Gobustan, sandy–aleurolite deposits of the Upper Maykop and Chokrak horizons are oil- and gas-bearing at Nardaran-Akhtarma, Umbaki, and Ajuveli areas, and besides said area, the Upper Maykop deposits are also oil- and gas-bearing at Sheitanud, Donguzdyk, Kaftaran, and Arzani areas, while Chokrak horizon bears oil and gas at Gyrkishlak and Cheildagh areas.

Commercial oil- and gas-bearing capacity is established for the III, IV, and V horizons in the Upper Maykop sequence, at the Umbaki anticline northeastern overthrust margin, where the III horizon, brought into development in 1951, is the most oil-saturated one. The Maykop suite III horizon is gas bearing in one of the northern margin tectonic blocks. Here, prospect well 23 showed gas spouter with primary yield of 500 thou. m^3/day with 10-mm choke.

At Eastern Ajiveli area, two prospect wells drilled at the fold northern margin, yielded by testing of the Maykop III horizon commercial oil flows of up to 15 t/day, and testing of the Chokrak horizon sandy layers gave heavy oil inflow of up to 5–7 t/day.

At Cheildagh area, commercial oil content of Maykop suite and Chokrak horizon was supported by drilling of separate wells. Commercial oil content of the Upper Maykop sandy–aleurolite horizons was revealed by drilling at Donguzdyk area, where one of the wells gave light oil inflow of up to 35 t/day.

The Maykop suite and Sarmatian stage deposits are prominent for their regional oil content in the Kur-Gabyrry interfluve and in the Ganja OGF.

In Ganja OGF, a series of minor commercial oil pools confined to Gazanbulagh, Dalmamedli, Naftalan, Ter-Ter, and Ajidere areas was found in the Maykop deposit sequence. Powerful oil and gas shows were noted by stripping of the Chokrak horizon at Duzdagh area and of the Sarmatian stage at Duzdagh and Barda areas.

At Naftalan area, prospect drilling revealed a number of oil-bearing horizons in the Maykop deposit sequence. Three horizons (I, the loamy, and II) contain remedial oil of 0.945–0.948 g/cm^3 density. Underlying, thicker sandy horizons IV, V, and VI contain commercial oil pools of 0.860–0.900 g/cm^3 density, but because of low permeability, relatively high initial well productions (40–60 t/day) within several days dropped down to 3–5 t/day.

Commercial oil flows from the Maykop suite bottom were obtained in well 21 at Zardab area and in well 28 at Shikhbagi area. Oil yield was 20 and 5 t/day of water in the first well, while the second one yielded 18 t/day of oil.

In the Talysh submountain region northeastern part, at Tumarkhanly area, two prospect well showed by drilling brief oil and gas kicks when the Chokrak horizon and Upper Maykop deposits were exposed.

The Chokrak Horizon is the second oil- and gas-bearing facility of the Oligocene–Miocene subcomplex. This horizon is being developed at Saadan area, where the first well was put into operation with 16 t/day yield. Further, the Chokrak horizon was tested at Amirkhanly area, where in some wells daily oil flow amounted to 10–15 t.

At Umbaki area, a pool of heavy oil that is run by separate wells in the fold western part is associated with the Chokrak deposits (Salayev 1961).

At Muradkhanly field, drill stem tester in well 27, drilled in fold crestal position, produced oil of up to 42 m^3/day, and well 18 gave commercial oil flow of up to 110 m^3/day produced from the Chokrak deposits.

The Karagan-Konk strata and the Sarmatian deposits within Siazan monocline were not targeted for prospecting works. These deposits were tested concurrently in a number of wells at Saadan, Siazan-Nardaran, and Zeiva areas. In many cases, minor oil flows were produced.

The Sarmatian deposits bear oil at Talabi area. Testing of well 12 at 4461 m depth gave oil flow yield of about 40 m^3/day from the Sarmatian deposits.

Surface oil and gas shows occur in the Kur-Gabyrry interfluve as fluid oil and free gas seeps, kir covers, oil-saturated sandstone and oily spots in rock fractures. Here, at Alachyg anticline northern edge, well 72/1 yielded 1.6 t/day of oil by testing the Middle Sarmatian age.

Deposits of the ***Pliocene*** oil- and gas-bearing complex are widely distributed in all depression zones of Azerbaijan. However, oil and gas content of this complex varies to a considerable extent as a function of its lithofacial composition.

Within the near-Caspian-Guba region and the Middle Kur Depression, the ***Lower Pliocene (PS)*** deposits are

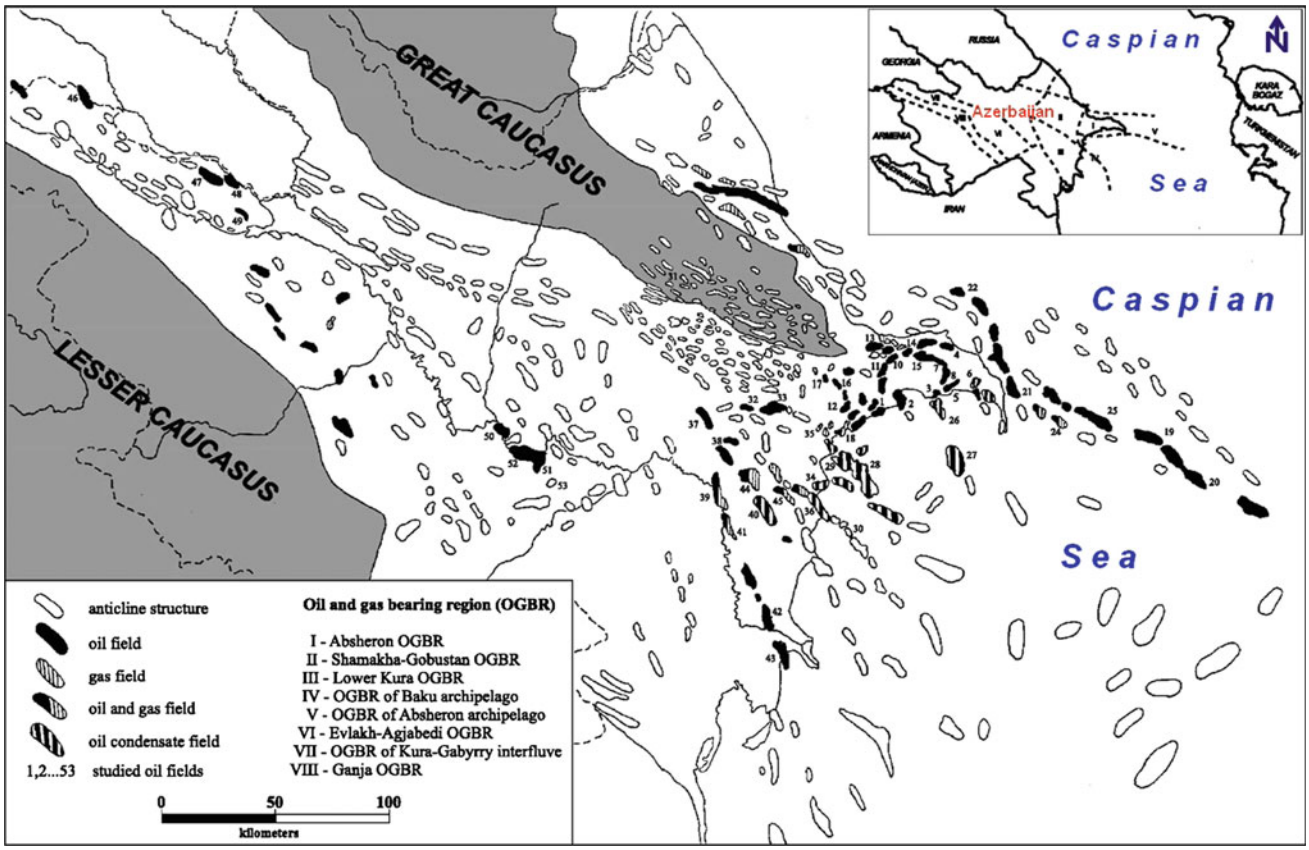

Fig. 2.17 Spacing array of oil and gas fields and potential structures in Azerbaijan

represented by coarse detrital facies and devoid of oil and gas signs. The PS principal oil- and gas-bearing facies are the Absheron and the near-Kur facies that have extensive areal development at the Absheron Peninsula, in Absheron archipelago, and in the Lower Kur Depression.

Within the Absheron oil- and gas-bearing region, oil and gas pools are non-uniformly distributed through the PS section. Maximal oil saturation of the PS section is found in the Absheron Peninsula central part (Balakhan, Surakhan, Bibi-Heybat), where the amount of productive horizons reaches 40 (Azizbekov et al. 1972, 1976; Mamedov et al. 2008).

Stratigraphically, the lower division suites, the Sabunchi suite, and the Balakhan suite upper part are the most oil- and gas-saturated suites of the Absheron Peninsula. The Balakhan suite lower horizons are mostly saturated by oil and gas at the southwestern Absheron fields (Bibi-Heybat, Lokbatan, Puta) and at marine areas (Gum Island, Bakhar, Neft Dashlary).

In the Absheron Peninsula northeastern part, at Shabandagh, and Atashkya fields, where the PS upper part is eroded, the upper division suites do not contain oil and gas pools.

Areal distribution of oil and gas pools is controlled by rock lithological composition and by structural and tectonic conditions. As clay content increases from east to west, dramatic drop in oil saturation of PS sequence takes place. Amount of gas-saturated formations increases with formation regional subsidence from north and northwest to southeast, and oil and gas pools are frequently replaced by predominantly gas condensate pools (Garadag, Zire, Janub-2, Bakhar, Shakh deniz).

Structurally and tectonically, the Absheron region oil and gas pools are confined to anticline highs that are grouped in seven large anticline belts. These anticline belts serve as oil and gas accumulation zones, and above 50 independent highs are found within their boundaries. About 30 anticline highs contain HC deposits that are being developed (Fig. 2.17).

The northern Absheron zone of oil and gas accumulation includes Khazri, Arzu, Dan Ulduzu, Garabagh, and Ashrafi large low-angle folds and a series of southwest-adjacent small anticline folds of Gilavar, Sevinj, Novkhany-deniz, and Gyanjlik. Commercial oil and gas condensate flows are found in the zone SE part at Ashrafi and Garabagh areas. The supra-Kirman sandy (SKS) and sub-Kirman (SK) suites

were productive at both areas. Prospect well 1 at Ashrafi area produced 640 thou. m^3/day of gas and 70 m^3/day of condensate from SK suite, with 20.6-mm choke. The SKS suite revealed oil and gas pool. Oil yield amounted up to 556 t/day and gas yield, to 27 thou. m^3/day.

Two prospect wells, drilled at Garabagh area, gave oil flows from SK and SKS suites as 846 and 700 thou. m^3/day, with 16-mm choke, respectively, and gas condensate yield as 24.6 and 83 m^3/day, respectively. The third well permitted to produce up to 300 t/day of gas from SKS suite, while the SK suite tops were gas-bearing ones (Jafarov et al. 2003).

The near-Absheron zone of oil and gas accumulation consists of brachyanticlinal folds: Gosha dash, Agburun-deniz, Absheron uplift, Darvin uplift, Pirallakhi Island, Gyurgan-deniz, and Janub. Oil and gas pools are found only in four latter folds. Within the Absheron area, commercial gas blowout was produced in well 4 by testing of the PS bottoms. Testing results of wells 11 and 21 in PS northeastern edge established the presence of commercial oil pool.

The Absheron-near-Balkhan zone of oil and gas saturation (the Absheron threshold subzone) represents a large stripe of anticlinal highs, also includes the Azerbaijan sector structures: Chilov Island, Palchyg Pilpilesi, Khali-Neft Dashlary, Oguz, Gyuneshli, Chirag, Azeri, and Kyapaz.

Neft Dashlary field holds a specific place among these oil and gas deposits because here all PS suites are oil- and gas-bearing. Up to 28 independent process facilities are distinguished in the most oil-saturated part of this oil field. Northwestward of Neft Dashlary, within Palchyg Pilpilesi and Chilov Island fields, commercial pools are found only in Kalin, sub-Kirmakin, and Kirmakin suites (Alizadeh et al. 1966).

Large Gyuneshli, Chirag, Azeri, and Kyapaz fields are located southeastward of the Neft Dashlary field.

Gyuneshli field is confined to a brachyanticlinal fold complicated by a series of transversal and longitudinal dislocations and by a buried mud volcano. Here, the principal oil-bearing facilities are the Balakhan suite X horizon and Pereriv ("Fasila") formation (Akperov and Kasymov 2003).

Chirag field and Gyuneshli field are confined to a brachyanticlinal fold complicated by a series of transversal and longitudinal dislocations. At this field, the Balakhan suite VI, VII, VIII, and X horizons, and Pereriv ("Fasila") formation are oil-bearing, whereas the Balakhan suite IV and V horizons in SKS and SK contain gas and condensate pools.

At Azeri field, the Balakhan suite VI and VIII horizons contain gas and condensate pools, while the suite IX and X horizons and Pereriv ("Fasila") formation contain oil pools that are being developed.

Kyapaz field is confined to a brachyanticlinal fold, and oil and gas pools were revealed in the Balakhan suite VI horizon and in Pereriv ("Fasila") formation.

The Buzovny-Zire oil and gas accumulation zone, located in the Absheron Peninsula eastern part, is found within the eastern Absheron depression. This subzone embraces Buzovny-Mashtagi, Kalin, and Zirya fields.

The largest oil and gas accumulation zone is situated in the Absheron Peninsula central part and stretches from the Absheron Peninsula northern seashore, continuing southward to the Caspian Sea. Here, Balakhan-Sabunchi-Ramany, Surakhan, Garachukhur-Zykh, Gum Island, Bakhar, ,and Shakh deniz fields are arranged. Said oil and gas condensate fields are confined to large anticlinal folds.

Within the Balakhan-Sabunchi-Ramany field, all sandy horizons, despite exposure of the PS suites, were commercially oil-bearing. The PS section revealed 28 oil-bearing horizons here: Ten of them are confined to the lower division suites and 18, to the upper division suites.

Within the Surakhan field, oil- and gas-bearing capacity scope measurably expands and here, overall amount of oil- and gas-bearing facilities becomes 56. Oil-bearing capacity scope narrows at the Garachukhur-Zykh field.

At Gum Island field, commercial oil and gas content starts from the Balakhan suite V horizon and continues to X horizon, inclusively. Pereriv ("Fasila") formation and other suites of the lower division are oil- and gas-bearing as well, to PS inclusively. Nearly all pools of the PS lower division have gas caps.

Binagady-Sulutepe-Shubany zone of oil and gas accumulation is the Absheron Peninsula most elevated tectonic zone. Here, PS deposits are eroded nearly to the Kirman suite, inclusively. Oil and gas pools are essentially confined to the SK and SKS, which thin out at the fold winged sections facing the Baku trough. Up to 9 development facilities are found in SK section within Binagady and Sulutepe fields.

The Bibi-Heybat oil field is confined to a separate brachyanticlinal fold situated southeast of Shubany anticline. Here, commercial oil and gas pools are found in all PS suites.

In Lokbatan-Kergez-Gyzyltepe-Shongar zone, PS is eroded to upper division bottoms. Oil and gas pools are found in latitudinally oriented highs of Lokbatan, Puta, Gushkhana, Shongar, and the northeast—in Kergez-Gyzyltepe and Saryncha-Gyulbakht highs (Alizadeh et al. 1966). The Garadagh high of basically latitudinal course is adjoined to this zone in Kergez-Gyzyltepe high area.

In this oil and gas accumulation area, the largest oil and gas condensate pools are confined to the VII horizon (an analog of the Absheron Peninsula Pereriv ("Fasila") formation) and to the Balakhan suite V and VI horizons. The Gara-Heybat field is situated in the Gyuzdek trough northern marginal part.

The Pliocene oil- and gas-bearing complex is also broadly developed within the Jeirankechmez depression of Shamakhy-Gobustan region that deepens and widens toward

the SCB. Basing on PS deposits, the following sedimentation zones Anart-Shikhigaya-Donguzdyk, Toragay-Kyanizadag-Sangachaldeniz, Khara-Zire Island, the Alyat Range, and Pirsaat-Sangi-Mughan-Dashly are prominent within this depression and at its marine extension.

At Anart area, up to nine sandy horizons were selected in the section exposed part, and in three of them, commercial gas production was obtained with 50–75 thou. m^3/day yields. At Shikhigaya area, by testing of wells 5, 16 and 18, gas production of 7, 50 and 40 thou. m^3/day was obtained, correspondingly. At Kaftaran, Gargabazar, and Donuzduk areas, intense oil shows were noted by drilling of stratigraphic test wells.

Utalgi-Kyanizadag-Sangachal-deniz-Khara-Zire Island zone is the most elevated and extended oil and gas accumulation subzone in Jeirankechmez zone and Baku archipelago. Crest parts of this subzone structure show 800–900 m washout in the PS section upper part. Large oil and gas fields are found here: Kyanizadag, Sangachal-deniz–Duvanny-deniz–Khara-Zire. The PS horizon VII is the most essential oil- and gas-bearing facility. At the Kyanizadagh area, oil yields of some wells amounted to 120–130 t per day. Large oil and gas pools with gas cap are under development within Sangachal-deniz, Duvanny-deniz, and Khara-Zire areas. At Khara-Zire area, large gas condensate and oil pools are being developed in the PS horizons V and VII. Separate wells of horizon V yielded 100 t of condensate and 500–800 thou. m^3/day of gas, and condensate flow from horizon VII amounted to 400–450 t and to 1.5 million m^3/day pf gas (Suleimanov and Mekhtiyev 2003).

Commercial oil and gas content of horizon VIII, the analog of the Absheron Peninsula NKP suite, was established for more plunged area of the Duvanny-deniz fold northeastern edge, where gas spouter with condensate was obtained. This horizon contains large gas condensate pools. The pools are noteworthy for their height and high coefficients of trap filling. Well initial daily yields were 100–200 t/day of oil, 500–700 thou. m^3/day of gas and up to 100–130 t/day of condensate.

Commercial oil and gas content in horizon V of the Duvanny-deniz fold northeastern edge was exposed by wells 35 and 361, where 300 t/day of oil and 0.5 million m^3/day of gas were produced, respectively. The sub-Kirmakin suite in most prospect wells is water-bearing. Positive result of up to 200 thou. m^3/day of gas was obtained for well 99.

Within the Bulla deniz fold northeastern edge, prospecting and exploratory drilling revealed the presence of gas condensate pools in the PS V, VII, and VIII horizons. Power gas (above 1.0 million m^3 per day) with condensate (up to 350 t/day) spouter was obtained in well 18 by testing of VII horizon. Initial well yields in the V horizon amounted to 200–450 thou. m^3/day of gas and 70–200 t/day of condensate and in the VII horizon, to 1.8 million m^3/day of gas with oil and condensate mixture of up to 300 t/day.

Southwest of Kyanizdagh, the Duvanny field is located, where the largest gas and condensate reserves are confined to the VII horizon.

The Alyat Range oil and gas accumulation zone is situated between the Shamakhy-Gobustan and the Lower Kur OGFs. The following anticlinal folds are confined to this oil and gas accumulation subzone: Dashmardan, Shokikhan, Durandagh-Baridash, Solakhai, Airantekyan, Goturdagh, Dashgil, and Alyat-deniz. Rather intense oil and gas shows (sometimes of commercial importance) were found by drilling and testing in a number of wells at the PS sandy layers in the Dashgil, Airantekyan, Solakhai, Goturdagh, and Dashmardan structures.

Commercial oil and gas accumulations were found in the central tectonic block and in the Dashgil fold northern edge, where the PS VII horizon produced oil yield of 75–100 t/day, and testing of the V horizon of the same area gave 25–30 t/day of oil and 100 thou. m^3/day of gas.

At Alyat-deniz area, commercial oil pools of the PS horizon VII are confined to SE of the fold periclinal part, which is separated by transversal ruptures in crestal position. Here, the horizon VII pool is under development, and yields of separate wells vary from 20 to 320 t/day.

Intense oil and gas shows, often of commercial importance, were found during drilling and testing of nearly all prospect wells of the large Solakhai structure northeastern edge. Here, four sand levels (I, II, III, and IV, according to local Solakhai marking) were distinguished from lower unexposed part of the PS sequence, so that three of them are oil-bearing, and some of this level wells yielded 5–7 t/day of oil. Multiple oil and gas shows in various Alyat range areas are associated with mud volcano gryphons and salsas.

The Lower Kur oil and gas accumulation zone is one of the prime oil- and gas-bearing regions of Azerbaijan. In the Lower Kur oil- and gas-bearing region, the PS deposits and partly the Akchagyl and Absheron stage deposits bear oil and gas. Twenty sand levels are delineated from the PS upper division section at Kyurovdagh area. Here, reference horizon XX of upper division is represented by conglomerates and is the age equivalent of the western Absheron VII horizon (by the Karadagh marking) and of the central and eastern Absheron Pereriv ("Fasila") formation.

The anticlinal zones are recognized in the Lower Kur Depression and extend further to the Baku archipelago, producing unified oil and gas accumulation zones. Specifically, such zones as Pirsaat-Hamamdagh are recognized that continues within the Baku archipelago to Dashly and Sabail structure. Here, the I Pirsaat, the II, and III sub-Pirsaat suites and the "Fasila" formation are oil- and gas-bearing. Individual wells yield up to 70 m^3/day of oil and 250 thou. m^3/day of gas.

Southeast of Pirsaat, within the Baku archipelago, prospect and exploratory drilling encompassed the Hamamdagh-deniz, Garasu, Aran-deniz, Dashly, and Sabail anticlinal folds. However, positive result for oil and gas content was obtained only in well 25, drilled in the elevated section of the Garasu fold northeastern edge, where oil free flow to surface from VII horizon amounted to 250 t/day, and gas flow was up to 300 thou. m^3/day. The VII horizon in the edge more subsided area was water-bearing.

The Kalamadyn-Mishovdag-Byuandovan zone embraces within the Baku archipelago such structures as Yanan-Tava-Atashgyakh and the Kyurovdagh-Neftchala subzone, which continues toward the Kyurdashy and Shirvan anticlinal folds within the sea boundaries.

Commercial oil and gas pools are found in its northwestern part, within the Kalamadyn, Mishovdag, and Galmaz anticlines.

At Mishovdagh structure, commercial oil and gas pools were found in the I, II, and III horizons and confined to the fold northwestern part. Commercial oil and gas flows were also obtained from horizon IV (well 37 up to 4 t/day). Well 64 of horizon VII produced up to 3 t/day of oil and well 36 of horizon XII, 2 t/day. The lowest horizon with commercial oil flow (well 62—up to 6 t/day) is horizon VIII of the PS upper division.

At Galmaz field, horizons I, II, and III contain gas pools. Commercial oil and gas content of horizon IV was found for well 15, drilled at the southwestern edge (oil yield is 20 t/day, and gas yield is 20 thou. m^3/day). Below horizon V, the PS section is clayey, but in horizons XII, XVII, and XX, separate oil- and gas-bearing sand units appear.

At Khydyrly-Byandovan potential area, the PS section has been studied to the lower division inclusively, but positive results were not obtained. The Absheron stage upper horizons produced commercial gas flows from 40 to 58 thou. m^3/day. Southeastern extension of the Kalamadyn-Byandovan anticlinal zone within the Baku archipelago displays oil and gas shows in Byandovan-deniz, Yanan-Tava-Atashgyakh, Kyurdashy, Mughan-deniz, etc., anticlinal folds, within mud volcano boundaries, but commercial oil and gas content of the PS section has not yet been determined.

At Kyursangi oil and gas field, oil and gas pools are confined to 7 sandy levels of the PS section upper part. Commercial oil flow of up to 30 t/day was obtained from well 68, horizon VIII, of the fold northeastern edge.

In the *Kyurovdagh-Neftchala subzone* of oil and gas accumulations, 20 sandy levels are localized in the PS upper division section, predominantly dissociated by clayey divisions. The largest oil pools are confined to sand level I.

Some sandy levels of the Akchagyl and Absheron stages are commercially oil- and gas-bearing in the framework of Kyurovdagh and Garabagly fields.

Southeast of Garabagly field, at the northeastern margin of large and asymmetrical Babazanan high, the PS upper part of up to 750 m thickness is washed out. Multiple natural oil and gas shows are noted in sand layers of the PS exposed part. Oil flow of 3–4 t/day yield was produced by testing of wells 3 and 5, drilled in the fold crest, while well 20 produced gas with initial daily yield of up to 20–30 thou. m^3. More powerful gas flows were obtained from sand levels of the Absheron stage middle division.

At Khilli field, the first commercial oil flow of up to 70 t/day yield was obtained from the PS horizon VIII. By testing horizons III, IV, and V, some wells produced from 3 to 10 t/day of oil.

At Neftchala field, oil pools were found in horizons I–VIII of the PS upper division. Unlike Kyurovdagh and Garabagly fields, oil pools are found at both fold edges. Here, oil commercial pools are found in the PS horizons I, II, and III, and in the middle Absheron sand levels that are confined to separated tectonic blocks.

Classification of pools and fields is extremely important for determination of formation conditions, assessment of oil- and gas-bearing capacity in individual regional and districts, and the selection of rational HC exploration, survey, and development methods.

Such well-known geologists like M.V. Abramovich, B.K. Babazade, F.M. Bagirzadeh, A.A. Bakirov, I.O. Brod, I.I. Potapov, M.F. Mirchink, A.A.Trofimuk, N. Yu. Uspenskaya, and others dealt with the classification of oil and gas pools.

They based their pool classifications on a number of morphological, structural, and genetic criteria.

The most acceptable classification for Azerbaijan oil and gas pools based on the analysis and critical assessment of existing classifications and on genetic principle has been developed by Babazadeh (1964, 2005).

HC pools found in the SCB are confined to the traps of two basic types: tectonically screened traps (Fig. 2.18) and stratigraphically/lithologically screened traps (Fig. 2.19). HC fields are as a rule related to the combined type (Fig. 2.20).

A rare type of oil field, confined to the Upper Cretaceous age volcanogenic elevation, buried in the Miocene and Pliocene–Anthropogenic deposits was discovered at Muradkhanly area (Fig. 2.21).

2.1.6 Assessment of Resources for Various Azerbaijan Stratigraphic Complexes

Peculiarities of spatial distribution of ultimate potential resources (UPR) of HC crude in the region are essentially determined by differences in oil and gas generation potential

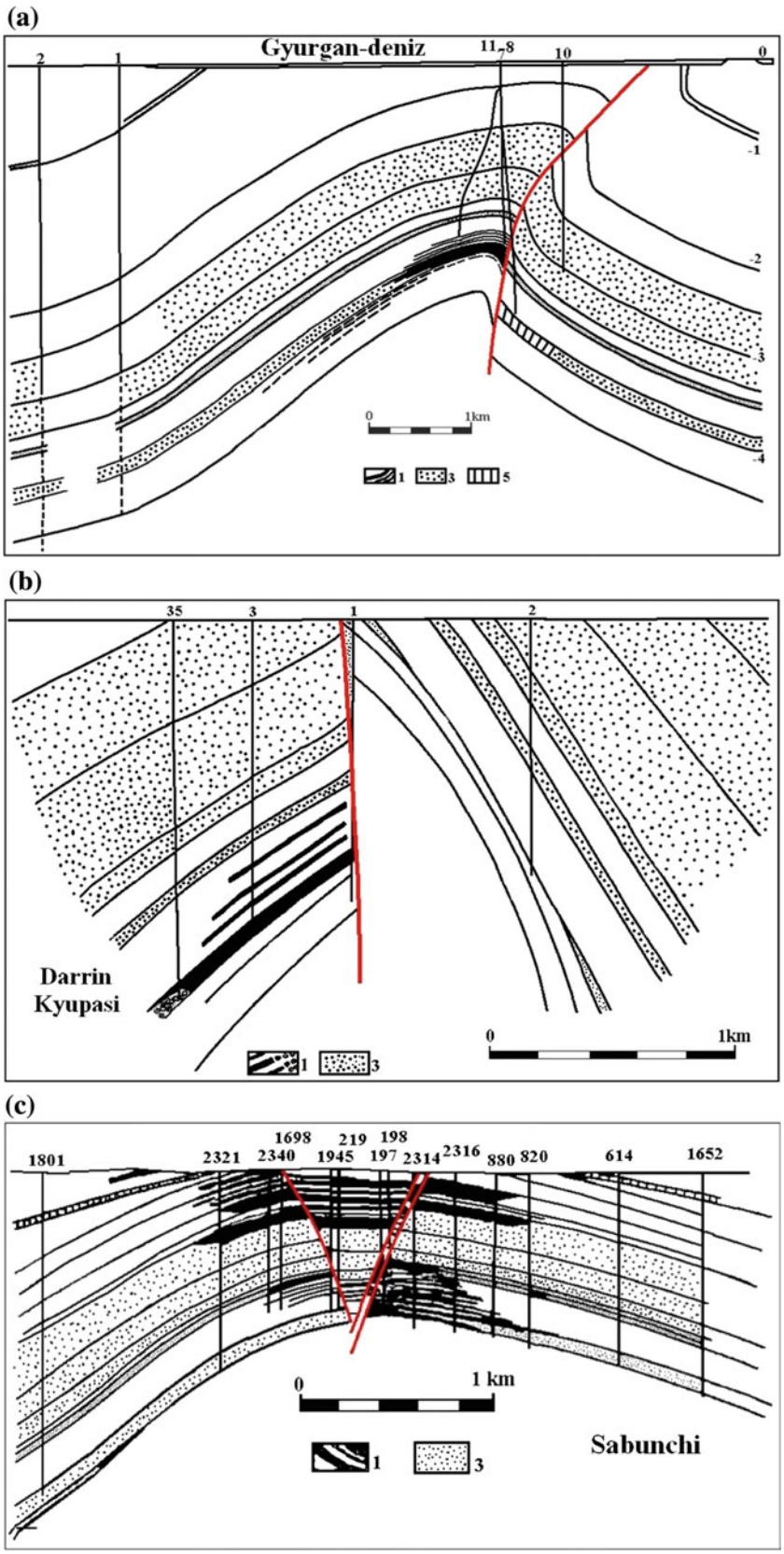

Fig. 2.18 Pool/field types in SCB: tectonically screened type. **a** Gyurdan-deniz, **b** Darrin Kyupasi, **c** Sabunchi

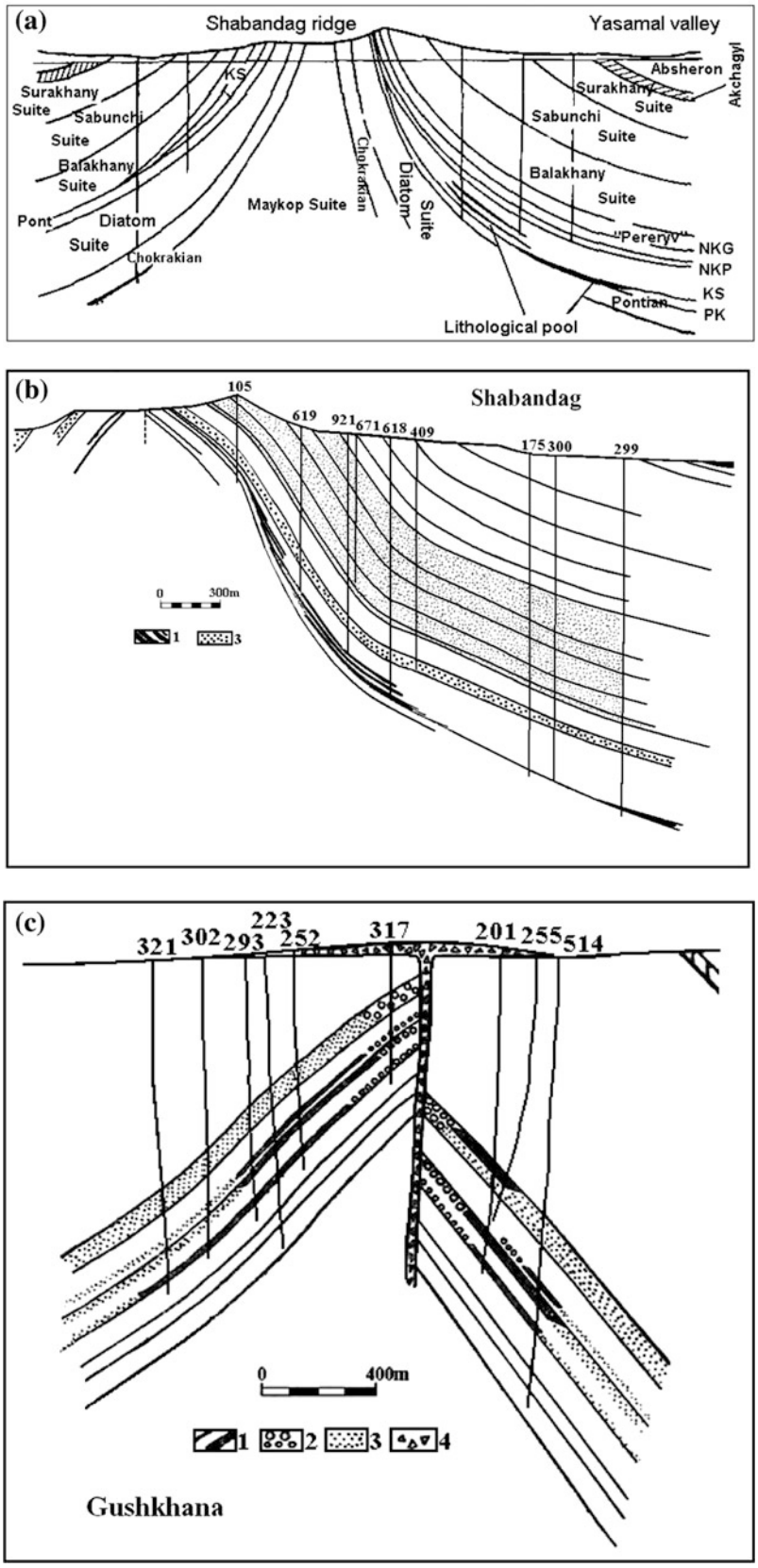

Fig. 2.19 Pool/field types in SCB: stratigraphically/lithologically screened type. **a** Yasamal Valley, **b** Shabandagh, **c** Gushkhana

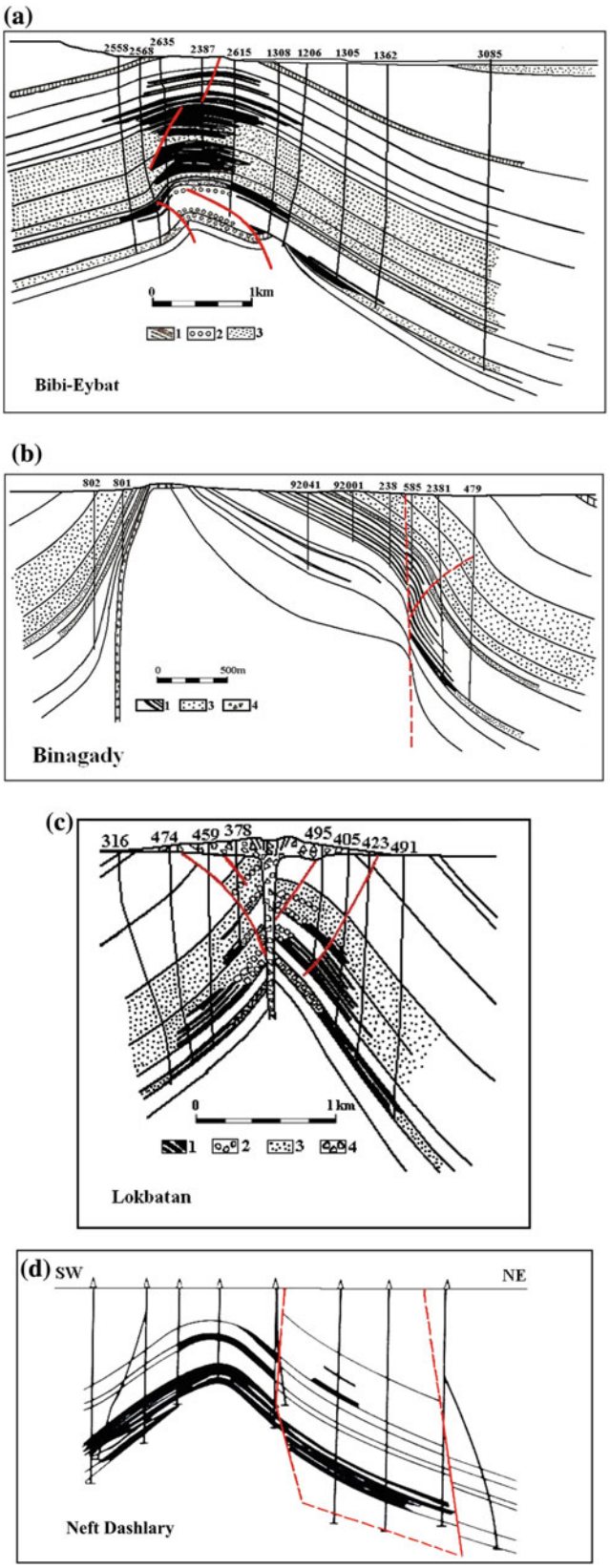

Fig. 2.20 Field types in SCB: combined type. **a** Bibi-Heybat, **b** Binagady, **c** Lokbatan, **d** Neft Dashlary

of the source rocks and in trap/reservoir parameters that control oil and gas accumulation scale.

The applied technique of assessment of oil and gas accumulation scale, or, in other words, assessment of HC resources, is based on the determination of relationship between basin geodynamic type, sedimentation rate, and resource density in sedimentary basins.

Density of HC resources at calculated areas was established, basing on the implementation of reference values for reasonably assured HC resources at a number of fields that are used by calculations with correcting analogy factors, taking into account difference in parameters that control oil and gas content at reference and calculated areas.

Hydrocarbon resources were estimated together with GEON Center (Russia) (D.A. Fedorov, L.E. Levin et al.) from the Jurassic, Cretaceous–Eocene, Oligocene–Miocene, and Pliocene deposits, using both internal (Pliocene, Oligocene-Miocene, Eocene, partly Cretaceous) and external references (Jurassic, partly Cretaceous ones).

The Jurassic deposits

Commercial oil resources were not found in the Jurassic deposits; here, the wells drilled demonstrated only oil and essentially gas shows of various intensity in the near-Caspian-Guba region. By virtue of the South Mangyshlak area with 29.5 thou. t/km^2 density of reference fuel (RF), these commercial reserves were taken as a reference area.

UPR calculations showed that the HC total reserves in the Azerbaijan sector of the Caspian Sea and on the Azerbaijan dryland consist of 0.41 billion tons of reference fuel (oil + gas + gas condensate). These resources have been estimated for a total potential area of 38.1 thou. km^2 (Fig. 2.22).

More than 75 % of HC resources in the Caspian region Jurassic system are found in the SCB, while 25 % of them fall on the Middle Caucasus (the near-Caspian-Guba region with adjacent Caspian marine area). The resources of 10 thou. t/km^2 density occupy the largest area (Fig. 2.22).

The Cretaceous and Eocene deposits

The Cretaceous and Eocene deposits of Azerbaijan contain minor oil pools at the Siazan monocline fields, in the Yevlakh-Agjabedi trough (Muradkhanly, Jafarly), and in the Kur-Gabyrry interfluve (Tarsdallyar). The Cretaceous–Eocene overall potential area on dryland and in the Caspian Sea of Azerbaijan is 74.5 thou. km^2, so that 30.3 relate to marine area and 44.2 thou. km^2 - to the dryland.

To assess the resources, several reference sites were selected in the Middle Kur Depression (2 sites) and in the near-Caspian-Guba region (1 site), with a density of proven

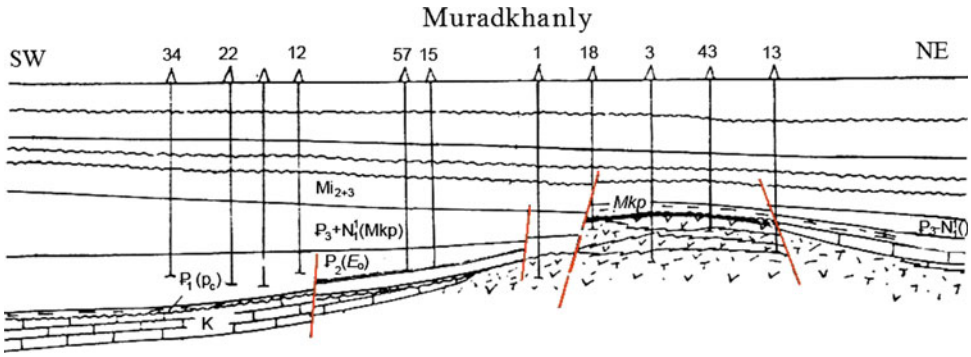

Fig. 2.21 Muradkhanly field. Oil pools are confined to weathering crust of the Upper Cretaceous volcanogenic rocks, and the Middle Eocene deposits are lithologically and tectonically screened at the fold SW edge

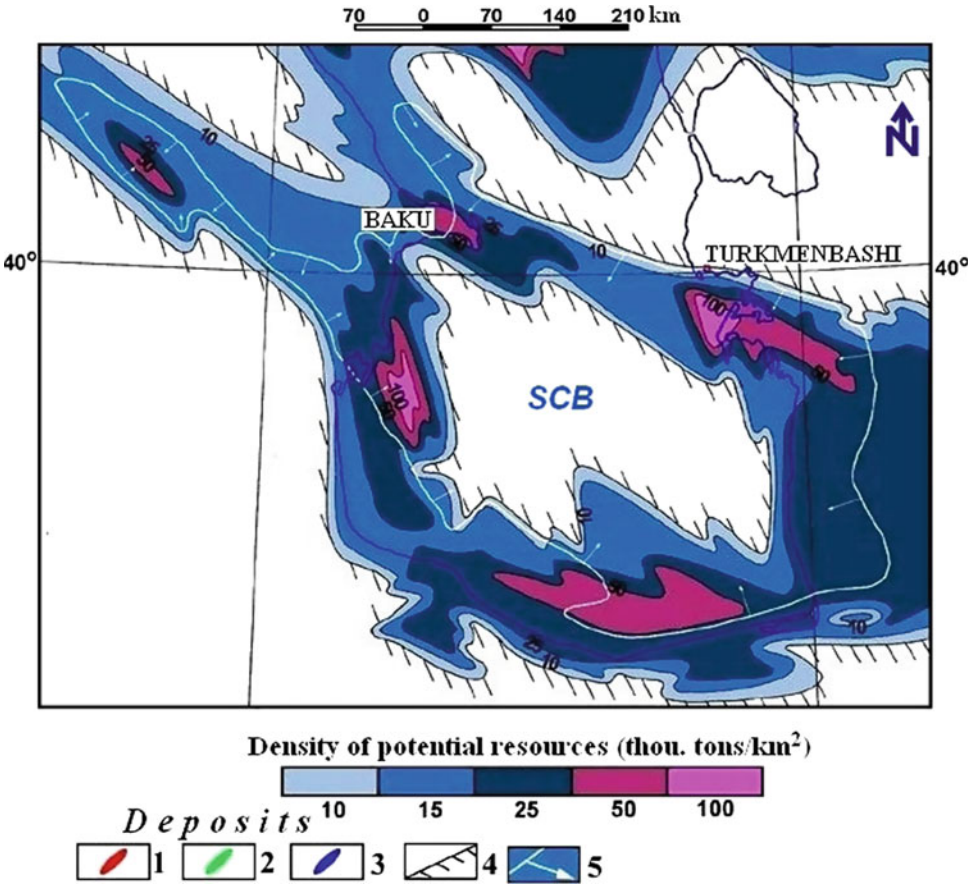

Fig. 2.22 Distribution map of potential hydrocarbon resources in the Jurassic deposits (Guliyev et al. 2003). *1* Oil; *2* gas; *3* oil–gas and gas condensate; *4* regions that are not HC prospecting promising; *5* outline of the region with deposit occurrence roof at below 7 km depth

reserves for sum of hydrocarbons equal to 11–50 thou. t/km^2.

Overall sum of estimated ultimate potential resources for the Azerbaijan Cretaceous–Eocene deposits is 2.15 billion tons of RF, where 1.28 billion tons relate to dryland and 0.87 billion tons of RF - to the marine shelf (Fig. 2.23). The South Caspian resources are estimated as 1.44 billion tons of RF.

The Oligocene–Miocene deposits

Oil and gas content of these Azerbaijan deposits has been proved for a number of regions (near-Caspian-Guba, Shamakhy-Gobustan, Ganja, Muradkhanly, etc.). But oil pools and their reserves are poor, correspondingly.

Estimated sum of Azerbaijan HC is 3.54 billion tons. It is the largest among the resources of the Caspian region

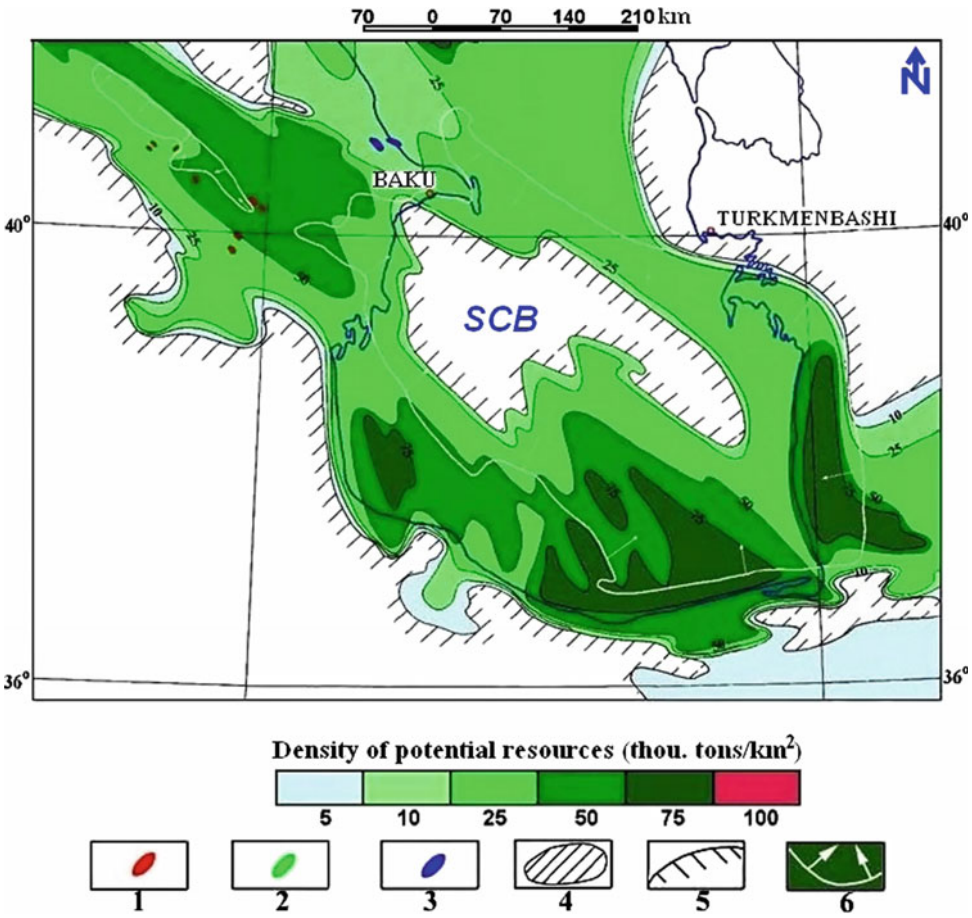

Fig. 2.23 Distribution map of potential hydrocarbon resources in the Cretaceous–Eocene deposits. *1* Oil; *2* gas; *3* oil–gas and gas condensate; *4* internal regions of partial Cretaceous–Eocene sediment denudation; *5* regions that are not HC prospecting promising; *6* outline of the region with deposit occurrence roof at below 7 km depth (Guliyev et al. 2003)

countries (nearly 50 % of the Oligocene–Miocene resources for the region). Most of the HC resources (85 %–3.05 billion tons) resides in the South Caspian Sea, where they are subdivided nearly equally between the offshore and the onshore parts (Fig. 2.24).

All in all, the Oligocene–Miocene resources of Azerbaijan marine zone, equaling 1.99 billion tons, constitute more than 56 % of all resources of this stratigraphic system.

Above half (55 %) of the Azerbaijan Oligocene–Miocene promising onshore and offshore areas is characterized by HC resources density of 20 thou. t/km^2 (see Fig. 2.24).

The Pliocene deposits

Overwhelming majority of Azerbaijan oil and gas fields is confined to the Pliocene deposits. Meanwhile, potential discovery of new HC accumulations is nowhere near exhausted, particularly in Azerbaijan offshore part, including the Caspian Sea deep section.

Reference sites have been chosen in Absheron and Lower Kur regions and at the Baku archipelago. Their density of commercial reserves varies from 25 (Jeirankechmez depression) to 910 thou. t/km^2 (Absheron), averaged value of HC density being 470 thou. t/km^2.

The Pliocene deposits of the Caspian Sea Azerbaijan section contain nearly 2.5-fold more (15.2 billion tons) of HC than those of the dryland (5.8 billion tons) (Fig. 2.25).

Cumulative review of hydrocarbon UPR distribution in stratigraphic systems of Azerbaijan dryland and Azerbaijan sector of the Caspian Sea is given in Table 2.19.

As seen, basic volume of oil and gas resources is concentrated in the Pliocene complex, i.e., 21 billion tons of RF, or nearly 78 % of the entire sum of hydrocarbons assessed for Azerbaijan as 27 billion tons of RF. In this, two-thirds of

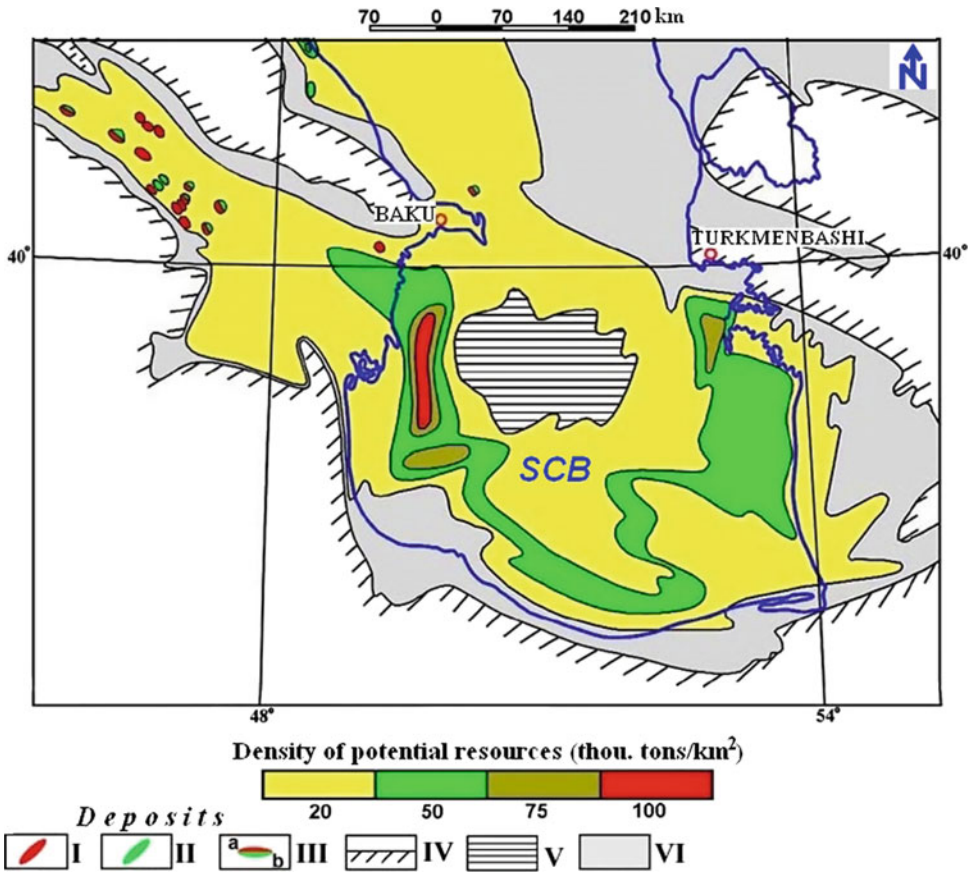

Fig. 2.24 Distribution map of potential hydrocarbon resources in the Oligocene–Miocene deposits. *I* Oil; *II* gas; *III* elevations with established intense flow of: *a* oil, *b* gas; *IV* outline of the Oligocene–Miocene system distribution; *V* system occurrence region at below 9 km depth. Density of potential resources has not been determined; *VI* region of low-thickness sediments, not HC prospecting promising (Guliyev et al. 2003)

these republican resources fall on the Caspian shelf (18.25 billion tons of RF).

2.1.7 Development Outlook of Oil and Gas Extraction in Azerbaijan

Azerbaijan is one of the oldest oil and gas recovery regions in the world, where commercial development of oil fields started already in the second half of the nineteenth century.

At present, 71 oil and gas fields are discovered on dryland and in the adjacent offshore Caspian Sea, and 54 of them are in operation. Azerbaijan depths have, so far, produced about 1 billion, 400 million tons of oil with condensate and about 500 billion m^3 of gas. At the same time, according to the Azerbaijan specialists' estimates, only remaining oil in place for operating fields amounts to above 2.4 billion tons, and the issue of oil and gas extraction is extremely pressing and challenging for the Republic (Aliyev and Bagirzadeh 1988; Abasov et al. 1999; Yusufzade 2000). The issue importance is also determined by the fact that oil sector of national economy is one of the principal donors ensuring currency supply to budget, and its development determines Azerbaijan economic well-being in no small measure.

The issue of further development of oil and gas extraction in Azerbaijan (mainly in the SCB) can be conditionally subdivided into two constituents: **engineering and geological**.

Engineering constituent includes advancement of development techniques and systems for both new and newly introduced fields.

For pools under development, the problem consists in advancement of techniques and systems for well development and operation, in application of potential and feasible novel technologies of oil and gas extraction aimed at efficiency enhancement for their redevelopment, as well as in drilling of horizontal and multilateral wells; application of productivity gain techniques in wells and enhanced oil recovery; recovery of operating well stock; and joint operation of productive facilities and some others.

The challenge for newly introduced fields is preparation and implementation of their development projects based on state-of-the-art achievements of oil and gas extraction theory and practice.

Geological constituent of the problem is mainly related to potential enhancement of commercial oil reserves that can be done at the expense of exploration and discovery of new oil fields and additional reservoir exploration of the already

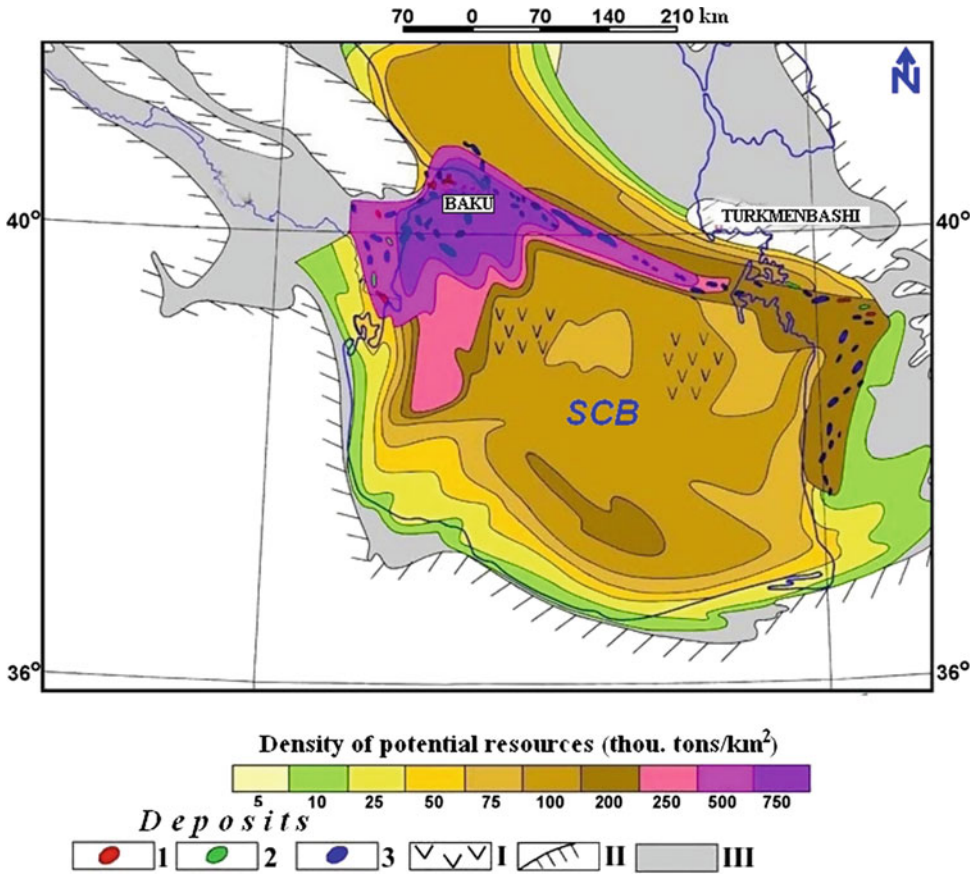

Fig. 2.25 Distribution map of potential hydrocarbon resources in the Pliocene–Quaternary deposits. *1* Oil; 2 gas; *3* oil–gas and gas condensate. *I* Regions of intense gas hydrate generation, hypothetical; *II* distribution outlines for the Pliocene–Quaternary deposits; *III* regions of low-thickness sediments, not HC prospecting promising (Guliyev et al. 2003)

Table 2.19 Ultimate potential geological resources (UPR) of Azerbaijan Meso-Cenozoic deposits (in billion tons of RF)

Geological age	Onshore	Offshore	Onshore + offshore
Pliocene	5.8	15.2	21.0
Miocene–Oligocene	1.5	2.0	3.5
Eocene–Cretaceous	1.3	0.9	2.2
Jurassic	0.25	0.15	0.4
Total sum	8.85	18.25	27.1

developed fields, i.e., this constituent is also subdivided into two groups: *long-run developed fields and novel regions, areas, and structures*.

The challenges for long-run developed fields are *detection of missed reservoirs and layers; search for satellite reservoirs; and exploration of new stratigraphic pays.*

Solution of the problem related to *detection of missed reservoirs and layers* is based on analysis and re-interpretation of the bulk of geological and geophysical materials intended to outline facilities and layers with hydrocarbon saturation that have not been developed in due time, either because of their intricacy or of some engineering reasons. Such cases can be met at Absheron fields.

Another challenge, whose solution will result in oil and gas extraction enhancement at old areas, is *search and exploration of satellite reservoirs*.

By oil and gas migration to the basic trap, they can get into stratigraphically, lithologically, and tectonically screened traps in peripheral sectors. These pools can have no common reservoir limits with principal pool and thus be omitted during prospecting and exploration. Therefore, detection and operation of these reservoirs is a reserve for production gain at old fields (Abasov et al. 1999).

Here, we should also assign the *search for hydrocarbon reservoirs at shallow depths,* including HC gas (essentially methane) accumulations of biochemical genesis in the SCB Quaternary–Upper Pliocene deposits of extreme thickness.

High gas saturation of the SCB surface deposits was noted by drilling of multiple wells and from mud logging data.

Another very important stage in enhancing the resources base of the republic oil and gas complex is search for hydrocarbons *at new stratigraphic pays*.

Azerbaijan oil and gas fields are mainly confined to the terrigenic Lower Pliocene stratigraphic complex, the "productive series" (PS). Despite large thickness of sedimentary filling and presence of good oil and gas parent rocks (source rocks), main hydrocarbon storage is focused in narrow stratigraphic range. Geological explanation of this phenomenon is based on the PS unique parameters: wonderful, stable areal, sandy (predominantly quartz) reservoirs; thick clay cap rocks with good insulating properties; pronounced brachyanticlinal folds with vertical migration channels (fractures, mud volcanoes); and high quality of source rocks (the Miocene–Paleocene); coincidence of fold formation time and migration phases (the Late Pliocene–Quaternary period).

At the same time, *the Paleogene–Miocene deposits* are the high-priority target of prospecting and exploration in the SCB. Their regional oil- and gas-bearing capacity triggers the necessity of development of new techniques for their prospecting and operation.

The Paleogene–Miocene deposits are the principal source rocks in the SCB Cenozoic sequence. At the same time, their regional commercial oil and gas content was defined.

However, despite reservoir discovery and development, potential of the Paleogene–Miocene deposits has been realized not to a full measure, which is essentially connected to limited porosity and permeability modalities and to the intricate structure of natural reservoirs for these sediments. Universal clay content (up to 90 %) of the Paleogene–Miocene deposits shows that generation conditions for large accumulations are very limited here, and for this reason, the bulk of HC is dispersed as small clusters.

Geophysical research and drilling results give grounds to assume that alternative type of reservoirs will serve as oil and gas receptacle in the Paleogene–Miocene deposits. It might be possible that HCs will be localized in the crushing, decompression, and fracturing zones. The traps of salt dome, tectonically screened, stratigraphic, and lithological types are also of interest. Potential production of shale oil might be related to these sediments.

Search for such kind of reservoirs demands much broader scope of modern geophysical and geochemical methods, specifically three-dimensional seismics and its modifications, as well as more detailed data processing and interpretation for these investigation techniques.

The *Mesozoic deposits* are still other search-prospective deposits. Methodical prospecting and exploration efforts for Mesozoic oil search in Azerbaijan were conducted within the recent 50–55 years. During this period, about 300 wells of overall meterage of nearly 950,000 m have been drilled for studying the Mesozoic deposits. Despite such a large drilling scope of prospecting and exploration wells, commercial oil and gas reservoirs were found only within the Siazan monocline (the near-Caspian-Guba region) and at Muradkhanly and Zardab areas (Middle Kur Depression). One of the reasons of low efficiency of geological prospecting survey is insufficient knowledge of the Mesozoic deposit structure.

Despite low efficiency of conducted research, perspective oil- and gas-bearing capacity and potential capacities of the Azerbaijan Mesozoic deposits are estimated rather high. It is witnessed by prolific oil and gas seeps to the surface and by oil and gas shows discovered by well drilling and testing. The mentioned oil and gas shows are associated both with the Jurassic and with the Cretaceous deposits.

The Mesozoic deposits are promising mainly in the near-Caspian-Guba, in the Shamakhy-Gobustan regions, and in the Middle Kur Depression.

The second group that can be denoted as "***novel areas and structures***" is subdivided into two groups of facilities, *the traditional and the non-traditional* ones.

We perceive structural anticlinal type traps, to which overwhelming majority of Azerbaijan-revealed HC reservoirs is related and which contribute to be the principal oil and gas exploration and prospect targets as *traditional* exploration targets.

The *non-traditional* traps are another group of structures. Among these, we classify the non-structural traps related to lithological thinning out and stratigraphic unconformity zones, the areas of PS regional thinning out, of unconformable overlapping of stratigraphic intervals, where accumulation of commercial-scale HC reserves is possible. *Riff massifs*, whose presence is predicted within the Middle Caspian Depression, are also classified as non-traditional.

The *zone of regional thrusts* is another target of exploration interest. Within the Southeastern Caucasus, a number of large regional nappes (mass overthrusts) are found. Established commercial HC reservoirs are related to some of them. Among them is the Siazan thrust with same-name field situated along it and confined to the underthrust Cenozoic complex and a number of oil- and gas-bearing areas (Amirkhanly, Chinarlar, and others).

Search for the reservoirs of indicated type demands, first of all, novel technologies of seismic survey.

The SCB was for a long time considered as predominantly oil-producing province. However, some objective facts such as OM type in HC-generating complexes, values of oil and gas factors, scope of gas outbursts from mud volcanoes, presence of large gas condensate fields, high quantity of HC gases dissolved in formation water, and, finally, exploration and prospecting results testify to high gas

saturation in the SCB depths and, respectively, to high search potentials for large gas reservoirs at deeper depths.

The PS structure located in the SCB central deeply subsided part is of primary importance in the search for gas condensate reservoirs. Here, geophysical methods permitted to find 15 large structures within borders of which discovery of gas condensate reservoirs with high gas condensate factors and possible oil rims of various sizes is suggested. Gas resources in these structures are assessed as tens of trillions m^3.

Implementation of all above-mentioned tasks is directly associated with exploration and prospecting efficiency. Their success is composed of such constituents as the sedimentary basin development concepts, HC genesis and formation of their pools, levels of geophysical research and quality of the result interpretations, and engineering level of well drilling.

The problem of contemporary oil and gas generation and sustainability of hydrocarbon resources is an important and warranting further investigation topic.

Wide applicability of *geochemical and hydrochemical techniques* can promote further search efficiency. It is in geochemical and hydrochemical parameters that the processes of chemical transformation of sedimentary rock substance and associated mass transfer and phase transitions find the most contrasting reflection.

It is important to conclude that choice of prospecting and exploration tendencies should be based not only on geological attractiveness of this or that facility but also on economic feasibility as well.

Economic analysis of the choice of prospecting and exploration tendencies is an important element of the entire geological survey process, and it should be based on the country's economic strategy.

2.2 Hard Economic Minerals

In Azerbaijan occur not only richest hydrocarbon deposits, but also most part of known hard economic minerals (e.g., Azizbekov et al. 1972; Atlas 2000; Ismailzadeh et al. 2005). We will consider here only main types of hard economic minerals (without building, optical, semi-precious, and ornamental stones, chemical raw materials, salt, and some other minerals).

2.2.1 Metallic Minerals

The deposits and occurrences of iron, chromite, and manganese ore are known to exist on the territory of Azerbaijan; however, the only iron ore deposits contain proved mineable reserves (Kashkay 1947; Mustafabeyli et al. 1964; Mustafayev et al. 1989). The titanium occurrences have been found in magnetite-bearing sandstone.

2.2.1.1 Iron

Iron ore formations play a substantial role in the metallogeny of Azerbaijan. Genetically, deposits of iron ore have been subdivided into segregation–magmatic, contact–metasomatic (magnetite skarn mineralization), hydrothermal–metasomatic (hematite mineralization), and sedimentary genetic types. The contact–metasomatic and hydrothermal–metasomatic types are the most prospective types of mineralization.

The proved mineable reserves of iron ore are concentrated within the Dashkesan ore region of the Lok-Garabagh (Somkhit-Agdam) metallogenic belt. The Dashkesan group of iron ore deposits is located in the Dashkesan region extending for 40 km to the southwest of Ganja city. The motor highway and railway link the Dashkesan, South Dashkesan, Damir deposits, and series of small deposits and occurrences close to Dardara village and on the slopes of the Ponakh-Chermez Mt. The Dashkesan deposit has been known from times immemorial. However, up to 1917, iron ore has been mined by primitive methods and geological studies were sporadic.

The mineable reserves of the Dashkesan deposit were estimated for the first time in 1933 and recalculated in 1954. The additional mineral exploration of the deposit from 1954 to 1966 has resulted in a discovery of the South Dashkesan iron ore deposit. At the beginning of the 1970s, exploration of the northern area of the Dashkesan deposit was conducted. Mineable reserves of iron ore have been approved by the State Commission on Reserves of Economic Minerals of the former USSR. Total reserves of iron ore of all categories were estimated at 278 million tons. The industrial exploitation of the Dashkesan deposit was initiated in 1954. The Azerbaijanian ore mining and processing enterprise was established. The iron ore deposits of the Dashkesan group have served as the source of raw materials for the metallurgical industry of the Transcaucasus. Iron concentrate was supplied until 1991 to the Rustavi Metallurgical Combine in Georgia. The proved mineable reserves of the Dashkesan group of iron ore deposits accounted for 234 million tons providing 90 years of life cycle of the mine based on annual mining capacity.

2.2.1.2 Magnetite Skarns

The Dashkesan group of iron ore deposits is confined to the Dashkesan syncline, located in the central axial part of the Dashkesan synclinorium, with pronounced intensive volcanic activity in the Bathonian and Kimmeridgian. The transition from the syncline to adjacent anticlines is fixed mainly by bends of beds and outcrops of the Upper Bajocian deposits represented by quartz porphyry and their tuffs with interbeds of tuff–sandstone. The deposits of the Bathonian stage from 450 to 800 m thick are composed of rocks of tuffogenous and tuffogenous–effusive formations.

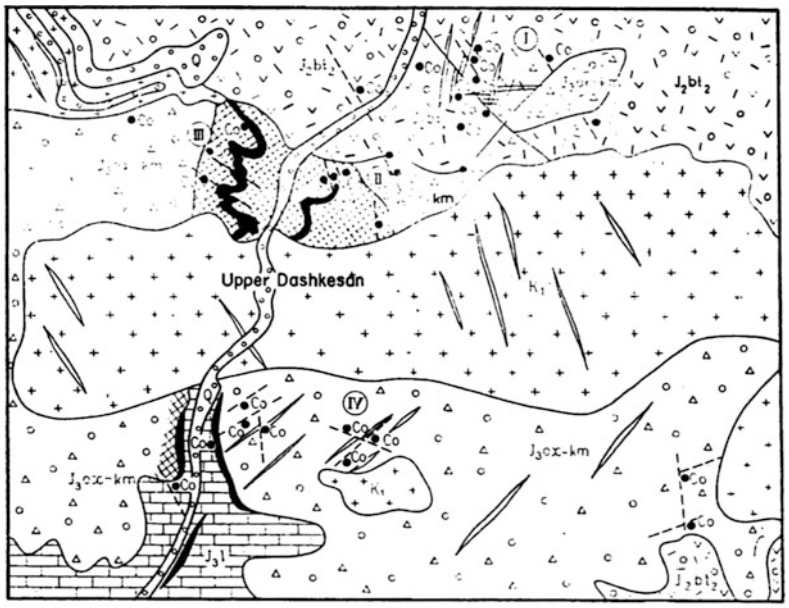

Quaternary fluvial deposits

Lower Cretaceous intrusive rocks (K_1)

Vein rocks of basic composition (K_1)

Marbled limestones of Lusitan age (J_3Lz)

Tuffs, lime tuffs, tuff-sandstones, pebbles, siltstones of Oxford-Kimmerian age ($J_3oxf + km$)

Tuffs, tuff-breccia, tuff-pebbles and tuff-sandstones alternating by separate flows of andesite and andesite-dacite porphyrites of the Upper Bathian age (J_2bt)

Hornfels

Cobalt-bearing tectonic zones

Scarn-iron fields

Occurrences of cobalt mineralization; I-northern cobalt deposits, II-north-eastern iron-cobalt deposits; III-north-western cobalt-bearing iron ore field; IV-southern iron-cobalt deposit

Fig. 2.26 Geological map of the central area of the Dashkesan ore district

The Upper Jurassic formations are represented by a thick series of volcanogenic and sedimentary rocks of the Callovian and Kimmeridgian stages. Tectonically, the ore region is confined to the jointing zone of the Murovdagh and Shamkir anticlinoriums of the general Caucasian direction and the Shamkir and Pantdagh cross-Caucasian uplifts. Combination of the two folded constructions forms the gentle Dashkesan synclinorium hosting various mineralization.

Two systems of the northwestern and northeastern faults complicated the structure of the ore region and served as the channels of intrusive magmatism. The Jurassic sedimentary formation was intruded by the polyphase and polyfacial Dashkesan intrusive massif confined to the abyssal fault along the axial part of the Dashkesan syncline. The deposits and occurrences of iron ore, cobalt, sulfide–arsenide, sulfides, alunite, pyrophyllite, kaolinite, and other mineralization of the region are genetically and spatially associated with this intrusive massif. Four phases of intrusion of magmatic rocks were delineated. The first phase is represented by gabbro, gabbro–diorites, syenite–diorites, and other basic magmatic rocks of neck and stock shapes. The most widespread rocks of the second phase outcrop on the area of more than 25 km^2 and are represented by granodiorites, adamellites, and banatites. Aplites and alaskites of the third phase have a limited distribution. The fourth phase of the intrusion is represented by numerous extended dykes of diabase porphyries and diabase. Cobalt mineralization of the ore region is paragenetically associated with these dykes. The iron ore mineralization is also associated by some geoscientists with these dykes. The intrusion of magmatic

rocks was accompanied by contact–thermal metamorphism of volcanogenic–sedimentary rocks. Metamorphic rocks are represented by hornfels, metasomatites, and marbles.

The rocks of hornfels facies are represented by pyroxene–scapolite, albite–pyroxene–scapolite, pyroxene–plagioclase, amphibole–pyroxene–plagioclase, biotite–pyroxene–plagioclase, and biotite feldspar varieties developed both above and under iron ore deposits. The thickness of hornfels and metasomatites varies from a range of 20–30 to 50 m. They are developed on volcanogenic rocks in contact zones of gabbroids and quartz diorites.

Marbles and marbled limestone have been formed by thermal and contact metamorphism of limestone. According to their chemical and physical properties, they meet the requirements of ornamental stones and flux limestone. The new Dashkesan deposit of white marble is being quarried now, and the Khoshbulag deposit of flux limestones with reserves of more than 57 million tons has been explored near the Dashkesan iron ore deposits.

Magnetite skarn deposits of the Dashkesan group are concentrated in the northern and southern zones of exocontacts of intrusive massifs. The massifs of latitudinal direction are spatially confined to the abyssal fault passing the axial part of the Dashkesan syncline. The Dashkesan and South Dashkesan deposits of submeridional direction are separated by the Goshgarchay River into the western and eastern parts (Fig. 2.26).

The Damir iron ore deposit is located southeast of the South Dashkesan gabbroid massif of submeridional direction. According to lithofacial analysis, the magnetite skarn mineralization is hosted by the rocks of calcareous series of the top sections of the Oxfordian–Lower Kimmeridgian age. The mineralization is localized in the nearshore lithofacies, where the volume of limestones varies from 0 to 30 %.

The character of localization of magnetite skarn mineralization is variable. In the northwestern area of the Dashkesan deposit, magnetite skarn mineralization overlies the marbled limestones. Its thickness gradually increases reaching 60 m by simultaneous reduction of the thickness of limestones. In the northeastern area, the mineralization occurs between hornfels and keratinized tuffites of the Callovian–Oxfordian series and volcanogenic series of the Kimmeridgian age. Similar types of occurrence were observed within the Damir iron ore deposit.

In general, magnetite skarn mineralization of the Dashkesan group of deposits is represented by 8–10 monoclinal stratified beds concordant by strike and dipping with host rocks. The maximum distance of skarns from the contours of the main intrusive massif is 2.5 km. The length of magnetite skarn deposits varies from 1900 to 4000 m in separate areas. The width of the deposit normally corresponds to the length, and in plan, the deposits have an isometric shape. The thickness of deposits varies from 4 to 40 m reaching a range from 100 to 200 m. Magnetite skarn deposits are characterized by a complicated integral structure due to a wide range of magnetite content from 0 to 90 % and a great variety of skarn types.

The stratified and lens-shaped deposits of economic value of up to 60 m thick extend from 100 to 2000 m. Massive deposits are subdivided into massive magnetite ores containing up to 90 % of magnetite and sulfide–magnetite ores containing up to 20 % of sulfide minerals. The content of iron ore in massive magnetite ores varies from 45 to 60 %. The texture of the ore is: (1) massive, (2) slaggy, and (3) porous. The sulfide minerals of disseminated texture and irregular shapes in the northwestern area of the deposit contain 50 % of chalcopyrite, 40 % of pyrite, 5 % of chalcosine, as well as rare bornite, sphalerite, and arsenopyrite. The sulfide ores of the northeastern part of the deposit contain from 70 to 95 % pyrite, up to 15 % chalcopyrite, 5 to 7 % arsenopyrite, and up to 5 % galenite, rare sphalerite, and bornite.

The massive magnetite ores of the South Dashkesan deposit contain up to 12 % of sulfides being represented by a range of 70–80 % of pyrite, up to 10 % of chalcopyrite, cobaltine, rare pyrrhotite arsenopyrite, glaucodote, bornite, sphalerite, and galenite. Sulfide–magnetite ore contains arsenic, vanadium, titanium, cobalt, zinc, manganese, tin, magnesium, copper, lead, molybdenum, nickel, silver, gallium, cadmium, bismuth, indium, and zirconium.

The deposits of the disseminated type also form beds and lenses and gradually transit into massive magnetite ores. The ores contain from 40 to 70 % magnetite, up to 25 % garnet, 5 up to 30 % calcite, and up to 1 % quartz, epidote, rare hematite, chlorite, dashkesanite, and actinolite. Manganese, gallium, tin, molybdenum, vanadium, titanium, copper, zinc, cobalt, and nickel are assayed in sulfide part of disseminated types of ores. The iron content in this type of ores reaches 30 %.

The contours of mineable iron ores in magnetite skarns are defined by the content of dissolved iron distinguishing massive magnetite ores with iron content of more than 45 %, magnetite skarns from 30 to 45 % of iron content, and ore skarns with iron content from 15 to 25 %. The share of massive magnetite ores of skarn type of total reserves varies from 30 to 50 %, reach magnetite skarns from 10 to 40 %, poor magnetite skarns from 6 to 13 %, and ore skarns from 2 to 4 %. Despite available infrastructure and sufficient mineable reserves of cobalt-bearing iron ore, the Dashkesan group of deposits did not involve to a full commercial exploitation. The open cast mining production has been sharply reduced owing to a low demand after a breakup of the former Soviet Union.

Smaller deposits of magnetite skarns are known to exist on the territory of the Gedabey and Ordubad ore regions. The Novo-Ivanovka occurrence is located within a range of 4–5 km to the northwest from Novo-Ivanovka village of the Gedabey

region. The mineralization is confined to the contact zones of the Lok-Garabagh limestones of the Upper Cretaceous age and volcanogenic–sedimentary rocks of the Eocene intruded by the post-Middle-Eocene granitoids of gabbroid and syenite–diorite phase. Small ore bodies contain fine-grained magnetite with admixture of pyrite. The iron content varies from 9 to 58.2 % and cobalt from 0.015 to 0.02 %. The cobalt mineralization is paragenetically associated with pyrite. The occurrence is of no present economic interest.

2.2.1.3 Hematite Ore

Hematite ore is known to exist in the Dashkesan ore region, being represented by the Alabashli deposit and a number of small occurrences. The deposit is located westward of Gyandja city close to the Alabashli railway station. The deposit is hosted by the Middle Jurassic volcanogenic and the Upper Cretaceous sedimentary formations overlaid by the Quaternary deposits. The Middle Jurassic volcanics are represented by tuff–sandstone, tuff–breccia, and tuff–conglomerates of the Bathonian stage exposed to hydrothermal alterations. The upper section of the Cretaceous system is represented by the formations of the Lower Coniacian, Turonian, and Santonian stages transgressively overlapping volcanogenic rock series of the Bathonian stage. The formations are complicated by a series of tectonic faults of various orientations. The mineralized zone of the Alabashli hematite deposit subsided concordantly with enclosing rocks and has a moderate dipping of 15°–20°. The mineralized zone is broken by faults defining the terrace structure of the deposit. The ore body occurs in the form of stratabound beds.

The ores are represented by massive red hematite and coarse–crystallic hematite of steel-gray color. Ore texture is impregnated and laminated, sometimes banded and breccia-shaped. Main ore minerals are hematite, hausmannite, hydroferrum oxide, pyrite, and chalcopyrite. The associated minerals are quartz, sericite, chlorite, epidote, calcite, alunite, and kaolinite. The chemical assay of samples shows 25 % of Fe_2O_3, 47 % of SiO_2, 1 % of TiO_2, a range of 0.12–0.74 % of sulfur, from 0.4 to 2.0 % of CaO, from 0.04 to 0.08 of Cr_2O_3, from 0.02 to 0.029 of zinc, 0.019 of copper, and from 0.012 to 0.2 of water-dissolved salts, all indicating the siliceous type of mineralization.

Hematite ores of the Alabashli deposit after enrichment on chemical composition and density can be used as a weighting ingredient of drilling muds. The proved reserves of hematite ore are estimated at 580,000 t. The geological prospecting and geophysical studies carried out in the vicinity of the deposit indicated additional reserve potential in the southeastern flank of the deposit. The stratabound hematite mineralization of up to 60 m thick has been proved to be hosted by rocks of volcanogenic series. Besides the Alabashli deposit, the Shamkir uplift also hosts typical hydrothermal manifestations of hematite of veinlet type in acid intrusions being characterized by monomineral composition.

The Chardakhli hematite occurrence is located within 2–3 km westward of the Alabashli deposit and confined to a contact zone of the Atabek-Slavyan plagiogranite intrusive massif with quartz porphyrites, where hematite mineralization is represented by stringers and lenses. Ore bodies are small and of a low economic value. A maximum content of ferrum in hematite ore is 60 %.

The Atabek hematite occurrence is confined to the endogenous contact zone of the Atabek intrusive massif of plagiogranites, which were transformed into secondary quartzites. Mineralization is represented by vertically dipping veins and lenses. Similar manifestations of hematite mineralization are developed in various parts of the contact zone of the plagiogranite intrusive massif. This type of hematite mineralization has not been studied in detail.

The titanium–magnetite-bearing mineral sand placers were observed along the coast of the Caspian Sea in the southeastern part of Azerbaijan up to the border with the Islamic Republic of Iran.

Magnetite sandstone

Numerous occurrences of magnetite sandstone are concentrated in the Lok-Garabagh metallogenic belt (Dashkesan, Shamkir, Khanlar ore regions) and stratigraphically confined to the volcanogenic series of the Bathonian age. More than twenty outcrops of magnetite sandstones were traced over a distance of 85 km along the coastal line of the Lower Bathonian paleosea. The occurrences in the form of beds and lens-shaped bodies have a variable thickness from 0.5 to 2 m and are traced over a distance from 10 to more than 1000 m.

The main ore minerals are magnetite, titanium–magnetite, ilmenite, rare hematite–ilmenite, hematite, and martite. Hypergene magnetite, goethite, hydrogoethite, and siderite are rare. Among sulfides, rare grains of pyrite and chalcopyrite are found. The content of magnetite in the form of rolled and angular grains from 0.1 to more than 1 mm varies from 30 to 90 %. According to the content of ore grains, reach (70–80 %) and poor (20–35 %) types of magnetite ore have been distinguished. The grade of titanium–magnetite which is the second ore mineral in titanium-bearing magnetite sandstone varies from 3 to 4 %. The content of ilmenite is from 2 to 3 %. Chlorite is the basic cementing mineral, while quartz, plagioclase, pyroxene, epidote, actinolite, and zircon are found as separate grains. The content of these cementing minerals varies from a range of 1–5 % to 30–50 %, and the quantum of cementing mass varies from a range of 3–12 % to 20–25 %.

The content of Fe_2O_3 in magnetite sandstone varies from 47.8 to 75.7 %, metallic ferrum from 33.4 to 53.0 %, and V_2O_5 from 0.36 to 0.46 %. A method of magnetic separation from magnetite sandstone is applied to obtain enriched iron ore concentrate grading 60 % of Fe_2O_3 and from 0.47 to 0.57 % of V_2O_5. The flotation method enables the extraction of 55 % of magnetite concentrate from the initial quantity of magnetite ore. The content of TiO_2 in magnetite concentrate varies from 9.6 to 10.68 %. The percentage of extraction of titanium varies from 43 to 64 %. The presence of titanium and vanadium in magnetite sandstone indicates the possibility of using these ores as metallurgical raw materials for high-quality steel. Favorable geological conditions suggest a discovery potential of large deposits of magnetite sandstone in various regions of the northeastern slope of the Lesser Caucasus.

2.2.1.4 Magnetite-Bearing Sands

Titanium placers of magnetite-bearing sands are traced along the coast of the Caspian Sea over a distance of 52 km from Lenkaran to Astara city representing iron ores of sedimentary type. The width of placers varies from 50 to 300 m. Further south, these sands are observed on the Iranian coast of the Caspian Sea. The mineral composition of the sands is represented by magnetite (21.5 %), titanium magnetite (63.2 %), hematite (2 %), chromite (0.5 %), and quartz and feldspar (12.8 %).

2.2.1.5 Chromites

The deposits and occurrences of chromites are confined to the ultrabasic rocks of the ophiolite belt of Azerbaijan. The total extent of the ophiolite belt within the Transcaucasus is about 260 km, from which nearly 160 km falls into Azerbaijan's territory. Tectonically, the ophiolite belt of Azerbaijan is confined to the Goycha-Garabagh tectonic zone of the Lesser Caucasus. Petrologically, ultrabasic rocks of the ophiolite belt are represented by peridotites (harzburgite), dunites, and pyroxenites, all reworked into serpentinites by metamorphism. While all massifs of ultrabasic rocks of the ophiolite belt of Azerbaijan are chromite-bearing, the majority of deposits and occurrences of chromite ores are confined to outcrops of dunites and, more rare, harzburgites. The major chromite mineralization in the Azerbaijanian part of the ophiolite belt was found within the Geydara and Kyazimbinin-Gavrilov deposits as well as the Zaydara, Nikolayev, Khotavan, and Ipak groups of occurrences.

The Geydara chromite deposit

The Geydara chromite deposit is one of the known chromite deposits in the Transcaucasus located in the watershed of the Soyutluchay and Istibulag rivers at an altitude of 2290 m above sea level. The deposit occurs on the contact of strongly serpentinized harzburgites with the massif of gabbro–amphibolites, which is hosted on the northeast by volcanogenic–sedimentary sequence of the Santonian age. The ore bodies of the Geydara deposit are confined to a lens-shaped massif of serpentinized dunites elongated in parallel with an archy contact of peridotites and gabbro–amphibolites. The length of the dunite massif is 350 m with a variable thickness from 0.5 to 15 m. Contacts of dunites with enclosing peridotites are gentle and rare. Chromite ore bodies of economic interest are represented by isolated nests of oval and, rarely, lens-shaped form, being located as a chain along the strike of dunites. Some elongation of ore nests along the strike and dip is observed. Minor chromite ore nests or bodies nearby the massive ore bodies are met in the form of spheroids, veinlets, and fracture fillings. A disseminated type of chromite mineralization is rare.

Five groups of ore bodies were distinguished within the Geydara chromite deposit. The most prominent ore zone on the southeast of the deposit contains around 40 nests of chromite ore. Chemical assay shows a range of 43.1–52.2 % of Cr_2O_3, 12.5–16.4 % of FeO, 5.77–5.94 % of SiO_2, 0.17–0.37 % of CaO, 0.01–0.03 % of SO_3, 0.01–0.02 % of P_2O_5, and ratio of CrO to FeO from 3.0 to 5.2 %.

Massive chromite ores of deposits and occurrences of Azerbaijan are characterized by the following average composition: from 42 to 54 % of Cr_2O_3, from 6 to 17 % of FeO, from 6 to 11 % of Al_2O_3, from 0.13 to 0.16 % of CaO, from 16 to 20 % of MgO, from 0.005 to 0.02 % of P_2O_5, and from 0.01 to 0.02 % of SO_3. Vanadium, zinc, cobalt, and nickel are associated ore minerals. Technological properties of massive chromite ore meet the highest requirements of the metallurgical industry and can be used for the production of ferroalloys. Chromite ores of impregnated and nodular types grading from 18 to 39 % of Cr_2O_3 and from 8 to 18 % of FeO can also be used for metallurgical purposes after appropriate enrichment. Field tests have proved that it is possible to obtain concentrates grading more than 50 % of Cr_2O_3 and more than 16 % of FeO. While mining and technological conditions of chromite ore development are generally favorable, additional mineral exploration and mineral economics works are required to determine their development.

The ophiolite belt of Azerbaijan constitutes a part of the large Pontian ophiolite belt extending through northern Turkey, Armenia, and Azerbaijan with known chromite deposits being exploited in Turkey. The proven reserves of the chromite deposits in Turkey vary from a range of 5000–20,000 t to more than 200,000 t. The similarity of the geological environment and tectonic regimes suggests a potential for discovery of new medium-sized chromite deposits in Azerbaijan.

2.2.1.6 Manganese

Only small deposits and occurrences of manganese ore are known to exist in the Lok-Garabagh and Araz tectonic zones of the Lesser Caucasus, on the southern slope of the Greater Caucasus and in the northern Gobustan. All occurrences of the Somkhit-Agdam tectonic zone are hosted by the Upper Cretaceous volcanics being characterized by exhalation–sedimentary and hydrothermal types of mineralization. The most known mineralization in this tectonic zone are the Molladjali deposit and Elvar occurrence in the Agjakend trough and the Dashsalakhli occurrence in the Gazakh trough of the Lesser Caucasus.

The Molladjali deposit is located close to the same village in favorable mining and geographic conditions. The deposit is hosted by volcanogenic and sedimentary rocks of the Upper Cretaceous: andesite–basalts and tuffs of the Coniacian and Lower Santonian stages, clayey–sandy horizon of the Upper Santonian stage, and marly limestone of the Campanian–Maastrichtian stages. Stratiform beds of ferromanganese ore occur in sandy–clayey rocks of the Upper Santonian stage on a contact with limestone of the Campanian stage. Ore bodies are elongated in the northwestern direction conformable with enclosing rocks and are traced as fragmented occurrences. The mineral composition of manganese ores shows a vertical upward zonation from siliceous manganese and ferromanganese varieties to more pure manganese ore in the middle of the mineralized section. The ferromanganese content, however, prevails toward the topmost sections. The deposit is subdivided into the northwestern, central, and southeastern areas.

In the northwestern area, ferromanganese beds are represented by several separated ore bodies from 0.3 to 3.0 m thick and from 45 to 90 m long. The total extent of this mineralized zone is more than 700 m. Chemical assay of ore shows from 0.3 to 16.71 % of MnO, 20.4 to 42 % of FeO, and 1.54 % of P_2O_5. In the southeastern area, the ore-bearing horizon contains two beds thicker from 0.2 to 0.5 m in the lower part and from 0.5 to 1.0 m in the upper part being separated by strongly limonitized sandy clays. Northwestward, the thickness of the upper ore bed increases up to 4 m. The grade of manganese varies within a range from 0.4 to 32 %.

2.2.2 Non-ferrous and Light Metals

2.2.2.1 Lead and Zinc

The lead–zinc deposits of Azerbaijan are characterized by variable genetic and morphological types being hosted by a wide spectrum of the Phanerozoic formations from the Devonian (Gyumushlug deposit) to the Miocene–Pliocene age. Artisanal mining and processing of lead/zinc ores existed in the nineteen century at the Mekhmana deposit of the Daghliq (Mountainous) Garabagh and the Gyumushlug deposit of the Nakhchivan AR. The geological prospecting and mineral exploration from 1950 to 1954 resulted in the discovery of the Agdara lead–zinc deposit in the Lesser Caucasus, a number of occurrences in Nakhchivan Autonomic Republic (AR) of Azerbaijan and in the Dalidagh intrusive massif in the Kelbadjar region. The discovery of the Filizchay giant deposit on the southern slope of the Greater Caucasus in 1958 triggered intensive exploration work for base metal mineralization in this previously unexplored region and follow-up discovery of the Katsdagh, Katekh, Sagator and some other deposits in Azerbaijan, the Gyzyldara and Gurdul deposits in Dagestan, occurrences of copper–zinc ores within the Azerbaijan territory of the southern slope of the Greater Caucasus, and also in adjacent areas of Dagestan. According to the estimation of some Azerbaijan and Russian geologists, Filizchay deposit by its commercial reserves is within five largest polymetallic deposits in the world. The base metal deposits in the Lesser Caucasus of hydrothermal type are generally of small size. The Agdara base metal deposit has been exploited until depletion and mining operations at the Gyumushlug deposit were ceased owing to political instability in the Mountainous Garabagh.

The metallogenic province of the Greater Caucasus

All known deposits and occurrences of base metals are hosted by the Lower and Middle Jurassic tectonic zones of mountainous folded system of the Greater Caucasus (Kurbanov et al. 1967; Azizbekov et al. 1972; Akberov et al. 1982; Hasanov 1982; Kurbanov 1982; Shirinov 1982; Agayev 1990; Atlas 2000; Ismailzadeh et al. 2008). The geological investigations and tectonic analysis of this tectonic zone distinguished southward the Metlyuta-Akhtichay, Tufan, Katekh-Gyumbulchay, and Zagatala-Kovdagh tectonic subzones. These subzones of a deep thrust-over-thrust nature have served as boundaries of structural–facial zones in the pre-collisional stage and currently represent large tectonic transversal elements of thrusting mature. The Jurassic tectonic zone of the mountainous system of the Greater Caucasus has experienced an intensive magmatism being represented by subvolcanic, hypovolcanic, and hyperabyssal bodies of gabbro and gabbro–diabases, as well as by subvolcanic and hypovolcanic intrusions of dacites, liparites–dacites, liparites, and, more rarely, by andesite–basalts and basalts.

The major structural control of mineralization in this tectonic zone belongs to transversal tectonic elements which divide longitudinal zones into a number of large transversal

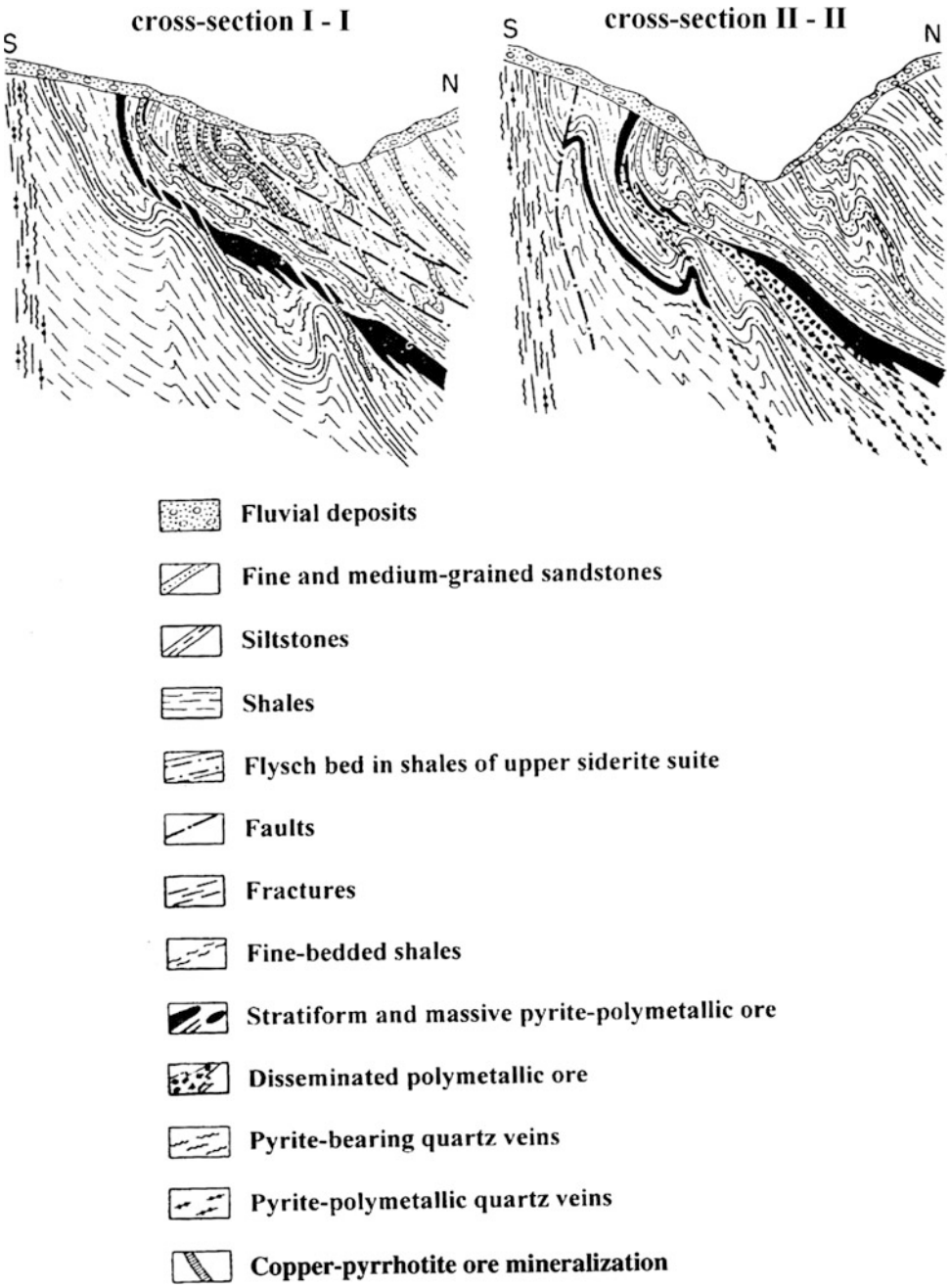

Fig. 2.27 Cross sections of the central (*I–I*) and eastern (*II–II*) areas of the Filizchay pyrite–polymetallic deposit

terrace uplifts and subsided blocks. On the recent erosional level, the crosscutting blocks are expressed as the north–northeastern or the north–northwestern vertical flexures being complicated by fragmented faults of a thrust–upthrust nature of the same directions.

The Filizchay complex ore deposit

The Filizchay deposit of base metals is hosted by terrigenous deposits of the Upper siderite and Khinalug suites of the Middle Jurassic which are crumpled into a large overturned to the south the sublatitudinal Karabchay anticline. The morphology of the ore deposit is rather simple being represented by a stratabound lens-like ore body with swells and pinches along the dip and strike of the ore body (Fig. 2.27). The ore body is dipping to the north at 40°–45° and on the top horizons at 60°–70° up to a vertical dipping. Unlike the roof, where the deposit is characterized by sharp and well-pronounced contours, its base has a more complicated structure.

Mineral composition of the ore body is quite monotonous comprising mainly of pyrite followed by sphalerite, galenite, and pyrrhotite. Chalcopyrite, marcasite, arsenopyrite, magnetite, and secondary copper sulfides are found in small

quantities. The cementing minerals are carbonates, quartz, and, to a lesser extent, chlorite and sericite. The ore contains more than twenty rare minerals.

Five types of ore have been distinguished within the Filizchay deposit based on the texture of the ore, namely (a) banded pyrite and pyrite–sphalerite–galenite; (b) massive pyrite; (c) impregnated pyrite and pyrite–sphalerite–galenite; (d) streaky and fracture fillings of pyrite, pyrite–sphalerite–galenite and pyrrhotite, and (e) massive copper–pyrrhotite.

The banded ores occur in a hanging side of the deposit and occupy most of the volume of the ore body. Massive pyrite ores with a minor admixture of chalcopyrite, sphalerite, and galenite are found together with banded ores and form lens-shaped areas in the top and bottom sections of the ore body.

The impregnated and disseminated pyrite–sphalerite–galenite type of ores occurs in the eastern part of the deposit forming the bodies of rather complicated form. This type of ores is characterized by a coarse-grained pyrite segregation of up to 1.0–1.5 cm of cubic and irregular form on the background of cementing material. Textural varieties of impregnated ores are defined by quantitative correlation of pyrite, cementing minerals, and content of polymetallic sulfides. Two extreme textural members are impregnated ores grading from 60 to 70 % of pyrite and ores grading from 20 to 30 % of pyrite.

The veinlets and fracture filling ores are developed in a lying side of the ore body on the eastern flank of the deposit and extend beyond its limits up to 2.0 km. This type of ore is overlain by banded and impregnated ores. Three textural varieties of mineralization are parallel to schistosity, net-like-breccia, and brecciated ores. The thickness of separate stringers and veins varies from 0.5 cm to 0.5 m.

Later massive pyrrhotite ores are developed exclusively in the eastern part of the deposit forming a single vein-shaped body located in a hanging side of massive pyrrhotite and partially among the impregnated and banded ores. Massive textural varieties prevail in the surficial part of the ore body; more abyssal horizons of the ore body are dominated by breccia texture being cemented by fine-grained pyrrhotite.

The deposit has been explored in detail by drilling and mining at four exploration levels. The technological types of ores include the primary ore (97.3 %), mixed (2.2 %), and oxidized ore (0.5 %). Technological properties of ores have been studied in laboratories, and two semi-industrial tests on selected flotation indicate a feasibility of obtaining 67.7 % of copper concentrate, 65.2 % of lead concentrate, and 86.1 % of zinc concentrate. Technology of complex reworking of pyrite concentrate enabled to obtain 90.3 % of lead, 92.0 % of zinc, 84.7 % of gold, 84.6 % of silver, 72.1 % of cobalt, 72.2 % of cadmium, 29.7 % of indium, and 10.4 % of selenium.

The deposit is planned to be exploitated by underground mining. The proven reserves of the deposit, the data on which are unavailable, were approved by the State Commission on Reserves of the former Soviet Union in 1983.

The Katsdagh pyrite–polymetallic deposit

The Katsdagh pyrite–polymetallic deposit is located northwest of the above-mentioned Filizchay deposit (Hasanov 1982). All ore zones of the deposit are confined to the Kekhnamedan abyssal upthrust–overthrust. The deposit is hosted by the Lower Siderite suite of the Middle Jurassic being represented by alternations of sandstone, sandy–clayey shales, and clayey shales. This sequence overlies the upper clayey series of the Khinalug suite dipping to the north at a variable angle from 20° to 65° (Fig. 2.28). The deposit is tectonically controlled by the Kekhnamedan fault which is separated into crushed and schistose zones of various degrees being exposed to hydrothermal metamorphism and sulfide mineralization. These structural units host dykes and sills of basic, intermediate, and acid compositions, which have been formed in two stages. The later stage of intrusive magmatism includes diabases, gabbro–diabases, andesite–porphyrites, andesite–dacites, dacites, and liparite–dacites.

Based on intensity of mineralization, the deposit has been subdivided into several mineralized zones. The most prominent zones I and IV have been traced in sublatitudinal direction parallel to each other over a distance of more than 2000 m. Comparatively, shallow ore zones of up to 60 m deep are represented by a series of subparallel ore-bearing fractures up to 50 m long. These fracture filling zones form echelon-like mineralized zones from 50 to 300 m long and occurring from each other at a distance from 30 to 50 m. The detailed mineral exploration within the most prospective zone I has revealed mineralized beds, lenses, and veinlets with an average thickness from 2.5 to 5 m and a maximum thickness from 10 to 16 m in their swellings. The ore bodies are composed of banded and massive ores of sulfide–polymetallic and copper–pyrrhotite composition, which are found in equal ratios. The stringer-impregnated type of mineralization of same composition prevails in other parts of the deposit. The major role in localizing mineralization belongs to the above-mentioned dykes and sills, which were exposed to an intensive hydrothermal–metasomatic alteration preceding the mineralization. These dykes and sills are considered to be the screens for large ore deposits. The presence of numerous shallow veins composed of all known mineral associations in all types of dykes indicates their preceding formation in relation to major mineralization time.

Massive, banded, and stringer-impregnated types of ores are the prevailing textural types of mineralization in the

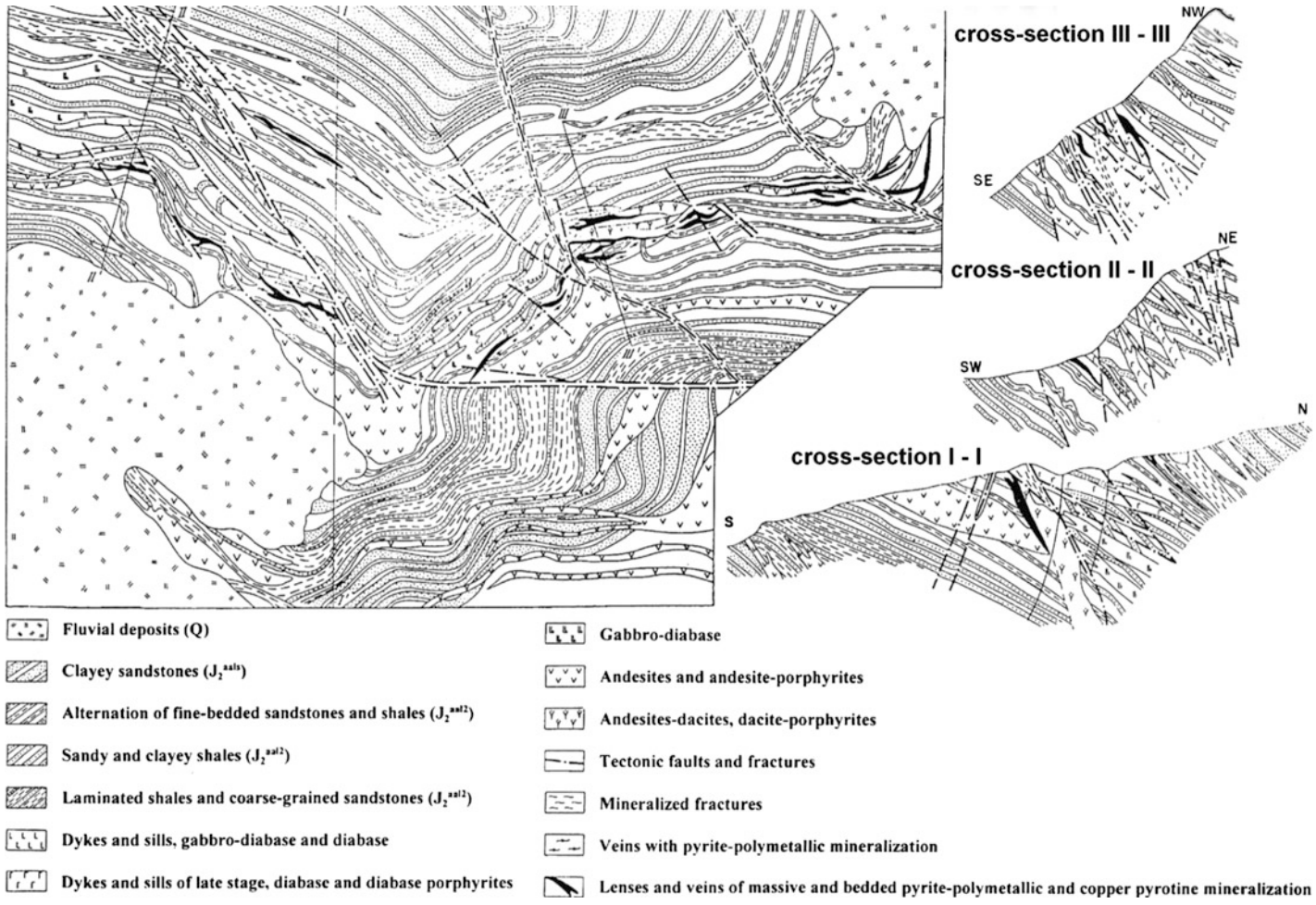

Fig. 2.28 Geological map and cross sections of the Katsdag pyrite–polymetallic deposit

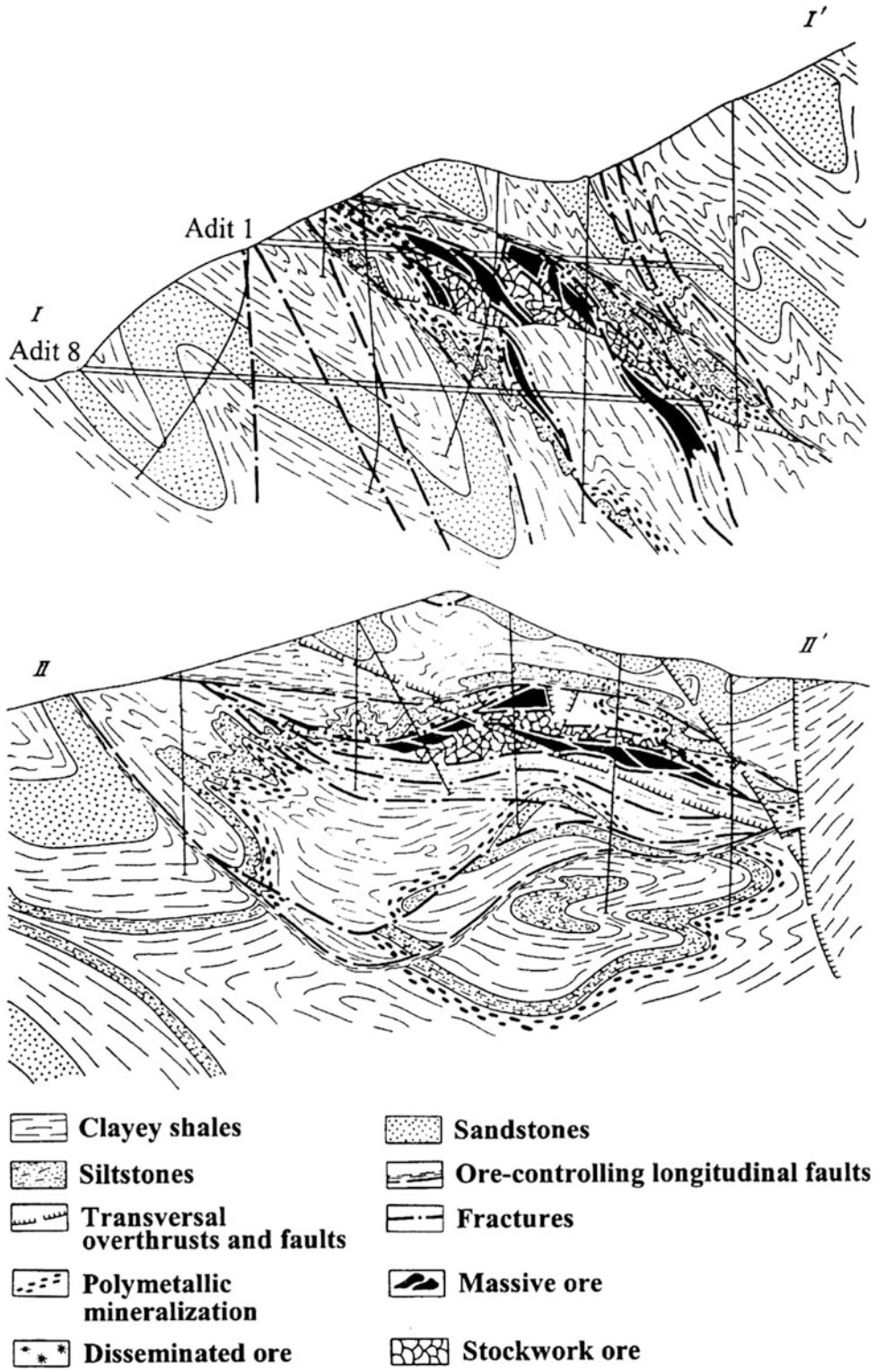

Fig. 2.29 Transversal (*I–I′*) and longitudinal (*II–II′*) cross sections of the Katekh polymetallic deposit

Katsdagh deposit. The banded type of mineralization includes mineral associations of copper–pyrrhotite and sulfide–polymetallic composition. Hydrothermal alterations of host rocks at the Katsdagh deposit which are accompanying or preceding mineralization are different from those in the Filizchay deposit. Unlike the Filizchay deposit, the hydrothermal alterations here are pronounced with the same intensity in hanging and lying sides of ore bodies. Differing from the Filizchay deposit, where the major hydrothermal alteration is carbonization, quartzitization, chloritization, and sericitization create a metasomatic column of facies of secondary quarzites around the ore bodies of the Katsdagh deposit.

Five ore bodies in the form of mineralized beds and lenses have been explored by drilling and mining within the Katsdagh deposit. Ore bodies have been traced and contoured on five horizons at a depth from 1800 to 2100 m level. The major ore-forming minerals are pyrrhotite, sphalerite, galenite, chalcopyrite, pyrite and rare arsenopyrite and cobaltite. Major metals are zinc, lead, copper, sulfur, silver, and associated cadmium and gold.

The Katekh polymetallic deposit

The Katekh deposit occurs in the Katekh-Gyumbulchay ore-bearing tectonic zone south of the Katsdagh deposit (Kurbanov 1982). Numerous clayed siderite and pyrite concretions from 1 cm up to 1.5 m size are hosted by flyschoid sandy–clayey formation of the Aalenian suite being subdivided into two large rhythms with regressive and transgressive structures.

Katekh anticline being located between transversal and longitudinal faults (Fig. 2.29). Three genetic types of sulfide mineralization are (a) diagenetic, (b) sulfide–polymetallic, and (c) polymetallic mineralization of vein type. The most prospective are the latest two types. By texture, the mineralization is subdivided into massive, impregnated, vein, and rudaceous ores. All these types of ores are spatially associated with each other and localized in the same ore zones being controlled by faults limiting the tectonic wedge. This tectonic wedge hosts three ore-bearing zones.

The major morphological type of sulfide deposits of the Katekh deposit are lens-shaped bodies complicated by longitudinal and crosscutting ore-controlling faults. Pyrite, galenite, sphalerite, chalcopyrite, arsenopyrite, secondary copper sulfides, marcasite, and pyrrhotite are the basic ore-forming minerals. Lead, zinc, silver, copper, gold, and cadmium are the major metals of commercial value.

Technological properties including enrichment of ores of the Katekh deposit have been studied on seven samples in laboratory conditions. Application of a scheme of collective–selective floatation enabled to obtain tradeable commodity concentrates with extraction of lead up to 85.5 %, 85.8 % of zinc, 33.2 % of copper, 76.2 % of gold, and 65.5 % of silver. The ore reserves of the Katekh deposit have been approved by the State Commission on Reserves of the former Soviet Union. The deposit was planned to be exploited by underground mining.

The Sagator polymetallic deposit

The Sagator deposit is located within a distance from 10 to 12 km northward from the Filizchay deposit. The deposit is hosted by terrigenous formations of the Pliensbachian and Toarcian suites of the Middle Jurassic. The deposit is confined to the development of aleuro-clayey series represented by intercalation of fine-bedded aleurolite–sandstone, clayey shales, and aleurolites.

Two natural ore types are massive copper–zinc and vein-type copper–pyrrhotite mineralization. Sphalerite, chalcopyrite, and pyrrhotite are the basic ore-forming minerals. Lead, zinc, silver, cobalt, and cadmium are the major metals of commercial value. Separate technological tests of three samples have been conducted on vein and massive ores as well as on admixture of these types of ore in a ratio 1:1. An appropriate technological scheme and ore enrichment regime enabling to extract up to 86.8 % of copper and 68.1 % of zinc have been developed and recommended.

The metallogenic province of the Lesser Caucasus

Polymetallic deposits and occurrences of the Lesser Caucasus are known to exist within the Lok-Garabagh, Ordubad-Zangazur, and Sharur-Djulfa metallogenic belts (Aliyev 1976; Azizbekov et al. 1976; Kerimov 1964; Kerimov et al. 1986; Ismailzadeh et al. 2008).

The Lok-Garabagh metallogenic belt

This metallogenic belt hosts one hydrothermal polymetallic deposit and numerous occurrences of vein type containing lead, zinc, and barite mineralization. The sporadic lead–zinc mineralization is mainly pronounced in small occurrences consisting of single veins or a series of small quartz and quartz–carbonaceous veins.

The Mekhmana base metal field

The Mekhmana copper–lead field contains reserves of commercial significance in the Lok-Garabagh metallogenic belt. The deposit is located near Mekhmana village of the Garabagh region. The artisanal mining of this deposit is recorded since the end of the nineteenth century.

The deposit occurs in a complex of volcanogenic–sedimentary rocks of the Middle Jurassic - Upper Cretaceous

and is hosted by the Middle Jurassic sedimentary rocks. The main structural unit of the deposit is a large anticlinal fold of the north–northwestern direction. The structure of the deposit and mineralization is controlled by a deep-seated tectonic fault being a channel of multiple magmatic activity during the Middle–Late Jurassic time. The magmatic series is represented by gabbro–diabase magma and subvolcanic intrusions of quartz porphyries of the Upper Bajocian, small intrusions of diorite–porphyries of the Late Jurassic, and finally quartz ore veins of the Mekhmana field. The youngest intrusive rocks are the Late Jurassic dykes of diorite–porphyrites in the eastern part of the deposit being localized in fragments of more late tectonic downthrusts. Around thirty ore-bearing quartz veins of the Mekhmana field are concentrated in a narrow strip of sublatitudinal direction corresponding to a bending area of anticlinal fold and localized in fracture fillings. The veins' volume is usually filled up by calcites, quartz, and ore-forming minerals intermixed with enclosed hydrothermally altered rocks. Ore minerals are mainly represented by galenite and sphalerite, which are closely associated with quartz and carbonates. Chalcopyrite, pyrite, marcasite, chalcosine, bornite, and secondary copper sulfides have a lesser distribution. Galenite and sphalerite in quartz veins and veinlets are met in the form of strips from 5 to 10 cm thick, large and small nests, stringers, and impregnations. The most typical banded texture of ores is followed by breccia, colloform, looped, and impregnated textures. As a rule, structure of ore accumulations is coarse-grained. Based on the content of lead and zinc, the ores have been divided into predominantly lead ores, predominantly zinc ores, and mixed lead–zinc ores. Associated metals are cadmium, silver, selenium, and tellurium.

The Ordubad–Zangazur metallogenic belt

This belt is a typical representative of the Late Alpine stage of development of the Lesser Caucasus, wherein various ore formations, typical to the pre-, syn-, and post-collisional stages, are present. All large polymetallic deposits are associated with a late stage of belt's development and concentrated within the western margin of the Megri-Ordubad granitoid massif. The deposits are typical examples of sulfide formation genetically linked with volcanites being the constituent part of a single volcanoplutonic complex. Small deposits and occurrences of sulfide–polymetallic type within the Ordubad ore region are spatially and genetically associated with the areas of hydrothermal–metasomatic alterations in enclosing volcanogenic rocks of the Lower Eocene which form a single basalt–andesite–liparite–dacite formation. The most intensive concentration of sulfide–polymetallic ores is linked with sulfate–fumarole fields of the central type being the products of post-magmatic activity of acid volcanites in subsequently differentiated basalt–andesite–liparite–dacite formations.

In spite of a common presence of sulfide mineralization in volcanites of acid composition, a distribution pattern of massive sulfide deposits is irregular. Large deposits of pyrites and pyrite–polymetallic ores are confined to local uplifts being expressed by closely converged volcanic structures of various types. The most typical are volcanic dome extrusions which are synchronous with volcanism of subvolcanic bodies. The tectonic and magmatic control of sulfide mineralization within this metallogenic belt has been studied in detail within the Agdara sulfide–polymetallic deposit in the northwestern part of the belt.

The Agdara sulfide-polymetallic deposit

The deposit is confined to the northern part of the core of the Agdara archy uplift which is composed of typical volcanic brachyanticlines appeared on the site of extrusive structures and volcanic domes. The core of the fold is composed of rocks of eroded pipes and prepipe facies. Wings and the eastern periclinal hinge of the old consist of more younger basic volcanites. Sulfide–polymetallic mineralization is concentrated within the core of the southern periclinal hinge of brachyanticline. The mineralization is controlled by a wide subvertical zone of intensive tectonic reworking. The core of ore-enclosing brachyanticline is intruded by subvolcanic bodies of liparite–dacite exposed to intensive hydrothermal–metasomatic alteration of secondary quarzites and propyllites.

Mineral exploration in the southern part of the brachyanticline has revealed massive sulfide mineralization underlined by secondary quarzites and overlapped by sedimentary–volcanogenic sequence. Two morphogenetic types of sulfide–polymetallic mineralization are stratabound massive and streaky-impregnated ores which occupy various structural positions, though spatially are closely associated with each other.

The stratabound bed of massive sulfides varies in thickness from 0.2 to 4.5 m and has been traced from the surface to a 65 m depth, where it reaches a range of 120–130 m length. Bend of the ore body on dip and extent repeat those of overlapping and enclosing sedimentary–volcanic rocks. Along the strike, the ore body has sharp contacts with underlying secondary quarzites. The roof structure of the deposit is more complicated. The morphology of streaky ores developed in a base of bed-shaped ore deposit is rather complicated.

Sulfide stringers from 1 mm to 1.5–2.5 cm form a complicated stockwork inside of areas of mineral concentrations where they coat fragments of mono-quarzites and sericite–quartzose rocks.

Major ore-forming minerals are pyrite (80 %), sphalerite (3–4 %), galenite (3 %), and chalcopyrite. The volume of bed-shaped deposit is composed of sphalerite (70–75 %), pyrite (5 %), chalcopyrite (10 %), and galenite (20–30 %). A certain vertical zonation in localization of sulfides is expressed by a prevalence of ferrum, copper, and lead sulfides in the lower part of the ore body and a domination of zinc and lead sulfides in the massive ores of the deposit upward. Secondary minerals are tennantite, tetraedrite, stromeyerite, bornite, molybdenite, chalcosine, cerussite, and covellite. The cementing minerals are quartz, sericite, alunite, barite, calcite, and chlorite. The formation of stringer-impregnated ores has occurred in two stages, where the initial stringers of quartz–pyrite–chalcopyrite and molybdenite composition have been crosscut by stringers of quartz–calcite and sphalerite–galenite composition. The deposit has been worked out and closed due to its depletion.

The Sharur-Djulfa metallogenic belt

The polymetallic mineralization within this metallogenic belt is known to exist in the Gyumushlug and Darridag-Paradash regions. The Gyumushlug ore region is situated in the area of the Paleozoic terrigenous–carbonaceous complex development and hosts the known Gyumushlug lead–zinc deposit and the Danzik and Sadarak small occurrences.

The Gyumushlug polymetallic deposit

The deposit was discovered at the end of the nineteenth century and has been exploited by the "Alagez" Joint Stock Company during a period from 1908 to 1916. The deposit is confined to the southwestern limb and core of the Gyumushlug anticline made up by limestone, clayey shales, marly limestone, and sandstone of the Givetian and Fransnian stages of the Devonian age. The Gyumushlug anticline has a complex tectonic structure due to intersection of lateral and transversal tectonic faults forming a clear block or mosaic structure.

The mineralization is strictly confined to limestone of the Givetian stage being localized in pre-ore meridional brecciated zones and also in interlayer space of limestone favorable for ore deposition. Structural and lithological factors have defined the existence of two morphological types of mineralization, namely steeply dipping crosscutting ore zones and stratabound mineralized beds.

Altogether, twenty four steeply dipping ore zones with a variable thickness from 0.4 to 6 m have been found in the deposit and only eight zones have been proved to be of an industrial importance. Clayey shales played a screening role in the formation of ore bodies enabling the localization of mineralization in the topmost sections of the limestone sequence. Industrial concentrations of lead and zinc have been found only in the lower horizons. The mineralization spreads toward from the fractures of a range of 25–30 m with a thickness of stratified mineralized lenses from 1 to 11.0 m. Veins, nests, and lens-shaped veins being accompanied by the areal of impregnated ores are distinguished in both morphological types of ores. The main initial ore minerals are galena and sphalerite; secondary minerals are pyrite, chalcopyrite, and secondary copper sulfides; rare minerals are boulangerite, boutnonite, and argenite; associated minerals are smithsonite, cerussite, limonite, covellite, chalcosine, anglesite and malachite; vein minerals are quartz, barite, calcite, rarely ankerite, dolomite, and gypsum.

The mineralization has concentrated in three stages being separated by the periods of tectonic movements. These stages are the main sulfide ore-forming stage, the galena–barite stage, and the galena–carbonate stage. According to texture peculiarities, massive, gneissose, brecciated, streaky, and impregnation ores have been distinguished, while massive ores have localized in ore zones and adjacent areas of stratabound mineralization streaky and impregnated ores have been met in the peripheral parts of ore bodies. The cemented, subgraphical, emulsioned, and replacement types of ore structures are distinguished. According to the chemical composition, three industrial types of ores, namely the prevailing lead type and lead–zinc types, have been identified. The polymetallic ores of the Gumushlug deposit are typical hydrothermal formations being concentrated under conditions of shallow depths and low temperatures.

The deposit has been explored by underground mining in combination with drilling. The reserves have been estimated. The deposit has been exploited since 1955, and up to now, the reserves of the I, II, and El ore areas have been nearly worked out. The ore-processing capacity of the Gumushlug processing plant used to be at around 50 t per day. The detailed geological prospecting and mineral exploration have identified further prospects of sulfide mineralization in the southeastern flank of the IV ore zone of the deposit. The reserves here have been estimated and the underground mining is visible from a single shaft. At present, the exploitation works have been suspended due to technical reasons. The remaining reserves as of January 1, 1991, were 133,000 tons of ore or 5800 lead metal.

2.2.2.2 Cobalt

Cobalt mineralization is closely associated with magmatic activity and has been found in many tectonic zones of Azerbaijan (Azizbekov et al. 1972; Atlas 2000; Ismailzadeh et al. 2005, 2008). The cobalt deposit of the Dashkesan ore region is paragenetically associated with the Dashkesan polyphase granitoid massif of the Upper Jurassic age. The deposit has been studied in details by mineral exploration

and has been partially worked out in the Lok-Garabagh zone. Cobalt mineralization has also been observed in sulfide ores of the Goshgardagh and Chanakhchi occurrences (Bajocian-Bathonian), hematite ore of the Novo-Ivanovka occurrence (Eocene), and others. In the Goycha-Garabagh tectonic zone, the prospects of cobalt mineralization are associated with hyperbasites and magnesite schists of the Late Cretaceous. In the Araz tectonic zone, cobalt mineralization is associated with skarns of the contact area of the Megri-Ordubad pluton of granitoids of the Early Eocene–Late Pliocene age. On the southern slope of the Main Caucasian ridge, cobalt mineralization has been found within the southern limb of the western part of the Tufan anticlinorium. Cobalt mineralization here occurs as isomorphic admixture to pyrite–coper–polymetallic ores of the deposits of the southern slope of the Greater Caucasus.

The Dashkesan ore region of the Lok-Garabagh metallogenic belt

The Dashkesan ore region is hosted by the Middle and Upper Jurassic sedimentary, volcanogenic–sedimentary, and volcanic rocks. These rocks are intruded by the Dashkesan polyphase granitoid massif, the exocontacts of which host metamorphic and contact–metasomatic rocks, hornblendes marbles, as well as barren and mineralized skarns.

Numerous dykes of mainly diabase diorite and plagioclase porphyrites have been found in the Jurassic

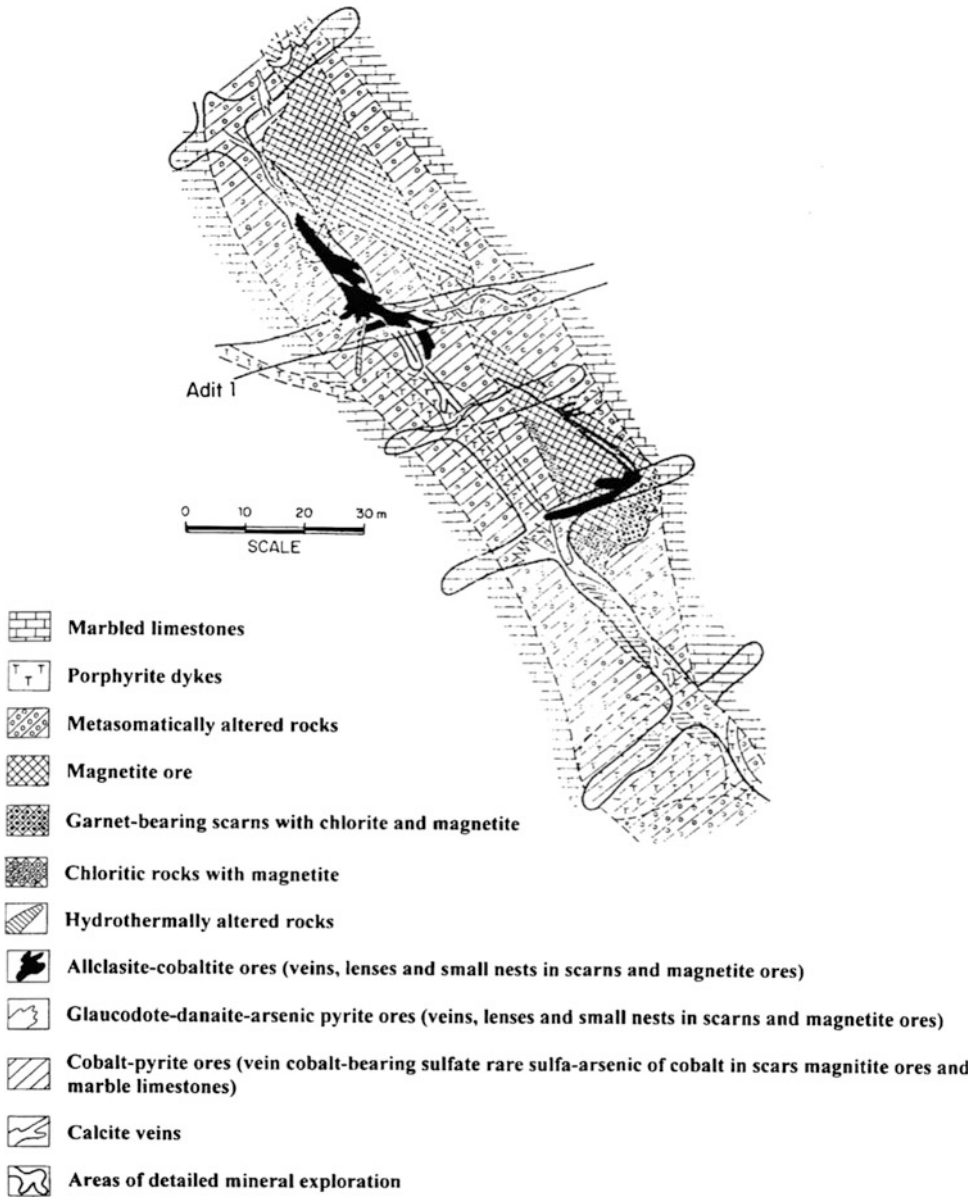

Fig. 2.30 Geological map of the SE area of the South Dashkesan iron–cobalt deposit

sedimentary rocks containing the intrusive massif. The presence of dykes inside of the granitoid massif is very rare. The main tectonic element is the Dashkesan anticline of the west–northwestern direction and associated numerous tectonic dislocations of variable age. Cobalt mineralization is also known to occur in the form of cobalt sulphoarsenide in the Dashkesan iron deposit of ore and in hydrothermal ore bodies beyond the skarns zones in the north deposit. Cobalt mineralization has been also found in a dispersed form in magnetite and as isomorphic admixture in pyrite.

By structural–geomorphological features and mineral associations, the following types of cobalt deposits and occurrences have been identified: (a) steeply dipping zones with sulphoarsenic cobalt mineralization (the north deposit of the Dashkesan ore region); (b) lenses and nests of sulphoarsenic cobalt concentration in magnetite skarns (the northeastern iron ore deposit); (c) steeply dipping zones bearing lenses and nests sulphoarsenic cobalt mineralization (Amamchay area); and (d) lenses and nests of cobalt–pyrite and sulphoarsenic cobalt mineralization in magnetite skarns (the South Dashkesan (Fig. 2.30) and Damir deposits).

The Amamchay cobalt deposit

The Amamchay cobalt deposit is located to the southwest from the South Dashkesan deposit. The character of ore mineralization has common features with that within the "north" and "northeastern" deposits. The deposit is hosted by marbled limestone of the Tusitanian suite of the Upper Oxfordian–Lower Kimmeridgian age up to 250 m thick.

Magnetite skarns series occurs in the upper section of limestone being cut by numerous dykes of porphyrites of the northwestern and, rarely, northeastern directions. In some places, brecciated and fractured matrix of dykes is substantially replaced by magnetite exposed to chloritization, epidotization, carbonatization, and pyritization, with associated cobalt mineralization. Some zones contain only cobalt mineralization along dykes without magnetite skarn mineralization. The most intensive cobalt mineralization up to 30 m thick has been found to occur in tectonically crushed and reworked areas of the deposit being a result of intensive tectonic activity and crosscutting dykes. Cobalt grade varies from 0.004 to 0.95 %. Cobaltite is met in a disseminated form, as fissure fillings and separate crystallic aggregates. Other ore minerals are pyrite, chalcopyrite, saffolorite, hematite, and molybdenite.

The Goycha-Hakeri metallogenic belt

Cobalt mineralization within this metallogenic belt has been identified in all types of magnesite schists of ultrabasic rock development in the Kelbadjar region, where the cobalt content varies from 0.001 to 1 %. It has been found that an increase of cobalt content in ultrabasic rocks is associated with an increase of magnesite. The maximum cobalt concentrations have been observed in olivine and less in enstatite. The increased cobalt content has been also observed in serpentinites in comparison with source peridotites.

The Ordubad-Zangazur metallogenic belt

Cobalt mineralization of the Kilit-Ketan occurrence in the Ordubad ore region has been found in exocontact of the Megri-Ordubad granitoid massif. The cobalt occurrence is hosted by the Upper Cretaceous sandy–argillitic series of the Lower Turonian, marly–argillitic series of the Lower and the Upper Coniacian, limestone of the Upper Coniacian, tuffogenous series of the Lower Santonian, limestone of the Upper Santonian, and marly–argillitic series of the Campanian age. Metasomatic rocks such as marbles, hornfels skarns, and epidosites were formed as a result of intensive magmatism in a strip from 200 to 1000 m long.

Cobalt-bearing sulfide mineralization is confined to the external margin of the Upper Cretaceous rocks surrounding the Megri-Ordubad intrusive massif, where mineralization has been traced over a distance of 2.5 km. Copper–cobalt mineralization is associated genetically with the post-magmatic activity of the Megri-Ordubad pluton. Epidote–garnet skarns of the most promising Ketam zone contain lenses, nests, and impregnations of sulfides. Mineral exploration by underground horizontal adits has been terminated due to security instability on the territory of the Nakhchivan AR.

2.2.2.3 Molybdenum

The deposits and occurrences of molybdenum ores in the Lesser Caucasus are concentrated within the Ordubad and Dalidagh ore regions (Azizbekov et al. 1972; Kerimov and Kerimov 1974; Babazadeh et al. 1990; Ismailzadeh et al. 2008). The majority of ore deposits of the copper–molybdenum formation are concentrated within the Megri-Ordubad intrusive complex confined to a large geoanticlinal uplift and representing the median massif in the definite stages of the geologic evolution. Molybdenum mineralization is mainly developed in intersection of longitudinal and northwestern faults with cross-faults of the northeastern direction. The large Misdag, Alchalig, and Diakhchay copper–molybdenum deposits of industrial type are mainly characterized by stockwork type of mineralization with the leading copper component.

Deposits with industrial molybdenum mineralization with a dominant molybdenum component of vein type are represented by either quartz veins and fissure fillings or veinlets

and stockworks with impregnated mineralization. The thickness of veins and veinlets varies from 0.1 to 1.0 m reaching a thickness of up to 2 m in swelling. The molybdenum content varies from 0.2 to 1.1 %. Associated ore minerals are copper (0.02–1.73 %), renium (0.04 % in molybdenite), selenium (0.06 %), and tellurium (0.02 %). The molybdenum deposits, unlike the copper–molybdenum deposits of the region, have limited reserves from 100 to a range of 1500–2000 tons of molybdenum metal.

The Paragachay deposit

The Paragachay molybdenum deposit is located in the central part of the Ordubad ore region and hosted by gabbro–diorites, diorites, and dykes of lamprophyres and diorite–porphyries. The mineralization is tectonically controlled by sublatitudinal (NW—280°–310°) and submeridional (NE—20°–60°) faults. The mineralization in the form of veins and veinlets is concentrated in sublatitudinal faults. Ore-bearing gabbro–diorites and diorites have been subjected to intensive hydrothermal–metasomatic alteration. The formation of ore mineralization at the deposit has occurred in the following five stages: (a) quartz–molybdenite early stage productive for molybdenum; (b) quartz–molybdenite–chalcopyrite stage productive for molybdenum and copper; (c) quartz–pyrite–chalcopyrite stage productive for copper; (d) quartz–galena–sphalerite stage; and (e) latest carbonate stage. Four quartz–molybdenite veins of industrial importance, namely Glavnaya, Novaya, Pyataya, and Srednya, have been exploited within the Paragachay deposit.

Unlike the Glavnaya (Bash or Major) vein, where the dyke-related mineralization demonstrates its continuity, the mineralization in the last three veins discontinues along their strike. The prospects of the Paragachay molybdenum deposit are associated with the lower horizons of the Yeni and Besh veins which can be opened by mine or adit from 2 to 2.5 km long. At present, due to unfavorable economic–technical conditions, the exploitation works have been suspended. The remaining mineable reserves of molybdenum as of January 1, 1999, are about 54,000 tons of molybdenum ore or 256 tons of molybdenum metal.

The Urumis molybdenum deposit

There are known to exist ten quartz–molybdenum veins distributed in the endocontact zone of the Megri-Ordubad pluton. The deposit occurs in gabbro–diorites, granodiorites, and quartz syenite–diorites with cutting dykes of granodiorite–porphyrites, diorite–porphyrites, lamprophyre, aplite, and pegmatites. Tuffs and tuffites of the Eocene in the southeastern part of the deposit have been changed into secondary quarzites in the contact zone with the intrusion.

The veins strike to the west–northwest at 270–290° and dip to the southwest at the angle from 50° to 70°. The average thickness is 0.4 m. The molybdenum content is from 0.001 to 0.1 % and that of copper from 0.06 to 0.7 %. The veins consist of milky-white quartz containing impregnations of pyrite, chalcopyrite, and molybdenite. Secondary hydrothermal alterations are expressed by silicification and sericitization. The veins have a banded texture and lens-shaped structure.

The northwestern part of the deposit contains mainly copper vein mineralization, which has been explored by short underground adits. The tense concentration of copper-bearing quartz veins within a narrow strip of 400 m wide and a shallow erosion depth suggests good development prospects. Mineral exploration also expects a possible increase of thickness and content of molybdenum in the southeastern flank of the deposit where mineralization has not been effected by erosion.

The Gekgyundur deposit

The deposit is hosted by intrusive rocks of the Megri-Ordubad pluton represented by rocks of the early adamellite intrusive phase and late quartz syenite–diorites and porphyry granosyenites being crosscut by dykes of diorites and granite–porphyries. The tectonic structure of the deposit is defined by the major Ordubad fault which divides two intrusive phases and the Vardanichay fault of meridional direction with adjacent zones of hydrothermal alteration.

The thickness of these zones with molybdenum mineralization varies from 0.5 to 1.2 m where molybdenum content is from 0.01 to 2.5 %. The zones are composed of loose chloritized and epidotized rocks. The molybdenum mineralization, except zone No. 1, is being controlled by the Vardanichay fault. The mineralization at zone No. 1 was traced up to 360 m deep on four horizons every 60 m by adits and by underground drilling wells. In some intervals of two horizons, this zone contains the industrial accumulations of molybdenum. The average thickness is 1.1 m, and the average grade of molybdenum is 0.44 %. Reserves are so far limited, while the identified further exploration is required to judge its economic prospects. The stockwork type of molybdenum–copper mineralization was suggested at a depth in the area of the Vardanichay fault, where the molybdenum content in individual samples from quartz stringers varies from 0.01 to 2.5 % and that of copper from 0.2 to 2.5 %.

The Dalidagh ore region

Molybdenum mineralization of this region is closely associated with the post-magmatic activity of the Dalidagh

intrusive massif. The early copper–molybdenum and most later polymetallic ore formations have been distinguished within the deposit. Structural position and localization of these ore formations are defined by a series of dykes which separated the enclosing rocks into two blocks.

The typical Teymuruchandagh molybdenum deposit of the Dalidagh ore region is confined to the northwestern exocontact of the Dalidagh granitoid intrusive massif composed of porphyry granosyenites, quartz syenite–diorites, and syenite–diorites. The regional west–northwest tending fault of a thrust nature with amplitude of 400 m was traced by the Istisu mineral springs and confined to the axis of the Dalidagh anticlinorium. The deposit is subdivided into the northwestern and southeastern blocks by a meridional fault. The most part of a subsided block is covered by thick flows of the Quaternary andesite–basaltic lava. Quartz molybdenum veins are confined to ruptures of shearing and fissures along the fault within the uplifted northwestern block.

Altogether, 41 quartz veins and zones of hydrothermally altered rocks have been identified within the deposit. The veins strike northeast with a variable limb from 30° to 85° and dip to the southeast and sometimes to the northwest at angles from 50° to 90°. Ore veins are mainly controlled by pre-ore dykes of diorite porphyrite composition. The thickness of veins and zones varies from 0.1 to 1.8 m. Molybdenum content varies from 0.01 to 0.2 %, copper from 0.01 to 0.3 %, lead from 0.001 to 1.83 %, and zinc from 0.01 to 0.74 %.

Veins of a lens from are separated in some places by stepped faults with amplitude of displacement from a range of 0.5–2.0 m up to 10 m. Veins are composed mainly of quartz; the main ore-forming minerals are pyrite, molybdenite, galenite, and sphalerite. Mineralization is represented by nests and stringers in quartz mass. Veins have brecciated and banded texture owing to imposition of late quartz–polymetallic and quartz–carbonate stage on quartz–molybdenite stage of mineralization. The secondary minerals are chalcopyrite, secondary copper sulfides, bornite, covellite, chalcosine, anglesite, cenissite, malachite, azurite, and limonite. Mining, technological, hydrogeological, and the relief conditions of the deposit are favorable enabling to develop the deposit by horizontal underground mining.

2.2.2.4 Alunites

Alunite resources are known to exist in the Zaglic deposit and the Seifali and Dugli occurrences (Azizbekov et al. 1972; Ismailzadeh et al. 2008).

The Zaglik deposit

The Zaglik alunite deposit is confined to the northeastern side of the Dashkesan syncline composed of volcanogenic and sedimentary formations of the Middle and Upper Jurassic being intruded by the polyphase Upper Jurassic granitoid massif. The deposit is known since the Middle Ages, when alum has been produced from alunites. The host volcanosedimentary sequence upward includes the Upper Bajocian porphyrites, agglomeratic lava, yellow tuff–sandstone, tuff–conglomerate, and tuff–sandstone which are overlain by a thin bed of argillites and sandstone. The cross section is followed by carbonate rocks of the Oxfordian and Lizitonian suites being covered by yellow tuffites and extrusive–effusive diabase porphyrites. The topmost volcanogenic section is subdivided into lower tuffogenic, lower effusive, upper tuffogenic, and upper effusive series with a total thickness of 600 m. The lower tuffogenic series of 250 m thick was subjected to intensive metasomatic reformations during the intrusive magmatism.

The composition of metasomatized rocks is changing over a distance from the intrusive massif reflecting the changes of a temperature regime. The metasomatic rocks are associated with the intrusion host magnetite skarns mineralization. Westward, these rocks transfer to silicified rocks and then into the alunites series with some propyllitization in the transition zone. Based on this zonation, the deposit has been subdivided into (a) northwestern alunite–iron ore area; (b) Alunitdagh alunite–siliceous area; (c) Kirvadagh alunite–propyllite area; (d) Zaglik alunite area; and (e) Western Zaglik kaolinite–alunite area.

The alunite series of rocks has a gentle (10°–15°) dip to the southwest. Thrusts up to 30 m uplifted the southern blocks in relation to the northern ones. Based on degree of alunitization, morphology, composition, and admixtures of ores, eight textural and structural types of mineralization have been distinguished in the alunite series of rocks. Besides alunite, the primary minerals of alunite rocks are kaolinite, propyllite, quartz, hematite, and limonite. The secondary minerals are chalcedony, opal, monothermite, zunyite, pyrite, diaspore, halloysite, corundum, fluorite, magnetite, ilmenite, sericite, chlorite, and barite.

The thickness of the upper alunite section varies from 4 to 39 m with an average thickness of 19 m. It has a limited distribution and pinches out within a short distance. The lower alunite section of the deposit has a wide distribution. Main minerals of industrial significance are alunite and quartz (95 % of the volume) and clayey minerals (5 %) represented by kaolinite, dickite, and halloysite. Less important weakly alunitized rocks are represented mainly by quartz, clayey minerals, volcanic glass, and hematite. Hydromicas, chlorite, calcite, and pyrite are observed in some places. Due to economic and technical reasons, the exploitation of the Zaglic alunite deposit is currently suspended. The remaining reserves were estimated as about 160,000,000 tons.

The Seifali alunite occurrence

This occurrence is located in the Shamkir region and confined to hydrothermally altered rocks of the Middle Jurassic (Bathonian) of the Alabashli iron ore deposit. Similar to the above Zaglic deposit, the alunite mineralization is likely to be hosted by the Upper Jurassic rock series. Major genetic types of mineralization are (a) titanium–magnetite sandstone; (b) intensively hematitized volcanogenic rocks; and (c) alunitized and kaolinized volcanogenic rocks. The cross section of this occurrence demonstrates a vertical zonation with distinguished downward in layers of (a) alunite–quartz with little content of dickite and kaolinite; (b) alunite–dickite–kaolinite–quartz; (c) argillite–sericite; and (d) propyllites. Gradual transitions are observed between these zones. The alunite content varies in a wide range from 9.52 to 57.0 %.

2.2.2.5 Bauxites

On the territory of Azerbaijan, bauxites have been initially found in the Sadarak region of the Nakhchivan AR in the Arpachay River basin. The mineral exploration within this river basin has identified the existence of the Geransgalasi, Gabakhyal, Myunkhbala-ogl, Gabakdagh, Sadarak, Danzik, and Kyarki bauxite occurrences. The occurrences are hosted by terrigenous–carbonate formations of the Devonian and Carboniferous systems and carbonate formations of the Permian and Triassic systems. Magmatism is weakly pronounced and represented by dykes and layered injections of diabase and gabbro–diabase. Bauxites and bauxite-bearing rocks are confined to the lower section of the Permian formation occurring on various rock formations of the Lower Carboniferous. The bauxite-bearing section is overlapped and underlies everywhere by carbonate rocks and outcrops on the surface in a form of two strips.

The specific feature of bauxites and bauxitic clays is their red and reddish brick color, clearly distinguished on a background of dark gray and black limestone. Bauxite-bearing rocks of gray and light-gray color are also met. The main morphologic type are layers with lens-shaped bodies. Leguminous, oolitic, and polytomorphic structures are typical. Conglomerate and brecciated varieties are met in some places. The bauxite-bearing layer has been traced over a distance from 1.5 to 2 km with a thickness from 2 to 13 m.

The Geran-galasi occurrence

The occurrence has been found on the left bank of Arpachay River, south of Ashagi Yaidji village in the periclinal part of the anticlinal fold. Two outcrops of bauxites are represented by red, reddish brown, gray, and greenish gray varieties in the upper part of bauxite-bearing section. The bauxite-bearing lateritic profile is represented by clayey, loose, and conglomerated rocks with typical leguminous, leguminous–oolitic, and pelitomorphic structures. The thickness of the profile varies from 2 to 8 m depending on a volume of loose sediments. The distribution of bauxites in the bauxite-bearing section is uneven. The lower part of the section is dominated by red bauxitic clays which tend to increase gradually upward reaching the even ratio with legumes in the middle part of the section. In the upper part, legumes dominate over cementing material. Bauxites with a silica module over 2.1, allites, and sialites are the major rocks in the section. The content of Al_2O_3 varies from 30 to 57 %. Mineralogically, bauxites of the Nakhchivan region are of metamorphosed type where the large part of goethite transformed into hematite, gibbsite discontinued to exist as trihydrate of aluminum and beohmite–diasporic association with corundum admixture had originated in bauxites. This occurrence is of mineralogical interest only.

2.2.2.6 Copper

Copper mineralization is the most widespread type of mineralization in the metallogenic provinces of the Azerbaijanian part of the Greater and Lesser Caucasus (Azizbekov et al. 1972; Atlas 2000; Ismailzadeh et al. 2005, 2008). Copper deposits are involved in all stages of metallogenic development of Azerbaijan and are characterized by a wide range of formational types. The most productive types of copper mineralization are pyrite and porphyry copper types. Copper deposits on the southern slope of the Greater Caucasus are of massive pyrite type. Copper deposits within the Lesser Caucasus are typical to all tectonic zones of Azerbaijan except the Goycha-Garabagh zone with its ophiolite belt where pyrite and porphyry copper formation types are dominant.

The metallogenic province of the Greater Caucasus

Copper deposits within the metallogenic province of the Greater Caucasus are concentrated mainly in the Zagatala-Balakan ore region. The proven reserves and resources of copper ore are associated with massive pyrite and copper–lead–zinc–pyrite types represented by stratiform deposits in sandy–shaley formation of Jurassic age (Kurbanov et al. 1967; Agayev 1982; Akberov et al. 1982; Azizbekov et al. 1972; Kurbanov 1982).

The Zagatala-Balakan ore region proved to host the large Filizchay and medium Katsdagh and Katekh deposits of pyrite–polymetallic ores of the copper–lead–zinc–pyrite type. Mineable reserves of the Sagator, Jikhikh and Karabchay deposits of copper–zinc ores of the copper–zinc–pyrite type have also been estimated. More detailed data on these deposits are given in the Lead and Zinc section. The industrial development of these copper deposits will be

feasible only by integrated utilization of large reserves of pyrite–polymetallic deposits. The extensive mineral exploration program for copper–pyrite mineralization within the southern slope of the Greater Caucasus has been launched following the discovery of the Mazimchay deposit.

The Mazimchay copper-pyrite deposit

The Mazimchay copper–pyrite deposit is located 20 km from Balakan city of Azerbaijan near the confluence of Balakhanchay and Mazimchay rivers at the altitude from 1500 to 2200 m. The deposit occupies an area from 6 to 7 km in a highly mountainous area with relief uplifts from 200 to 1200 m. The Mazimchay deposit is located within a distance of 500–600 m to the south from the Katsdagh pyrite–polymetallic deposit. The combined proved reserves of these two deposits can serve as the additional raw material base of the Filizchay mining and processing enterprise in the future.

Tectonically, the Mazimchay deposit is located at the intersection of the Tufan and Sarbash tectonic zones of the Greater Caucasus being separated by the Kekhnamedan deep-seated fault of overthrust nature of 1.5 km wide. Numerous crosscutting sills and dykes of diabase porphyrites, liparite–dacites, and gabbro–diabase hosting copper–pyrite and pyrite–polymetallic ores have been found within the deposit. The deposit is confined to the southern overturned limb of the Katsdag anticline composed of sandy–shaley formations of the Katsdagh series of the Pliensbachian and Toarcian suites of the Lower Jurassic. Coarse-laminated rocks of this series are saturated by magmatic formations such as lava–basalts, spilites, and diabases and have been subdivided into three seams.

The lower seam is represented mainly by dark-gray clayey shales with separate beds of laminated sandstone. In the top of the seam, there are pockets of thin flysch. The middle seam consists of clayey shales enriched by accumulations of concretions, syngenetic with sedimentation, and globular segregations of pyrite and pirrhotite of economic interest. The upper seam is characterized by rhythmic intercalation of sandstones, aleurolites, and clayey shales with an increased thickness of sandstones upward of the section. The total thickness of the section varies from 1950 to 2200 m.

The structure of the deposit is tectonically complex. Rocks of the Katsdagh series are crumpled in longitudinal linear folds and cross-flexures intensively complicated by cleavage along axial plane, zones of plastic flow, and tectonic faults. Faults of sublatitudinal and northwestern extension are united into two systems. The sublatitudinal faults are generally conformable with a lamination of overthrusts being concentrated in a strip of 500 m wide in parallel to a large Kekhnamedan fault, passing to the south of the deposit. Upthrusts–overthrusts with a large thickness enclose dykes and sills of diabase and ore-bearing zones including that of the Mazimchay deposit. The thick ore-bearing zone of the Mazimchay deposit is confined to a zone of hydrothermally altered and crumpled rocks with a stringer-impregnated mineralization of pyrrhotite–chalcopyrite composition. This mineralized zone of sublatitudinal direction has been traced over a distance of 5 km with distinct swells and pinches along its strike and dip. The thickness of two separate ore bodies of vein type with saturated stringer and fissure filling mineralization varies from 0.6 to 14 m.

Lens-shaped bodies of massive ore have also been observed within this zone. As a rule, massive pyrrhotite–chalcopyrite ores transform into stringer and fissure filling/impregnated ores of the same composition along the strike of this zone. Morphologically, ore bodies have tape and lens form with slightly pronounced contacts and metasomatic processes within enclosing rocks. The grade of copper in ore-bearing dykes is higher than that in ores of sandy–shaley formations.

Pyrrhotite in association with chalcopyrite has been observed as stringers and small lens-shaped bodies and pyrite in a disseminated form. The share of quartz, calcite, ankerite, biotite, and other rock-forming minerals in the fissure-impregnated types of ores is at a range of 80–85 %. The grade of major mineral component, copper, varies from 0.55 to 13.3 % with an average grade of 2.33 %. Associated minerals are cobalt, bismuth, gold, silver, and sulfur. Technological feasibility study on flotation enrichment of a 500 kg sample has proved recovery of 97.6 % of copper in 27.2 % copper concentrate and pyrrhotite–pyrite product with 37 % of sulfur content and 38.1 % of sulfur extraction. The associated metals of copper concentrates are 50.2 % of gold, 59.1 % of silver, 73.5 % of bismuth, and 63 % of cobalt. The combined share of noble metals (gold, silver) and bismuth in copper concentrate substantially increases the value of this product.

The detailed mineral exploration has been conducted by a combination of underground mining openings and adits, drilling, and underground geophysics. The inferred reserves of copper ore and copper metal have been estimated. By reserve/resource categorization scheme, the deposit is rated as a medium-class copper deposit. The deposit is planned for development by underground mining upon availability of investment.

The metallogenic province of the Lesser Caucasus

The metallogenic province of the Lesser Caucasus hosts the copper deposits of massive copper–pyrite and porphyry copper types as well as polymetallic deposits with a major

copper component of various genetic types (Kerimov 1964; Azizbekov et al. 1972; Kerimov and Kerimov 1974; Aliyev 1976; Kerimov et al. 1986; Babazadeh et al. 1990; Kerimov et al. 1996).

The Lesser Caucasus is generally characterized by a complex polymetallic and polycyclic metallogeny being defined by various patterns of spatial distribution of various metals including copper, lead, zinc, molybdenum, mercury, antimony, and gold. The Lesser Caucasus is known as one of the ancient areas of copper ore development. At present, numerous places of ancient production and reworking of copper ores at the Alaverdi, Shamlig, Miskhana, Gedabek, Zangazur, and Shanardara ores are known to exist within the Azerbaijanian part of the Lesser Caucasus.

In the proximity to the Azerbaijanian part of the Lesser Caucasus, development of the Gafan and Alaverdi copper–pyrite, Gafan and Agarak copper–molybdenum deposits in Armenia and the Madneul copper deposit in Georgia is being continued. The large-scale geological mapping and mineral exploration programs within the Azerbaijanian part of the Lesser Caucasus have proved high prospects for copper and copper-bearing polymetallic mineralization. Based on the results of these works, the following prospective metallogenic zones have been delineated:

- The Lok-Garabagh metallogenic belt includes the Gazakh, Gedabek, Dashkesan, Murovdagh, Mekhmana, and Garabagh ore regions hosting the Gedabek, Garadagh, Khar-Khar, Goshgarchay, Gyzylbulagh, Damirli, Khachinchay, and Zardaryn deposits of massive copper–pyrite, porphyry copper, and complex polymetallic ores.
- The Goycha-Hakera metallogenic belt includes the Kelbadjar and Lachyn ore regions.
- The Kelbadjar-Gochaz metallogenic belt with its Dalidagh ore region.
- The Gafan metallogenic belt.
- The Ordubad-Zangazur metallogenic belt with the Ordubad ore region hosting the Diakhchay, Shalala, Geygel, Paragachay and other deposits of porphyry copper and copper–molybdenum ore.

Brief overview of major types of copper deposits in the above-mentioned ore regions of Azerbaijan is provided below.

The Gedabek ore region

The Gedabek copper–pyrite deposit with associated gold is located to the northwest of Gedabek district center in the exocontact zone of the Gedabek granitoid massif of the Jurassic–Early Cretaceous age and gabbroids of the Late Jurassic age.

The deposit is hosted by volcanogenic formations of the Lower Bajocian, the Upper Bajocian series of quartzose plagioporphyries, effusive pyroclastic formations of the Bathonian stage, strongly schistosed tuffogenous–sedimentary deposits of the Callovian–Oxfordian stage, and carbonate deposits of the Lusitanian stage. As a result of magmatic activity, the carbonates of the Lusitanian stage have been transformed into vesuvian–garnet–wollastonite and mixed skarns. The process was accompanied by the formation of quartz diorites and numerous dykes of plagioclase, diorite, and diabase porphyrites and, rarely, of aplite and kersantite. Tectonically, the deposit is confined to the anticlinal fold of the northwestern direction complicated by parallel faults and fractures. The complex tectonic position of the deposit has favored concentration and localization of various mineralization. The mineralization was mostly found in secondary quarzites of mono-quarzites of mono-quartz, quartz–sericite and quartz–kaolinite facies, and, partially, hornfels around a local volcanoplutonic structure. These ore-bearing secondary quarzites of sedimentary and subvolcanic nature are overlaid by a series of epidotized, keratinized, and chloritized formations and their pyroclasts, frequently with impregnated sulfide mineralization represented mainly by pyrite and, rarely, chalcopyrite.

Morphological types of ore bodies are stocks and lenses of high-grade massive pyrite ores and large stockworks of stringer-impregnated fissure filling ores of poor grade. Stocks and lenses of massive ores are represented by covellite–bornite–chalcosine–chalcopyrite–pyrite association of minerals, sometimes with galenite and sphalerite. Stringer-impregnated ores of large stockworks contain chalcopyrite–chalcosine–quartz–pyrite association, in some places, with barite, covellite, bornite, and native copper. Major metals of copper–pyrite ores are copper, gold, and silver, and associated minerals are lead, zinc, molybdenum, cobalt, and others. Six individual stocks with a length from first tens to several hundred m and a width up to several tens of m are known within the deposit. These stocks have been expoitated by the Siemens Company before 1917. The stringer-impregnated type of mineralization with relatively poorer grades of metals in stockworks usually frames stocks of high-grade ores. Limonite, sulfur, melakonite, manganese oxides, malachite, azurite, chrycolla, gypsum, melanterite, and epsiolite are found in the oxidation zone of ore bodies. A zone of cementation is rather distinctive containing covellite, rare chalcosine, and native copper with native silver and cuprite in some places. Substantial remaining reserves of gold, copper, and silver have been evaluated in mine dams and tailings of ancient and old mining workings of the deposit.

The scale of stringer-impregnated type of mineralization with presence noble metals, favorable, geographic,

economic, and mining-technical conditions define high prospects of the Gedabek deposit for mining investment.

The Novo-Gorelovka deposit

The Novo-Gorelovka deposit of copper–zinc ores is known since the end of the nineteenth century in the Gedabek region. The deposit is hosted by the Upper Bajocian quartz plagioporphyries as well as volcanoclastic and volcanic formations of the Bathonian stage of the Middle Jurassic with a total thickness up to 600 m. This volcanogenic formation is intruded by the Novo-Gorelovka Late Jurassic granitoid massif composed mainly of quartz diorites. In the exocontact zone of this massif, rocks of the Bathonian suite are intensively silicificated, sericitized, epidotized, and ferrunginated. Tectonically, the deposit is confined to the anticlinal fold of the second order, dislocated by the Novo-Gorelovka fault of a dome structure. The fault is likely to play an essential role in localization of mineralization.

The ore body of a stock shape contains mainly sphalerite and chalcopyrite. Marcalite, pyrrhotite, galenite, chalcosine, and hydroferrum oxide are the secondary minerals. Quartz and barite are major cementing minerals. The texture of ore is massive. Chalcopyrite forms nests and stringers. The deposit is genetically associated with post-magmatic activity of the Novo-Gorelovka intrusive massif. The deposit requires additional mineral exploration to judge its economic prospects.

The Battibulagh copper–mercury deposit

The Battibulagh copper–mercury deposit is known to occur in the Gedabek ore region since 1850. Mineral exploitation has been conducted by Siemens Company during 1910–1911 and 1916–1917. The deposit occurs in volcanogenic formations of the Lower Bajocian suite with a thickness more than 300 m being intruded by the pre-Bathonian Atabek-Slavyan plagiogranites. Intensive hydrothermal alteration of volcanogenic formations is represented by sericitized, silicificated, kaolinized, and epidotized rocks. Rocks of vein type are represented by dykes of diabase porphyries and, rarely, of diabase. Tectonically, the deposit is confined to the northern limb of anticlinal fold of latitudinal direction. The Gedabek ore-controlling fault of submeridional direction plays an essential role in the structure of the deposit and localization of mineralization.

The impregnated type of ores is mainly of quartz–pyrite composition and that nest-vein type of enargite–barite composition. Impregnated ores are widespread though the intensity of mineralization is gradually decreasing with a depth. Major ore minerals are chalcopyrite and enargite. The nest-vein type of mineralization forms irregular nests, lenses, and veins among quartz–sericite rocks. The main ore minerals are enargite, and pyrite, chalcopyrite, galenite, sphalerite, and barite are found rarely. Main cementing minerals are sericite, rarely quartz, and kaolinite. Enargite–barite ores are characterized by a limited development on a depth yielding to impregnated pyrite ores. The deposit requires further exploration to identify its economic prospects.

The Garadagh porphyry copper deposit

The Garadagh porphyry copper deposit is located in the Gedabek ore region, 600 m to the west–southwest of Chanlibel village and 30 km from the adjacent Shamkir railway station. The deposit is confined to the eastern part of the large Atabek-Slavyan massif of plagiogranites which serves as an intrusive frame of porphyry copper system. The area of the deposit is characterized by a complex geological structure and is composed of andesites, andesite–porphyrites, liparite–dacite porphyries, and their rudaceous facies of the Upper Bajocian age. These volcanic rocks are intruded by the Atabek-Slavyan massif of plagiogranites, small stocks of quartz–diorite porphyries, and subvolcanic bodies of liparite–dacite porphyries and are crosscut by a series of dykes of diabase and quartz–diorite porphyrites. Tectonically, the area of the deposit is confined to the knot of intersection of the Maarif-Khar-Khar-Chanlibel fault of submeridional extent with faults and fractures of the northeastern and the northwestern orientation, which defined its stockwork inner structure.

The thickness of the cementation zone varies within 20–80 m reaching 130 m in some places. The zone of secondary pyrite enrichment is of economic interest. The grade of copper and molybdenum varies from 0.4 to 1.0 % and from 0.001 to 0.1 %, respectively. Small nests and stringers of turquoise of practical interest have been observed at the boundary of the zone of leaching and the zone of cementation. The zone of primary ores is represented by secondary quarzites, partially silicificated diorites–porphyrites, plagiogranites with impregnated thin stringers and small nests of pyrite, rare chalcopyrite, and more rare—molybdenite.

The major metals of economic interest are copper and molybdenum, with associated gold and silver. Exploration drilling has contoured the ore body with a variable barite copper grade from 0.3 to 0.45 %. The thickness of the productive section varies from 200 to 250 m with an average content of copper from 0.64 to 0.68 % and that of molybdenum from 0.005 to 0.006 %. By reserve/resource categorization scheme, the deposit is regarded as a medium by its reserves and as a large deposit by its projected resources. Feasibility studies on floatation scheme of ore enrichment indicate the extraction of combined copper–molybdenum concentrate with a recovery of copper at 88 % and

molybdenum at 50 % with associated gold and silver. Laboratory tests on heap-leaching of ores of the Garadagh deposit indicate a good recovery of copper with low grades.

The deposit is planned for development by open-pit mining. Favorable geographic and economic conditions place the deposit into a category of highly prospective targets for investment of exploitation works. The Gedabek ore region also hosts the Maarif, Beyuk-Kalachy, Maschit, and other small occurrences of porphyry copper.

The Murovdagh ore region

The Murovdagh ore region hosts a number of copper and molybdenum, lead, zinc, and other mineral deposits and includes the Goshgarchay and Gyzyl-Arkhach ore fields. The Goshgarchay ore field includes the Goshgarchay deposit, Goshgardagh occurrence of porphyry copper, and the Chanakhchi and Zivlyan occurrences of copper–pyrite ores. The Gyzyl-Arkhach ore field hosts the Gyzyl-Arkhach, Kechaldag, Djamilli, Elbekdash, and other occurrence of porphyry copper.

The Goshgarchay ore field

The Goshgarchay ore field is located in the central part of the northwestern flank of the Murovdagh anticlinorium made up of the Lower Bajocian andesite–basalt subformation and differentiated basalt–andesite–rhyolitic formation. The Goshgarchay porphyry copper deposit of this ore field is a typical example of porphyry copper mineralization of the whole Murovdagh ore region.

The Goshgarchay deposit

The Goshgarchay porphyry copper deposit is located within a distance of 10–12 km to the southwest from Khoshbulag village of the Dashkesan region. The deposit is mainly composed of the Bajocian volcanogenic formations being intruded by rocks of the Goshgarchay granitoid massif. Rocks of volcanogenic series are represented by effusive plagioclase–pyroxene, plagioclase, and diabase basalts, andesite–basalts, andesites, and their pyroclasts. Intrusive rocks include gabbro, gabbro–diorites, diorites, quartzose diorites, and porphyry granodiorites. Steeply dipping multiple dykes of diorite, quartz–diorite, and gabbro–diabase porphyrites are cutting the above intrusive and volcanic rocks.

The intermediate zone consists of quartz–sericite–chloritic facies of secondary quarzites, occupying an area of 1200 m in length by a range of 400–600 m in a width. Porphyry copper mineralization of vein-impregnated type is distinctly superimposed on this facies of secondary quartzites. The third external zone is represented by propylitic facies of secondary quarzites hosting streaky-impregnated stockwork ores and quartz and carbonate veins with disseminated pyrite, chalcopyrite, and molybdenum mineralization.

The stockwork body of the central part of the deposit occupies an area of 0.4 km^2 in the apical and peripheral parts of the intrusive massif of porphyry structure hosting ten enriched areas of copper mineralization with a copper grade above 0.3 %. The largest area is of 0.12 km^2 in size. These mineralization zones are hosted and intercalated by barren and slightly mineralized rocks with copper grading up to 0.2 %. These enriched areas on the surface are likely being combined at a depth into a unified ore body of a stockwork type with a complex morphology.

The grade of copper varies from 0.2 to 2.5 % with an average grade of 0.4 % with associated molybdenum, gold, silver, and cobalt. The grade of gold in some intervals is more than 1.0 ppm and that of silver is from 2.5 to 40 ppm, which are well correlated with a copper content for porphyry type deposits.

Along with a stockwork type of mineralization in the southern and southeastern parts of the deposit, the vein type of copper mineralization indicates some prospects of buried porphyry mineralization. The rare "Mantas" type of mineralization typical for numerous porphyry copper deposits of Peru and Chile is represented by chalcosine in association with quartz, calcite, and epidote which fill cavities has been observed in the deposit. The vertical profile of mineralization varies from 600 to 700 m. This deposit of economic interest is a target for investment and development.

The Garabagh ore region

The Garabagh ore region includes the Gyzylbulagh, Mekhmana, Gyulyatag, Damirli, Khachynchay, Agdara, and Gazanchay porphyry copper and the Khazinadagh copper–pyrite deposit and occurrences. The ore region is located in the southeastern part of the Lok-Garabagh tectonic zone and confined to a knot of intersection of the Agdam anticlinorium and the Dalidagh-Mekhmana uplift. The Garabagh ore region is characterized by a spatial linkage of various genetic and morphological types of sulfide mineralization. The ore region is hosted by the Middle–Upper Cretaceous sedimentary and volcanogenic–sedimentary rocks dislocated by faults of the northwestern, northeastern, and sublatitudinal directions and by intrusive massifs. The Damirli, Gyulatag, Khachinchay, and Agdara deposits and occurrences of porphyry copper are confined to exo- and endocontact zones of the Djanyatag intrusive massif of gabbro–diorite–granodiorite formation which intruded the Jurassic volcanites and, in some places, is unconformably overlain by more recent Cretaceous formations.

The Damirli porphyry copper deposit

The Damirli porphyry copper deposit is located within two km southeast of the Damirli village of the Ashderin district. The deposit is confined to the endo–exocontact zone of the Djanyatag intrusive massif. The mineralization is hosted by silicified and pyritized rocks of the granitoid massif and volcanic rocks of intermediate composition. These rocks are intruded by subvolcanic bodies of andesite–dacite and liparite–dacite porphyries being transformed into secondary quarzites. The structure of the deposit is complex being crossed by a series of closed faults of the northwest–submeridional and northeast–sublatitudinal directions with crosscutting dykes of granodiorite–porphyries, liparite–dacites, andesite–dacites, and diorites.

The deposit is represented by stockwork bodies of fissure filling-impregnated type with pyrite–molybdenite–chalcopyrite association, sometimes with chalcosine, bornite, and covellite. The area of development of copper mineralization is around a range of 5–6 km^2 being from 1.8 to 2.2 km wide and more than 3 km long. The deposit also includes six quartz–vein zones with gold sulfide mineralization traced over a distance from 4.5 to 8 km. The grade of gold is up to 5 ppm and that of silver is up to 91 ppm. The grade of copper in fissure filling and disseminated types of ore varies from 0.1 to 0.8 %, molybdenum from 0.001 to 0.2 %, gold from 0.1 to 0.2 ppm, and silver from 4 to 6 ppm.

Mineral exploration by drilling and geophysics has proved the extension of fissure filling and disseminated types of copper and molybdenum mineralization to a depth over 300 m. Given the large reserves of copper ore despite its relatively low grades, the deposit constitutes a target for open-pit mining in the future.

The Khachinchay porphyry copper deposit

The Khachinchay deposit of porphyry copper is located within 9 km northwest of Agdam city in the south–southeastern contact zone of the Djanyatag granitoid massif. The deposit is confined to the archy part of the local Eddikhirman brachyanticline of the Garabag uplift composed of intermediate and acid volcanics of the Middle and Upper Jurassic being intruded by stocks of granitoids. The mineralization is hosted by quartz diorites and diorites of the southern endocontact zone of the Djanyatag granitoid massif and, partly, by the Early and Middle Bathonian andesite–dacites and liparite–dacite porphyries.

The deposit is represented by a stockwork body of low-graded copper–molybdenum ores with associated gold and silver of higher grades confined to an area of conjunction of faults of the northwestern and northeastern directions. Numerous dykes of andesites, diorite–porphyrites, liparite–dacite porphyries and liparite, as well as hydrothermally altered rocks have been found within the deposit's area.

The total area of distribution of fissure filling and disseminated types of sulfide of mineralization is around 0.8–1.0 km^2 and that of the mineralized stockwork is 800–1000 m by 300–400 m. Copper grade varies from 0.1 to 0.6 %, molybdenum from 0.003 to 0.02 %, gold 2.2 ppm, and that of silver up to 30–40 ppm. The deposit did not undergo a detailed mineral exploration; however, given the intensity and character of sulfide mineralization, prospects of enclosing volcanic rocks for future discoveries of porphyry copper mineralization are very high. The other porphyry copper occurrences in the Garabagh ore region are very similar to the Damirli deposit. Given a widespread distribution of porphyry copper mineralization in exo- and endocontact zones of the Djanyatag intrusive massif, favorable tectonic and geologic environment, as well as positive results of geological, geophysical, and geochemical exploration, the Garabagh ore region represents one of the highly prospective targets for discovery of new porphyry copper mineralization of large scale.

The Ordubad ore region

The Ordubad ore region constitutes a part of the Mekhmana-Zangazur tectonic subzone hosting a number of known porphyry copper and molybdenum deposits. The region is sharply distinguished from other zones of the Lesser Caucasus and includes the known copper–molybdenum belt part of which is observed on the territory of the Nakhchivan AR of Azerbaijan.

Porphyry copper deposits of the Ordubad ore region were localized within the western part of the Megri-Ordubad granitoid massif, where the Paragachay, Diakhchay, Misdag, Goygel, Geydagh, Gekgyundur, Shalalag, and other deposits were found. The detailed mineral exploration and estimation of reserves has been completed only within the Paragachay deposit. The reserves and prospects of the rest of the deposits are unknown. At present, the exploitation of the Paragachay copper–molybdenum deposit has been suspended due to economic problems.

The Diakhchay deposit

The Diakhchay porphyry copper deposit is located in the central part of the Diakhchay ore field in the upper streams of the Ordubadchay River. The deposit is enclosed in monzonites, granodiorites, quartz diorites, granosyenites, quartz syenite–diorites, and granodiorites–porphyries being intruded by crosscutting dykes of granite–porphyries and diorite–porphyries. The mineralization is tectonically controlled by the Ordubad deep-seated fault being accompanied

by a zone of metasomatic rocks from 1.2 to 1.5 km wide. The major stockwork zone represents a system of fractures, fissure fillings, and impregnation of molybdenite, chalcopyrite, and pyrite in quartz syenite–diorites in a contact area in the south with hydrothermally altered gabbro–diorites and adamellites.

The stockwork zone is elongated along dykes of granodiorite porphyry or along a contact of intrusive rocks of various phases over a distance of up to 2 km. The thickness of the zone tends to increase in the areas of dykes jointing. Relatively intensive hydrothermal–metasomatic changes in the form of local feldspartization, biotitization, silicification, and sericitization are observed in tectonically reworked parts of the zone along contacts with dykes. The major ore minerals are copper and molybdenum of fissure filling and disseminated types. On the surface, the zone has been traced over a distance of 600 m. A width of the mineralized zone is 140 m with the most intensive mineralization from 40 to 100 m.

Mineral exploration of the deposit by drilling and adits indicates a copper grade on the surface from 0.66 to 1.3 % up to 2.0 % and that of molybdenum from 0.001 to 0.003 %. The grades of copper and molybdenum tend to decrease with a depth with 0.7 % of copper and 0.0022 % of molybdenum. The mineralization has been traced up to a depth from 350 to 400 m.

The Sarkidagh and Fakhlidara occurrences of copper–molybdenum ores were found in the northwestern and southeastern parts of the Diakhchay ore field, respectively. The occurrences are represented by stockwork zones with a variable copper grade from 0.4 to 2.44 % and a molybdenum grade from 0.01 to 0.02 %. The proximity of these occurrences to the Diakhchay deposit increases the economic prospects of the Diakhchay copper–molybdenum ore field for future development.

The Misdagh deposit

The Misdagh deposit is located in the Ordubad region on the southwestern slope of the Zangazur ridge in the upper streams of the Vanandchay River. The deposit is confined to the endocontact of the Megri-Ordubad granitoid massif and is basically composed of quartz, monzonites, monzonite diorites, diorite syenites, diorites, and gabbro–diorites. Major structural elements are tectonic faults and associated fractures of submeridional and northwestern directions. The mineralization tends to be associated with separate fractures, dykes, and zones of jointing of the northeastern direction. The deposit is represented by a series of numerous closed steeply dipping ore zones including 18 prospective zones concentrated within an area of 0.3 km^2. The distance between zones varies from a range of 15–20 to 100–150 m. On the surface, the mineralized zones have been traced from 300 to 700 m with a variable thickness from 0.5 to 10 m. Most part of the zones strikes in the northeastern direction and dip at 60°–85° northwest. On the recent erosion level, these zones were traced to a depth of more than 350 m. Ore bodies are represented by veins and stockworks characterized by frequent swells and pinches of veins. The thickness of lenticular ore bodies in swells is increasing up to 40 m and is reducing up to 0.5 m in pinches.

Distribution of major metals in the ore bodies is irregular. The grade of copper varies within a wide range from 0.2 to 7.2 % with an average grade from 1.3 to 2.5 %. Associated metals of economic importance are molybdenum, cobalt, and gold in some veins. Major ore minerals are magnetite, chalcopyrite, sphalerite, galenite, pyrrhotite, and cubanite and those of the oxidation zone are malachite, azurite, bornite, chalcosine, limonite, goethitte, and hydroferrum oxide. A high content of copper in veins and fissure zones is accompanied by accumulation of disseminated copper mineralization in host rocks with a copper grade from 0.1 to 0.4 % that substantially increases the economic prospects of the deposit. Due to complex mining and geological conditions, the deposit has not been studied at a depth.

The Geygel deposit

The Geygel deposit is located within 8 km northeast of the Nyurgyut village in the watershed of the Zangazur ridge. The deposit is subdivided into the northern, central, and southern areas. Mineralization of stockwork type is confined to rocks of the granodiorite–porphyry phase of the Megri-Ordubad intrusive massif being intruded by dykes of granodiorite porphyries. The deposit is tectonically controlled by a system of faults and fractures of submeridional (20° NE) and northwestern (270°–290° NW) direction being healed by dykes of diorite porphyrites and granite–porphyries, respectively. More intensive mineralization has been observed within the central part of the deposit containing five ore-bearing zones of sublatitudinal direction and several hundred meters long. Almost all stages of mineralization typical for porphyry copper deposits of the Ordubad ore region are present in this deposit. The central area of the deposit is considered to be of economic interest owing to commercial concentration of porphyry copper–molybdenum mineralization.

The Geydagh deposit

The Geydagh porphyry copper deposit is located in the confluence of the Alindjachay and Gilyanchay rivers. The area of the Geydagh deposit hosts the Khanaga-Ortakend and Bashkend occurrences as well as the major Djadakhli,

Dikyurt, Muradkhanli, and Gyumushdara individual stockwork ore bodies localized in intensively dislocated and hydrothermally altered andesite–dacite porphyrites, quartz–syenite–diorites, tuff–sandstone, tuff–gravelites, and other rocks. The length of ore bodies varies from 390 to 500 m and the width from 200 to 470 m. Copper–molybdenum mineralization has been traced at a depth from 420 to 680 m. The average content of copper in ore bodies varies from 0.28 to 0.66 % and that of molybdenum from 0.008 to 0.011 %. Associated lead–zinc mineralization is confined to selvages and dykes of diorite–porphyries. Galenite and sphalerite are mainly of fissure filling and disseminated types. A thickness of mineralized intervals varies from 16 to 50 m grading 0.35 % of lead and 1.19 % of zinc. The inferred reserves of copper have been estimated. The deposit requires additional mineral exploration to judge its economic prospects.

The Gekgyundur deposit

The Gekgyundur deposit is confined to a zone of intensive jointing along the main Ordubad and Vardanichay faults composed of rocks of early adamellite phase of the Megri-Ordubad intrusive massif and late quartz syenite–diorites, porphyry granosyenites being intruded by dykes of diorite, and granodiorite–porphyries. The ore-bearing zone is confined to a contact area of granodiorites and was traced from 1200 to 1500 m long and from 480 to 600 m wide. Mineralization is presented by stringer-impregnated, stockwork, and vein types. The major stockwork of the deposit with copper mineralization reaches a thickness up to 168 m grading 0.85 % of copper.

On the southwest flank of the deposit, the thickness is decreasing being split into several steeply dipping bodies with a thickness from 14.5 to 28 m found at a spacing interval from 200 to 300 m. The grade of copper in these bodies varies from 0.53 to 0.65 % and that of molybdenum does not exceed 0.001 %. Similar situation is observed on the northeastern flank of the deposit where three individual bodies have been traced from 300 to 500 m with a thickness from 10 to 20 m. The grade of copper is from 0.74 to 0.77 % and that of molybdenum is up to 0.001 %. Such morphology of the stockwork deposit is defined by its tectonic position and peculiarities of internal structure of the ore-bearing zone of the deposit. Chalcopyrite, molybdenite, and pyrite are the basic ore minerals. Secondary minerals of copper are covellite, bornite, malachite, and chrysocolla. Copper reserves are unknown.

The Shalala deposit

The Shalala deposit is hosted by quartz and syenite–diorites of the second intrusive phase of the Megri-Ordubad granitoid massif. The deposit is represented by a zone of stockwork mineralization of up to 300 m wide and 800 m long hosting four closed ore bodies of a complex morphology with a thickness from 7 to 100 m. Basic ore minerals, chalcopyrite, bornite, molybdenite, and pyrite, form impregnations and stringers. The content of copper in the ore bodies varies from 0.11 to 7.8 %. The most intensive mineralization was found in an isolated ore body of up to 300 m from 410 m deep with an average thickness of 41.5 m. The average grade of copper is 0.5 % and that of molybdenum is 0.006 %. Two zones with a thickness of 30 and 14 m were found in interdyke interval running in parallel to the major ore body. The grade of copper is up to 0.84 % and that of molybdenum is from 0.005 to 0.025 %. Further mineral exploration is likely to lead to new discoveries of porphyry copper–molybdenum mineralization of economic interest.

The Darridag-Paradash ore region

This region represents the area of development of the Oligocene–Early Miocene volcanism associated with concentration of numerous small-scale occurrences of ferrous metals. Copper mineralization in this region is close to one of the most productive copper sandstone types. Numerous occurrences of copper of the Ashabi-Kahf group are confined to rocks of volcanosedimentary series of the Oligocene age along the north–northeastern flank of the Nakhchivan superimposed trough being controlled by the Nakhchivan Fault. Three copper-bearing beds within the Oligocene rocks form a copper belt of up to 60–70 km long hosting around twenty areas with a high copper mineralization. The number of copper-bearing beds within this belt varies from one to four with a variable thickness from 0.6 to 9.0 m. The grade of copper in beds varies from 0.25 to 1.56 %. Impregnated copper mineralization is represented by native copper, cuprite, chalcosine, azurite, and malachite. The Ashabi-Kahf group of occurrences is of potential economic interest owing to a polymetallic character of mineralization.

Mercury

Mercury mineralization is present in all metallogenic provinces of Azerbaijan, but its intensity is uneven in various zones due to tectonic faults separating different structural and formational zones of the Greater and Lesser Caucasus (Kashkay et al. 1970; Azizbekov et al. 1972; Suleimanov and Babazadeh 1974; Kashkay and Nasibov 1985). Mercury deposits are traced in the form of isolated zones or chains along the extended folded and tectonic structures of the Lesser Caucasus. Based on a distribution pattern of mercury mineralization, the southern, central, and the northern zones of mercury mineralization have been distinguished within

Table 2.20 Classification of mercury deposits and occurrences in Azerbaijan

Formational type	Mineral type	Typical mineral associations	Host rocks	Structural and orphological types	Shape of ore bodies	Hydrothermal alterations	Sample of deposits and occurrences
Mercury	Magnesite–carbonaceous	Cinnabar Pyrite Chalcopyrite Bornite Orpigment Magnetite Millerite Quartz Calcite Dolomite Dikkite Alkerite	Serpentinite Magnetite Schists Andesite–dacite Sandstone Argillites	Lenses and veins in tectonically reworked areas along and in intersection of faults and structural zones	Lenses, veins	Magnesite, Schists Silicification Argilization	Shorbulag Agkaya Agyatag Sarydash Kamyshly Nagdolychay Chilgyazchay Guneyplin
Mercury	Carbonate–cinnabar	Cinnabar Pyrite Chalcopyrite Realgar Quartz Calcite	Limestone	Lenses and veins along steeply dipping tectonic dislocations and fractures	Lenses and pillars of complex morphology	Silicification Pyritization Calcitization	Narzali Arzuni Dumanli Millin and other deposits
Antimony–mercury	Quartz–carbonate–antimony–cinnabar (gasper type)	Cinnabar Antimony Pyrite Realgar Barite Orpigment Chalcopyrite Quartz Calcite Dolomite Dikkite Hydromicakaolinite	Limestone Volcanogenic Rudaceous Rocks Sandstone	Lenses-bearing veins and pillars along steeply dipping thrusts and interbeds' fractures	Stratiform and pillar-like veins	Silicafication, pyritization, argillization, jasperization	Levchay Novolev Eliz-gel
Antimony–arsenic		Realgar Antimony Quartz				Horfelns Selicitization Silicafication	Deveboyin Turschsuin

the Lesser Caucasus. Analysis of numerous data on distribution patterns of mercury mineralization identified the stratigraphic–lithologic, structural, and magmatic factors.

Mercury mineralization has been found in rocks of various lithology and stratigraphic intervals. The oldest mercury mineralization is associated with the Middle Jurassic volcanogenic formations and the most recent with the Mio-Pliocene tuffs and dykes of liparite–dacites. The intensity of mercury mineralization tends to increase from the Middle–Upper Jurassic–Lower Cretaceous deposits to the Upper Cretaceous formations. The Lower Senonian volcanosedimentary formations overlain by the Upper Jurassic limestone have been proved to be the most productive stratigraphic section hosting around 70 % of known mercury deposits in Azerbaijan. The major lithological varieties of the Upper Cretaceous interval are magnesite schists, limestone, conglomerates, rudaceous tuffs, sandstone, breccia, and clayey–siliceous rocks. Classification of mercury deposits and occurrences of Azerbaijan is given in Table 2.20.

The Shorbulag deposit

The deposit occurs in volcanogenic formations of the Bathonian suite, sedimentary–volcanic rocks of the Lower Senonian stage and intrusive rocks of ultrabasic, basic, and acid composition. Ultrabasites are represented by serpentinized dunites and peridotites of a lens shape elongated along tectonic faults of the northwestern direction. Mercury mineralization is controlled by tectonic dislocations of thrust type and hosted by tectonically reworked, crushed, schistose, and loose rocks being subjected to intensive silicification, carbonatization, and other hydrothermal metasomatic alterations. The major enclosing environments of mercury mineralization are hydrothermal metasomatic carbonate rocks. In some areas, cinnabar is confined to crushed and altered

porphyrites, argillites, as well as talcose and carbonatized serpentinites. Cinnabar is the main ore mineral with a limited presence of chalcopyrite and pyrite. Steeply dipping fissures filled by calcite and quartz create mercury-bearing zones in various directions.

In ore-bearing zones, cinnabar is observed in the form of impregnations, small nests, selvages, stringers, and other accumulations of various shapes. Among seven ore-bearing zones of the deposit, the first, third, and fourth zones have been found to be the most prospective. The position of the first zone is closely controlled by a fault along a contact of serpentinites with sedimentary–volcanogenic rocks of the Lower Senonian hosting a lens of magnesite schists with intensive cinnabar mineralization. The structural position of the third zone is very similar to that of the first zone. Mineralization here is represented by frequent impregnations and thin and short stringers of cinnabar in hydrothermal metasomatic carbonate and quartz rocks and altered porphyrites. Mineralization of cinnabar in the most extended fourth zone is confined both to listvenites and to dykes of diabase porphyrites occurring among listvenites. Ore bodies have irregular complex pillar and column shape elongated along the main ore-controlling fault dipping gently to the southeast. The grade and reserves of mercury in this deposit are not available.

The Agkaya deposit

The deposit is hosted by volcanosedimentary sequence of the Lower Senonian represented by silicified brown argillites with interbeds of tuff–sandstone, porphyrites, tuffs and quartz–sericite–chlorite shales and thick pelitomorphic limestone of the Upper Senonian age outcropped in the northwestern part of the deposit. Intrusive rocks are represented by serpentinized peridotites, gabbroids, stockwork bodies of diorite porphyrites, granodiorites and the recent Mio-Pliocene andesites, andesite-dacites, and rare liparites forming dykes and stockworks. The deposit occupies a small part of the Agkayachay anticlinorium and is confined to a zone of intersection of tectonic faults dividing the Geydara-Almali anticline and the Chichekli-Kongur syncline located to the north.

Mercury mineralization has been found in listvenites and metasomatic varieties of listvenites. In six ore-bearing zones discovered in the Agkaya deposit, only three ore bodies have been studied on the surface. The grade, reserves, and prospects of the deposit are unknown.

The Agyatag deposit

The deposit contains three areas of mercury mineralization confined to the Agyatag tectonic block. The first mineralized area is composed, mainly, of the Santonian tectonic breccia, jasperous brown argillites, dacites, serpentines, and listvenites. The distribution of mercury mineralization of stringer-disseminated type within the only ore body in this area is very uneven. The second ore area is also confined to a crossing tectonic block and composed, mainly, of tectonic breccia, listvenites, and dacites. Similar to the first area, the mercury mineralization of irregular stockwork shape is being structurally controlled by tectonic fault of upthrust–overthrust nature. The geologic and tectonic environment of the third mineralized area is very similar to that of the above two areas. The morphology of ore bodies within the deposit is rather complex reflecting an uneven distribution of mercury mineralization. In most cases, ore bodies are of column, pillar, lens, or irregular complex shape.

The major textural types of mercury ore are brecciated, impregnated, massive, crustal, veined, and earthy, where the first four types are dominant. Main ore mineral of the deposit is cinnabar, with quartz and calcite as cementing minerals. Secondary minerals are pyrite, arsenopyrite, rare chalcopyrite, sphalerite, hematite, and schwazite. Hypergene minerals are represented by metacinnabarite, linolite, scorodite, malachite, eruzite, chalcosione, and covelline. The grades and reserves of the deposit are unknown.

The Gamishli deposit

The deposit is located at a distance of 1.5–2.0 km to the south from Gamishli village of the Kelbadjar region on the left bank of the Levchay River. The deposit occurs in schistose, silicified, and partially brecciated sandy–calcareous–clayey deposits of the Santonian suite dislocated by numerous longitudinal and rare near-meridional faults with accompanied schistose serpentinites and gabbroids.

The deposit is confined to a recumbent contact of the Garabagh fault of upthrust–overthrust nature, where mercury mineralization in a form of scattered small impregnations of cinnabar was localized in silicified, brecciated, and pyritized listvenites being traced in latitudinal direction along the overthrust strip dipping at (60°–80°) to the north. A total thickness of a zone of altered, schistose, and unconsolidated rocks varies from 50 to 100 m reaching 200 m. This zone has been traced over a distance of 10 km running via the Tala occurrence till the middle stream of the Bulandyhsu River.

The ore body dips to the northeast at 50°–60° being composed of silicified, strongly brecciated and pyritized listvenites hosting fine disseminations, small nests, and thread stringers of cinnabar. The proved mercury reserves of this ore body up to a depth of 30 m are 20 tons. The size of the second ore body on the surface is 140 m^2, and the average mercury content is 0.17 %. Mercury mineralization

is hosted by silicified and brecciated listvenites bearing everywhere fine disseminations and impregnations of cinnabar, rare chalcosine, chalcopyrite, pyrite, ezurite, and malachite. A hanging side of the ore body is composed of silicified, brecciated, and pyritized argillites and a recumbent side of schistose serpentinites. The proved mercury reserves of this ore body up to a depth of 36 m are 22 tons.

The Chilgyazchay deposit

The deposit is located in the midstream of the Chilgyazchay River basin southeast of the Mt. Agkaya. The geological environment of the deposit in its southwestern part consists of the Cenomanian sandy–clayey sequence overlain by a seam of fine and medium clastic conglomerates. The mineralization is being controlled by the Nagdalichay upthrust hosting a thick zone of ore-bearing breccias overthrusted on tectonically reworked argillites. Industrial concentrations of mercury mineralization are confined to feathering fractures of the Agyatag-Nagdalichay fault with a pronounced role of structural–lithologic factors. The tectonic features of the deposit are mostly of the dominated Caucasian and cross-cutting meridional directions. These dislocations are accompanied by silicification, kaolinitization, limonitization, brecciation, and crushing of host rocks. Mercury mineralization within the deposit is confined to tectonic breccias, mainly formed by red jasperous argillites of the Santonian age. A lens-shaped body along the Chilgyazchay fault of up to 40 m thick has been found.

The Narzali deposit

The deposit is located 350–400 m east of the Kalafalikh village on the eastern flank of the Chilgyaz syncline. The deposit is hosted by coarse-grained terrigenous formations of the Coniacian–Santonian age, terrigenous–carbonaceous series of the Campanian and Maastrichtian ages of the Upper Cretaceous, and clayey–carbonaceous formations of the Paleogene. Coarse-grained terrigenous series of the Coniacian–Santonian age have been intruded by undifferentiated serpentinized ultrabasic rocks and gabbroids. Two close outcrops of small stocks of diorite, quartz, and plagiogranite have been observed in the northeastern part of the deposit. Metasomatic rocks are represented by listvenites and listvenitized rocks observed in the northern and northeastern part of the deposit along a tectonic zone and in a contact zone of serpentinized ultrabasic rocks with the Santonian terrigenous rocks. The deposit is spatially related to a zone of the Sultangoyunuchan (Kalafalikhchay) upthrust being characterized by a complex tectonic structure. Mercury mineralization of high grades was found in several small ore bodies occurring among limestone. These ore bodies are being controlled by steeply dipping faults and fractures of different directions. Morphologically, ore bodies of stratabound, nest, lens, vein, and irregular types have been found in various sections of a limestone interval along the strike. Grades and mercury reserves have not been reported.

The Levchay deposit

The Levchay deposit is located in the central part of the Garagaya-Elizgel anticlinal zone and composed of intensively dislocated and partially crushed sandy–clayey and calcareous rocks of the Upper Cenomanian age and subvolcanic formations (andesite–dacites, liparite–dacites) and their tuffs of the Mio-Pliocene. Rich accumulation of mercury was observed in the western part of the deposit coinciding with a submergence of the Aghdash anticlinal fold to the west. Three ore bodies with mercury and one ore body with antimony mineralization have been delineated and evaluated in the upper sections of the central part of the deposit.

All these bodies of stockwork, complex lens or irregular shape, and morphology are confined to a submersible part of the anticline. The archy part of the anticline is composed of crushed limestone transformed into jasperoids along a zone from 50 to 150 m wide. The ore bodies are confined to knots of intersection of meridional and latitudinal faults. Main ore minerals are cinnabar, antimonite, stibcinite, valentinite, realgar, orpigment, and metacinnabarite. Other minerals are calcite, quartz, bitumen, and gypsum.

2.2.2.7 Tungsten

The distribution of wolfram mineralization on the Azerbaijan territory is rather limited. For instance, are known several tungsten occurrences near the Kilit village of the Ordubad ore region of the Nakhchivan AR as well as in the central part of the Lesser Caucasus region in the Geydara, Konurdagh, Sarigash, Nadirkhanli and Nadjafli districts. The mineralization tends to be associated with the hyperbasitic belt development with adjacent outcrops of metal-bearing small intrusions of the Neogene age and skarn type mineralization in contact zone of the Dalidagh intrusive massif. The mineralization is represented, mainly, by scheelite in quartz veins, aplites, and veins of the Kilit and Dalidagh granitoid massifs. Heavy concentrations of scheelite have been panned in the Kelbadjar region in the basin of the Terter River and in upper streams of the Ildrimsu River and in the Nakhchivan AR in the Kilitchay-Pazmarachay area.

The Darridagh (Djulfa) arsenic deposit

The deposit is hosted by the Campanian and Maastrichtian limestone and marls, sandstone, and clays of the Danian

stage and the Pliocene, tuffogenous–sedimentary rocks with basal conglomerates of the Middle and Upper Eocene and volcanogenic–rudaceous rocks of the Lower and Middle Oligocene, which construct the Darridagh anticlinal fold of the northwestern strike. The northeastern limb of this anticlinal fold hosts interbedded intrusive massif of hornblende diorites. The mineralization in the northern part of the deposit is represented by realgar–orpigment ores of stockwork type, in the central part by antimonite ores of nest type and in the southern zone near arsenic source, by realgar of disseminated type. Arsenic mineralization tends to be controlled by fractures of near-meridional direction.

Main proved reserves of the deposit are concentrated in the southwestern part of the Darridagh mountain ridge in the Campanian–Maastrichtian and the Eocene marls and sandstone being controlled by a tectonic fault crossing the axial part of the Darridagh anticlinal fold. The ore body is represented by a nearly vertical stockwork which tends to widen with a depth. Four main mineral types of ores have been distinguished within the deposit. The first type is represented, mainly by realgar with slight admixture of antimonite. The second mineral type has the highest quality of ores, but observed more rarely than the first one. Orpigment predominates in mineral composition with minor realgar. The third mineral type of high quality of ores is observed rarely. Mineralogically, it is represented by finely disseminated orpigment of yellowish–greenish color with films of black earthy melnikovite. The fourth mineral type of low quality of ores and of any industrial importance is represented by slightly enriched host rocks.

The Djulfa (Darridagh) deposit

The geologic and structural position of the deposit is in "Arsenic" section above. Antimonite mineralization within the Djulfa deposit was found in three areas of the deposit where it is paragenetically associated with arsenic and other mineralization. The northwestern area of the deposit hosts the main reserves of arsenic ores where antimonite is observed in a form of small admixtures. The antimony grades in this area are very poor. The southeastern area is represented by mineral springs where antimonite is accompanied by realgar and orpigment. The antimony hydrogen (SbH_3) content in arsenic-bearing mineral springs of the Darridagh deposit is about 0.005 % and that in mineralized host rocks is minor. The central area of the deposit hosts nests, impregnated, and disseminated types of ore where the grade of antimony reaches 8 %. In the mineral composition of antimony ore, realgar has a subordinate position; secondary minerals are anhydrous and complex oxides of antimony represented by valentinite, servantinite, and stibcinite.

The Levchay deposit

The geologic and structural position of the Levchay deposit is given under "Arsenic" section above. Antimony mineralization was found in significant concentrations in a form of minor admixtures in mercury ore bodies and in independent accumulations. The antimony ore body of 1.5 m thick has been open by adit No. 1. The thickness of the ore body tends to increase with a depth reaching a range of 8–10 m at a depth of adit No. 6 which is 50 m downward from the level of the first adit. The main mineral of the ore body is antimonite which forms solid veins, stringers, lenses, and impregnations. The secondary minerals are cinnabar realgar, valentinite, and servantite. Quartz is the main vein mineral. Calcite in a form of stringers in silicified limestone is subordinate. Bitumens and clayey minerals are observed somewhere. The antimony content is about 5 %.

2.2.3 Gold

Gold mining in the Transcaucasian territory including the Lesser Caucasus has been known for a long time. According to historical data, some gold-bearing areas were developed in VI-I centuries BC. Geological research, mapping programmes, and mineral exploration have led to a discovery of gold deposits and occurrences and associated genetic presence of gold in ores of copper–pyrite, porphyry copper, and copper–polymetallic deposits of Azerbaijan (Babazadeh and Malyutin 1967; Azizbekov et al. 1972; Abdullayev et al. 1979; Kurbanov et al. 1981; Kerimov et al. 1983, 1996; Hasanov and Aliyev 1984; Suleimanov and Guliyev 1986; Suleimanov et al. 1986; Mansurov 1998; Atlas 2000; Ismailzadeh et al. 2008).

In the Azerbaijanian part of the Lesser Caucasus, gold mineralization is typical for the following metallogenic belts:

- The Lok-Garabagh belt: gold–sulfide and gold–sulfide–quartz mineralization;
- The Goycha-Hakeri belt: gold–sulfide–carbonate–quartz and gold–sulfide–quartz mineralization;
- The Kelbadjar-Gochaz belt: gold–sulfide quartz mineralization;
- The Ordubad-Zangazur belt: gold–sulfide and gold–quartz mineralization;
- The Gafan belt: gold quartz mineralization.

The Lesser Caucasus region is characterized by spatial combination of development of gold, copper, lead, zinc, silver, molybdenum, and other mineralization typical for regions with rejuvenated tectonic activity and magmatism.

Due to this spatial overlapping of gold, porphyry copper, copper–pyrite, copper–polymetallic, and other types of mineralization, the Lesser Caucasus is treated as a polymetallic gold-bearing metallogenic province with a complex polycyclic metallogeny. A spatial and genetic relationship of gold mineralization with subvolcanic magmatic formations of various compositions has also been identified.

An important role of structural control in localization of gold in fractured zones and blocks of volcanoplutonic constructions has been noted and proved. There are some prospects of discovering of new types of gold–sulfide mineralization in jasperoids and dolomites of carbonate series, carbonaceous shales, and secondary quarzites. Major morphological types of gold mineralization are steeply dipping veins and stockworks and those of gold–sulfide mineralization are gently dipping interbedded bodies and stockworks. The following four formational types of gold and gold-bearing complex ores have been distinguished: (a) gold deposits of gold–sulfide, gold–sulfide–quartz, gold–sulfide–carbonate–quartz, and gold–quartz ore formations; (b) gold-bearing deposits of complex copper–gold ore and gold–copper–polymetallic ores where gold is one of the basic components; (c) deposits of copper sulfides, massive copper, and porphyry copper types with substantial associated gold; and (d) porphyry copper deposits with gold traces.

The most productive terrains are magmatic formations of pre- and post-collisional stages associated with concentrations of polymetallic, copper, and molybdenum ores. The geochronologic dating of gold mineralization indicates a wide range in a concentration of gold ore found in all stages of the Alpine metalogenic epoch and pronounced in the Lesser Caucasus metallogenic province from the Bajocian to the Pliocene. Several small gold placers are represented by scattered alluvial, fluvial terrace, and alluvial–proluvial types being characterized by irregular gold distribution. The most prospective Gazakh, Gedabey, and Garabagh gold-bearing districts with proved gold reserves were found within the Azerbaijan part of the Lok-Garabagh metallogenic belt. Highly prospective occurrences of gold and complex gold-bearing ores were identified within the Dashkesan, Geygel, and Murovdagh ore regions and the Shusha-Fizuli potential area.

The Gazakh ore district

The Gazakh ore district is located in the northwest segment of the Lok-Garabagh zone covering the northeastern part of Ijevan-Gazakh transformal gold-bearing fractured zone from 26 to 30 km long. This ore district includes the Dagkesaman gold–copper–polymetallic deposit gold occurrences, numerous points of gold mineralization, geochemical halos, and small gold-bearing placers.

The Dagkesaman gold deposit

The deposit is represented by steeply dipping gold-bearing quartz veins containing ore intervals of a "pillars" type with a high content of gold. Gold is associated with quartz and pyrite, chalcopyrite, sphalerite, galenite, and other sulfides. More close association of gold is with quartz and chalcopyrite. The basic metal is gold with associated silver, lead, zinc, and copper. The ratio of gold to silver within the deposit is 1:4. Favorable geologic and structural position of the deposit, the cut-off grade, and scope of gold ore mineralization - all these factors indicate high prospects for its economic development.

The Gedabey ore district

The district belongs to the northern part of the Megri-Gedabey gold-bearing structure of a submeridional direction. The district incorporates the Gosha gold–sulfide and Gedabey copper–gold deposits with estimated gold reserves, the Garabagh and Khar-Khar, Maarif, Gizildja, Barum-Barsum, and Berezin deposits of fissure filling and disseminated types in porphyry copper deposits as well as the Itgirlan, Mundjukhlu, Badakend, and other occurrences of gold and gold–silver ores.

The Gedabey copper-gold deposit

The deposit of copper–pyrite type is known to occur in secondary quarzites being represented by fissure filling and disseminated sulfide–quartz mineralization of chalcopyrite–pyrite–quartz polymetallic formation of stockwork type, and partly by stocks and lenses of massive copper–pyrite ores. The major ore body of stockwork type and large size contains adjacent ore bodies with high copper and gold grades. The major metals are copper, gold, and silver. Given the favorable geologic and structural position of the deposit, the intensity and scope of mineralization, grades, and reserves, the Gedabey deposit constitutes the primary target for open-pit mining.

The Gosha gold deposit

The Gosha gold–sulfide deposit is confined to the Gosha anticline located on the northwest flank of the Shamkir uplift. The deposit is hosted by layered porphyrites intercalated with bands of their pyroclasts, quartz porphyries, and their tuffs. The volcanic section is intruded by quartz–diorites and a subvolcanic body of liparite–dacites of the Upper Jurassic age. Crosscutting dykes of diabases, andesites, and, rarely, liparite–dacites are widely developed within the deposit. The deposit is structurally controlled by a dense network of faults and fractures of the northwestern,

northeastern, submeridional, and sublatitudinal directions with gold-bearing metasomatites.

Ore bodies are represented by extended subparallel hydrothermally altered zones, quartz–sulfide veins, stockworks, and fissure filling and disseminated types of mineralization. Higher grades of gold were found in quartz–sulfide veins, mineralized zones, and stockworks. The main ore minerals are pyrite and native gold; secondary minerals are sphalerite, chalcopyrite, galenite, bornite, and coverlite. Other minerals are quartz, carbonate, sericite, chlorite, and kaolinite. Hydrothermal alterations are represented by schistosity, kaolinization, sericitization, and chloritization. The basic precious components are gold and silver having irregular distribution patterns. Gold mineralization was traced over 400 m deep by underground mining (Atlas 2000).

Reserves of gold and silver have been proved to be economic for development by underground mining. The adjacent Itgirlan, Mundjukhly, Shikhabat, and other gold and gold–silver occurrences on the flanks of the Gosha deposit enhance the prospects of the deposit. The Gedabey ore district is made up of the Paleozoic carbonaceous shales containing steeply dipping multiple quartz veins with sulfide mineralization and is considered potentially prospective for discovering of gold mineralization of black shale type. A wide distribution of geochemical halos of gold and hydrothermal metasomatites including gold-bearing secondary quarzites enhances the prospects of the Gedabey ore district for new discoveries of complex polymetallic deposits of base and precious metals.

The Garabagh ore district

The Garabagh ore district represents a part of the Lok-Garabagh metallogenic zone being confined to the Khachinchay-Terter uplifted isolated block of the northeastern part of the Dalidagh-Mekhmana transformal uplift. The ore district has been developed in the Middle Upper in the Jurassic volcanogenic, volcanosedimentary, and the Cretaceous terrigenous–carbonaceous formations. Mineralization is genetically associated with intensive volcanic activity during the Jurassic time being traced by numerous volcanostructural constructions. The most typical Djanyatag intrusive massif is composed mainly of quartz diorite, banatites, tonalites, and its varieties. Dykes of granite–porphyry, liparites, and granodiorite–porphyries are widely developed within the massif. A rather intensive gold mineralization has been superimposed on massive sulfide, copper–polymetallic, and porphyry copper mineralization. A clear zonation and distribution of porphyry copper, gold, gold–copper–polymetallic, and copper–gold deposits have been traced from the east to the west within the Garabagh ore district. The Garabagh ore district incorporates the Gyzylbulagh copper–gold and Mekhmana gold–copper–polymetallic field, the Damirli porphyry copper deposit, the Khatinbeyli, Sampas, and Eddikhirman groups of gold–sulfide–quartz occurrences, gold-bearing placers in the valleys of the Terter, Kabartichay, Gyulyatagchay, and Khachinchay rivers, as well as numerous halos of gold, copper, lead, zinc, molybdenum, and other metals.

The Gyzylbulagh deposit

The Gyzylbulagh copper–gold deposit is hosted by sedimentary–volcanogenic formations of the Middle–Upper Jurassic represented by polymictic conglomerates, tuff–sandstone of the Callovian–Oxfordian stage, lithoclastic tuffs of andesites of the Bathonian stage and covers and lithoclastic tuffs of liparite–dacites and andesite porphyrites of the Bajocian stage. This volcanosedimentary sequence is intruded by subvolcanic bodies, dykes of andesites, andesite–basalts and liparite–dacites and small intrusions of quartz diorites and diorite porphyrites of the Late Jurassic age. A dense network of faults and fractures has defined a block structure of the deposit. Mineralization is confined to a thick zone of crushed and schistose rocks in liparite–dacite porphyrites and their detrital facies. Two ore bodies are represented by elongated irregular stockworks hosting dense fissure filling stringer, impregnated, and nest-shaped mineralization. Ores are mainly represented by pyrite, pyrite–chalcopyrite, and quartz–pyrite–chalcopyrite mineral associations. The basic ore minerals are chalcopyrite, pyrite, and native gold; secondary minerals are sphalerite, bornite, galenite, marcasite, melnikovite, and arsenopyrite. Gold of irregular and isometric form has been found in chalcopyrite and pyrite as inclusions. The basic precious components are gold, silver, and copper.

Feasibility studies on technological properties and enrichment of ores in laboratory and semi-industrial conditions have proved the applicability of gravitational–floatation technology of ores reworking for obtaining conditional gravitational gold-bearing and floatational copper–gold concentrates. Mineral exploration by underground mining and drilling has proved the existence of reserves of gold, silver, copper, and other associated minerals of industrial categories suitable for development by open-pit mining. Stripped rocks of overburden have been found to be suitable raw material for production of rock aggregates and vitrified ceramic products.

The Mekhmana field

The Mekhmana gold–copper–polymetallic field contains more than 30 ore-bearing veinlet zones and veins. The detailed mineral exploration has been carried out over four

major veins. Calcite–quartz veins contain galenite and sphalerite mineralization of disseminated, nest types, and stringers of massive sulfide ore. Ores are mainly of gold–silver–copper and lead–zinc-bearing types. The major metals are lead, zinc, silver, and gold with associated cadmium, selenium, and tellurium. More detailed description of the Mekhmana deposit is given in (Atlas 2000). Given the intensity and scope of mineralization, the Garabagh ore district is referenced as one of the highly prospective targets for noble and complex polymetallic deposits of the Lesser Caucasus region.

The Goycha-Hakeri metallogenic zone

This zone is located southward of the Lok-Garabagh metallogenic belt coinciding with the ophiolite belt of the Lesser Caucasus. The geological structure and mineralization are defined by abyssal fault being traced by outcrops of ophiolite rocks. The zone is characterized by the development of early, middle, and late stages of endogenous mineralization of the Alpine epoch being represented by chromite, gold–sulfide–quartz, and arsenic–antimony–mercury formations.

The Azerbaijanian part of the Goycha-Hakeri metallogenic belt contains a part of the Zod and Tutkhun deposits, the Soyutluchay, Gilichli-Alchalilg, and other groups of gold–sulfide–quartz and gold–sulfide–carbonate–quartz occurrences and the small Soyutluchay placer gold deposit. The zone is potentially prospective for discovery of deposits of finely dispersed gold in jasperoids and antimony–mercury deposits and occurrences. The larger part of gold reserves of the Zod gold–sulfide–quartz deposit is located in the Kelbadjar district of Azerbaijan at the border with Armenia.

The Tutkhun deposit

The Tutkhun gold–sulfide–quartz deposit is also located in the Kelbadjar district and includes the Gazikhanli, Agzibir, Gizilistan, Zargulu, and Galaboynu group of gold-bearing areas. The deposit is confined to the area of junction of the Goycha-Garabagh tectonomagmatic zone with the Dalidagh-Mekhmana transformal uplift. Gold mineralization was found along the longitudinal Agyatag-Zod strip of hyperbasites and granitoids. The deposit occurs in volcanic rocks of intermediate and alkaline composition and terrigenous–sedimentary rocks of the Cretaceous and Paleogene ages being intruded by complex ultrabasic and basic intrusions of the pre-Upper Cretaceous and alkaline magmatic rocks of the post-Middle Eocene. Widely developed metasomatites are represented by quartz–kaolinite, quartz–sericite, and mono-quartz facies of secondary quarzites.

The dominant part of gold–sulfide–quartz veinlets and veins is confined to granitoid massif. Ore bodies in steeply dipping vein zones of pillars and pipe shape are confined to areas of junction of faults and fractures of various limbs. The basic ore minerals are quartz, pyrite, galenite, sphalerite, tetraedrite, native gold, molybdenite, antimonite, and burnonite, and secondary minerals are carbonates, chalcopyrite, sericite, and chlorite. The major economic components are gold with associated silver, tellurium, bismuth, and antimony. Despite limited mineral exploration, the geologic and structural position of the deposit coupled with the intensity and scope of gold mineralization, wide distribution of metasomatic rocks, and a presence of gold occurrences on the flanks of the deposit contribute all to high prospects of the deposit for gold and complex polymetallic gold–silver-bearing ores.

The Agduzdagh deposit

The Agduzdagh deposit occurs in the upper streams of the Zarchay River in the Kelbadjar district. Mineralization here is associated in andesites, andesite–dacites, liparite–dacites, and their detrital facies. Morphologically, ore bodies are represented by steeply dipping vein zones and veins. Three major veinlet zones out of more than 30 vein zones and veins have been identified within the deposit. Hydrothermal alterations are expressed by schistosity, sometimes by kaolinization, carbonatization, serialization, and, in some places, by fine-dispersed pyritization. The main minerals of ore bodies are quartz, which occupies from 80 to 95 % of the volume being followed by calcite and kaolinite. Ore minerals are rare being represented by pyrite, magnetite, chalcopyrite, sphalerite, and other minerals. The major metal is gold with associated silver. Distribution of gold and silver is extremely uneven. Gold mineralization has been estimated by geophysics to extend to a depth from 600 to 800 m. The deposit has been explored on the surface and by underground mining up to a depth from 80 to 120 m. Based on estimated reserves of gold and vein quartz suitable for fluxes raw material, the prospects of the deposit for economic development are quite high. The Dalidagh ore district incorporates several gold–copper–molybdenum and gold–sulfide–quartz occurrences of vein type and gold–copper-bearing area in secondary quarzites (monoquarzites). Given the favorable geologic position, scale, and intensity of mineralization, the prospects of the Dalidagh ore district for development of gold and complex gold-bearing ores are very high.

The Ordubad ore district

The Ordubad ore district is located in the Ordubad-Zangazur metallogenic belt of the Nakhchivan AR occupying a vast territory of the western endo–exocontact zone of the Megri-Ordubad granitoid massif with multiple phases of magmatic activity. This ore district is characterized by a rather intensive complex polymetallic mineralization, forming substantial concentrations and various combinations of copper, molybdenum, lead, zinc, gold, and silver metals. The Agdara, Nasirvaz, and other deposits and occurrences of gold–copper–polymetallic formation and the Aport (Agyurt), Piyazbashi, Shakardara, Mundara, and other deposits and occurrences of the Ordubad group of gold–sulfide–quartz formation are the major targets for economic development within the Ordubad ore district.

The Aport (Agyurt) deposit

The deposit is confined to the area of intersection of the major Ordubad fault of the northwestern direction and the Vanandchay-Misdagh fault of the northeastern direction. The area of the deposit is composed of rocks of the Megri-Ordubad intrusive massif represented by granosyenites, quartzose, and quartzless syenite–diorites, and aplite–diorites. Quartzose syenite–diorites are prevalent. Ore bodies within the deposit are represented by zones of veins in hydrothermally altered rocks and by quartz–carbonate veins. Eight zones of veins out of twenty ore zones, which were identified within the deposit, have been studied in detail.

By its mineral composition, the deposit corresponds to gold–sulfide–quartz formation. The basic ore-forming minerals are pyrite and chalcopyrite; secondary minerals are magnetite, pyrrhotite, tennantite–tetraedrite, native gold, sphalerite, molybdenum, and others. Gold in ores is characterized by extremely irregular distribution. The basic economic metals of ores are gold, silver, and copper. Gold mineralization was traced to a depth of over 400 m by mineral exploration. The reserves of gold and silver have been evaluated. A gravitational–floatational technological scheme of ore processing has been worked out. A wide distribution of gold-bearing metasomatites, presence of a number of deposits with proved silver and gold reserves, and adjacent prospective occurrences in a favorable geological setting all substantiate high prospects of the area of the deposit for discovering new deposits of gold and gold-bearing complex polymetallic ores. By mining, technical, and geological conditions, the deposit is suitable for underground mining.

The Gafan metallogenic belt

The Gafan metallogenic belt is located in the southwestern part of Azerbaijan on the border with Armenia and includes the Vejnali ore district. Copper–polymetallic mineralization of stringer-impregnated type was found on the extent of ore-bearing zones of the Gafan deposit including the Vejnali quartz–gold deposit.

The Vejnali deposit

The Vejnali deposit is located at the territory of the Zangelan district on the border with Armenia and incorporates twenty-five gold-bearing vein zones. Proved mineable reserves have been so far evaluated within six vein zones. Ore veins and zones of the deposit are mainly represented by quartz–sulfide and, rarely, by quartz–carbonate–sulfide veins and hydrothermally altered disintegrated and brecciated rocks. Sulfides are dominated by pyrite with subordinate chalcopyrite. Arsenopyrite, tennantite, sphalerite, tellurium–bismuth, and native gold are met in low grades. Basic components of commercial value are gold, silver with associated copper, tellurium, and bismuth. A gravitational–floatational technological scheme of ores processing has been worked out enabling to obtain a high percentage of gold (96.5 %) and silver (97.4 %) extraction.

2.2.4 Non-metallic Minerals

Azerbaijan possesses abundant resources of non-metallic minerals which play an essential role in economic development of the country and constitute a substantial part of the mineral resources base in terms of a number of explored deposits, proved and potential reserves, and a variety of mineral types. The main genetic types of deposits of non-metallic minerals on the territory of Azerbaijan are endogenous, exogenous, and metamorphogenic, but a majority of the deposits belongs to a group of exogenous–sedimentary origin incorporating rock salt, gypsum, anhydrite, and phosphorites and all kinds of carbonate raw material, clays, sands, and sand–gravel deposits. Reserves of major non-metallic minerals and building materials of Azerbaijan are provided in Table 2.21. Distribution of non-metallic mineral deposits and occurrences in Azerbaijan is shown in Fig. 2.31.

2.2.4.1 Chemical Raw Materials

The deposits of chemical raw material group incorporate sulfuric pyrite, rock salt, dolomites, phosphorites, and barite.

Table 2.21 Reserves of non-metallic minerals and construction materials in Azerbaijan (Atlas 2000)

No.	Non-metallic minerals	Unit	Number of deposits	Reserves
1	Gypsum	Million tons	2	40.3
2	Anhydrite	Million tons	1	18.1
3	Alum	Million tons	5	5.6
4	Benthonite clay	Million tons	2	99.3
5	Saw stone, including	Million m^3	65	570.2
	Limestone,	Million m^3	54	512.7
	Sandstone,	Million m^3	1	0.44
	Tuff and tuff–sandstone,	Million m^3	9	51.0
	Travertine	Million m^3	1	6.1
6	Facing stone, including	Million m^3	23	58.3
	Limestone,	Million m^3	2	7.4
	Marbled limestone,	Million m^3	13	27.6
	Porphyrite,	Million m^3	1	0.92
	Travertine,	Million m^3	2	14.42
	Tuffs,	Million m^3	1	0.94
	Gabbro,	Million m^3	1	2.03
	Conglomerate,	Million m^3	2	3.23
	Teschenite	Million m^3	1	1.76
7	Cement raw mineral, including	Million tons	10	373.7
	Limestone	Million tons	4	242.02
	Clay,	Million tons	4	120.07
	Trass,	Million tons	1	4.56
	and volcanic ash	Million tons	1	7.05
8	Rock salt	Million tons	4	1301.6
9	Dolomites	Million tons	2	10.02
10	Quartz and quarzites	Million tons	2	7.59
11	Flux limestone	Million tons	1	50.8
12	Limestone for soda production	Million tons	1	244.6
13	Zeolite	Million tons	1	12.5
14	Quartz sands	Million m^3	3	20.0
15	Ceramic raw material	Million tons	2	19.0
16	Barite	Million tons	2	0.38
17	Pyrofillite	Million tons	1	6.5
18	Porcelain stone	Million tons	1	3.4
19	Bituminous sands	Million tons	3	3.5
20	Building stone, including	Million m^3	26	152.6
21	Clays	Million tons	94	191.7
22	Gravel–sand	Million m^3	68	1059.3
23	Building sand	Million m^3	16	68.0
24	Perlite–pumice	Million m^3	2	6.6
25	Mineral pigments	thou. tons	2	46.4
26	Iodine–bromine water	thou. m^3/day	5	250.5
27	Fresh underground water	thou. m^3/day	59	6 758.9
28	Mineral water	thou. m^3/day	29	19.8

Fig. 2.31 Distribution of non-metallic mineral deposits and occurrences in Azerbaijan (Atlas 2000)

NON-METALLIC DEPOSITS AND OCCURRENCES

PYRITE
45. Chiragidzor deposit
37. Chiragidzor-Toganali deposit
46. Toganali deposit

PHOSPHORITES
89. Geran galasi occurrence
88. Gumushlug occurrence

ROCK SALT
98. Nekhram deposit
93. Nakhchivan deposit
91. Pusyan deposit

DOLOMITE
99. Nekhram deposit

BENTONITE
10. Dashsalakhli deposit
9. Ali Bayramli deposit
7. Kaimakhli deposit
41. Upper Agdjakend deposit
15. Shamkhor deposit
18. Shikhandag deposit

FLUX LIMESTONE
43. Khachbulag deposit

KAOLIN AND REFRACTORY CLAYS
17. Chardakhli deposit
19. Gotul deposit
34. Kara-Murad occurrence
29. Anshapur deposit
28. Agekhush deposit
30. Danaer deposit
27. Zaglik occurrence
38. Mirzik deposit
32. Karabulakh deposit

SECONDARY QUARTZITES
20.. Kizildjin deposit
31. Getashen deposit
35. Chovdar deposit

PYROPHILLITE
39. Kirvakar (Sharukar) Deposit

ANDALUSITE
100. Paragachay deposit

SERPENTINE
53. Geidara zone
55. Zaidara zone
59. Nikolaev zone
60. Kiazimbin zone

TUFF-SANDSTONES
94. Daralin deposit

TUFF
57. Kilisalin deposit

MARBLED LIMESTONE AND MARBLE
90. Ulya-Novashen deposit
68. Vararak deposit
73. Zariinbakh deposit
74. Gorov deposit
85. Arakul deposit
5. Kazma-Kryg deposit
2. Akhchai deposit
4. Tengin deposit
44. Dashkesan deposit
76. Shushin deposit
65. Gulabli deposit

SAND AND GRAVEL
70. Bagramtapin
101. Lenkoran deposit
16. Mingechaur deposit
61. Boglypain occurrence
58. Khovatayoccurrence
54. Adjaris occurrence
62. Dzhamard occurrence
56. Leusky occurrence

ASBESTOS
71. Ipyak occurrence
52. Geidara occurrence

LIMESTONE AND CLAYS
42. Karadang deposit
11. Dash-Salakhlin deposit
14. Upper Oksuzli deposit
63. Chobandag deposit
13. Aidag deposit
72. Shushikend deposit

TRASS, VOLCANICASH, PUMICE
8. Kaimakhli deposit

GYPSUM
47. Upper Agdjakend deposit
48. Monashid deposit
50. Dostagir deposit
96. Shakhtakhtin deposit
97. Azazin deposit

CALCIUM CARBONATE
21. Kirovabad deposit
51. Mardakert deposit
12. Kazakh occurrence
22. Khailar occurrence

DIMENSTION AND FACING STONE
33. Guzdek deposit
40. Karadag deposit
82. Dovlyaterlin deposit
6. Dashsalakhlin deposit
64. Shakhbulag deposit

TRAVERTINE
95. Shakhtakhtin deposit
92. Buzgov deposit

PERLITE AND OBCIDIAN
67. Kechaldag deposit
66. Deve-gezu small deposit (obcidian)

GLASS SAND AND QUARTZ FOR GLASS INDUSTRY
49. Adjavelin deposit
3. Cuba deposit
24. Khyrdalan deposit
23. Geokmalin deposit
26. Kirmakin deposit
25. Stepan Rasin deposit

OPTICAL MINERALS
78. Martunin occurrence
75. Minishend (Archinprak) Occurrence
77. Ningin occurrence
69. Agkend (Siptakshen) Occurrence
79. Aranzamin occurrence
84. Tsakur deposit
80. Bagyin-Bashin area
81. Eoku area

CRYSTALLINE QUARTZ
1. Khavanchai, Komsomolsk Group of occurrences

AGATE
36. Adjikend group of deposits
87. Eivazlin deposit
86. Gurdzhulu occurrence
83. Gara-kishlak occurrence

Mineral commodities	Deposits under exploitation	Mineral occurrences
Pyrite		
Rock salt		
Dolomite		
Phosphorite		
Bentonite		
Flux limestone		
Kaolin and refractory clays		
Seconday quartzlites		
Pyrrophillite		
Andalusite		
Serpentive		
Asbestos		
Building materials and expanded clays		
Trass, volcanic ash, pumice		
Gypsum		
Calcium Carbonate		
Dimension and facing stones		
Travertine		
Tuff-sandstones		
Tuff		
Marbled limestone		
Gravel, sand		
Perlite and obcidian		
Ballasts		
Craft and semi-precious stones (agante)		
Opticla minerals		
Crystalline quartz		
Glass sand and quartz for glass industry		

Compiled by: Bairamov A.A., Gadzhiev T.G., Agakishibekova R.R. and Nagiev A.N.

Sulfuric Pyrite

Sulfuric pyrite is contained in all ore widespread formations of the Lesser and Greater Caucasus of Azerbaijan. The deposits of sulfur–pyrite, polymetallic, and copper–polymetallic ores of pyrite formation have an economic value. The deposits where sulfuric pyrite is the constituent of complex ores have been described in the section "Metallic minerals" above. All known large sulfuric pyrite deposits are concentrated within the Lesser Caucasus and confined to positive structures. These deposits are characterized by similar conditions of formation being confined to a series of quartz plagioporphyries of the Upper Bajocian age. Accumulations of sulfuric–pyrite ores of this series are linked with subvolcanic facies of the Upper Bajocian volcanism being represented by plagiogranite–porphyries.

The ore-enclosing quartzose plagioporphyries and their subvolcanic facies are distinguished by a high intensity of hydrothermal–metasomatic changes which have led to the formation of secondary quarzites. The formation of sulfur–pyrite deposits has occurred simultaneously with post-magmatic hydrothermal–metasomatic processes. The largest accumulation of sulfur–pyrite ores in Azerbaijan belongs to the Chiragideresi-Toganali group of deposits. The Chiragideresi, Chiragideresi-Toganali, and Toganali deposits and some occurrences are closely connected with each other owing to similar geologic and structural positions and chemical and mineral composition. The deposits differ from each other by morphology of ore bodies and textural types of ores. The deposits are hosted by volcanogenic–sedimentary rocks of the Middle Jurassic represented by quartzose plagioporphyries and being overlaid by the Cretaceous volcanogenic and volcanogenic–sedimentary formations. The deposits of sulfide pyrite ores are confined exclusively to quartzose plagioporphyries.

The Chiragideresi deposit

Sulfuric pyrite ores of this deposit with a high sulfur content are enclosed in stockworks of complex irregular shape and are widespread within the deposit. The contours of ore bodies are easily distinguished by a sharp decrease of a sulfur content. Other morphologic types of mineralization are nests and lenses. Out of seven ore stockworks known within the deposit, four ore stockworks have been mined out during the periods from 1905 to 1918 and intermittently from 1923 to 1968.

The Toganali deposit

Ore bodies of the Toganali deposit are localized in the upper part of quartzose plagioporphyries series near a contact with overlapping rocks of volcanogenic series. Mineralization of high grades and finely disseminated and impregnated types is concentrated in the upper sections of the quartzose plagioporphyries series and decreases with a depth. Small nests of massive pyrite mineralization are observed in some places.

The Chiragideresi-Toganali deposit

Ore bodies of the Chiragideresi-Toganali deposit represent a transition type of mineralization from impregnated ores of the Toganali deposit to massive ores of the Chiragideresi deposit forming stratabound a lens-shaped deposits of 120–300 × 100–400 m size. Sulfide mineralization in the above three deposits is basically represented by pyrite, with an exception of the Chiragideresi deposit wherein a presence of copper–zinc ores (chalcopyrite, sphalerite, tetrahedrite) has been observed. Marcasite, magnetite, ilmenite, hematite, and galenite are found sporadically. Massive and brecciated textures are typical for continuous ores and vein and impregnated textural types for discontinued mineralization with lower grades.

Besides, the above-mentioned deposits, the Slavyan, Gandzazar, and Gyulyatag sulfuric pyrite occurrences are known to exist in the Agdara district of the Lesser Caucasus. Mineralization is represented by vein-impregnated types with rare veins and lenses. The grade of sulfur varies from 15 to 18 % reaching 30 % in areas of continuous mineralization. A widespread distribution of ore-bearing quartzose plagioporphyries on the territory of Azerbaijan suggests high prospects for discovering of new deposits of sulfuric pyrite ores.

Phosphorites

Despite the absence of large deposits of phosphorites on the territory of Azerbaijan, an increased phosphorization has been identified in terrigenous–carbonaceous formations of the Middle and Upper Devonian in the Nakhchivan AR, in the Upper Cretaceous formations in the area of the southeastern submersion of the Greater Caucasus and in the Maykop suite of the Shdmakha-Gobustan area. A weak phosphorization was observed in the Middle Jurassic sandstone and the Upper Cretaceous conglomerates in the southern slope of the Greater Caucasus. Detailed exploration on the territory of the Nakhchivan AR has identified a presence of phosphorites in a cross section of the Famennian and Frasnian stages of the Upper Devonian in the East Arpachay River basin. The sequence is represented by alternation of clayey shales, limestone, quartzites, and sandstones. The interbeds of phosphorites are confined to beds of clayey shales with a variable thickness from 5 to 40 m.

Five neighboring areas of phosphorite-bearing rocks have been distinguished within the Arpachay River basin. Phosphorite-bearing seams strike in concordance with

enclosing series of rocks in the northwestern direction at the angle of 320°–340° dipping to the southwest with the angle from 25° to 45°. In some areas, the number of phosphorite-bearing beds varies from 3 to 17 with a thickness from 0.2 to 0.7 m each. Three natural types of phosphorites, namely the dominant oolitic, nodules, and phosphoritized host rocks, were distinguished within this area. The content of P_2O_5 varies in wide ranges for different strata from 1.17 to 15.75 %. The content of P_2O_5 in the most representative Gerangalasi occurrence varies from 3 to 8 % in eight phosphorite-bearing intervals, 5 to 8 % in three intervals of the Gumushlug occurrence, and 15.75 % in the fourth seam of the Ayvazkhan occurrence.

Barite

Around twenty barite deposits and occurrences that have been found on the Azerbaijan territory are represented by a vein type and often confined to marginal parts of anticlinoria in volcanogenic formations of the Middle Jurassic. The Chovdar, Gushchu, Zaglik, Bayan, and other barite deposits are located within the Shamkir anticlinorium. The Chaikend, Azad, Bashkishlak, and other deposits are confined to the Goygel uplift, and the Tonashen barite deposit was found within the Agdam anticlinorium.

A distribution of barite mineralization is controlled by relatively large faults and adjacent fractured zones, originated in archy zones of anticlines and in axial planes of folds. These fractured and compression zones of 5–6 m thick are often accompanied by brecciation and intensive hydrothermal alteration pronounced by silicification, kaolinization, sericitization, and chloritization. Typical morphological types of barite mineralization are veins and fissure fillings. A total number of barite-bearing veins within the barite deposits of Azerbaijan vary from ten to twenty, except the Chovdar and Bashkishlak deposits where the number of veins varies from 30 to 45. The veins of mainly northwestern direction are normally steeply dipping with variable angles from 40° to 85°. A thickness of veins varies normally from 0.15 to 2.0 m with an increased thickness in swellings of the Chovdar deposit up to 6 m. A general length of veins varies from 200 to 500 m with an exceptional length of some veins at the Chovdar exposit from 1000 to 1500 m.

A specific feature of barite-bearing veins at the Chovdar, Bayan, and some other deposits is their clear morphology stipulated by an alternation of barite veins with barren intervals. Hydrothermal alterations of host rocks along barite-bearing fractures are represented by quarzitization, calcitization, epidodization, sericitization, and chloritization. Textural varieties include foliated, latticed, and cellular types of barite in the upper sections of ore veins and cryptocrystalline and dense varieties in the lower sections. Well-formed crystals of barite are rare. Barite is the major ore mineral, and rarely associated minerals are quartz, calcite, fluorite, and fine-disseminated galenite. Within the Chovdar, Bashkishlak, and Bayan deposits, the concentration of galenite increases noticeably in the lower sections of barite-bearing veins. Minor pyrite, chalcopyrite, tennantite–tetraedrite, and sphalerites are observed in paragenesis with galenite.

A vertical zonation in all barite deposits is being traced by a dominant barite mineralization in the upper parts of veins through gradual transition to a lead–barite mineralization in the middle part to a completely polymetallic mineralization in the bottom sections of veins. Downward, barite is gradually replaced by quartz and, partially, by calcite and in lower sections by noticeable fluorite in association with polymetallic mineralization. The content of $BaSO_4$ varies from 70 to 95 %, density from 3.7 to 4.5 g/cm^3, CaO from 5 to 10 %, SiO_2 up to 10 %, and Fe_2O_3 from 1 to 2 %.

Zeolites

Zeolites are widely used in industry as sorbents, molecular sieves, catalysts for drying and refining of gas, extraction of valuable admixtures, filters of natural water, and other purposes. Among natural zeolites, the most valuable industrial varieties are highly siliceous clinoptilolites, mordenites, erionites, and chabasites. These minerals of zeolite group are widespread in Azerbaijan in volcanogenic–pyroclastic and sedimentary rocks of the Upper Cretaceous and Tertiary ages.

The Aidagh zeolite deposit

The deposit has been found 7 km northwest of Tauz town near the Baku-Tbilisi railway in carbonaceous–tuffogenic rocks of the Campanian stage of the Upper Cretaceous. The zeolite-bearing strata is represented by massive fine-grained heat tuffs of light, light-cream, and light-green colors, which has been raced over a distance of 2000 m with a variable thickness from 10 to 80 m with a dipping angle from 15° to 40°. The main minerals are clinoptilolite, quartz, and calcite with associated biotite and chlorite. The detailed mineral exploration has contoured two beds of zeolite-bearing tuffs with proven reserves of 10 million tons.

The average content of clinoptilolite is 30.4 % in the upper layer and 63.3 % in the lower bed. The central part of the deposit shows a high content of clinoptilolite from 60 to 99 %. The average chemical composition of the productive strata is 60 % of SiO_2, 1.24 % of MgO, 11.92 % of Al_2O_3, 2.12 % of K_2O, 1.4 % of Fe_2O_3, and 5.77 % of CaO. A lead content varies from 0.001 to 0.01 %.

There are good prospects for increased reserves of zeolite-bearing heated tuffs at the Aidagh deposit and the Upper Cretaceous trass bluish tuffs within the Koroglu deposit in the Gazakh district. A chain of zeolite occurrences similar to the Aidagh deposit was traced on the northeastern slope of the Lesser Caucasus. The presence of large reserves of analcimite enhances the value of these occurrences for zeolite production. Besides the Upper Cretaceous

formations, the Tertiary formations of the Talysh Mts. area contain zeolites in volcanogenic–sedimentary formations of the Paleogene–Neogene age. Beds of heated tuffs, tuffites, and traces among the Pliocene rocks are of special interest for zeolites. Prospects for zeolites are also associated with the Paleogene volcanogenic–sedimentary rocks in the Nakhchivan fold area and in the Kelbadjar superimposed trough.

Mineral Pigments

Geologic prospecting for mineral pigments on the territory of Azerbaijan has succeeded by discovering the large Danaeri and Chovdar deposits in the Dashkesan district and the Mirzik deposit in the Khanlar district. The deposits are hosted by hydrothermally altered rocks of volcanogenic series of the Middle Jurassic age. Pigments are related to a group of ferrum-oxide pigments corresponding to clayey ocher.

The Chovdar deposit

The deposit is located at a distance of 19–20 km southwest of the Ganja railway station partially coinciding with the Chovdar barite deposit. Technological properties of mineral ochers, occurring in stratified layer from 4 to 8 m thick, comply with the State's standards. The remaining reserves of ochers grading 32 % of Fe_2O_3 are 38,000 tons.

The Mirzik deposit

The deposit is located on the southern end of Mirzik village of the Khanlar district. The deposit of clayey ocher of golden color is confined to a large tectonic fault of the northwestern direction and gentle dip from 10° to 20°. A faults zone is filled with limonitized epidote–chlorite disintegrated rocks of lemon-golden-yellow color. Enclosing rocks as a result of supergenous processes have been completely reworked and transformed into dispersal ocher mass. Technological tests of paints made from the above pigments have showed good gentle coverage and susceptibility of vanish. The remaining reserves of the deposit are 8000 tons of ocher with a content of Fe_2O_3 from 40 to 49 %. The detailed mineral exploration for increasing the reserves has identified the new Danaeri and Sariyal deposits of orchres with a variable Fe_2O_3 content at the Danaeri deposit from 35 to 50 %. Other targets for development of mineral orchres are pigments of secondary origin known in the Jabrail district near Sumgayit city.

The Dashveisal occurrence

The occurrence is located 2.5 km northwest of the Jabrail district center in deluvial–eluvial sediments. A pigment-bearing layer from 0.5 to 3 m thick consists of detrital material with a clayey fraction of 48.57 %. The minerals are hydromicas, quartz, kaolinites, apartite, hematite, limonite, and calcite. The chemical composition is 46.88 % of SiO_2, 19.62 % of Al_2O_3, 9.38 % of Fe_2O_3, 8.44 % of CaO, 4.13 % of MgO, and 1.23 % of SO_3. Pigments of this occurrence are clayey ocher which is a raw material for dark-red paints of covering ability 20.4 g/m^2 and oil capacity of 27.18 %. Light-pink cement resistable to atmospheric erosion was obtained by pigments in addition to white clinker in quantity from 2.5 to 10 %. Proved reserves are estimated at 40,000 tons.

The Sumgayit occurrence

The occurrence is located on the right slope of the Sumgayit River valley, 20 km northwest of the Khyrdalan town being represented by red clays of the Tertiary age. The seam of clays with a thickness of 8 m is traced over a distance from 2.5 to 3 km. Clays are compact, of a red color with various shades; a clayey fraction is 98 %. Chemical composition is 54.88 % of SiO_2, 18.52 % of Al_2O_3, 7.78 % of Fe_2O_3, 3.13 % of MgO, 0.81 % of CaO, and 1.17 % of SO_3. Covering ability is 2.25 g/m^2, and oil capacity is 25.3 %. Pigments of this occurrence are related to clayey red types suitable for production of colored cement and linoleum. Proved reserves are estimated at 1 million tons. Other prospective areas of Azerbaijan for mineral pigments of various types, colors, and shades are colored varieties of the Tertiary clays of the Shamakhy-Gobustan foothill zone, hematites of the Alabashli area in the Shamkir district, and limonitized clays of the Nakhchivan AR.

References

Abasov, M.T., Kuliyev, G.G. and Jabbarov, M.J., 1999. Feasibility to employ multicomponent seismic survey in South Caspian Basin. *Geophysical Reading Dedicated to Memory of N.I. Shapirovsky*, 11-12 March, Baku, 41-43 (in Russian).

Abdullayev, R.N., Ismailov, A.I. and Kerimov. A.F., 1979. Gyzylbulagh caldera – A new volcano-tectonic morphostructure in the Mekhmana ore district. *Izvestiya*, *Acad. Sci. Azerb*., Ser.: Earth Sci., No. 4 (in Russian).

Abramovich, M.B., 1955. *Prospecting of Oil and Gas Deposits*. Aznefteizdat, Baku (in Russian).

Abrams, M.A. and Narimanov, A.A., 1997. Geochemical evaluation of hydrocarbons and their potential sources in the western South Caspian depression, Republic of Azerbaijan. *Marine and Petroleum Geology*, **14**, 451–468.

Agayev, S.A., 1982. On the peculiarity of structure conditions and zonation of Filizchay pyrite-polymetallic field. *Proceed. of TSNIGRI*, Moscow (in Russian).

Agayev, S.A., 1990. *Stratigraphy of the Jurassic Deposits of Azerbaijan* (*Greater Caucasus*). Baku (in Russian).

Akberov, M.A., Samedov, A.M., Mamedov, H.Sh. and Mamedov, I.A., 1982. On the peculiarities of morphology and natural types of ores in the Filizchay deposit. *Proceed. of TSNIGRI*, Moscow (in Russian).

Akperov, N.A. and Kasymov, A.A., 2003. Condition of depletion of reserves oil suite interruption in the Guneshli deposit. *Azerbaijan Oil Industry*, No. 11, 13–18.

Akhmedov, G.A., 1957. *Geology and Oil-Bearing of Gobystan*. Aznefteizdat, Baku (in Russian).

Akhmedov, A.M., Yusufzadeh, Kh.B., Tziger, B.M. and Tagiyev, E.A., 1973. *New Oil and Gas Deposits of Azerbaijan*. Azerb. Govern. Publ. (in Russian).

Aliyev, A.G., 1949. *Petrography of Tertiary Deposits of Azerbaijan*. Aznefteizdat, Baku (in Russian).

Aliyev, A.G. and Akhmedov, G.A., 1958. *Oil and Gas Reservoirs of Mesozoic and Tertiary Deposits in Azerbaijan*. Azerneftneshr, Baku (in Russian).

Aliyev, A.I., Bagirzadeh, F.M., Buniyatzadeh, Z.A. et al., 1988. *Oil and Gas Bearing of Azerbaijan Republic*. Элм, Баку (in Russian).

Aliyev, A.G. and Daidbekova, E.A. 1955. *Sedimentary Rocks of Azerbaijan*. Aznefteizdat, Baku (in Russian).

Aliyev, G.A., Akhmedbeyli, F.S., Ismailzade, A.D., Kangarli, T.H. and Rustamov, M.I. (V.E. Khain and Ak.A. Alizadeh, Eds.), 2005. *Geology ofAzerbaijan*, Vol. IV: Tectonics. Nafta-Press, Baku (in Russian).

Aliyev, I., Gadiyeva, T., Fasanov, F., Zohrabova, V., Nabiyev, M., Pashaly, N., Sarajalinskaya, T., Safarov, I., Seidov, A., Kheirov, M. and Efendiyeva, E. (Ak.A. Alizadeh, Ed.), 2005. *Geology of Azerbaijan*, Vol. **II**: *Lithology*. Nafta-Press, Baku (in Russian).

Aliyev, S.A., 1982. *Map of Thermal Flows of Depression Zones of Azerbaijan*, Scale 1:500,000. Mapping Factory, Leningrad.

Aliyev, S.A., Mukhtarov, A.Sh., Bagirly, P.J. et al., 2002. Geothermal investigations in Azerbaijan. In: (Ak.A. Alizadeh, Ed.) *Geology of Azerbaijan*, Vol. **V**, Physics of the Earth. Nafta-Press, Baku, 229–263 (in Russian).

Aliyev, V.I., 1976. Iron pyrite formations of the Lesser Caucasus. *D. Sci. Thesis*, Baku (in Russian).

Alizadeh, A.A., Akhmedov, G.A., Akhmedov, A.M. et al., 1966. *Geology of Oil and Gas Deposits of Azerbaijan*. Nedra, Moscow (in Russian).

Alizadeh, A.A., Akhmedov, G.A. and Zeinalov, M.M., 1972. *Mesozoic Deposits of Azerbaijan*. Nedra, Moscow (in Russian).

Alizadeh, A.A., Akhmedov, G.A. and Aliyev, G.-M.A. et al., 1975. *Estimation of Oil-Generating Properties of Meso-Cenozoic deposits in Azerbaijan*. Elm, Baku (in Russian).

Alizadeh, A.A., Salayev, S.G. and Aliyev, A.I., 1985. *Scientific Estimation of Perspectives Oil&Gas Bearing of Azerbaijan and South Caspian and Direction of Prospecting Works*. Elm, Baku (in Russian).

Atlas of Mineral Resources of the Escap Region, 2000. Vol. **15**, Geology and Mineral Resources of Azerbaijan. *United Nations*, N.Y.

Avdusin, P.P., 1952. *Rock Structure and Facies of Middle Pliocene of the Eastern Transcaucasian*. Acad. Sci. USSR, Moscow (in Russian).

Azizbekov, Sh.R., Alizadeh, K.A., Shikhalibeyli, E.Sh. and Gadjiev, T. G. (Eds.), 1972. *Geology of the USSR*, Vol. **47**, Azerbaijan Republic. Nedra, Moscow (in Russian).

Azizbekov, Sh.R., Agakishibekova, R.R., Alizadeh, A.A., Alizadeh, K. A., Aliyev, M.M., Akhmedov, A.M., Akhmedov, G.A., Bairamov, A.S., Gadjiev, T.G., Zhouze, B.P., Zaitseva, L.V., Kashkay, M.A., Mekhtiyev, Sh.F., Sultanov, A.D., Khalilov, A.G., Shikhalibeyli, E. Sh., Efendiyev, G.H. and Yakubov, A.A. (Eds.), 1976. *Geology of the USSR*, Vol. **47**, Azerbaijan Republic. Economic Deposits. Fossil Fuels (Oil and Gas). Moscow, Nedra (in Russian).

Babazadeh, V.M. (Ed.), 2005. *Mineral Raw Resources of Azerbaijan* (*Generation Conditions, Location Peculiarities, and Scientific Basis of Prognosis*). Nafta-Press, Baku (in Russian).

Babazadeh, V.M., Makhmudov, A.I. and Ramazanov, V.H., 1990. *Copper and Molybdenum Porhyrite Fields in Azerbaijan*. Azerneshr, Baku (in Russian).

Babazadeh, V.M. and Malyutin, R.S., 1967. Structure conditions and localization of gold mineralization within the Agduzhdagh ore field (Lesser Caucasus). *Scient. Notes of Azerb. State Univ*., Ser.: Geol.-Geogr., No. 2 (in Russian).

Babazadeh, B.K., 1964. *Classification of Oil and Gas Pools and Deposits of Azerbaijan and Rational Methodology of their Prospecting*. Nedra, Moscow (in Russian).

Bagirzadeh, F.M., Kerimov, K.M. and Salayev, S.G., 1987. *Deep Structure and Oil&Gas Bearing of the South Caspian MegaBasin*. Azgosisdat, Baku (in Russian).

Bailey, N.J.L., Guliyev, I.S. and Feyzullayev, A.A. 1996. Source rocks in the South Caspian. *Proceed. of the AAPG/ASPG research symposium "Oil and Gas Petroleum Systems in Rapidly-Subsiding Basins"*. Baku, Azerbaijan, 409–421.

Buryakovsky, L.A., Djevanshir, R.D. and Aliyarov, R.Yu., 1986. *Geophysical Methods of Investigating Geofluid Pressures*. Elm, Baku (in Russian).

Chung, K.-T., Ssu-Ching, C., Tit, Y. W., Ying-Sing, L., Cheng-I, W., and Ming, W.C., 2000. Mutagenicity Studies of Benzidine and Its Analogs: Structure-Activity Relationships. *Toxicological Sciences*, **56**, 351–356.

Collister, J.W. and Wavrek, D.A., 1996. δ13C Compositions of saturate and aromatic fractions of lacustrine oils and bitumens: Evidence for water column stratification. *Org. Geoch*., **24**, Nos. 8/9, 913–920.

Dadashev, A.A., Feyzullaev, A.A. and Guliyev, I.S., 1986. Vertical zonation of oil and gas generation from the data of isotope composition of carbon methane from mud volcanoes of Azerbaijan. *Express-Information*, *Ser. Oil&Gas Geology and Geophysics*, No. 6, 24–26 (I Russian).

Eppelbaum, L.V., Kutasov, I.M. and Pilchin, A.N., 2014. *Applied Geothermics*. Springer, Heidelberg – N.Y. – London.

Feyzullayev, A.A., Guliyev, I.S. amd Tagiyev, M.F., 2001. Source potential of the Mesozoic-Cenozoic rocks in the South Caspian Basin and their role in forming the oil accumulations in the Lower Pliocene reservoirs. *Petroleum Geosciences*, **7**(4), 409–417.

Feyzullayev A. A. and Lerche, I., 2009. Occurrence and nature of overpressure in the sedimentary section of the South Caspian Basin, Azerbaijan. *Energy Exploration & Exploitation*, **27**, No. 5, 345–366.

Feyzullayev, A.A., Tagiyev, M.F. and Lerche, I., 2008. Tectonic Control on Fluid Dynamics and Efficiency of Gas Survey in Different Tectonic Settings. *Energy Exploration and Exploitation*, **26**, No. 6, 363–374.

Gorin, V.A., 1934. On the problem of stratigraphic division of Productive Series of the Absheron peninsula. *Azerbaijan Oil Industry*, No. 3, 70–72 (in Russian).

Gorin, V.A., 1958. Genetic zones of the oil&gas bearing of the South Caspian Depression and oil and gas origin. *Doklady Acad. Sci USSR*, Vol. **122**, No. 4 (in Russian).

Gubkin, I.M., 1934. *Tectonics of South-Eastern part of the Caucasus in connection with Oil and Gas Bearing of this Region*. ONTI, Leningrad-Moscow (in Russian).

Guliyev, I.S. and Feyzullaev, A.A., 1996. Natural hydrocarbon seepages in Azerbaijan. Near Surface Expression of Hydrocarbon Migration. *AAPG Hedberg Research Conf*. April 24–28, Vancouver, British Columbia, Canada. Memoir 1996, 63-70.

Guliyev, I.S., Fransu, U., Muller, R., Feyzullaev, A.A. and Mamedova, S.A., 1991. Geological-geochemical peculiarities of oil and gas bearing of Alpine intermountain basins. *Geochemistry*, No. 1, 148–156 (in Russian).

Guliyev, I.S., Levin, L.E. and Fedorov, D.L., 2003. *Hydrocarbon Potential of the Caspian Region* (*System Analysis*). Nafta-Press, Moscow-Baku (in Russian).

Guliyev, I., Radjabov, M., Feyzullayev, A. and Gambarov, Yu., 1989. On the searching of petroleum fields in the South Caspian Basin at

the depth of 7–12 km. *Proceedings of session, dedicated 50-s anniversary of Geology Institute of Az. Nat. Acad. of Sc*. Baku. Elm, 40-46 (in Russian).

Gurgey, K., 2003. Correlation, alteration, and origin of hydrocarbons in the GCA, Bahar, and Gum Adasi fields, western South Caspian Basin: geochemical and multivariate statistical assessments. *Marine and Petroleum Geology*, **20** (10), 1119–1139.

Hasanov, M.A., 1982. Peculiarities of structure of the Katsdagh pyrite-copper polymetallic deposit. *Proceed. of TSNIGRI*, Moscow (in Russian).

Hasanov, R.K. and Aliyev, A.A., 1984. Some features of structure and mineralogical-geochemical peculiarities of ores in the Gyzylbulag field. *Proceed. of TSNIGRI*, Moscow (in Russian).

Huseynov, D.A., Aliyeva, E., Nummedall, D., Guliyev, I. and Friedmann, J., 2004. Oil Source Rocks in the Lower Pliocene Deltaic-Lacustrine Successions in the South Caspian Basin. *Proc. AAPG Hedberg conference "Sandstone deposition in lacustrine environments: Implications for exploration and reservoir development"*, May 28–21, 2004, Baku, Azerbaijan, in CD.

Inan, S., Yalcin, N., Guliyev, I., Kuliyev, K. and Feisullayev, A., 1997. Deep petroleum occurrences in the Lower Kur Depression, South Caspian Basin. Azerbaijan: an organic geochemical and basin modeling study. *Marine and Petroleum Geology,* **14**, Nos. 7/8, 731–762.

Ismailzadeh, A.D., Mustafayev, G., and Rustamov, M. (Ak.A. Alizadeh, Ed.), 2005. *Geology of Azerbaijan*, Vol. **3**: *Magmatism*. Nafta-Press, Baku (in Russian).

Ismailzadeh, A.,D. Mustafayev, Q.V., Abdullayev, Z.B., Mamedov, M. H., Nagiyev, V.H., Mahmudov, A.I. and Aliquluyev, Q.Q. (Ak.A. Alizadeh, Ed.), 2008. *Geology of Azerbaijan*, Vol. **VI**: *Mineral Resources*, Nafta-Press, Baku (in Russian).

Jafarov, P.P., Gadjiev, S.G. and Alimuradov, Sh.E., 2003. Peculiarities of geological structure of Absheron archipelago in the light of new data. *Azerbaijan Oil Industry*, No. 12. 14–18 (in Russian).

Kashkay, M.A., 1947. *Basic and Ultrabasic Rocks of Azerbaijan*. Baku (in Russian).

Kashkay, M.A., Aliyev, V.I., Mamedov, A.I. et al., 1970. *Petrology and Metallogeny of Magmatic Formations in the Tutkhun Basin*. Baku (in Russian).

Kashkay, M.A. and Nasibov, T.N., 1985. Mercury zones of the Sevan-Akera structure in the Lesser Caucasus. *Geology of Ore Deposits*, No. 6 (in Russian).

Katz, K.J., Richards, D., Long, D. and Lawrence, W., 2000. A new look at the components of the petroleum system of the South Caspian Basin. *Jour. of Petroleum Science and Engineering*, **28**, 161–182.

Kerimov, A.D., 1964. *Petrology and Ore-Bearing Granitoid Intrusive of Mekhmana*. Baku (in Russian).

Kerimov, A.D. and Kerimov, F.A., 1974. Structure-genetic peculiarities of the copper-molybdenum field in the Gey-Gel region. *Izvestiya, Acad. Sci. Azerb*., Ser.: Earth Sci., No. 2 (in Russian).

Kerimov, A.F., Aliyev, A.A. and Hasanov, R.K., 1996. Geological-structural peculiarities and conditions of formations of the copper-gold Gyzylbulag deposit. Baku (in Russian).

Kerimov, A.F., Zamanov, Yu.D. and Musayev, Sh.D., 1986. Criterion of mineralization of pyrite-polymetallic deposits in volcanic regions. *Trans. of Workshop "Geology. Geochemistry and Ore-Bearings of the Lesser Caucasus and Talysh"*, Baku (in Russian).

Kerimov, K.M. and Pilchin, A.N., 1986. Geothermal regime of the sedimentary cover of depression areas of Azerbaijan and Caspian Sea. *Azerbaijan Oil Industry*, No. 1, 9–13 (in Russian).

Kerimov, A.F., Shekinsky, E.M., Musayev, Sh.D. and Zamanov, Yu. D., 1983. The types of gold mineralization of Azerbaijan. Proceed. of the All-Union Geological Conf., Moscow (in Russian).

Khalilov, N.Yu. and Imanov, A.A., 1980. Prognosis of anomaly high pool pressure in the process of prospecting drilling. *Geology of Oil and Gas*, No. 5, 41–45 (in Russian).

Klosterman, M.J., Abrams, M.A. Aleskerov, E.A., Abdullayev, E.N., Guseinov, A.N. and Narimanov, A.A., 1997. Hydrocarbon system of the Evlakh-Agdzhabedi depression. *Azerbaijan Geology*, No. 1, 89–118.

Korchagina, Yu.I., Guliyev, I.S. and Zenalova, K.S., 1988. Oil-Gas parent potential of deep seated Meso-Cenozoic deposits of South Caspian Depression. In: *Problems of Oil and Gas Bearing of the Caucasus*. Nauka, Moscow, 35–41 (in Russian).

Kurbanov, N.K., 1982. Integrated prospecting and principles of searching complex pyrite-copper-polymetallic deposits in the Alpine geosyncline belt of the Greater Caucasus. *Proceed. of TSNIGRI*, Moscow (in Russian).

Kurbanov, N.K., Mamedov, E.M. and Aliyev, A.A. et al., 1981. Cyclical mineral formation (origin) of complex gold-pyrite deposits of the Lesser Caucasus. *In: Geological-Commercial Types of Gold-Ore Fields. Proceed. of TSNIGRI,* Moscow (in Russian).

Kurbanov, N.K., Zlotnic-Khotkevich, A.G., Romanov, V.I. et al., 1967. On the peculiarity of pyrite-polymetallic mineralization of the southern slope of the Greater Caucasus. *Proceed. of TSNIGRI*, Moscow (in Russian).

Lerche, I. et al., 1997a. Geohistory, thermal history and hydrocarbon generation history of the north-west South Caspian basin. In*: Evolution of the South Caspian Basin: Geologic Risks and Probable Hazards*, Nafta-Press, Baku, 50–103.

Lerche, I., Alizade, Ak., Guliyev, I., Bagirov, E., Nadirov, R., Tagiyev, M. and Feizullaev, A., 1997b. *South Caspian Basin: Stratigraphy, Geochemistry and Risk Analysis*. Nafta-Press, Baku.

Mamedov, P.Z., Guliyev, Q.Q., Kadirov, F.A., Shikhalyev, Y.A., Guliyev, I.S., Aliyeva, E.H., Feyzullayev, A.A., Dadashov, F.Q., Kheirov, M.B. and Tagiyev, M.F., 2008. (Ak.A. Alizadeh, Ed.), 2008. *Geology of Azerbaijan*, Vol. VII: *Oil and Gas*. Nafta-Press, Baku (in Russian).

Mansurov, M.I., 1998. Structure and texture peculiarity of ores of the Gosha gold-pyrite field. *Abstr. of Conf. "Mineral Resources of Azerbaijan"*, Baku State Univ., Baku (in Russian).

Mekhtiyev, Sh.F., 1956. *Problems of Oil Origin and Forming Oil Deposits of Azerbaijan*. Acad. Sci. Azerb., Baku (in Russian).

Mekhtiyev, Sh.F., Mirzadjanzadeh, A.H. and Aliyev, S.A., 1971. *Geothermal Investigations of Oil and Gas Deposits*. Nedra, Moscow (in Russian).

Mekhtiyev, Sh.F., Mirzajanzadeh, A.Kh., Aliyev, S.A., Bagbanly, E.A. and Motyakov, V.I., 1960. Geothermal Regime of Oil and Gas Deposits. Azerneftneshr, Baku (in Russian).

Mukhtarov, A.Sh., 2011. Structure of thermal flow of sedimentary complex of the Southern Caspian Basin. D. Sci. Thesis, Inst. of Geology, Azerbaijan Acad. of Sci., Baku (in Russian).

Mustafabeyli, N.A., Liberzon, I.M. and Akhmedov, D.M., 1964. Main features of distribution of endogeneous fields in the Dashkesan ore zone. In: *Periodic Distribution of Mineral Deposits*. Nedra, Moscow (in Russian).

Mustafayev, H.V., Magribi, A.A., Shiraliyev, A.B. et al., 1989. Periodic distribution and formation of ore deposits in Azerbaijan. *Proceed. of Conf. Dedicated to the 50th Anniver. Of the Inst. of Geology of the Acad. Sci. of Azerb*. Elm, Baku (in Russian).

Peters, K.E., Moldowan, J.M., Shoell, M. and Hempkins, W.B., 1986. Petroleum isotopic and biomarker composition related to source rock organic matter and depositional environment. *Org. Geochem*., **10**, 17–27.

Salayev, S.G., 1961. *Oligocene-Miocene Deposits of the South-Eastern Caucasus and their Oil and Gas Bearing*. Acad. Sci. Azerb., Baku (in Russian).

Salayev, S.G., Guseinov, G.A. and Solomonov, B.M., 1964. *Geology and Oil and Gas Bearing of Precaspian Tertiary Monocline*. Azerneshr, Baku (in Russian).

Shykhaliyev, Yu. A., Feyzullayev, A.A. and Lerche, I., 2010. Pre-drill overpressure prediction in the South Caspian Basin using seismic data. *Energy Exploration & Exploitation*, **28**, No. 5, 397–410.

Shirinov, A.M., 1982. Geological structure and conditions of ore localization in the Jigien pyrite-copper-polymetallic field. *Proceed. of TSNIGRI*, Moscow (in Russian).

Sofer, Z., 1984. Stable carbon isotope compositions of crude oils: application to source depositional environments and petroleum alteration. *Amer. Assoc. of Petroleum Geologists Bull*., **68**, 31–49.

Suleimanov, S.M. and Babazadeh, V.M., 1974. *Geology of Mercury Deposits in the Lesser Caucasus*. Azerneshr, Baku (in Russian).

Suleimanov, S.M. and Guliyev, T.B., 1986. Morphology and structure position of the body of the Vejnaly ore field. *Scient. Notes of the Azerb. State Univ*., Ser.: Geol.-Geogr., No. 3 (in Russian).

Suleimanov, Sh.A. and Mekhtiyev, I.P., 2003. On some problems appearing by exploitation of gas-condensate-oil deposit Khere-Zire-deniz. *Azerbaijan Oil Industry*, No. 12, 18–24 (in Russian).

Suleimanov, S.M., Sitcovsky, I.N. and Aliyev, M.K., 1986. Gold manifestation in the field of volcanic quartz porhyrities in Touus region. *Scient. Notes of the Azerb. State Univ*., Ser.: Geol.-Geogr., No. 3 (in Russian).

Suleimanova, S.F. and Atayeva, E.Z., 2002. Sedimentology and stratigraphy of oil and gas bearing deposits Gunashly, Chirag and Azeri (Absheron archipelago). *Azerbaijanian Geologist. Scient. Bull*., No. 7, 109–123.

Tagiyev, M.F., Nadirov, R.S., Bagirov, E.B. and Lerche, I., 1997. Geohistory, thermal history and hydrocarbon generation history of the north-west South Caspian basin. *Marine and Petroleum Geology,* **14**, No. 4, 363–382.

Weber, V.V., 1947. *Oil&Gas Bearing Facies and their Role Oil Deposit Generation*. Lengostoptekhizdat, Leningrad (in Russian).

Yusufzade, Kh.B., 2000. Conditions and perspectives of evolution of hydrocarbon exploitation in Azerbaijan. *Azerbaijan Oil Industry*, Nos. 11–12, 29-34 (in Russian).

Yusufzade, Kh.B., Kasumov, K.A. Alexandrov, B.L. and Dergunov, E. N., 1976. Study and prognosis of anomaly high pool pressure by data of log geophysics. *Azerbaijan Oil Industry*, No. 5, 1–8 (in Russian).

Petrophysical Support of Geophysical Studies 3

3.1 Use of Geological Data

A preliminary model is devised to represent the geological objective when preparing a geophysical project for the given area. Otherwise, it is impossible to select the set of methods and interpretation procedure. The latter is revised before interpreting, if necessary. The initial development of a model of the medium is the most important stage, since the results of interpretation and the investigation in general depend to a considerable degree upon its quality.

Any model must comply with two conflicting requirements, i.e., (a) reflect the essential features (indicators) of the object for modeling and (b) be sufficiently simple to use.

A model of the medium is an integrated and, if possible, formalized representation of the geological and geophysical data concerning the target and host rocks (Movshovich et al. 1987; Kozlovsky and Krivtsov 1988). Hence, a model of the medium can be seen as a symbolic informational model. The background is no less important than the target object itself and should also be considered in the model in detail. The details should correspond to the scale of investigation. In addition, various noise effects should be taken into account.

In many cases, the characteristics of geological media for open (one-stage) regions testify to the expediency of employing stochastic models. However, geophysical fields as random functions may contain regular components of an impulse or periodic nature. If we ignore tasks involving area mapping by statistical characteristics of the field, which as a whole are considered random, the most important geological problems remain. These involve the extraction of a regular component from its associated noise. This component may correspond to magnetized gabbroid or low-magnetic acid intrusions, a zone of hydrothermal alterations, skarn–magnetite or pyrrhotite containing lens, etc.

According to Bosch et al. (2015), combined rock physics and seismic inverse problem is a powerful tool in mapping uncertainties associated with various steps of modeling and observations involved in the inference of such reservoir parameters as saturation, porosity, and shale fraction. Sometimes it is possible to analyze different physical parameters (for instance, temperature and pressure) by using some common approaches (e.g., Kutasov and Eppelbaum 2015) that enables to simplify development of combined physical–geological models.

The regular component cannot be revealed without applying certain modeling notions. Such targets as large orebodies are usually rare, and it is always a problem to determine their statistical characteristics. This has generated the need for developing a special system of processing and interpretation of the results of geophysical investigations. Such a system makes it possible to extract anomalies from the combination of anomalies and noise on the basis of a deterministic approach to the object under study (the anomaly) and a probabilistic approach to the remaining salient features of the medium and geophysical observations regarded as noise.

The deterministic study of geophysical targets is facilitated by restricting the geometric approximations of the objects belonging to the main classes under investigation.

3.2 Use of Petrophysical Data

The sources used for devising a model of this medium include geological data, information from studies of physical properties, geophysical observations obtained in adjacent areas, and the results of solving problems of the same type under similar conditions.

When studying geological descriptions and documentation obtained from the region and in other areas with the target object, the key geological factors which define the geological pattern need to be identified. The model must take all these factors into account. Any well-explored geological object related to the target (structural facial zone, tectonic block, structure, ore field, orebody, etc.) may serve as a model for the object under investigation. Thus, an examination of the geological data can provide a concrete idea of the possible classes of objects occurring in the area under

A.A. Alizadeh et al., *Geosciences of Azerbaijan*,
Regional Geology Reviews, DOI 10.1007/978-3-319-40493-6_3

study, their geometry, composition, and relationships to the host rocks.

A petrophysical variability of Azerbaijan territory is well-known (e.g., Ismailzadeh et al. 1983a, b; Gadjiev et al. 1984; Aliyev et al. 2005a, b; Alizadeh 2012). It caused the necessity of careful studying physical properties of rocks before (and during) any geological–geophysical examination.

The regional ore controls are larger ore-bearing and ore-distributing structures and, therefore, are related to their corresponding regional boundaries of physical properties. This makes it possible to study the behavior of the pre-Alpine basement to detect large metallogenic crust blocks. For regional prospecting, deepness in homogeneities may be approximated by simple deterministic models as a function of available knowledge. It serves to apply deterministic methods of quantitative interpretation provided they are adapted to the complex observation surface and other complicating factors. Some lithological and stratigraphic boundaries and tectonic lines, mineral deposit borders, and intervals of hydrothermal alterations may also be considered as references within the areas under detailed investigation.

It should be emphasized that many peculiarities of geological structure (for example, plicative and disjunctive dislocations) affect different mineral resources, including oil and gas and in underground water (Eppelbaum and Khesin 2012).

Analysis of the data shows that in most cases the types of geometric approximations of objects are restricted to a comparatively small number of classes. This determines the shared features of their models and the possibility of an integrated approach to their study.

Geophysical investigation of the mountainous and piedmont regions is complicated by rapidly changing media and a great number of near-surface anomaly sources. The changeability of mountainous regions along the lateral is accompanied by their rapid change along the vertical.

Characteristically, petrophysical variability is typical of geologically identical rocks. The erosion of young mountainous structures causes a considerable change in near-surface associations. Physical properties of rocks occurring close to the Earth's surface may not, therefore, be the same as those of deep-seated rocks of the same composition and age. Consequently, the measurements of physical properties of the rocks located in the upper portion of a section should be treated with great care, especially when they are extrapolated to the depth. There is, however, a need for a shallow survey, since the majority of the deposits occur in the upper portion of a section. When investigating deeper horizons, the effect of this rapidly changing portion should be corrected by taking into account its true parameters. All these factors call for special attention to the physical properties of rocks and ores measured on samples taken from the surface, in their natural bedding, drill cores, or mines. Their determination should be carried out on the basis of the observed geophysical fields. The variability of physical properties makes it possible to derive additional information, and single out the specific ore characteristics by petrophysical investigations.

Through an integrated approach to investigation and interpretation, the physical properties of the material can be used to develop an integrated petrophysical model of the medium. For example, the process of compiling a petromagnetic model is analogous to the use of data on other physical properties for a similar purpose.

In open areas, if the petromagnetic study is conducted at the same time as the magnetic survey on the same scale, and a petromagnetic map is drawn up, the latter represents a petromagnetic model of the surface area under investigation (Ismailzadeh et al. 1983a, b). The need to construct several petromagnetic sections presents no problems in this case. The petromagnetic data obtained from core samples and deep mines are especially crucial since they are not distorted by near-surface alterations. The determination of magnetic properties by correlating the observed field with the known geological section deserves special attention.

When no petromagnetic data are available for the area under investigation (which will be an exception to the rule in the future), the data on magnetic properties of similar rocks in adjacent areas and on objects analogous with the target can be used, including those obtained from interpretation results. Naturally, the quality of a petromagnetic model in this case will be markedly lower. This may affect the quality of interpretation and progress in solving the problem overall. A range of variability of physical properties for different objects is shown in Eppelbaum and Khesin (2012).

A petromagnetic model of a medium must yield the magnetic characteristics of all the rocks and their varieties occurring in the region. All stratified rock masses and compact geological bodies (including mineral deposits) should have corresponding average values of magnetic parameters with confidence limits. The same applies to the zones of altered rocks. The magnetic characteristics of the geological objects which do not outcrop onto the area under exploration, but are possible at a certain depth and are known to occur in adjacent areas should not be ignored either. When geophysical data obtained in neighboring or similar areas are employed, this can be used to develop a model of the medium to define deeper portions of the section in the area under investigation (even on a smaller scale), when the intensity and shape of magnetic anomalies over the objects are similar to those sought for.

To develop a petromagnetic model, the total magnetization should be computed of the individual structural-material associations using the available geological classification. However, if the classification does not conform to the results of the analysis of petro- and paleomagnetic data on the

section, a model must be devised that incorporates these petromagnetic features. In this case, the weighted average magnetization is calculated for certain rock complexes that have comparable magnetic property values or magnetization direction (within the same paleomagnetic zone). The explosive index of magmatic rocks, i.e., the pyroclast percentage may be of use when computing the weighted average values of their total magnetization, since pyroclastic rocks are characterized by a lower magnetic susceptibility κ and natural remanent magnetization (NRM), J_n as compared to the lavas.

When dealing with oblique magnetization, it is crucial to determine the direction of magnetization: The intensity and especially the type of anomaly depend on the inclination angle of the object's redundant magnetization.

Alexeyev (1976) examined the magnetization of an arbitrary triaxial ellipsoid in the Earth's magnetic field $\boldsymbol{T}_0$. Under certain simplifications, the limiting cases for this body are a vertical bed, a thick horizontal bed and a horizontal circular cylinder. The above bodies had sufficiently high-magnetic susceptibility to be magnetized almost in parallel to the active field. The angular error was less than 1.5° at $\kappa = 0.05$ SI unit and less than 3° at $\kappa = 0.1$ SI unit.

Therefore, we can assume that for all examined values and any shape of a body, a vector equality for the induced magnetization ($\boldsymbol{J_i}$) is valid:

$$\boldsymbol{J_i} = \kappa \boldsymbol{T}_0 \tag{3.1}$$

Note that for higher values of magnetic susceptibility ($\kappa > 0.08 \div 0.10$ SI unit) vector $\boldsymbol{J_i}$ is not parallel to vector $\boldsymbol{T}_0$. As is generally known, a sphere is magnetized parallel to the active field independently of the magnetic susceptibility value.

3.2.1 Analysis of Some Paleomagnetic Parameters

Paleomagnetic data investigations can contribute considerably to the analysis of magnetic survey results since they characterize certain general features of the magnetization distribution.

Paleomagnetic investigations assist us in obtaining some unique 'stumps' of past geomagnetic field configurations. Some geodynamic and tectonic information derived from the paleomagnetic field analysis cannot be received by any other geophysical or geological method (Eppelbaum 2015).

For example, data from a detailed paleomagnetic examination of the Lesser Caucasus indicate that the remanent magnetization of the Mesozoic volcanites is parallel or antiparallel to the induced magnetization, and the zones of the inverse polarity ($\boldsymbol{J_n}$) usually correspond to relatively weakly magnetized intervals of the geological section.

The Cenozoic volcanogenic series of the Talysh and Pre-Talysh have other characteristics. Here, direct polarity is dominant in the Eocene section. However, the most magnetized basaltoids of the Kosmalyan series are divided into two parts: (1) trachyandesites, andesite basalts, basalts, and tufogens with a total average thickness of 0.7 km of direct magnetization (Middle Eocene), and (2) andesite basalts, gabbro dolerites with a total average thickness of 0.8 km of inverse magnetization (Lower Eocene). The vector sum of these values determines the presence of a very complex magnetic field ΔT observed on the Earth's surface and at various levels above it.

At the same time, the Neogene-Quaternary lava sheets in the central part of the Lesser Caucasus are characterized by frequent alteration of paleomagnetic zones of different polarities. Magnetic field modeling indicated that by upward continuation of the magnetic field (computed on the basis of Poisson's integral) and an airborne magnetic survey carried out at certain altitudes (also computed on the basis of 3D modeling), the magnetic anomalies caused by the flat-laying Cenozoic bodies with different directions of natural remanent magnetization (NRM) were significantly attenuated (Khesin et al. 1996). This conclusion is congruent with the observed magnetic data analysis and confirms that paleomagnetic data can be employed for an overall estimate of magnetic prospecting possibilities and for qualitative and quantitative examination of magnetic data.

When analyzing magnetic properties, it is common practice to use the induced magnetization $\boldsymbol{J_i}$ alone, since the remanent $\boldsymbol{J_n}$ is assumed to be comparatively small. In this case, it is sufficient to have information on the magnetic susceptibility of the host rocks and the target objects. However, in contrast to current opinion, the presence of remanent magnetization is often the general rule, rather than the exception to the rule (Affleck 1964; Khesin et al. 1983; Eppelbaum et al. 2004), especially for volcanogenic and intrusive rocks. Here, it may take on a higher value and a direction different from that of the modern geomagnetic field. The remanent magnetization is vector added to the induced magnetization.

With the advent of induction susceptibility meters (kappameters), magnetic susceptibility became easier to measure. These measurements have now been generalized to common practice. Remanent magnetization has become the subject of paleomagnetic investigations. The aims, objects, and nature of the results of these investigations do not adhere to the requirements of magnetic prospecting involving the value and the direction of the total vector

$$\boldsymbol{J} = \boldsymbol{J_i} + \boldsymbol{J_n} \tag{3.2}$$

Here, $\boldsymbol{J_n}$ is the NRM. Interestingly, many papers describing the results of paleomagnetic investigations do not present any data on NRM.

As paleomagnetic experience has shown, scattering is typical of the initial directions of $\boldsymbol{J_n}$, i.e., directions of NRM on a stereoprojection. They are often scattered over the whole field of stereoprojection, and sometimes reverse orientations occur. After eliminating the unstable components of remanent magnetization by various methods (such as demagnetization, thermomagnetic cleaning), the directions come together to form a rather narrow area of the stereoprojection. The average direction defines the orientation of the ancient magnetic field in the rock formation period, which is different from the modern field $\boldsymbol{T}_0$.

However, the chaotic behavior of the initial directions of $\boldsymbol{J_n}$ suggests that the average total magnetization defined from formula (3.2) will not appreciably deviate from the direction of $\boldsymbol{T}_0$ in terms of direction averaging. This supposition was confirmed by a paleomagnetic investigation in the Gedabey district of the Lesser Caucasus (Khesin et al. 1983). Over the course of this study, the initial materials were processed using formula (3.2) for 600 samples of volcanogenic and intrusive rocks of acid to basic composition from the Middle and Upper Jurassic, which are the primary sources of anomalies in the region (Fig. 3.1).

The total vector of magnetization $\boldsymbol{J}$, in spite of its chaotic nature and the presence of reverse directions of $\boldsymbol{J_n}$, lies nearly parallel to the modern geomagnetic field $\boldsymbol{T}_0$ (the average deviation is 5° for declination, and 1° for inclination). Similar calculations employing paleomagnetic data for magmatic rocks of the Mesozoic and Paleogene within the area of the whole Lok-Garabagh (Somkhet-Agdam) zone (Lesser Caucasus), and the Gedabey district within it yielded similar results. The magnetization of acid and basic intrusives along the field $\boldsymbol{T}_0$ was reinforced in the literature (Dukhovsky et al. 1970). This is probably a general postulate. It is confirmed by many years' experience studying magnetite deposits in the Krasnoyarsk area of the Altai-Sayan Mts. (B.M. Afanasiev, private communication).

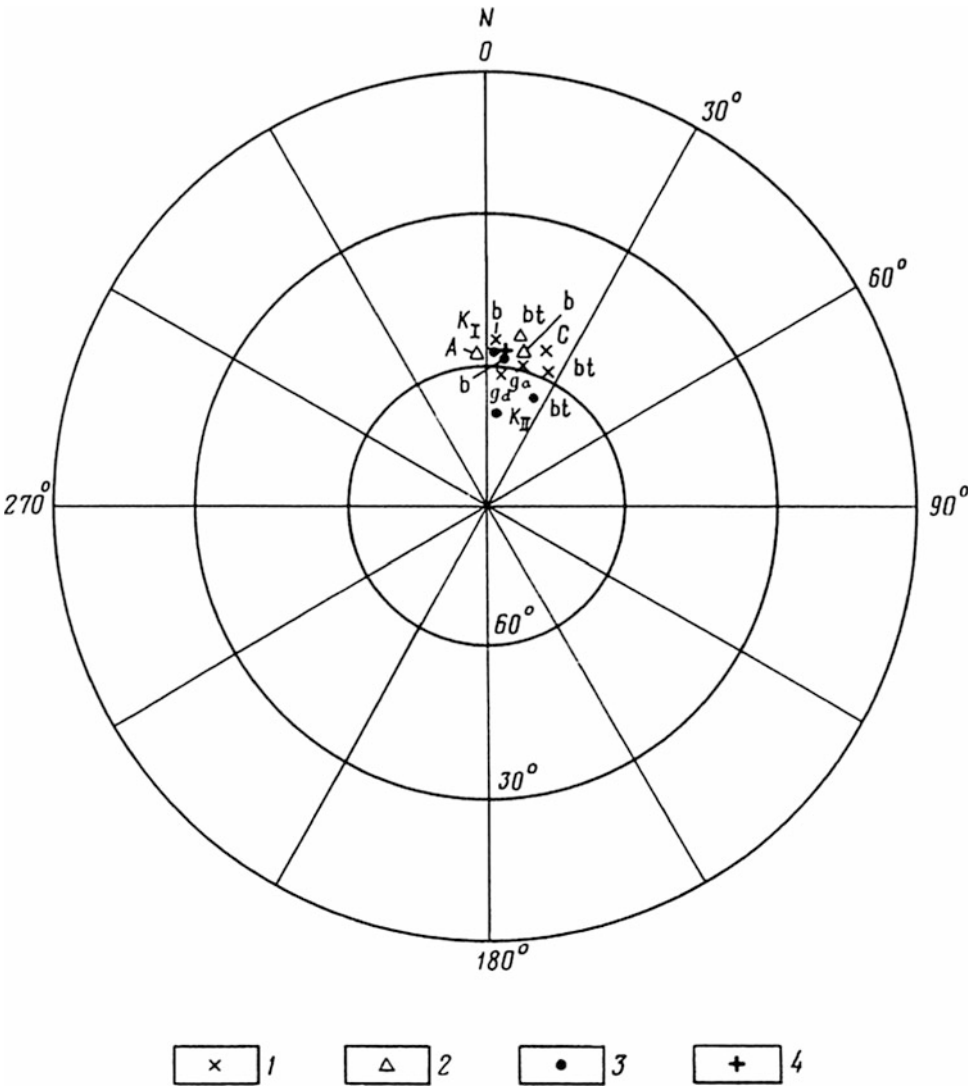

Fig. 3.1 Stereoprojections of average directions of magnetization $\boldsymbol{J} = \boldsymbol{J_i} + \boldsymbol{J_n}$ for volcaniclastic and intrusive rocks in the Gedabey district (Lesser Caucasus) of Azerbaijan (Khesin et al. 1983). Directions of rock magnetization at the following values of J, A/m: *1* <0.2 (<200 × 10^{-6} CGS), *2* 0.2 ÷ 1.0 (200 ÷ 1000 × 10^{-6} CGS), *3* >1.0 (>1000 × 10^{-6} CGS) *4* Direction of the modern geomagnetic field. *b* and *bt* are effusive and pyroclastic Bajocian and Bathonian rocks, respectively; *C* are the plagiogranites of Slavyansky intrusion; K_I are the gabbro and gabbro-diorites of phase I of the Gedabey intrusion; K_{II} are the diorites and quartz diorites of phase II; *A* is the quartz diorites and diorites of Aitaly intrusion; g_d and g_a are granodiorites and granoaplites of sheet intrusions, respectively

Thus, the inclination angle of magnetization may be regarded as a fixed parameter for interpretation under conditions of oblique magnetization.

Investigators should make sure that the condition

$$\boldsymbol{J} \parallel \boldsymbol{T}_0 \tag{3.3}$$

is fulfilled for typical rocks in each region subjected to magnetic survey if not both the magnetic susceptibility and the NRM vector must be studied.

The total magnetization direction can be estimated if we know the factor $Q = J_n/J_i$ and the rough direction of $\boldsymbol{J_i}$. Formula (3.2) makes it easy to obtain the expression:

$$\tau = \arctan \frac{Q \sin \upsilon}{1 + \cos \upsilon}, \tag{3.4}$$

where ν is the angle between vector $\boldsymbol{J_n}$ and vector $\boldsymbol{T}_0$, and τ is the angle between vector $\boldsymbol{J}$ and vector $\boldsymbol{T}_0$.

To determine angle τ, we plotted a nomograph (Fig. 3.2) for values $\upsilon = 0 \div 30^\circ$ ($\boldsymbol{J_n}$ and $\boldsymbol{T}_0$ are roughly parallel) and for $\upsilon = 150 \div 180^\circ$ ($\boldsymbol{J_n}$ and $\boldsymbol{T}_0$ are roughly antiparallel). In this situation, the direction of $\boldsymbol{J_n}$ with an angle of 30° does not fall outside the cone around $\boldsymbol{T}_0$. From the nomograph, it follows that in the first case the direction of the total vector

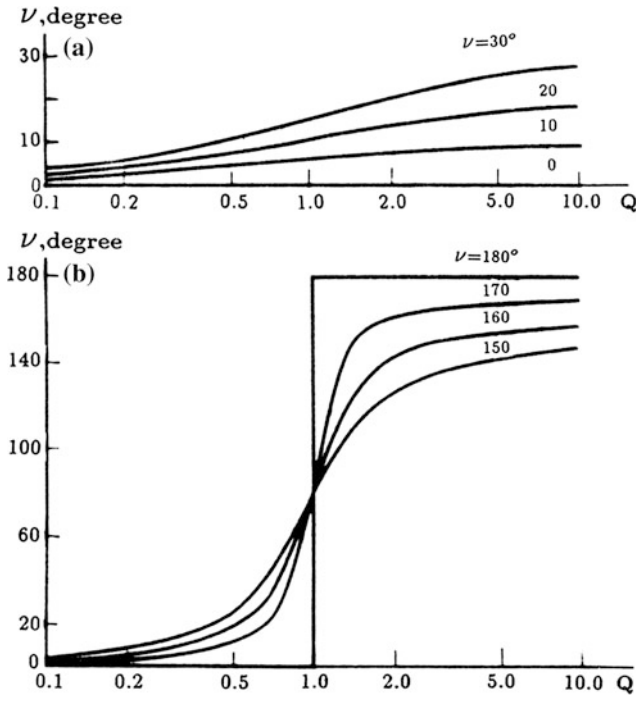

Fig. 3.2 Nomograph to determine the deflection angle τ of the magnetization vector $\boldsymbol{J}$ from the geomagnetic field vector $\boldsymbol{T}_0$ by a known angle τ between $\boldsymbol{J_n}$ and $\boldsymbol{T}_0$ vectors, and the Q factor $\left(Q = \frac{J_n}{\kappa T_0}\right)$: **a** $0^\circ \leq \upsilon \leq 30^\circ$; **b** $150^\circ \leq \upsilon \leq 180^\circ$ (Khesin et al. 1996)

($\boldsymbol{J}$) is within the cone since it has a more acute angle $\tau < \upsilon$ for all values of Q; the lower the Q factor is, the smaller the angle will be. In the second case, antiparallelism holds for higher values of Q, whereas for smaller ones $\boldsymbol{J}$ is roughly parallel to the vector $\boldsymbol{T}_0$. The most unfavorable situation is at $Q = 0.7, 1.5$, when the direction of vector $\boldsymbol{J}$ is markedly different from the $\boldsymbol{T}_0$ direction. For rocks characterized by such Q values and a reversed polarity of vector $\boldsymbol{J_n}$, the total vector is calculated by formula (3.2). For the first and second cases, it can be computed using a simple approximate formula

$$\boldsymbol{J} = \boldsymbol{J_i}(1 \pm Q) = \kappa \boldsymbol{T}_0(1 \pm Q). \tag{3.5}$$

The parallel vectors $\boldsymbol{J_n}$ and $\boldsymbol{T}_0$ have a positive sign and a negative sign when they are antiparallel.

Analysis of magnetic survey results and calculation of the direct magnetic effects require treatment of the local anomalous object's redundant magnetization with respect to the host medium. In contrast to excess density, redundant magnetization is a vector quantity. For purposes of calculation, all the components of magnetization vectors for both the local bodies and the host medium must be known. If the magnetization vectors of the body and the medium (of two adjacent objects) are parallel, and more specifically if condition (3.3) is fulfilled, the redundant magnetization modulus is the simple difference in absolute values of these vectors, and its direction is parallel to the direction of the initial vectors. When the magnetization vectors for the body and the medium are not parallel, the redundant magnetization components must be computed.

The NRM direction in rocks depends on the influence of quite a number of components which were formed during different geological time intervals. These can be altered as a result of certain physical and chemical processes. Therefore, care is required when selecting the magnetization direction as a fixed parameter for interpretation, and needs to be confirmed on a statistically significant sample. The constancy of the magnetization direction (accurate up to 20°) must be verified not only for the search objects, but also for the host rocks. The above is easy due to the fact that induced magnetization has a constant direction, and NRM, when measured on rock samples, varies randomly with respect to a certain average value. Therefore, the direction of their average sum, especially if $Q < 1$, will be close to that of the present geomagnetic field in the area under investigation.

For a better understanding of the appearance and further evolution of the NRM over the evolution of the Earth, it is important to analyze the conditions during the early Earth's formation and evolution. This analysis can provide a clear picture of the causes of primary magnetization formation and its possible changes (Pilchin and Eppelbaum 1997).

3.2.2 Results of Some Regional Paleomagnetic Examinations

The results of paleomagnetic investigations were compiled for the general paleomagnetic scale of the Mesozoic–Cenozoic of Azerbaijan (Ismailzadeh et al. 1983b). This scale was updated by Guseinov (1988) on the basis of analysis of the Lower Jurassic and Aalenian deposits of the Lesser Caucasus (the generalized data are shown in Fig. 3.3).

The Jurassic-Cretaceous, Paleogene, and Neogene deposits are divided into 19, 22, 6, and 5 paleomagnetic zones of direct and inverse magnetization, respectively. This can be used to define the geological sections and stratigraphic position of some floors more accurately. The most significant was the correlations for the barren productive series of the Middle Pliocene (Balakhan floor) within western Absheron, the Lower Kur Depression and its northern frame (Jeirankechmez depression). It was shown that the thicknesses of the same paleomagnetic zones in the above depressions are much greater than on the western Absheron with its commercial multihorizon oil, gas, and gas-condensate deposits. Thus, the oil and gas potential of these depressions noted by geologists was supported by the paleomagnetic examination. Regional paleomagnetic analysis testifies to the relationship between the productive series of Azerbaijan, the Shirak series of Georgia, and the red sequence of Turkmenistan. This provides additional data for investigation of oil and gas in these regions given the relationships and spatial changes of the series identified by paleomagnetic techniques. Paleomagnetic identification of the Upper Bajocian deposits of the Lesser Caucasus (where an inverse magnetization prevailed) and the same zones of inverse polarity identified in the Northern Caucasus are presented in Fig. 3.4.

An interesting example of paleomagnetic correlations can be found between the Lower Eocene deposits and the most distant regions of Azerbaijan, i.e., Nakhchivan in southwest and Talysh in southeast. It was shown through the strong Paleogene correlations for these regions that the lower part of the Lower Eocene is absent in Talysh.

The use of paleomagnetic data for paleotectonic reconstructions in Azerbaijan and surrounding regions is of great importance (e.g., Asanidze and Pecherskiy 1979; Asanidze et al. 1980; Camps et al. 1996; Khalafly 2006; Eppelbaum and Khesin 2012). Table 3.1 lists results obtained by paleomagnetic groups under the supervision of T. A. Ismailzadeh for the Lesser Caucasus, the southern slopes of the Greater Caucasus and the Northern Caucasus (here D is declination and I is the inclination).

Table 3.1 provides the coordinates of the ancient magnetic poles and paleolatitude for areas of the Lesser Caucasus: 22–26°. Thus, in the Middle–Late Jurassic the Lesser

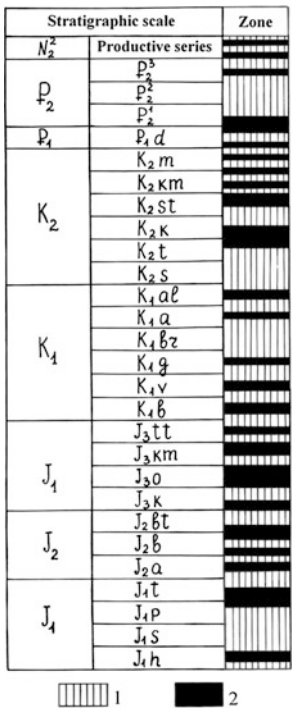

Fig. 3.3 Generalized paleomagnetic scale of the Mesozoic–Cenozoic of Azerbaijan. *1* Direct magnetization and *2* Inverse magnetization

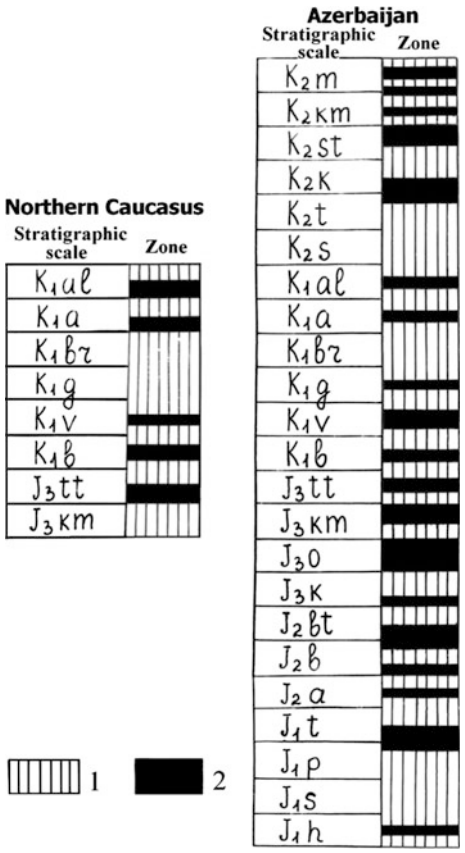

Fig. 3.4 Regional correlation of the Mesozoic paleomagnetic sections. *1* Direct magnetization and *2* Inverse magnetization

Table 3.1 Average directions of ancient magnetization for different regions of Azerbaijan and northern Caucasus

Sampling area	Age	Average direction of J_n, degrees	
		D	I
Lesser Caucasus			
Dashkesan	J_2–J_3	0	40
Garabagh	J_2–J_3	25	40
Khodjavend	J_2–J_3	20	48
Lachin	J_3–K_1	30	50
Southern slope of the Greater Caucasus			
Khizi	K_1–K_2	350	45
Northern Caucasus			
Krasnogorskii	J_1–K_1	343	55
Kislovodsk	K_1	340	50

Caucasus was 14–18° more to the south of its modern location. In terms of longitudes, the Lesser Caucasus can be seen as separate blocks that rotated in relation to each other. Data presented by Asanidze and Pecherskiy (1979) confirmed that in the Jurassic and Early Cretaceous the Greater and Lesser Caucasus were located about 15–20° to the south of their modern location.

The paleomagnetic directions of the Lower Jurassic rocks of the Lesser Caucasian region and Jurassic rocks of the Greater Caucasian region are close to those of the Eurasian continent. Analysis of the available paleomagnetic data suggests that the deviation between the Jurassic and the Lower Cretaceous declinations may have been caused by the turning of the Lesser Caucasian region anticlockwise toward the Greater Caucasian region.

The values of the paleolatitudes of the Jurassic and Cretaceous rocks of the Lesser Caucasian region are similar and differ from the paleolatitudes of the Greater Caucasian region by 8–10°. Consequently, during the Middle and Later Mesozoic the Lesser Caucasian region practically did not change its latitude position.

Paleomagnetic examination of the Paleogene and Eocene deposits in Talysh and Nakhchivan shed light on the rotation of the Lesser Caucasian Plate anticlockwise 30–40° toward the Greater Caucasus. In addition, the plate was divided into separate blocks which turned relative to each other [confirmed later by Khalafly (2006)]; obviously, the horizontal transitional displacements of the Lesser Caucasian region which finished in the Jurassic were not renewed. Paleomagnetic research in the Lesser Caucasus within Turkey (Van der Voo and Channel 1980) indicates that the Turkish territory rotated toward the north of Eurasia. Thus, all the territory of the Lesser Caucasus, beginning from the Jurassic, turned at the angle of 30–40° anticlockwise to the Greater Caucasus. This rotation ended for the most part by the beginning of the Late Eocene.

3.2.3 Analysis of Other Physical Parameters

The procedures for assessing the density σ, electric resistivity ρ, polarizability η, and other physical nonvector properties are generally analogous to the procedures described above for petromagnetic data, but are simpler. Note once again that the complexity of the terrain relief may be of use in determining such an important feature as the effective density of the medium under study. This forms the basis for the well-known method suggested by Nettleton (1940), in which the Bouguer anomalies are calculated for different intermediate layer densities. The curve which is least correlated with the relief profile corresponds to the mean density of rocks in the upper portion of the section. Various methods for determining the density with respect to mountainous conditions were described by Parasnis (1966), Berezkin (1967), and Varlamov and Filatov (1983), and as for other physical properties, they are described in various studies including reference books (Tarkhov 1980; Kobranova 1986; Nikitsky and Glebovsky 1990). Electric parameters can best be estimated by parametric measurements at outcrops (in situ) and electric sounding in the investigated sections. The possibility of determining the density by the results of measurements at different levels of horizontal mines (adits, drifts) and by borehole gravimetric measurements is also worth mentioning (Veselov 1986). All the above-mentioned methodologies were widely applied for the determination of physical properties in different regions of Azerbaijan (Ismailzadeh et al. 1983a, b; Khesin et al. 1996; Eppelbaum and Khesin 2012). Density can be also determined by making use of the gravimetric measurement grouping method. This involves a group of additional measurement points located around a point of the network. The last methodology was successfully applied in the Gyzylbulagh gold–copper deposit in the Daghliq (Mountainous) Garabagh region of Azerbaijan (Khesin et al. 1993).

In many cases, it is advisable not to estimate physical properties by their correlation with others. For instance, when dealing with rapidly changing rocks of various compositions in mountainous regions, the correlation coefficient between the velocity and density for intrusive and volcanogenic rocks in the Lesser Caucasus varies from 0.1 ÷ 0.2 to 0.5; i.e., the correlation is negligible (Detkova and Shopin 1969). This is related to the pronounced porosity of igneous associations.

An example of a study on the physical properties in the Gyzylbulagh gold–pyrite deposit (Mekhmana ore region of the Lesser Caucasus) is presented in Table 3.2. In this table, density and magnetic susceptibility were assessed by

Table 3.2 Physical properties of rocks and ores in the Gyzylbulagh gold–pyrite deposit (Garabagh, Azerbaijan)

Age	Lithology	σ, g/cm^3		κ, 10^{-5} SI		ρ, Ohm•m		λ, W/m• °C	
		Average	Range	Average	Range	Average	Range	Average	Range
Q_3	Alluvial soil, clay and loam	–	–	50	13–125	–	–	–	–
Q_1	Deluvium conglomerates, pebbles, brecciated rocks	–	–	500	350–1080	–	–	–	–
J_3k–J_3o	Calcareous sandstone	2.64	2.62–2.66	260	39–760	–	–	–	–
	Silicified calcareous sandstone	2.66	2.63–2.67	690	480–1030	–	–	–	–
	Limestone	2.56	2.53–2.59	10	1–20	–	–	–	–
J_2bt	Andesite–dacite porphyrite	2.47	2.27–2.59	1400	115–4800	–	–	2.80	2.44–3.0
	Andesitic porphyrite	2.59	2.48–2.73	3260	810–69000	700	140–1200	–	–
	Intensely silicified andesitic porphyrite	2.45	2.36–2.56	210	30–660	–	–	2.87	2.72–3.0
J_2b	Liparite–dacite porphyrite	2.48	2.38–2.55	590	210–1750	450	400–500	2.84	2.73–2.94
	Tuff breccia	2.52	2.42–2.60	1630	580–4130	–	–	–	–
	Silicified brecciated lava	2.30	2.20–2.56	24	0–100	–	–	–	–
J_3	Dike of andesite–basalt composition	2.72	2.64–2.90	1050	450–2130	–	–	3.20	3.03–3.50
	Malachitized rock with rare inclusion of magnetite	2.55	2.46–2.73	8750	1880–26300	320	140–500	–	–
	Veinlet-disseminated pyrite–chalcopyrite ore	3.13	2.80–3.54	14	2–31	8	1–20	3.97	3.50–4.19
	Dense-impregnated chalcopyrite ore	3.20	2.90–3.74	19	6–29	–	–	4.5	4.30–4.84
	Massive chalcopyrite ore	3.50	3.10–4.0	15	13–19	1	0.1–5	5.7	5.14–7.30

Eppelbaum (1989), the resistivity data are from Novikova et al. (1983), and measurements of thermal conductivity were performed under the supervision of S.N. Ginzburg in TzNIGRI (Moscow).

Geophysical studies of the mountainous areas are complicated by rapidly changing media and the great number of near-surface anomaly sources. Even for medium-scale areal surveys of the northeastern part of the Lesser Caucasus, up to 5 or 6 petrophysical variables (according to the classification of the Institute of Geology, St. Petersburg) can be found in a 4 km^2 cell (Karkoshkin 1979). The petrophysical survey of the Gedabey mining district of the Lesser Caucasus showed that an area of 700 km^2 prospected on a scale of 1:50,000 had 17 petromagnetic and 11 petrodensity gradations. The changeability of mountainous regions along the lateral is accompanied by their rapid change along the vertical (Fig. 3.5).

An interesting investigation of compressional wave velocity versus pressure in volcanoclastic rocks of the Shamakhy-Ismailly blocks of Azerbaijan was carried out by Safarov (2006). A fragment of this investigation is presented in Fig. 3.6.

In hydrocarbon, geology estimation of the relative water volume change ($\Delta V/V_0$) can be used to characterize dilatancy in sedimentary rocks and rock layers. From this point of view, it also seems important to analyze the variable volume $\Delta V/V_0$ (V and V_0 are volume and initial volume, respectively) in relation to maximal porous pressure for sedimentary layers in different regions with varying thermodynamic regimes (Eppelbaum et al. 2014) (Fig. 3.7).

Advantage of using both P_0 and T_0 parameters (where P is the real pressure, P_0 is the lithostatic or hydrostatic pressure, T is the temperature, T_0 is the normal temperature [the normal temperature for matter is determined using the condition for the equilibrium line ($V/V_0 = 1$)]) in analyzing the thermodynamic conditions of porous fluids is the elimination of the dependence on depth of such parameters as K_{aP} (coefficient of abnormality of pressure defined as $K_{aP} = P_{\mathrm{AHSP}}/P_0$), K_{aT} (coefficient of abnormality of temperature defined as $K_{aT} = T/T_0$), the excess of pressure ($P - P_0$), the excess of temperature ($T - T_0$), etc. (Kerimov and Pilchin 1986). In fact, both the excess of pressure and the excess of temperature could have the same values at different depths, which would obviously produce different effects and create problems in interpreting these values together. In order to avoid such problems, it was suggested (Pilchin 1983) to use dimensionless relative values $(P - P_0)/P_0$ and $(T - T_0)/T_0$ for the analysis of P- and T-conditions of porous fluids which are compatible for data analysis and not depth dependent. For example, the scatter plot composed of values

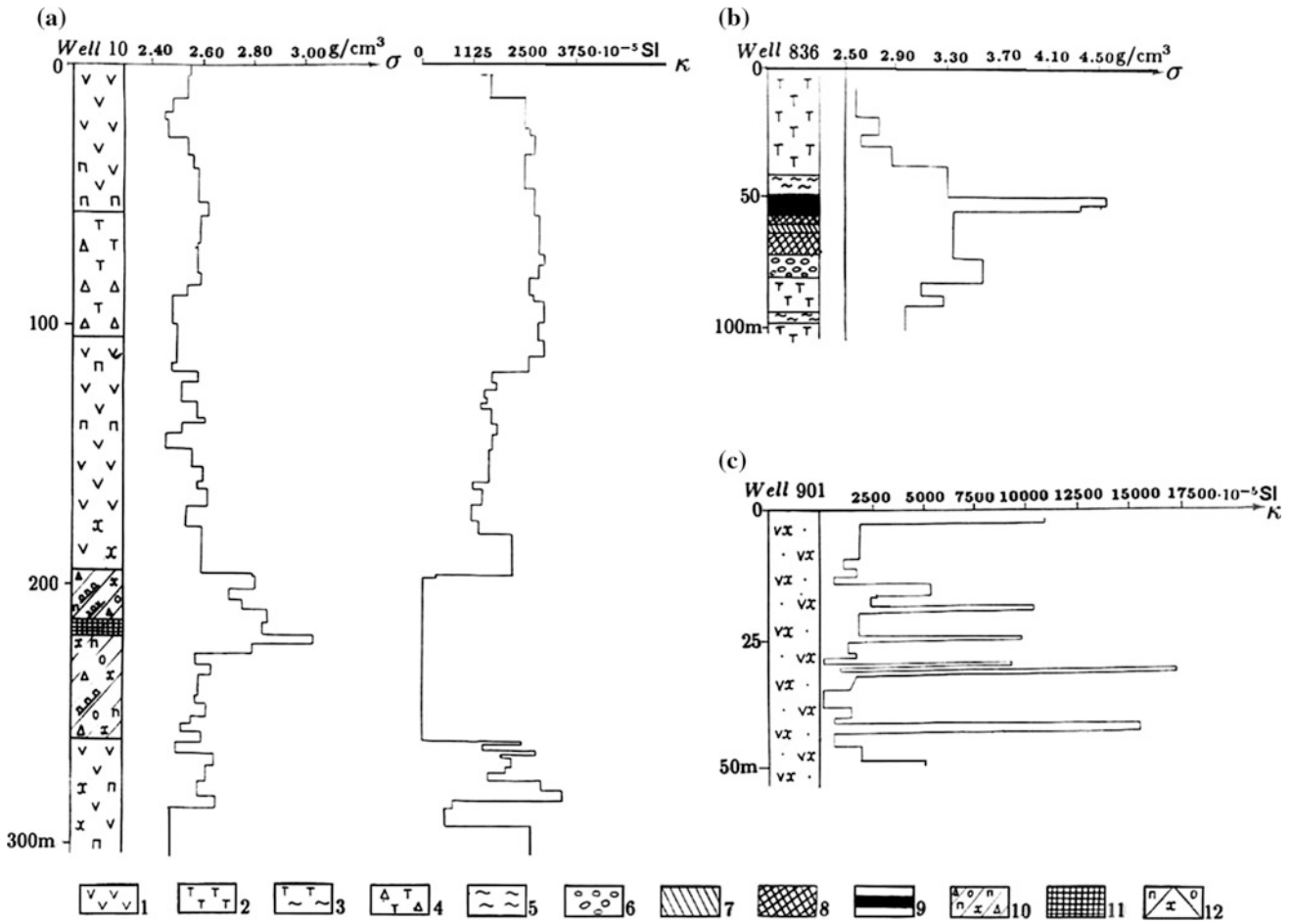

Fig. 3.5 Petrophysical variation in cores (NE Lesser Caucasus) (Khesin et al. 1996). **a** Gyzylbulagh gold–pyrite deposit, **b** Dashkesan iron deposit, **c** Uchbulag (Murut) site. *1* Porphyrites; *2* Slightly altered tuffs; *3* Hornfelsed tuffs; *4* Tuff breccias; *5* Hornfels; *6* Garnet skarns; *7* Magnetite-garnet skarns; *8* Lean skarn-magnetite ore; *9* Rich skarn-magnetite ore; *10* Zone with phenocrysts, nests; *11* Intervals of pyrite and chalcopyrite massive ore occurrence; *12* Pyritization, chloritization, and silicification

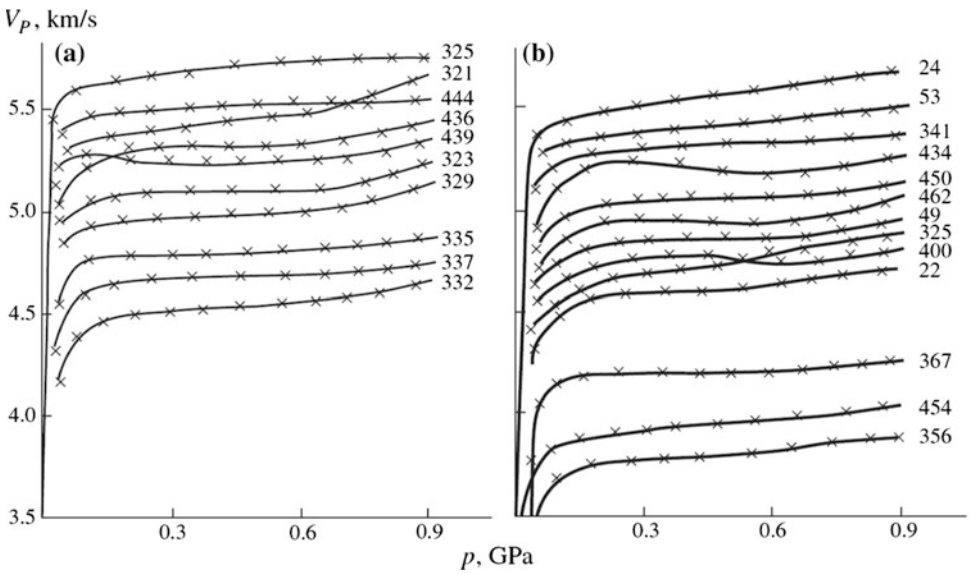

Fig. 3.6 Compressional wave velocity versus pressure in sedimentary carbonate rocks of the Shamakhy–Ismailly blocks: mudstones (356, 367, 454), limestones (24, 53), and sandstones (22, 49) of the Shamakhy block; clayey limestones (325, 341, 400, 434, 450, 462), sandy limestones (321, 323, 326, 329, 436, 439, 444), and marls (332, 335, 337) of the Ismailly block (after Safarov 2006)

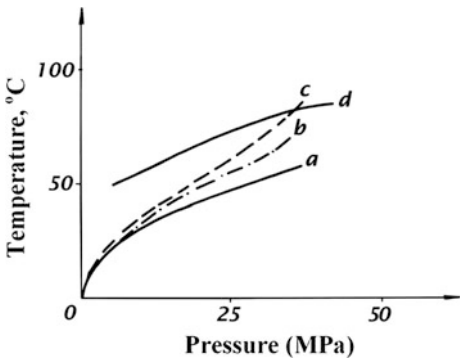

Fig. 3.7 Changes in a unit of volume of water (V/V_0) under different temperatures and pressures for hydrocarbon well 558 of the Duvanniy Sea area (offshore Azerbaijan): **a**—*Curve* of conditions for water at $V/V_0 = 1.00$; **b**—*Curve* of conditions in the well with unloading of layer from excess water (V_2/V_0); **c**—*Curve* of conditions in the well without unloading of layer from excess water (V_1/V_0); **d**—*Curve* of condition of water with $V/V_0 = 1.01$ (Eppelbaum et al. 2014)

$(P-P_0)/P_0$ and $(T-T_0)/T_0$ from measurements at various depths of the Kyurovdagh area of the Lower Kur Depression presented in Fig. 3.8 shows the strong correlation for the area between these relative values, with a correlation coefficient of $r = 0.77 (n = 159)$. However, there was no correlation found between values of $(P-P_0)$ and $(T-T_0)$.

Figure 3.9 displays a correlation between porosity, permeability, and density observed up to the depth of 6 km in

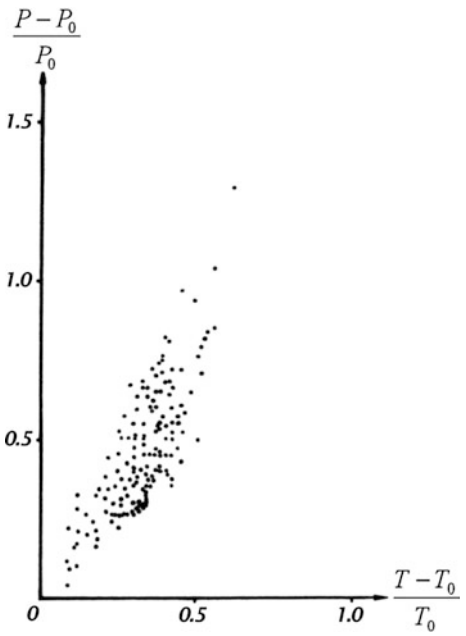

Fig. 3.8 Scatter plot of values $(P-P_0)/P_0$ versus $(T-T_0)/T_0$ for oil and gas fields in the Kyurovdagh area of the Lower Kur Depression (Eppelbaum et al. 2014)

sandstones of Baku archipelago and predicted up to depths of 6–9 km (Djevanshir 1987).

A separate attention must be paid to calculation of Curie point depth (CPD) and depths of lower edge occurrence of magnetized bodies (LEOMB) (e.g., Pilchin and Eppelbaum 1997). These parameters are important for the development of physical–geological models in the process of 3D magnetic field modeling (Eppelbaum et al. 2014). At the same time, the CPD and LEOMB parameters may significantly differ (Table 3.3). The main reasons of this phenomenon are described in detail in Eppelbaum et al. (2014).

The correlation between the physical properties of metamorphic rocks also breaks down. For instance, ultrabasic rock serpentinization leads to a sharp increase in their magnetization and to a simultaneous decrease in their density. Generally, it is not worthwhile to compute the density according to the density/velocity correlation for regions abundant in igneous and metamorphic rocks. The computation of the gravitational field by this type of density model will, however, be effective in the case of sediment section, where this correlation is reliable enough.

To determine physical properties, the position of the sampling interval, the representivity of the sample, and the number of measurements for statistical processing and stable results all need to be taken into account. For instance, according to Kotlyarevsky, who investigated 20 intrusive massifs in Uzbekistan, the effective magnetization obtained by aeromagnetic prospecting is consistent with the magnetization calculated from at least 200 samples (Khesin et al. 1983).

Statistical processing makes it possible to determine the uniformity of the data sample; it indicates whether to make additional petrophysical differentiations or, on the contrary, to combine certain subassociations and associations according to their physical properties (Ismailzadeh et al. 1983a, b; Gadjiev et al. 1984, 1985). The average characteristics (arithmetic average for a normal distribution and geometric average for a lognormal one) and their confidence intervals are selected on the basis of testing the hypotheses concerning the laws of distribution. The weighted values of the physical properties thus obtained can be attributed to their corresponding geological associations or structural–material complexes, and their distribution can be refined later by physical–geological modeling (Vakhromeyev and Davydenko 1987).

Beside physical properties utilized in studying regional geophysics and economic minerals, some environmental geophysical parameters are of a great interest. For instance, investigation environmental radioactivity of Talysh and southern slope of the Greater Caucasus are shown in Fig. 3.10.

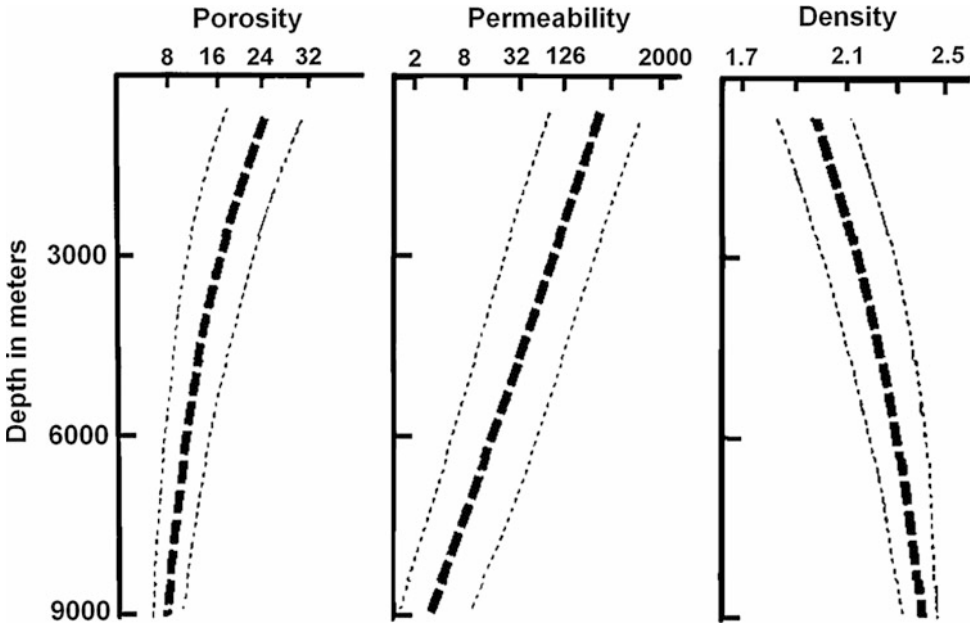

Fig. 3.9 Generalized variations of porosity (in percent), permeability (in millidarcies), and density (in g/cm^3), versus depth, in sandstones of the Baku archipelago. Upper and lower boundaries of range of values are shown by *narrow lines*; the *bold lines* represent average values (after Djevanshir 1987, with technical modifications)

Table 3.3 CPD (H_C), depths of isotherms (473 and 673 K) and lower edges of magnetized bodies (H_m) in the Middle Kur Depression, Azerbaijan (after Pilchin and Eppelbaum 1997)

Name of magnetic anomaly	Depth of 473 K isotherm, km	Depth of 673 K isotherm, km	H_C, km	H_m, km
Ismailly	5.5–6.5	14–16	25–30	14
Shamkir	5.0–6.0	12–13	18–22	20
Sarkyar	5.5	13–14	22–24	18
Borsunly	5.5–6.5	14–15	24–28	16
Lyaky	5.5–6.5	15–17	30–32	22
Karajaly	5.5–6.5	15–17	30–32	14
Sor-Sor	6.0–7.9	16–17	30–34	13
Ragimly	6.0–7.0	16–17	32–34	12
Imishly	7.5	20–22	44–46	11
Comushly	7.5	19–21	42–44	14
Saatly	7.5	18–19	40–42	9
Goyarkh	5.5–6.6	14–15	24–26	16
Bashkarvand	5.5–6.5	15–16	26–28	10
Gindarch	5.5–6.5	15–16	25–30	15
Beilagan	6.5–7.0	15–16	25–30	26
Birmay	6.5–7.5	19–20	42–44	7

Other effective example of environmental features examination is studying physical properties of such interesting geological phenomenon widely distributed in Azerbaijan as mud volcanism (e.g., Guliyev 1992; Feyzullayev et al. 2005b; Kadirov et al. 2005). Results of non-conventional penetration tests at the active Dashgil mud volcano (see also Chap. 7 in the Volume I "Geology") are presented in Kopf et al. (2009). Some results of this investigation are shown in Fig. 3.11.

3.3 The Formation of an Indicator Space

When developing a model of a medium, the most important issue is to compute the anomalous effects from objects of various classes against the background of a host medium field (or to apply suitable data available in the literature) and to compare them with observed anomalies from similar objects. Comparison of the results serves to correct the model and determine the criteria for singling out the targets. This criterion is a quantitative indicator (such as field value, dissection, and gradient) exceeding the critical level only in the presence of the target.

Effects caused by the targets are often weak under complex conditions and, therefore, one has to use poor criteria. Hence, the probability of misinterpretation (i.e., missing the target or erroneous conclusion as to its presence) increases. By implementing an integrated approach to geophysical study, the risk of making the wrong decision can be considerably lessened. For example, if a weak anomaly[1] is detected using three points, and the mean square of the anomaly in each method is equal to the noise dispersion, the interpretation reliability for separate methods amounts to 0.61 and for the set of three methods it reaches 0.87 (Eppelbaum 2014).

The use of indirect indicators; i.e., the effects caused not by the objects proper (for example, orebodies), but by larger geological bodies (ore-controlling structures, etc.) which are

[1]A weak anomaly is a relative notion. Under very strong noise typical of open areas the anomaly may have large amplitude, but is considered to be weak, since it has to be separated from the noise field background of the same intensity.

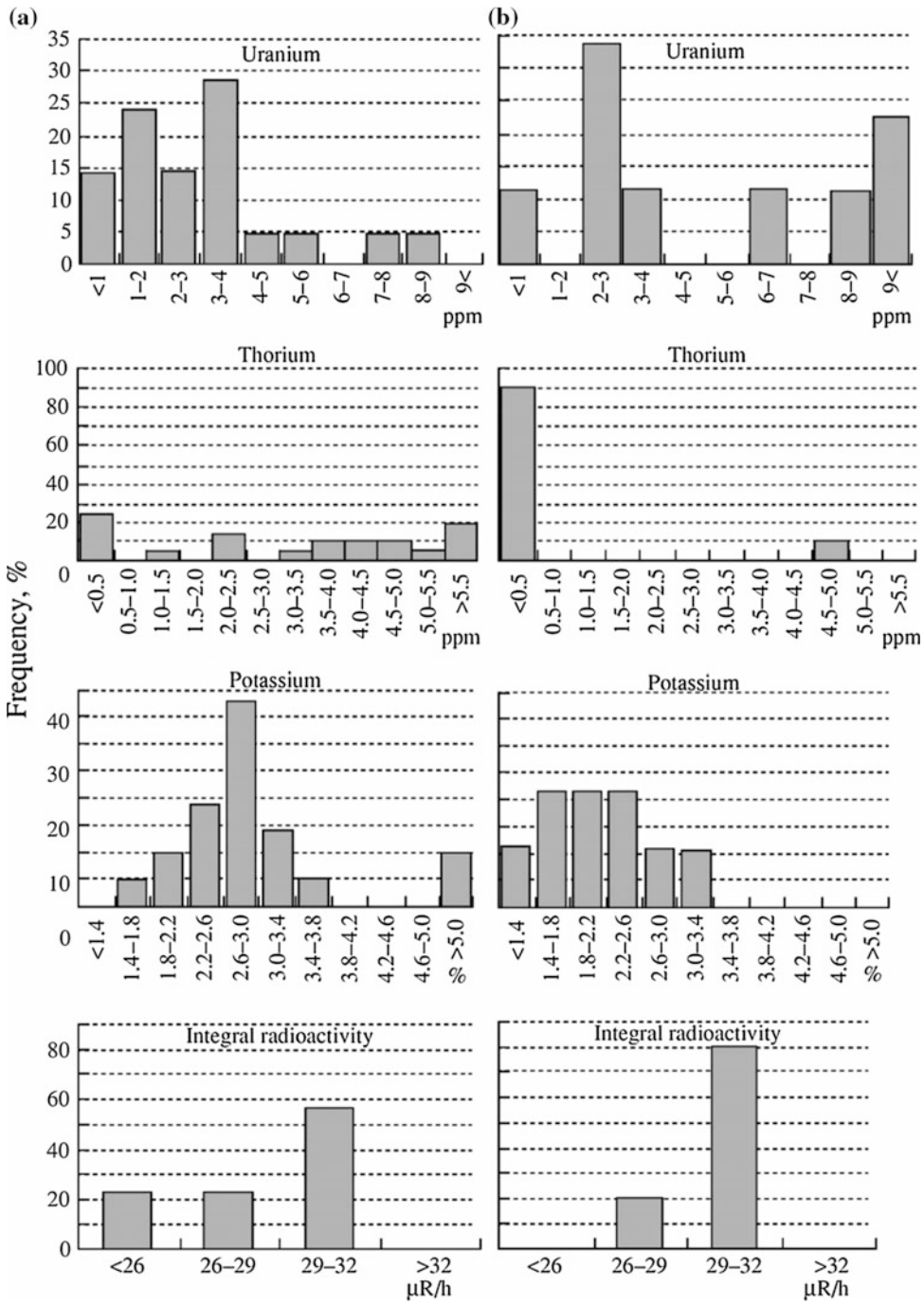

Fig. 3.10 Histograms of the distribution of radioactive elements and integral radioactivity in Oligocene clays of the **a** Talysh and **b** Greater Caucasus regions (after Feyzullayev et al. 2005a)

spatially or genetically related to them, also reduces the interpretation error. Finally, secondary indicators, in other words, derived quantities (Borovko 1979) such as various initial field transforms and their combinations (smoothed values of a field, its variability, predominant strike of isolines, etc.) are also of major importance. In many cases, the secondary indicators are far more important than the initial observed field. It is common knowledge that a rare combination of many features is a salient characteristic of large deposits and their significant secondary indicator.

However, too many indicators is a negative factor which affects both labor output and interpretation. At the same time, there are cases where the number of indicators or standards reaches hundred or more. This is the reason why the selection of the most essential features is crucial in developing a model of the medium. In this situation, after critical analysis, geophysical experience in solving similar problems under similar conditions is called for. It is worth mentioning that as a rule, only a few methods are integrated in practice; nevertheless, positive results of integration are

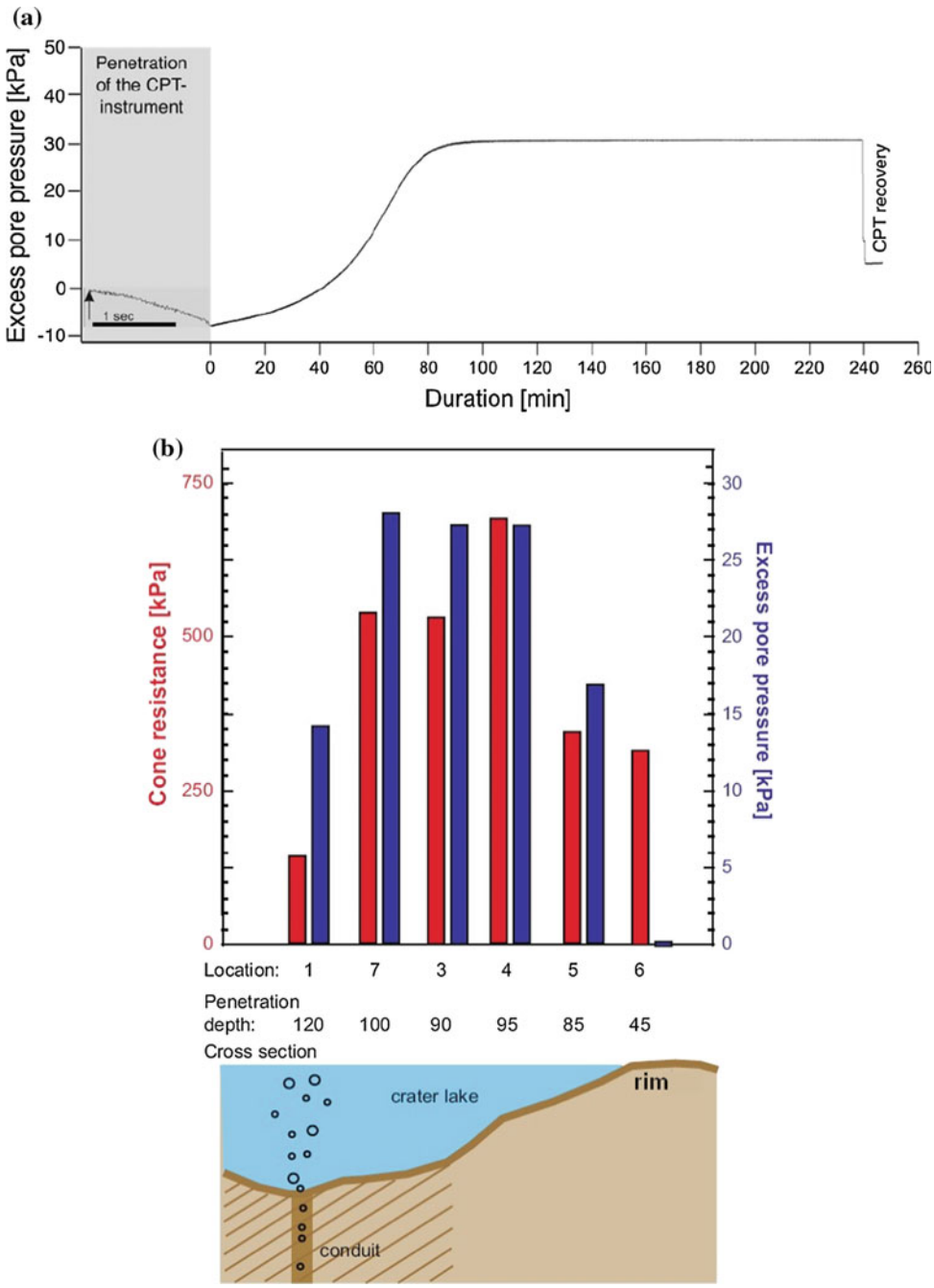

Fig. 3.11 CPTU results showing cone resistance and pore pressure. **a** Pore pressure evolution during insertion (*gray shading*) and long-term at location #7; **b** Diagram of cone resistance upon insertion and excess pore pressure taken 30 min after deployment at each location. Note different y-axis (*left*: cone resistance, *right*: pore pressure) in (**a**) and (**b**), and variable x-axis with *gray shading* (only 1.5 s of CPTU penetration vs. white area of long-term pore pressure response in (**a**) (after Kopf et al. 2009)

well-known (Berezkin et al. 1978; Parasnis 1986; Brodovoi 1989; Nikitin 1993; Eppelbaum et al. 2004, 2011; Eppelbaum and Khesin 2012). As shown in (Eppelbaum 2014), a simple analysis testifies to the great interpretative capabilities of a set consisting of at least two independent methods.

In regional investigations, one and the same set of methods can in principle be employed to study objects of various classes which control different types of mineral resources. Of special interest is a shared approach to predicting the presence of ore and oil and gas on the basis of geophysical data, by relating discoveries of non-conventional oil and gas deposits in mountainous regions to igneous and metamorphic findings (Eppelbaum and Khesin 2012). Table 3.4 illustrates these fundamental potentialities.

Secondary indicators are usually obtained from initial field transformations. Therefore, when developing a model of a medium, secondary indicators should be selected. Methods of obtaining them, their types, and especially their transformation parameters should be specified as well. Experience and theoretical calculations show that the results

Table 3.4 Revealing common controls of ore and oil and gas deposits by geophysical methods

Geological controls (Fluid conductors and hosts of mineral deposits)	Predominant location		Typical geophysical methods and their results	
	Mineralization	Hydrocarbons	Methods	Field patterns and geometry of sources
Deep faults	Pinnate joining	Faults zones to neighborhood	Gravity and magnetic prospecting	Gradient zones, local anomaly chains, linearly elongated anomalies
Overlap-overthrust structures	Volcanogenic and sedimentary rock masses	Sedimentary rock masses	Seismic exploration	Gently sloping reflecting boundaries
			Gravity prospecting	Extrema on cover edges
Intersection of longitudinal and transcurrent fractures	Local structures	Regional structures	Gravity and magnetic prospecting	Interference pattern
Igneous rocks concealed highs, their contacts with sedimentary rocks	Exomorphic and endomorphic zones of intrusives	Eroded volcanic structures, sedimentary rock pinching-out zones	Magnetic and gravity prospecting	Anomalies of circular and ring shapes
			Seismic exploration	Zones of zero reflection
Porous and fractured metamorphites (secondary quartzite, serpentinites, shales)	Scattered bodies	Continuous filling	Magnetic and gravity prospecting	Field decreasing (excluding magnetic maxima over serpentinite)
			electric prospecting	conductivity anomalies
Hydrothermal alteration and pyritization zones	Pyritization zones	Below pyritization zone	Magnetic prospecting	Linear field decrease
			Electric prospecting	Increased polarizations
Brachy-anticlines flexures in terrigeneous-carbonate deposits	Northeastern flanks of structures	Eastern and Northeastern flanks of structures	Electric prospecting, seismic exploration	Contact flexures of media with various physical properties

of transformation depend on parameters, rather than on the type of transformation. Generally, the parameter selection must comply with requirements of maximum efficiency of the ultimate solution to the interpretation problem. But since concrete requirements entail certain difficulties, parameter selection is usually confined to the analysis of changes in the model signal during transformation and to the evaluation of the related cost.

The choice is determined by the increase in the signal-to-noise ratio and preservation of as much accumulated information as possible. Of prime importance are indicators that are strongly correlated in the presence of the target and are weakly so (up to negligible) in its absence. The difference in the correlation of indicators is the major source of information about their presence or absence.

Thus, when selecting standards, we are interested in the objects which are well explored not only by geological, but also by geophysical methods involving various transformations, and the study of the relations between indicators, which enables the development of a standard indicator space. As a rule, there are not a large number of objects, but they should be found and used to devise a model of the medium. This highlights the extreme importance of the accumulation and analysis of prior geological and geophysical information for developing a model of a medium. Another approach is computer modeling of geological situations and their respective indicator spaces; i.e., the creation of simulation models.

We will not dwell on the quantitative criteria for integrated interpretation. It is simply worth noting that routine qualitative criteria are also integrated since geological problems that can be solved using one geophysical method are very rare, whereas a combination of only two methods considerably expands the possibilities of geophysical data interpretation. A number of papers dealing, for the most part, with the principles of joint interpretation of gravity and magnetic fields have made this point clear-cut. For instance, it is expedient to consider qualitative criteria to single out and trace faults, which are among the main targets of geophysical investigation. It is possible not only to isolate and trace the zones of fracture by some typical indicators in the magnetic and gravity fields, but also to assess their types. The main indicators of various faults reflected in magnetic and gravity fields are summarized in Table 3.5.

Thus, the results generated from a model of the medium should be as follows:

(1) Specification of classes of objects under investigating the definition of the geological, petrophysical, and geometrical characteristics of typical objects in these classes and corresponding characteristics of host media;

Table 3.5 Magnetic and gravity fields over faults (after Eppelbaum and Khesin 2012)

Types of fractures	Geological characteristics	Reflections in fields
Faults—channels for magma flow	Fractured zones filled with basic rocks	Linearly elongated positive anomalies
	Intrusions or volcanic centers localized along fractured zone	Chain of near-isometric maxima, or sometimes minima
Contemporaneous (growth) faults	Abrupt changes in lithological composition, facies, and deposit thickness on both sides of a fault	Change of sign or behavior of the same sign field at the fault
Faults fixing vertical displacement of blocks	Abrupt changes of boundary positions separating a section into individual structural facial complexes	Zone of high-field gradients (an additional criterion is an abrupt change in occurrence depth for upper or lower anomalous mass edges)
	Crush zone due to differentiated movement of conjugated blocks along the fault	Chain of linearly elongated magnetic and gravity minima coincident in plan
Faults fixing horizontal displacement of blocks	Horizontal rock displacement determined by comparing age, and structural and facies features of rocks on both sides of a fault	Rupture and echelon displacement of zones with linearly elongated anomalies, abruptly inflected isolines

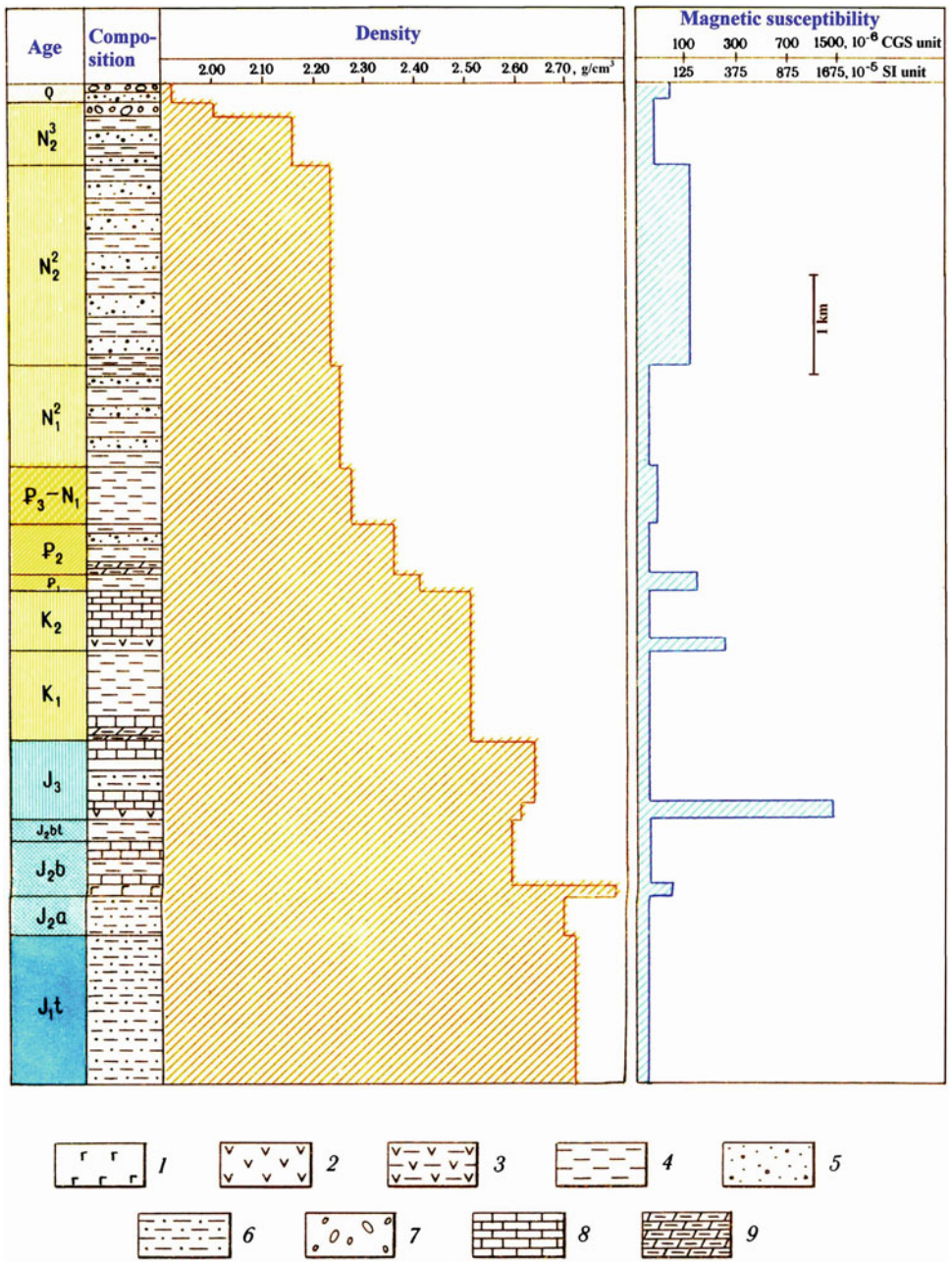

Fig. 3.12 Generalized petrophysical column for the southern slope of the Greater Caucasus mega-anticlinorium and the adjacent area of the Pre-Caucasus. *1* Basalts, andesito basalts and diabases, *2* Andesites, *3* Volcanogenic-sedimentary rocks, *4* Clays, *5* Sands, *6* Sandy-clay deposits, *7* Coarse gravels and conglomerates, *8* Limestone and dolomites, *9* Marl

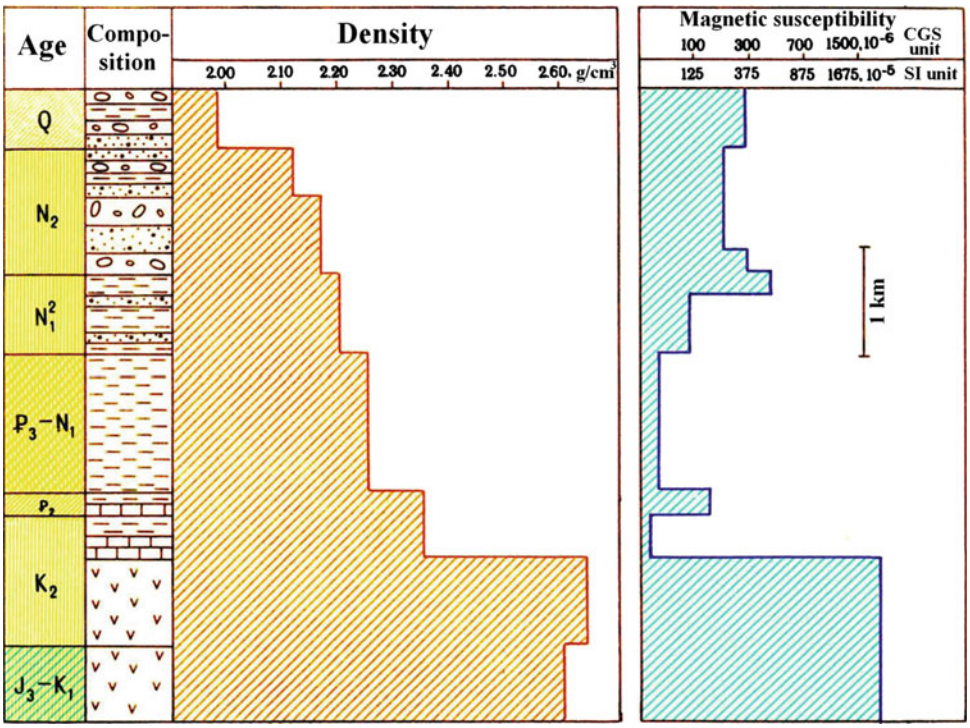

Fig. 3.13 Generalized petrophysical column for the Kur mega-sinclinorium

(2) identification of the features from the observed field (and from other geophysical fields) and a set of indicators associated with the targets; determination of the methods and estimates of their anomalous values; and
(3) interpretation criteria for singling out the targets according to the given field (and other geophysical fields) and/or to a set of indicators.

It is generally good practice to summarize the results of a model of medium in a table containing geological, petrophysical, geometric, and geophysical data on the targets and host media, the key indicators of these objects and their identification criteria. These should be presented as generalized sections with the computed field charts placed above them.

It is also worthwhile presenting parts of the model in the form of petrophysical and/or schematic geological maps that highlight the geological objects that are the probable sources of anomalies and exclude all other objects. These complete data graphic models can be represented as block diagrams.

Naturally, a model of the medium can only partially reflect reality. The greater the accuracy and completeness of the analysis, and the better the use of existing data, the more reliable it is and the more robust the analogies drawn from it. Clearly, a model of a medium is a complex hypothesis of unknown features in the geological structure in the investigation area and its likelihood of containing a certain mineral. Uncertainty is always present (and must be present) in a model. The aim of subsequent field data interpretation is to reduce this uncertainty and to test the hypotheses by applying the criteria (Goltzman 1971).

In the petrophysical sequence of the Greater Caucasus mega-anticlinorium (together with the adjacent area of the Pre-Caucasus) (Fig. 3.12), five density steps were defined (Khesin and Eppelbaum 2007): (1) Quaternary (σ_{aver} = 1.95 g/cm^3), (2) Paleogene–Neogene (σ_{aver} = 2.23 g/cm^3), (3) Cretaceous (σ_{aver} = 2.48 g/cm^3), Bajocian–Upper Jurassic (σ_{aver} = 2.62 g/cm^3), and Lower Jurassic–Aalenian (σ_{aver} = 2.72 g/cm^3). Thus, in the section four petrodensity boundaries were found with the following density contrasts at the interfaces (top-down): +0.28, +0.25, +0.14, and +0.10 g/cm^3.

As a whole, the geomagnetic sequence of the Greater Caucasus mega-anticlinorium is characterized by low values of magnetic susceptibility ($\sigma_{aver} = 80 \times 10^{-6}$ CGS unit), which increase sharply only for volcanogenic and volcanogenic-sedimentary associations. An analysis of magnetic susceptibility behavior revealed three petromagnetic floors: (1) Pliocene–Quaternary (coarse molasse) with $\sigma_{aver} = 100 \times 10^{-6}$ CGS unit, Eocene–Miocene (fine molasse)—$\sigma_{aver} = 60 \times 10^{-6}$ CGS unit and Jurassic–Cretaceous—$\sigma_{aver} = 30 \times 10^{-6}$ CGS unit.

The upper (uppermost) part of the Kur Depression sequence is represented (Fig. 3.13) by rocks of low density and Jurassic-Cretaceous associations relate to the middle density class only at the bottom of the sequence. Here, three petrodensity floors could be identified: (1) Quaternary (σ_{aver} = 1.98 g/cm^3), (2) Palaeogene–Neogene (σ_{aver} = 2.18 g/cm^3), and Jurassic–Cretaceous (σ_{aver} = 2.62 g/cm^3). These floors are interrupted by two petrodensity boundaries (top-down): +(0.20 and 0.44) g/cm^3.

The current stage of the Kur Depression investigation reveals three petromagnetic floors: (1) Pliocene–Quaternary ($\sigma_{aver} = 300 \times 10^{-6}$ CGS unit), (2) Eocene–Miocene ($\sigma_{aver} = 100 \times 10^{-6}$ CGS unit), and (3) Cretaceous (volcanogenic and volcanogenic-sedimentary deposits with $\sigma_{aver} = 1500 \times 10^{-6}$ CGS unit). It should be noted that the first two floors are similar to the floors found for the Greater Caucasus mega-anticlinorium, but the magnetic susceptibility of the corresponding geological associations in the Kur Depression is significantly higher.

The sequence of the Lesser Caucasus mega-anticlinorium is characterized by low differentiation of density at the vertical (Fig. 3.14) that complicates clear identification of the petrodensity boundaries. Initially, three petrodensity floors were described: (1) Quaternary (molasses and river deposits)—$\sigma_{aver} = 1.98$ g/cm^3, (2) Upper Bajocian–Neogene —$\sigma_{aver} = 2.57$ g/cm^3, and (3) Precambrian–Lower Bajocian —$\sigma_{aver} = 2.65$ g/cm^3. The values of the petrodensity jumps at the boundaries (top-down) are +0.57 and +0.08 g/cm^3, respectively. The presence of Quaternary lavas eliminates the first jump. It should be noted that the available density characteristics of the Beyukkishlak metamorphic schists (outcropping in the core of the Shamkir anticlinorium—Proterozoic?) do not allow to distinguish these very ancient associations in the studied petrodensity floors (Karkoshkin 1979). At the same time, the density of these associations in Armenian territory testifies to the heightened values of this parameter (Nikolsky et al. 1975). Apparently, the Upper Precambrian–Lower Paleozoic decreases in density

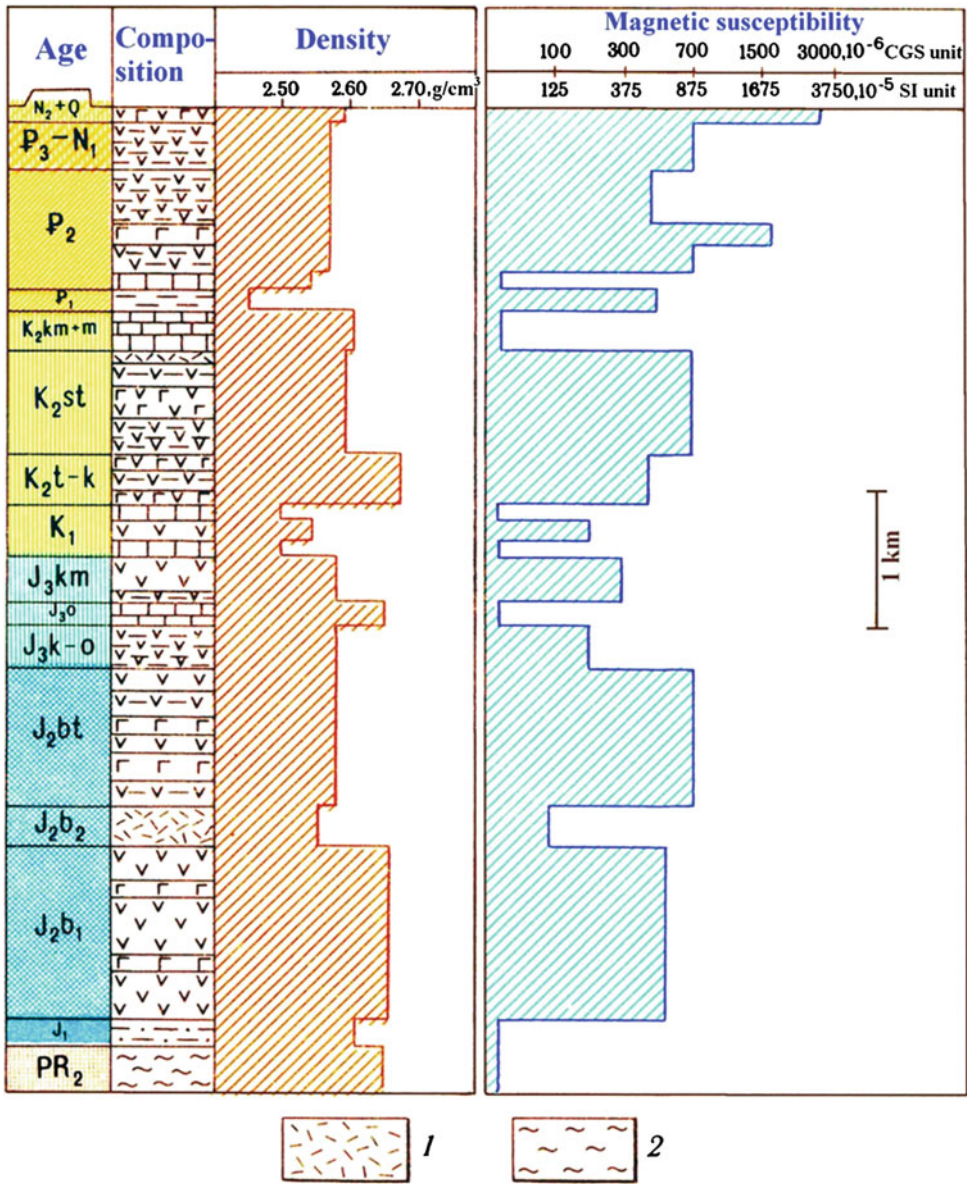

Fig. 3.14 Generalized petrophysical column for the Lesser Caucasus mega-anticlinorium. *1* Liparites and plagio-liparites, *2* Metamorphized schists (other symbols are the same as in Fig. 3.12)

compared to overlying rocks from south to north (right up to inversion).

The petromagnetic sequence of the Lesser Caucasus mega-anticlinorium is highly differentiated and is abundant in magnetic and high-magnetic associations (Fig. 3.14). In the sequence, there are six petromagnetic floors: (1) Eocene–Quaternary ($\kappa_{aver} = 700 \times 10^{-6}$ CGS unit), (2) Upper Cretaceous–Paleocene ($\kappa_{aver} = 100 \times 10^{-6}$ CGS unit), (3) Upper Cretaceous ($\kappa_{aver} = 700 \times 10^{-6}$ CGS unit), (4) Upper Jurassic–Lower Cretaceous ($\kappa_{aver} = 250 \times 10^{-6}$ CGS unit), (5) Middle Jurassic ($\kappa_{aver} = 600 \times 10^{-6}$ CGS unit), and (6) Paleozoic–Lower Jurassic ($\kappa_{aver} = 10 \times 10^{-6}$ CGS unit).

In the Nakhchivan folded region, three petrodensity floors were identified (Fig. 3.15): (1) Neogene ($\sigma_{aver} = 2.17$ g/cm^3), (2) Upper Cretaceous–Oligocene ($\sigma_{aver} = 2.51$ g/cm^3), and (3) Paleozoic–Jurassic ($\sigma_{aver} = 2.65$ g/cm^3). The jumps on these two petrodensity boundaries (top-down) are +0.34 and 0.14 g/cm^3. Analysis of magnetic susceptibility behavior served to delineate five floors (Fig. 2.15): (1) Oligocene–Miocene ($\kappa_{aver} = 100 \times 10^{-6}$ CGS unit), (2) Eocene ($\kappa_{aver} = 1500 \times 10^{-6}$ CGS unit), (3) Upper Cretaceous–Paleocene ($\kappa_{aver} = 50 \times 10^{-6}$ CGS unit), (4) Jurassic ($\kappa_{aver} = 1500 \times 10^{-6}$ CGS unit), and (5) Paleozoic ($\kappa_{aver} = 10 \times 10^{-6}$ CGS unit).

In the petrodensity sequence of the Talysh anticlinorium, four floors were detected (Fig. 3.16): (1) Pliocene ($\sigma_{aver} =$

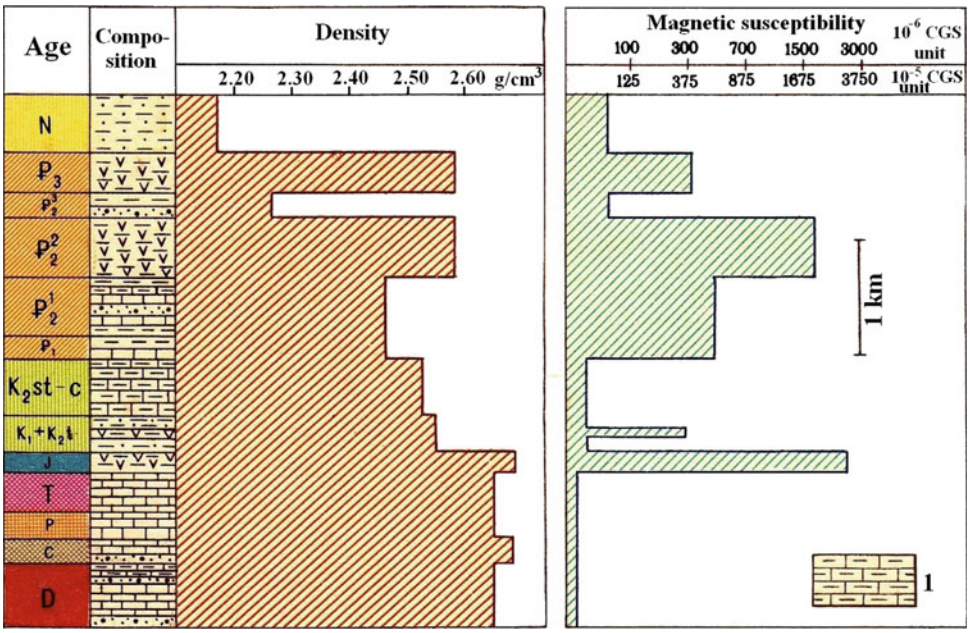

Fig. 3.15 Generalized petrophysical column for the Nakhchivan folded region. *1* Carbonate-terrigeneous rocks

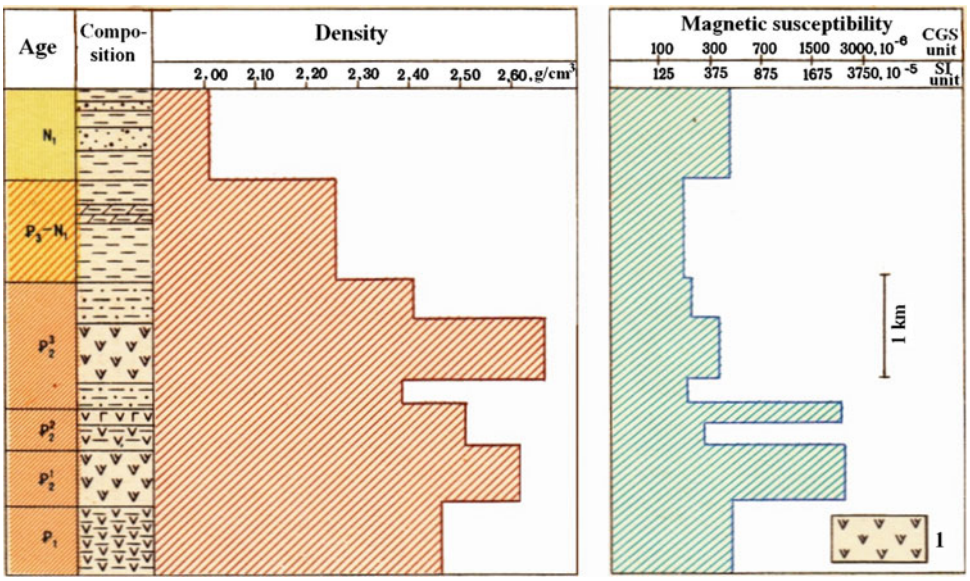

Fig. 3.16 Generalized petrophysical column for the Talysh anticlinorium. *1* Trachyandesites and trachybasalts

Table 3.6 Density properties of sedimentary samples selected in the western part of the South Caspian depression (total number of analyzed samples: 1200) (after Gadjiev 1965)

Rock	Suite	Density (min-max), g/cm^3
Clay	Maykop	1.86–2.11
Clay	Diatomaceous	1.84–2.10
Clay	Productive Series (PS)	1.73–2.30
Clay	Absheron	1.64–2.22
Clay	Akchagyl	1.67–1.97
Clay	Selected from a depth of 1167 m	2.25
Quaternary deposits		1.70–2.11
Mud volcanic breccia		1.90–2.19
Sandstone		2.04–2.53
Marls		2.06–2.60

2.00 g/cm^3), (2) Oligocene–Miocene (σ_{aver} = 2.25 g/cm^3), (3) Eocene (σ_{aver} = 2.53 g/cm^3), and (4) Paleocene (σ_{aver} = 2.45 g/cm^3). The discontinuity jumps (top-down) are +0.25, +0.28, and −0.08 g/cm^3, respectively.

In the petromagnetic sequence of the Mountainous Talysh, two floors were found (Fig. 3.16): (1) upper (Eocene–Neogene) $\kappa_{aver} = 300 \times 10^{-6}$ CGS unit, and (2) lower (Paleocene–Middle Eocene) with $\kappa_{aver} = 700 \times 10^{-6}$ CGS unit. It is significant that the Kosmalyan suite with its high-magnetic susceptibility (about 1700×10^{-6} CGS unit) and residual magnetization (about 1900×10^{-6} CGS unit) (Ismailzadeh et al. 1983b) is divided into intervals of direct (Middle Eocene) and reverse (Lower Eocene) magnetization. This fact confirms earlier conclusions about the nature of negative magnetic anomalies in this region (Khesin and Eppelbaum 2007).

Some density characteristics of samples (sedimentary rocks) withdrawn in the South Caspian Depression are presented in Table 3.6.

3.4 Common Characteristics of Petrophysical Boundaries and Geological Associations

Density characteristics patterns, together with some common peculiarities, can have both shared and distinct features (Fig. 3.17).

The shared feature of all these sequences is the presence (typical of all geostructures) of two petrodensity boundaries: (I) between the Quaternary (sometimes Neogene–Quaternary) deposits and the underlying denser associations ($\Delta\sigma$ = 0.2–0.3 g/cm^3), and (II) the boundary between Cenozoic and Mesozoic associations ($\Delta\sigma_{aver}$ consists of 0.14–0.44 g/cm^3). However, the latter boundary in the sequence of the Lesser Caucasus mega-anticlinorium is poorly defined since $\Delta\sigma_{aver}$ reaches only 0.05 g/cm^3. Here the reference horizon of lower density and magnetization are liparites and plagio-liparites of the Upper Bajocian.

As a whole, the densest rocks are typical of intrusive formations in the pre-, syn- and post-collisional stages. The rock density of intrusive formations in the pre-collisional stage ranges approximately from 2.80 to 2.95 g/cm^3 (excluding Bajocian plagiogranites whose chemical consistency leads to a density of 2.50–2.60 g/cm^3). The density of the intrusive formations of the syn- and post-collisional stages ranges on average from 2.70 to 2.85 g/cm^3 and thus should be included in the class of heightened density.

The density of intrusive formations in the pre-accretional stage has a clear tendency to decrease the class of middle density (σ_{aver} = 2.65–2.75 g/cm^3). The intrusive formations of this stage have the lowest density (σ_{aver} = 2.55–2.60 g/cm^3).

The rocks composing effusive formations mainly belong to the class of heightened (σ_{aver} = 2.70–2.85 g/cm^3) and middle (σ_{aver} = 2.50–2.70 g/cm^3) density. Rocks of heightened density are typical of the effusive formations of the early Alpine mobilization stage. The density of the later stages gradually decreases, and rocks of the orogenic stage can almost completely be assigned to the class of low density (σ_{aver} = 2.45–2.60 g/cm^3).

Among the background sedimentary deposits, the densest (σ_{aver} = 2.60–2.75 g/cm^3) are the sand-shale associations of the mega-anticlinorium of the Greater Caucasus, as well as carbonate deposits of the Late Jurassic–Early Cretaceous. The tendency for decreased density from the early to late stages is also present here.

The Pre-Alpine associations (metamorphic shales of the Upper Proterozoic and subplatform terrigeneous-carbonate Paleozoic deposits) belong to the middle density class.

As a first approximation, a geomagnetic sequence can be divided into three floors corresponding to the main tectonic stages. The lower floor (Pre-Jurassic) is represented mainly by terrigeneous carbonate associations penetrated by acid intrusions and is practically non-magnetic. One exception is the volcanogenic association revealed in the Shamkir anticlinorium of the Lesser Caucasus. The middle floor (Mesozoic-Eocene), within which basic and middle consistency thick volcanites develop, is distinguished by its heightened magnetization. The upper floor (Post-Eocene) represented mainly by the terrigeneous deposits of the sedimentary cover is characterized by a lower magnetization (although in the some areas Neogene–Quaternary lavas with high magnetization have developed).

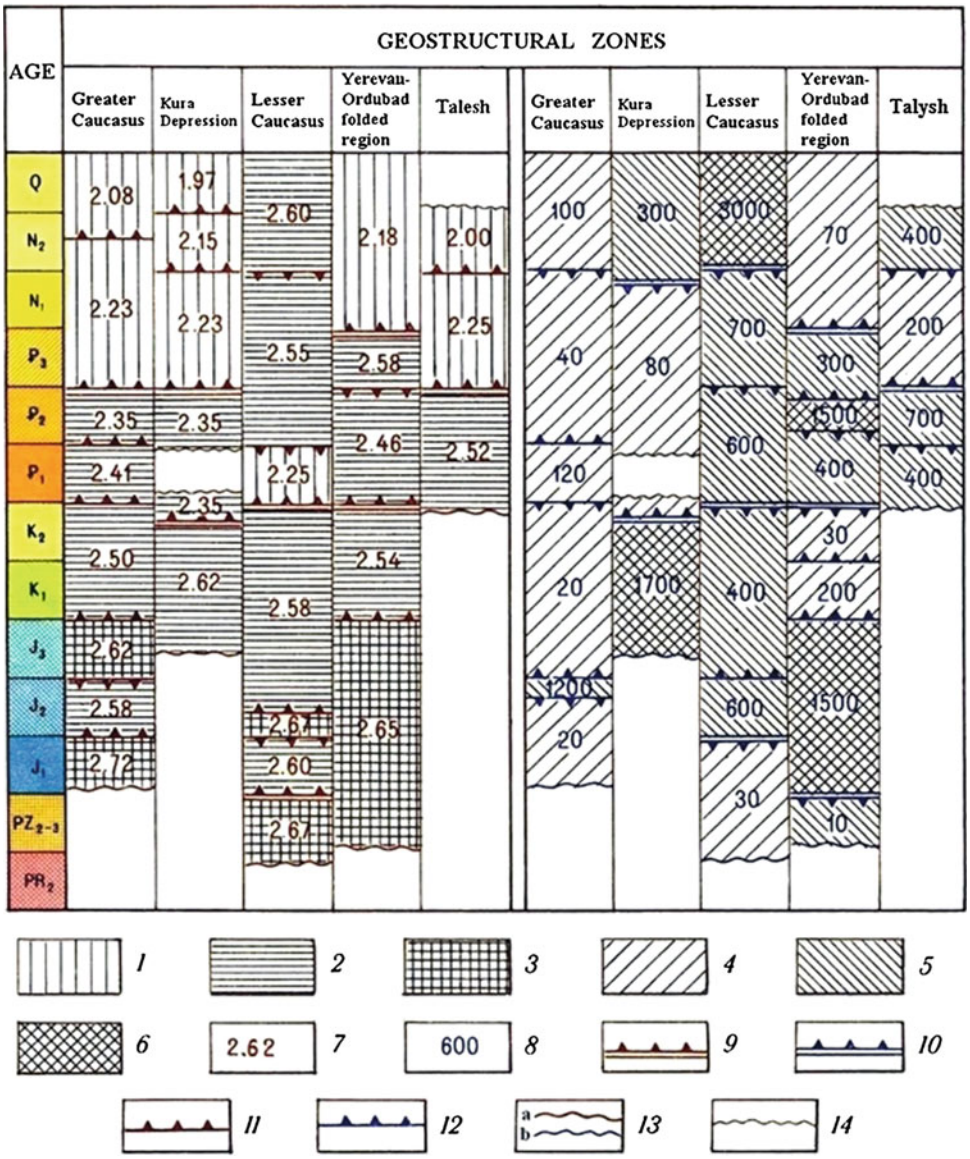

Fig. 3.17 Determining petrophysical floors of Azerbaijan (after Alexeyev et al. 1989, with modifications). Intervals of average density values, g/cm^3: *1* 1.95–2.30, *2* 2.31–2.60, *3* 2.61–2.90; intervals of average magnetic susceptibility values, 10–6 CGS: *4* 0–250, *5* 251–700, *6* >700; *7* Average value of density, g/cm^3; *8* Average value of magnetic susceptibility, 10^{-6} CGS; clearer petrophysical boundaries: *9* Density, *10* Geomagnetic; less clear petrophysical boundaries: *11* Density, *12* Geomagnetic; *13* Lower boundary of density (**a**), and magnetization (**b**) investigations; *14* Boundary of petrophysically unknown section. *Note* The *arrows* in 9–12 are oriented in their direction of density or decreasing magnetization

It should be noted that in the intermediate floor, the volcanogenic associations of the Middle Jurassic have the highest average magnetic susceptibility (in the Lesser Caucasus, their thickness attains approximately 4 km), and less thick volcanites of the Upper Cretaceous. The residual magnetization of these rocks is parallel or antiparallel to the induced magnetization; in the zones of inverse magnetization typically there are relatively low-magnetic associations.

The Cenozoic volcanogenic associations of the Talysh and Pre-Talysh as well as the lava covers in the central part of the Lesser Caucasus have a different characteristic. Here, paleomagnetic zones of different polarities alternate. Computations indicate that the upward continued magnetic anomalies (associated with the gently sloping Cenozoic associations) were rapidly damped.

The lavas are characterized by the largest values of magnetization compared to piroclastic associations of the same consistency. Magnetization of hyperbasites is approximately proportional to their degree of serpentinization (at the same time, the hyperbasite density decreases by degree of their serpentization).

Analysis of the sequence of the main petrodensity and petromagnetic geostructures of Azerbaijan (Fig. 3.17) thus suggests that these floors are correlated in terms of age, but the average values of their physical characteristics and relations differ. Obviously, this is caused by the different histories of these geostructures' geological developments. Nevertheless, the physical parameters can be assessed by creating 3D physical–geological models of the Earth's crust of Azerbaijan (Chaps. 4–6) and 3D models of hydrocarbon (Chap. 7) and ore deposits (Chap. 8).

References

Affleck, J. (Special Editor), 1964. Special issue on magnetic methods. *Geophysics*, **29**, No. 4.

Alexeyev, V.V., 1976. Development and improvement of the magnetic anomalies interpretation methods under conditions of inclined magnetization and sloping relief (a specific example of Belokan-Zagatala ore district (Azerbaijan), southern slope of the Greater Caucasus), *Ph.D Thesis*. Mining Institute, Dnepropetrovsk (in Russian).

Alexeyev, V.V., Gadjiev, T.G., Karkoshkin, A.I. and Khesin, B.E. (T. A. Ismailzadeh and B.E. Khesin, Eds.), 1989. *Gravity and Magnetic Anomalies of Azerbaijan and Their Geological Interpretation*, Printing Map Factory, Leningrad (in Russian).

Aliyev, G.A., Akhmedbeyli, F.S., Ismailzade, A.D., Kangarli, T.H. and Rustamov, M.I. (V.E. Khain and Ak.A. Alizadeh, Eds.), 2005a. *Geology of Azerbaijan*, Vol. **IV**: Tectonics. Nafta-Press, Baku (in Russian).

Aliyev, S.A., Aliyev, C.S., Askerhanova, H.Q., Balakishibeyli, Sh.A., Qasanov, A.O., Qasanov, A.B., Zolotovichaya, T.A., Ismailzade A. D., Isayeva, M.I., Kadirov, F.A., Mukhtarov, A.Sh., Rzayev, A.Q., Cafarov, I.B. and Khalafly, A.A. (Ak.A. Alizadeh, Ed.), 2005b. *Geology of Azerbaijan*, Vol. V: *Physics of the Earth* (in Russian).

Alizadeh, Ak.A. (Ed.). 2012. *Modern Problems of Geology and Geophysics of the Caucasus*. Nafta-Press, Baku.

Asanidze, B.Z. and Pecherskiy, D.M., 1979. Paleomagnetic investigations of the Jurassic rocks of Georgia and Northern Caucasus. *Izvestiya, Earth Physics*, **10**, No. 10, 77-92 (in Russian).

Asanidze, B.Z., Pecherskiy, D.M. and Adamiya, Sh.A., 1980. Results of paleomagnetic investigations of the Paleozoic rocks of the Caucasus. *Izvestiya, Earth Physics*, **16**, No. 9, 90-109 (in Russian).

Berezkin, V.M., 1967. *Calculation of Terrain Relief and Intermediate Layer Effects in Gravity Prospecting*. Nedra, Moscow (in Russian).

Berezkin, V.M., Kirichek, M.A. and Kunarev, A.A., 1978. *Application of geophysical survey methods for direct oil and gas prospecting*, Nedra. Moscow (in Russian).

Borovko, N.N., 1979. *Optimization of Geophysical Investigations in Ore Deposit Prospecting*. Nedra, Leningrad (in Russian).

Bosch, M., Bertorelli, G., Alvarez, G., Moreno, A. and Golmenarez, R., 2015. Reservoir uncertainty description via petrophysical inversion of seismic data. *The Leading Edge*, No. 9, 1018-1026.

Brodovoi, V.V., 1989. Searching and prospecting of useful deposits: Copper. *In*: (Brodovoi, V.V., Ed.), *Borehole and Mining Geophysics*, Vol. **II**, Nedra, Moscow, 190-208 (in Russian).

Camps, P., Ruffet, G., Shcherbakov, V.P., Shcherbakova, V.V., Prevot, M., Moussine-Pouchkine, A., Sholpo, L., Goguitchaichvili, A. and Asanidze, B., 1996. Paleomagnetic and geochronological study of a geomagnetic field reversal or excursion recorded in Pliocene volcanic rocks from Georgia (Lesser Caucasus). *Physics of the Earth and Planetary Interiors*, **96**, 41-59.

Detkova, N.V. and Shopin, Yu.G., 1969. Estimation of correlation between the elastic wave velocity and the density for magmatic and metamorphic rocks in the ore-bearing regions of the Altai and Lesser Caucasus. *Problems of Applied Geophysics* (*Voprosy Razvedochnoi Geofiziki*), **9**, 160-163 (in Russian).

Djevanshir, R.D., 1987. Relationships between clay minerals, low temperatures, high pore pressures, and oil and gas reservoirs at great depths in the Baku Archipelago, U.S.S.R. *Jour. of Petroleum Science and Engineering,* **1**, 155-162.

Dukhovsky, A.A., Ilayev, M.G. and Kronidov, I.I., 1970. *Geophysical Investigations / Methodological Instructions for Geological Survey on a 1:50,000 Scale*. Nedra, Leningrad (in Russian).

Eppelbaum, L.V., 1989. The development of methods for processing and interpretation of natural geophysical fields in prospecting for pyrite ores under mountainous conditions. *Ph.D Thesis*, YuzhVNIIGeofizika (Baku, Azerbaijan) and Institute of Geophysics (Georgian Acad. of Sciences), Tbilisi, 1989 (in Russian).

Eppelbaum, L.V., 2014. Four Color Theorem and Applied Geophysics. *Applied Mathematics*, **5**, 358-366.

Eppelbaum, L.V. (Ed.), 2015. Introduction to *New Developments in Paleomagnetism Research*. Ser: Earth Sciences in the 21st Century, Nova Science Publisher, NY, vii-viii.

Eppelbaum, L.V., Alperovich, L., Zheludev, V. and Pechersky, A., 2011. Application of informational and wavelet approaches for integrated processing of geophysical data in complex environments. *Proceed. of the 2011 SAGEEP Conference*, Charleston, South Carolina, USA, **24**, 24-60.

Eppelbaum, L., Ben-Avraham, Z. and Katz, Y., 2004. Integrated analysis of magnetic, paleomagnetic and K-Ar data in a tectonic complex region: an example from the Sea of Galilee. *Geophysical Research Letters*, **31**, No. 19, L19602.

Eppelbaum, L.V. and Khesin, B.E., 2012. *Geophysical Studies in the Caucasus*. Springer.

Eppelbaum, L.V., Kutasov, I.M. and Pilchin, A.N., 2014. *Applied Geothermics*. Springer, Heidelberg – N.Y. – London.

Feyzullayev, A.A., Kheirov, M.B., Aliyev, Ch.S., Abbasova, S.B. and Aliyev, K.A., 2005a. *Lithology and Mineral Resources*, **40**, No. 4, 376-385.

Feyzullayev, A.A., Kadirov, F.A. and Aliyev, C.S., 2005b. Mud volcano model resulting from geophysical and geochemical research. *In*: (G. Martinelli and B. Panahi, Eds.), *Mud Volcanoes, Geodynamics and Seismicity,* 251-262.

Gadjiev, R.M., 1965. Deep Geological Structure of Azerbaijan. Azerneshr, Baku (in Russian).

Gadjiev, T.G., Karkoshkin, A.I., Khesin, B.E., Alexeyev, V.V., Potapova, E.I. and Salekhli, T.M., 1984. *Petrodensity Characteristics of Geological Associations in Azerbaijan*. Azerneshr, Baku (in Russian).

Gadjiev, T.G., Karkoshkin, A.I., Khesin, B.E., Alexeyev, V.V., Potapova, E.I., and Salekhli, T.M., 1985. *Petrodensity Map of the Azerbaijan SSR. Scale 1:500,000*. Map Printing Factory, Leningrad.

Goltzman, F.M., 1971. *Statistical Models of Interpretation*. Nauka, Moscow (in Russian).

Guliyev, I.S., 1992. A Review of Mud Volcanism. *Report. Azerbaijan Academy of Sciences, Inst. Geology*. 1-65.

Guseinov, A.N., 1988. Paleomagnesim of the Jurassic and Cretaceous deposits of the eastern part of the Lesser Caucasus. *PhD Thesis*, Inst. of Geology, Baku, Azerbaijan (in Russian).

Ismailzadeh, T.A., Gadjiev, T.G., Khesin, B.E., Karkoshkin, A.I., Alexeyev, V.V. and Metaxa, Kh.P., 1983a. *Petromagnetic Map of the Azerbaijan SSR*, *Scale 1:500,000*, Printing Map Factory, Leningrad.

Ismailzadeh, T.A., Gadjiev, T.G., Khesin, B.E., Karkoshkin, A.I., Alexeyev, V.V. and Potapova, E.I., 1983b. *Petromagnetic Characteristics of Azerbaijan*. Elm, Baku (in Russian).

Kadirov, F.A., Lerche, I., Guliyev, I.S, Kadyrov, A.G., Feyzullayev, A. A. and Mukhtarov, A.Sh., 2005. Deep structure model and dynamics of mud volcanoes, southwest Absheron Peninsula (Azerbaijan). *Energy Exploration & Exploitation*, **23**, No. 5, 307-332.

Karkoshkin, A.I., 1979. Petrophysical characteristics of the Somkhet-Agdam zone (in connection with ore prognosis from the geophysical data). *Ph.D Thesis*, Leningrad State University (in Russian).

Kerimov, K.M. and Pilchin, A.N., 1986. Use of geothermics data for prognosis of abnormal stratum pressure and oil and gas perspectives at great depths. *In*: (Kerimov, K.M., Ed.), *Combined Interpretation of Geological-Geophysical Data with the Goal to Search Oil and Gas Presence at Great Depths*. Baku Book Publ., Baku, 25-36 (in Russian).

Khalafly, A.A., 2006. *Paleomagnetism and Some Problems of the Shear Deformations of the Lesser Caucasus*. Takhsil, Baku (in Russian).

Khesin, B.E., Alexeyev, V.V. and Eppelbaum, L.V., 1993. Investigation of geophysical fields in pyrite deposits under mountainous conditions. *Jour. of Applied Geophysics*, **30**, 187-204.

Khesin, B.E., Alexeyev, V.V. and Eppelbaum, L.V., 1996. *Interpretation of Geophysical Fields in Complicated Environments*. Kluwer Academic Publishers (Springer), *Ser.: Modern Approaches in Geophysics,* Boston - Dordrecht - London.

Khesin, B.E., Alexeyev, V.V. and Metaxa, Kh.P., 1983. *Interpretation of Magnetic Anomalies in the Conditions of Oblique Magnetization and Rugged Topography*. Nedra, Moscow (in Russian).

Khesin, B.E. and Eppelbaum, L.V., 2007. Development of 3-D gravity/magnetic models of Earth's crust in complicated regions of Azerbaijan. *Proceed. of the 69th EAGE Conference*, P343, London, Great Britain, 1-5.

Kutasov, I.M. and Eppelbaum, L.V., 2015. *Pressure and Temperature Well Testing*. CRC Press (Taylor & Francis Group). London - N.Y.

Kobranova, V.N., 1986. *Petrophysics*. Nedra, Moscow (in Russian).

Kopf, A., Stegmann, S., Delisle, G., Panahi, B., Aliyev, C.S. and Guliyev, I., 2009. In *situ* cone penetration tests at the active Dashgil mud volcano, Azerbaijan: Evidence for excess fluid pressure, updoming, and possible future violent eruption. *Marine and Petroleum Geology*, **26**, 1716-1723.

Kozlovsky, E.A. and Krivtsov, A.I., 1988. Modeling of ore deposits: Trends and targets. *Soviet Geology*, No.8, 3-8 (in Russian).

Movshovich, E.B., Knepel, M.N. and Cherkashin, M.S., 1987. *Formalization of Geological Data for Mathematical Processing*. Nedra, Moscow (in Russian).

Nettleton, L.L., 1940. *Geophysical Prospecting for Oil*. McGraw-Hill, N.Y.

Nikitin, A.A.,1993. *Statistical Processing of Geophysical Data*. Series of Advanced Geophysics, Russian Experience, No. 22, Electromagnetic Research Centre, Moscow (in Russian).

Nikitsky, V.E. and Glebovsky, Yu.S. (Eds.), 1990. *Magnetic Prospecting. Geophysicist's Manual*. Nedra, Moscow (in Russian).

Nikolsky, Yu.I., Milai, T.A. and Kogan, L.Z., 1975. *Geological-Geophysical Studies of the Tectonics, Magmatism, and Metallogeny of the Caucasus*. Nedra, Leningrad (in Russian).

Novikova, O.V., Muradkhanov, S.A., Karkoshkin, A.I. et al., 1983. Unpublished report "Construction of geological-geophysical etalons for various types of ore objects for north-eastern slope of the Lesser Caucasus (within territory of Azerbaijan)". Azerbaijan Geol. Assoc., Baku (in Russian).

Parasnis, D.S., 1966. *Mining Geophysics*. Elsevier, Amsterdam.

Parasnis, D.S., 1986. *Principles of Applied Geophysics*, 4th ed., revised and supplemented. Chapman & Hall, London.

Pilchin, A., 1983. *Geothermal regime of Earth's crust of the Kura depression and its influence on pressure distribution in it*. Ph.D Thesis, Inst. of Geophysics of the Georg. Acad. of Sci., Tbilisi (in Russian).

Pilchin, A.N. and Eppelbaum, L.V., 1997. Determination of magnetized bodies lower edges by using geothermal data. *Geophysical Jour. International*, **128**, No.1, 167-174.

Safarov, I.B., 2006. Petrophysical properties of rocks in seismogenic crustal blocks of the southeastern Greater Caucasus and their geological and geophysical interpretation. *Izvestiya*, *Physics of the Solid Earth,* **42**, No. 3, 260-270.

Tarkhov, A.G. (Editor), 1980. *Electrical Prospecting. Geophysicist's Manual*. Nedra, Moscow (in Russian).

Van der Voo, R. and Channel, J.E.T., 1980. Paleomagnetism in orogenic belts. *Rev. Geophys. Space Phys*., **18**, 455-481.

Vakhromeyev, G.S. and Davydenko, A.Yu., 1987. *Modeling in Applied Geophysics*. Nedra, Moscow (in Russian).

Varlamov, A.S. and Filatov, V.G., 1983. *Determination of the Density of Rocks and Geological Objects*. Nedra, Moscow (in Russian).

Veselov, K.E., 1986. *Gravimetric Survey*. Nedra, Moscow (in Russian).

Regional Geophysical–Geological Zonation

4

The regional geological–geophysical zonation may be subdivided into: (1) the development of new geophysical maps (cross sections) for the region under study, (2) qualitative and semiquantitative analysis of geophysical data (including different schemes of geophysical data processing and transformation), (3) quantitative analysis of geophysical anomalies (inverse solution) and preliminary regioning, and (4) compilation of final geophysical–geological maps. Let us successively consider these stages with application to the territory of Azerbaijan.

4.1 Development of New Geophysical Maps (Cross Sections)

4.1.1 Gravity Field

The development of novel exact geophysical maps (cross sections) basing on new obtained data and reinterpretation of some old data is of great importance. A bright example of such new map compilation is the development of new Bouguer gravity map of the Caspian Sea and adjacent areas (Lodzhevsky and Kadirov 2001) (Fig. 4.1). This gravity map was constructed on the basis of Dehghani and Makris (1983), Gravity map of the USSR (1990), and Kadirov (2000a).

The gravity map is characterized by anomalies of various geometries and amplitudes. The anomaly field of the northern part of the basin is represented by the area of increased horizontal gradients subparallel to the strike of the Caucasus. In the northwestern part of the SCB, there is a vast gravity minimum with amplitude reaching 125 mGal. The central part of the basin is represented by a gravity minimum and by an isometric maximum of the gravity field in the southwest and in the southeast (Safidrud and Godin uplift). The area of increased gradients from the Alborz mountains to the south up to the deepwater part of the basin is typical for the southern part of the SCB. The area of the Central Alborz is characterized by a negative anomaly (−120 mGal) (Kadirov and Gadirov 2014).

4.1.2 Remote Sensing

Today, the origin and evolution of the Caucasus are mainly explained in terms of plate tectonics (e.g., Khain and Ryabukhin 2002). In a brief review, Kopf et al. (2003) noted that the present-day Caucasus is dominated by thrust faulting due to continental collision. From the Jurassic to the Paleogenic eras, subduction of the Tethyan seafloor occurred along the southern margin of the Turkish and Iranian blocks, resulting in calc-alkaline arc volcanism and a wide back-arc basin system. The spread of the Red Sea began during the Early Miocene, and the Arabian Plate migrated northward, accompanied by a reduction in width of the Tethys. After its closure (~20 Ma), subduction shifted to the north. As a result of the indentation of the Arabian block, the continuous back-arc basin was separated, and the oceanic crust only remained in the Black Sea and the southern Caspian Sea. The continuous northward drift of the Anatolian Plate led to initial continental collision expressed by the formation of the Lesser Caucasus and the subsequent resurrection of the Greater Caucasus during the Middle Pliocene. Currently, continental convergence continues at a rate of up to ~20–30 mm/year (e.g., Reilinger et al. 2006) along strike-slip faults, where most of the modern tectonic activity is localized (Fig. 4.2). Reilinger et al. (2006) note the tendency for motion rates to increase from west to east along strike of the Main Caucasus thrust (MCT) (≈120° azimuth). Besides this, there is little change in the magnitude of velocity estimates across the Lesser Caucasus along transects perpendicular to the Caucasus range. Taking into account the low level of seismic activity within the Lesser Caucasus, Reilinger et al. (2006) propose to imply block-like, counterclockwise rotation of the Lesser Caucasus resulting in increased convergence from west to east along the MCT.

Without hesitation, the GPS data constructions (e.g., Reilinger et al. 2006; Kadirov et al. 2008) must be coordinated with other remote sensing data or regional geophysical field distribution. For example, the map of deep-seated lineaments (Fig. 4.3) (which is undeservedly little used) shows very interesting tectonic patterns for Azerbaijan and adjacent

A.A. Alizadeh et al., *Geosciences of Azerbaijan*,
Regional Geology Reviews, DOI 10.1007/978-3-319-40493-6_4

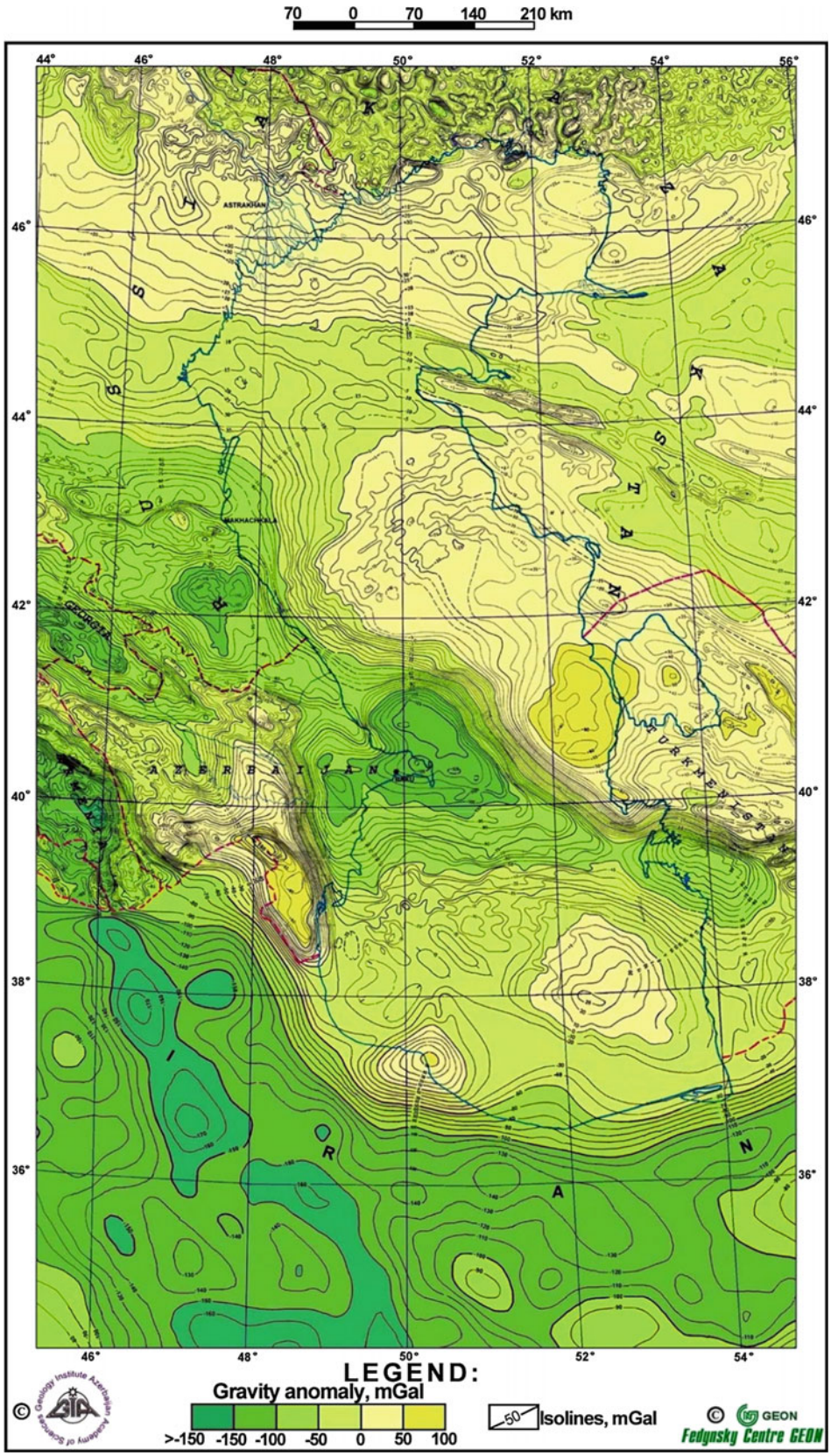

Fig. 4.1 Caspian region: Bouguer gravity map (Lodzhevsky and Kadirov 2001)

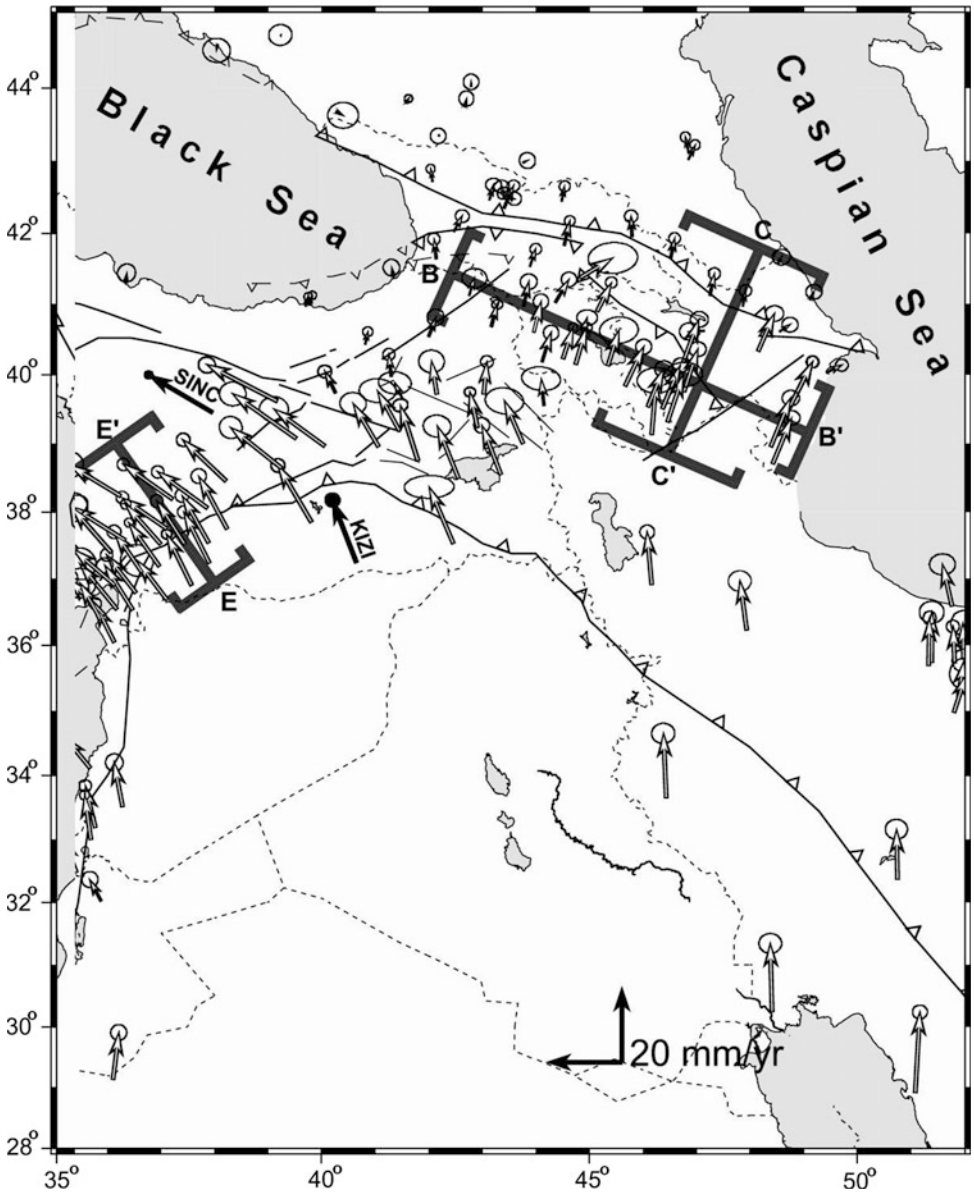

Fig. 4.2 Map showing GPS velocities with respect to Eurasia Locations and widths (*brackets*) of velocity profiles along and across strike of the Greater Caucasus (B′–B, and C′–C, respectively), the eastern Anatolian fault (E–E′) (fragment of Fig. 3 from Reilinger et al. (2006), with minor modifications)

regions. Besides other peculiarities, the intersection of deep faults was detected at the northern point of sharp tectonic wedge where the destructive Spitak earthquake of 1988 (coordinates: 40°49′ N, 44°15′ E) took place.

Gadjiev et al. (1989) identified this feature from this map of the Caucasus (Fig. 4.3) by calculating the lithospheric heterogeneity at different depths. The sum total length of the lineaments within square cells with different sides (corresponding to cubic blocks of different depths) served as a measure of heterogeneity (Khesin et al. 1996).

Note that this map of the deep structure of the Caucasian lithosphere (Fig. 4.3) is consistent with the depiction of horizontal gradients of isostatic and lithospheric gravity anomalies shown in Fig. 4.4.

Figure 4.5 illustrates more detailed example—the relation between hydrocarbon accumulations in the Kur basin and regional faults (faults location was obtained from Landsat data analysis). The map shows many faults with different orientations and styles of movement (sublatitudinal, Caucasian, anti-Caucasian, submeridianal, etc.) and depths of occurrence (from pre-Mesozoic to the younger Cenozoic). These findings were used to examine the fault systems and oil and gas content in Eastern Azerbaijan (Zeynalov 2000).

4.1.3 Thermal Field

Geothermally, Azerbaijan is one of the most investigated regions of the world (e.g., Mekhtiyev et al. 1960, 1971; Sukharev et al. 1969; Yakubov and Atakishiyev 1973; Lebedev and Tomara 1981; Aliyev 1988; Kerimov et al. 1989; Aliyev and Aliyev 1995; Pilchin and Eppelbaum

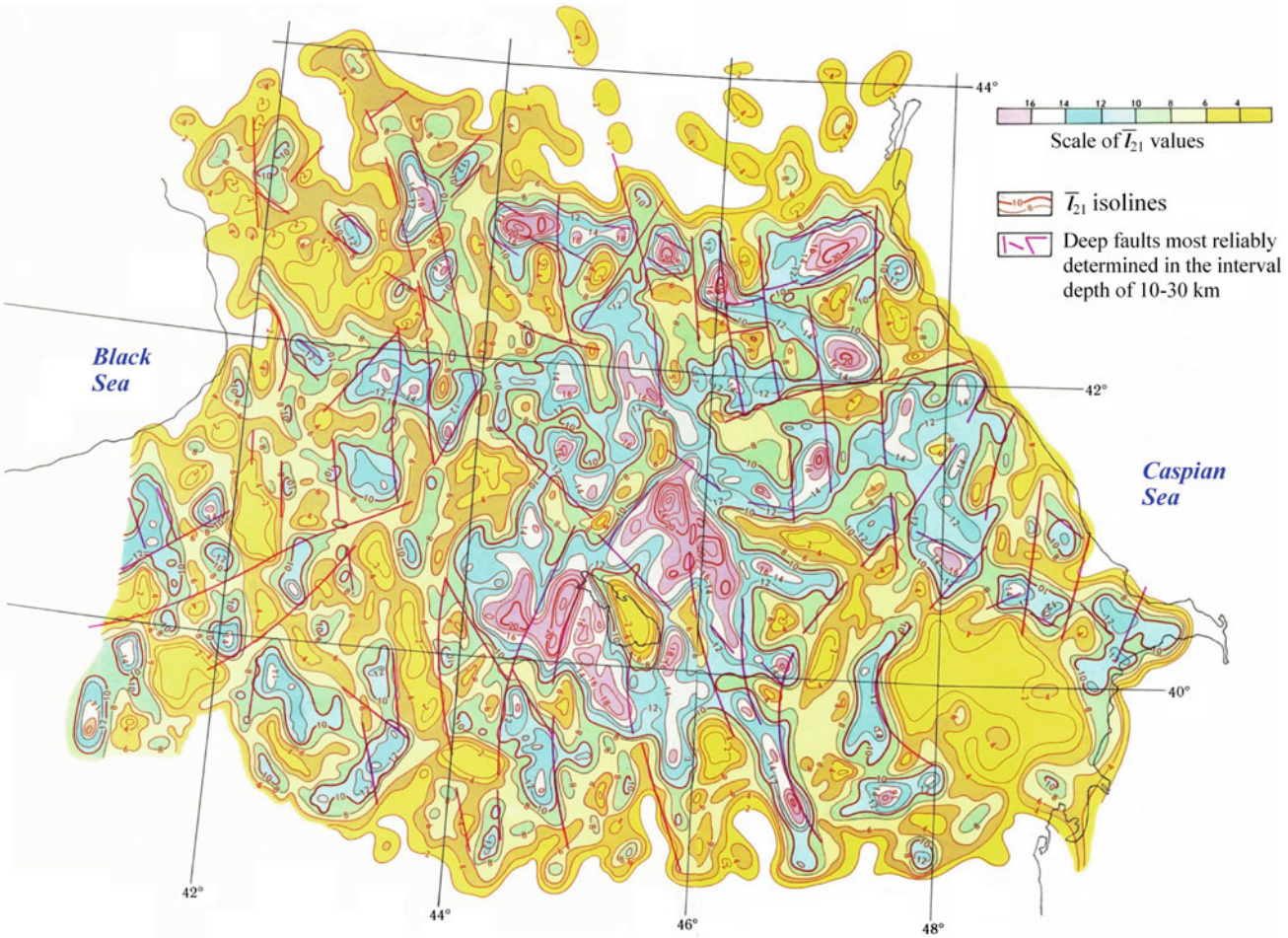

Fig. 4.3 Deep structure of Azerbaijan and adjacent regions (the cut at ≈10 km in depth) according to the satellite data analysis (after Gadjiev et al. 1989)

1997; Aliyev and Mukhtarov 2000; Rustamov 2001; Aliyev et al. 2005a, b; Mekhtiyev et al. 2003; Mukhtarov 2004, 2011, 2012; and Eppelbaum et al. 2014).

The many year's results of heat flow measurements on the territory of Azerbaijan are generalized in Fig. 4.6. This map is of great interest not only for studying deep structure and geological–geophysical mapping, but also for searching economic minerals (first of all, hydrocarbons) in this region.

Comparison of vertical and horizontal geothermal gradients at depths of 0–4 km and 0–6 km is shown in Figs. 4.7 and 4.8, respectively.

4.1.4 Radioactivity

Numerous radioactive measurements have been carried out in the territory of Azerbaijan (e.g., Ch. Aliyev and Zolotovitskaya 1996, 2000; Ch. Aliyev et al. 2001; Zolotovitskaya 2003; Ch. Aliyev and Zolotovitskaya 2005; and Ch. Aliyev et al. 2012) (see also Chap. 9 of this Volume).

The study of the radon concentration (anomalies) presents a special interest not only from the environmental point of view.

Considering the impact of other geological factors on the distribution of radon, it is necessary to note that radon is an admixture component and is emitted from the subsoil to the surface in hydrocarbon, nitrogen, and carbon dioxide gas flows. Prevalent pathways of vertical (subvertical) migrations are high-permeable zones of deep faults that usually are expressed by high thermal flows. Taking that into account, the radon distribution map was compared with deep faults and earthquake epicenters in Azerbaijan area (Fig. 4.9) and with a map of temperature distribution at 5000 m depth (Mukhtarov 2011). This comparison reveals a correlation of studied parameters confirming theoretical and some lateral assumptions (Ch. Aliyev et al. 2012).

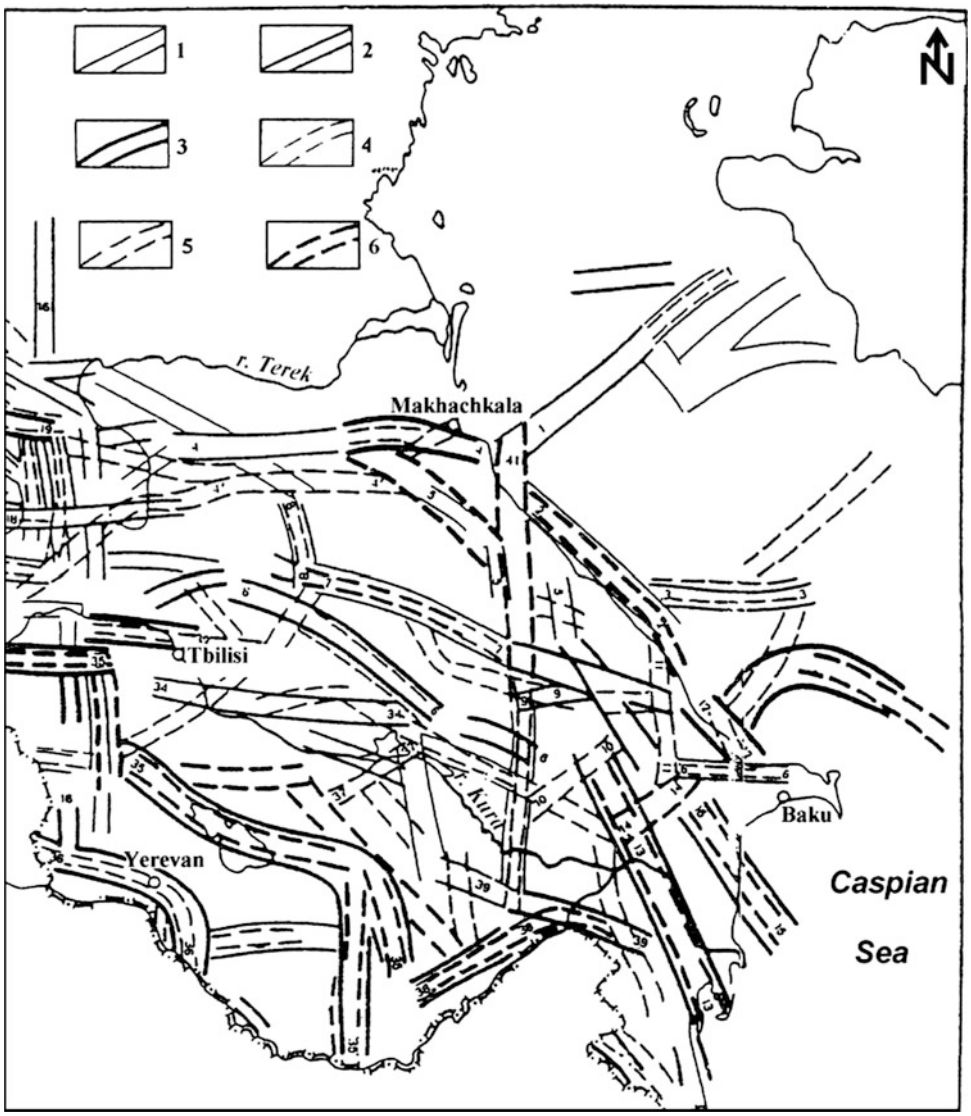

Fig. 4.4 Diagram of horizontal gradients of isostatic and lithospheric gravity anomalies (after Gorshkov and Niauri 1984, with small modifications). Zones of horizontal gradients of isostatic anomalies in mGal/km: (*1*) 0.5–1, (*2*) 1–2, (*3*) 3, zones of horizontal gradients of lithosperic anomalies in mGal/km: (*4*) 0.5–1, (*5*) 1–2, (*6*) 2

4.1.5 Paleomagnetic Analysis

Paleomagnetic data are an important source for paleotectonic reconstructions (e.g., Gorodnitsky et al. 1978; Tauxe et al. 2009). It should be noted that some geodynamic and tectonic problems cannot be solved by any other geophysical or geological method (Eppelbaum and Katz 2015). The reduction of the location of the magnetic pole for different terranes at different times can serve to evaluate regional rotation and the relative displacement of these terranes. Issayeva and Khalafly (2006) carried out an important paleomagnetic study of this type. It was revealed that the regions of the Lesser and Greater Caucasus and Iran rotate clockwise through about 20–30° with respect to the magnetic meridian, and the North Anatolia rotates anticlockwise through about 30–40° (Fig. 4.10).

The average coordinates of the paleomagnetic poles for Azerbaijan, Georgia, Armenia, Turkey, and Iran were compared to the Russian Platform and showed that these regions have been connected to the Eurasian continent since the Upper Eocene. The Lesser Caucasus has moved 5–7° to the south with respect to the Eurasian continent.

4.1.6 Deep Seismic Sounding Reinterpretation

Examples of the deep seismic sounding (DSS) reinterpretation for two DSS profiles crossing Azerbaijan are shown in Chap. 5 (Figs. 5.1, 5.2, and 5.3) (Pavlenkova 2012). Besides this, Chaps. 5 and 6 contain other seismic profiles crossing the Kur Depression and South Caspian basin.

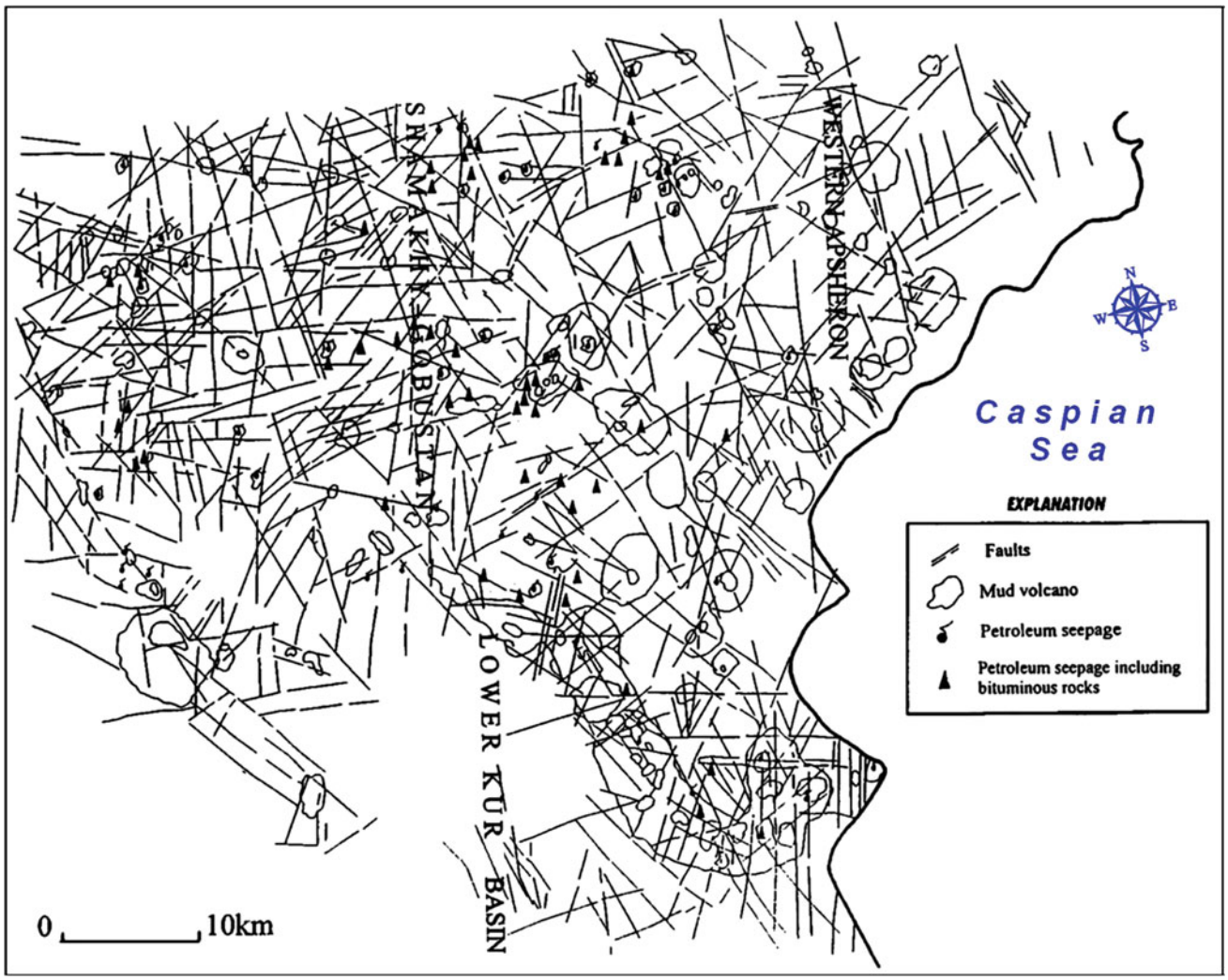

Fig. 4.5 Map of faults from analysis of Landsat data for central-eastern Azerbaijan (after Zeynalov (2000), with minor modifications)

4.2 Qualitative and Semiquantitative Analysis of Geophysical Data

The calculation techniques should be decided upon when developing the initial model of the medium. After the fieldwork is completed, the set of interpretation techniques can be corrected as a function of the particular types of anomalies that were observed. This set of calculations includes techniques to obtain the parameters of a certain class of model bodies typical to the area under survey. The techniques should meet the following criteria: applicability to the specific conditions of the geophysical investigation, in particular under the oblique polarization and rugged terrain relief characteristic of open areas in central and low latitudes, independence of the normal background level, and the choice of the origin of coordinates. The optimal techniques are those which can successfully obtain the above-mentioned parameters. Of special interest is the geophysical field interactive modeling (e.g., Kadirov 2000a; Eppelbaum and Khesin 2012).

The parameters should be determined using a combination of techniques, so that independent data on the parameter values can be obtained. When the 2D condition is satisfied, the calculations should ideally be carried out along a series of profiles in the mid-portion of the anomaly, where the field isolines are nearly parallel. The results should then be averaged. This will ensure higher validity in determining the parameter values.

To obtain the anomalous body parameters, the first stage involves interpolation selection methods (the method of characteristic points, the tangent method, the areas method, etc.). These make it possible to obtain a large number of parameters in a fairly simple way. The next stage involves the methods of singular points and analytical continuation,

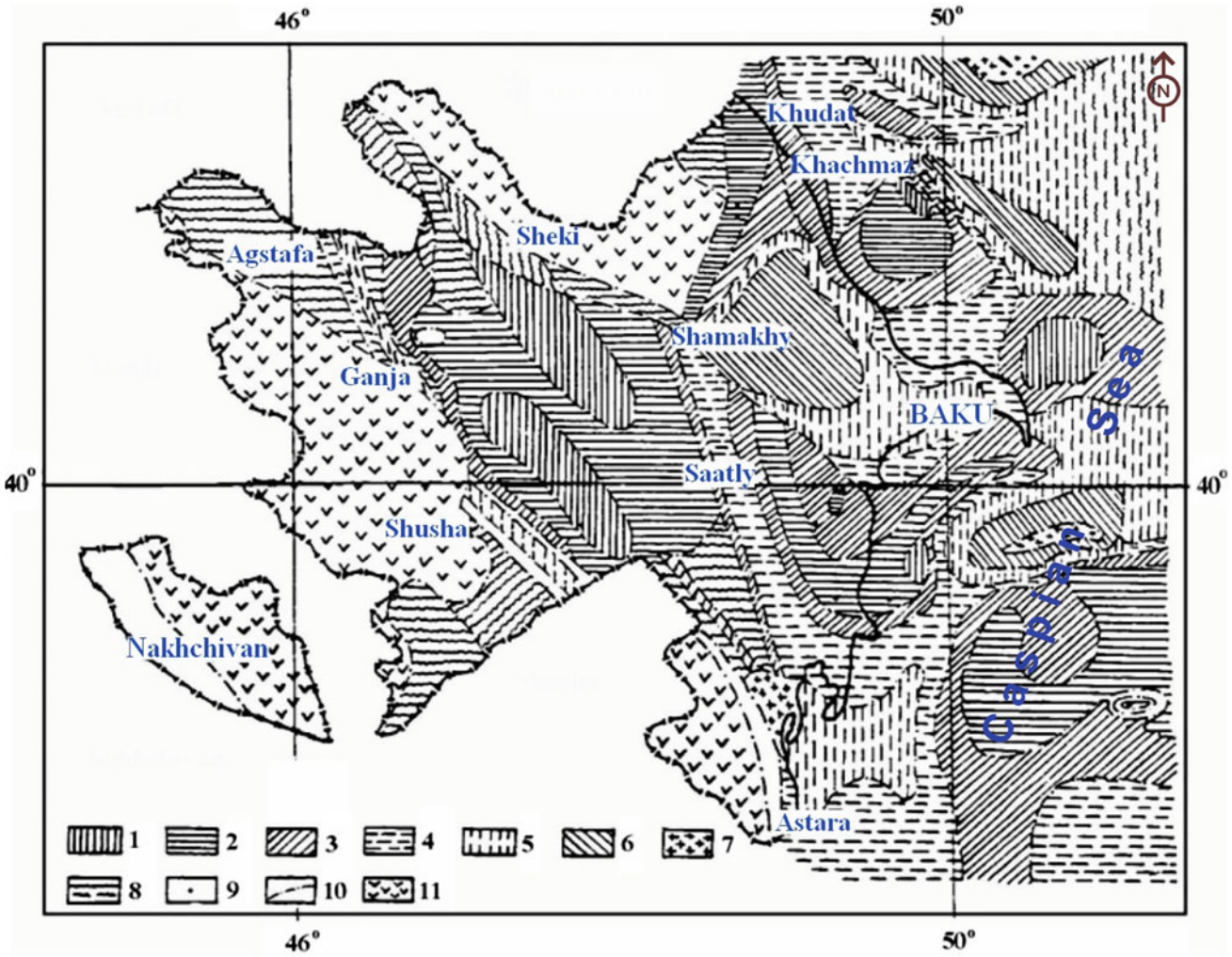

Fig. 4.6 Sketch map of heat flow of Azerbaijan. Heat flow in mW/m^2: (*1*) 0–29; (*2*) 20–30; (*3*) 30–40; (*4*) 40–50; (*5*) 50–70; (*6*) 70–90; (*7*) 90 and higher; (*8*) uncertain; (*9*) heat flow measurement points; (*10*) heat flow zone boundaries; and (*11*) folded mountain structures (Aliyev and Aliyev 1995)

because by this time, the researcher already has the necessary information about the quantitative characteristics of the object. Comparing the results obtained by the methods of interpolation selection to those obtained through the method of singular points will yield a more reliable and valid classification of singular points. The same applies to the method of analytical continuation. In this case, because the range of the upper edge occurrence depth is known, one can avoid the risk of field continuation into the vicinity of the sources.

The selection methods are used at the final stage of (Khesin et al. 1993), when a sufficient amount of data on the object parameters has been acquired. These data enable important corrections and modifications in the initial medium model, thus forming an initial approximation to make the selection: the better the initial approximation, the faster the selection.

The initial approximation involves tracing the average parameters obtained by the above techniques onto the section (scheme) plotted when developing the initial model of the medium with previous data. The information on the sources' shapes and dimensions provides a rationale for selecting the type of approximating expression. The mean-square divergence in the parameters, with prior information and fieldwork experience taken into account, is used to impose constraints on the range of possible values of the parameters.

4.2.1 Magnetic Data Analysis

It is valuable to compare the average parameters obtained by a statistical approach to the results of a deterministic

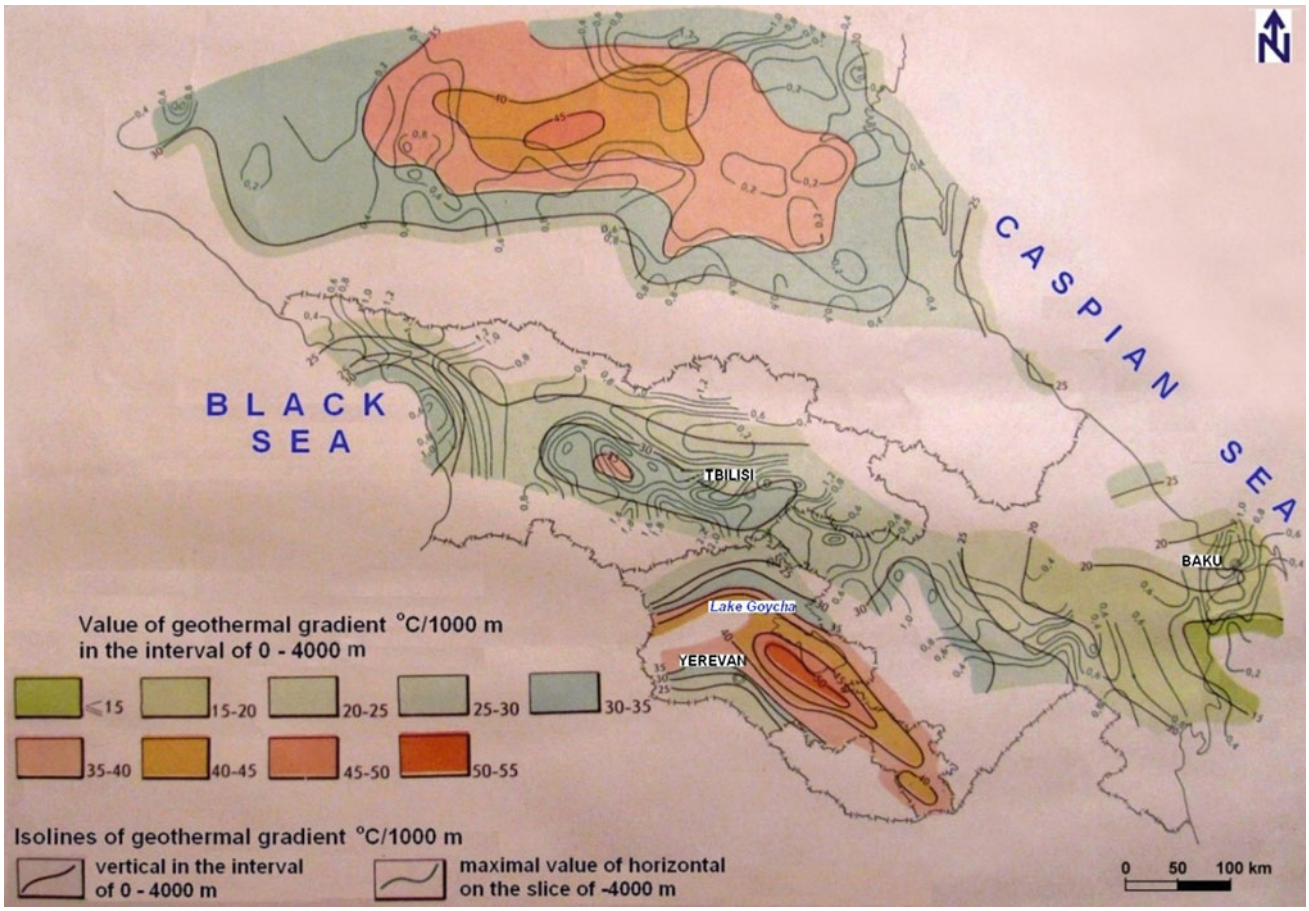

Fig. 4.7 Values of vertical and horizontal geothermal gradients at depths of 0–4000 m in the Caucasian region (after Kerimov et al. 1989)

interpretation. The technique worked out by Klushin and Tolstikhin (1961) estimates the average occurrence depth of magnetized masses by computing the normalized autocorrelation function $R_n(\tau)$ of a field with sources represented by a set of thin vertical beds. The average depth of the upper edge of magnetized sources was calculated by the following formula:

$$\bar{h} = \frac{1}{\pi}\int_0^\infty R_n(\tau)\mathrm{d}\tau = \frac{\tau_e}{\pi}, \tag{4.1}$$

where $\tau_e$is the autocorrelation radius.

We obtained $\bar{h}$ value of 4.3 km which is close to the average depth of the magnetic field's singular points. This technique was applied to the meridional profile through Western Azerbaijan (Fig. 4.11) and confirmed Paffenholtz's (1959) geological concepts.

The rugged relief in Azerbaijan means that various methods should be used to estimate different heights of geophysical field observations. The topographic mass attraction may be of no use, for example, for magnetic investigations directed at singling out a magnetized body among non-magnetic host rocks or for electric exploration to locate conducting ores in a high-resistance medium. In any case, however, the distorting effect of a non-horizontal observation line takes place when the object differs from the host medium by contrasting properties and causes an anomalous vertical gradient.

It is well known that for the purpose of estimating the usefulness of reduction to the common level, the degree of anomaly distortion can be approximated from the formula for any component of the recorded field

$$\Delta U = \frac{\partial U}{\partial z}\Delta H, \tag{4.2}$$

where $\partial U/\partial z$ is the vertical derivative of the field, and ΔH is the relative elevation of the flight height (observation line), i.e., the terrain clearance of the aerial survey.

In aerial surveys along sinuous (in the vertical plane) routes and ground surveys, the sinuosity effect, i.e., reducing observations to horizontal or inclined planes, is theoretically necessary. It substantiates the solution to certain problems associated with quantitative determination of anomalous body parameters in that neglecting the effect of variation in

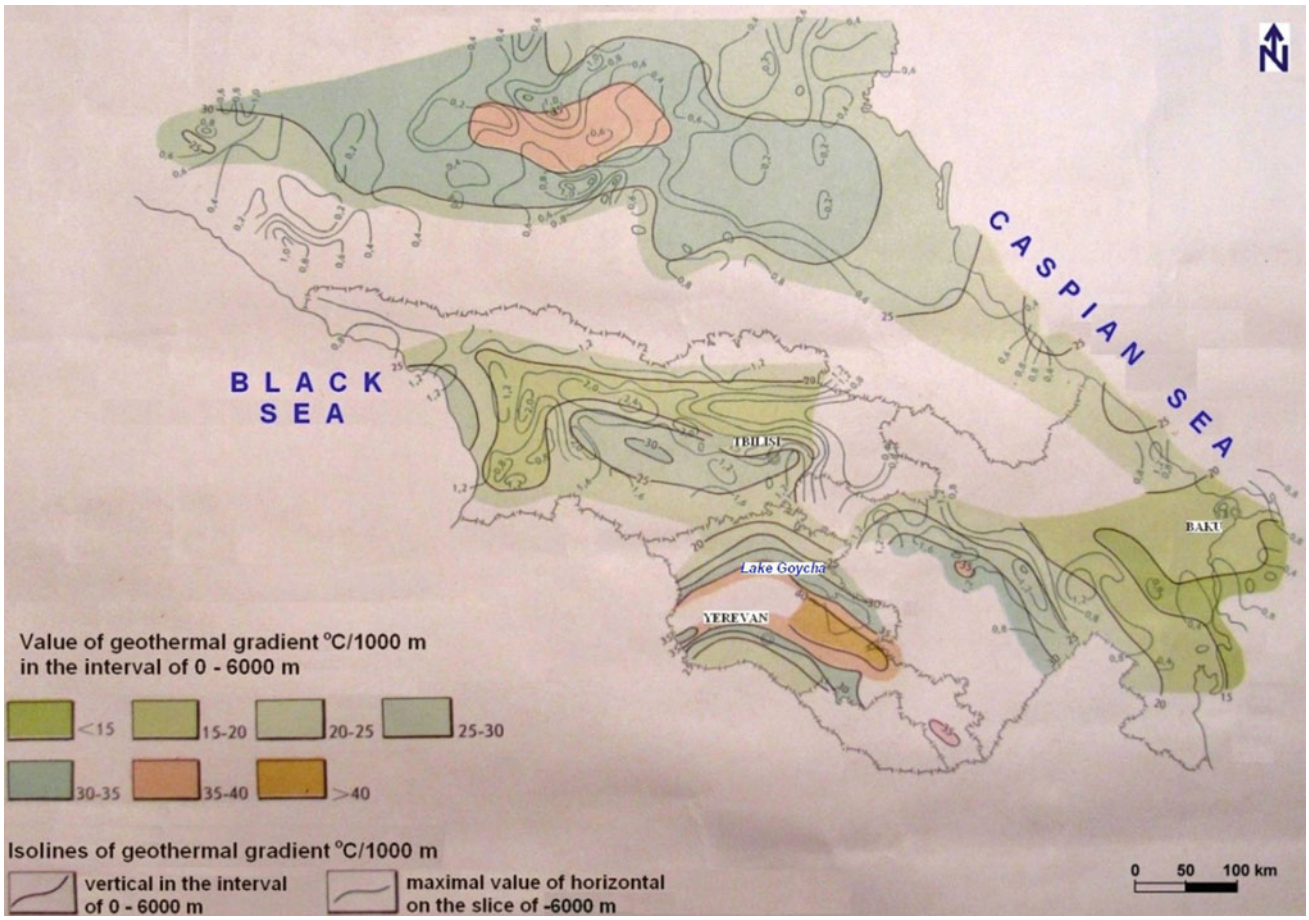

Fig. 4.8 Values of vertical and horizontal geothermal gradients at depths of 0–6000 m in the Caucasian region (after Kerimov et al. 1989)

the observation point heights may introduce errors into the interpretation. Hence, the reduction level should be as close to the acting masses as possible, and if required, several levels should be selected.

Within areas in which the surface profiles have close inclination angles, distortions of the field and its transforms due to the relief also occur. This means there is no need to carry out reduction to the plane if the preliminary regioning of the main forms has determined the dominant dips of the routes.

Subsequent analysis of the field and its transforms should be executed independently within the singled-out areas. Note that the results relate to fictitious bodies of identical forms, and the sizes are similar to those of the real anomalous bodies (Khesin et al. 1996). The evidence shows that the positions of fictitious and real bodies in plane do not differ greatly (max. 0.4 of body depth for a relief dip angle up to 30°). This is not essential for shallow-seated objects. When the relief is very complex in certain plots, it may be necessary to reduce the field to the plane, which should be inclined and as close as possible to the relief.

A general case of the complexity of the physical properties and the geophysical anomaly polygon distribution can be found in the Caucasus. Take for example the magnetic anomaly distribution in the Lok-Garabagh (Somkhit-Agdam) tectonic–magmatic zone of the Lesser Caucasus (Fig. 4.12).

Even within the limits of this zone, the magnetic anomaly distribution does not correspond to a normal or lognormal distribution that fits either the Pearson criterion or the less rigid Kolmogorov criterion (Yaglom and Yaglom 1973). Interestingly, in the observed magnetic field distribution, the average values are close to the dispersion. This is specific to the Poisson distribution which represents the physical nature of anomalies as rare events.

The similarities in anomalies ΔT and Z_a for the Kur Depression can be explained by the northern (≈45°) dip of the disturbing bodies approximated by thin beds (Khesin et al. 1996). This assumption is corroborated by the regional geological sections through the Kur megasynclinorium. For instance, in the upper part of the sedimentary cover, there are large northern sharply dipping faults. In many cases, these faults form a plateau whose depth curls to the north. Thus, the magnetic anomaly bodies occurring in the Kur Depression section at a depth (mainly in the Ganja region) were exposed by tectonic forces oriented to the north. Hence, the

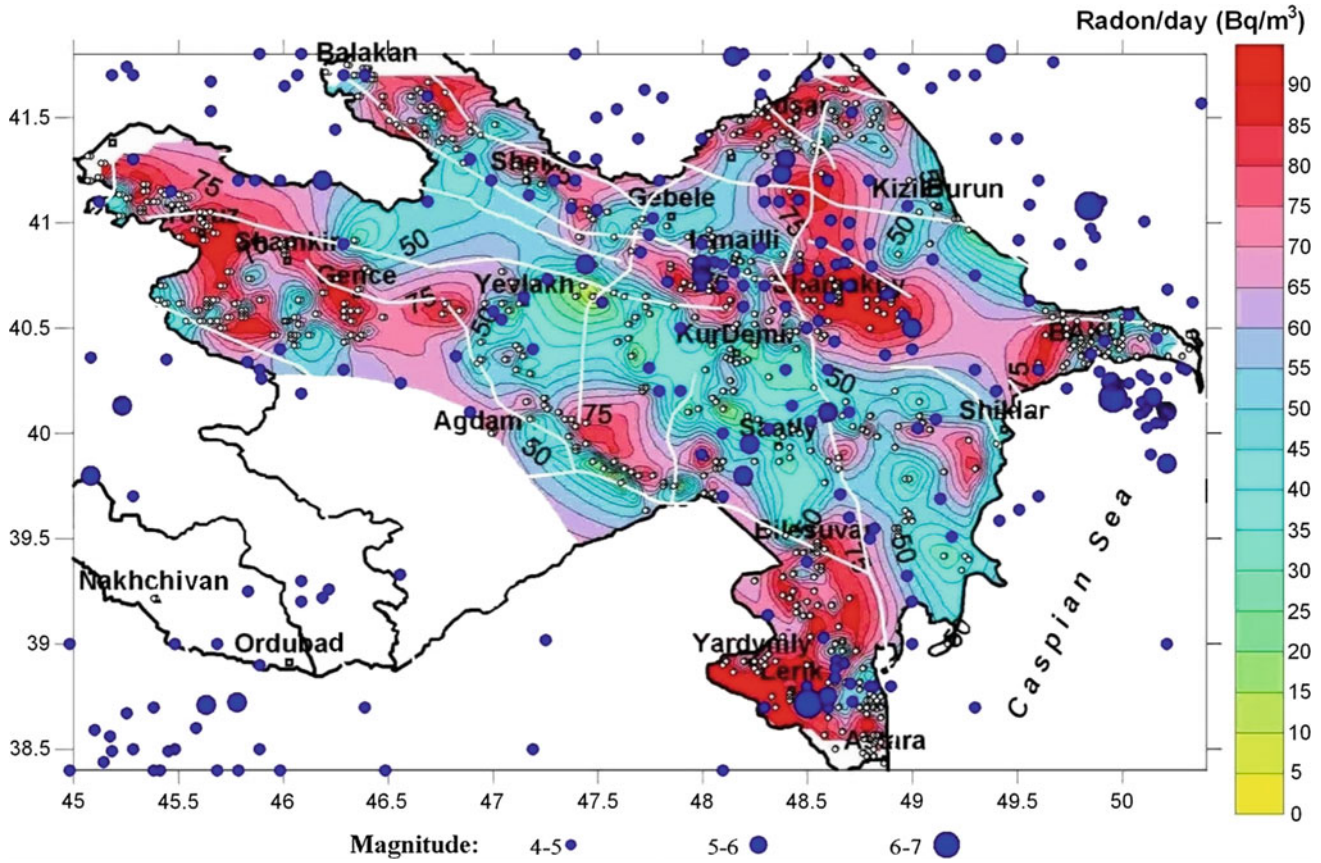

Fig. 4.9 Map of comparison of radon field of Azerbaijan with deep faults and epicenters of sensible earthquakes. *White lines* designate position of deep faults (Ch. Aliyev et al. 2012). Map of earthquake epicenters in Azerbaijan was taken from Kadirov et al. (2008)

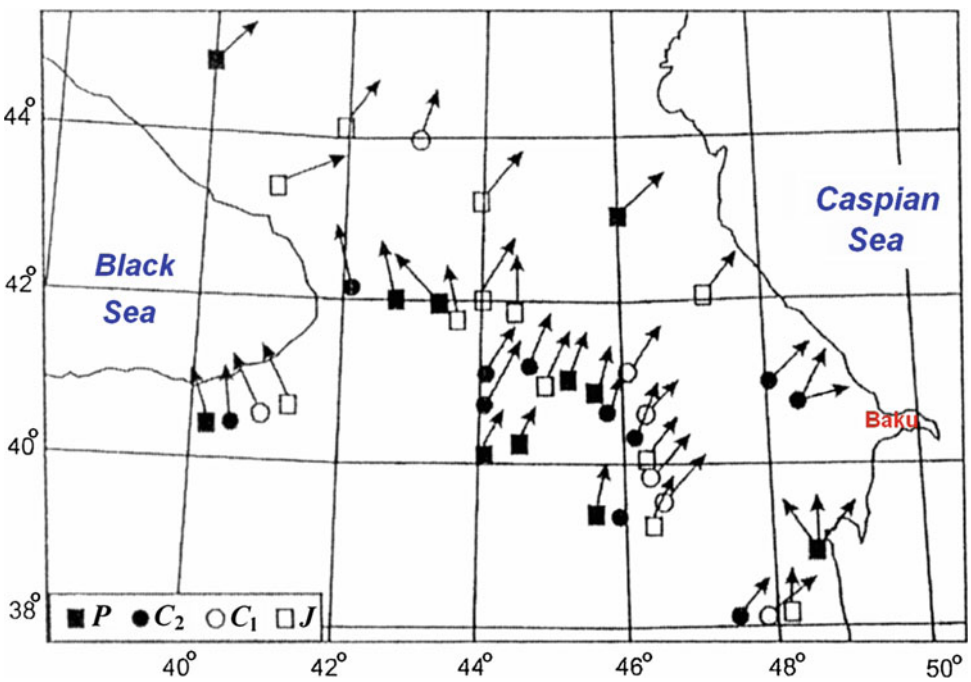

Fig. 4.10 Distribution of paleomagnetic vectors for the Mesozoic–Cenozoic rocks of Azerbaijan and adjacent areas (after Issayeva and Khalafly 2006, with some modifications). *P*—Paleogene, C_2—Late Cretaceous, C_1—Early Cretaceous, and *J*—Jurassic

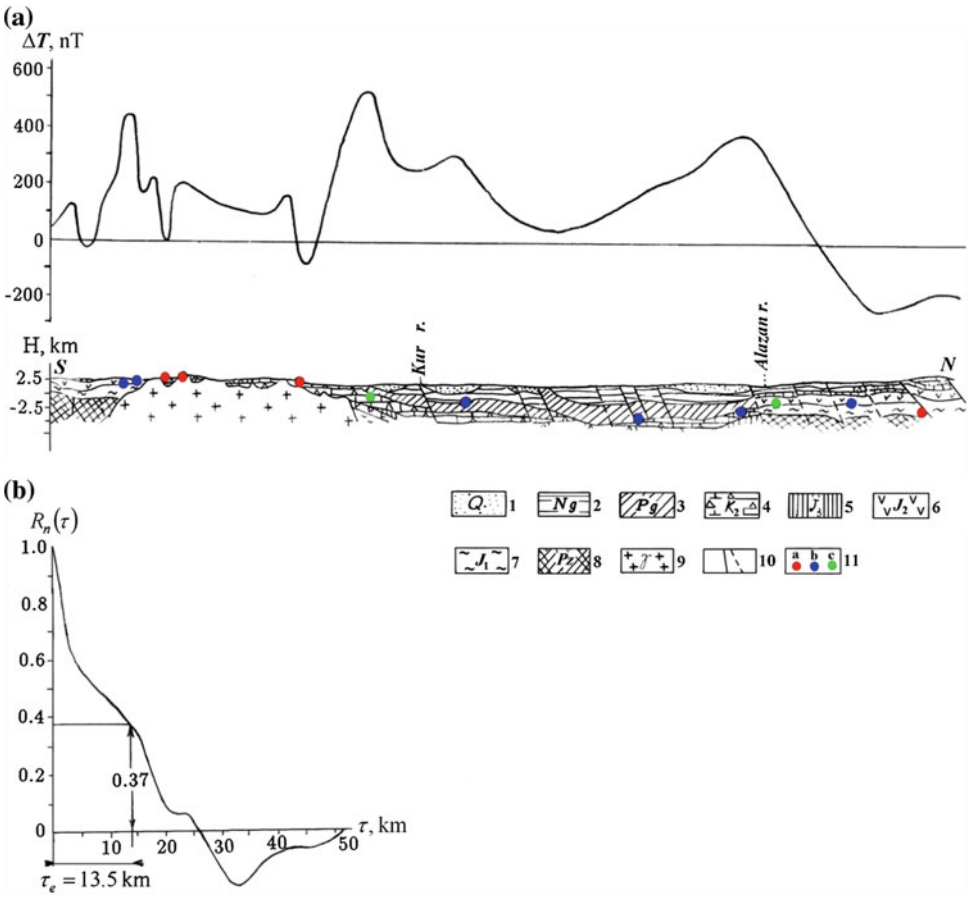

Fig. 4.11 Determination of the average occurrence depth of magnetized masses by the autocorrelation function of the magnetic field along the Gedabey-Belakan profile (Khesin et al. 1996): (**a**) ΔT plot, (**b**) the plot of the autocorrelation function. Deposits: (*1*) Quaternary, (*2*) Neogene, (*3*) Paleogene, (*4*) Upper Cretaceous, (*5*) Upper Jurassic, (*6*) Middle Jurassic, (*7*) Lower Jurassic, (*8*) Paleozoic, (*9*) intrusive rocks of the granodiorite series; (*10*) disjunctive dislocations; and (*11*) singular points of the magnetic field with the following magnetization values: **a** up to 0.5×10^{-3} CGS, **b** from 0.5 to 1×10^{-3} CGS, **c** larger than 1×10^{-3} CGS

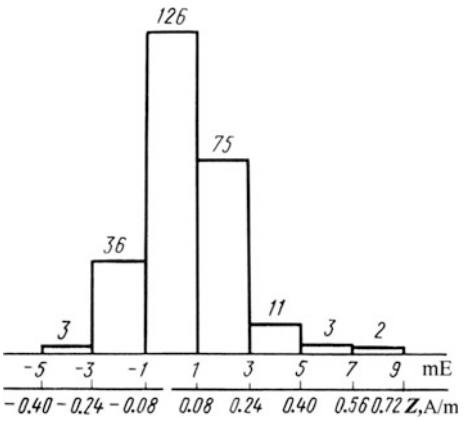

Fig. 4.12 Histogram of residual magnetic anomaly (Z component) distribution (after upward continuation to the level of 25 km) for the Lok-Garabagh zone of the Lesser Caucasus (Eppelbaum and Khesin 2012). *Values* over the histogram intervals show the frequencies of magnetic anomalies

magnetic data examination confirms the opinion of Peyve et al. (1980) and certain other investigators as to the significant role of tangential movement and the subduction of the Lesser Caucasus under the Greater Caucasus structure.

A map of predominant trends of magnetic anomaly distribution (Fig. 4.13) could be also used for regional tectonic–structural examination. Note that selected four trends (0°–45°, 45°–90°, 90°–135°, and 135°–180°) are sufficient for the description of map of any complexity.

There are several advantages of the direct use of topographic maps for geological purposes which are well known in geomorphology. Topographic data (digital terrain models) are used to determine topographic corrections in geophysics. Furthermore, the data on the terrain relief (height field) can be a source of additional geological information in processing and interpreting geophysical observations.

To summarize, the application of height field transformations enhances the informativity of a set of geophysical investigations practically without any expenditure, since the terrain height data need to be calculated for topographic effects. These transformations of the digital terrain model can be executed together with the geophysical field conversion using programs developed for computing field entropy, and curvature or the standard deviation. Obviously, the spatial distribution of the entropy values will be close to the distribution of the SSI parameter.

Various techniques of averaging are used to single out regional isometric anomalies in Azerbaijan. These include

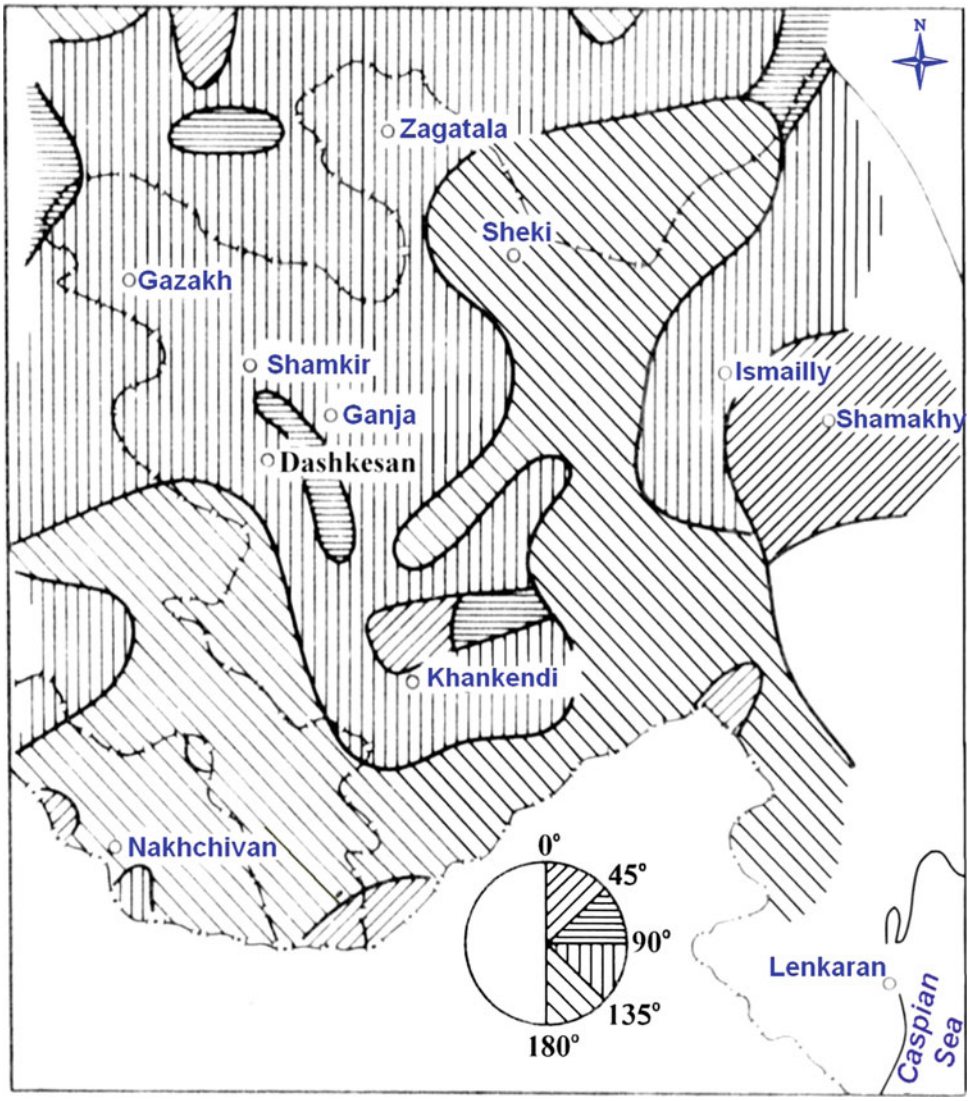

Fig. 4.13 Map of predominant trends of magnetic anomalies in Azerbaijan and adjacent regions (after Eppelbaum and Khesin 2012, with small modifications)

the method developed by Tikhonov and Bulanzhe (1945) who initiated the extensive implementation of transformations. Other techniques that are applicable are analytical upward continuation and smoothing with polynomials. However, averaging of fields with asymmetric distributions using the conventional techniques may result in distorting the regional component by the intensive local anomaly. Therefore, it is recommended to apply the method of quantiles, in particular, the median method (Borovko 1971). The 50 % quantile, the median, corresponds to the middle of the variation series composed of sequentially increasing field values within the transformation cell. To differentiate isometric anomalies by the median method, the radius r of the sliding window is chosen according to

$$r = \sqrt{r_1 r_2}, \tag{4.3}$$

where r_1 and r_2 are the radii of field features to be separated (regional and local objects, respectively) using half of their amplitude.

Usually, the transformation cell (sliding window) size should be larger than the local noise, less than the background features, and closer (or slightly higher) than the expected signal. Since there is always a correlation of results when overlapping the neighboring cells by a sliding window, it is not recommended to reduce the computation step to more than half a radius of the transformation cell.

Kunin (1968) proposed a relationship between the average area radius r and the continuation height H for the gravitational field, leading to a good fit of this transformation:

$$r \approx (2.5 \div 3)H. \tag{4.4}$$

The comparison of regional component charts of Azerbaijan obtained by averaging and upward continuation corroborates this conclusion regarding the magnetic field as well (Fig. 4.14).

Usually, the choice of transformation technique is up to the researcher. A clear physical sense of the transformation by upward continuation suggested by Andreyev and Klushin (1962), and its comparability with aircraft observations testify to the advantages of this method. However, the uncontrollable influence of the discarded residual term in Poisson's integral often turns out to be very high.

In informal calculations, along with their fundamental advantages, productivity plays an important role in the selection of the type of conversion. The median method is attractive from this standpoint. Actually, the assumption of compensation of random deviations from the average within the limits of the transformation cell (averaging method) may not hold true in smooth fields, whereas for sharply varying fields, polynomial smoothing is completely inapplicable. The results of application of the sliding average method, as shown by Borovko (1971), are more dependent on the anomaly amplitude than those of the median method. This method demonstrates very high productivity, which was confirmed by its application in Azerbaijan (Eppelbaum 2012).

High reliability can basically be attained in geophysical field regioning and reveal regional structures through areal autocorrelation analysis. However, the results of this method are highly dependent on the field description interval and the size of a sliding window. In addition, this analysis is accompanied by a significant loss of the area on the map edges and only yields general results, which rarely or never have individual value.

4.2.2 Gravity Data Analysis

The difference field ("ring" anomalies) $\Delta g_{B(8-20)}$ which is present to a significant extent in the mountain-folded regions reflects the influence of the internal structure and inhomogeneities of the consistency of the metamorphic basement (Baikalian folded basement) and deeply occurring (and buried) parts of intrusions in the Kur Depression, in general the influence of Mesozoic associations (Khesin et al. 1996). This map is shown in Fig. 4.15.

An informational parameter can be effectively applied for the regional gravity field processing (Eppelbaum 2014). It is well known that the South Caspian basin (*SCB*) is one of the main hydrocarbon provinces in the world (Mamedov et al. 2008). The satellite gravity data of the *SCB* were obtained from the World Gravity DB as retracked from Geosat and ERS-1 altimetry (e.g., Sandwell and Smith 2009). A highly positive factor is that these observations were made with regular global 1-min grids, and the error of gravity data computation for the newly arrived data is estimated at 1.0–1.5 mGals (Sandwell et al. 2013). The gravity data retracked to the Earth's surface are close to free-air gravity and can be effectively applied to the tectonogeophysical zonation (Eppelbaum and Katz 2011). The compiled gravity map (Fig. 4.16a) shows the gravity pattern within the *SCB* and southwest land bordering. The gravity data are ranging from −180 up to +420 mGals, and the anomalies in the center of the *SCB* are not brightly expressed. After application of the informational approach (Eppelbaum 2014), the image was significantly transformed (Fig. 4.16b) and the gravity anomalies in the *SCB* can be effectively recognized (it should be noted that in the both maps, the same color pattern was applied).

Such a satellite imaging of various geophysical fields (gravity, magnetic, infared, etc.,) in different scales is a powerful interpretation tool of the nearest future.

One of the most effective gravity field transformations in Azerbaijan was demonstrated in Kadirov (2000b). Gravity data acquired in the Shamakhy-Gobustan and Absheron oil- and gas-bearing regions (Fig. 4.17) were filtered using a Hartley transform (HT) and Butterworth filter (BF).

Figure 4.18 shows the Bouguer gravity map of the study area. The gridded square constructed on the basis of the Bouguer gravity data set has 32 × 32 elements both in the west-to-east and south-to-north directions, with the grid interval taken every 5 km in both directions.

The Eastern Azerbaijan negative anomaly with an extreme value at −140 mGal covers the Absheron-Gobustan area; this type of anomaly is not the characteristic of areas of high topography. The Dubrar relative maximum, stretched along the southeast slope of the Greater Caucasus, is located in the northwest part of the area. Another non-extensive relative maximum zone goes in the direction from the Yavany Mt. to the Sangachal locality. The axis of this anomaly is stretched parallel to the direction of the Greater Caucasus axis. Some of the local anomalies are overshadowed by the regional anomalies clearly outlined in the map.

The 2D HT of a real function $f(x, y)$ is defined (after Hartley 1942) as:

$$H(u,v) = \int_{-\infty}^{\infty} \int_{-\infty}^{\infty} f(x,y)\mathrm{Cas}(ux) \cdot \mathrm{Cas}(vy)\mathrm{d}x\mathrm{d}y, \quad (4.5)$$

where $\mathrm{Cas}(ux) \cdot \mathrm{Cas}(vy) = \cos(ux - vy) + \sin(ux + vy)$.

The ideal low-pass BF is given by (Kulhanek 1976):

$$H_B(k) = \frac{1}{\sqrt{1 + \left(\frac{k}{k^c}\right)^{2n}}}, \quad (4.6)$$

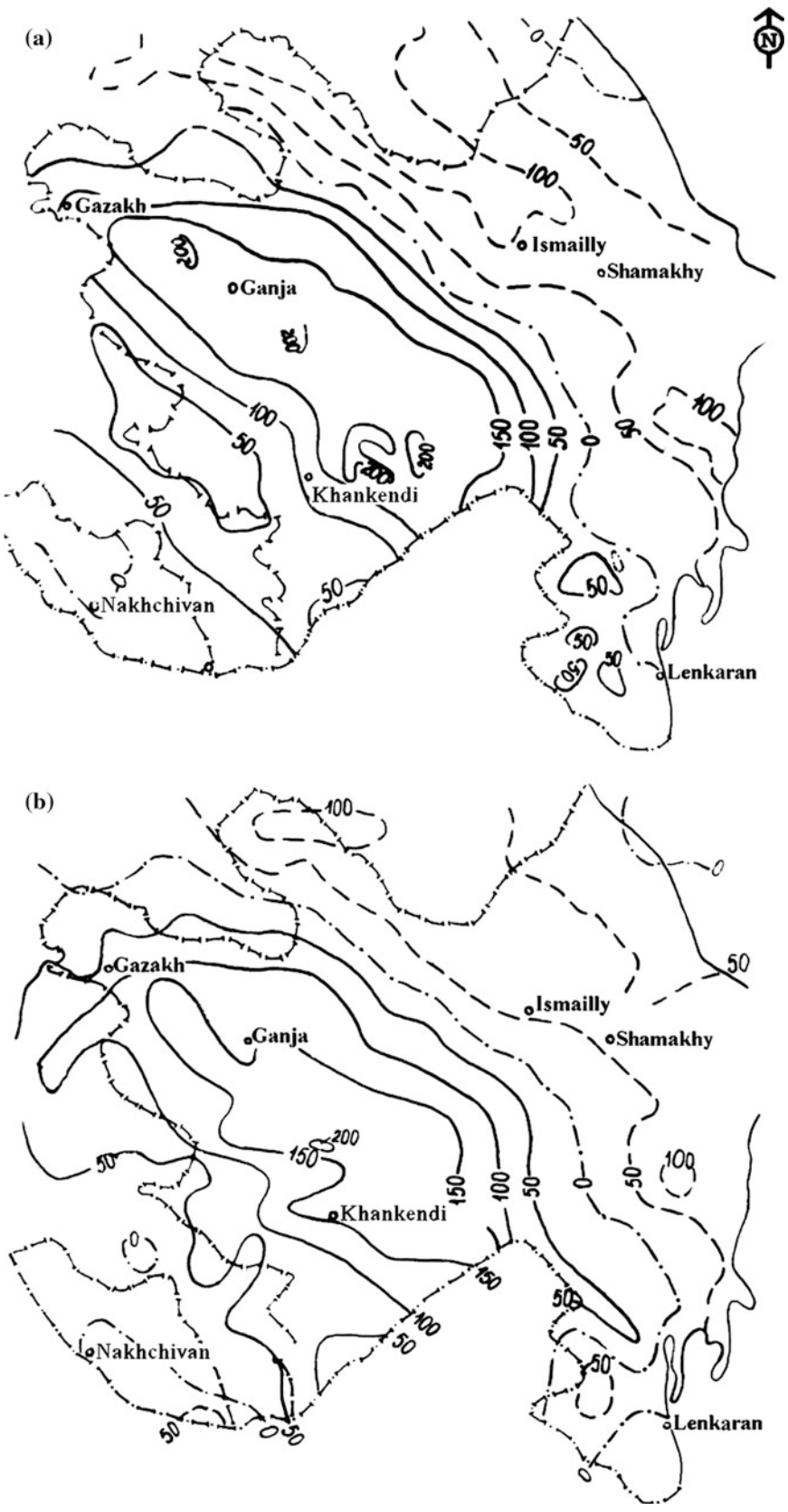

Fig. 4.14 Singling out the regional component of the magnetic field in Azerbaijan: (after Eppelbaum and Khesin 2012). **a** average within a radius of 60 km; **b** continued upward to a height of 25 km. Isolines in nanoTesla: (*1*) zero, (*2*) positive, (*3*) negative

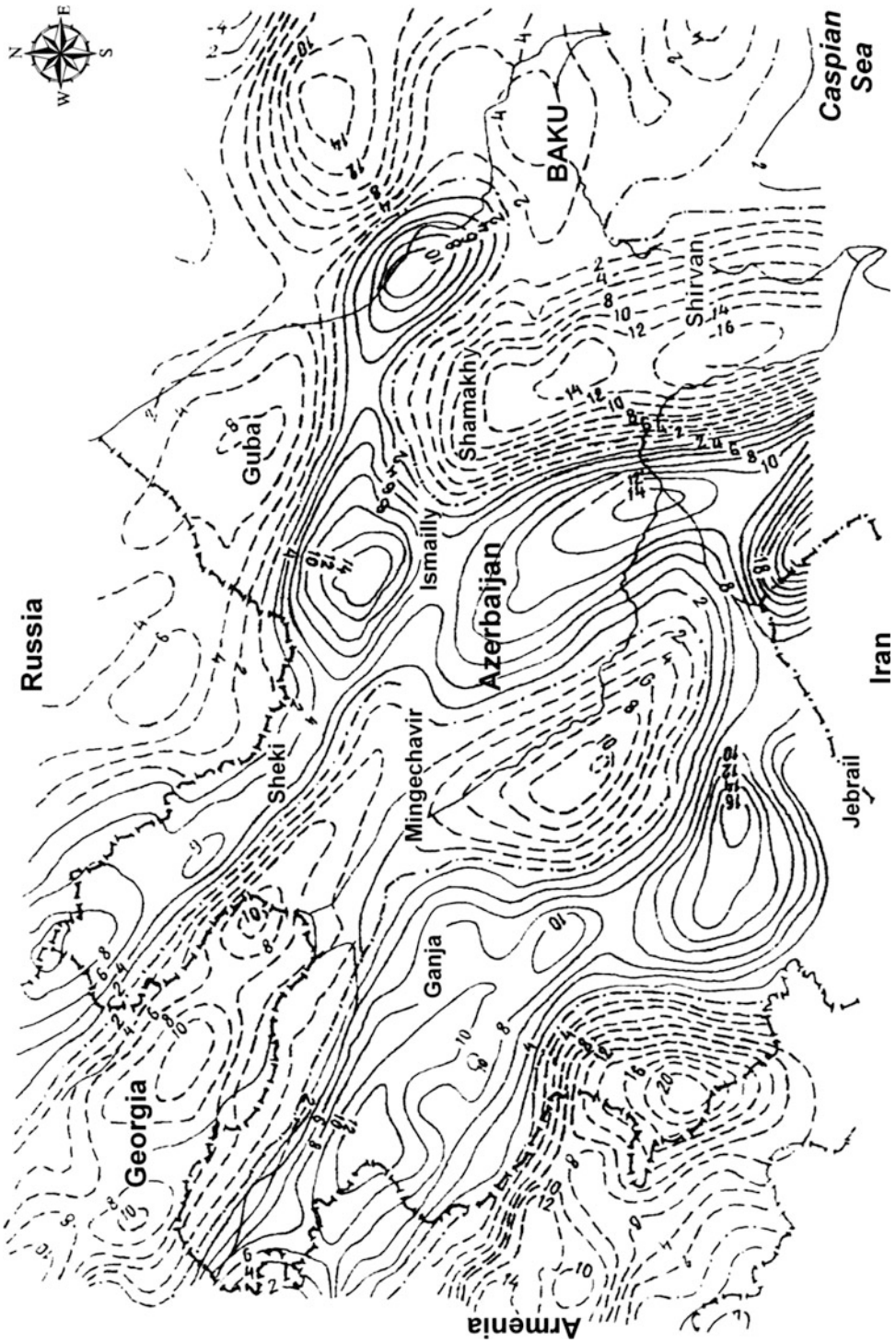

Fig. 4.15 Map of difference Δg_{8-20} anomalies computed as the difference between upward continued fields in the Bouguer reduction (terrain correction was computed with a radius of 200 km and the density of the intermediate layer was defined as 2.67 g/cm^3) at heights of 8 and 20 km, respectively (Khesin et al. 1996; Kadirov 2000a; Gasanov 2001)

where $k = \frac{2\pi}{\lambda}$ is the wave number, $k_c = \frac{2\pi}{\lambda^c}$ is the cutoff wave number, and n is the degree of the filter. In this study, n was taken to be equal to 1. The procedure of filtering is using the HT transform, the gridded gravity data are converted to space–frequency Hartley domain. In this domain, row by row followed by column by column Butterworth filters are applied using a suitable cutoff frequency. Then, the produced filters are multiplied by the spectrum of data in the Hartley domain. Finally, by taking the inverse transform, the mathematical processing was returned to the space domain (Kadirov 2000b).

The calculated power spectrum curve (by the use of Fourier transform (FT)) is displayed in Fig. 4.19. The power spectrum of the gravity data shows a cutoff wave number

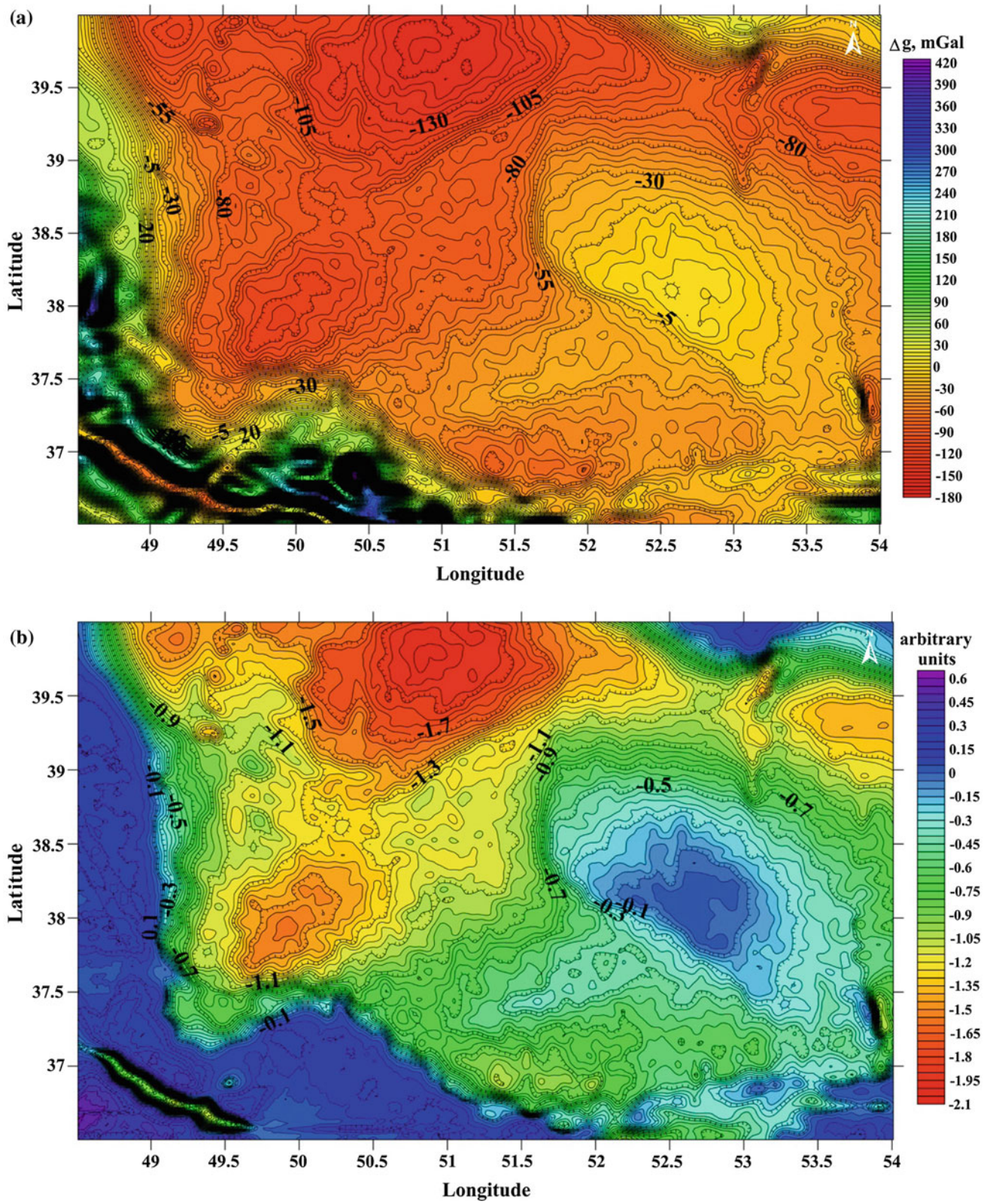

Fig. 4.16 **a** Satellite gravity map of the South Caspian basin and its SW border compiled on the basis of Geosat and ERS-1 altimetry data (Eppelbaum 2014). **b** Map of the informational parameter I_i transformed from the map shown in Fig. 4.16a (Eppelbaum 2014)

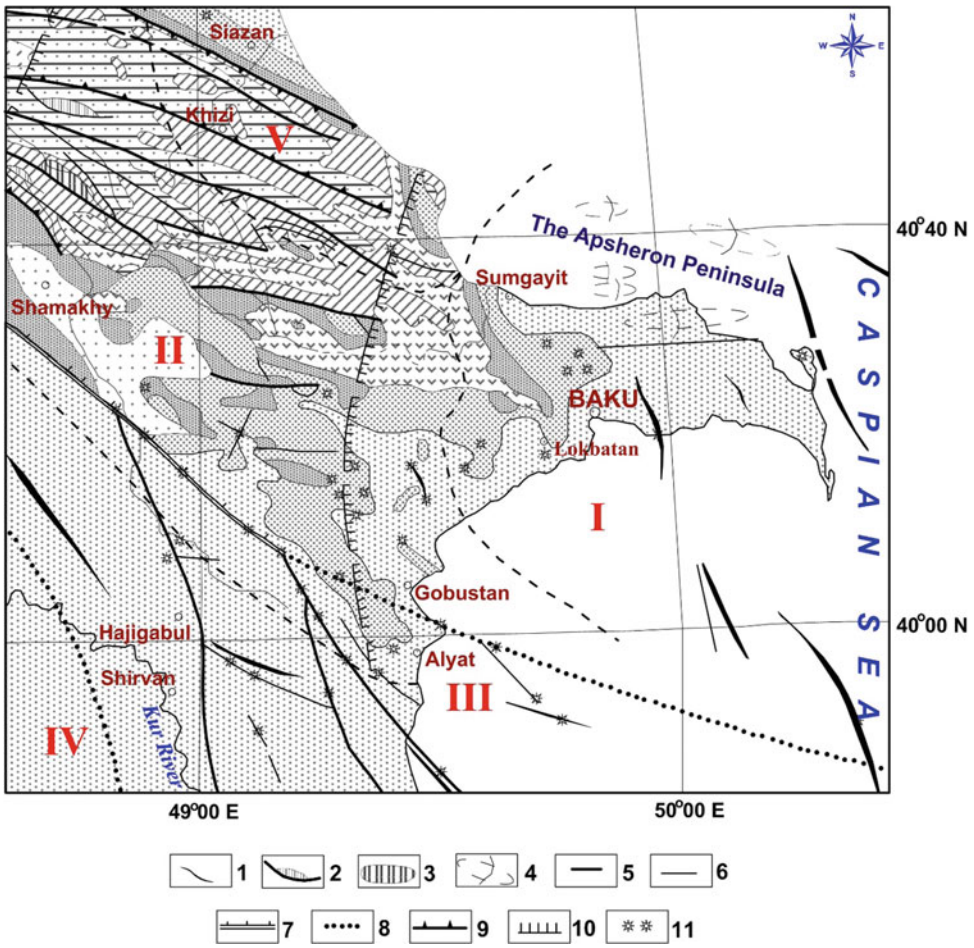

Fig. 4.17 Tectonic–geological scheme of the study area. Alpine orogenesis subcomplexes: (*1*) early orogenesis subepoch ($O_1^1 AP_3 - N_1$), (*2*) early orogenesis upper epoch ($O_1^2 A N_1^2 - N_1^2$), (*3*) late orogenic epoch up to 800 m ($O_2 A N_2^3 \ N_2^3 - Q$), and (*4*) late orogenic epoch 800 m and greater (O_2). Structural elements, fold types, and dislocations with a break in continuity: (*5*) axes of large anticlinal folds, (*6*) scale-shaped folds, (*7*) tectonic nappe, (*8*) buried folds, (*9*) normal faults with thousands of meters of amplitude, (*10*) normal faults with hundreds of meters of amplitude, (*11*) crustal faults manifested at the surface by thrusts and overfaults, (*12*) buried faults, (*13*) thrusts and overfaults with thousands of meters of amplitude, (*14*) buried flexure, (*15*) mud volcano. Oil- and gas-bearing regions: *I*—Absheron region, *II*—Shamakhy-Gobustan region, *III*—Baku archipelago, *IV*—Lower Kur region, *V*—near-Caspian region (after Kadirov 2000b, with modifications)

separating two domains of high- and low-wavelength information. The low- and high-wave number parts of the power spectrum, associated with deep and shallow gravity sources, were taken as representing the regional and residual anomalies, respectively. Two linear segments shown in the plot are suggestive of the existence of discrete density boundaries, with the slopes being the estimates of their mean depths (Bhattacharyya 1966; Spector and Grant 1970). The present power spectrum indicates a depth of 24.5 km for the long-wavelength component and a depth of 3.2 km for the short-wavelength component. These depth values are well-correlated with the results of seismic studies previously carried out in the region.

The cutoff wave number is determined by the crossing point of fitted straight lines approximating the power spectrum data in the high- and low-wavelength domains. A cutoff wave number of k_c is found from the c power spectrum.

Figure 4.20 shows the results of low-pass filtering arranged for a k_c 0.142 km^{-1} wave number. The gravity minimum north of Absheron is reflected in the regional Bouguer anomaly map. The results of the high-pass filtering process are shown in Fig. 4.21. A large positive anomaly is evident northwest of the region from Sumgayit to Siazan, the so-called Dubrar positive anomaly. A maximum local anomaly value of 7 mGal is noted in the Khizi locality. Another extensive positive anomaly lies parallel to the Greater Caucasus axis covering an area from the Yavany Mt. to Sangachal, where the highest value is equal to 3 mGal. In the southwest, a large positive anomaly located within the

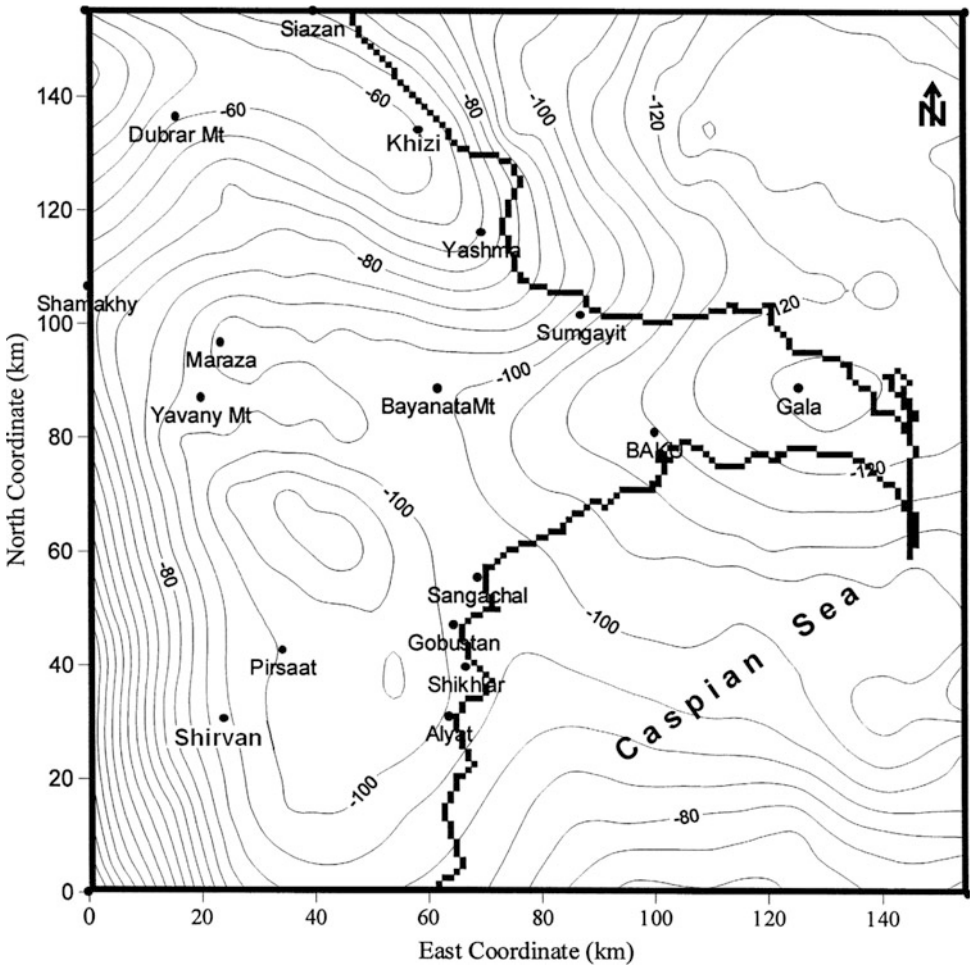

Fig. 4.18 Bouguer gravity map for the study area. Contour interval is 5 mGal (Kadirov 2000a)

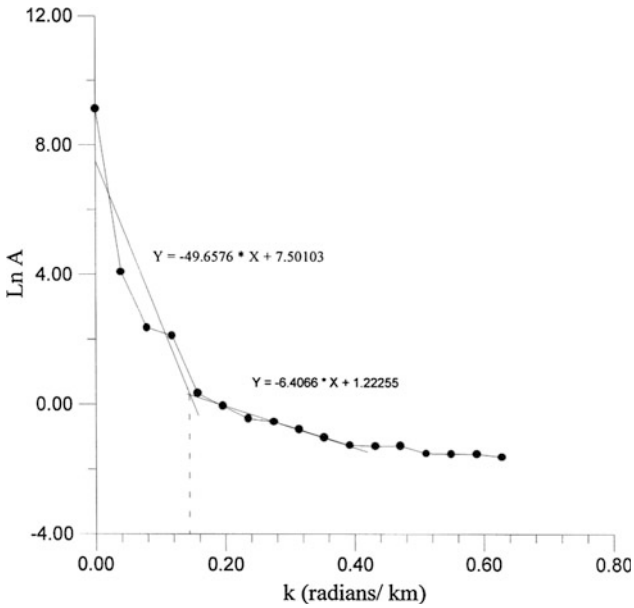

Fig. 4.19 Power spectrum of the Bouguer gravity anomaly in the study area (Kadirov 2000b)

Kur Depression is noted. The Absheron-Central Gobustan negative anomaly (as low as −7 mGal) is seen to the east and south of the Dubrar Mt. positive-anomaly region. The Absheron negative anomaly extends toward the north. A row of closed negative anomalies begins from Gobustan and goes toward Shamakhy. The results of the high-pass filtering through the FT are shown in Fig. 4.22. As can be seen, the contours shown in Figs. 4.21 and 4.22 are very similar ones.s

The depth occurrence of the pre-Mesozoic crystalline basement surface has been studied with the aim of interpreting the gravity anomalies in the Absheron and the Shamakhy-Gobustan regions. The density versus depth relationship in the part of the Earth's crust overlying the crystalline basement can be approximated by a quadratic function (Bhaskara Rao 1986). The computed function for the area under study is shown in Fig. 4.23.

The depth map of the basement in Fig. 4.24 is estimated from the inversion of the "residual" gravity field constrained with the density model (Fig. 4.23) by using the GR3DSTR program (Bhaskara and Ramesh 1991).

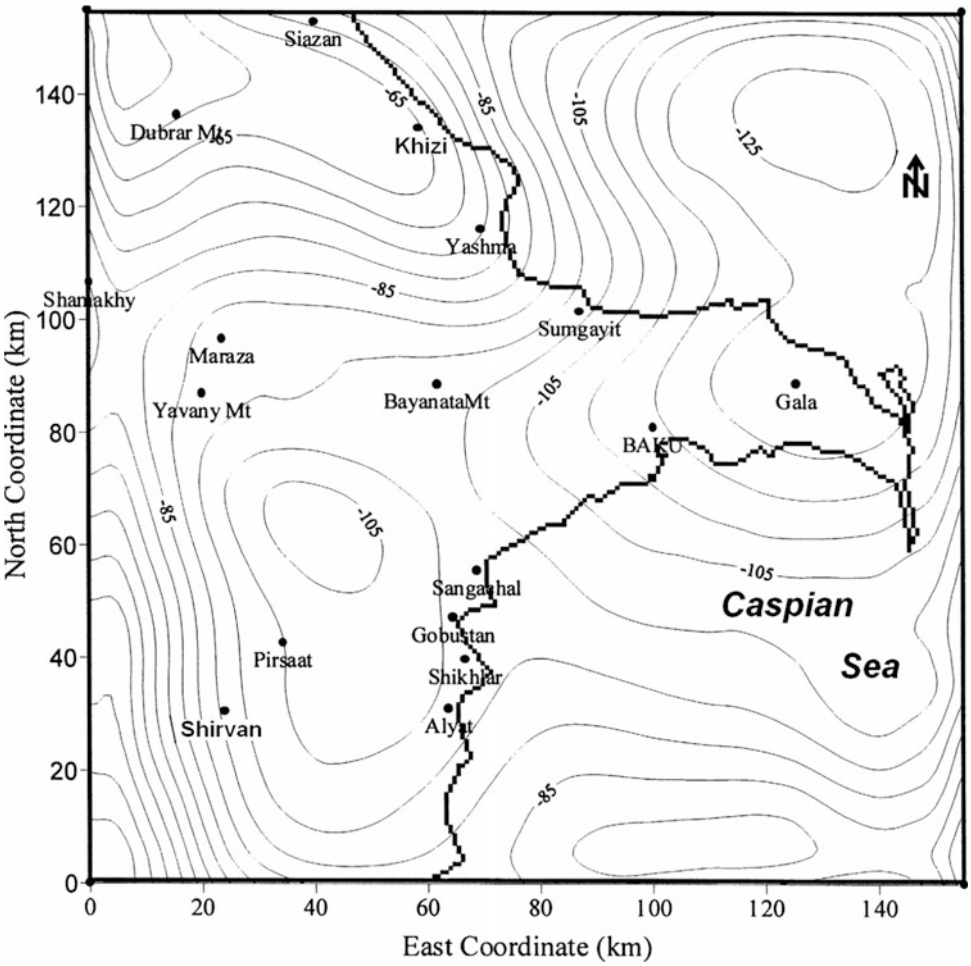

Fig. 4.20 Results of the low-pass filtering of the gravity data on the study area using 2D HT (Kadirov 2000b)

Calculations for the basement depth maps were performed at specified 10 iterations. The recalculated gravity effect based on the depth-to-basement map (Fig. 4.24) is shown in Fig. 4.25. Apart from the regional shift of 30 mGal, the map agrees well with the regional-anomaly map. As can be seen, higher values on the map correspond to the Yavany Mt.—Alyat area where the mean depth is around 23 km. The mean depths in the Absheron Peninsula and the Dubrar zone are 20 and 6 km, respectively. The data presented are well-correlated with the results of seismic exploration (e.g., Aksyonovich et al. 1962; Gadjiyev 1965; Radjabov 1978).

Regional gravity anomalies in the Caucasus-Caspian region were successfully studied in Kadirov (2004).

Upward continuation of gravity data is widely used in geophysics. It can be used, for example, to enhance the signal of deeper sources when shallower ones are present. Mantle anomalies of the gravity field ("geodynamic reduction") obtained through the elimination of impact of the upper layers is determined by analytical continuation into the upper half-space—to the altitude of more than 50 km (Kaban 2000; Kadirov 2000a, b). Values of depth of occurrence of abnormal bodies calculated with logarithm of the power spectrum determined by analytical continuation of regional gravity field allow to make a conclusion about the necessity of application of these anomalies as reflectors of mantle gravitation effect (Kadirov 2000a). Gravitation model of the region may be considered as one of the main factors of geodynamic constructions.

Kadirov (2004) applied the Hartley transform (Hartley 1942) for upward continuation of the gravity data on the Caucasus-Caspian regions, recalculation of gravity anomalies for different heights, and computation of horizontal gradient of gravity field for unmasking some regional tectonic–structural peculiarities.

Gravity field in the studied area in the Bouguer reduction (Fig. 4.26) includes the territory of the Middle and the South Caspian and territories of Azerbaijan, Georgia, Armenia, south of Russia, west of Turkmenistan and Kazakhstan as well as eastern Anatolian and northern Iran. The gravity map in the Bouguer reduction is constructed with the value of the interstitial layer density of 2.67 g/cm^3. Normal value of the gravity was calculated by the Helmert Eq. 1909 with account of amendment—14 mGal. While calculating the Bouguer anomalies, relief of the locality was taken into

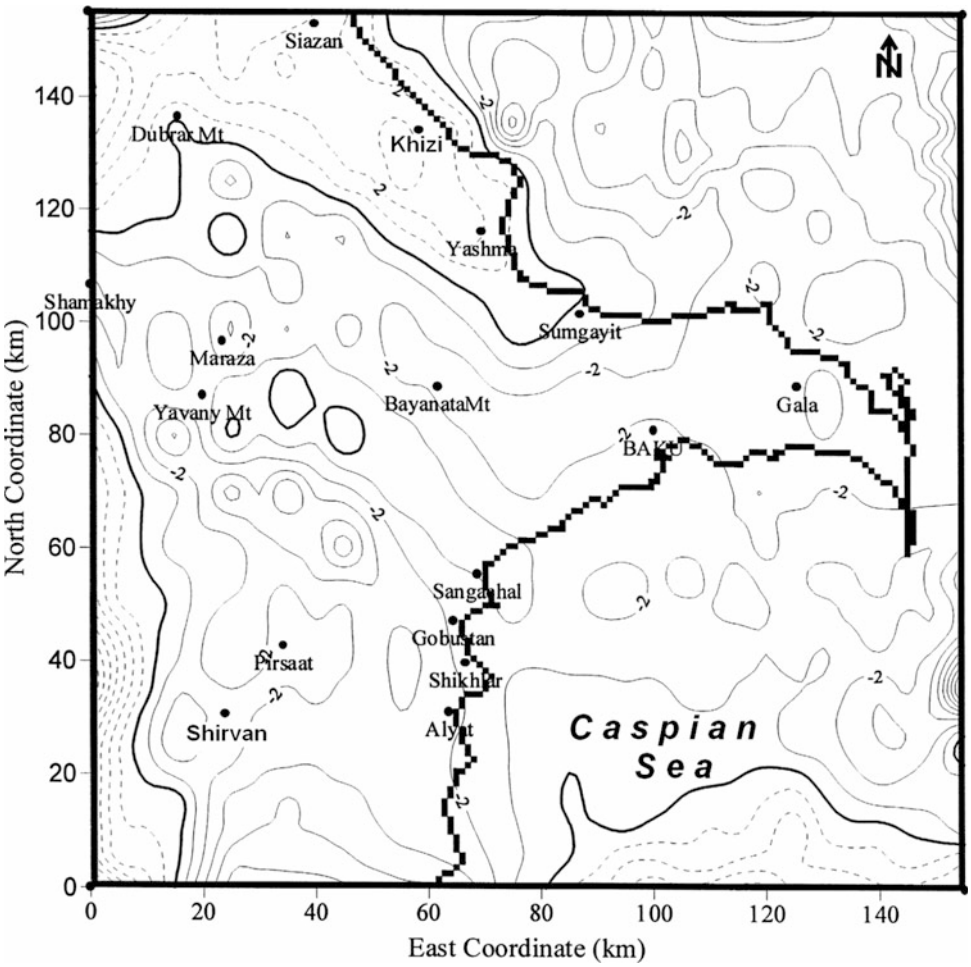

Fig. 4.21 Results of the high-pass filtering of the gravity data on the study area using 2D HT. *Dashed* and *solid lines* show positive and negative local anomalies, respectively (Kadirov 2000b)

account (R = 200 km). For the offshore areas, the gravity map is constructed with account of amendments for the surrounding relief and for the seafloor topography (Gravity map of the USSR 1990). In the summary map of the Bouguer anomalies in the investigated region, one can identify a pan-Caucasian background of negative anomalies. A vast positive regional anomaly occupies a part of the Middle Caspian and a part of territories of Turkmenistan and Kazakhstan (Aktau-Bekdash-Turkmenbashy). This maximum is adjacent to Dagestan, East Azerbaijan, and Tcheleken minimums linked with each other by a narrow line. From the west, the East Azerbaijan minimum is limited by the Azerbaijan maximum. The latter with values of the gravity varying from 0 to 100 mGal is mainly associated with the Lower Kur Depression and partially spreads over the Talysh Mts. This maximum has two "fingers" in the form of narrower relative maximums (anomalies from 0 to 50 mGal). One of them stretches northward and connects with the Alazan zone. Another one goes northwestwards through the city of Ganja as far as Tbilisi and spreads over a narrow line of uplifts along the northwest margin of the Lesser Caucasus.

Regional anomalies of the gravity field in the Caucasus-Caspian region are investigated by recalculation of data of the gravity field for different altitudes. In the zone of frequency, the gravity field at a height of z is calculated by the product of 2D spectra of the input function and weight function:

$$F_u(u, v, -z) = A(u, v) \exp\left(-z\sqrt{u^2 + v^2}\right), \quad z > 0, \quad (4.7)$$

where $F_u(u, v, -z)$ is the result of analytical continuation to the height in the frequency zone, $A(a, v)$ is the spectrum of the input function, and u and v are the spatial frequencies in x and y directions, respectively (Blakely 1995).

The spectrum of the input function is calculated with the application of Hartley transform (Hartley 1942; Sundararajan 1995; Kadirov 2000a). And further with the help of reverse Hartley transform, we return to the spatial zone. Recalculation of gravity anomalies was carried out for altitudes 20, 50, and 100 km. In compliance with geologic–geophysical investigation, one may suppose that the first altitude corresponds approximately to the average depth of the surface of a "basaltic" layer. The second altitude

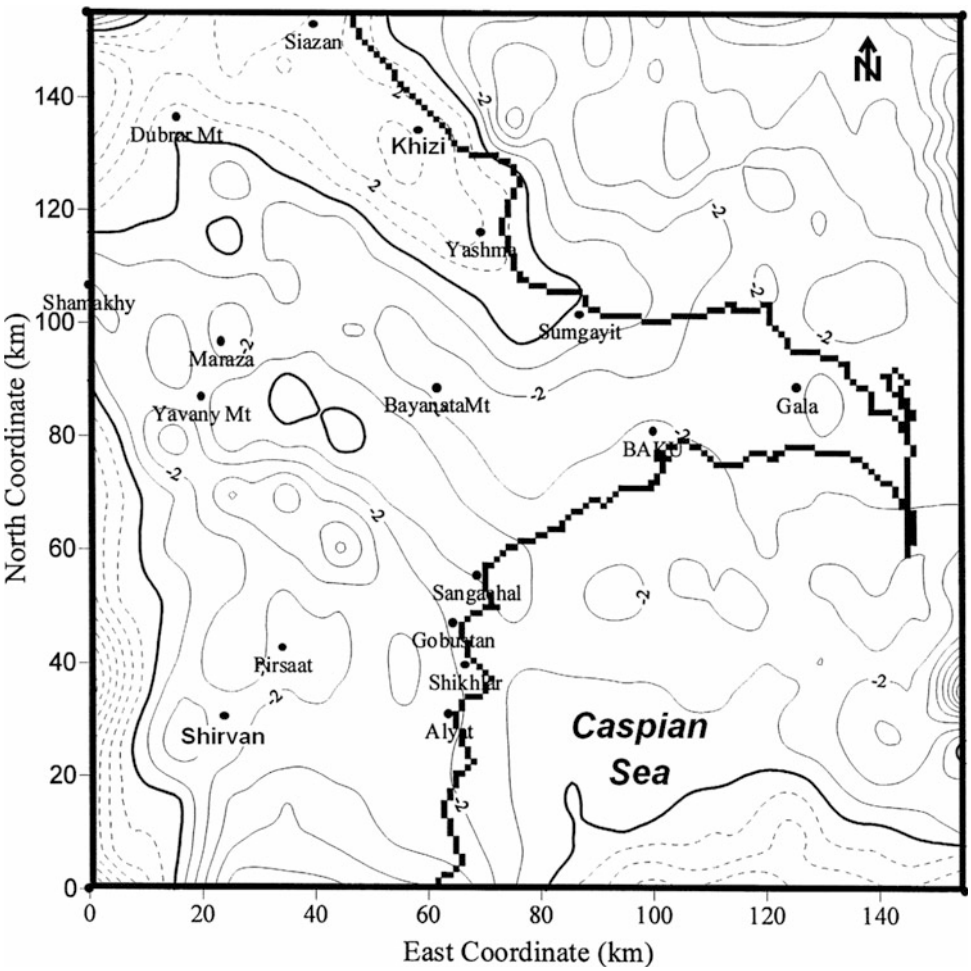

Fig. 4.22 Results of the high-pass filtering of the gravity data on the study area using 2D FT. Dashed and solid lines show positive and negative local anomalies, respectively (Kadirov 2000b)

corresponds to the depth of Moho discontinuity occurrence. Other altitude corresponds to depth in the upper mantle. For this reason, they are taken by us for "geodynamic reduction." Figure 4.27 demonstrates gravity anomalies of the region recalculated for the altitude of 20 km. Negative and positive anomalies are marked by continuous and dotted lines. The southeast of the Caspian Sea, Kara-Bogaz bay, and Aktau and Bekdash districts are overlapped by a positive anomaly (+40 mGal). The central part of this isometric anomaly is situated in Bekdash where values of amplitude are up to 60 mGal. Other positive anomalies are observed in Talysh (20 mGal), Safidrud (5 mGal), and 30 km to the west of Okerem (5 mGal).

Figure 4.28 shows the distribution of the gravity field in the Caucasus-Caspian region recalculated for the height of 50 km. The isoline contour interval is 5 mGal. Preservation of the north Absheron minimum recalculated for the height of 100 km in the maps of gravity anomalies demonstrates that this regional minimum is linked partially with density boundaries located below the Moho discontinuity (Kadirov 2000a). Comparison of gravity anomalies determined by possible density boundaries in the upper mantle with results of the investigation by other methods of the mantle structure is of a certain interest.

One can see that the Bekdash positive anomaly is preserved with the amplitude of 25 mGal. Relative maximum manifests itself in Talysh and in the south of the Caspian Sea. In the Lesser Caucasus and in the Absheron Peninsula, one can observe gravity minimums. Most of the regional anomalies are linked with the change of depth of the Moho discontinuity occurrence.

Distribution of gravity anomalies at the altitude of 100 km is shown in Fig. 4.29. At the altitude of 100 km, minimum of the gravity field is −105 mGal and maximum is +8 mGal. Gravity anomalies of the region recalculated to the height of 100 km indicate that the gravity field became much simpler and is displaced in the south direction of the center of the above-mentioned large negative anomalies. Regional anomalies for these cases are linked with the depth of occurrence of the layer surface in the upper mantle. Isolines of the regional anomaly in the Lesser Caucasus are bended in Khankendi in the northeast direction. In the Absheron Peninsula, negative anomaly is preserved. Maximums of the gravity field in Talysh and Safidrud and the southeast

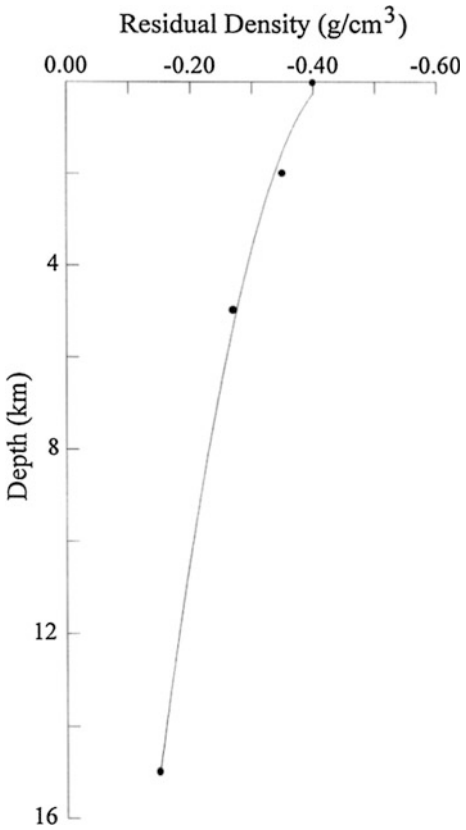

Fig. 4.23 Approximation of density versus depth data for the study area by a quadratic function

Caspian are united into one relatively positive anomaly. The anomaly in the Absheron Peninsula preserves its Caucasian orientation.

On the base of analysis of data of the gravity field recalculated for the height of 100 km as well as anomaly of velocity of the propagation of seismic waves in the asthenosphere, heat field in the surface of the mantle under the eastern part of the Absheron Peninsula, one should anticipate intensive disconsolidation of the matter in the asthenosphere (Vinnik 1976; Shengelaya 1984; Kadirov 2000a). In other words, these results allow to suppose that regional anomalies of the gravity field (recalculated for the height of 100 km and corresponding to the depth of asthenosphere) in the Absheron Peninsula are determined by the properties of the upper mantle.

Deep subvertical boundaries in the territory of Azerbaijan and adjacent regions were detected by computing gravity field horizontal gradient in different modifications (Kadirov 1998, 2004).

Value of a total horizontal gradient of the gravity field in Azerbaijan varies between 0 and 5.63 mGal/km. Maximum calculated values of the horizontal gradients for Azerbaijan are >1.5 mGal/km (Kadirov 2000a). Figure 4.30 demonstrates shaded relief map of total horizontal gradients of the gravity field in the Caucasus-Caspian region. Field of the gradients is a rather complex picture. One can clearly see superposition of gradient zones of different intensity and width. To identify interblock boundaries, there were determined horizontal gradients of gravity anomalies which are maximums. The identified values are united nearly everywhere into extended zones corresponding to the boundaries of the blocks. In the shaded relief map of total horizontal gradients of the gravity field, one can clearly see the plan of location of subvertical contacts of rocks of a different abnormal density.

Figure 4.31 demonstrates a map of total horizontal gradients of a regional field, recalculated for the altitude of 20 km and its shaded relief map. In the shaded relief map of the horizontal gradients of the regional field, there were shown lines corresponding to vertical boundaries. Figure 4.32 demonstrates that the pre-Caucasian (Makhachkala-Turkmenbashy), Siazan, major-Caucasian, pre-Lesser Caucasian (Kur Depression), Lagich-Kyzylagach, Dilidjan-Lachin-Ardabil, and north Ajinohur faults find their reflexing in the regional anomaly of the gravity field, recalculated for the altitude of 20 km (Gadjiyev 1965; Borisov 1967; Shikhalibeyli 1996). The zone of the crushing by these faults may be related to the depth of occurrence of the "basaltic" layer. A number of longitudinal and cross-linear elements in the distribution of maximums of the horizontal gradient of the gravity field manifest themselves as well. A linear trend in the distribution of maximums of horizontal gradients of the gravity field—the Agdash linear element stretching from the north to the south as far as 150 km—is of a certain interest. In the north deep, faults cut into this linear element in the south slope of the Greater Caucasus.

4.2.3 Thermal Data Analysis

Computation of vertical and horizontal gradients of temperature field is widely applied tool for revealing some desired geological–geophysical peculiarities (e.g., Somerton 1992; Beardsmore and Gull 2001; Eppelbaum et al. 2014).

When defining temperature at intersection points of rectangular grid, horizontal gradients are calculated using finite difference method. Map of distribution of total horizontal geothermal gradients at 5000 m depth is shown in Fig. 4.33. It may be seen from this map that the maximal values of total horizontal gradients correspond to active regional fault zones (Mukhtarov 2012). Besides this, some examples of thermal data analysis are also shown in Chap. 5 of this volume.

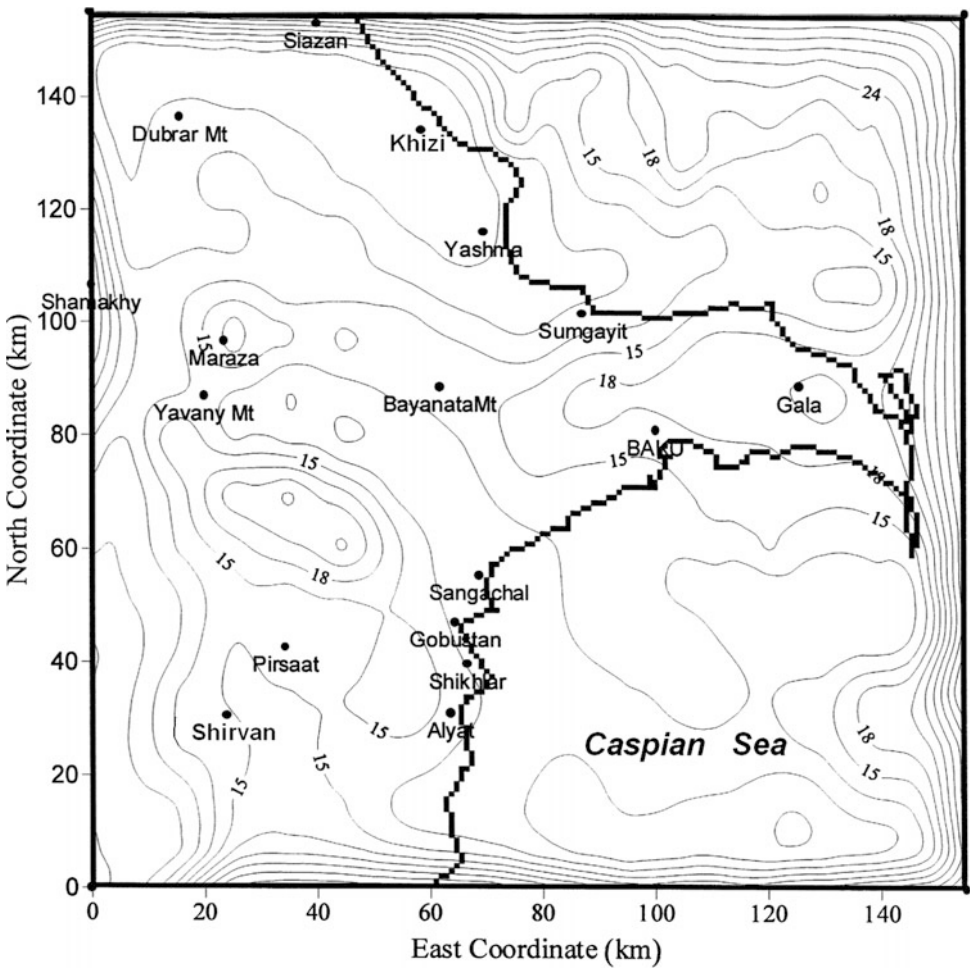

Fig. 4.24 Basement contour map of the study area derived from 3D modeling of gravity anomalies using a quadratic density function. Contour interval is 3 km (Kadirov 2000b)

4.2.4 Topography Data Analysis

Geological regularities, which manifest themselves in mountainous relief structures, can be highlighted by treating the height field of the area with the techniques employed in geophysical field analysis. For example, Borovko (1971) presented an effective application for anomalous object by the predominant strikes of relief isohypses. Later (Khesin et al. 1996) showed that this transformation can identify a very important indicator of endogenic deposits of various compositions and origins (Fig. 4.34). Large deposits tend to occur in the corners of blocks having a predominant strike of isohypses that differs from the Caucasus as the whole. This led to the recommendation to drill deep test wells in the mountainous regions of Azerbaijan.

The relief complexity, which was described above, governs the spatial distribution of topographic corrections and can be estimated by a map of the specific sinuosity of height isolines. Khesin et al. (1983) proposed applying the specific sinuosity of isolines (*SSI*) to characterize the complexity of a geophysical field.

It is calculated as follows: (1) the total length of isolines (L) for a given field is computed within a sliding area, (2) area S on the sliding cell is calculated, and (3) the parameter

$$SSI = KL/S, \tag{4.8}$$

is computed, where K is the scale factor for converting L into kilometers and S into square kilometers. The *SSI* parameter is measured in km/km^2, and the value obtained refers to the center of this cell.

In order to identify the general features of geophysical fields (and the height field as well), it is often advisable to calculate tertiary indicators, i.e., SSI by formula (4.8), the length of dislocations obtained by sliding window calculations (Khesin et al. 1996).

The SSI distribution (Fig. 4.35) reflects certain geological features of the region. Interestingly, this chart correlates rather well with the map of seismic activity (Riznichenko et al. 1983).

The role and significance of various indicators in the indicator space is different when the goal is regioning. Here,

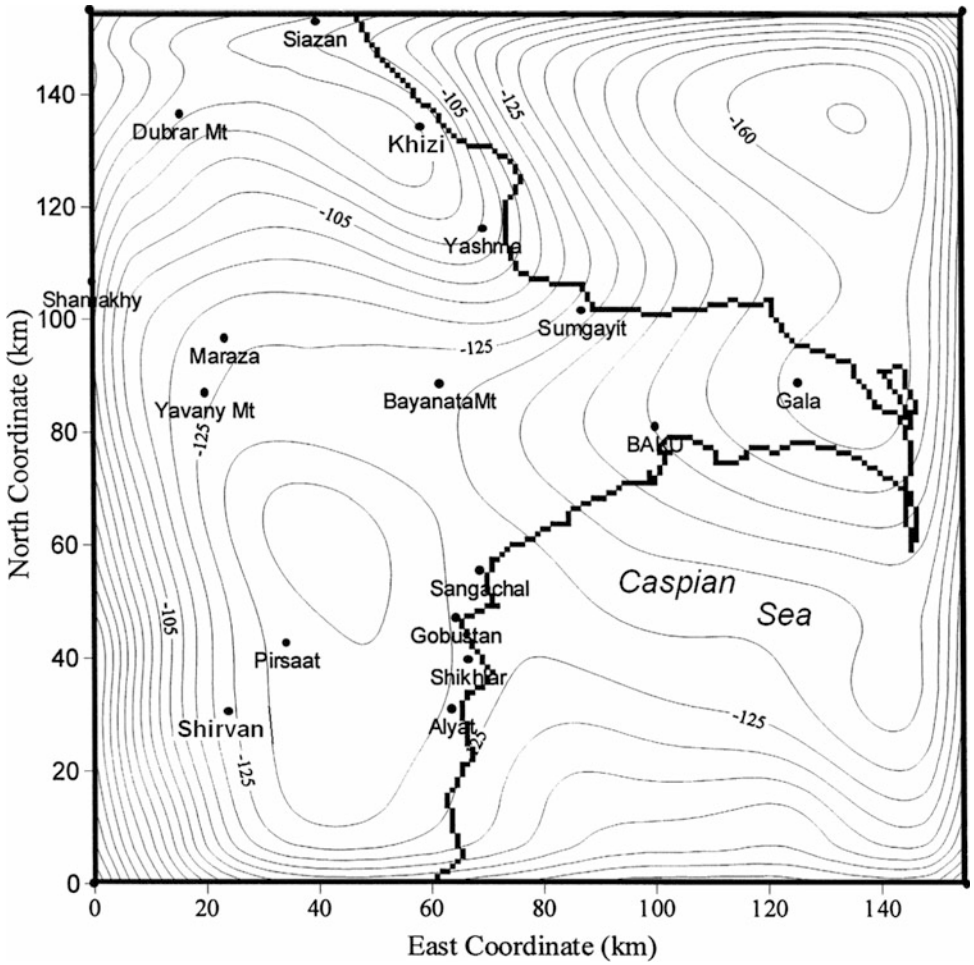

Fig. 4.25 The calculated gravity anomalies of the sedimentary basin with the 3D prism program. Contour interval is 5 mGal (Kadirov 2000b)

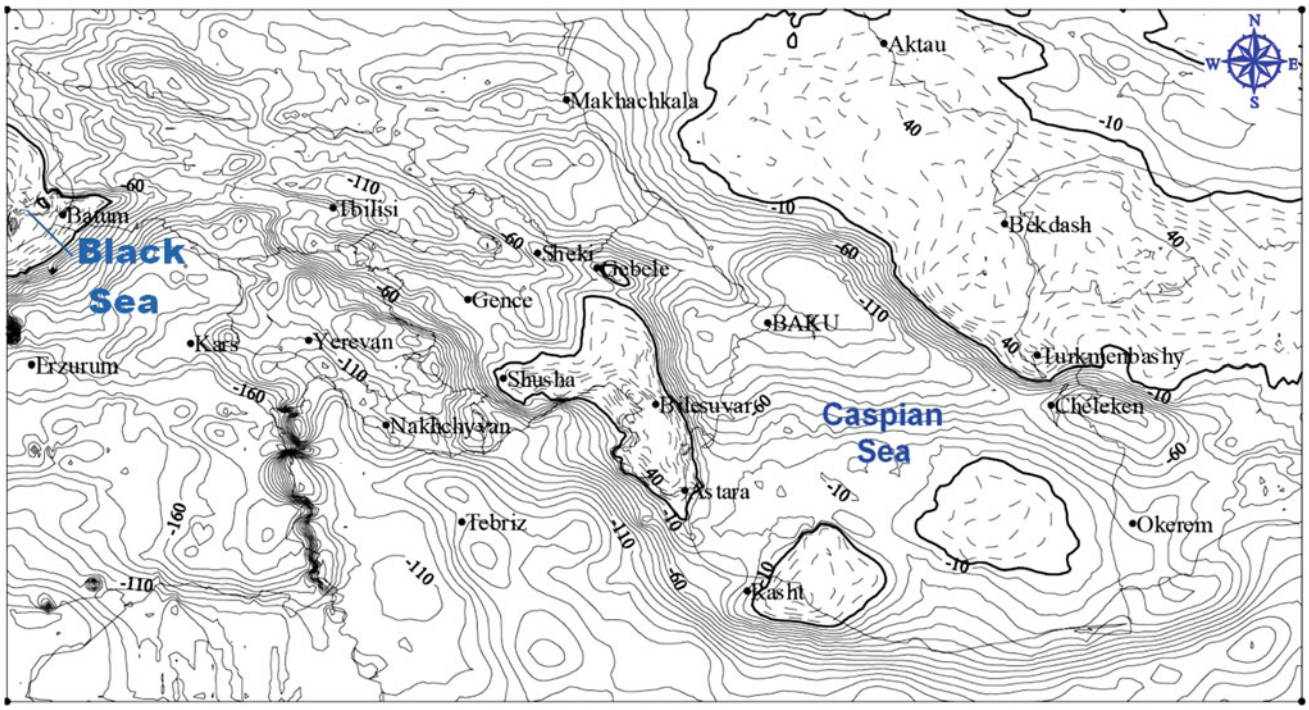

Fig. 4.26 Bouguer gravity map of the Caucasian-Caspian region (Kadirov 2004)

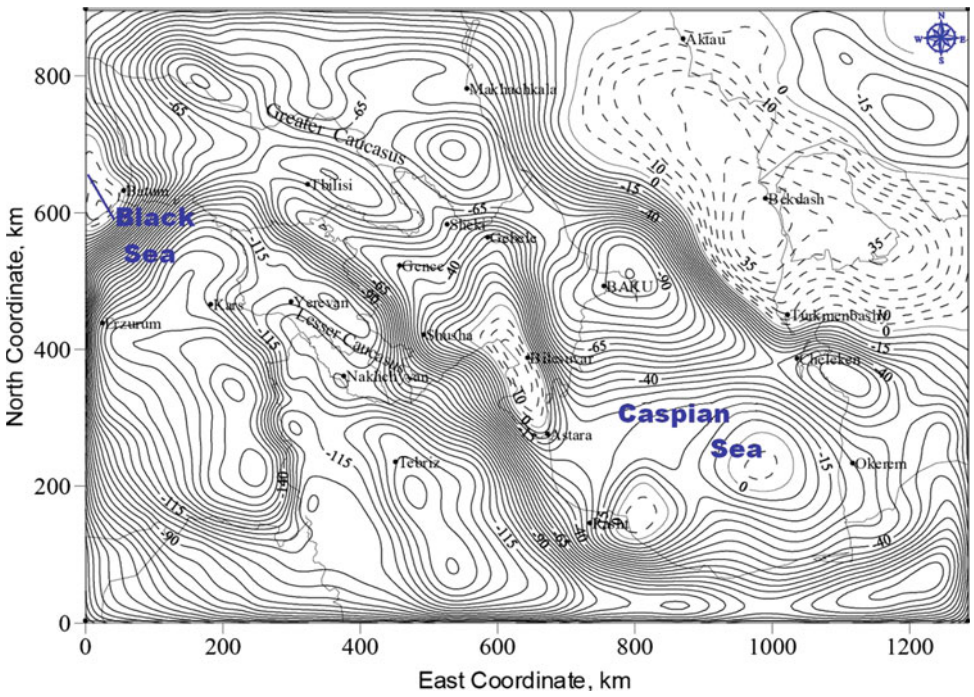

Fig. 4.27 Distribution of gravity field in the Caucasian-Caspian region upward continued to altitude of 20 km. Isolines density: 5 mGal (Kadirov 2004)

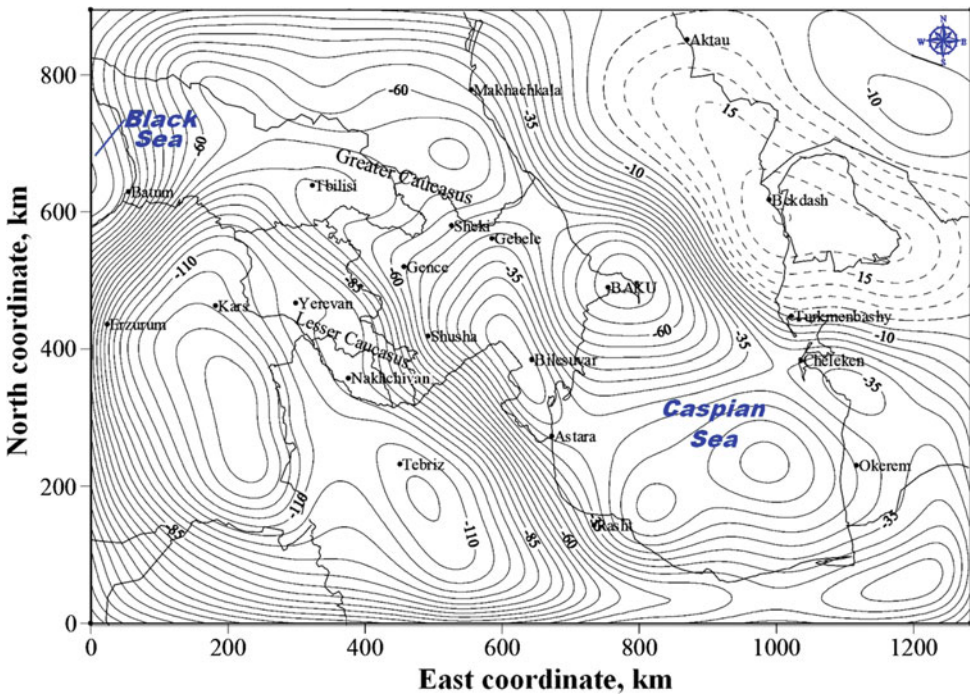

Fig. 4.28 Distribution of gravity field in the Caucasian-Caspian region upward continued to altitude of 50 km. Isolines density: 5 mGal (Kadirov 2004)

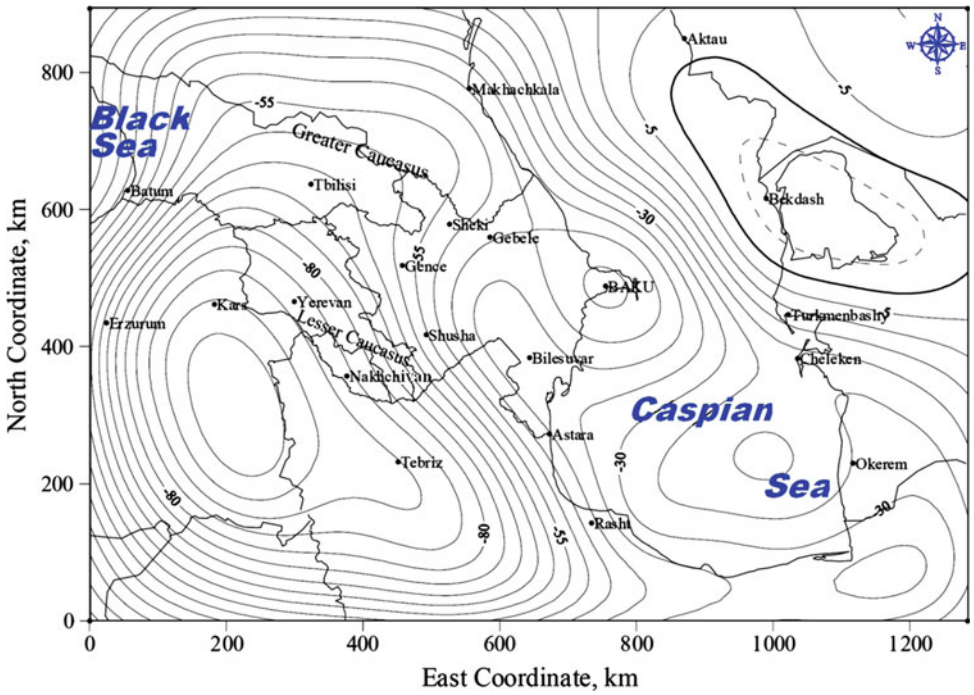

Fig. 4.29 Distribution of gravity field in the Caucasian-Caspian region upward continued to altitude of 50 km. Isolines density: 5 mGal (Kadirov 2004)

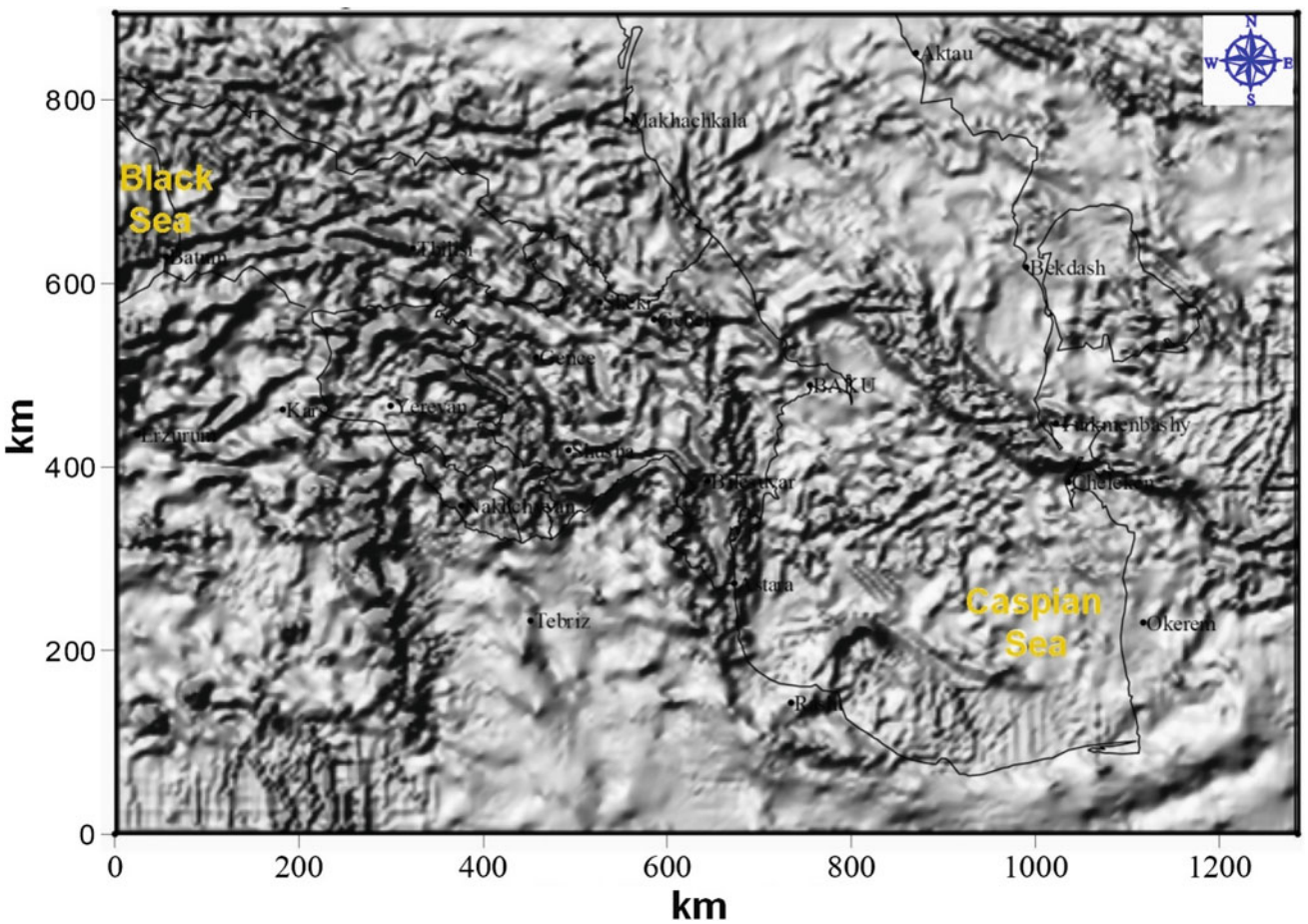

Fig. 4.30 Shaded relief map of total horizontal gradients of gravity field in the Caucasian-Caspian region upward continued to altitude of 20 km (horizontal and vertical light position angles were taken as 135° and 45°, respectively) (Kadirov 2004)

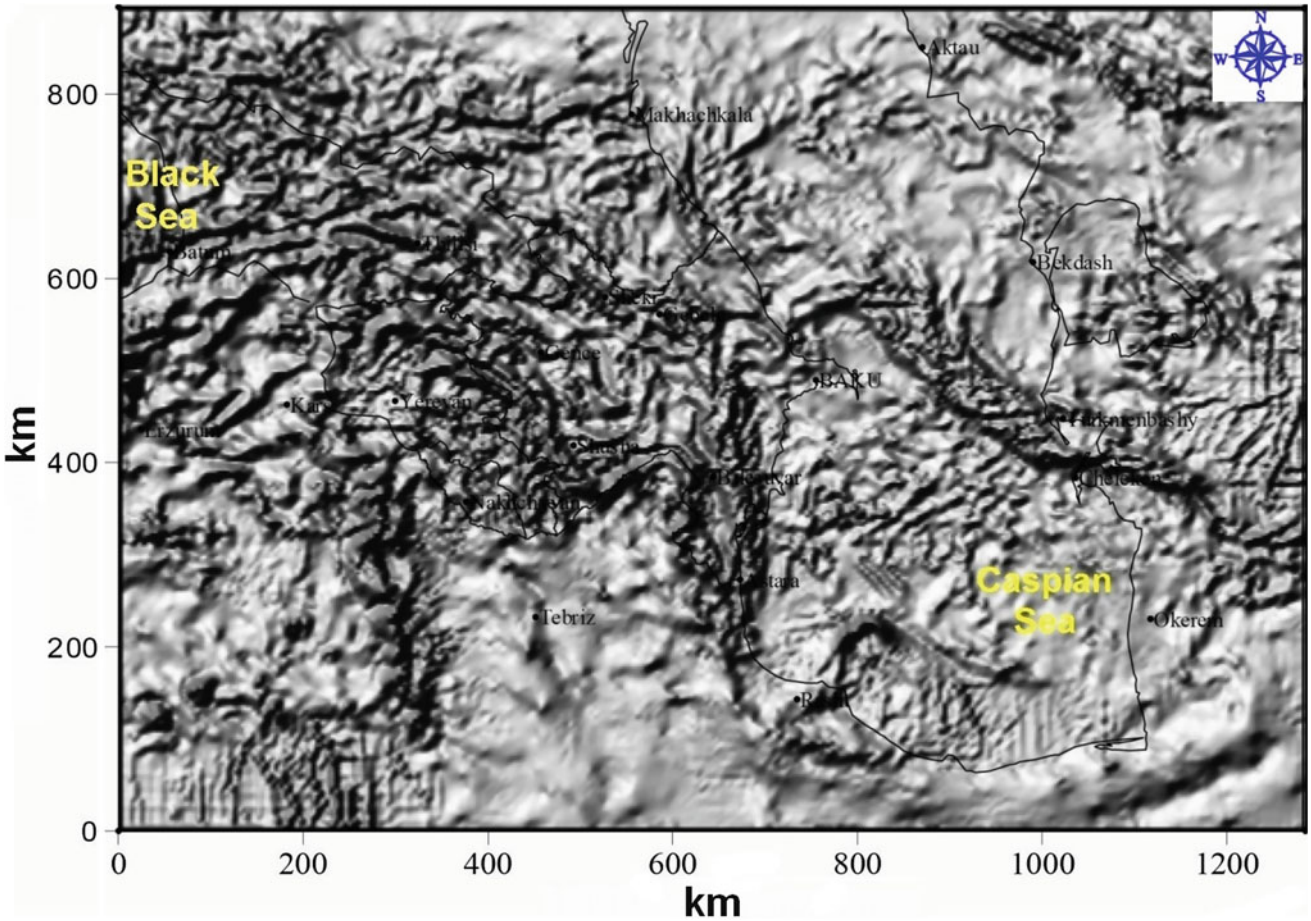

Fig. 4.31 Shaded relief map of total horizontal gradients of gravity field in the Caucasian-Caspian region upward continued to altitude of 20 km (horizontal and vertical light position angles were taken both as 45°) (Kadirov 2004)

regions with different signs and intensity of the field are mainly singled out by maps of the initial field and the field on a number of levels of the upper semi-space incorporating local and difference anomalies. Field region boundaries and other linear elements are traced by horizontal gradients and predominant strike isoline maps using the initial field and regional-anomaly maps and employing local elongated anomalies from corresponding charts. The local anomalies are singled out by maps of local and difference anomalies on the basis of the horizontal gradient map. These together give an idea of the depth extension of the sources.

4.3 Quantitative Analysis and Regioning

To enhance reliability when calculating the anomalous object parameters, techniques that measure different individual elements of the anomaly or the curve as a whole should be applied jointly. These include the methods of interpolation selection, singular points, analytical continuation, and selection based on approximation optimization. The optimum combination is determined by the specific nature of the region under survey and the nature of the material. For example, the density of the observation network and the accuracy of the field measurements impose certain restrictions on the method of singular points. The results of this method also depend on the noise fields of the sources occurring above the singular points of the objects being localized.

The applicability of methods under rugged terrain relief is not, in most cases, a decisive one if the observed anomaly is initially converted into a horizontal or inclined plane. The need for anomaly reduction is determined by the chosen set of techniques.

A system of advanced potential and quasi-potential geophysical field interpretation has been presented in Khesin et al. (1983, 1996), Eppelbaum and Khesin (2012) and

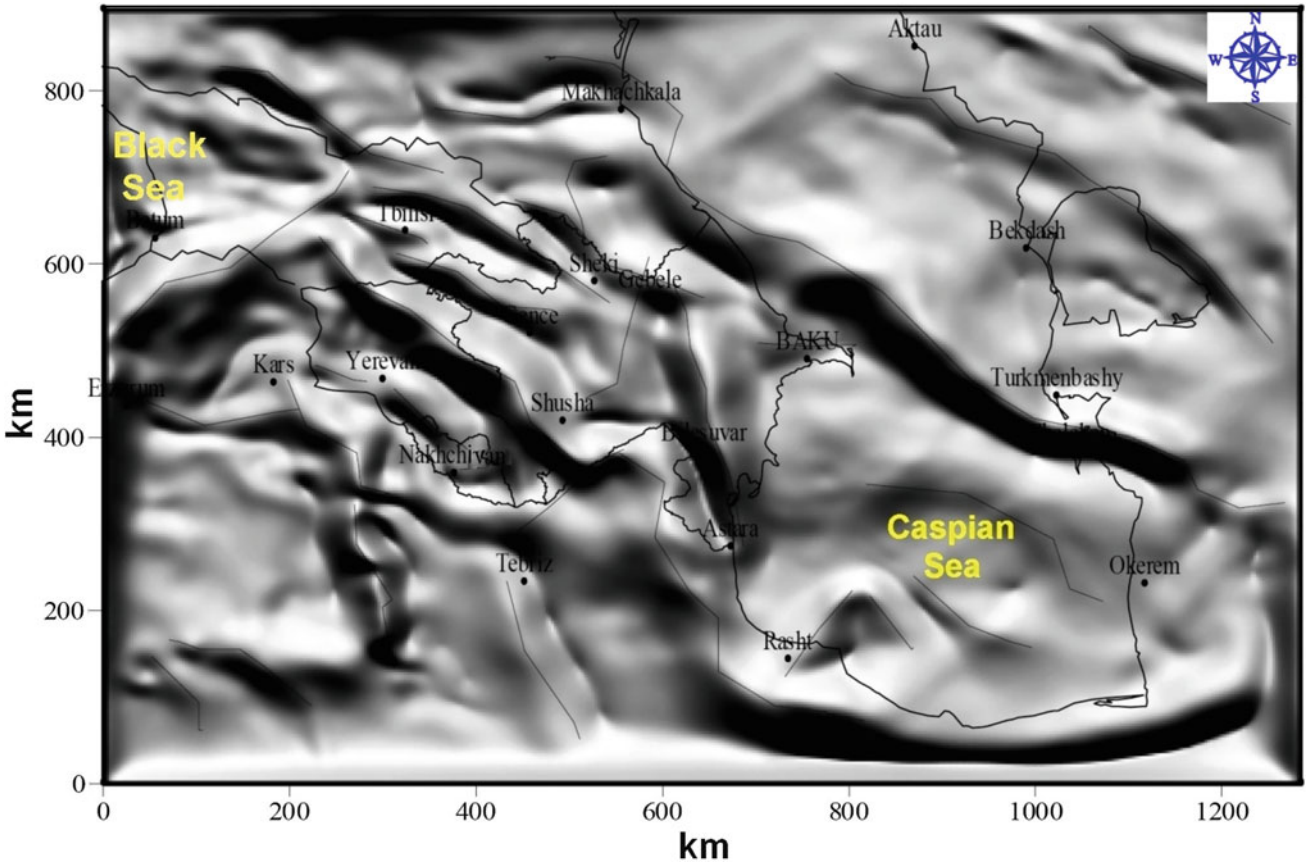

Fig. 4.32 Shaded relief map of full horizontal gradients of gravity field in the Caucasian-Caspian region upward continued to altitude of 50 km (horizontal and vertical light position angles were taken for 45° and 50°) (Kadirov 2004)

Eppelbaum et al. (2014). A key element of this system is a quantitative analysis of magnetic anomalies in conditions of inclined relief, oblique magnetization, and unknown level of the normal magnetic field. Let us consider several examples of the magnetic anomaly interpretation in complex regions of Azerbaijan.

Figure 4.36a exemplifies the use of the tangent method and the method of characteristic points, whereas Fig. 4.36b presents the method of characteristic areas (for the inclined thin bed model) applied for airborne magnetic data analysis in the Big Somalit area (northwestern Azerbaijan).

The Guton magnetic anomaly is situated in NW Azerbaijan (southern slope of the Greater Caucasus), near the border with Russia (Fig. 4.37). A detailed quantitative interpretation of this anomaly was carried out along fifteen profiles crossing this anomaly. The results along one of these profiles (the anomalous body was approximated by a thick inclined bed) are shown in Fig. 4.38 (here, improved tangent, characteristic point, and areal methods were applied). The methodology is described in detail in Khesin et al. (1996). The data indicate that the anomalous body is characterized by comparatively low magnetization (250 mA/m), considerable vertical thickness (about 30 km), and a steep dip of the lateral contacts. Analytical continuation and singular point methods applied on the same profiles gave similar results (Fig. 4.39). The characteristics of this anomalous body testify to the intermediate-acid composition of this target (intrusion). The interpretation of the significant vertical thickness of this body agrees with the geothermic data on the depth of the Curie discontinuity in this area (about 30 km) (Eppelbaum et al. 2014).

The outcroppings at the Earth's surface formed subvolcanic and subintrusive bodies of different consistencies which are apparently fragments of this large magmatic massif penetrating the upper part of the section along the extended faults of the common Caucasian direction. This

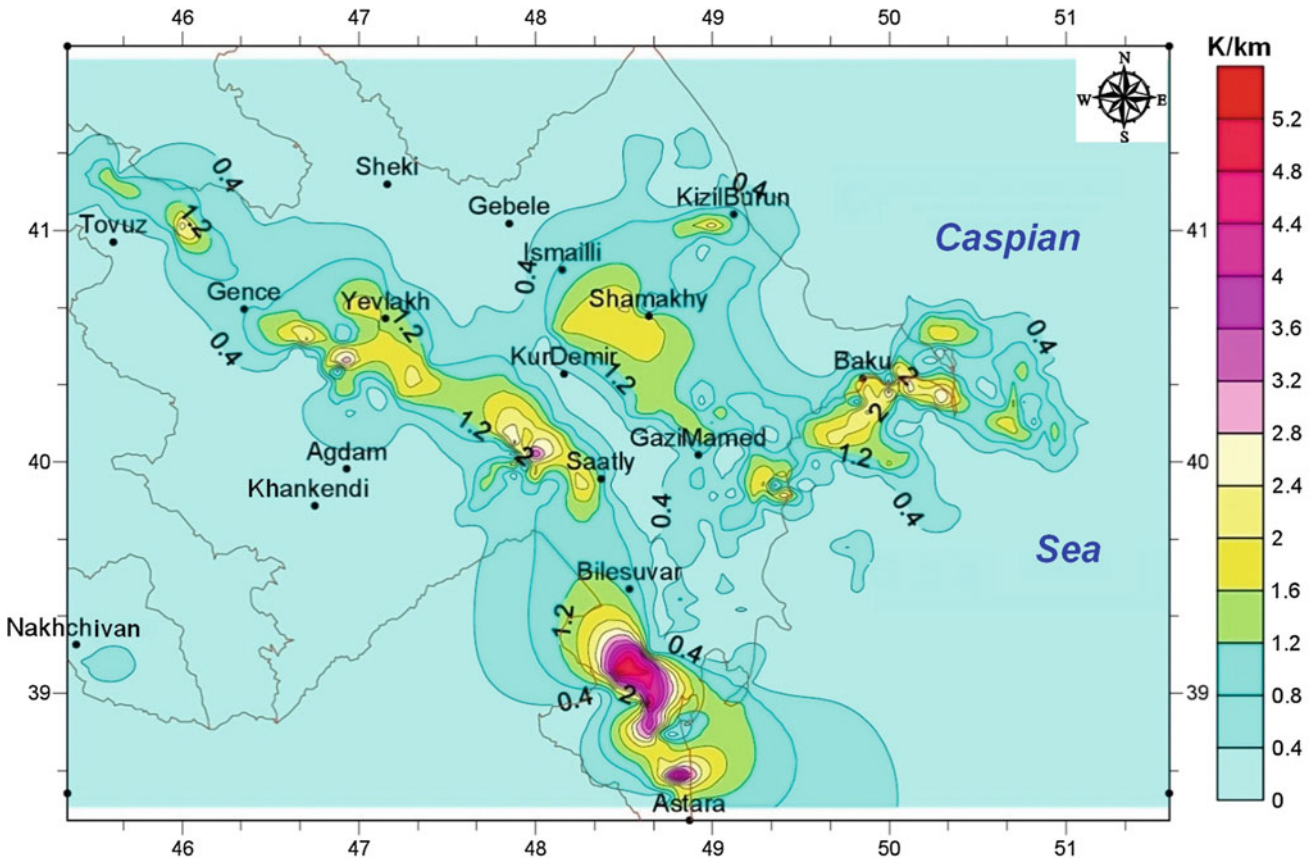

Fig. 4.33 Map of the total horizontal gradients of temperature field for Azerbaijan (for the depth of 5 km (Mukhtarov 2012)

magmatic focus is associated with the rich pyrite–polymetallic deposits of the Belakan-Zagatala ore field and possibly other areas in the Greater Caucasus (Ismailzadeh et al. 2005; Eppelbaum and Khesin 2012).

4.4 Compilation of Final Geophysical–Geological Maps

To delineate the ore mineralization associated with intrusive magmatism, the structures shown in Fig. 4.40 are especially instructive. They are presented as series of local anomalies corresponding mainly to the basic phases of granodiorite intrusive bodies.

The complex geological structure of Azerbaijan governs its highly intricate gravity and magnetic fields which reflect the effects of outcropped and deeply buried bodies and structures. Thus, to identify anomalies arising from a range of geological sources, both the observed geophysical fields and their various transformations must be used. Therefore, the legend of such a deep structure map must include a classification of spatial features (regional and local anomalies), geomorphological features (isometric anomalies, elongated anomalies, or ledges), and the signs and intensities of geophysical fields.

The regional minima of the same component outline the prospective oil and gas regions. The lower density of the Cenozoic terrigenous rock masses (2.0 ÷ 2.3 g/cm^3) unambiguously defines the regions of lower density at depth (gravity minima) as having the largest accumulation of sedimentary rock masses. The latter are promising as regards oil and gas resources in the Palaeogene–Miocene and Pliocene–Quaternary deposits. These regions are characterized by the conjunction of the Guba-Khachmaz and Iory-Agrichay zones with the Kobustan-Lower Kur zone in the east, and the Evlakh-Agjabedi zone (negative field regions 1, 5, 6, and 14, respectively, in Fig. 4.41).

The regioning scheme of the gravitational field in Azerbaijan as compared to the regional steps of the magnetic field is shown in Fig. 4.41. Regional peculiarities of the gravitational

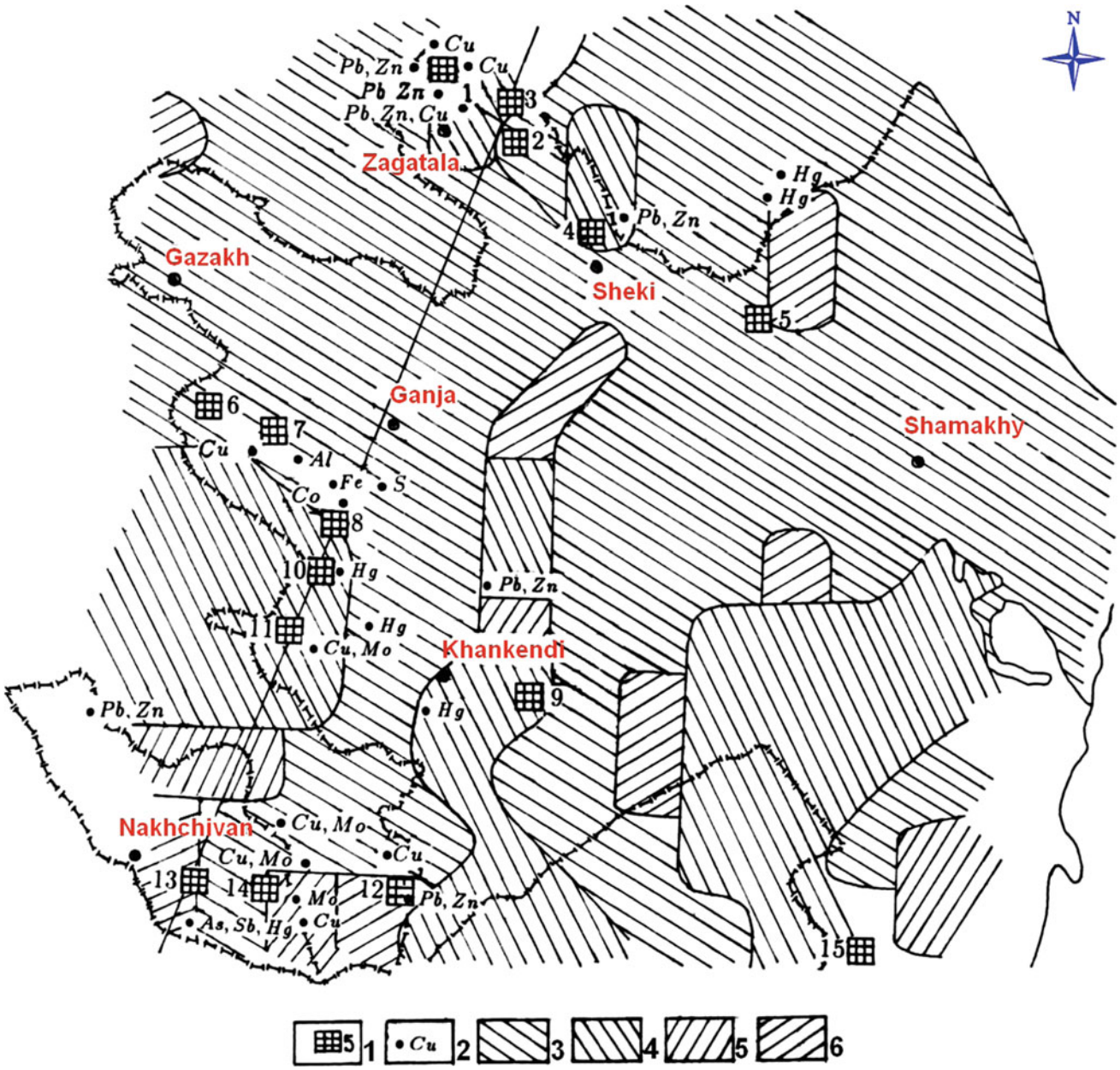

Fig. 4.34 Test well drilling site pattern in mountainous regions of Azerbaijan (after Khesin et al. 1996, with small modifications). (*1*) sites recommended for test well drilling and their numbers; (*2*) ore deposits; predominant courses of terrain relief isohypses: (*3*) WNW, (*4*) NNW, (*5*) NNE, and (*6*) ENE

and magnetic fields determine the regional factors of both oil and gas and ore control. The Shamkir-Gedabey-Dashkesan ore zone and the Mekhmana ore district (Lesser Caucasus), and the Belakan-Zagatala ore field (Greater Caucasus) which were identified on the basis of systematic geophysical studies, as well as the Kutkashen-Ismailly district (the Greater Caucasus), which has potential endogenic mineralization according to a number of indicators (Azizbekov et al. 1972; Eppelbaum and Khesin 2012), are controlled by the positive difference field $\Delta g_{B(8-20)}$ (see Fig. 4.15) that corresponds to zones 8 and 2, respectively, as shown in Fig. 4.41.

Accumulated experience shows the importance of performing independent regioning using initial field and regional-anomaly maps. Comparing the results in a unified

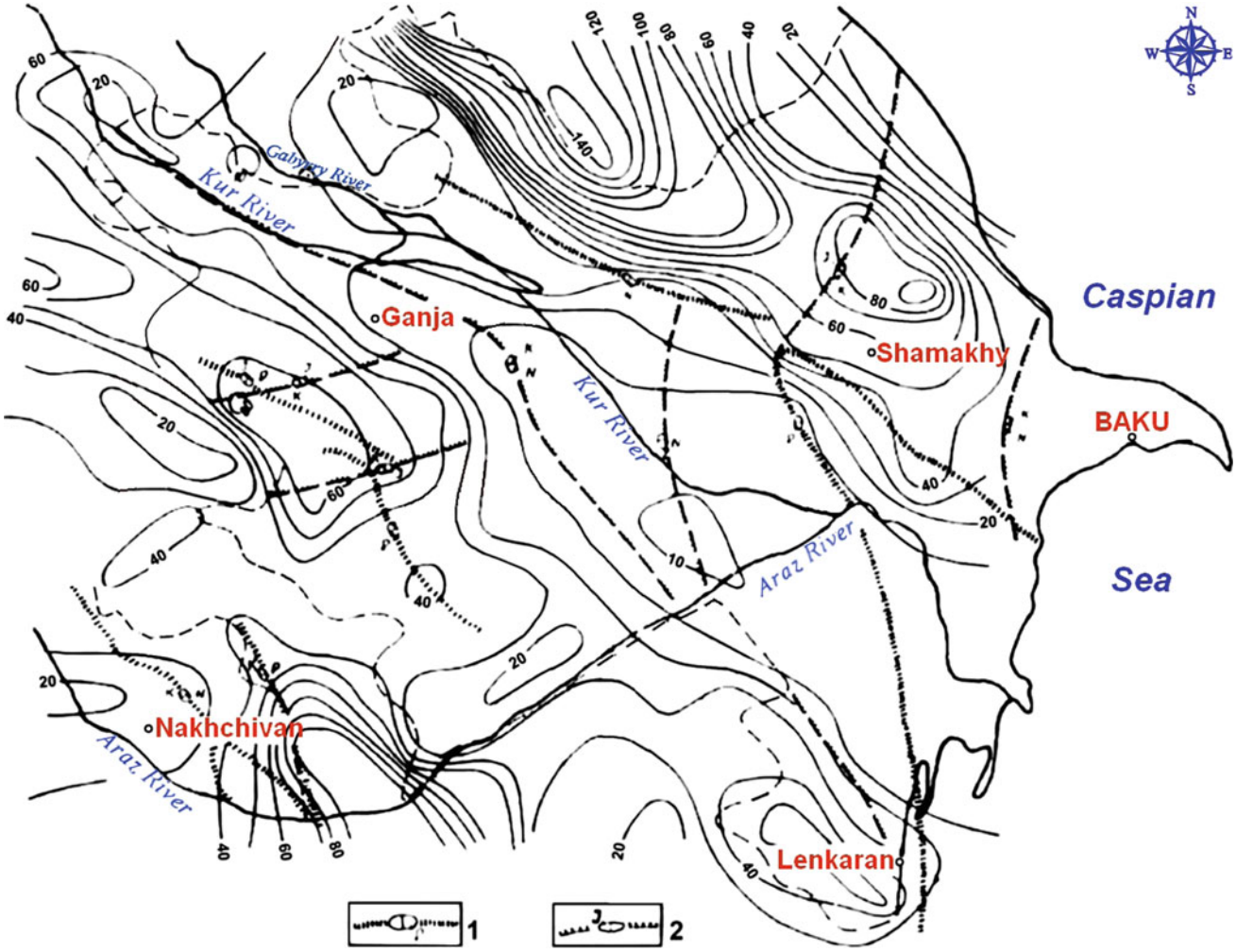

Fig. 4.35 Map of equal lengths of isohypses for the topography of Azerbaijan (after Khesin et al. 1996). (*1*) deep fault (*dots* show buried paths of the fracture); (*2*) flexures (on the surface as shown by *solid lines* and buried as shown by *dashed lines*); indices point to the expected section interval dissected by fractures

scheme makes it possible to determine common features and differences in deep structure elements and in the upper portion of the section, and reveal the elements (primarily, disjunctive dislocations, and blocks) that manifest themselves at the different structural stages.

The transforms reflecting the degree of heterogeneity of the field such as anomalous coefficients, dispersion, and entropy are the most useful for singling out field areas in open regions. In different areas, these parameters can take on different geological meanings. They are also appropriate for solving more specific problems, in particular in the regioning of separate portions by the degree of heterogeneity of their lithological complexes. Here, it makes sense to compute the specific sinuosity of the isolines.

The map of gravity–magnetic anomalies (Fig. 4.42) shows both these minima since the problem of their nature can be solved at the stage of anomaly examination (Alexeyev et al. 1989; Eppelbaum and Khesin 2012).

A description of gravity anomalies was based on the following: (1) difference fields ("ring" anomalies) $\Delta g_{B(8-20)}$ and $\Delta g_{B(4-10)}$ computed as the difference between upward continued fields in the Bouguer reduction (terrain correction

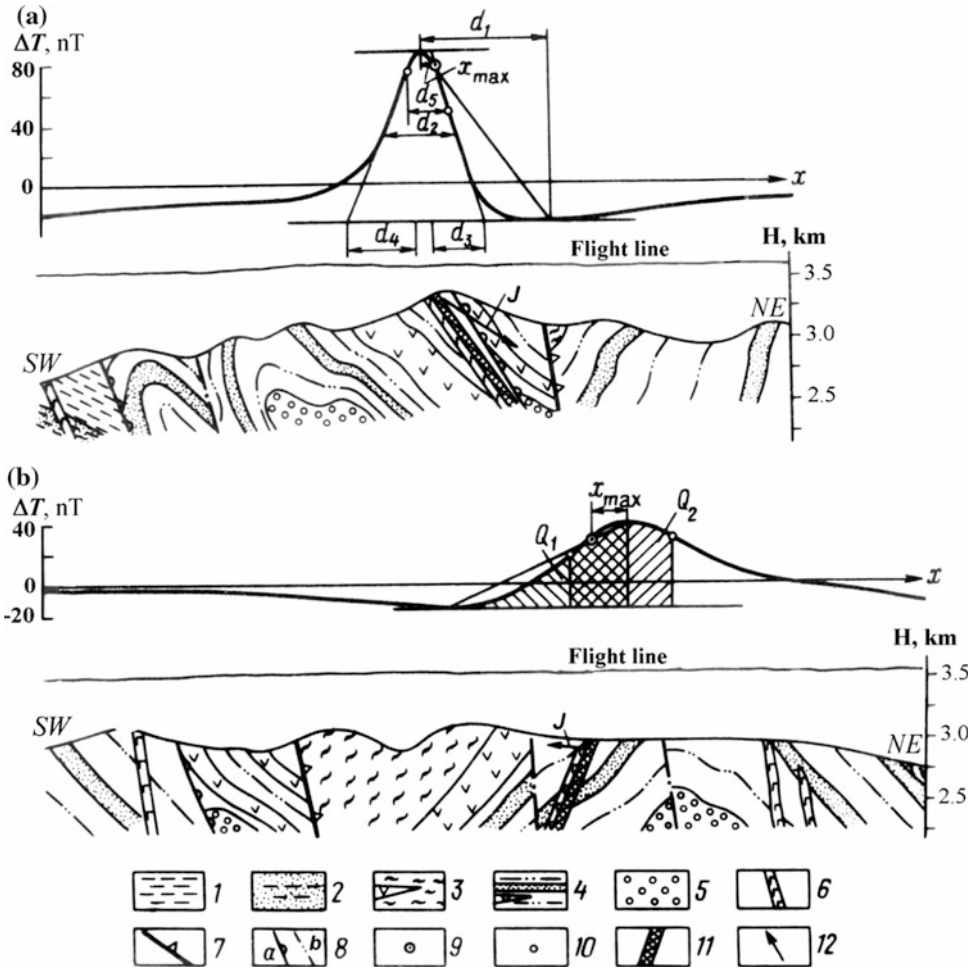

Fig. 4.36 Examples of quantitative interpretation of ΔT plots along profiles 171 (**a**) and 181 (**b**) in the area of the Big Somalit (southern slope of the Greater Caucasus) (Khesin et al. 1996). (*1*) Yalakhkam suite J_2aal_2; (*2*) Zainkam suite J_2aal_1; (*3*) Nagab suite J_1toa_3; (*4*) Tseilakhan suite J_1toa_3; (*5*) the Lower and Middle Toarcian suite J_1toa_{1-2}; (*6*) dikes of the gabbro–diabasic association; (*7*) the Main Caucasian upthrust–overthrust; (*8*) ore controlling (**a**) and ore distributing (**b**) upthrust–overthrusts; (*9*) Reford's point; (*10*) inflection points; (*11*) anomalous body according to the interpretation results; (*12*) obtained direction of the magnetization vector

was computed with a radius of 200 km, and the density of the intermediate layer was defined as 2.67 g/cm^3) at heights of 8 and 20, 4 and 10 km, respectively, (2) the residual field $\Delta g_{B(0-4)}$(local anomalies were calculated as the difference between the initial land Bouguer gravity and this field continued upward to a height of 4 km), and (3) horizontal gravity gradient field at a height of 2 km ($\Delta g_{x(2)}$).

These features were analyzed on the basis of the following descriptors.

I. The residual field $\Delta g_{B(0-4)}$ in the mountain-folded regions reflects the influence of near-surface Alpine structures composed of volcanogenic and volcanogenic–sedimentary associations, and intrusions (both outcropping to the Earth's surface and near-surface), and in the Kur Depression as regards the distribution of dense inhomogeneities of the upper part of the sedimentary floor.
II. The peculiarities of difference field ("ring" anomalies) $\Delta g_{B(8-20)}$ were described in Sect. 4.2.2.
III. Significant anomalies of $\Delta g_{x(2)}$ should be taken into consideration by delineation and examination of regional gravity anomalies.

These descriptors were determined on the basis of analysis of petrophysical parameters (see Sect. 4.1) as well as data on density of metamorphic foundation outcropped in Armenian territory.

According to Nikolsky et al. (1975), basement outcrops in Armenia are characterized by the following average density values: Aparan (2.80 g/cm^3), Arzakan (2.76 g/cm^3), Lok (2.76 g/cm^3), Eranos (2.87 g/cm^3), Nyuvadi (2.80 g/cm^3), and Akhum (2.63 g/cm^3). It should be noted that the Shamkir (Beyukkishlak) protrusion, located in Azerbaijanian territory 20 km east of Akhum, is also characterized by an average density of 2.63 g/cm^3.

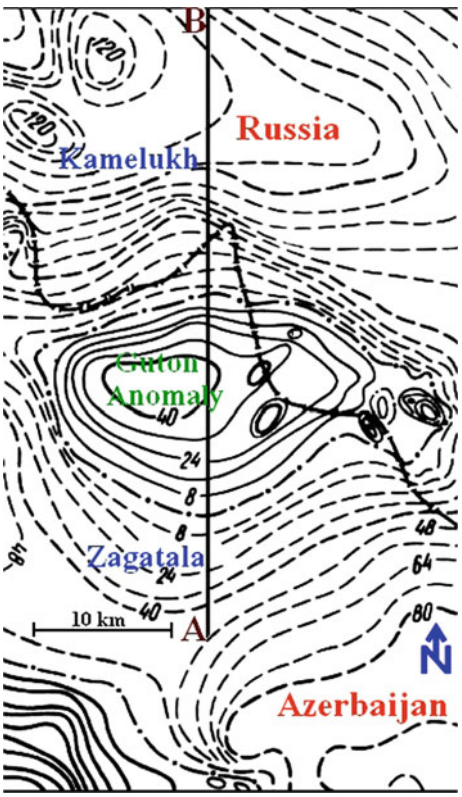

Fig. 4.37 Guton magnetic anomaly (results of an airborne survey) on the southern slope of the Greater Caucasus. The map shows the total magnetic field ΔT (isolines are given in mA/m) and the location of interpreting profile **A–B** (Eppelbaum and Khesin 2012)

At the same time, the density of separate types of rocks composing these protrusions may vary considerably. For instance, muscovite and sericite–quartz shales have a density of 2.66 (Aparan) to 2.79 g/cm^3 (Lok), quartzite from 2.60 (Lok) to 2.67 g/cm^3 (Nyuvadi), phyllite from 2.63 (Akhum) to 2.84 g/cm^3 (Arzakan), greenstone rocks (plagioclase porphyrites, tuff-sandstone, etc.) from 2.71 g/cm^3 (Lok) to 2.83 g/cm^3 (Aparan), gneisses from 2.60 g/cm^3 (Arzakan) to 2.94 g/cm^3 (Nyuvadi), limestone and marble from 2.66 g/cm^3 (Aparan) to 2.78 g/cm^3 (Arzakan), and amphibole shales from 3.00 g/cm^3 (Aparan) to 3.03 g/cm^3 (Eranos).

In the Shamkir (Beyukkishlak) cericite-muscovite-graphite outcrop, shales were found with comparatively low density (which is typical for the average density of the Baikalian series) (Azizbekov et al. 1972). An analogical situation was identified on the Akhum outcrop where at the Earth's surface, phyllite clay shales representing the less metamorphosed part of the geological section were identified (Nikolsky et al. 1975). Thus, despite this variability in density, the average density of the rocks composing the pre-Alpine foundation in SW Azerbaijan can be estimated as 2.80 ± 0.05 g/cm^3.

For the Armenian territory, the regional gravity map $\Delta g_{B(reg)}$ was constructed by a methodology that included using points of outcropped metamorphic basement (6 points), boreholes that crossed the basement (7 points), and other data. This map as a whole coincides with the $\Delta g_{B(8)}$—map obtained by analytical continuation of the surface gravity field to a height of 8 km (the absolute levels of these maps are different) (Sirotkina and Nikolsky 1971). It can be suggested that analogical correspondence is correct and for the Lesser Caucasian part of Azerbaijan territory. Thus, the $\Delta g_{B(8)}$ map mainly reflects the variations of the upper surface and inhomogeneities of the consistency in the pre-Alpine metamorphic floor and deeper layers of the Earth's crust; the effects of the Alpine floor are weakly present in this map. Therefore, the difference field $\Delta g_{B(8-20)}$ ("ring anomalies") primarily reflects the influence of the internal structure and inhomogeneities of the consistency of Baikalian and possibly the pre-Baikalian floor. In addition, as regards the transition from the Lesser Caucasus to depression regions, the difference field mainly represents the structure and consistency of the Mesozoic associations which act here as a dense basement.

Thus, the anomalies in the $\Delta g_{B(0-4)}$ map indicate local (close to the Earth's surface) objects; anomalies recognized in the $\Delta g_{B(8-20)}$ map represent some regional (deep) objects. The $\Delta g_{B(4-10)}$ map has a pattern similar to $\Delta g_{B(8-20)}$, but with a more differentiated field.

To examine regional magnetic anomalies, the following measures were used: field ΔT (in the Middle Kur Depression —field Z_a) at 6 and 10 km and the $\Delta T(Z_a)$ horizontal gradient field at 2 km. Attempts to reveal local magnetic anomalies as a residual field of $\Delta T_{(0-6)}$ or $\Delta T_{(0-10)}$ were unsuccessful because of the considerable difference in the observed magnetic field in the Lesser Caucasus. Therefore, local magnetic anomalies were selected directly in the initial field, and magnetic maxima were singled out irrespective of whether they were found in a positive or negative field. Magnetic minima were identified in a similar fashion. Some of these minima were conjugated with the corresponding maxima in relation to the oblique magnetization typical of the Azerbaijan territory. Other minima corresponded to objects with a low magnetization or reversely magnetized targets.

In the $\Delta g_{B(8-20)}$ map intensive (first tens of mGals) and extended (first hundreds of km) gravity, ledges were identified that split the areas of positive and negative field. Similar ledges were identified in the $\Delta g_{B(4-10)}$ map. The intensive linear

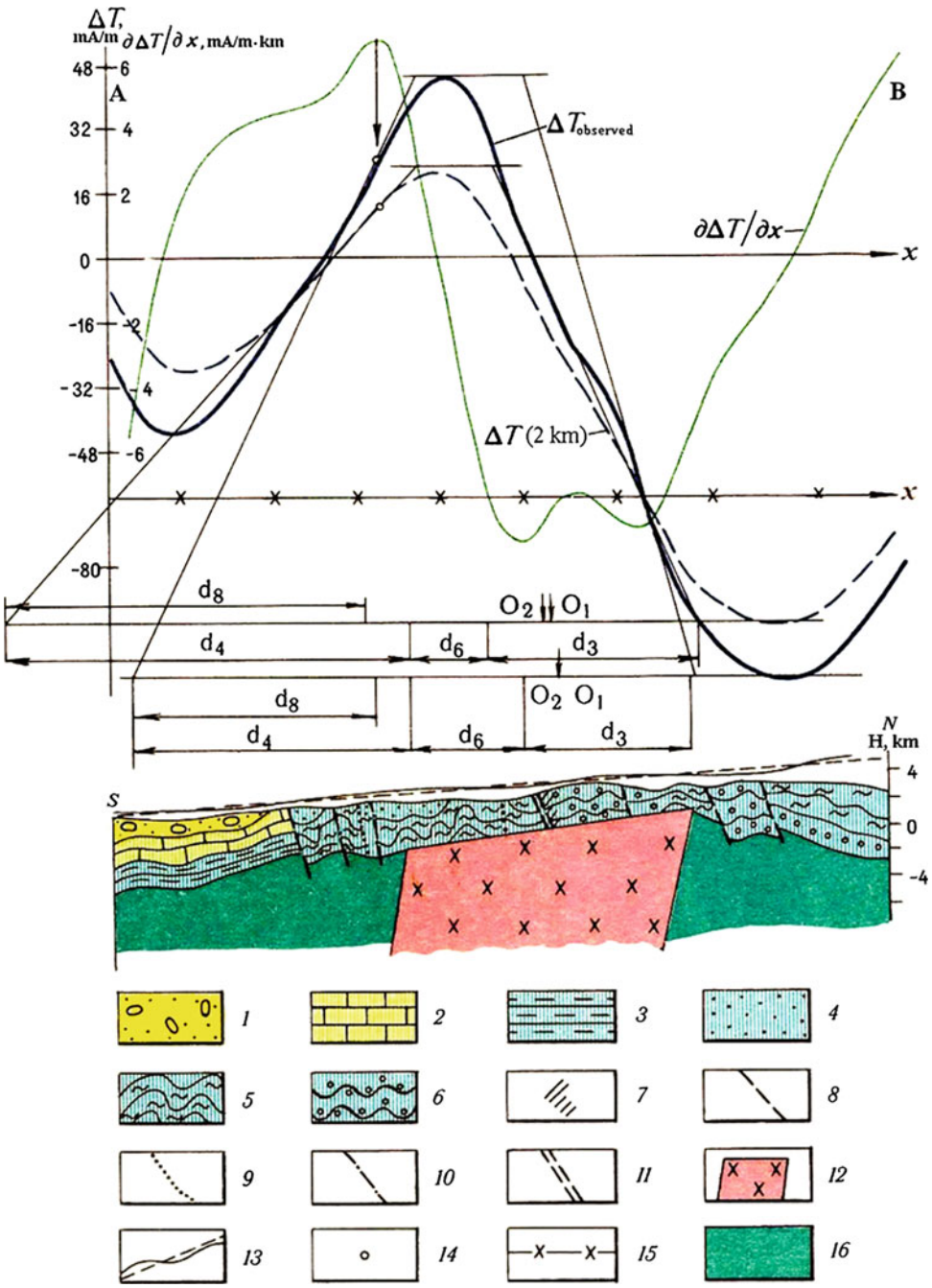

Fig. 4.38 Interpretation of ΔT graphs on two levels along profile 28 through the Guton anomaly (southern slope of the Greater Caucasus) (Khesin et al. 1996). (*1*) recent alluvial deposits; (*2*) limestones, tuff sandstones, clay shales (*K*); (*3*) mudstones, tuff sandstones (J_3); (*4*) monolith clay shales and coarse-grained tuff sandstones (J_2); (*5*) sandy-clay shales with horizons of sand flysch, metamorphosed clay shales, and sandstones (J_2); (*6*) phyllitizated clay shales, sandstones, spilites (J_1); (*7*) dikes and sheet bodies of the gabbro–diabasic association (J_2); (*8*) regional upthrust–overthrusts; (*9*) upthrust–overthrusts separating the longitudinal tectonic steps of the second order; (*10*) upthrust–overthrusts complicating the longitudinal tectonic steps; (*11*) transverse fractures; (*12*) magmatic intrusion of intermediate-acid composition according to the interpretation data (in non-segmented $J_{1–2}$ complex); (*13*) the lines of flight and averaging inclined *straight line*; (*14*) inflection point of the plot ΔT nearest to the maximum on the *left*; (*15*) corrected zero line of the plots ΔT; O_1 and O_2 are locations of the origin (middle of the anomalous body's upper edge) obtained from $x_{un–r}$ to $x_{un–l}$, respectively; (*16*) $J_{1–2}$ complex

maxima or minima correspond to them in the horizontal gravity gradient map. Axes of these ledges are shown in the map of gravity–magnetic anomalies (Fig. 4.42) as two bold colored lines: brown from the side of the positive field and green from the side of negative one; arrows in the green line are oriented toward the block of lesser density. Less intensive (several mGals) and less extended gravity ledges are represented by an analogous symbol with lines of less density.

Regional magnetic steps were identified by analysis of $\Delta T_{(10)}$ and $Z_{a(10)}$ maps by taking into consideration the map of the horizontal magnetic gradient $\Delta T(Z_a)$ at 2 km. Axes of these ledges are depicted in this map (Fig. 4.42) as two bold colored lines: Blue is from the side of positive field, and red is from the side of negative field; arrows on the red line are oriented toward the side of the block with lesser magnetization (Eppelbaum and Khesin 2012).

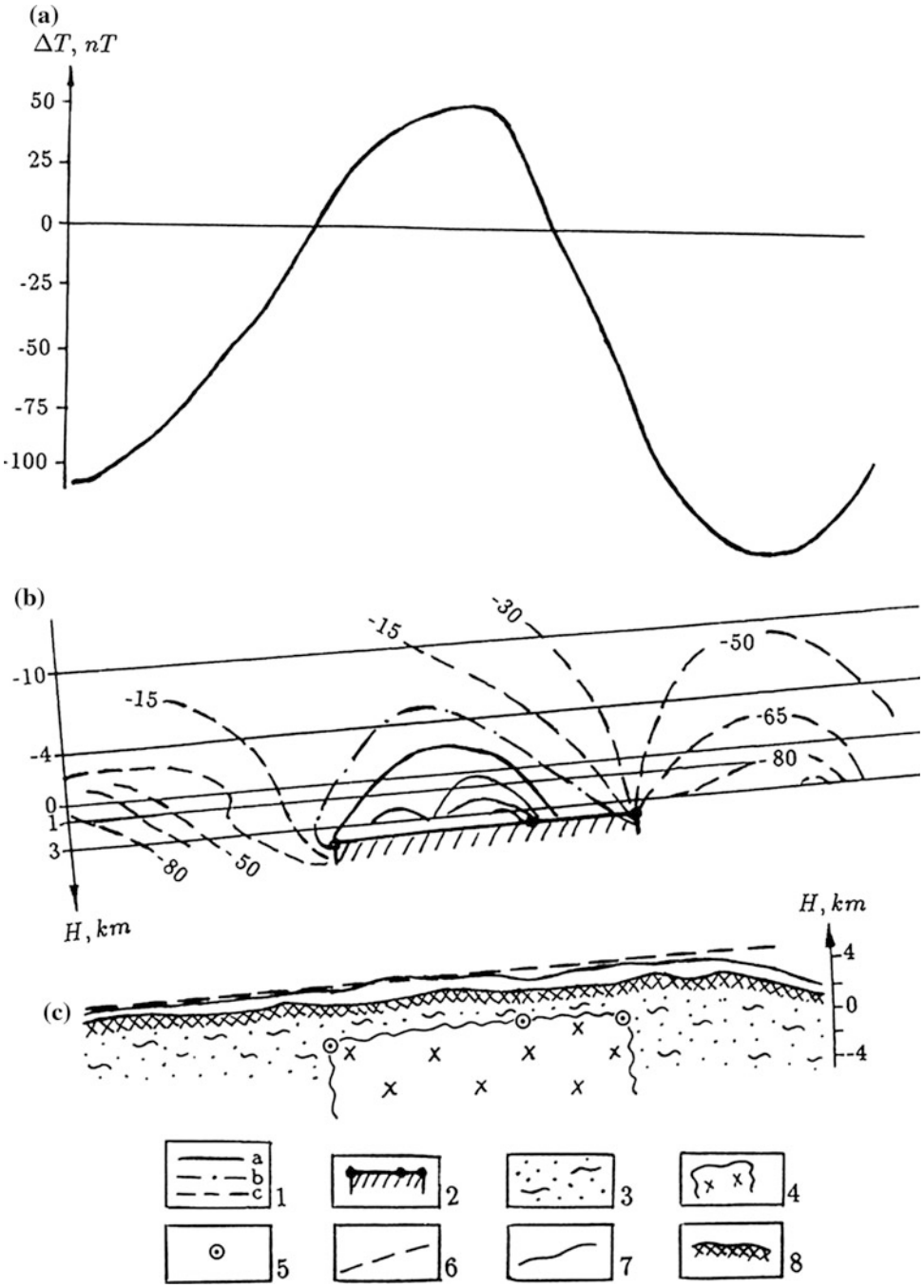

Fig. 4.39 Example of interpretation of the Guton anomaly implementing analytical continuation and singular point methods (Eppelbaum and Khesin 2012). **a** plot of ΔT; **b** an isoline chart based on the results of analytical continuation in an inclined half-space; **c** a schematic section of the anomalous object. (*1*) isolines, nT: **a**—positive, **b**—zero, **c**—negative; (*2*) magmatic intrusion of an intermediate-acid composition (according to the interpretation results); (*3*) the upper edge of the anomalous object, obtained by the method of analytical continuation (*black points* show logarithmic peculiarities of the field); (*4*) singular point; (*5*) inclined straight line approximating the observation profile

Regional gravity maxima and minima (with intensity up to 20 mGals) as revealed in the $\Delta g_{B(8-20)}$ map are contoured by the points with values approximately equal to half the extremal values.

In the map (Fig. 4.42), they are shown as solid bold brown (maxima) and green (minima) lines, respectively, with arrows oriented to the side of decreasing field. Within certain contours are located several (1 to 3–4) anomalies of $\Delta g_{B(4-10)}$ but are not shown to make the map pattern more legible.

Local gravity and magnetic maxima indicated, respectively, in maps $\Delta g_{B(0-4)}$ and $\Delta T\,(Z_a)$ are represented by points with the half maximum of the corresponding extremum. The

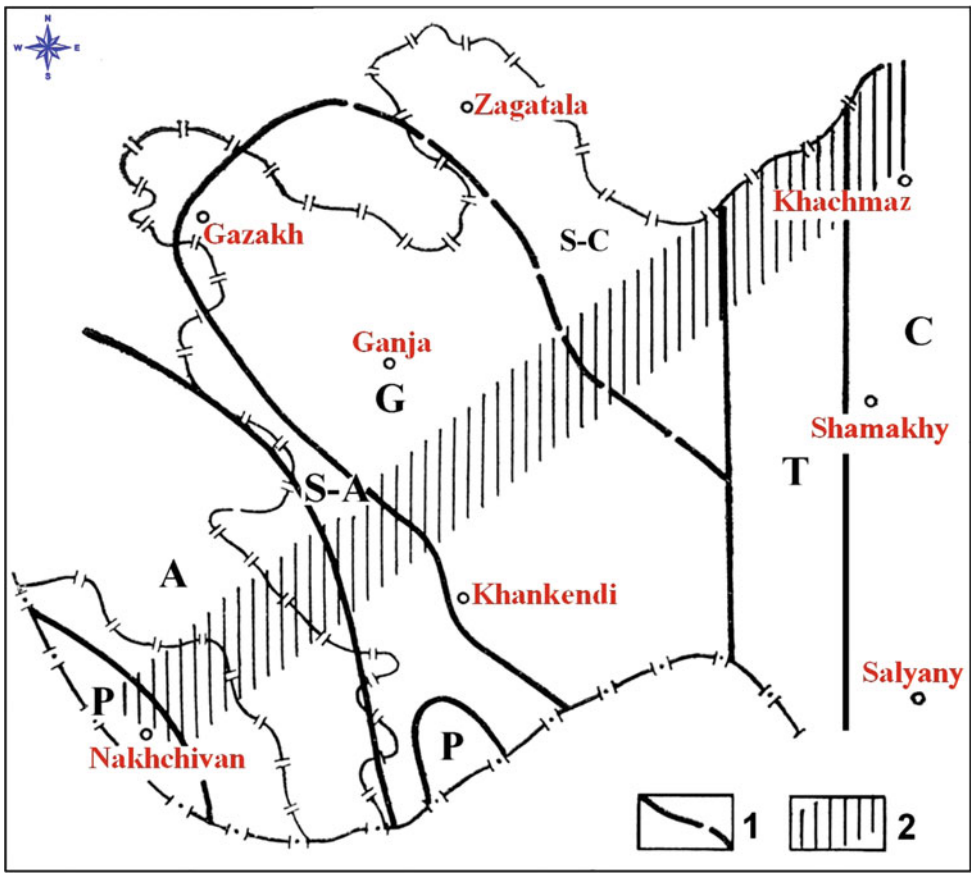

Fig. 4.40 Geophysical data of the Azerbaijan tectonic regioning (after Khesin et al. 1996). (*1*) boundaries of tectonic units, (*2*) the largest zone of anti-Caucasus dislocations delineated in most geophysical maps

maxima and minima are divided into intensive (exceeding the absolute value of 3–4 mGals and 300–400 nT) and less intensive (intensity of 1–2 mGals and 100–200 nT).

In the map (Fig. 4.42), intensive local gravity maxima are depicted by the dense dark shading surrounded by a brown line, and intensive minima are indicated by the dark green line. Less intensive local gravity maxima in a positive field are shown by light brown shading contoured by a brown line; the same maxima in a negative field are represented by light brown shading surrounded by a green line. Similarly, less intensive gravity minima are shown by light green shading surrounded by a green line in a negative field and a brown line in a positive field.

A similar system of symbols was applied to depict local magnetic anomalies: Intensive maxima are shown by dark blue shading surrounded by a blue line in a positive field and red in a negative field. The less intensive maxima are shown by light blue shading surrounded by blue or red lines depending on the sign of field in which the maximum appears. The local magnetic minima are shown as dark or light red shading depending on field intensity and a red or blue contour line depending on the sign of surrounding field.

The points of high intensive magnetic maxima and minima (exceeding 2000 nT in absolute value) are presented, respectively, by a blue cross and a bold red dot (imitating the tail and head of an arrow—magnetization vector).

Fig. 4.41 Comparison of gravity field regioning and regional steps of magnetic field mapping (after Khesin et al. 1996). (*1*) Axes of intense extended gravity steps distinguished in the $\Delta g_{B(8–20)}$ and $\Delta g_{B(4–10)}$ difference fields and the horizontal gradient field obtained from Δg_B at a level of 2 km; (*2*) axes of marked gravitational steps distinguished in the same fields; (*3*) axes of regional magnetic steps distinguished in the magnetic field at a level of 10 km and in the field of its horizontal gradient at a level of 2 km; (*4*) $\Delta g_{B(8–20)}$ positive gravity field blocks and zones; (*5*) $\Delta g_{B(8–20)}$ negative gravity field blocks and zones; (*6*) weak boundaries of $\Delta g_{B(8–20)}$ positive or negative gravity field areas; (*7*) gravitational step number (beginning and end of a step are indicated); (*8*) magnetic step number; (*9*) number of $\Delta g_{B(8–20)}$ positive or negative gravity field zones and blocks. *Note* The *arrows* on the symbols show the direction to the blocks of lower density or magnetization

The areas or intersections of local gravity and magnetic anomalies are shown by combined symbols: strips of corresponding color and shading intensity oriented in a NE direction at an angle of 45°.

On the basis of a combined analysis of gravity and magnetic fields, selected areas for deep drilling were charted (Fig. 4.43).

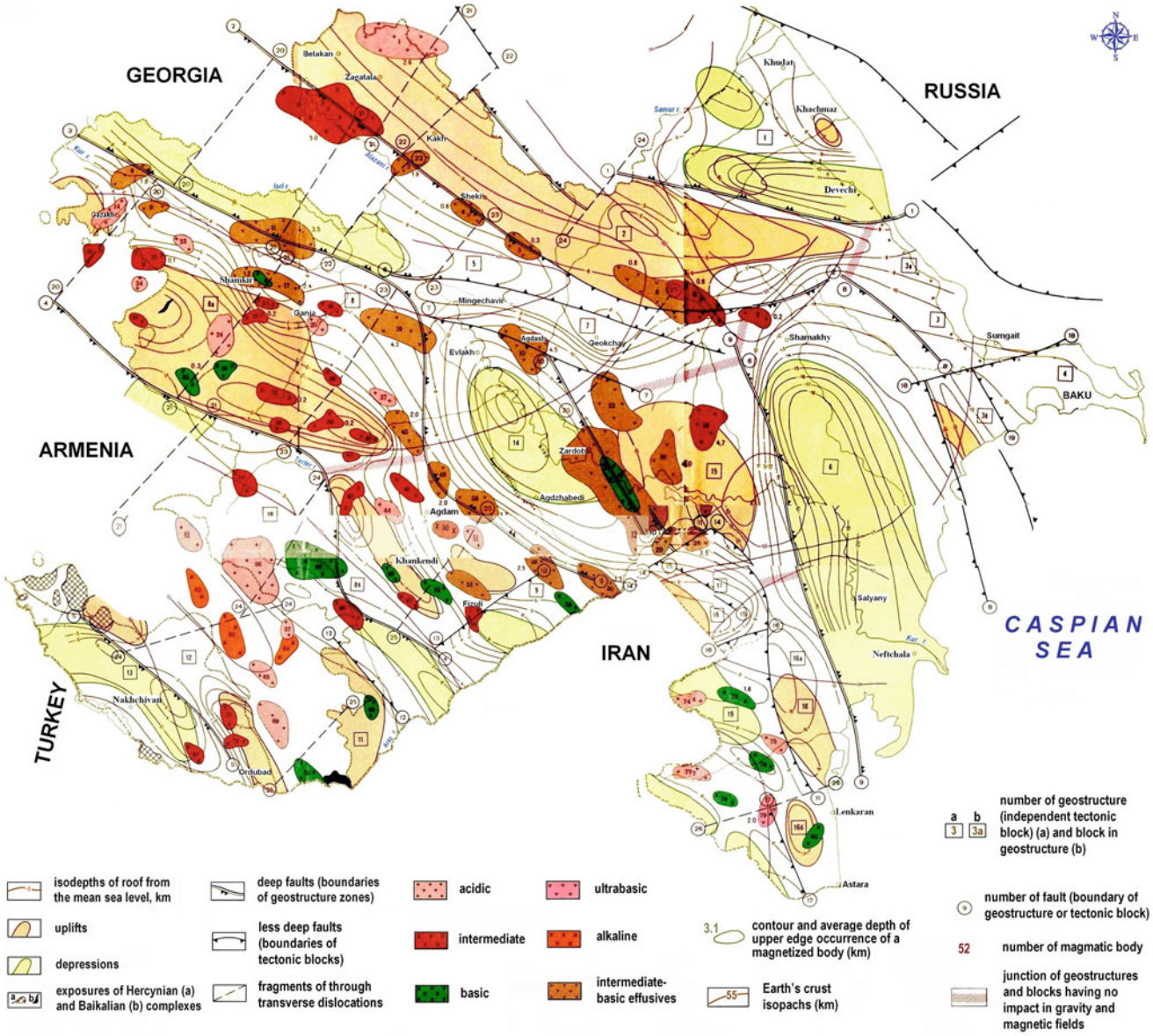

Fig. 4.42 Map of the deep structure of Azerbaijan with its adjacent regions according to gravity and magnetic data (after Alexeyev et al. (1989); Eppelbaum and Khesin (2012) with small modifications, geology after Azizbekov et al. (1972)

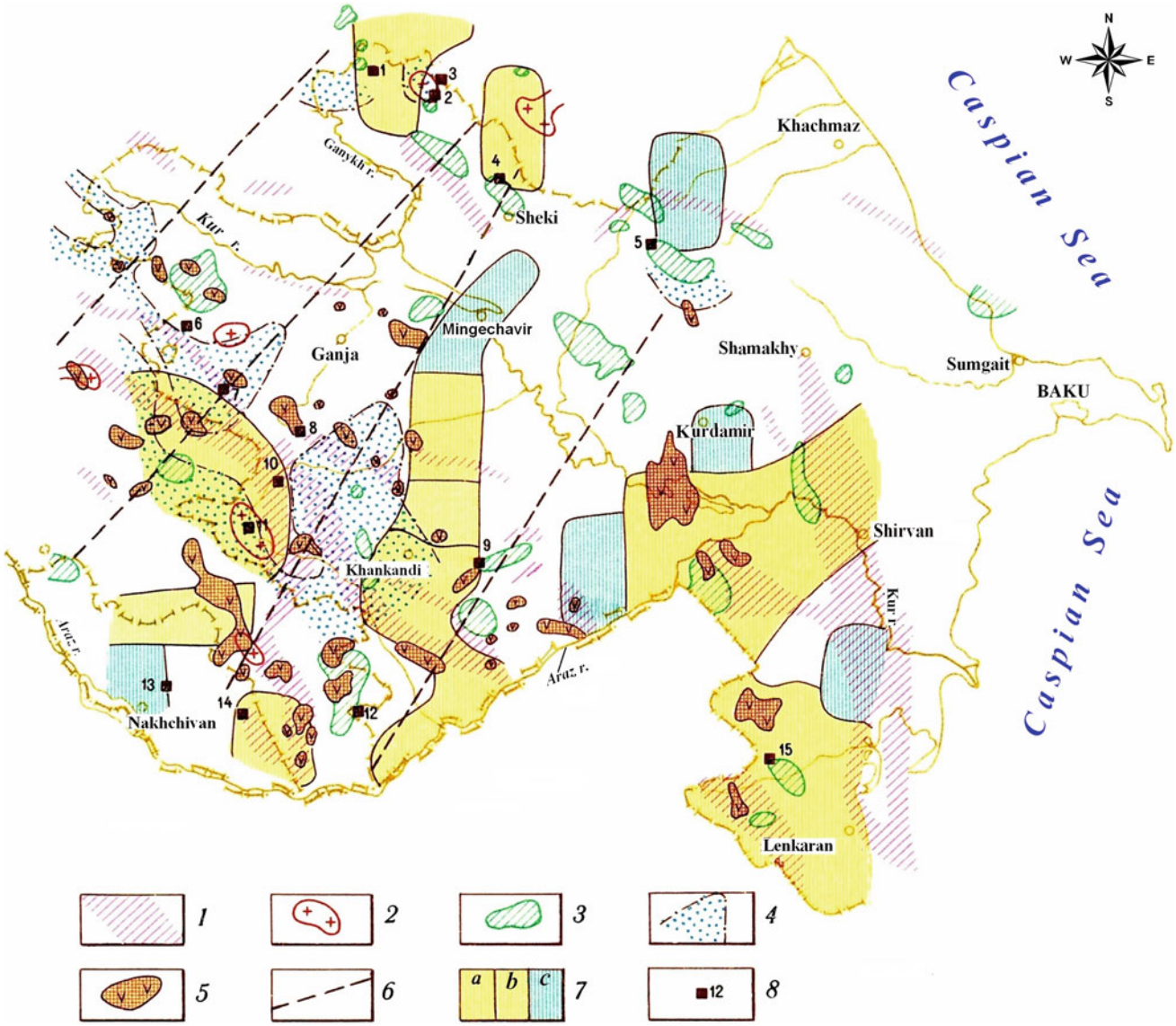

Fig. 4.43 Location of areas for deep drilling in Azerbaijan derived from integrated examination of geophysical fields (Khesin et al. 1996; geology is mainly from Azizbekov et al. 1972). (*1*) Zones of large faults detected by the use of the highest gradients of the gravity field in the Bouguer reduction, (*2*) acid intrusions revealed by negative local gravity anomalies, (*3*) dome-shaped structures or areas of basic rock development revealed by positive local gravity anomalies, (*4*) uplifts of basic and middle magnetized generations found after determination of singular points in the reference aeromagnetic net, (*5*) areas of basic rock development corresponding to local magnetic anomalies, (*6*) transversal faults marked by local magnetic anomalies, (*7*) neotectonic blocks corresponding to areas with anomalous (different from common Caucasian) strikes of relief isolines: **a**—NNW, **b**—NNE, and **c**—NEE, and (*8*) areas of recommended reference boreholes and their numbers

References

Aksyonovich, G.I., Aronov, L.E., Galperin, E., Kosminskaya, I.P. and Gegelgants, A.A., 1962. *Deep Seismic Sounding in Central Part of the Caspian Sea*. USSR Academy of Sciences, Moscow, (in Russian).

Alexeyev, V.V., Gadjiev, T.G., Karkoshkin, A.I. and Khesin, B.E., 1989. *Gravity and Magnetic Anomalies of Azerbaijan and Their Geological Interpretation*, (Ismailzadeh, T.A. and Khesin, B.E., Eds.), Printing Map Factory, Leningrad (in Russian).

Aliyev, Ch.S., Feyzullayev A.A. Valsangiacomo, C., Hoffmann, M., Baghirli, R.J. and Veliyeva, F.F., 2012. Radon problem in Azerbaijan: results of indoor measurements and its nature. In: (Alizadeh, Ak.A., Ed.), *Modern Problems of Geology and Geophysics of the Caucasus*. Nafta-Press, Baku, 52-71.

Aliyev, Ch.S. and Zolotovitskaya, T.A., 1996. Results of radiometric investigations. *In*: (Kerimov, K.M., Ed.) *Geophysical Investigations in Azerbaijan*, Sharg-Garb, Baku, 386-389 (in Russian).

Aliyev, Ch.S. and Zolotovitskaya, T.A., 2000. Radioactivity of Eocene rock complexes in the Central Talysh. *Izvestiya, Acad. Sci. Azerb*., Ser.: Earth Sci., No. 1, 67-72.

Aliyev, Ch.S. and Zolotovitskaya, T.A., 2005. Comparison of gamma-field with geological structure, geophysical fields, oil&gas bearing, and seismicity. *In*: (Ak.A. Alizade, Ed.), *Geology of Azerbaijan*, Vol. **V**, Physics of the Earth, Nafta-Press, 292-312 (in Russian).

Aliyev, G.A., Akhmedbeyli, F.S., Ismailzade, A.D., Kangarli, T.H. and Rustamov, M.I. (Khain, V.E. and Alizadeh, Ak.A., Eds.), 2005a. *Geology of Azerbaijan*, Vol. **IV**: Tectonics. Nafta-Press, Baku (in Russian).

Aliyev, S.A., Mukhtarov, A.S., Bagirli, R.J. et al., 2005b. Geothermal studies in Azerbaijan. In: (Alizadeh, Ak.A., Ed.), *Geology of Azerbaijan.* Vol. V: *Physics of the Earth*. Nafta-Press, Baku, 229-263 (in Russian).

Aliyev S. et al. (2001) Radioactive fields of mud volcanoes of Azerbaijan. *Geophysics News in Azerbaijan*, **3**, 25-32.

Aliyev, S.A., 1988. Geothermal fields of depression zones of the South-Caspian Depression and their relation with oil and gas bearing capacity. *D.Sci. Thesis*, Geol. Inst. Azerb. Acad. Sci., Baku (in Russian).

Aliyev, S.A. and Aliyev, A.S., 1995. Heat flow in depression of Azerbaijan. In: (M.L. Gupra and M. Yamano, Eds.), *Terrestrial Heat Flow and Geothermal Energy of Asia*. Oxford & IBH Publishing Co. PVT. Ltd., New Delhi.

Aliyev, S.A. and Mukhtarov, A.S., 2000. Geothermal studies in the borehole. In: (Ak.A. Alizadeh, V.E. Khain and A.D. Ismailzadeh, Eds.) *Saatly Superdeep Well. Studies of Deep Structure of the Kur Intermountain Depression Based on Materials of Drilling of Saatly Superdeep Well SG-1*. Nafta-Press, Baku, 213-233 (in Russian).

Alizadeh, Ak.A. (Ed.). 2012. *Modern Problems of Geology and Geophysics of the Caucasus*. Nafta-Press, Baku.

Andreyev, B.A. and Klushin, I.G., 1962. *Geological Interpretation of Gravity Anomalies*. Gostoptekhizdat, Leningrad (in Russian).

Azizbekov, Sh.A., Alizadeh, K.A., Shikalibeyli, E.Sh. and Gadjiev, T.G. (Eds.), 1972. *Geology of the USSR*, *Azerbaijan*, Vol. **XLVII**, Nedra, Moscow (in Russian).

Beardsmore, G.R. and Gull, J.P., 2001. *Crustal Heat Flow: A Guide to Measurement and Modelling*. Cambridge, Cambridge Univ. Press.

Bhaskara Rao, D., 1986. Modelling of sedimentary basins from gravity anomalies with variable density contrast. *Geophys. J. R. Astron. Soc*., **84**, 1, 207-212.

Bhaskara Rao, D. and Ramesh Babu, N., 1991. A fortran-77 computer program for three-dimensional analysis of gravity anomalies with variable density contrast. *Comput. Geosci*., **17**, 655-667.

Bhattacharyya, B.K., 1966. Continuous spectrum of the total magnetic anomaly due to a rectangular prismatic body. *Geophysics*, **31**, 97-121.

Blakely, R.J., 1995. *Potential Theory in Gravity and Magnetic Applications*. Cambridge Univ. Press.

Borisov, A.A., 1967. *Deep Structure of the Territory of the USSR According to Geophysical Data*. Nedra, Moscow (in Russian).

Borovko, N.N., 1971. *Statistical Analysis of Spatial Geological Regularities*. Nedra, Leningrad (in Russian).

Dehghani, G.A. and Makris, J., 1983. The gravity field and crustal structure of Iran. *Geodynamic Project* (*Geotraverse*) *in Iran*. Final Report. 51. Geological Survey of Iran, 50-68.

Eppelbaum, L.V., 2012. Geophysical Studies in the Caucasus (1925 – 2012): Initial, Basic and Modern Stages. *Trans. of the 8th EUG Meet.*, Geophysical Research Abstracts, Vol. **14**, EGU2012-1341, Vienna, Austria, 1-3.

Eppelbaum, L.V., 2014. Estimating informational content in geophysical observations on example of searching economic minerals in Azerbaijan. *Izvestiya* (*Proceedings*), *Acad. Sci. Azerb. Rep.*, Ser.: Earth Sciences, Nos. 3-4, 31-40.

Eppelbaum, L. and Katz, Y., 2011. Tectonic-Geophysical Mapping of Israel and eastern Mediterranean: Implication for Hydrocarbon Prospecting. *Positioning*, **2,** No. 1, 36-54.

Eppelbaum, L.V. and Katz, Yu.I., 2015. Paleomagnetic Mapping in Various Areas of the Easternmost Mediterranean Based on an Integrated Geological-geophysical Analysis. *In*: (Eppelbaum L., Ed.), *New Developments in Paleomagnetism Research,* Ser: Earth Sciences in the 21st Century, Nova Science Publisher, NY, 15-52.

Eppelbaum, L.V. and Khesin, B.E., 2012. *Geophysical Studies in the Caucasus*. Springer, Heidelberg –N.Y. –London.

Eppelbaum, L.V., Kutasov, I.M. and Pilchin, A.N., 2014. *Applied Geothermics*. Springer, Heidelberg – N.Y. – London.

Gadjiyev, R.M., 1965. *Deep Geologic Structure of Azerbaijan*. Azerneshr, Baku (in Russian).

Gadjiev, T.G., Nechayev, Yu.V., Potapova, E.I., and Sattarova, V.M., 1989. *The Map of Deep Structure of the Caucasus According to Cosmic Data*. Map Printing Factory of the Ministry of Geology of the USSR, Moscow.

Gasanov, A.G., 2001. *Deep Structure and Seismicity of Azerbaijan in Relation to Hydrocarbons Prognosis*. Elm, Baku (in Russian).

Gorodnitsky, A.M., Zonenshain, L.P. and Mirlin, E.G., 1978. *Reconstructions of the Continents in Phanerozoic*. Nauka, Moscow (in Russian).

Gorshkov, A.I. and Niauri, G.A., 1984. Reflection of fault tectonics of the Caucasus in zones of horizontal gravity anomaly gradients. *Izvestiya*, *Acad. Sci. USSR, Physics of the Earth*, **20**, No. 9, 699-704 (in Russian).

Gravity map of the USSR, 1990. Scale 1:2,500,000, Ministry of Geology. Moscow.

Hartley, R.V.L., 1942. A more symmetrical Fourier analysis applied to transmission problems. *Proc. IRE*, **30**, No. 2, 144-150.

Ismailzadeh, A. D., Mustafayev, G. V., & Rustamov, M. I. (Ak. A. Alizadeh, Ed.). (2005). Geology of Azerbaijan, Magmatism (Vol. III). Nafta-Press, Baku (in Russian)

Issayeva, M.I. and Khalafly, A.A., 2006. Paleomagnetic Studies of the Caucasian Segment of the Alpine Fold Belt. *In:* (Ismailzadeh, A.T., Ed.)*, Proceedings of the International Workshop on Recent geodynamics, Georisk and Sustainable Development in the Black Sea to Caspian Sea Region* (Baku, 2005), American Inst. of Physics, Melville, N.Y., 132-135.

Kaban, N.K., 2000. Gravity model of lithosphere and geodynamics. In: *Recent Tectonics, Geodynamics and Seismicity of the Northern Eurasia*. Probel, Moscow, 267-290 (in Russian).

Kadirov, F.A., 1998. Geological interpretation of full horizontal gradients of the gravity field in Azerbaijan. *Izvestiya, Acad. Sci. Azerb*, Ser.: Earth Sciences, No. 5-6, 129-134 (in Russian).

Kadirov, F.A., 2000a. *Gravity Field and Models of Deep Structure of Azerbaijan*. Nafta-Press, Baku (in Russian).

Kadirov, F.A., 2000b. Application of the Hartley transform for interpretation of gravity anomalies in the Shamakhy–Gobustan and Absheron oil- and gas-bearing regions, Azerbaijan. *Jour. of Applied Geophysics*, **45**, 49-61.

Kadirov, F.A., 2004. Gravity models of lithosphere in the Caucasus – Caspian region. In: (Alizade, Ak.A., Ed.), *South Caspian Basin: Geology, Geophysics, Oil and Gas Content.* Nafta-Press, Baku, 107-122.

Kadirov, F.A. and Gadirov, A.H., 2014. A gravity model of the deep structure of South Caspian Basin along submeridional profile Alborz–Absheron Sill. *Global and Planetary Change*, **114**, 66-74.

Kadirov, F.A., Mammadov, S.A., Reilinger, R. and McClusky, S., 2008. Some new data on modern tectonic deformation and active faulting in Azerbaijan (according to Global Positioning System Measurements). *Izvestiya, Acad. Sci. Azerb*., Ser.: Earth Sciences, No. 1, 82-88.

Kerimov, K.M., Pilchin, A.N., Gadjiev, T.G. and Buachidze, G.Y., 1989. *Geothermal map of the Caucasus, Scale* 1:1,000,000 Baku, Cartographic Plant No. 11 (in Russian).

Khain, V.E. and Ryabukhin, A.G., 2002. Russian geology and the plate tectonics revolution. *Geological Society*, *Special Publications*, London, **192**, 185-198.

Khesin, B.E., Alexeyev, V.V. and Eppelbaum, L.V., 1993. 3-D modeling of gravity and magnetic fields as a final stage of application of effective interpretation system of geophysical data under difficult geological conditions. *Geoinformatics*, **4**, No.3, 177-188.

Khesin, B.E., Alexeyev, V.V. and Eppelbaum, L.V., 1996. *Interpretation of Geophysical Fields in Complicated Environments*. Kluwer Academic Publishers, *Ser.: Modern Approaches in Geophysics*, Dordrecht – Boston - London.

Khesin, B.E., Alexeyev, V.V. and Metaxa, Kh.P., 1983. *Interpretation of Magnetic Anomalies in the Conditions of Oblique Magnetization and Rugged Topography*. Nedra, Moscow (in Russian).

Klushin, I.G. and Tolstikhin, I.N., 1961. Singling out linear tectonic dislocations in geophysical maps. *Geology and Geophysics*, No.6, 98-103 (in Russian).

Kopf, A. Deyhle, A., Lavrushin, V.Y., Polyak, B.G., Gieskes, J.M., Buachidze, G.I., Wallmann, K., and Eisenhauer, A., 2003. Isotopic evidence (He, B, C) for deep fluid and mud mobilization from mud volcanoes in the Caucasus continental collision zone. *Intern. Jour. of Earth Sciences*, **92**, 407-425.

Kulhanek, O., 1976. *Introduction to Digital Filtering in Geophysics*. Elsevier, Amsterdam.

Kunin, N.Ya., 1968. Problems of singling out the observed gravity field components for structural-tectonic regioning (as applied to the Southern Kazakhstan), *In: Geophysical investigations in Kazakhstan*. Kazakh. Geoph. Inst., Alma-Ata, 76-88 (in Russian).

Lebedev, L.I. and Tomara, G.A., 1981. Some peculiarities of distribution of heat flow in the South Caspian. In: *Geothermometers and Paleotemperature Gradients*. Nauka, Moscow, 156-161 (in Russian).

Lodzhevsky, M.I. and Kadirov, F.A., 2001. *Caspian Region: Bouguer Gravimetry Map*. Scale 1:1,000,000. Fedynsky Centre GEON & Geol. Inst. of the Azerb. Acad. of Sci.

Mamedov, P.Z., Guliyev, Q.Q., Kadirov, F.A., Shikhalyev, Y.A., Guliyev, I.S., Aliyeva, E.H., Feyzullayev, A.A., Dadashov, F.Q., Kheirov, M.B. and Tagiyev, M.F., 2008. (Ak.A. Alizadeh, Ed.), 2008. *Geology of Azerbaijan*, Vol. VII: *Oil and Gas*. Nafta-Press, Baku (in Russian).

Mekhtiyev, S.F., Mirzadjanzade, A.H. and Aliyev, S.A., 1971. *Geothermal Studies of Oil and Gas Fields*. Nedra, Moscow (in Rissian).

Mekhtiyev, S.F., Mirzadjanzade, A.H., Aliyev, S.A. et al., 1960. *Thermal Regime of Oil and Gas Fields*. Azerneftneshr, Baku (in Russian).

Mekhtiyev, S.F., Hasanov, F.D. and Mukhtarov, A.Sh., 2003. Radiogenic heat generation and heat flow in the South-Caspian Basin. *Bilgi,* No. 3, 99-105 (in Russian).

Mukhtarov, A.Sh., 2004. Heat flow distribution and some aspects of thermal field formation in the Caspian region. In: (Ak. A. Alizadeh, Ed.), *South Caspian Basin: Geology, Geophysics, Oil and Gas Content*. Nafta-Press, Baku, 165-172.

Mukhtarov, A.Sh., 2011. Structure of thermal flow of sedimentary complex of the Southern Caspian Basin. *D.Sci. Thesis*, Inst. of Geology, Baku (in Russian).

Mukhtarov, A.Sh., 2012. Models of distribution of temperatures in sedimentary section of the South Caspian Basin. In: (Ak.A. Alizadeh, Ed.), *Modern Problems of Geology and Geophysics of the Caucasus*. Nafta-Press, Baku, 214-230.

Nikolsky, Yu.I., Milai, T.A. and Kogan, L.Z., 1975. *Geological-Geophysical Studies of the Tectonics, Magmatism, and Metallogeny of the Caucasus*. Nedra, Leningrad (in Russian).

Paffenholtz, K.A., 1959. *Geological Essay of the Caucasus*. Acad. of Sci. of Arm. SSR, Yerevan (in Russian).

Pavlenkova, G.A., 2012. Structure of the Caucasus' earth crust along the deep seismic sounding profiles Stepnoe-Bakuriani and Volgograd-Nakhchivan (results of initial data re-interpretation). *Izvestiya*, *Physics of the Earth*, No. 5, 16-25.

Peyve, A.V., Zonenshayn, L.V., Knipper, A.L. et al., 1980. *Tectonics of the Northern Eurasia. Explanation Notes to Tectonic Map of the Northern Eurasia, Scale 1:5,000,000.* Nauka, Moscow (in Russian).

Pilchin, A.N. and Eppelbaum, L.V., 1997. Determination of magnetized bodies lower edges by using geothermal data. *Geophysical Journal International*, **128**, No.1, 167-174.

Radjabov, M.M., 1978. Study of the structure of the earth's crust-consolidated complex of the Azerbaijan using deep seismic sounding and refracted wave-correlation method data. In: *The Structure of the Earth's Crust and Upper Mantle in the Central and East Europe*. Naukova Dumka, Kiev, 205-211 (in Russian).

Reilinger, R., McClusky, S., Vernant, P. Lawrence, S., Ergintav, S., Cakmak, R., Ozener, H., Kadirov, F., Guliyev, I., Stepanyan, R., Nadariya, M., Hahubia, G., Mahmoud, S., Sakr, K., ArRajehi, A., Paradissis, D., Al-Aydrus, A., Prilepin, M., Guseva, T., Evren, E., Dmitrotsa, A., Filikov, V., Gomez, F., Al-Ghazzi, R. and Karam, G., 2006. GPS constraints on continental deformation in the Africa-Arabia-Eurasia continental collision zone and implications for the dynamics of plate interactions. *Jour of Geophysical Research,* **111**, B05411, 1-26.

Riznichenko, Yu.V., Khesin, B.E. and Metaxa, Kh.P., 1983. Relation between seismicity and magnetic field according to observations in Azerbaijan. *Izvestiya*, *Acad. Sci. Russ.,* Ser.: Physics of the Solid Earth, No.1, 3-14 (in Russian).

Rustamov, R.I., 2001. Geothermal regime of the South Caspian Sea region. *Azerbaijan Oil Industry,* Nos. 4-5, 28-32 (in Russian).

Sandwell, D.T., Garcia, E., Soofi, K., Wessel, P. and Smith, W.H.F., 2013. Towards 1 mGal Global Marine Gravity from CryoSat-2, Envisat, and Jason-1. *The Leading Edge*, **32**, No. 8, 892-899.

Sandwell, D.T. and Smith, W.H.F., 2009. Global marine gravity from retracked Geosat and ERS-1 altimetry: Ridge Segmentation versus spreading rate. *Journal of Geophysical Research*, **114**, B01411, 1-18.

Sirotkina, T.N. and Nikolsky, Yu.I., 1971. Method of successive geological approximations by interpretation of geophysical fields in ore regions (on example of Armenia). *Methods of Exploration Geophysics,* No. 12, 36-44 (in Russian).

Somerton, W.H., 1992. *Thermal Properties and Temperature Related Behavior of Rock/Fluid Systems*. Developments in Petroleum Science, **37**. Elsevier, Amsterdam.

Spector, A. and Grant, F.S., 1970. Statistical models for interpreting aeromagnetic data. *Geophysics*, **35**, 293-302.

Shengelaya, G.Sh., 1984. *Gravity Models of the Caucasus' Earth crust*. Nauka, Moscow (in Russian).

Shikhalibeyli, E.Sh., 1996. *Some Problems of Geological Structure and Tectonics in Azerbaijan*. Elm, Baku (in Russian).

Sukharev, G.M., Taranukha, Y.K. and Vlasova, S.P., 1969. Thermal flow from Azerbaijan subsoil. *Soviet Geology,* No. 8, 146-153 (in Russian).

Sundararajan, N., 1995. 2-D Hartley transforms. *Geophysics*, **60**, 262-265.

Tauxe, L., Banerjee, S.K., Butler, R. F. and van der Voo, R., 2009. *Essentials of Paleomagnetism*: *Web Edition*. http://magician.ucsd.edu/essentials/WebBook.html

Tikhonov, A.N. and Bulanzhe, Yu.D., 1945. On the gravity field averaging. *Izvestiya, Ser. Geoph.*, USSR Acad. Sci., No 2 (in Russian).

Vinnik, L.P., 1976. *Investigations of the Earth's Mantle by Seismic Methods*. Nauka, Moscow (in Russian).

Yaglom, A.M. and Yaglom, I.M., 1973. *The probability and Information*. 2nd ed., revised and supplemented. Nauka, Moscow (in Russian).

Yakubov, A.A. and Atakishiyev, I.S., 1973. *Geothermal Studies of Oil and Gas Fields of Absheron*. Azerneshr, Baku (in Russian).

Zeynalov, G.A., 2000. Importance of remote-sensing data in structural geologic analysis of oil-and gas bearing regions of Azerbaijan. *Natural Resources Research*, **9**, No. 4, 307-313.

Zolotovitskaya, T.A., 2003. Mechanisms of formation of radionuclide contamination at the oil fields of Azerbaijan. *In*: (N. Birsen, and K. K. Kadyrzhanov, Eds.), *Environmental protection against radioactive pollution*. Kluwer Acad. Publ., NATO Science Series, Earth & Environmental Sci., Vol. **33**, 74-77.

5 Deep Structure of Azerbaijan Derived from Combined Geophysical–Geological Analysis

5.1 Brief Geological–Geophysical Background

The complexity of Azerbaijan's territory geological structure stems from its location in the Alpine-Himalayan tectonic belt (AHTB) (e.g., Khain 2000; Aliyev et al. 2005a, b; Leonov 2008; Alizadeh 2012; Eppelbaum 2015; Kadirov et al. 2015). The NE part of Azerbaijan is a fragment of the Pre-Caucasian foreland filled by Cenozoic terrigenous sediments. A heterogenic Nakhchivan folding system is located in the SW part, where carbonate Paleozoic strata and Cenozoic magmatic formations are mixed. At the mega-anticlinorium of the Greater Caucasus, stratified Cenozoic and Mesozoic thick (predominantly, sedimentary) strata are presented. The prevalence of Mesozoic magmatic formations is typical of the mega-anticlinorium of the Lesser Caucasus. The Kur megasynclinorium, dividing the Greater and Lesser Caucasus, is characterized by an accumulation of thick (up to several kilometers) Cenozoic terrigenous sediments. The Talysh anticlinorium is located on the SE flank of the Kur Depression, where Paleogene magmatic associations are widely distributed (Aliyev et al. 2005a; Ismailzadeh et al. 2005).

According to Khain (2000), the most ancient Pre-Baikalian (this complex is termed as Cadomian in western publications (Khain 2007)) structural complex is characterized by a submeridional strike. A less metamorphosed Baikalian complex is rumpled to latitudinal folds in separate areas. The Caledonian complex is practically unknown. The Hercynian complex is characterized by a Caucasian strike identical to the overlying Mesozoic rocks.

The Alpine tectonomagmatic cycle is characterized by more complete geological data. As a whole, for Azerbaijan territory is typical the frequently changing geological associations on the vertical and lateral axes, the presence of multivarious fold and fault structures of different orders, and regional and local metamorphism (Alizadeh 2012). All these factors make the development of reliable models of these media sufficiently complex.

The first models of the Earth's crust of Azerbaijan were put forward in the mid-1960s (Gadjiev 1965; Tzimelzon 1965; Shekinsky et al. 1967). First, generalized velocity models of the Azerbaijanian's Earth' crust have been developed by Radjabov (1977). These models were subsequently evaluated in the works of Tzimelzon (1970), Azizbekov et al. (1972), Shikhalibeyli (1972), Shikhalibeyli and Grigoriants (1980), Khain (1984), Alexeyev et al. (1988), and later by Khesin et al. (1993, 1996). Rappel and McNutt (1990) studied the regional compensation of the Greater Caucasus using the Bouguer gravity. Sarker and Abers (1998) attempted to apply *P* and *S* wave tomography for examination of the Greater Caucasus deep structure. After that new models developed on the basis of gravity field analysis were presented in Kadirov (2000a, b).

Some significant regional peculiarities of the deep structure of Azerbaijan and adjacent Caspian area are reflected in the following: Pilchin and Eppelbaum (1997), Mangino and Priestley (1998), Artyushkov et al. (2000), Gasanov (2001), Jackson et al. (2002), Kaban (2002), Allen et al. (2003), Brunet et al. (2003), Ulomov (2003), Glumov et al. (2004), Guliyev and Panachi (2004), Ismailzadeh et al. (2004), Mamedov (2004), Mukhtarov (2004), Knapp et al. (2004), Aliyev et al. (2005a, b), Babayev and Gadjiev (2006), Eppelbaum and Pilchin (2006), Kadirov (2006), Khalafly (2006), Reilinger et al. (2006), Saintot et al. (2006), Artyushkov (2007), Khain (2007), Leonov (2008), Ricketts et al. (2008), Mamedov (2008, 2009), Mamedov et al. (2008); Egan et al. (2009), Green et al. (2009), Mosar et al. (2010), Yetirmishli et al. (2011), Alizadeh et al. (2012), Eppelbaum and Khesin (2012), Koulakov et al. (2012), Pavlenkova (2012), Yetirmishli and Kazimova (2013), Forte et al. (2013), Mederer et al. (2013), Ruban (2013), Kadirov and Gadirov (2014), Abdullayev et al. (2015), Eppelbaum

A.A. Alizadeh et al., *Geosciences of Azerbaijan*,
Regional Geology Reviews, DOI 10.1007/978-3-319-40493-6_5

(2015), Kadirov et al. (2015), Sharkov et al. (2015), and others.

We will present some examples of geophysical investigation separately for the Azerbaijanian land and sea.

5.2 Azerbaijan: Land

5.2.1 Seismic Data Analysis

Seismic data analysis plays now an important role in development of physical–geological models of deep structure. We will consider both two main approaches: deep seismic sounding and seismotomography.

5.2.1.1 Deep Seismic Sounding

Review of main recent publications in this field was presented in Sect. 5.1. Here, we will show the last examples of reinterpretation of deep seismic profiles crossing Azerbaijan territory (Pavlenkova 2012) (Figs. 5.1, 5.2 and 5.3).

Profiles of deep seismic sounding (DSS) 'Stepnoe-Bakuriani' and Volgograd-Nakhchivan were carried out by the Ministry of Geology of the former USSR in 60s of the last century (Yurov 1963; Krasnopevtseva et al. 1970). These profiles cross the Greater Caucasus (Fig. 5.1) and till the present time are sole DSS profiles (Figs. 5.2 and 5.3) intersecting across the strike the Greater Caucasus and surrounding regions of Azerbaijan. Therefore, reinterpretation of these profiles is of great interest.

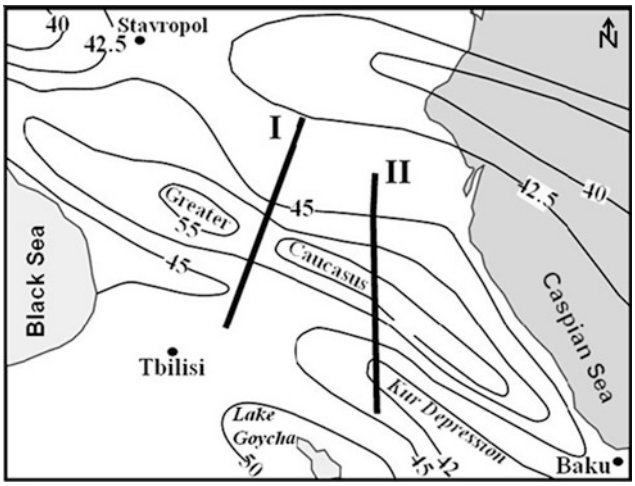

Fig. 5.1 Scheme of location of deep seismic sounding profiles: Stepnoe-Bakuriani profile (**I**) and southern part of the Volgograd-Nakhchivan profile (**II**) and map of the Moho discontinuity of the Greater Caucasus (after Rezanov and Shevchenko 1978; Pavlenkova 2012, with small modifications)

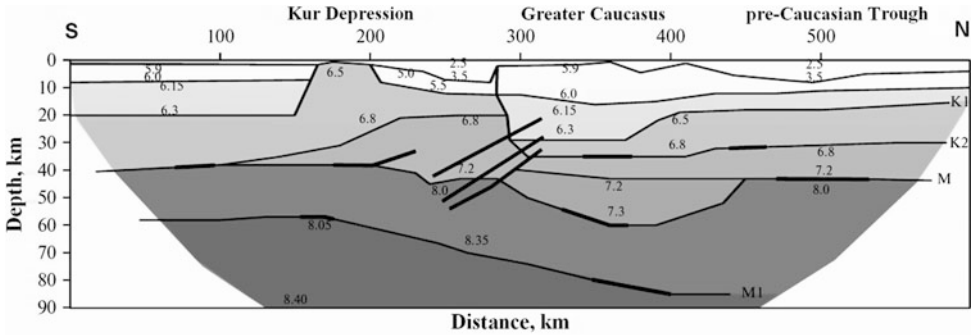

Fig. 5.2 New velocity section along the profile Stepnoe-Bakuriani (**I**). Other captions are presented in Fig. 5.1. M boundary shows the Earth's crust bottom, M1 is the wave reflected from the mantle boundary; K1 and K2 are the boundaries inside the Earth's crust. *Thin lines* represent the boundaries between layers with different seismic velocities (km/s), *thick line* represent the reflecting areas (Pavlenkova 2012)

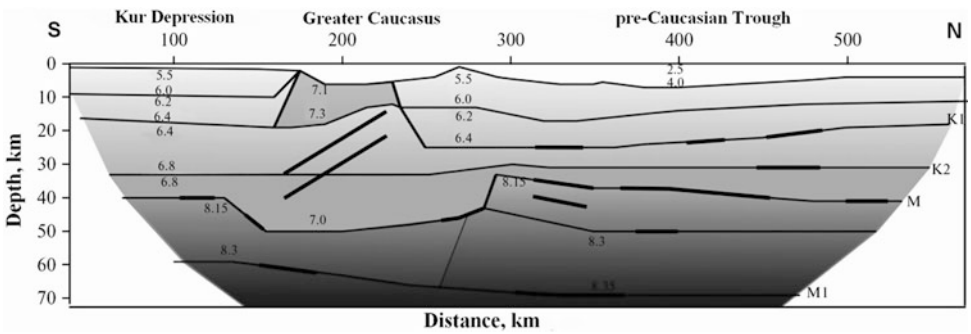

Fig. 5.3 New velocity section along the southern part of profile Volgograd-Nakhchivan (**II**). Other captions are presented in Figs. 5.1 and 5.2 (Pavlenkova 2012)

In general, the new velocity sections indicate that the tectonic movements generating the Caucasian Mountainous System (CMS) were a complex combination of horizontal and vertical movements covering entire all the Earth's crust and upper mantle. The boundary M1 in the upper mantle and ramps in the southern part of the CMS is relicts of the subhorizontal movements (Pavlenkova 2012).

Seismic sections of regional and composite profiles provide enough space for reconstruction of the main features of the tectonic development and sedimentation conditions. Information obtained from seismic sections and updated by available geological–geophysical and well information was used by us for compiling of some seismostratigraphic sections (Fig. 5.4). The tracing of regional surfaces of unconformity on seismic sections has a principal meaning not only for deep structure analysis, but also for the historical–genetic analysis. The unconformity surfaces between sequences control the majority of revealed and forecasted non-anticlinal traps in the region outlining the applied aspect of their study (Guliyev et al. 2003).

5.2.1.2 Seismotomography of the Azerbaijanian Earth's Crust

Seismic tomography as one of the methods for Earth deep structure analysis allows (on the basis based on the travel time of elastic waves from earthquakes) to obtain an independent information about structure and physical properties of Earth's crust and mantle. The development of new algorithms and methodologies, the use of the new recording equipment, and improvement of computational methods allow more efficiently and accurately restore the velocity structure of the upper layers of the Earth. Together with geological and geophysical (magnetic, gravity, and thermal data, and magnetotelluric sounding) data, the tomographic model is used for construction of integrated geological–geophysical model. Just the velocity model is the tool which can be used for revealing interrelations between geophysical field parameters and concrete depth intervals (Koronovsky 2000).

Novel information obtained on the basis of cooperative analysis of recalculated velocity models with geological–tectonic maps significantly improves the present notions about deep geological structure peculiarities and geodynamic processes (Tarakanov 2006).

Methodology of investigation: A Brief description

Aim of the tomographic inversion consists in detailed analysis of velocities and absorbing properties of the medium. Such investigations are based on the travel time of the first arrivals or observed amplitudes for a set of pairs

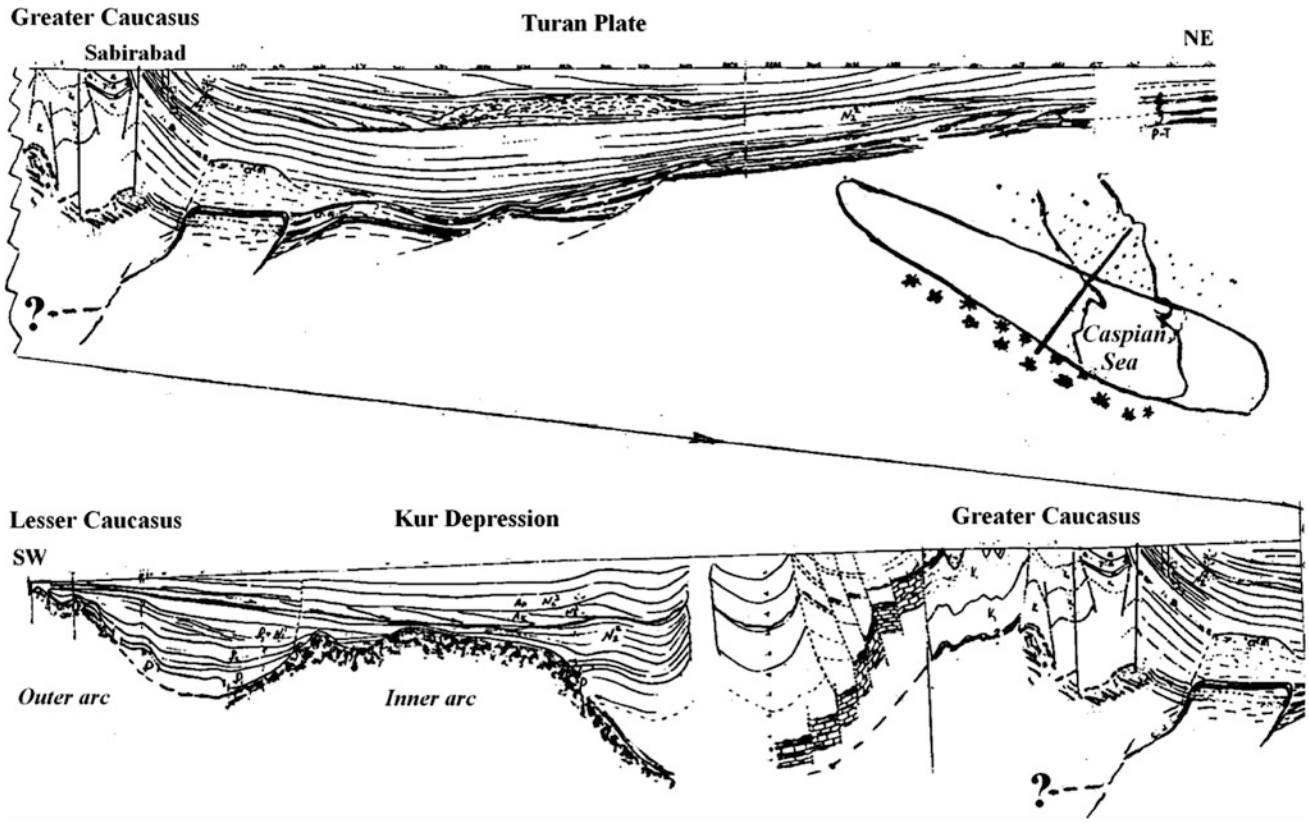

Fig. 5.4 Regional seismic–stratigraphic section through Turan Plate, southeastern troughs of the Greater Caucasus, Kur Depression, and Lesser Caucasus (after Mamedov 1991)

'receivers–sources'. Any geometry of sources and receivers can be applied. The sole limitation consists of that the seismic rays should create a common net; each point of the observed medium must be crossed by seismic rays in all directions (Fig. 5.5). At a first step of the tomographic inversion, selection of initial velocity model (and absorbing model for amplitude inversion) must be created (Adamova and Sabitova 2004). Further interpretation realizes in two stages: (1) solving direct problem and (2) solving inverse problem (Richter 1958; Firbas 1987).

In this investigation, a leading role was played by "TomoTetraFD" software—program for computing 3D velocity models on the basis of seismotomography method developed at the Inst. Geosphere Dynamics of the Russ. Acad. of Sci. (Usoltseva 2004). This software allows to restoring velocity structure on the basis of analysis of discrepancies of ray tracing containing information about anomalous zones in all the way of wave propagation.

For sorting of events, Kissling's and Roecker's criteria were used (Abers and Roecker 1991; Barber et al. 1996). In the investigation process were considered seismological parameters about the characteristics of local earthquakes and travel time of *P* and *S* waves registered by the telemetric station net for the period of 2004–2014 (Fig. 5.6). Parameters of hypocenters (coordinates and depth of focus, time of event generation and travel times of *P* and *S* waves) were received from the catalogs of Republic Center of Seismological Service. Based on the geometry of earthquake focus location and seismological station disposition, depth of the investigation may consist up to 60 km (Kazymova and Kazymov 2010; Yetirmishli et al. 2011).

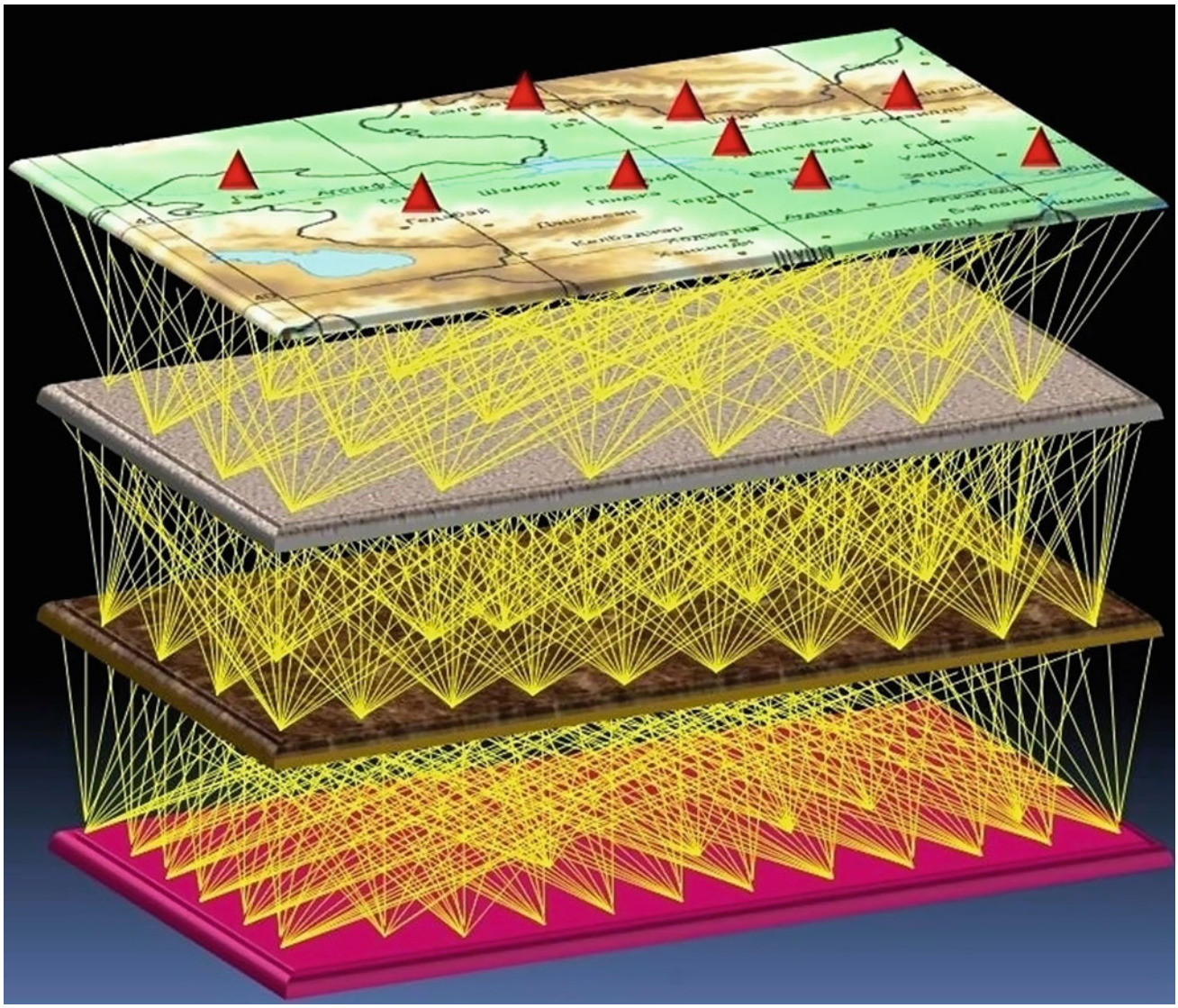

Fig. 5.5 3D scheme of seismic ray distribution in tomographic inversion (Yetirmishli and Kazimova 2013)

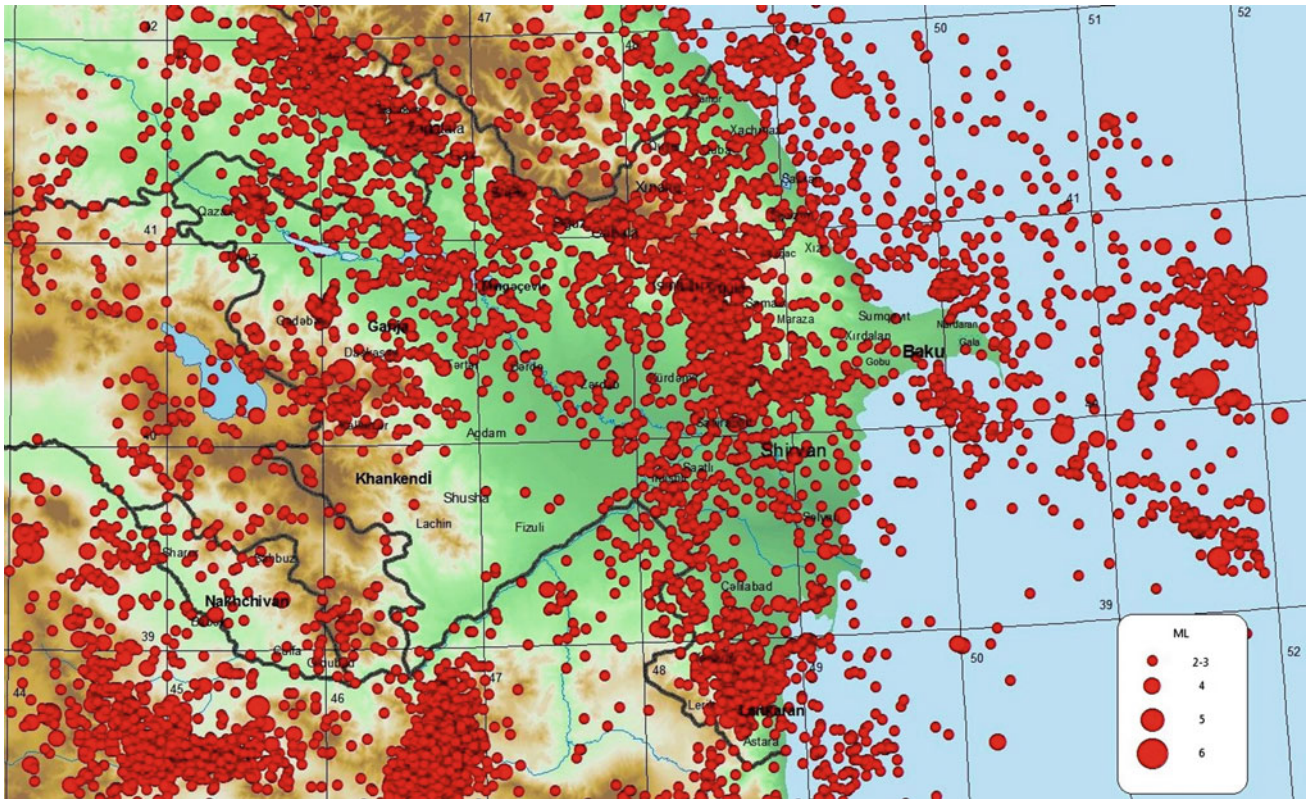

Fig. 5.6 Map of epicenters of the region under study for the period of 2004–2014 with ml ≥2.0 (from materials of Yetirmishli, F. Kadirov and S. Kazymova)

In the process of velocity model computation, 4 input files were utilized: (1) coordinates of usable seismological stations, (2) 1D velocity model, (3) travel time of seismic waves from focus to station, and (4) main file jointing all input and output arrays. The main criterion of velocity model optimization was selected the closeness of rms residuals (deviation of travel wave times from the used velocity model) for all rays to zero.

The investigated volume up to the depth of 60 km was divided on layers with a thickness of 2 km in the depth interval of 0–10 km and thickness of 5–10 km in the depth interval of 10–60 km. Data of 35 seismological stations of Azerbaijan cover all the regions under study (Fig. 5.6) were analyzed.

After numerous iterations were carried out, 1D models for *P* and *S* waves shown by thick red line in Fig. 5.7. Dash black line shows a velocity model utilized at present for calculations earthquake hypocenters.

Seismotomographic investigation has been performed in three stages. At the first stage, an initial data set was analyzed. At the second stage, calculation of optimal 1D velocity layered model by the use of 'Velest' software was carried out and stability of the obtained model was checked. Simultaneously with selection of 1D model has been performing re-estimation of hypocenter parameters and time in the source in the 1D model and calculation of temporary corrections.

The third stage (most important) consisted of checking resolving capacity of the available data set and construction of 3D velocity model. For computation of 3D velocity field, the program TomotetraFD was used. In this program, a classic seismotomographic method for the case when sources and receivers are within the investigating region is realized. Calculation of seismic ray trajectories has been carried out by the finite difference method.

The obtained 3D model is linear quasi-continuous function (velocity function discontinues at concrete depths), and in horizontal direction is continuous (Usoltseva et al. 2010). Figures 5.8, 5.9, 5.10, 5.11, 5.12, and 5.13 display horizontal slices of 3D velocity models at different depths in the region under study

Basing of the geological–geophysical data of the region under study, at the depth interval of 1–3 km a clear boundary caused by transition of sedimentary rocks to volcanogenic ones, was revealed. This depth interval relates to rocks of Lower and Middle Jurassic age which presented by limestone with clay interbedding, marl, sandstone, tuffs, mudstone, and dolomites. In the depth interval of 4–6 km, a transition from porphyry olivine–pyroxene–plagioclase basalts to andesite basalts of Lower Cretaceous (Radjabov

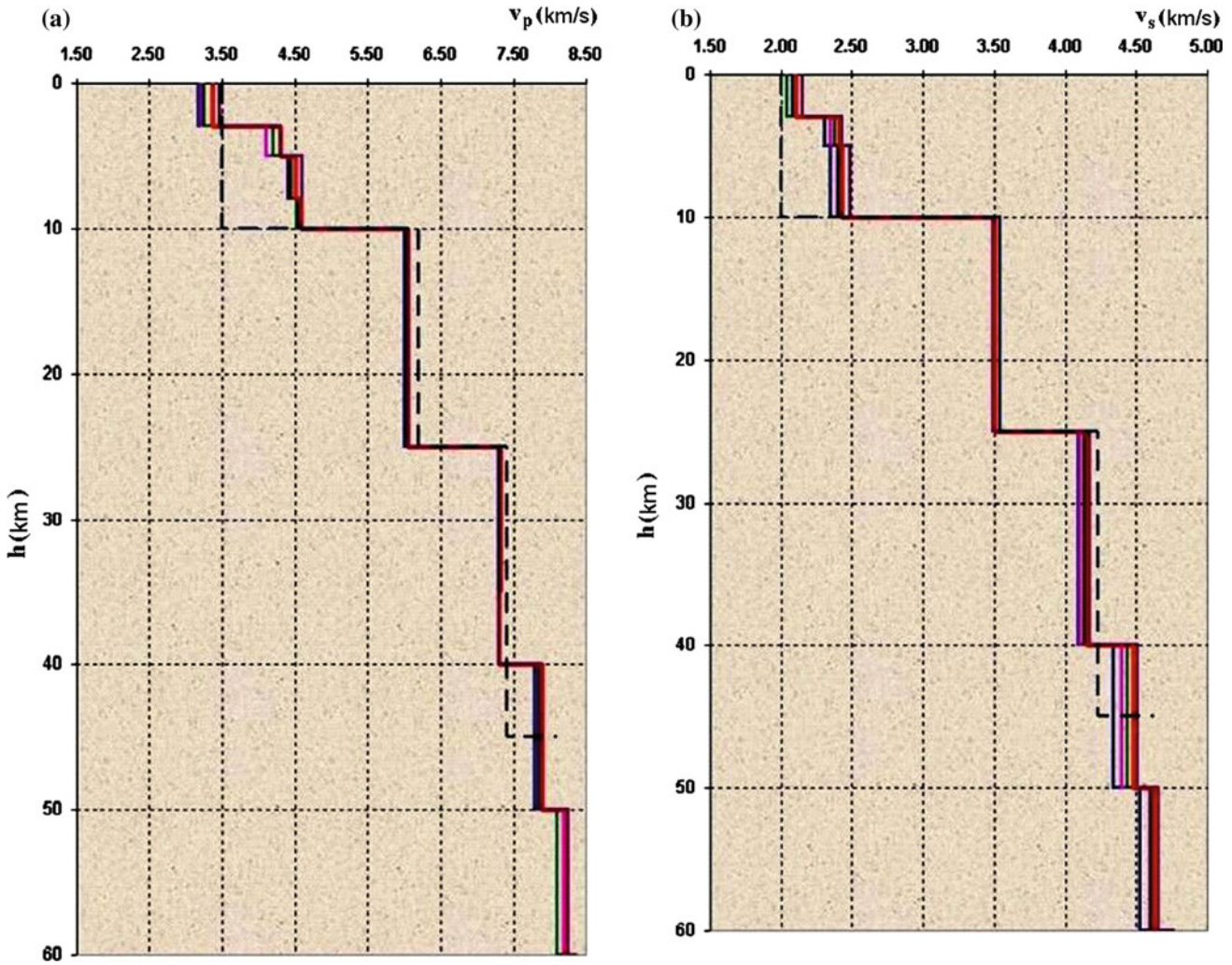

Fig. 5.7 1D velocity model of compressional (**a**) and shear (**b**) waves (Yetirmishli and Kazimova 2013)

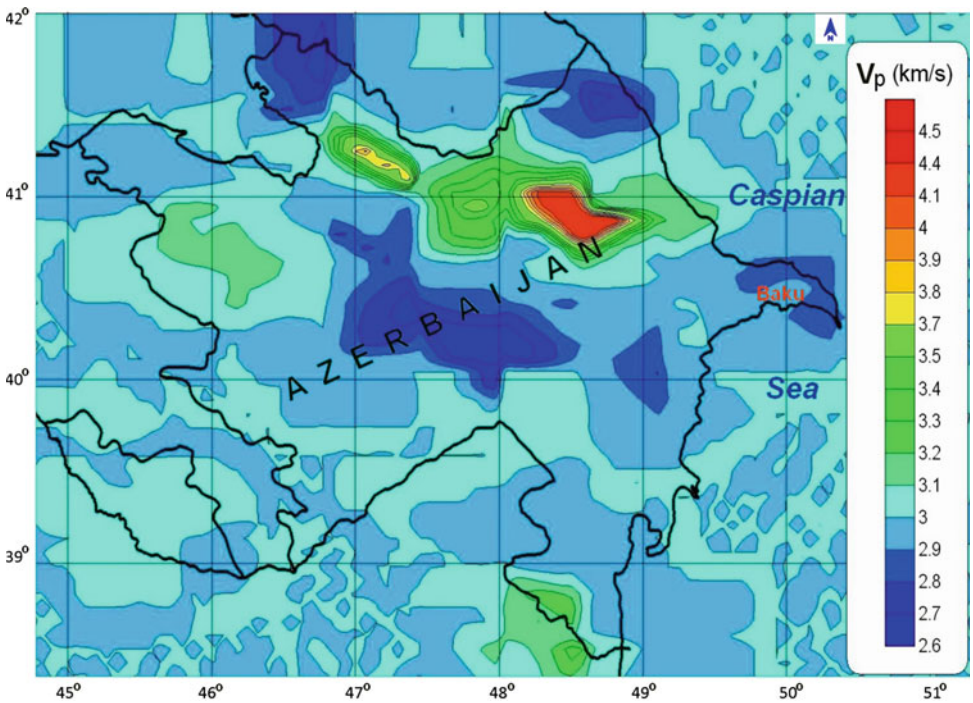

Fig. 5.8 Horizontal slice of velocity model for the territory of Azerbaijan at the depth of 1 km (Yetirmishli and Kazimova 2013)

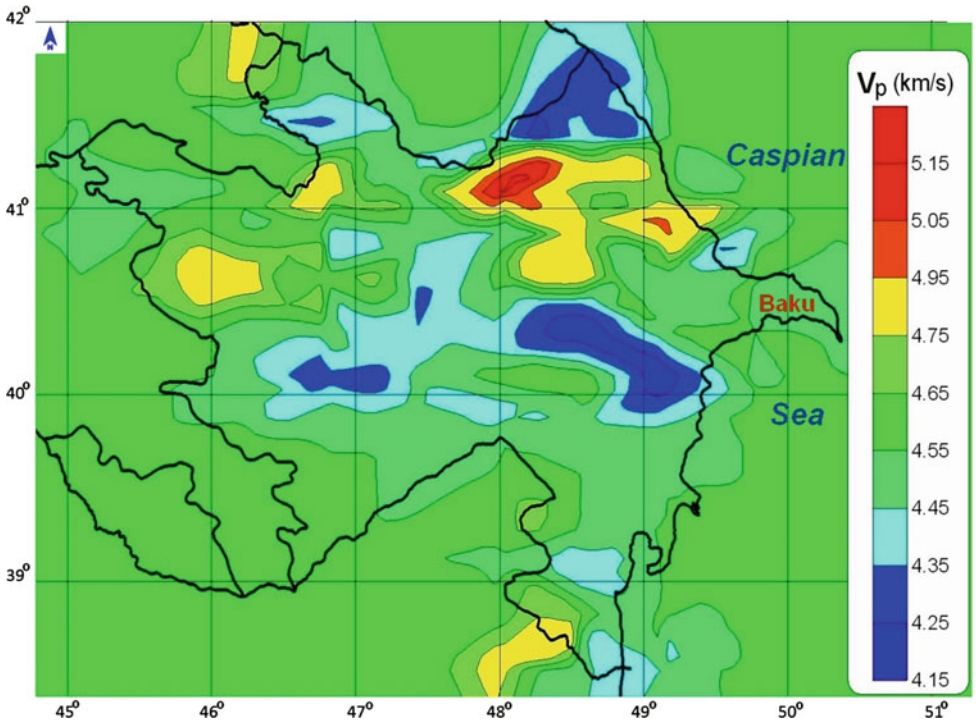

Fig. 5.9 Horizontal slice of velocity model for the territory of Azerbaijan at the depth of 5 km (Yetirmishli and Kazimova 2013)

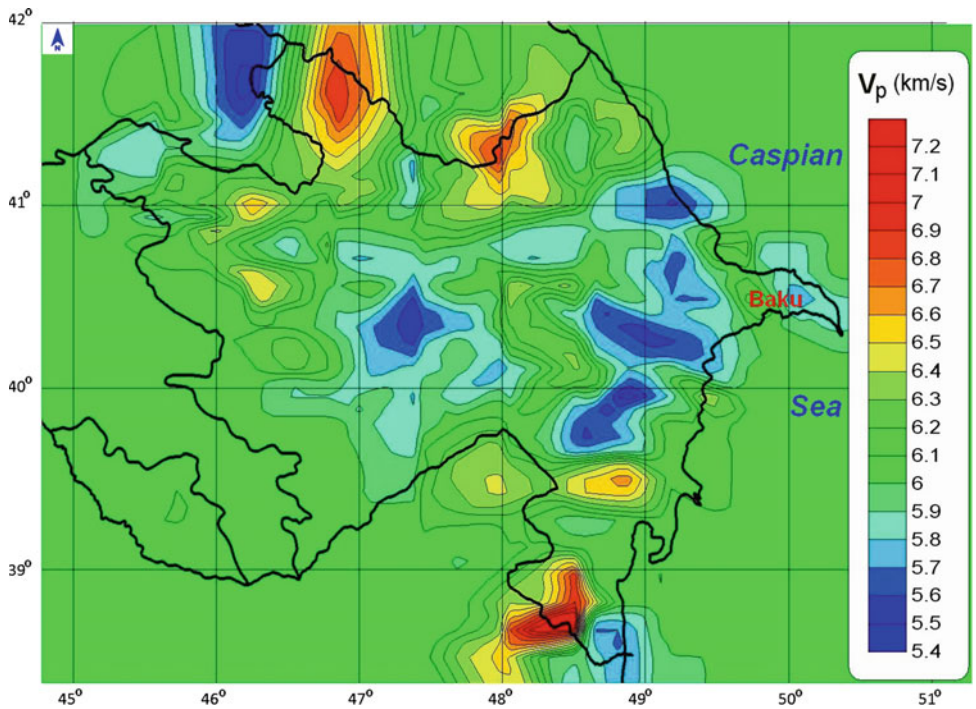

Fig. 5.10 Horizontal slice of velocity model for the territory of Azerbaijan at the depth of 10 km (Yetirmishli and Kazimova 2013)

1974) was observed. At the depth of 7 km, a boundary at which is being transition from andesites to dacites and plagiorhyolites, their tuffs, and pumice breccia, was found. At the depth interval of 7–10 km, a roof of pre-Alpine basement was revealed. In this interval seismic velocity decreasing in the Evlakh-Agjabedi and Kurdamir-Saatly zones of the Middle Kur Depression (this fact confirms the presence of rock fracturing and decompression zone) was observed. At the depth of 15 km, also a geological boundary was detected. Here, seismic velocities increase from 5.9 to 6.4 km/s (it is known that velocities of 6.0–6.2 km/s correspond to granites, and 6.5–6.7 km/s—to basalts).

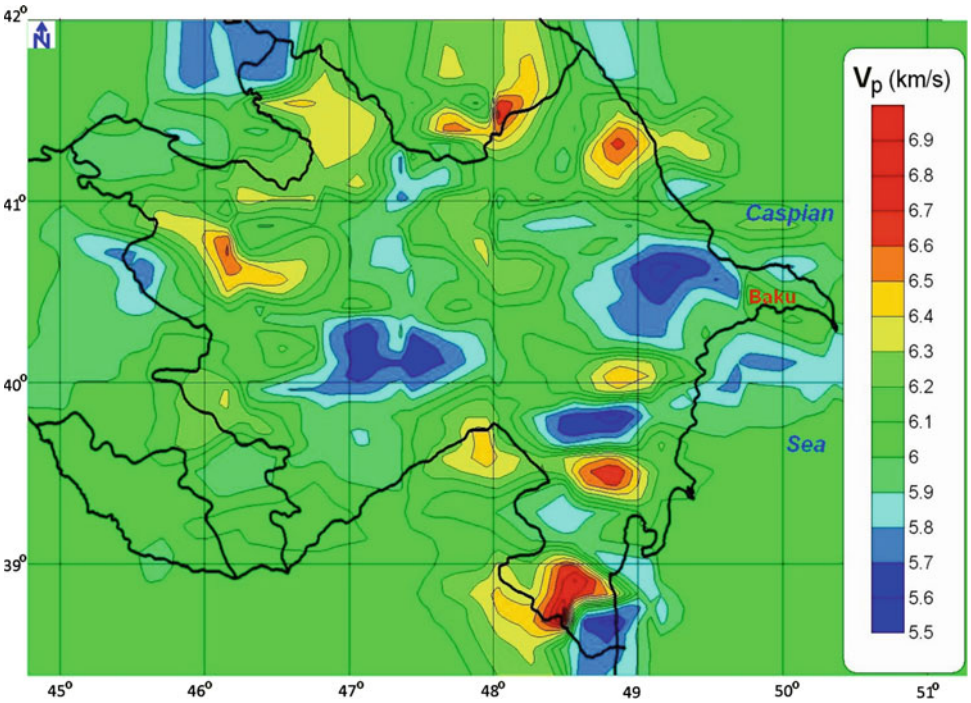

Fig. 5.11 Horizontal slice of velocity model for the territory of Azerbaijan at the depth of 15 km (Yetirmishli and Kazimova 2013)

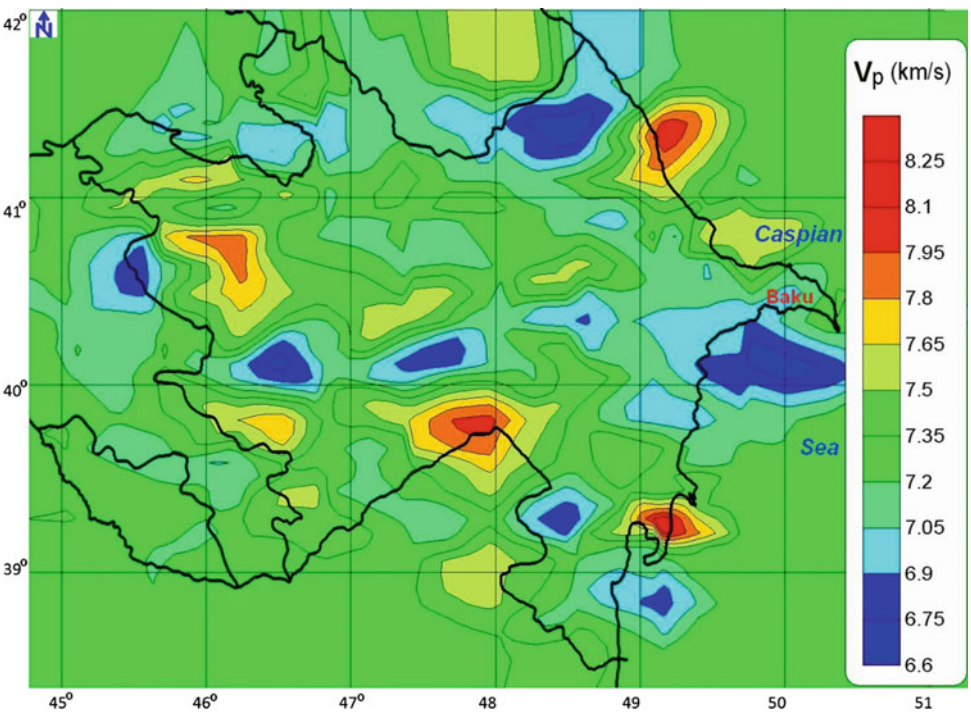

Fig. 5.12 Horizontal slice of velocity model for the territory of Azerbaijan at the depth of 25 km (Yetirmishli and Kazimova 2013)

It is important to underline that not all velocity boundaries in the volcanogenic strata are associated with the rock composition changing. Some boundaries induced by different stress condition of geological matter at the depth, with superposition of metamorphic processes, rheological fracturing, and some other processes. We can suggest that these depths reflect an upper surface of substrate from metamorphized rocks of pre-Alpine basement, and in separate zones—from consolidate volcanogenic and metamorphized associations of Mesozoic age.

Based on the obtained data, we can note that 1st interval (0–10 km) relates to the Cenozoic–Mesozoic boundary in sedimentary cover and is characterized by velocities of 2.8–5.9 km/s, 2nd interval (10–25 km) associates with a roof of

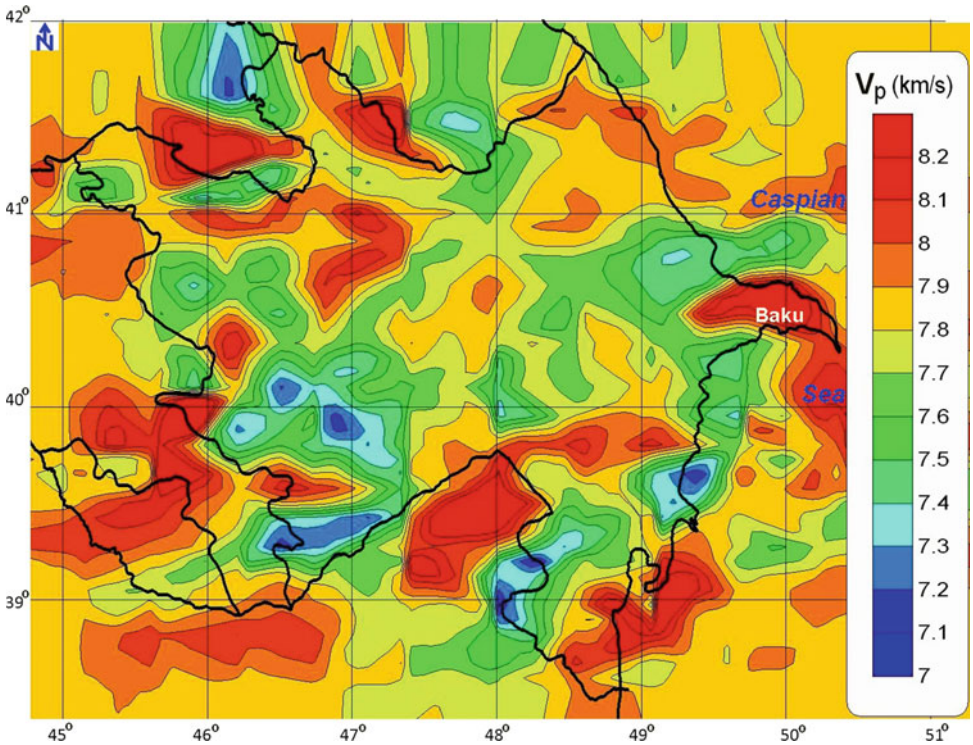

Fig. 5.13 Horizontal slice of velocity model for the territory of Azerbaijan at the depth of 40 km (Yetirmishli and Kazimova 2013)

consolidated Earth's crust ("granitic" layer) with velocities of 6.0–7.3 km/s, 3rd (25–40 km) with velocities of 7.4–7.8 km relates to "basaltic" layer, and 4th (≈40 km and deeper) with velocities of 8.0–8.2 km associates with the Moho discontinuity. The above-mentioned computations were used for development of 3D maps of "granitic" (Fig. 5.14a), "basaltic" (Fig. 5.14b) and Moho (Fig. 5.14c) discontinuities.

5.2.2 Thermal Data Analysis

Thermal data analysis plays an important role in the deep structure unmasking in different regions of the world (Lyubimova 1968; Turcotte and Schubert 1982; Eppelbaum et al. 2014).

It is well known that all deep structure analysis of thermal data began from development of a map of neutral layer distribution of the region under study. Such a map was developed by Mukhtarov (2011) (Fig. 5.15).

The analysis of soil temperature data recorded by meteostations in Azerbaijan revealed that the temperature recorded at the depth of 3.2 m is very close to the temperature of neutral layer. Within the limits of measurement error, it can be assumed that it is equal to the temperature of the neutral layer. It was found that neutral layer temperature in Azerbaijan varies within the range 5.8–18.1 °C. The lowest neutral layer temperatures (from 5–6 to 10–12 °C) are observed in the Caspian Sea water area and in high-altitude areas (Fig. 5.15). High-temperature area of the neutral layer were observed in the Kur Depression (from 16 to 19 °C).

At this depth, the amplitude of annual temperature variations is reduced to minimum and average annual temperature closely approaches the temperature of the neutral layer, its footwall lays at the depth of around 20 m where temperature stabilizes and does not change (Mukhtarov 2011). Lower temperatures of the neutral layer are explained by the impact of the water masses.

On horizontal section of about 2000 m, the lowest temperature was observed at the area Garamaryam (38 °C) (Ajinour oil- and gas-bearing region), Agamamedli (39 °C), Yevlakh-Agjabedi oil- and gas-bearing region, Nakhchivan (39 °C), Absheron oil- and gas-bearing region and Bulla deniz (40 °C), and oil- and gas-bearing area of the Baku archipelago (Fig. 5.16).

Maximum temperature (110 °C) at this section is observed in Arkevan-Lenkaran-Astara region. Local temperature maximums (80.4 °C) are also observed in Bibi-Heybat and Garachukhur-Zikh areas of Absheron oil- and gas-bearing region. Low temperature area extends from the northwest to southeast and covers depression areas of the considered region. At the same local temperature, maximums (70–95 °C) are observed in the deepest part of the depression in deepwater part of the Caspian Sea (Mukhtarov 2011).

Temperature field distribution is in general similar at the 4000 m (Fig. 5.16) and 6000 m (Fig. 5.17) horizontal sections. It is necessary to note that the computed isotherms to a

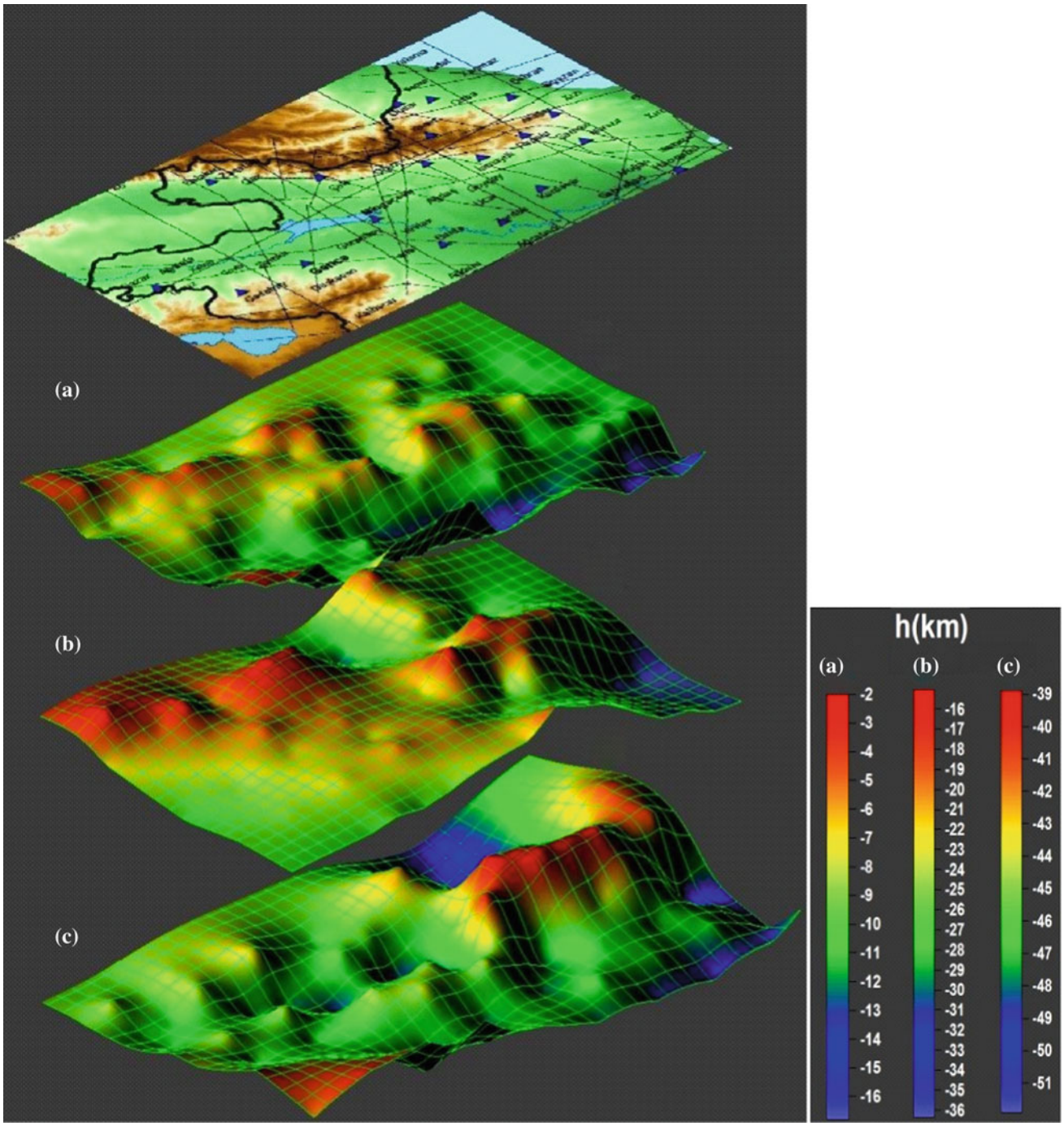

Fig. 5.14 3D scheme of depths distribution for "granitic" (**a**), "basaltic" (**b**), and Moho (**c**) boundaries obtained from interpretation (after Yetirmishli and Kazimova 2013, with small modifications)

certain degree correspond to structural contours and reflect main tectonic peculiarities of the region. At the same time, it is noticeable that regional structures are well defined at deeper levels (4000–6000 m), while local structural elements become distinct closer to the surface (2000 m).

Temperature change is determined both by structural and lithological, hydrogeological, and other factors. For example, the increase of shale content in the section results in the drop of temperature, while the increase of sand content has an opposite effect, which is related to their thermal

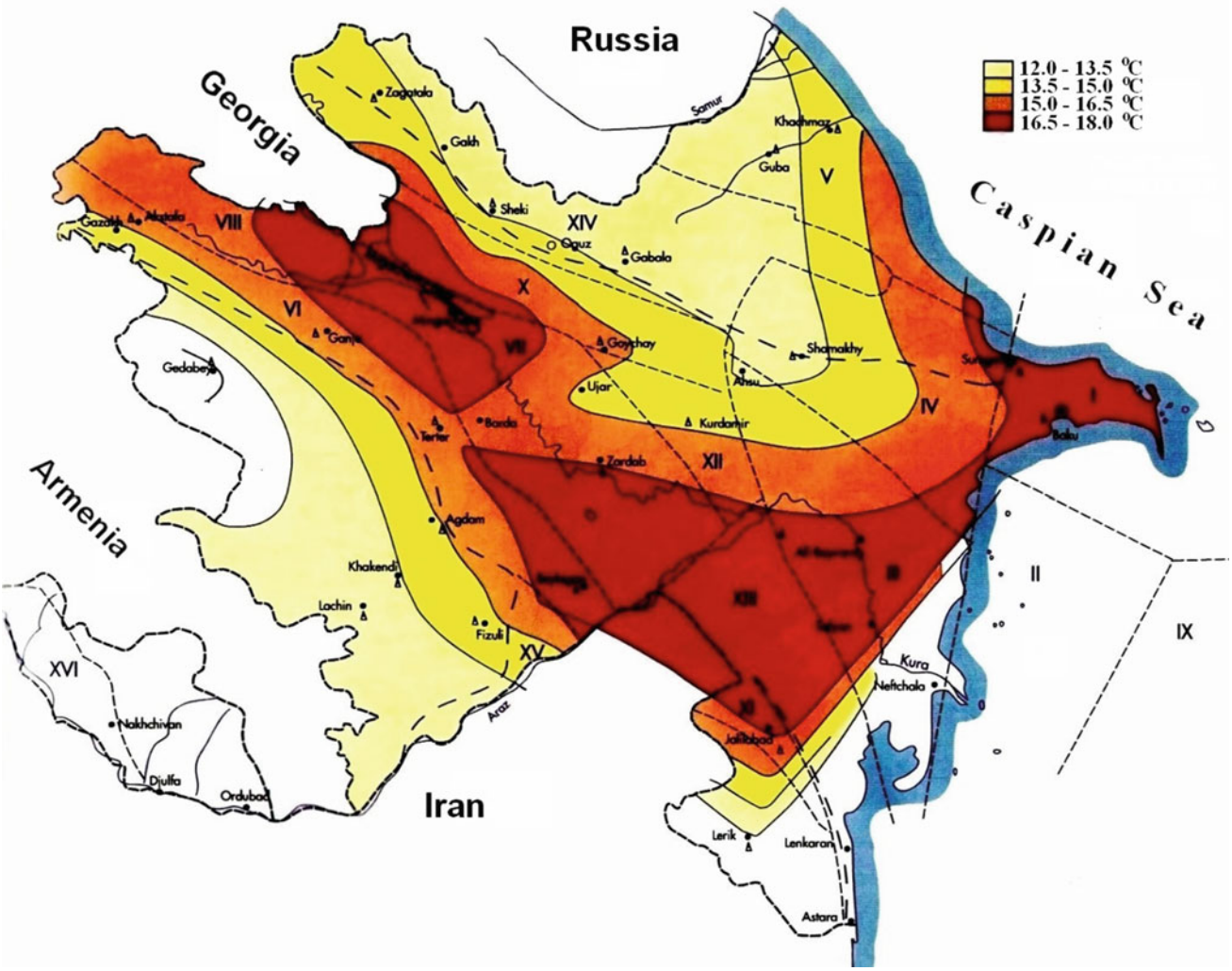

Fig. 5.15 Map of neutral temperature layer distribution for the territory of Azerbaijan (Mukhtarov 2011)

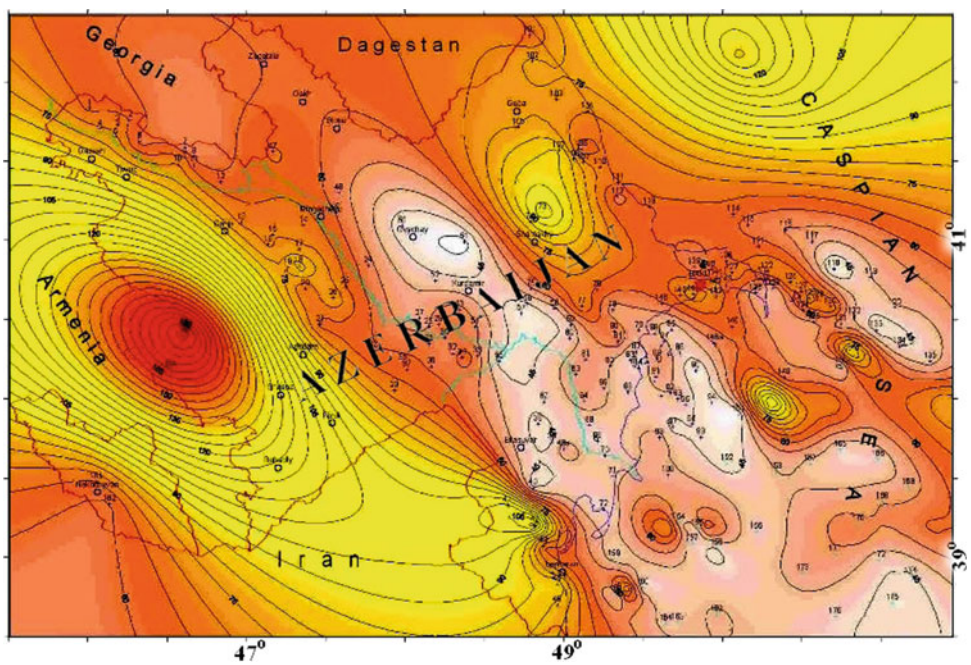

Fig. 5.16 Map of temperature field distribution at the depth of 2000 m (after Mukhtarov 2011)

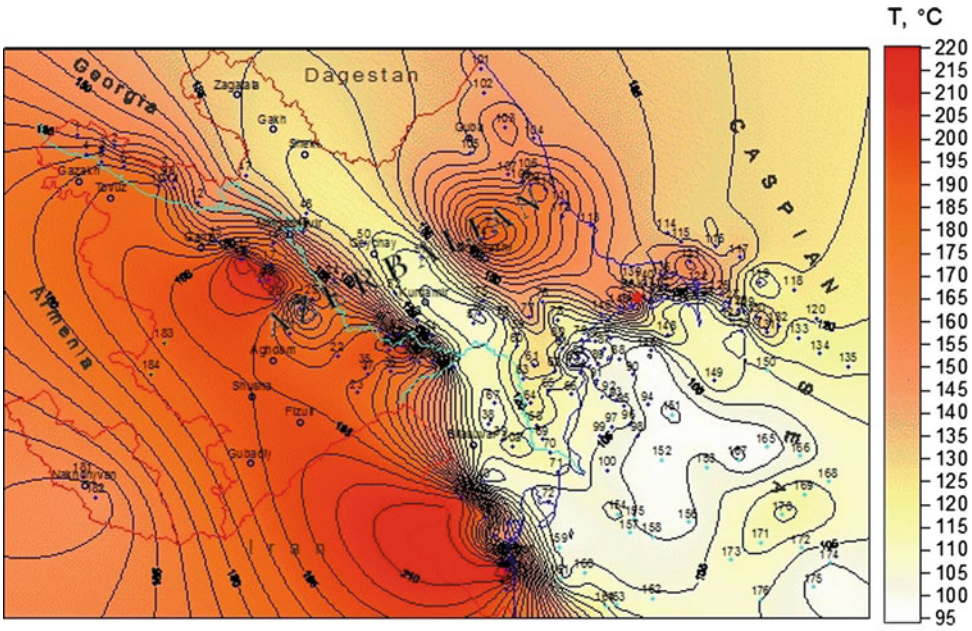

Fig. 5.17 Map of temperature field distribution at the depth of 6000 m (after Mukhtarov 2011)

conductivity (an ability to conduct heat). Filtration of surface water also results in temperature decrease and rise of ground water increases the temperature.

At 6000 m elevation section (Fig. 5.17), temperature also decreases from the sides of the depression (180–160 °C) toward deeper parts (110–100 °C). In the center of the depression minimum temperatures extend in the southeast direction from 120 to 100 °C (Mukhtarov 2011)

Mukhtarov (2011) map of temperature distribution at the roof of Mesozoic associations (Fig. 5.18) is of great importance for the deep structure analysis.

All the thermal maps (here only small part of the developed thermal maps is presented) play an important role in the deep structure analysis.

5.2.3 Magnetotelluric Data Analysis

H.D. Jafarov with collaborators made a significant contribution to studying Azerbaijan deep structure by the use of magnetotelluric sounding (e.g., Jafarov et al. 1967).

In 1988–1991, observations of telluric and magnetic field variations were conducted at three points on a profile perpendicular to the Greater Caucasus (Trofimov 1995). One of these sites, KSN is located at the northern slope of the ridge in the vicinity of Kusnet village (Guba region, Azerbaijan). Example of such observations is shown in Fig. 5.19. These observations were utilized both for deep studying of the Greater Caucasus and analyzing geodynamic activity.

On the basis of analysis of numerous magnetotelluric measurements, Gugunava (1988) developed a map of the longitudinal conductance of the crustal inverted layer in the Caucasus (Fig. 5.20).

According to Gugunava (1988), the Caucasian crust contains several electrically conducting units: (1) the sedimentary cover (up to 15–20 km thick), (2) relicts of magma chambers within mountainous regions, and (3) the asthenosphere. This model was later confirmed by Spichak (1999). Chamber relicts were detected in the form of an oblate ellipsoid at a depth of about 20 km (Greater Caucasus) and as isolated lenses at a depth of 10–20 km (Lesser Caucasus). A crustal asthenosphere underlies the Transcaucasus (0–20 km thick) and attains maximal thickness beneath the Greater and Lesser Caucasus. High conductivity reflects the increased temperature at its depth; its highest values were detected in the southeastern prolongation of the Absheron Peninsula (Fig. 5.20), where increased geothermal gradients were measured (e.g., Kerimov et al. 1989; Mukhtarov 2011).

5.2.4 Gravity Data Analysis

The method of iterative selection is widely applied in practice of gravity field analysis. This method is used when researcher has the possibility to construct an initial model of the geological section. A criterion of selection is coincidence of observed and calculated fields (if the developed geophysical model corresponds to available geological criteria). Different approaches in terms of realization of selection method are exist (e.g., Tikhonov and Arsenin 1977; Bulakh et al., 1984; Bulakh 2000). Mathematically, the applied methodology corresponds to the problem of minimization of multiparametric functional.

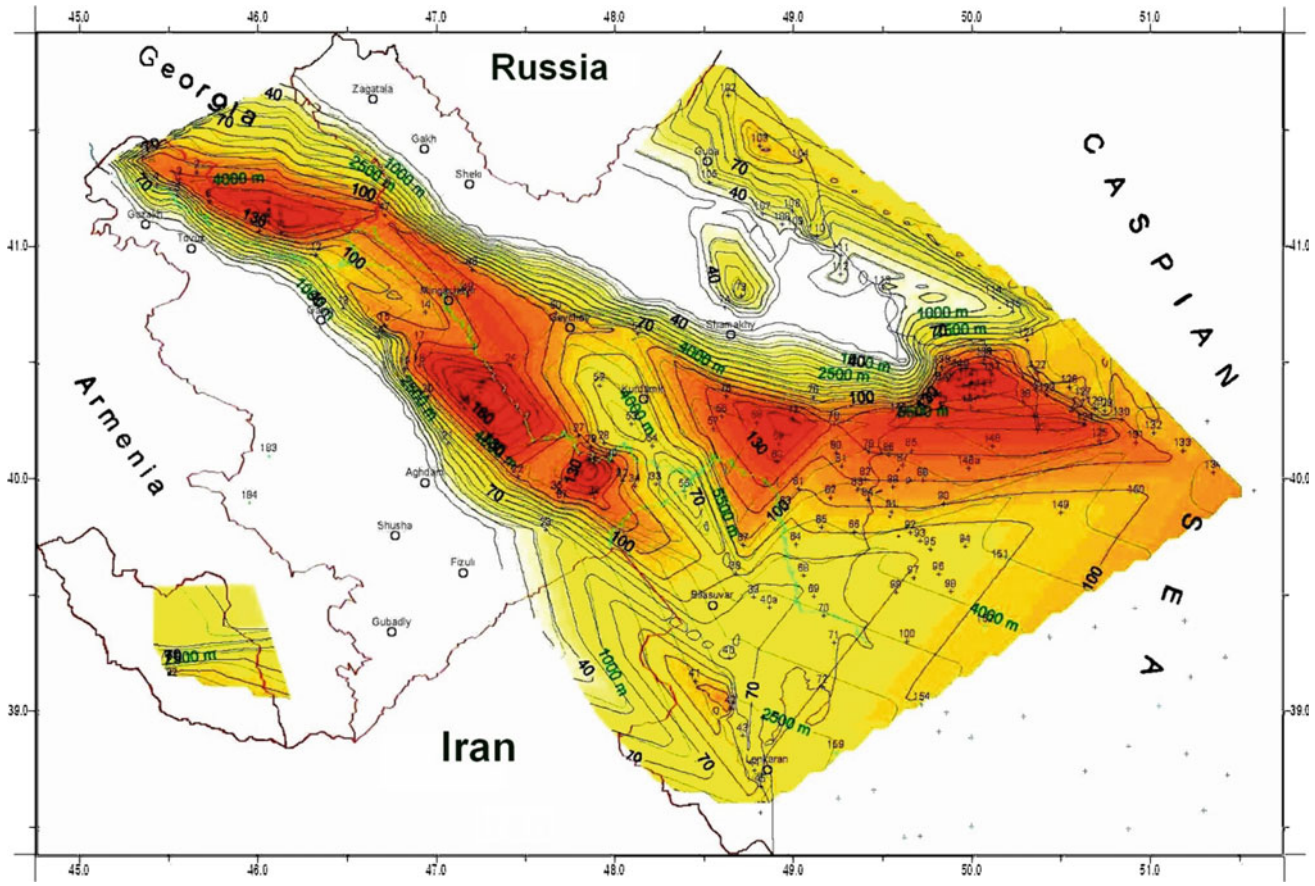

Fig. 5.18 Map of temperature distribution at the roof of Mesozoic rocks in Azerbaijan (Mukhtarov 2011)

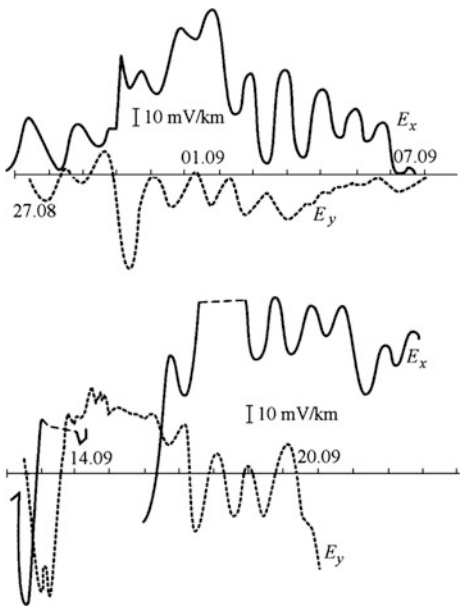

Fig. 5.19 Long-period variations in the telluric field at the KSN site in the Guba region of Azerbaijan (Trofimov 1995)

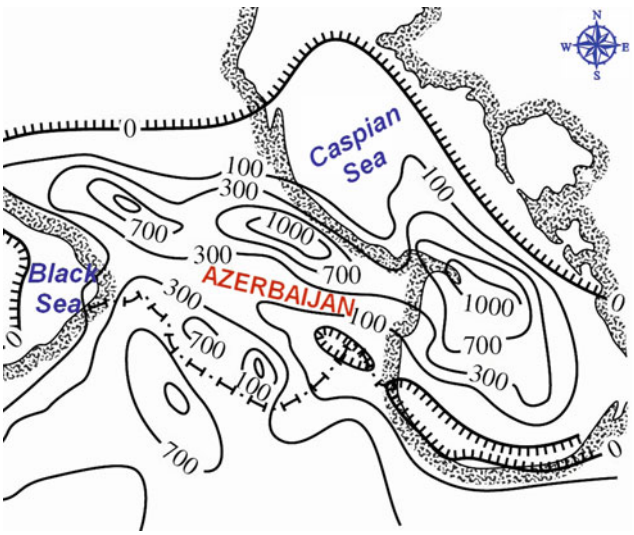

Fig. 5.20 Map showing the longitudinal conductance (in Siemens) of the crustal inverted layer in the Caucasus (after Gugunava 1988, with small modifications)

5.2.4.1 Physical–Geological Model Along the Profile Masally-Poilu

The gravity model along the studied profile was constructed applying a forward modeling process including the fit of the initial model to the observed gravity profile, recalculation of the anomaly, and comparison of the modeled and observed anomalies. This procedure was repeated until the calculated and observed anomalies were considered sufficiently alike (based on data uncertainties and model resolution), adjusting the model parameters in such a way in order to improve the matching between the observed and modeled anomalies.

With the aim to study, the deep structure of the Kur Depression gravity modeling along the profile DSS-3 (Masally-Poilu) has been conducted by the interactive selection method (Shikhalibeyli et al. 1990; Kadirov 2000b; Aliyev et al. 2005a) (Fig. 5.21).

In the SE part of the studied region, the interpreting profile crosses the Mughan monocline, and in NW part—the pre-Lesser Caucasian trough.

For composing the initial model of this profile, the geological–geophysical sections constructed on the basis of the DSS were utilized (Gadjiev 1965; Krasnopevsteva 1984; Baranova et al. 1991; Kadirov 2000b).

Figure 5.21 shows gravity graphs of observed anomaly (solid line), computed from the initial model (dotted line), and computed from the final model (point line). In the right part of this profile, sufficient discrepancy between the observed and computed (from initial model) gravity fields was observed. The gravity effects difference here consists of 70 mGal that indicates to deficit of masses in the initial model.

On the basis of analysis of observed and computed gravity curves in the right part of this profile, some additional contact boundaries and mantle bodies were introduced. The determined upper edges of the mantle bodies with redundancy density of +0.3 g/cm^3 occur here at the depths of 12.5 and 11 km (with corresponding width of 12.5 and 11 km) (Kadirov 2000b).

In the left part of profile, sometimes non-significant disagreement of observed and computed graphs was detected. This disagreement was removed by changing of configuration of the consolidated crust of the roof of the Tovuz-Ganja uplift of crystallic basement.

Taking into account the results of gravity modeling, the geological section of the Earth's crust within the DSS profile No. 3 is revised as follows. On the surface of consolidated crust along the profile were delineated two large uplifts

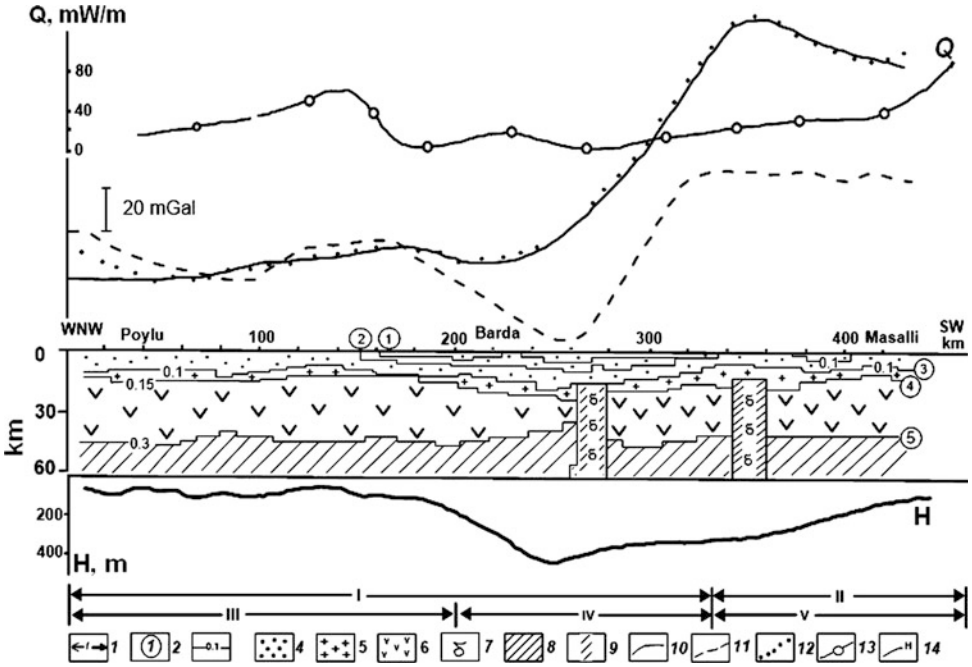

Fig. 5.21 Gravity model along the profile Poylu-Masalli. The values of density differences are in g/cm^3. (*1*) zonation carried out by geological data: *I*—pre-Lesser Caucasian depression; *II*—Mughan monocline; for deep horizons: *III*—Tovuz-Ganja uplift, *IV*—Evlakh-Agjavedi depression, *V*—Bilyasyvar-aradonlin uplift; (*2*) contact boundaries in the Earth's crust and upper mantle (digits in *circles*): 1, 2—in sedimentary strata, (*3*) surface of consolidated crust, (*4*) "basaltic" layer, (*5*) Moho discontinuity; (*6* and *7*) density boundaries in the upper mantle; 3—redundant densities at contact boundaries; (*4*) Meso-Cenozoic rocks; (*5*) rocks of consolidated crust; (*6*) basic rocks; (*7*) mantle's matter; (*8*) mantle; (*9*) deep faults; gravity field: (*10*) observed, (*11*) computed from initial model, (*12*) computed from the selected model; (*13*) graph of thermal flow density; and (*14*) thickness of the Quaternary deposits (Kadirov 2000b)

reflected in Tovuz-Ganja and Bilasuvar-Karadonly gravity highs. The depths of the boundary of consolidated crust in axial parts are 7 and 4 km, respectively. In the area of Evlakh-Agjabedi trough, the computed depth of the consolidated crust is 18.5 km. The Evlakh-Agjabedi trough is clearly appeared and in the subsurface layers: here are found troughs and on the bottom of the productive series and on the Cenozoic bottom. The boundary "basalt" along the profile repeated the form of consolidated crust and its depth in axial parts is as follows: Tovuz-Ganja zone—14 km, Evlakh-Agjabedi—22 km, and Bilasuvar-Karadonly—12 km. At the same time, the Moho boundary occurs reversely with two superincumbent boundaries in the most part of this profile. The Moho boundary rises only in the zone of the Bilasuvar-Karadonly maximum. In the Tovuz-Ganja zone, depth of the Moho discontinuity is about 47 km (to NW along the profile, the depth increases up to 52 km), in Evlakh-Agjabedi—39 km, and in Bilasuvar-Karadonly—41.5 km.

In Fig. 5.21, graphs of the thermal flow distribution (Q) (Aliyev 1988) and changing of thickness of Quaternary (H) deposits (Mamedov 1984) along the profile are also shown.

In the thermal flow distribution along the profile, Aliyev (1985, 1988) is marked a change of its level by transition from Tovuz-Ganja zone to Evlakh-Agjabedi zone that testifies to differences in the geotectonic evolution. The highest thermal flow values (50–70 mW/m^2) along the profile are typical for the comparatively young Tovuz-Ganja tectonic–magmatic zone, structures of which were formed in Meso-Cenozoic. The middle and low thermal flow values (20–40 mW/m^2) were observed in the Evlakh-Agjabedi and Bilasuvar-Karandonlin zones and indicate the ancient consolidation of the region.

The developed physical–geological section along the profile DSS No. 3 indicates that the region beginning from the axis of Evlakh-Agjabedi trough and to east including Bilasuvar-Karandonlin zone subjected to a common by genesis appearance of magmatism in the pre-Baikal time. The presence a residual gravity anomaly of 70 mGal (in the initial model) in the right part of profile and changing the observed anomaly comparing with the left part of profile may be explained by presence of ancient massif embedded from the mantle. Revealing by the way of gravity modeling, additional boundaries of mantle–lithospheric bodies and their small areal distribution testify to the fact that the crystallic basement was destructed by deep faults (Shikhalibeyli et al. 1990).

Scheme of distribution of thicknesses of Quaternary deposits along this profile (Mamedov 1984) indicates the contrast movement at the neotectonic stage. It continues to rapidly raise the Bilasuvar-Karandonlin zone whereas on both sides of it—to the Caspian Sea in the east, and to the Evlakh-Agjabedi trough in the west, an intense subsidence is observed.

5.2.4.2 Physical–Geological Model Along the Profile Agjabedi-Zardab-Mususli-Karamaryam

Deep structure of the Kur Basin was studied by various researchers (e.g., Gadjiev 1965; Azizbekov et al. 1972a; Radjabov 1977; Krasnopertseva 1984; Abbasov 2002; Mamedov et al. 2008). However, majority of these works were based on the classic fixist theory of basin formation. According to the 'plate tectonics' concepts (e.g., Khain 2005), the Kur Depression and framing mountain massifs of the Greater and Lesser Caucasus are the result of complex combination of the lithosphere horizontal and vertical motions. Thus, we can propose that formation of the subsided (Kur Intermountain Depression) and uplifted (Greater and Lesser Caucasus) regions of the Earth's crust is the result of the horizontal displacements and collision of the Arabian and Eastern European plates (Reilinger et al. 2006).

Here was realized an attempt to construct the gravitation model of the Kur basin deep structure basing on the aforementioned ideas. Special field study along the earlier compiled seismic profile of Agjabedi-Zardab-Myusyusli-Karamariyam was carried out (Fig. 5.22). Gravimetric and geodetic measurements on this profile were made at the every 250 m at 350 points.

The sedimentary section along the investigated profile is composed by Mesozoic, Paleogene, Neogene, and Quaternary rocks. First 45 km of profile (from Agjabedi to Zardab area) the regional gravitation field is influenced by SE parts of Alazan-Middle Kur minimum (Yevlakh-Agjabedi trough of crystalline basement) and the rest part of profile—by the western termination of Azerbaijan gravity maximum (combined influence of the Geokchay-Mingechavir and Saatly-Kurdamir projections of the crystalline basement) (Gadjiev 1965; Azizbekov et al. 1972a, b).

Results of deep seismic data analysis were utilized for construction of a geological-geophysical model of a first approximation. In this model, the geological section was constructed on the basis of the seismic profile of Agjabedi-Zardab-Mususli-Karamaryam and represented by six contact boundaries: foot of the Quaternary deposits (Absheron), boundary between the Neogene and Paleogene deposits foot of the Eocene deposits, foot of the Mesozoic deposits, surface of the "basaltic" layer, and Moho discontinuity. Such boundaries as "basaltic" layer and Moho discontinuity are compiled in their initial variant mainly by gravity data (Gadjiev 1965; Tzimelzon 1965; Azizbekov et al. 1972a). Average seismic velocity in the Absheron stage strata is 2.5 km/s, in another three boundaries—3.5 km/s, in Mesozoic—4 km/s. At the section interval between the Mesozoic complex and consolidated crust, the seismic velocities increase up to 5.2 km/s. The most part of Mesozoic boundary along the profile has boundary velocity of 6.2 km/s. Boundary velocities on the "basaltic" surface

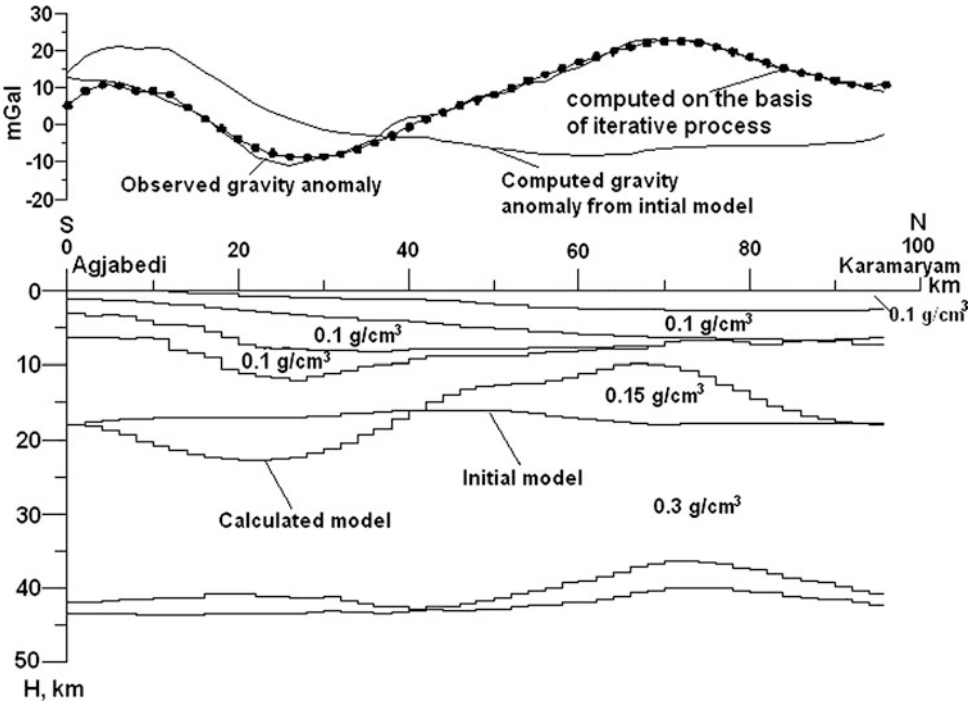

Fig. 5.22 Gravity model along the meridional profile Agjabedi-Karamaryam (Central Azerbaijan). The values of density differences are given in g/cm^3 (Kadirov 2000b)

vary from 6.5 to 7.3 km/s. Boundary velocities weakly change for the "Moho" discontinuity and consist of 8.1 km/s (Radjabov 1977; Krasnopertseva 1984; Baranova et al. 1991).

Density model for the upper part of the initial model was constructed on the basis of available density data for the sedimentary rocks. While constructing the model, some density generalization has been applied, i.e., a number of small density heterogeneities were replaced by common average parameters. The density acquired through the correlation linkage between the density of rocks and propagation velocity of *P* waves therein. To construct regional density model of the environment along the profile, the data of the DSS and density characteristics of the enclosing complex of rocks at normal and high *P-T* terms (Salekhli 1993) were applied.

Change of density determined by depth increase may be considered linear at small depth intervals whereas at a significant variation of depth change, this parameter corresponds to the exponential law. Density of deeper layers was determined by values of propagation velocities of *P* waves (determined experimentally) at high pressures and temperatures (Balakishibeyli et al. 1996). Density contrast for the boundary "basalt" is assumed as +0.15 g/cm^3 and for the Moho discontinuity— as +0.3 g/cm^3 (Balakishibeyli et al. 1996; Aliyev et al. 2005a).

To select the geometry, about 60 iterations were done, and to select density of the bodies, about 20 iterations were applied. Difference between the observed and calculated fields is not great (about 3 mGal) at a distance of 38 km.

Figure 5.22 demonstrates gravity curves of the observed anomaly (solid line), calculated from initial model of the section (dotted line), and final model from the presented geological–geophysical section (dotted line).

5.2.5 Combined Gravity–Magnetic Analysis

On the basis of our experience, it was recognized that gravity, magnetic, and especially combined gravity–magnetic modeling is a powerful tool for studying the variable deep structure of Azerbaijan (e.g., Kadirov, 2000b; Eppelbaum and Khesin 2012). This study must be preceded by a combined qualitative and advanced quantitative gravity/magnetic data analysis supported by integrated examination of available geological, seismic, magnetotelluric, and thermal data, and utilization of numerous magnetic, paleomagnetic, and density properties of geological samples from the region under study. Final product of such an investigation is development of series of 2.5 and 3D ***Physical-Geological Models*** (***PGM***)s. These ***PGM***s can be used not only for substantiation of various types of prospective economic deposits, but also to delineation of the tectonic–structural factors affecting the long-term seismological prognosis (Eppelbaum and Khesin 2012).

5.2.5.1 Preferences of Integrated Interpretation

Gravity–magnetic data processing is generally intended to reduce and eliminate noise factors of different origins and intensities. The main problem faced by qualitative interpretation is to single out a desired target, whereas quantitative

interpretation needs to determine and refine the target parameters. Thus, geological problems need to be resolved in terms of: (1) the capabilities of the geophysical method selected for measurements of the field containing the information required, (2) the physical properties of the medium under study and their capability to generate detectable signals (anomalies), and (3) the methods for data processing and interpretation, namely their ability to extract information from geophysical fields and reveal the effects from the geological targets. Figure 5.23 presents a general flowchart for the analysis and synthesis of geophysical data for complex regions. Each step in this flowchart is divided into substeps with more concrete formulation (Eppelbaum and Khesin 2012).

Estimation of efficiency of integrated interpretation from the probabilistic and information points of view is considered in detail in Eppelbaum (2014a). Interestingly, that from analysis of a classical "four-color problem" follows that two independent geophysical method application theoretically are sufficient for successive mapping of the area of any geological complexity (Eppelbaum 2014b). Undoubtedly, this fact supports the theoretical basement of 3D combined gravity–magnetic field modeling.

5.2.5.2 Short Description of the Employed Algorithm

The *GSFC* (Geological Space Field Calculation) program was developed for solving a direct 3D gravity and magnetic prospecting problem under complex geological conditions (Khesin et al. 1996; Eppelbaum and Khesin 2004). This program has been designed for computing the field of Δg (Bouguer, free-air or observed value anomalies), components of magnetic field ΔZ, ΔX, ΔY, total magnetic field ΔT, as well as second derivatives of the gravitational potential under conditions of rugged relief and oblique magnetization. The geological space can be approximated by (1) 3D, (2) semi-infinite bodies, and (3) those infinite along the strike closed, left-hand (LH) non-closed, right-hand (RH) non-closed, and open bodies.

The program has the following main advantages (besides above-mentioned ones): (1) simultaneous computing of gravity and magnetic fields; (2) description of the terrain relief by irregularly placed characteristic points; (3) computation of the effect of the earth–air boundary directly in the process of interpretation; (4) modeling of the interpreting profiles draping over rugged relief or at various arbitrary levels (using characteristic point description); (5) simultaneous modeling of several profiles; and (6) description of a large number of geological

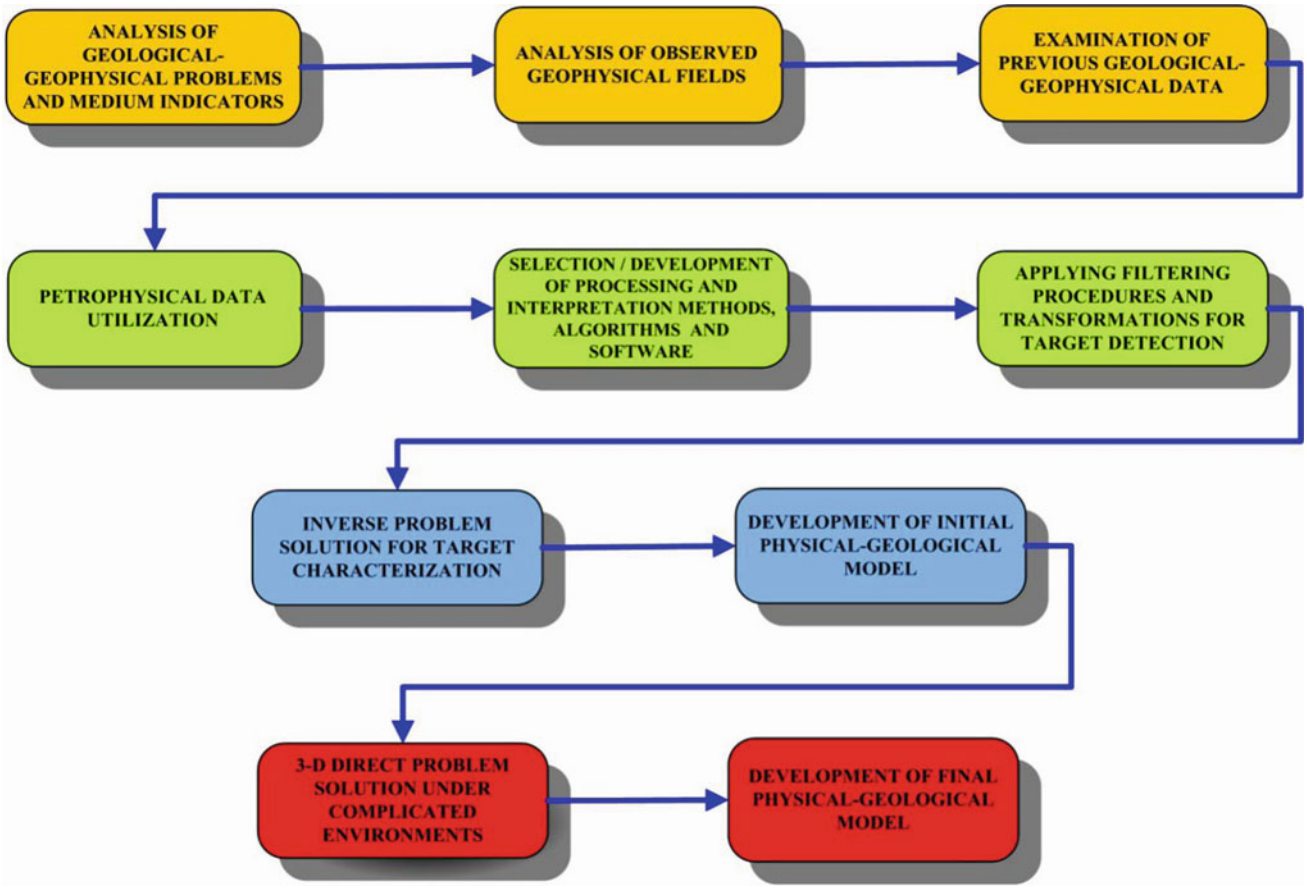

Fig. 5.23 Interpretation of geophysical fields under complex environments: a general scheme

bodies and fragments (up to 1000). The basic algorithm realized in the GSFC program is the solution of the direct computation of gravity and magnetic effects from the horizontal limited in the strike polygonal prism (Eppelbaum and Khesin 2004). In the developed algorithm, integration over a volume is realized on the surface limiting the anomalous body.

The advantage of the interactive computer selection system is that it eliminates the need for a great number of iterations, which are inevitable in automated selection algorithms that use successive parameter variation searches within a specified range.

Nevertheless, systems of automatic selection of geophysical fields (for the gravity field this approach was developed by Goldshmidt et al. (1981) and Bulakh et al. (1984) have certain limitations. First the selection must be meaningful: e.g., changes in physical properties and 3D geometrical parameters should be carried out in defined numerical and space intervals. These limitations stem primarily from the program. However, there are more serious issues. Take the example of a 3D integrated gravity and magnetic selection over a comparatively simple section consisting of ten geological bodies. Each geological body has three petrophysical variables (density, magnetization, and inclination of the magnetization vector), geometric variables (left-hand (y_1) and right-hand (y_2) end faces of the body) and, finally, its geometric parameters in the plane of geological section. The number of points (variables) to describe bodies in the plane of section a priori is unknown. For simplicity and given that many of these points are calculated twice by the contouring objects, the number of these points can be assuming to be ten. To calculate the number of possible combinations of all variables by combined 3D modeling, we need to calculate the approximate ranges of the variables (Table 5.1). Obviously, these ranges are relative and only estimate the number of combinations.

Applying known combinatorial analysis (e.g., Riordan 2014), for one body we have the number of combinations $C_{30}^1 \cdot C_{60}^1 \cdot C_{24}^1 \cdot C_{30}^1 \cdot C_{30}^1 \cdot C_{100}^1 \approx 4 \times 10^9$. Correspondingly, for ten bodies, we have $\approx 4 \times 10^{90}$ combinations. Obviously, such a number of combinations considerably complicate an automatic 3D-integrated gravity–magnetic modeling even using supercomputers.

Table 5.1 Calculation of the number of possible combinations of variables (Eppelbaum 2015)

Variable	Interval of changing	Ranging	Number of combinations
Density (g/cm^3)	2.30–2.60	0.01	30
Magnetization (mA/m)	0–3000	50	60
Inclination of magnetization (°)	0–360	15	24
Left-hand end face, y_1/x_m^a	0–20	nonlinear	30
Right-hand end face, y_2/x_m	0–20	nonlinear	30
Geometrical coordinates of geological body in the plane of geological section	min 10 points	–	min 10·10

[a] x_m is the maximum length of interpreting profile

5.2.5.3 Description of Interpretation Methodology

The most complete description of the interpretative process structure was given by Strakhov (1976). An interpretation process may be roughly subdivided into the following stages: (1) summarizing prior information; (2) sequential analysis, and (3) geological synthesis.

The development of 3D ***PGM*** is usually performed using these three stages.

The first stage (summarizing prior information) is as follows:

(A) First of all, the main geological–geophysical conception of tectonic development of the region under study must be analyzed and adopted (without it, the process of ***PGM*** construction will be not successive and logical). Construction of geological section includes compilation of all intrusive, effusive, and other associations, as well as faults and the surface of folded foundation on the basis of geological data within a strip of 15–20 km (in some cases—20–40 km) wide. The interpreting section is located in the middle of this strip. Undoubtedly, geophysicist–interpreter must have a good knowledge of the region under study.
Such a section characterizes the upper portion of the Earth's crust with a thickness from 2–3 to 5–8 km from the Earth's surface to the Baikalian basement. Deeper parts of the intrusive bodies and certain faults are formed by extrapolation of the available constructions, general geological considerations, and the results of previous geophysical analyses.

(B) A preliminary petrophysical model of the section is developed. Here, all the geological bodies acquire density and magnetization values according to the preceding petrophysical data analysis and results of geophysical field interpretation. When no data are available on the magnetization direction, it is assumed to be parallel to the normal geomagnetic field in the region under study. Further, the magnetization direction is refined in the process of physical–geological modeling. Density properties are received from the borehole sample examination and converted from the seismic data by the known method (e.g., Barton 1986). The petrophysical model includes deep-seated layers (slabs) of the Earth's crust: (1) the "basaltic," (2) the intermediate between the crust and the upper mantle, and (3) the upper mantle. Their surfaces are constructed and physical properties are associated with them according

to the data from previous seismic, magnetotelluric, thermal, and other geophysical studies. Paleomagnetic data examination may be of a high significance.

(C) The initial (preliminary) petrophysical model includes hidden bodies as well. Their location, thickness, depth, density, and magnetization are obtained from the quantitative analysis of magnetic and gravity fields as well as from seismic data examination.

The second stage (sequential analysis) includes application of combined gravity and magnetic field modeling along the interpreting profiles using 3D *GSFC* program. Each time the gravity–magnetic effects from different bodies, groups of bodies and the total computed model are displayed and compared to the observed gravity and magnetic fields. Using the results of this comparison, the changes that match the gravity and magnetic effects into the model of the medium are introduced. The computations and comparisons of fields and model modifications are repeated until the desired fit between the computed and observed fields is obtained.

Then, a regional gravity (and sometimes magnetic) field is roughly selected. As a rule, the densities of deep-seated complexes are not changed; the modifications only affect the shape of their roof. Next, geophysical fields of local bodies are selected. If necessary, this is followed by a verification of the regional fields and the fields of the local bodies.

At each computational step, a separate analysis of gravity and magnetic fields is carried out. Geometrical coordinates of geological bodies are verified in the subsequent steps and then introduced into the model. This procedure leads to an integrated qualitative and quantitative interpretation for anomalous gravity and magnetic fields. The modeling completes when the computed gravity and magnetic fields coincide accurately with the observed fields. All this modeling process must be carried out in a full compliance with the known geological principles.

The third stage (geological synthesis) involves a detailed geological interpretation of these models. A 3D ***PGM*** of the area under investigation is developed based on the geological data obtained at the previous stages and qualitative and quantitative geophysical data examination. This yields the final physical–geological sections, and the models are characterized by a more complete rendering of the geological targets, including crustal blocks, intrusions, faults, and economic deposits.

The geological interpretation of the geological associations, complexes, and local bodies of the constructed (final) petrophysical model does usually not consist of a hard problem since in the implementation of the interactive selection system almost all the bodies in the ***PGM*** acquire some specific geological content. The geological nature of new sources introduced into the model during the iterative modeling and reflected either in the initial geological section, or in the initial ***PGM***, is determined according to the similarity of their physical properties, dimensions, and depth of occurrence with respect to the known targets. The age of the bodies is determined according to their interrelations with the surrounding (host) rocks.

5.2.5.4 Application of 3D Combined Gravity–Magnetic Field Modeling in Azerbaijan (Land)

A simplified tectonic map of Azerbaijan with interpreting magnetic–gravity profiles is shown in Fig. 5.24. Advanced interpretation methods (improved modifications of tangents, characteristic point methods, and areal method) were applied to study magnetic and gravity anomalies along all profiles surrounding SuperDeep borehole SD-1 in Saatly area of Azerbaijan. A fragment of this interpretation along the profile 18 is shown in Fig. 5.25. First of all, note that the behavior of the magnetic ΔZ curve and graph $\partial \Delta g_B / \partial x$ is very simular that testifies to the fact that these anomalies are due to the same geological objects. A quantitative analysis of the magnetic curve allowed to delineate two magnetic targets. The main target apparently is a source of the Talysh-Vandam gravity anomaly (its upper edge coincides with the data obtained by SD-1 drilling) (Aliyev et al. 2005b). The obtained data were utilized by construction of a ***PGM*** of first approximation for 3D combined physical–geological modeling (Eppelbaum and Khesin 2012).

Integrated physical–geological model of the Saatly Superdeep borehole

For many years, the dominant point of view in Azerbaijan was that in the Kur Depression separating the mega-anticlinoria of the Greater and the Lesser Caucasus, thick sedimentary deposits were present in the crystalline pre-Alpine basement, and these structures were divided by subvertical deep faults. On the buried uplift of the basement, hypothesized on the basis of high densities and velocities of elastic waves, the Saatly superdeep borehole SD-1 was designed in 1965; the drilling was began in 1977 and stopped in 1991 (Popov and Kremenetsky 1999). The drilling area was selected using the analysis of seismic profiles 9, 16, and 18 (see Fig. 5.24) as well as regional gravity field analysis (Gadjiev 1965; Tzimelzon 1965).

However, analysis of the magnetic properties of rocks and the magnetic survey results showed that the basement was not magnetized, and a large part of the geological section of the Middle Kur Depression was occupied by Mesozoic magmatic associations of basic and intermediate composition with high magnetization (Eppelbaum and Khesin 2012). These mainly Jurassic associations are widely distributed in the northeastern part of the Lesser Caucasus.

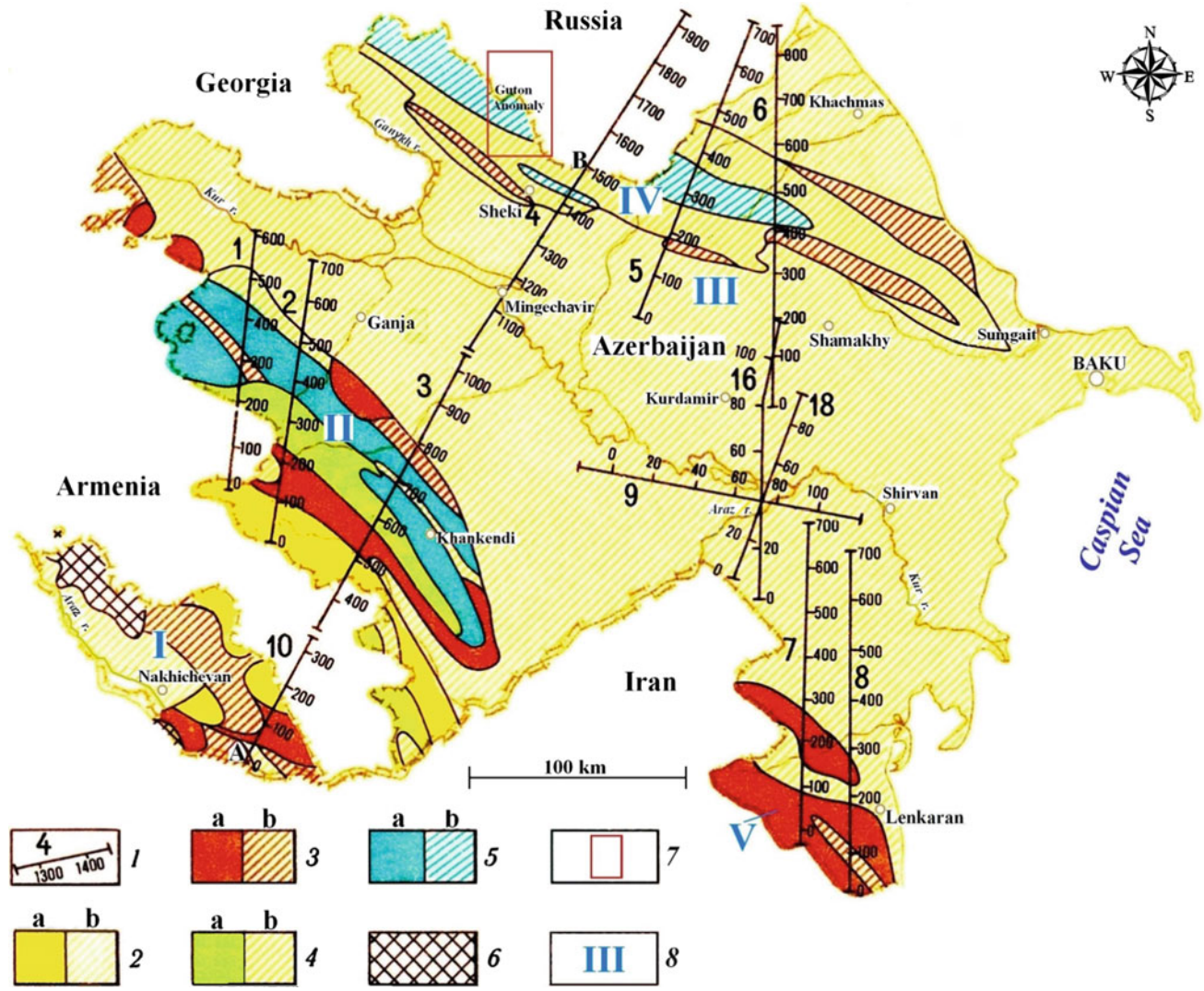

Fig. 5.24 Areal map of main profiles used for physical–geological modeling in Azerbaijan and adjacent regions. (*1*) profiles and pickets, (*2*) Pg_3–Q: (*a*) orogenic magmatic associations, (*b*) background sedimentary deposits, (*3*) K_2–Pg_2: (*a*) pre-orogenic magmatic associations, (*b*) background sedimentary deposits, (*4*) J_3–K_1: (*a*) magmatic associations of the Late Alpine substage, (*b*) background sedimentary deposits, (*5*) J_1–J_2: (*a*) magmatic associations of the Early Alpine substage, (*b*) background sedimentary deposits; (*6*) Pz deposits, (*7*) contour of the Guton magnetic anomaly, (*8*) tectonic regions: *I*—Nakhchivan folding region, *II*—SE part of the Lesser Caucasus mega-anticlinorium, *III*—central and SE parts of the Kur megasynclinorium, *IV*—SE part of the Greater Caucasus mega-anticlinorium, and *V*—Talysh anticlinorium

They have a deep-seated gently sloping underthrust under the sand–shale thick series of the Greater Caucasus Jurassic.

The validity of the interpretation was fully confirmed by the results of the SD-1 drilling (Fig. 5.26). The borehole exposed Mesozoic volcanogenic rocks at a depth of 3.6 km and did not reach its bottom even at 8.2 km (Alexeyev et al. 1988).

An examination of the gravity and magnetic fields was carried out for profiles 9, 16, and 18 (with seismic and thermal data) and were used to determine the main features of a spatial geological–geophysical model of the Earth's crust for the SD-1 area (Fig. 5.27). The diagram shows the main sources of gravity and magnetic anomalies in the eastern part of the area where SD-1 is located, and in the western part where the Zardab magnetic maximum was found. The magnetic and gravity field analysis (including 3D modeling of these fields) together with petrophysical data provided additional evidence to account for the Ganja regional magnetic maximum (Eppelbaum and Khesin 2012).

The SD-1 was halted at a depth of 8.2 km. Given the location of the lower edge of the magnetized masses and by analogy of this geological section to ones in the Lesser Caucasian, it is likely that magmatic rocks occur down to 10 km (compatible with the Lower Bajocian rocks of the Lesser Caucasus).

Obviously, the main source of the Talysh-Vandam gravity maximum is associated with underlying high-density

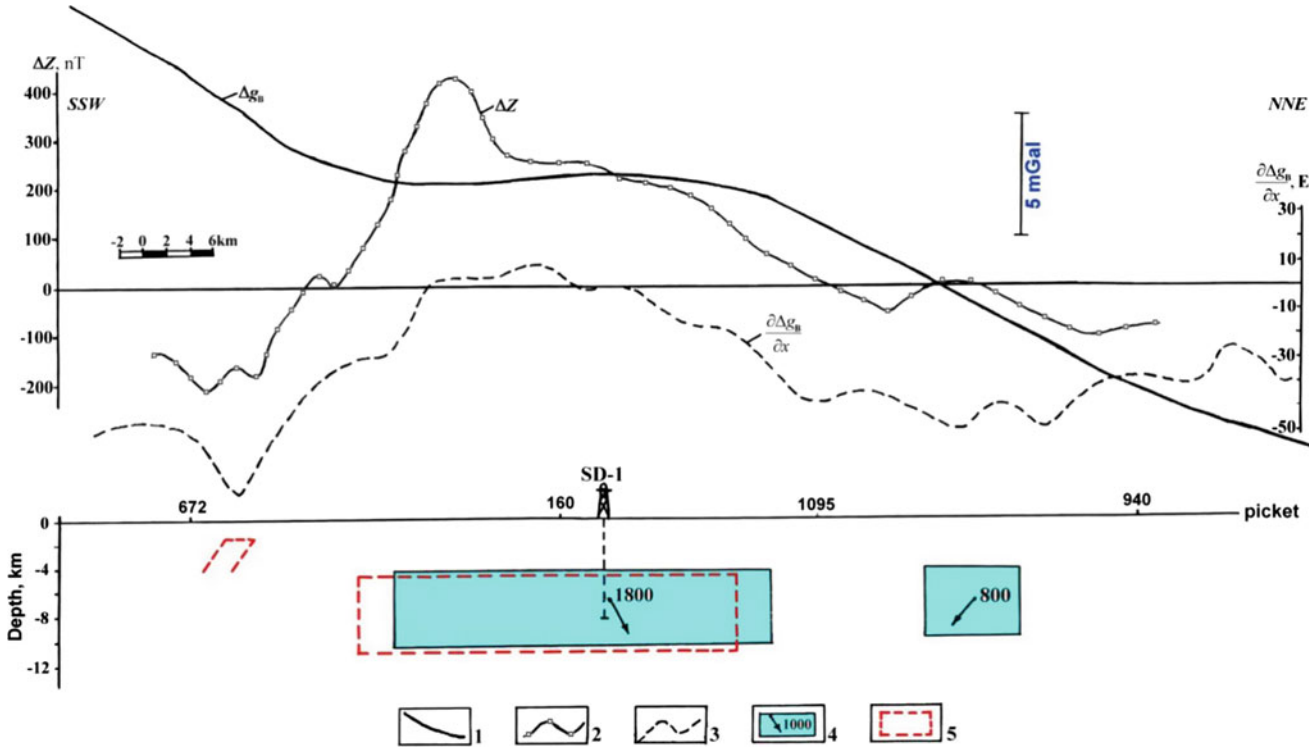

Fig. 5.25 Fragment of gravity and magnetic fields analysis along the profile 18 (Eppelbaum and Khesin 2011). (*1*) gravity field Δg_B, (*2*) magnetic field ΔZ, (*3*) first horizontal derivative of the gravity field $\partial \Delta g_B / \partial x$, (*4*) contour of determined magnetized body and position of magnetization vector, and (*5*) contour of body determined by analysis of $\partial \Delta g_B / \partial x$

strongly metamorphized and initially chiefly sedimentary associations of the non-magnetic or low-magnetic Pre-Baikalian floor (this floor has a submeridional strike in the Russian and African platforms). The depth of the upper edge of these highly dense rocks is estimated at 9.5 km.

Thus, SD-1 has yet to discover (these drilling operations may or may not be continued) the source of the Talysh-Vandam regional gravity anomaly, but it has identified the origin of the Ganja magnetic maximum. This has enormous importance not only for the analysis of the tectonic–magmatic evolution of the Caucasus region (Alizadeh et al. 2000), but also for evaluating the potential of ore- and oil- and gas-bearing prospecting. For example, the geomagnetic models can extend prospecting of oil deposits in the Middle Kur Depression that are associated with zones of protrusions of Mesozoic magnetoactive associations. Many geophysical methods have mapped these dense Mesozoic associations, but only magnetic prospecting revealed basic and middle consistency magmatites (Eppelbaum and Khesin 2011).

3D magnetic–gravity modeling along the profile 1

A visual example of 3D combined modeling of gravity and magnetic fields along the profile 1 (see scheme of profiles presented in Fig. 5.24) is shown in Fig. 5.28. Profile 1 crossing the Lesser Caucasus illustrates the very complex geological structure of this region. This profile stretches along the line Mez-Mazra - Gedabey - Dzegam-Jirdakhan. The Late Alpine effusives in the ***PGM***s compose an ophiolite zone (relic of the ocean crust). It is thought that the same rocks occur in the NE immersion of the Lesser Caucasus. Pre-orogenic and orogenic intrusive and effusive rocks are fixed in the southern parts of the ***PGM***.

Thick sedimentary deposits are developed in northern part of this profile. A smooth high of the Moho discontinuity is observed from south to north from a depth of 52 km up to 42 km (Eppelbaum and Khesin 2012). Such a Moho boundary behavior on the whole agrees with the latest data of deep seismic profile reinterpretation (Pavlenkova 2012). Depths of the magnetized body's lower edges were estimated on the basis of various geophysical field analyses, but mainly on the basis of thermal and magnetic data examination (Pilchin and Eppelbaum 1997). Here were revealed such classes of disturbing objects as acid intrusions of lower density and magnetization, basic magmatic rocks of increased density and magnetization, and fault zones. It was determined that the clearest density boundaries were associated with the base of the Cenozoic sedimentary strata and, to a lesser degree, with the base of the Alpine complexes. According to the performed modeling, geomagnetic boundaries are associated mainly with the roof and bottom of the Mesozoic floor of heightened magnetization.

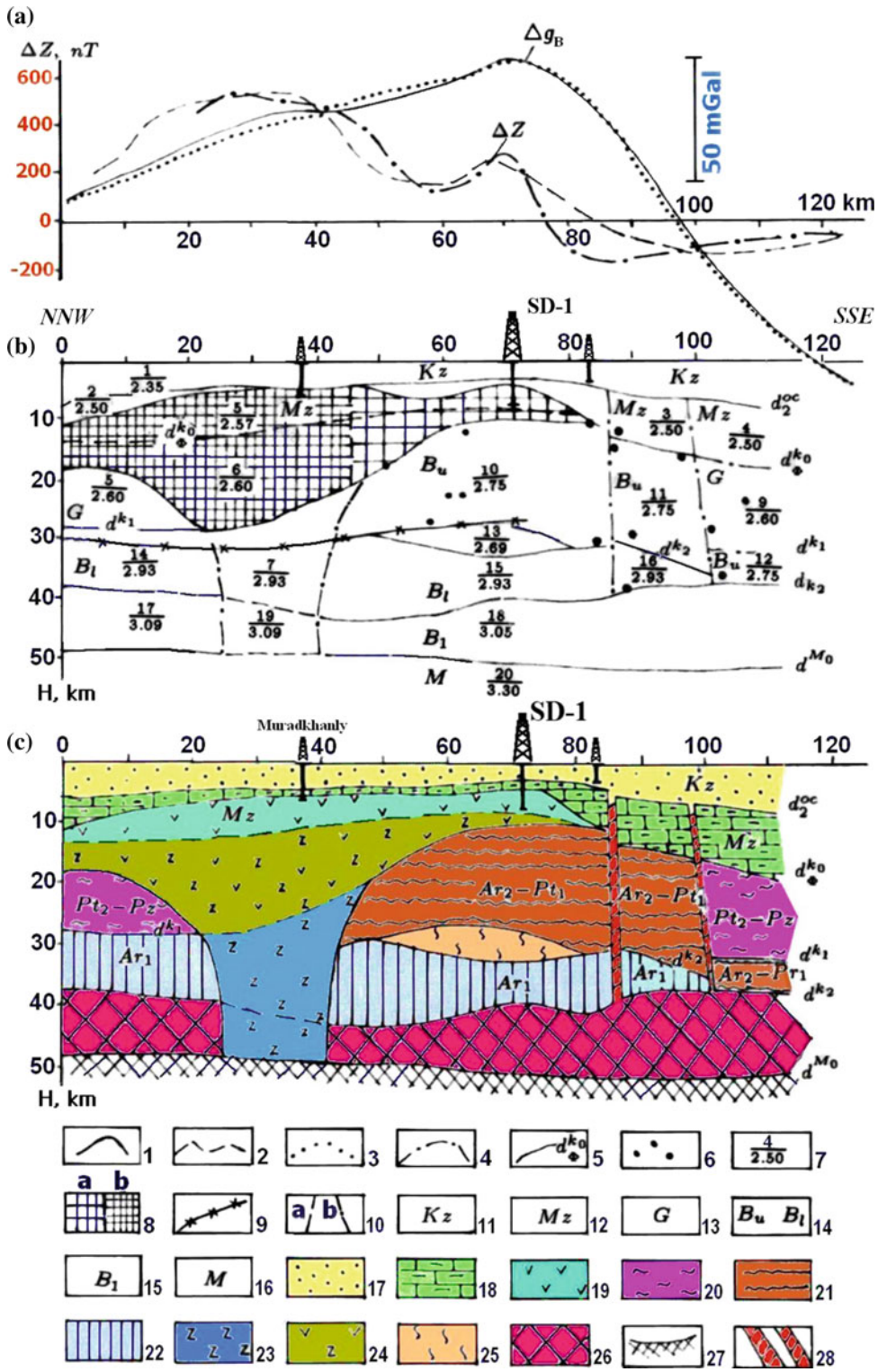
(a)
ΔZ, nT
600
400
200
0
-200
Δg_B
ΔZ
50 mGal
20
40
60
80
100
120 km
(b)
NNW
SSE
SD-1
H, km
Kz
Mz
G
Bu
Bl
B1
M
(c)
Muradkhanly
SD-1
H, km
Kz
Mz
Pt2 – Pz
Ar2 – Pt1
Ar1

◀ **Fig. 5.26** Deep geological section of the Earth's crust in the SD-1 area (profile 9 in Fig. 5.24). **a** gravitational and magnetic fields, observed and computed by the model **b**; **b** petrophysical model; **c** geological model (after Khesin et al. 1996, with modifications). Observed curves: (*1*) Δg, (*2*) ΔZ; curves computed by the model **b**: (*3*) Δg, (*4*) ΔZ; (*5*) boundaries of the velocity and the density inhomogeneities and their indices; (*6*) diffraction points; (*7*) body number (numerator) and density value, g/cm^3 (denominator); (*8*) geological bodies with a magnetization of 2500 mA/m (*a*) and 2800 mA/m (*b*); (*9*) projection of Curie surface on the basis of geothermal data; (*10*) subvertical boundaries of bodies on the basis of magnetic (*a*) and gravitational (*b*) fields; (*11*) Cenozoic; (*12*) Mesozoic; (*13*) *G* complex (velocity analog of the "granitic" layer); (*14*) B_u and B_l subcomplexes of *B* complex (complex *B* is the "basaltic" layer velocity analog); (*15*) B_1 complex (presumably basite and eclogite composition); (*16*) *M* complex (presumed peridotite composition); (*17*) Cenozoic complex: mainly terrigenous deposits; Mesozoic complex: (*18*) terrigenous–carbonaceous formations, (*19*) mainly effusive associations of basic and intermediate composition; (*20*) mainly Baikalian complex (Pt_2-Pz): metamorphic (primarily terrigenous) associations (the presence of younger deposits is possible in the upper part); (*21*) Pre-Baikalian complex (Ar_2-Pt_1): mainly gneisses and marbles; (*22*) ancient complex (Ar_1): gneisses and amphibolites; (*23*) root of the basic magmatism; (*24*) undivided effusive–intrusive complex; (*25*) rock complex of a low density (serpentinization zone ?); (*26*) complex of associations corresponding to crust-to-mantle transition; and (*27*) upper mantle roof position; (*28*) large fault zones

The geomagnetic model along the meridional profile 16 is significantly different from sublatitudinal profile 9 (see locations of profiles in Fig. 5.24). At the same time, the gravity field along the profile 16 is smoother. Obviously, these differences in potential geophysical fields reflect the specificities of the deep structure of the source of the Talysh-Vandam gravity maximum which is composed of a submeridional strike of deeply occurring masses with superfluous density and a sublatitudinal strike of younger magnetoactive associations.

The examination indicates that the area of the Talysh-Vandam gravity maximum is highly inhomogeneous in terms of geological structure, and individual elements of the gravity maximum—anomalies of second order—reflect a different genesis in areas of Earth's crust and suggest that they developed apart from one another (Eppelbaum and Khesin 2011).

A visual example of 3D combined interactive modeling of gravity and magnetic fields along stakes 700–1350 of profiles 3–4 (see scheme presented in Fig. 5.24) is shown in Fig. 5.29. This profile crosses the Lesser Caucasus, the Middle Kur Depression and comes to an end at the submountainous zone of the Greater Caucasus. An initial ***PGM*** was constructed on the basis of drilling data, analysis of seismic data and petrophysical material as well as advanced examination of magnetic and gravity anomalies. An important role played here determined values of the Curie point depth and lower edges of magnetized bodies (see Table 7.1 in Chapter 7 of the present volume). It explains, for instance, comparatively not deep occurring of non-magnetic rocks in SW part of the investigated profile.

As it can be seen from this figure there is, despite the complex geological section, obtained a good agreement between the observed and computed magnetic and gravity fields.

Results of 3D combined interactive modeling along the profile A–B (profiles 10, 3, and 4)

Regional profile A–B (its location is shown in Fig. 5.24) is composed of three profiles (10, 3, and part of profile 4), starts near the town of Djulfa (Nakhchivan Autonomic Republic (AR) of Azerbaijan), crosses Armenian territory, subsequently traverses the Azerbaijanian territory, and ends near the town of Sheki (near the border with Georgia) (Fig. 5.30). It is the most important profile and this ***PGM*** will be described in detail.

In this ***PGM***, the decrease in the Earth's crust is observed within the Kur Depression. The surface of the "basaltic" layer displays the most uplift in the area of the core of the Lesser Caucasus mega-anticlinorium, where effusive formations of the pre-collisional stage are found.

The upper part of the geological section visually reflects the stages of geological formation in Azerbaijan. Orogenic granodiorite–porphyric and pre-orogenic gabbro–monzonite–diorite-intrusive formations developed in the beginning of the SW profile (Nakhchivan region); orogenic effusive dacite–andesite–basaltic formation are found—SE of the town of Istisu, and orogenic sedimentary deposits (molassa) in the Kur Depression, to a thickness of 4–5 km.

Associations of pre-orogenic effusive formations are present in: (1) the SW part of this profile where they occur on subplatform terrigenous–carbonate deposits, (2) in the transfer area from the Lesser Caucasus to the Kur Depression, and (3) in the southern slope of the Greater Caucasus immersion.

The syn- and post-collisional effusive formations are outcropped in the Lesser Caucasus in the middle part of profile. These formations create a so-called ophiolitic zone. Physical–geological modeling indicates that these formations can occur under young sedimentary deposits in the Kur Depression and under Lower–Middle-Jurassic sand–shale associations of the pre-collisional stage of the Greater Caucasus (where these formations were underthrusted as a result of tectonic processes).

In the Lesser Caucasus, there are presumed to be thick buried intrusives of post-collisional gabbro–diorite–granodiorite formations. Intrusives of these formations are usually metalliferous. Sedimentary deposits of the post-collisional stage are exposed in separate areas of the Lesser Caucasus and more widely present on the southern slopes of the Greater Caucasus.

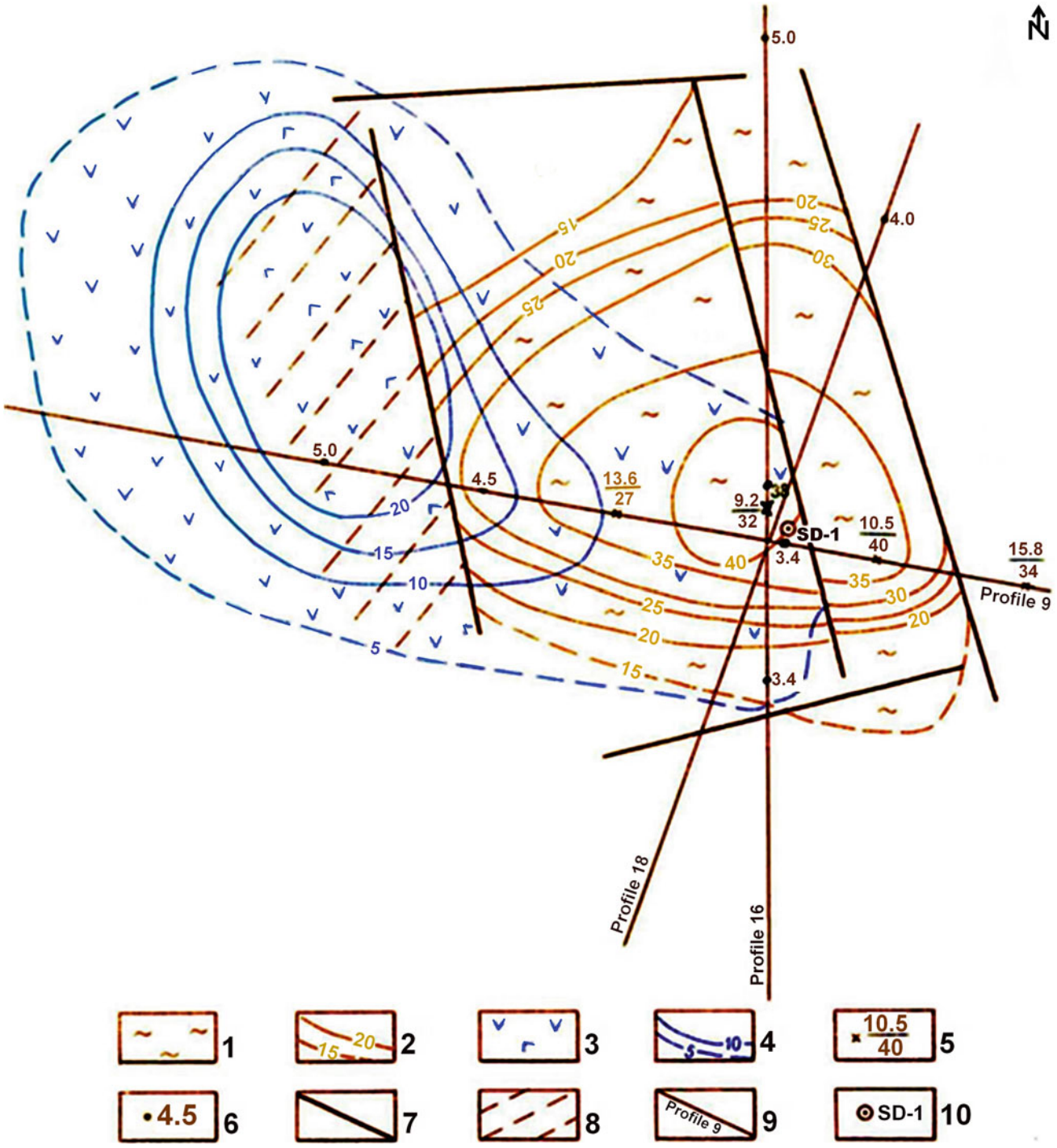

Fig. 5.27 Main elements in the 3D physical–geological model for the SD-1 area (the location of profiles 9, 16, and 18 is shown in Fig. 5.24) (Khesin and Eppelbaum 2007). (*1*) Pre-Baikalian (Ar_2-Pr_1?) rock associations of heightened density (initially mainly sedimentary), (*2*) total isopachs of Pre-Baikalian associations including Ar_2-Pr_1 (*solid line* is reliable, *dashed line* is proposed), (*3*) highly magnetized Mesozoic magmatic rocks of basic and intermediate composition, (*4*) isopachs (km) of Mesozoic magmatic rocks (*solid line*—reliable, *dash line*—proposed), (*5*) depth of occurrence (km) of roof (numerator) and lower boundary (denominator) of Ar_2-Pr_1 uplift, (*6*) depth of occurrence (km) of Mesozoic magmatic rocks, (*7*) major faults—boundary of blocks, (*8*) projection of root zone of basic magmatism, (*9*) interpretation profiles, and (*10*) SD-1 location

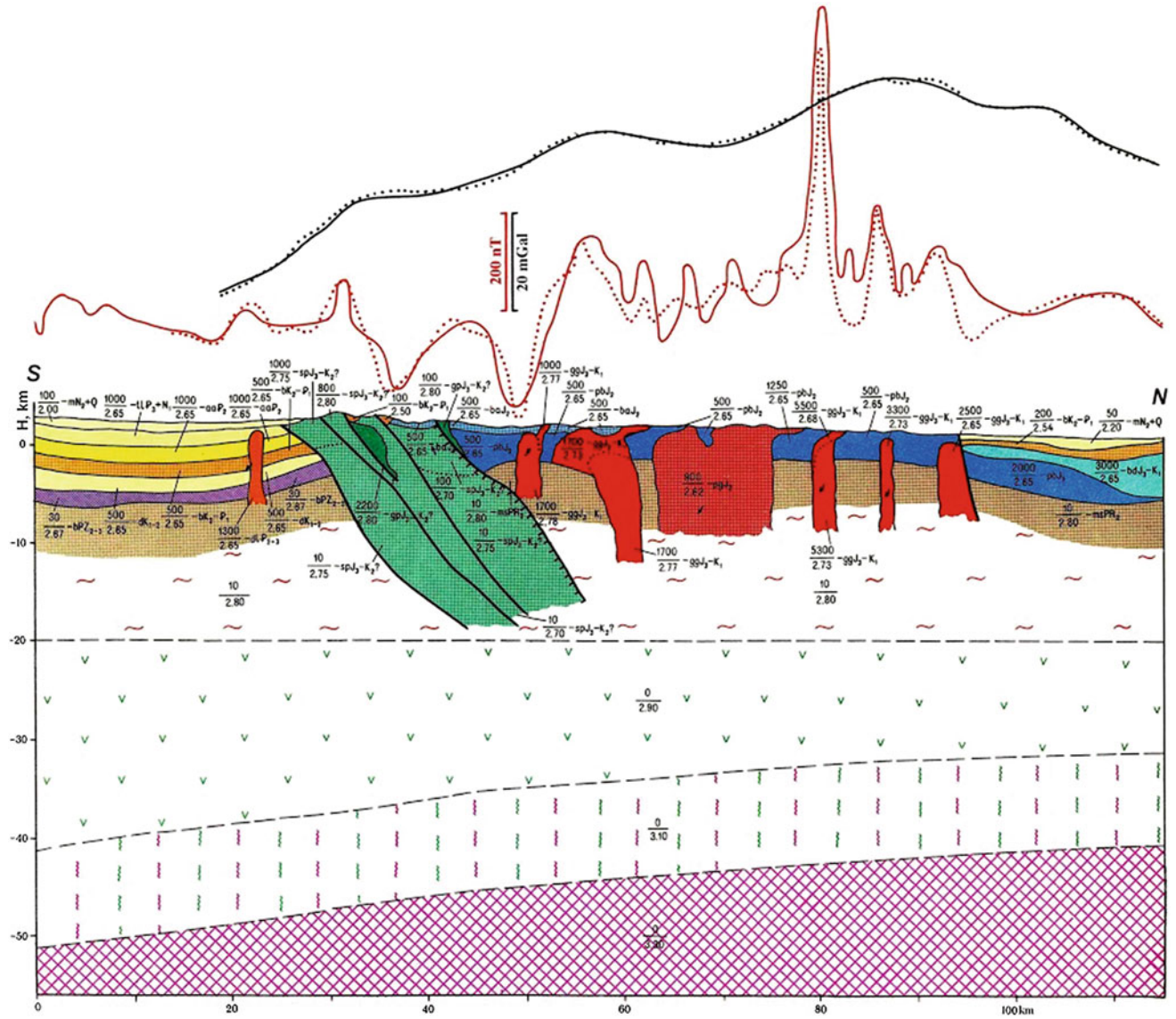

Fig. 5.28 3D modeling results along the profile 1 (location of this profile is shown in Fig. 5.24) (Eppelbaum and Khesin 2011)

Finally, effusive associations of the pre-collisional stage are (as was mentioned earlier) found in the core of the Lesser Caucasus mega-anticlinorium. The presence of these associations was predicted as well in the middle part of the Kur Depression below the syn- and post-collisional effusives. Pre-collisional sedimentary deposits exist in the Greater Caucasus, where their thickness attains 7–8 km.

Results of 3D combined interactive modeling along the profiles 2, 5, and 6

The pre-Alpine basement is closest to the Earth's surface in the vicinity of the ophiolitic zone, where it depth is only 1–1.5 km. Other physical–geological models have been developed. Profile 2 stretches along a line Lake Karagel-Dashkesan-Beyuk-Kasik (Fig. 5.31), profile 5—along a line Kutkashen-Shakhdagh Mt. - Chakh-Chakh village (Fig. 5.32), profile 6—Aghsu-Lagich-Gusar (Fig. 5.33). Profiles 7 and 8 (not presented in the book) stretch along the lines Kyalvazchay-Lerik-Jalilabad, and Shandankalasi Mt.-Masally, respectively.

The ***PGMs*** presented in models 1, 2, 5, and 6 show clearly fixed pre-collisional meganticlinorium's cores of the Lesser and Greater Caucasus with Jurassic associations. These associations are identified in the Lesser Caucasus as effusive basaltic–andesite–plagioliparite and basaltic–andesite formations, and in the Greater Caucasus–Lower–Middle Jurassic as sand–shale associations. The surface of

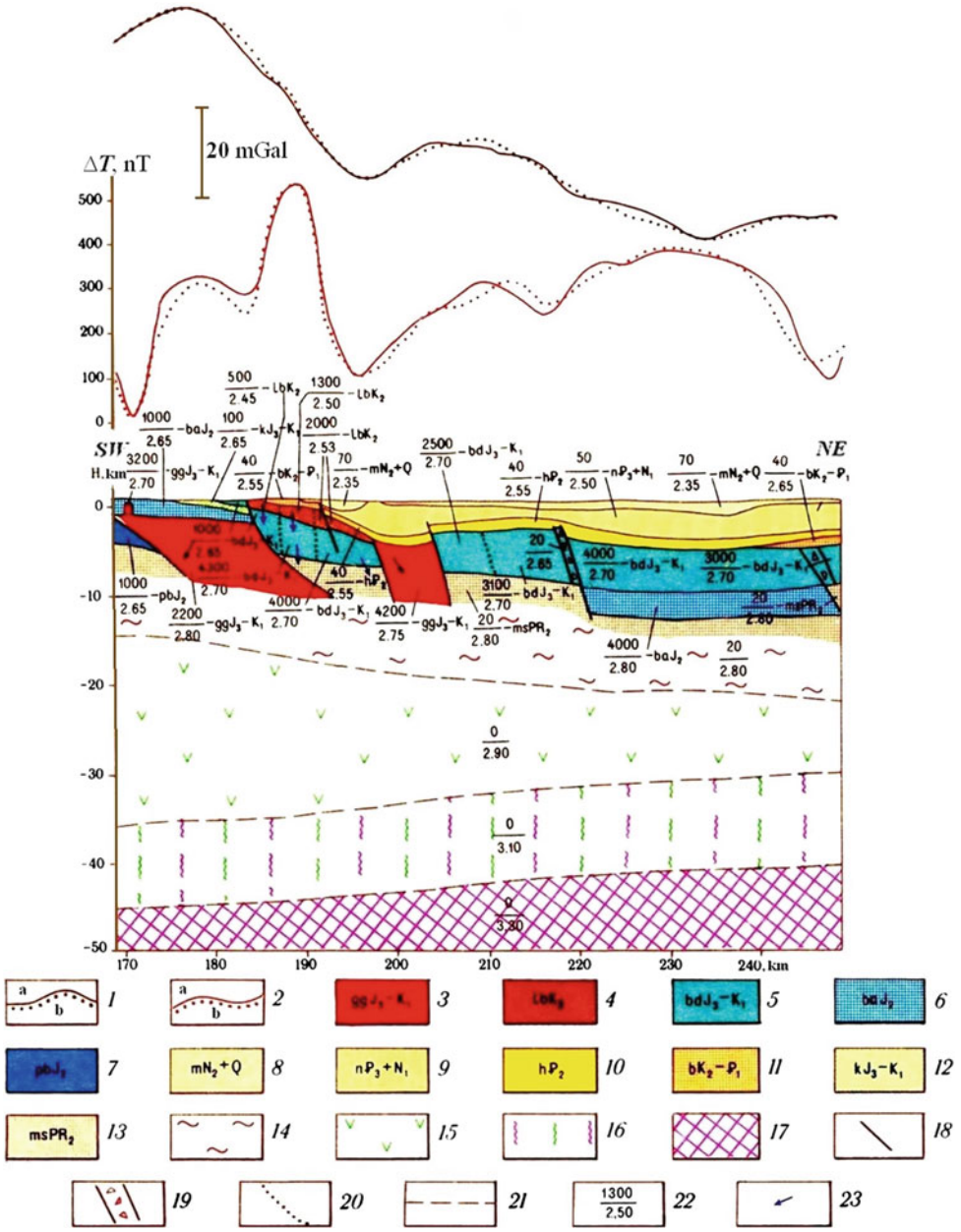

Fig. 5.29 Construction of a physical–geological model (for stakes 700–1350 of profiles 3–4; location of profiles is shown in Fig. 5.24) (after Khesin et al. 1996). (*1*) gravity field Δg_B: *a*—observed, *b*—computed; (*2*) magnetic field ΔT: *a*—observed, *b*—computed; (*3*) intrusive gabbro–diorite–granodiorite association; (*4–6*) effusive associations: (*4*) liparite–basaltic; (*5*) basalt–andesite–dacitic; (*6*) basalt–andesitic; (*7*) basalt–andesite–plagioliparitic; (*8–13*) background sedimentary deposits: (*8*) upper molassic; (*9*) lower molassic; (*10*) terrigenous; (*11*) terrigenous–carbonaceous, in some places flyschoid; (*12*) carbonaceous–sandy, reef rocks; (*13*) metamorphic schists and other metamorphites; (*14–16*) deep-seated complexes: (*14*) granites and gneisses, in some places amphibolites; (*15*) basic rocks; (*16*) basic rocks; (*17*) uppermantle peridotites; (*18*) faults, upthrusts; (*19*) crush zones; (*20*) boundaries of physical properties changing within the same geological association; (*21*) boundaries of physical properties changing along all geological section; (*22*) physical properties (numerator = magnetization, mA/m, denominator = density, g/cm^3); and (*23*) direction of the magnetization vector other than the averaged geomagnetic field inclination for the region

the Pre-Alpine foundation occupies the highest position in these cores.

The syn- and post-collisional effusive formations in the ***PGMs*** 1 and 2 (Lesser Caucasus), as in the ***PGM*** along line A–B, compose an ophiolitic zone. It is presumed that the same formations occur in the NE submersion of the Lesser Caucasus. In ***PGMs*** 5 and 6 (Greater Caucasus), their wide evolution can be predicted by the results of 3D combined gravity–magnetic modeling under the pre-collisional Lower–Middle-Jurassic sand–shale deposits of the Greater Caucasus (occupying this position as a result of overthrust), as well as under young deposits of the Kur Depression.

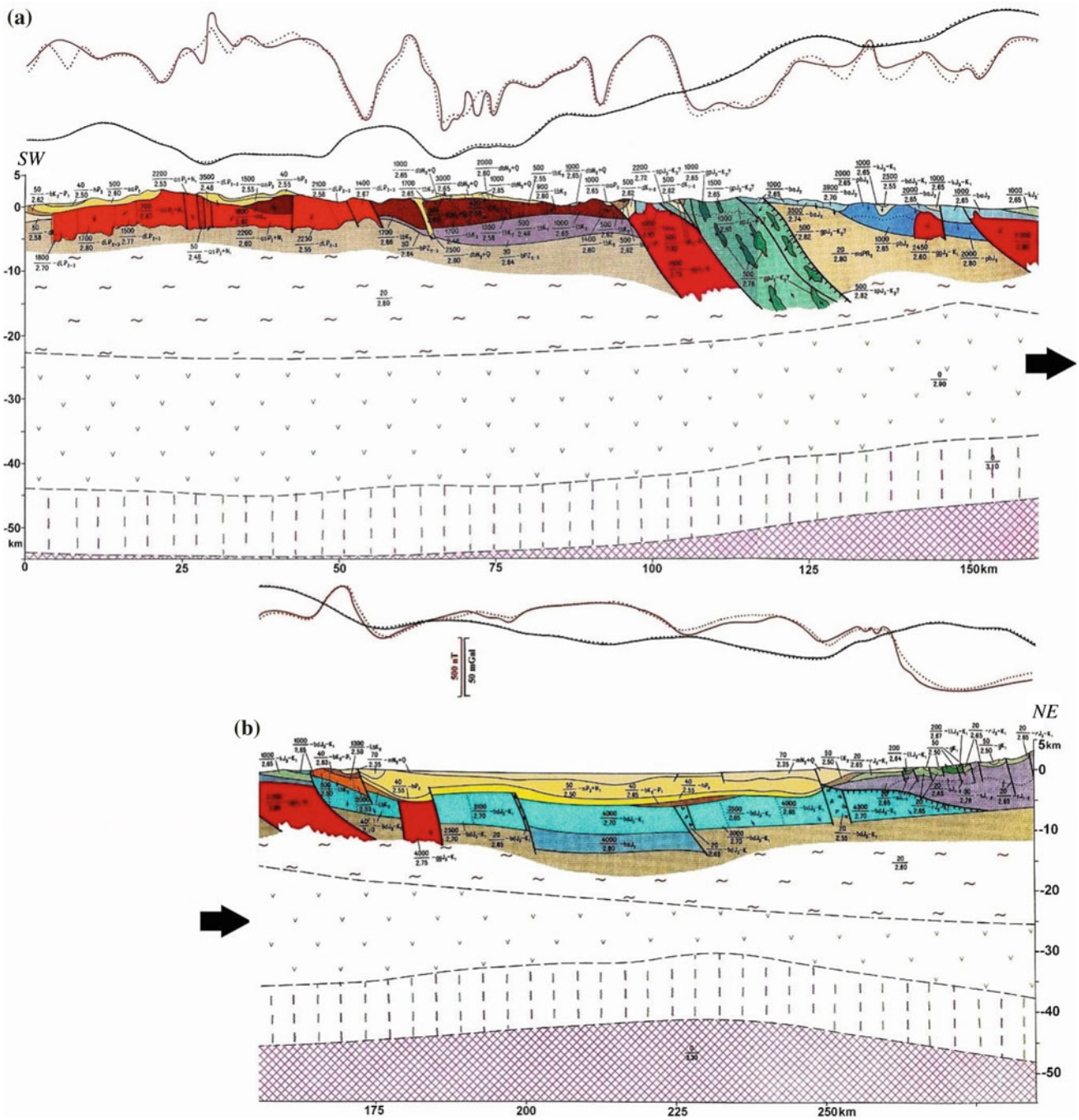

Fig. 5.30 Three-dimensional modeling results along the profile A–B (location of the profile is shown in Fig. 5.24) (Eppelbaum and Khesin 2011)

Pre-orogenic and orogenic intrusive and effusive formations are located in the southern parts of ***PGMs*** 1 and 2. Sedimentary deposits of these stages developed in the northern parts of profiles 1 and 2, and in southern and northern parts of profiles 5 and 6.

In the northern parts of profiles 5 and 6 at a depth of 9–10 km are associations of significant magnetization, presumably related to tuff–terrigenous subplatform associations of the Middle–Late Paleozoic.

The behavior of the Moho discontinuity in the aforementioned ***PGMs*** on the whole agrees with the ***PGM*** along direction A–B. In ***PGMs*** 1 and 2 a smooth uplift of the Moho discontinuity can be observed from south to north at the depth of −52–54 km up to −42 km. In the ***PGMs*** 5 and 6, its behavior is more complex: In ***PGM*** 5 (from SE to NW), there is an uplift from −44 to −41 km (under the area of the abovementioned overthrust), then submersion to a depth of −58 km (below the area of conjunction of

Fig. 5.31 Three-dimensional modeling results along the profile 2 (location of the profile is shown in Fig. 5.24) (Eppelbaum and Khesin 2011)

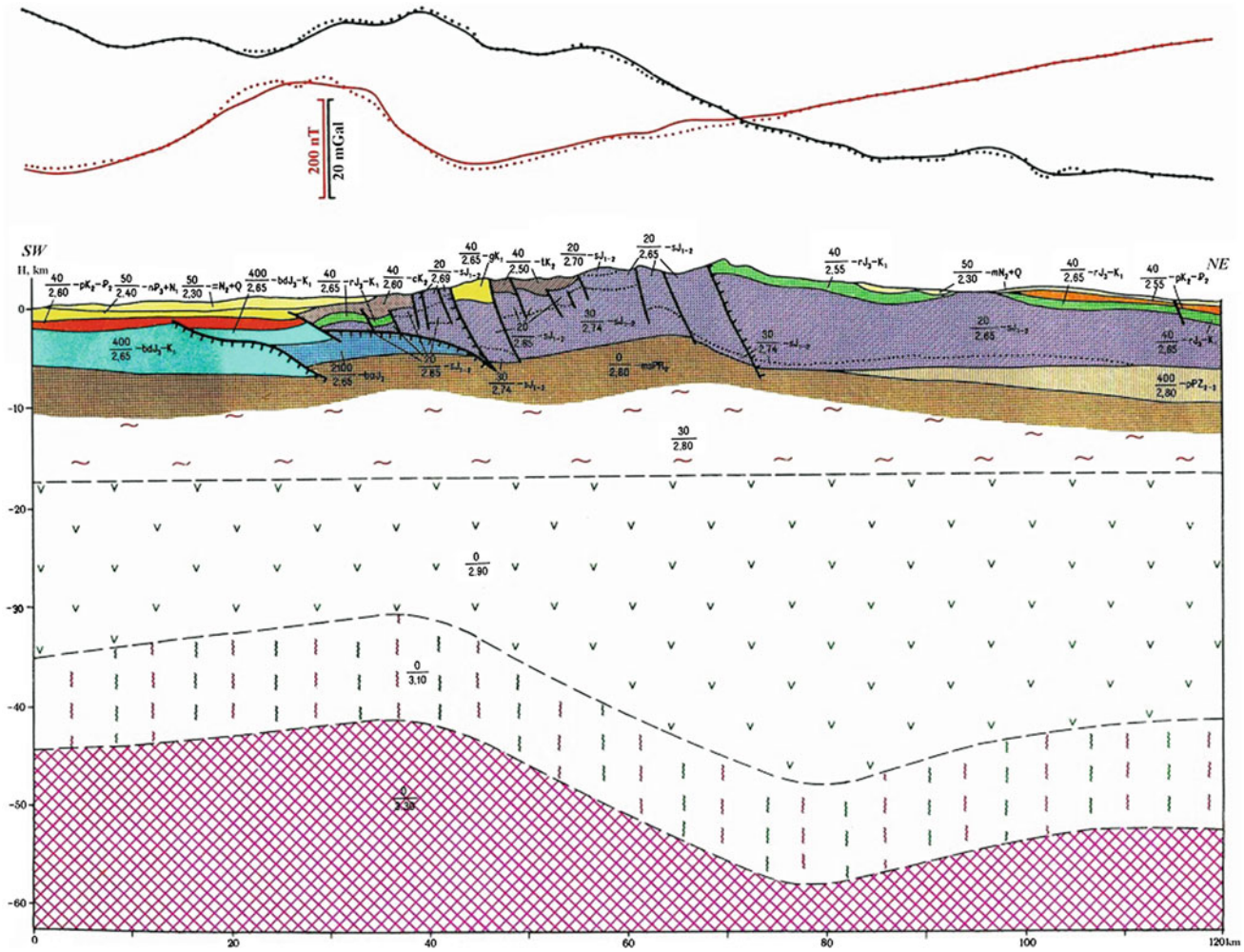

Fig. 5.32 Three-dimensional modeling results along the profile 5 (location of the profile is shown in Fig. 5.24) (Khesin and Eppelbaum 2007)

anticlinoria of the Main Ridge and Side Ridge) and then an uplift to a value of −52 km; in the ***PGM*** 6 (from north to south), there is a stepped submersion from a depth of −47 to −60 km (under the same conjunction area) and then a smooth uplift to a depth of −58 km.

An interesting peculiarity of the southern part of ***PGM*** 2 is the presence of a zone of strong rock decompaction in the root parts of the Dalidagh intrusive massif with values from −4 to −17 km and a horizontal thickness of 30 km. This decompaction zone produces the greatest Kelbadzhar-Dalidagh gravity minimum. This large "granite room" apparently was a source of pre-orogenic and orogenic granitoid magmatism.

PGM 7 and 8 are located in the Talysh geostructural zone (see scheme in Fig. 5.24). There is a Moho uplift from south to north (from −52 to −42 km and from −44 to −31 km, respectively) and as well as to the east (on the side of the Caspian Sea).

Within the Talysh zone, buried intrusive bodies from ultrabasic to acid consistency were delineated. Applying 3D gravity–magnetic modeling, surface trachite–trachiandesite–trachibasalt effusive formations that are widely present at the surface were divided into blocks of differing magnetization and (or) density. These blocks, apparently, have tectonic contacts. The bodies of gabbro–syenitic and gabbro–monzonite–diorite formation were characterized quantitatively.

Captions for the physical-geological models

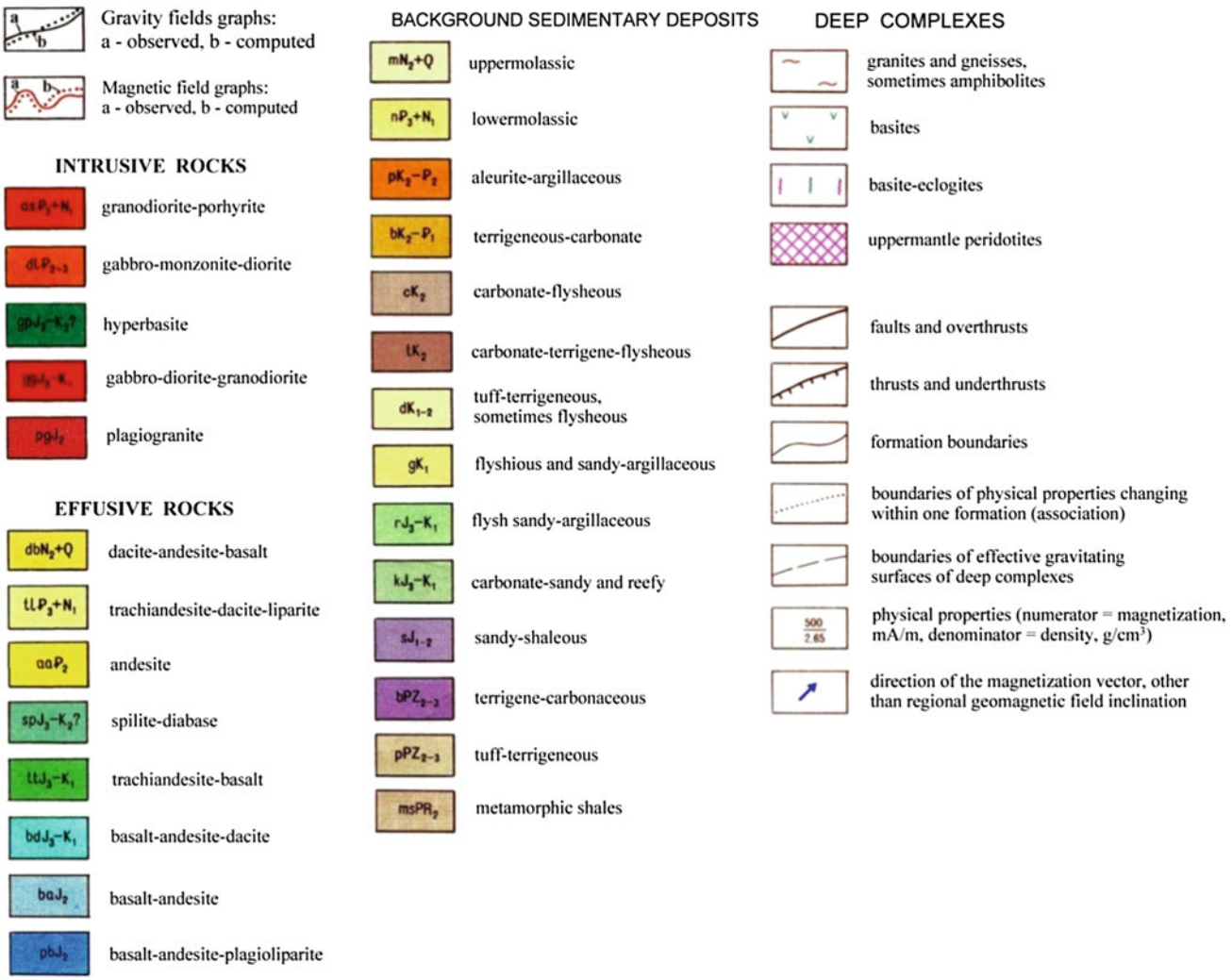

5.3 Azerbaijan: South Caspian Basin

5.3.1 Seismic Data Analysis

The South Caspian basin (SCB) occurs within intra-continental settings, but is poorly understood in terms of the mechanisms that have controlled their subsidence history (Fig. 5.34), with a depth to basement exceeds 20 km (Shikhalibeyli and Grigoriants 1980; Brunet et al. 2003; Egan et al. 2009; Abdullayev et al. 2015). Despite the fact that it is widely accepted that the SCB was initiated by Mesozoic back-arc extension related to the subduction of the Tethys Plate (e.g., Zonenshain and Le Pichon 1986), more than half of the 20 km subsidence presently observed occurred within the tectonic framework of the evolution of the Alpine-Himalayan tectonic belt (Egan et al. 2009).

Analysis of physical-geological section presented in Fig. 5.35 indicates that the depth to the Moho discontinuity varies from about 60 km, beneath the onshore South Caspian region, to approximately 30 km beneath the deepest part of the SCB. Based on seismic velocity data, it has been suggested that the 'granitic' crustal layer is absent in the central part of the basin (Mangino and Priestley 1998). This could be because the crust is of oceanic origin, although it is thicker than normal oceanic crust. Another appropriate model suggests that it could be continental crust of which the upper section has been removed by erosion or faulting, or it could be thinned and intruded continental crust (Egan et al. 2009). Zonenshain and

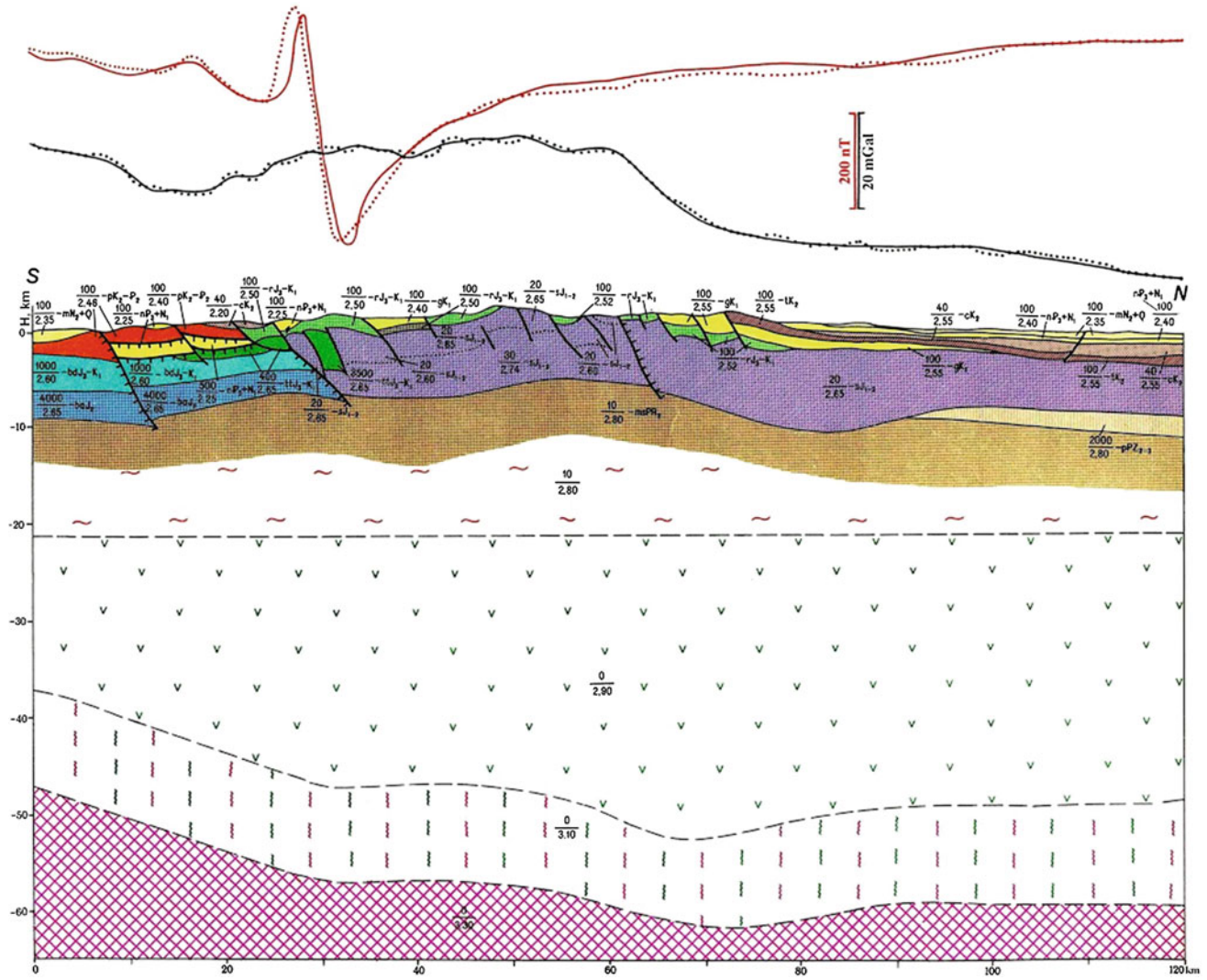

Fig. 5.33 Three-dimensional modeling results along the profile 6 (location of the profile is shown in Fig. 5.24) (Khesin et al. 1996)

Le Pichon (1986) proposed that the crust beneath the SCB is of continental origin but has been subjected to high pressures and high temperatures, such that the granite rocks of the continental basement were metamorphosed to become eclogite. From earthquake studies the SCB crust appears to be a relatively rigid and aseismic block within the framework of the Alpine-Himalayan orogenic belt (Priestley et al. 1994), which is further evidence for a rheological difference between the crust of the SCB and that of the surrounding region (Mangino and Priestley 1998; Egan et al. 2009).

It should be noted that Mamedov's (2008) seismogeological profile (SW–NE orientation) (Fig. 5.36) is a basis for many tectonic and geophysical reconstructions. Depth of Moho discontinuity in the SCB central part also is found about 30 km.

More detailed seismic time section is presented in Chap. 5 of Volume I (see Fig. 5.38a in Chapter 5). Analysis of this section indicates that Caspian Sea level lowering on the Jurassic and Cretaceous boundaries confirmed by the shore line displacement to south and southwest that caused a deposition of terrigene sediments on the shelf area.

Figure 5.37 shows time section along the submeridional profile in the South Caspian basin. In this section, consolidated crust is characterized by thickness of 8–10 km, and it is fluently submerses to side of the Turan Platform. According to Mamedov (2004), interpretation in the area of Absheron ridge over the consolidated crust is observed a tectonic congestion of Mesozoic and Palaeogene strata similar to accretional prism image in subduction zones.

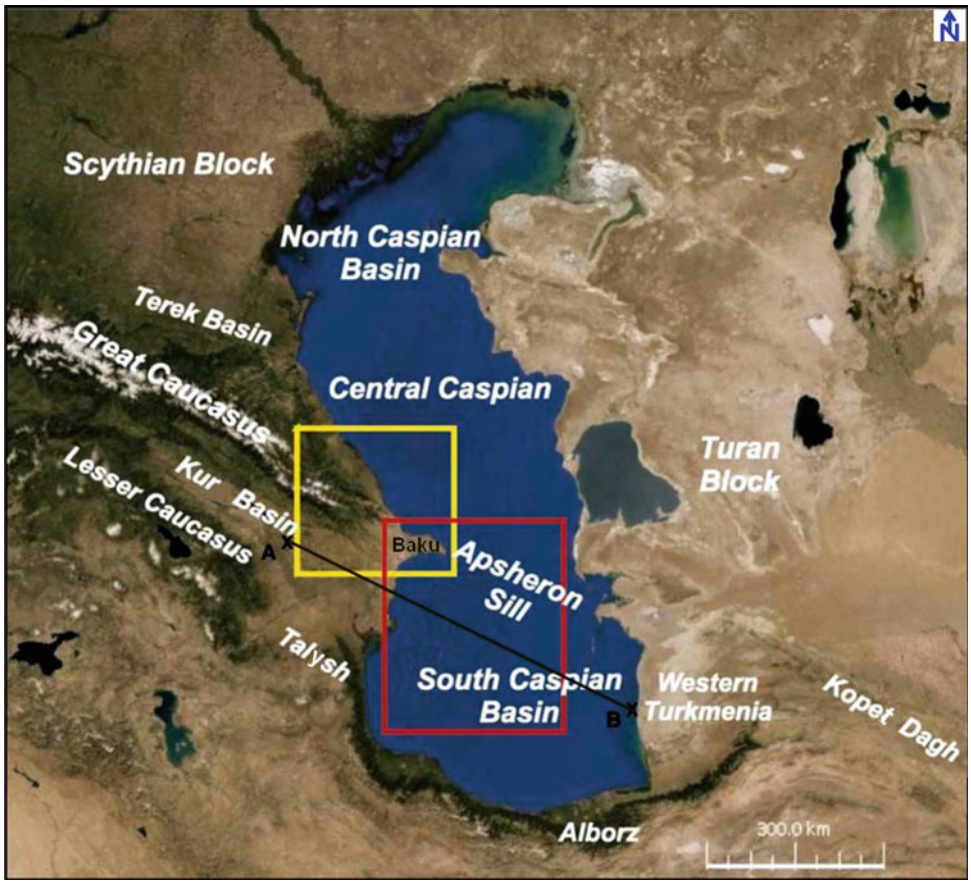

Fig. 5.34 Map of SCB and surrounding regions showing general location of onshore (*yellow box*) and offshore (*red box*) study areas (background image courtesy of NASA World Wind). Points A and B and *black line* designate position of investigated profile (after Egan et al. (2009), with small modifications)

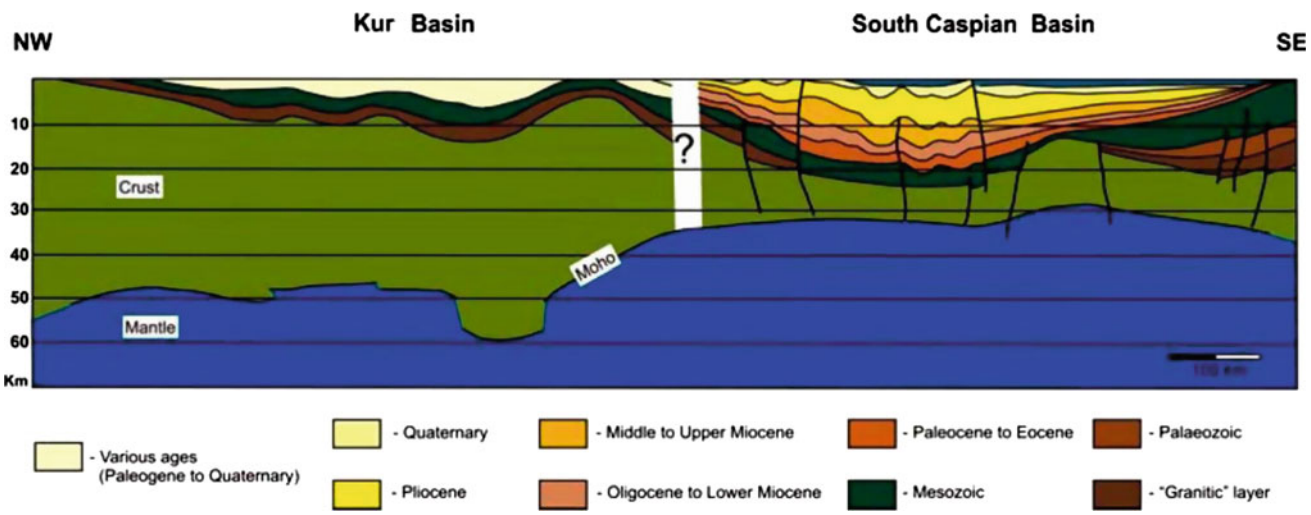

Fig. 5.35 Regional crustal-scale cross section through the Kur and South Caspian basins (Egan et al. (2009) adapted seismic constructions of Baranova et al. (1991) and Mamedov (1992)

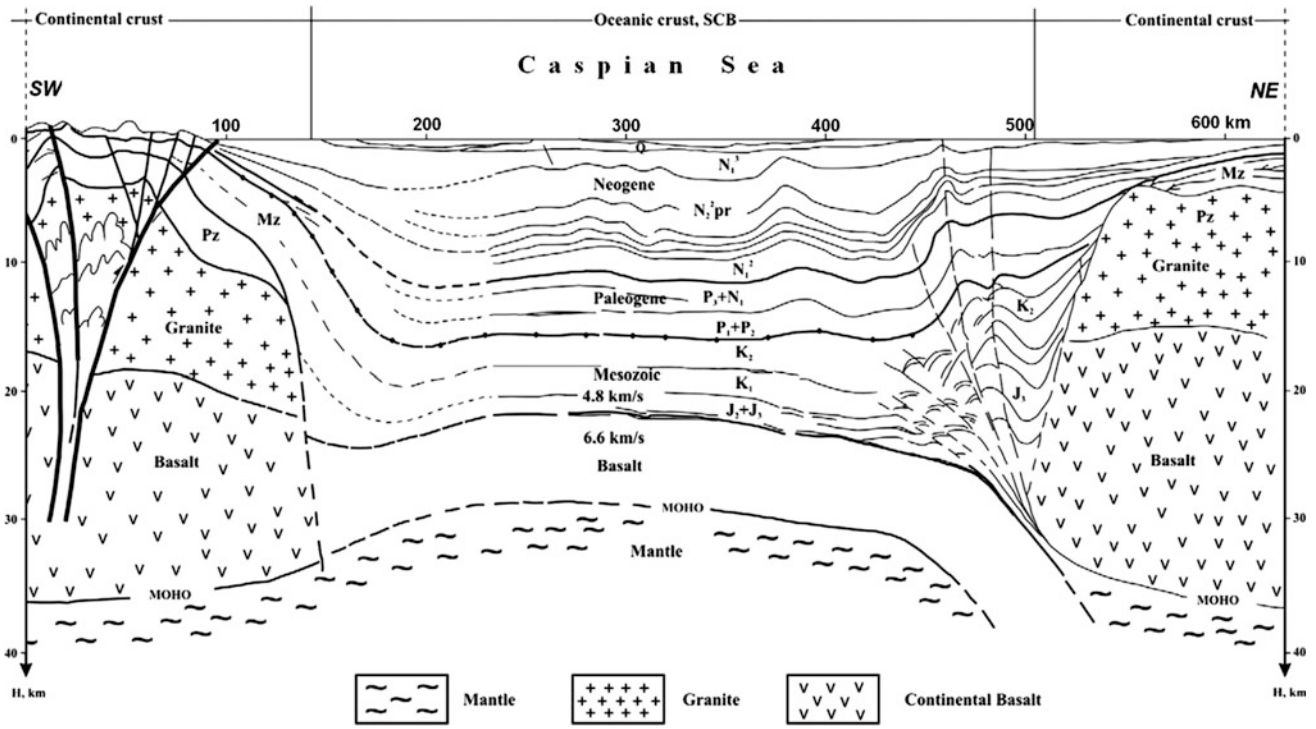

Fig. 5.36 The seismic–geologic cross section along a regional profile from the Alborz (SW) to the Absheron Sill (NE) (after Mamedov 2008)

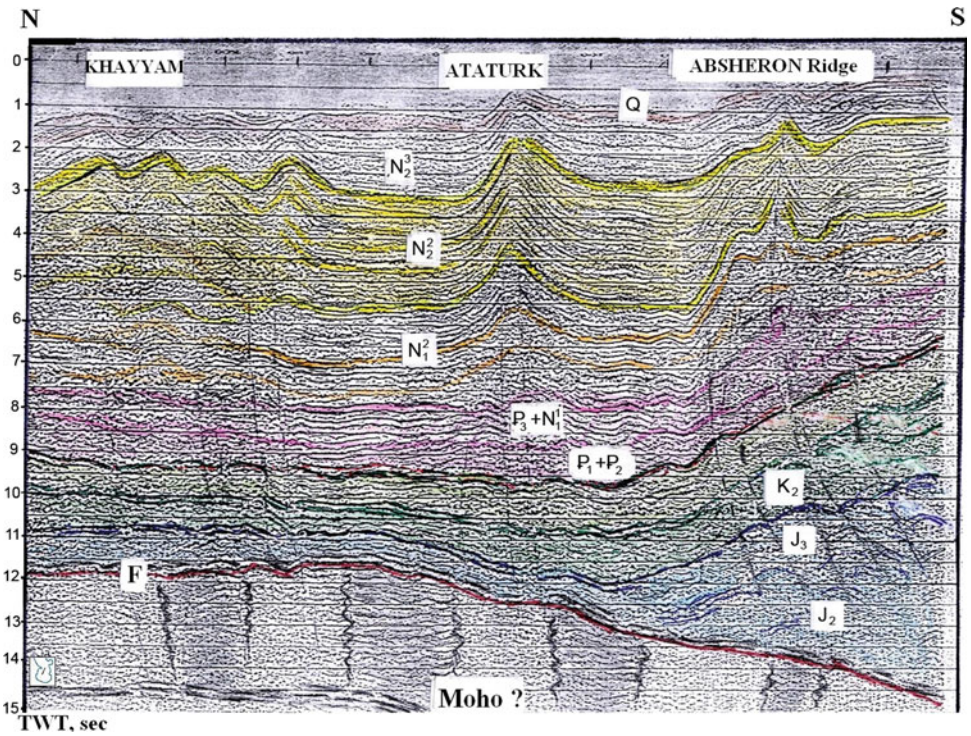

Fig. 5.37 Seismic time section of the profile crossing western part of the SCB (after Mamedov 2004). 'F' designates a top of crystallic basement

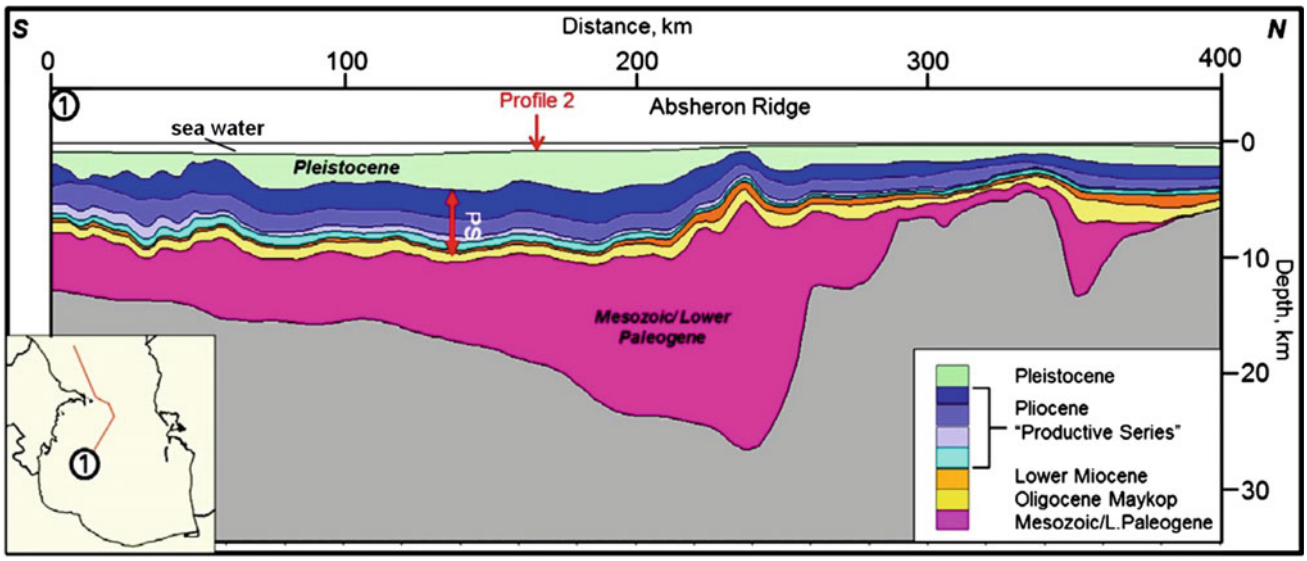

Fig. 5.38 Geoseismic profile 1 through the SCB and the Absheron ridge showing the variable thicknesses across the profile (Abdullayev et al. 2015)

An effective seismic model was presented by Abdullayev et al. (2015) (Fig. 5.38). This profile runs approximately north–south and is built up of available surface sets of various 2D reflection seismic profiles, some of which are ultradeep 2D TWT profiles. It is broadly similar to the profile modeled in Green et al. (2009) but differs by being constructed to avoid structurally complex parts of the Absheron ridge. The model consists of nine layers, corresponding to seismically mappable intervals covering the Jurassic to the present (Fig. 5.38). A portion of the profile, north of the Absheron ridge, represents continental crust of the SCB, while the southern portion is located over the SCB crust. The profile is characterized by an increase in thickness, from south to north, in the SCB portion of Mesozoic–Lower Palaeogene age. The full profile was subjected to a restoration with 'FlexDecomp' software initially with constant β-factors, based on the assumption of changing crustal types across the profile. The northern portion of the profile includes significant crustal shortening under the Absheron ridge and cannot be confidently restored using this methodology.

Abdullayev et al. (2015) on the basis of analysis of reflection seismic and some other data have developed a map of depth to the crystallic basement (Fig. 5.39).

5.3.2 Gravity Field Analysis

The main structural elements of the SCB are illustrated in Fig. 5.40. The central part of the basin, unlike its periphery, is practically aseismic with earthquakes primarily confined to the borders (Ambraseys and Melville 1982; Priestley et al. 1994; Mangino and Priestley 1998; Jackson et al. 2002; Ulomov 2003). Despite the observed, extremely low values of heat flow in the SCB, some small areas of higher flow are likely related to the activity of mud volcanoes (Yakubov et al. 1971; Mukhtarov 2004).

Recently, new seismic data have been acquired providing new constraints on basin structure and formation history. However, as a whole, the problem of the origin of the basin as a unified structure (Artyushkov 1993, 2007; Khain 2005) and assumptions about the subduction of lithosphere of the South Caspian underneath the mid-Caspian (Khalilov et al. 1987; Allen et al. 2003; Knapp et al. 2004; Granath et al. 2000; Mamedov 2008; Egan et al. 2009; Green et al. 2009) still remain disputable. The purpose of this study has been to propose a crustal model and describe some characteristic of the crustal structure of the SCB along a regional profile from the Alborz to the Absheron Sill, integrating available seismic data with the Bouguer gravity anomaly along the profile. The analysis of deep structure along the selected profile has been combined with an analysis of earthquake focal mechanisms and GPS velocity data to evaluate the active tectonics and geodynamic evolution of the basin.

Tectonic–structural scheme of the SCB region and its surrounding is of high complexity. Its generalization is presented in Fig. 5.40 where line of the investigated profile A–A is shown.

A new map of the Bouguer gravity field of the SCB has been developed by Kadirov and Gadirov (2014) on the basis of Dehghani and Makris (1983), Gravity map of the USSR (1990), Kadirov (2000b) (Fig. 5.41).

The gravity field is characterized by anomalies of various geometries and amplitudes. The anomaly field of the northern part of the basin is represented by the area of

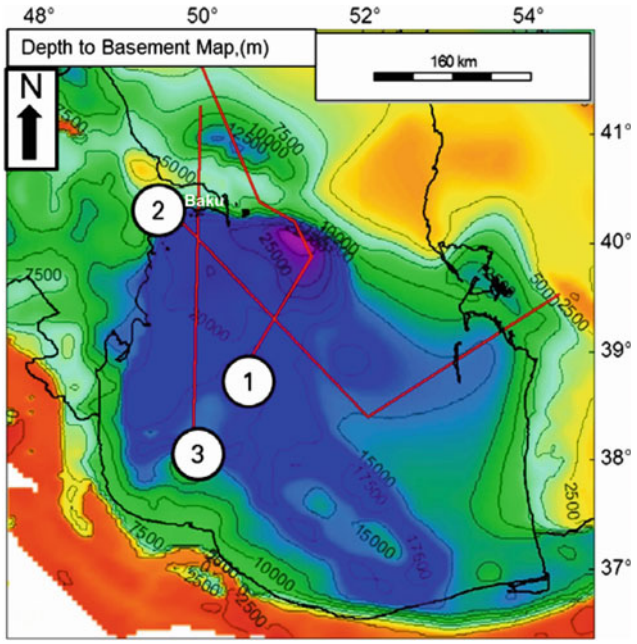

Fig. 5.39 Depth to basement map integrating reflection seismic and published data (Glumov et al. 2004; Abdullayev et al. 2015)

increased horizontal gradients subparallel to the strike of the Caucasus. In the northwestern part of the SCB, there is a vast gravity minimum with amplitude reaching 125 mGal. The central part of the basin is represented by a gravity minimum and by an isometric maximum of the gravity field in the southwest and in the southeast (Safidrud and Godin uplift). The area of increased gradients from the Alborz Mountains to the south up to the deepwater part of the basin is typical for the southern part of the SCB. The area of the Central Alborz is characterized by a negative anomaly (−120 mGal).

A model profile has been generated, which extends for almost 650 km from southwest Central Alborz range toward the northeast in the mid-Caspian (see Fig. 5.40). The initial model has been created by Mamedov (2008) and, later, utilized in models of Brunet et al. (2003) on the basis of the recent ultradeep 20-s TWT cross sections integrated with published data on deep seismic sounding and earthquake analysis (Aksenovich et al. 1962; Baranova et al. 1991; Allen et al. 2003; Jackson et al. 2002; Brunet et al. 2003; Knapp et al. 2004; Babayev and Gadjiev 2006).

The density values used in our model for the crust and upper mantle were selected from published data, while the mantle density was set at 3300 kg/m^3. The developed initial model demonstrated that there was a sequence of zones with excessive mass (0–62 km and 220–500 km) along the profile. Calculated values of the gravity field from the initial geological and geophysical models did not explain well the observed gravity field. The largest discrepancies appeared to be in the intervals of 10–65 km (54 mGal-100 mGal), 260–485 km (40–55 mGal), and 605–630 km (35–54 mGal). For compensation of the observed gravity field, a selection of density boundaries (upper boundary of "basaltic" layer of oceanic and continental crust and Moho surface) was conducted until providing the least discrepancy between the observed and selected values of the gravity field. The final gravity model, topography, and observed and calculated Bouguer gravity anomaly along the studied profile are demonstrated in Fig. 5.42. There is a general correlation between the geometry of layers' boundaries and topography along the profile, namely the boundary between the Neogene and Paleogene and the boundary between the Paleogene and Mesozoic.

The best-fit new model (Fig. 5.42) introduces a dense "basaltic"-type crust boundary only 6 km thick in places close to Absheron Sill (location about 480 km) and draws it as downgoing below the Absheron Sill, therefore suppressing the crust–mantle boundary. Isostatic compensation in this model therefore will occur in the mantle. Unlike previous models of Granath et al. (2000), thickness of this thin dense crust is not kept constant, but is variable, and increases to 10–12 km to the south around in the middle of SCB. Best fit also substitutes very thick sediment pile from the Mesozoic wedge by upper crustal "granitic layer," which also supported by seismic observations. Our best-fit basement surface is taken to be a deepest interpreted seismic reflector in Green et al. (2009), which is generally shallower than in the initial model by about 5 km across all of the profile and ranges between 16 and 20 km. Our best-fit model also puts maximum depth to sediments layer underneath Absheron Sill to about 22–25 km as opposed to 30 km from some places in the initial model.

Modeled "bending" of the oceanic crust, in both initial and best-fit models, can explain large gravity north of 480 km. Values of gravity without less dense downgoing slab and thickened continental crust north of Absheron Sill will not achieve a fit and therefore may be less reasonable.

The thickness of the Mesozoic layers in the middle part of the profile is ∼8 km, which increases northward reaching the peak value (∼20 km) in the Absheron-Pribalkhan Sill rather stays than constant as in Granath et al. (2000). Subduction underneath the Absheron-Pribalkhan Sill is accompanied by the sliding of the sediments from the basaltic layer, forming accretionary wedge, which can be observed on ultradeep seismic profiles (Knapp et al. 2004) and some of the increased thickness is clearly the result of shortening.

Green et al. (2009) also state, that while, some of the anomalous thickening is a result of shortening, especially close to the Absheron Sill, a geographically larger part of the thick is believed by to be original feature. This feature according to authors is caused by Mesozoic rifting followed by thermal subsidence and sediment loading in the post-rift phase following the formation of the basin in Late Jurassic. Forward lithosperic modeling performed by Green et al.

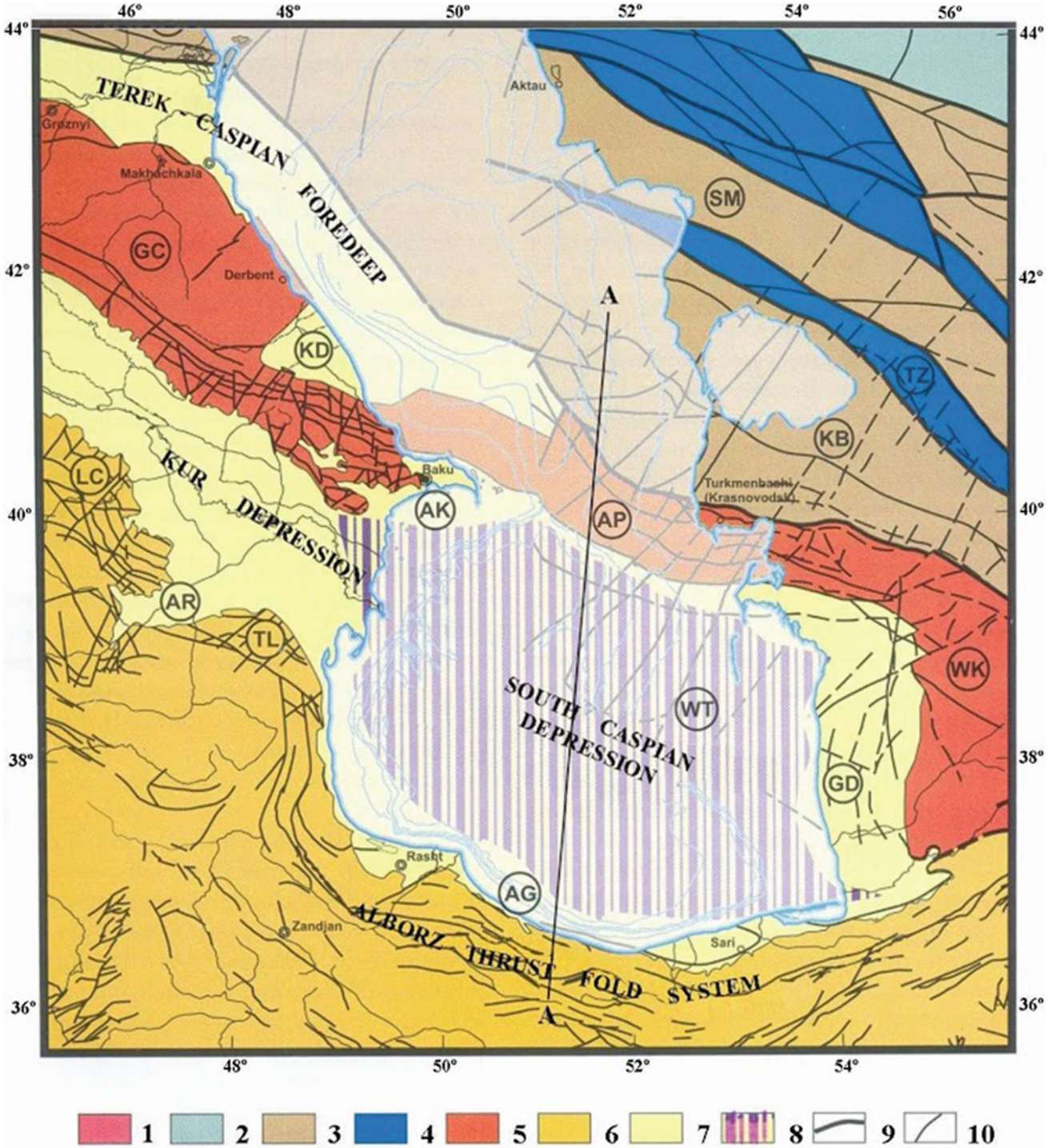

Fig. 5.40 Major structural elements of the SCB (on the basis of Khain 2005). The basement of platform areas (1–4): (*1*) Early Precambrian, (*2*) Baikalian, (*3*) Hercynian, (*4*) Early Cimmerian; the Alpine folding-cover systems (*5*, *6*): (*5*) Greater Caucasus and Kopetdagh, (*6*) Lesser Caucasus, Talysh, Alborz; (*7*) foredeeps and troughs; (*8*) troughs with a crust of an oceanic type; (*9*) fault corresponding borders of large structures; and (*10*) other relevant faults. The major structures (letters in circles): TZ—Tuarkyr zone, KB—Middle-Caspian-Karabogaz anteclise, KD—Gusar-Devechi trough, AK—Absheron-Kobustan trough, AP—Absheron-Pribalkhan Sill, WK—West Kopetdagh zone, LC—fold system of the Lesser Caucasus, AR—Lower-Aras flexure, TL—Talysh zone, AG—Alborz-Gogran foredeep, WT—west Turkmen trough, GD—Gogran Dagh-Okarem zone, GC—Greater Caucasus folds system, SM—South Mangyshlak-Ustyurt system of troughs; AA—Location of profile forming the basis of this research investigation (after Kadirov and Gadirov 2014)

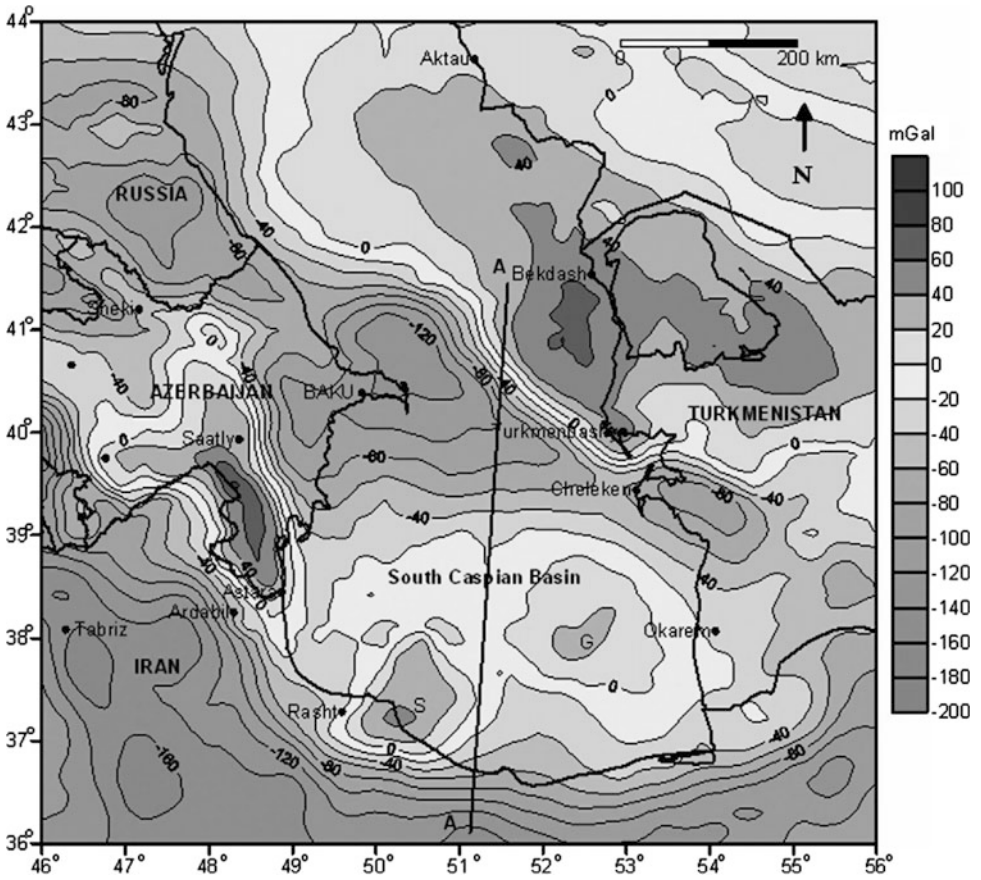

Fig. 5.41 Map of Bouguer gravity anomalies of the SCB; S—Safidrud uplift, G—Godin uplift (after Kadirov and Gadirov 2014)

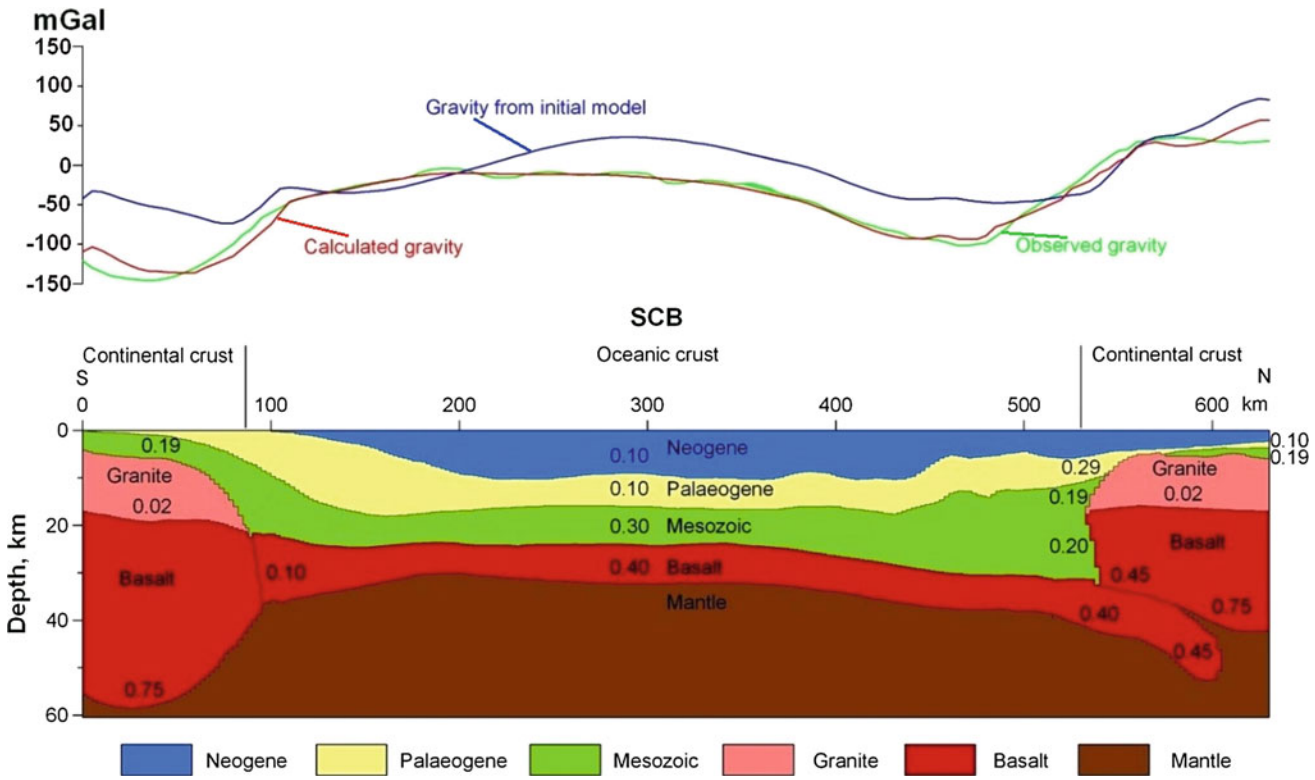

Fig. 5.42 Gravity model and topography along meridional profile Alborz-Absheron Sill. The values of density differences are in g/cm^3 (after Kadirov and Gadirov 2014)

(2009) also supports existence of thin (6 km) oceanic crust with high values of stretching β-factor south of Absheron Sill, increasing in thickness to the south. This crustal variation has been modeled in Fig. 5.42 to achieve the best fit.

There are of course other possible combination of densities and depths to achieve the best fit; however, the proposed crustal model for is supported by modeling and observation from Green et al. (2009) and better describes a geological scenario than initial model.

The gravity model matches the observed gravity field of profile 1 (Fig. 5.43b), which supports the presence of denser, 'oceanic-type' crust (5–7 km) underneath the northern portion of the SCB, below and to the north of the Absheron ridge. This gravity observation is also well supported by reflection seismic and earthquake observations (Kadirov et al. 2008; Kadirov and Gadirov 2014). This area corresponds to large negative Bouguer anomaly (Fig. 5.43a) and is best modeled as a root of South Caspian crust that has displaced the normal lithospheric mantle, creating a large isostatic anomaly, as shown in Granath et al. (2000).

The southern part of the profile has a very small negative Bouguer anomaly and can be modeled with thicker (+10 km) and less dense crust (we used lower continental crust densities of 2800 kg/m^3). The values of the Bouguer gravity field slowly increase toward positive values, south of the SCB.

5.3.3 Magnetic Field Analysis

The SCB as a whole is characterized by a smoothed positive magnetic field intensity which decreases to the south along the common abrupt subsidence of the surface of crustal basement and a sharp increase in sedimentary Mesozoic–Cenozoic complexes. In the western part of the SCB (area of the Baku archipelago), there are a large number of local positive and negative anomalies of small intensity (up to 100 nT) reflecting geological peculiarities of the sedimentary association structure (Fig. 5.44).

The geological nature of the regional magnetic maximum in the central part of the SCB is still being debated.

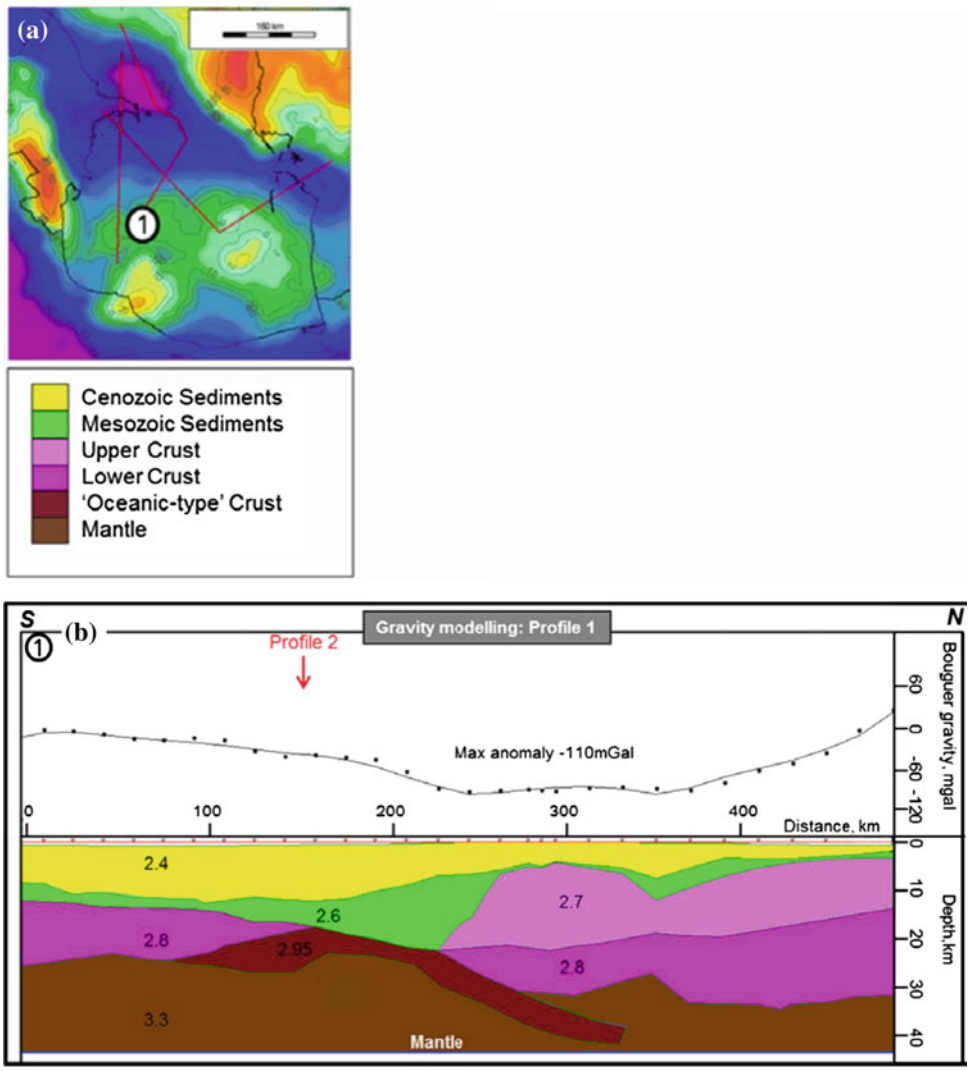

Fig. 5.43 Gravity map in the Bouguer reduction of the SCB and surrounding areas (**a**) (after Kadirov and Gadirov 2014) and gravity modeling results of profile 1 (**b**) showing the observed (*dotted line*) and modeled (*solid line*) Bouguer gravity anomaly (after Abdullayev et al. 2015, with small modifications)

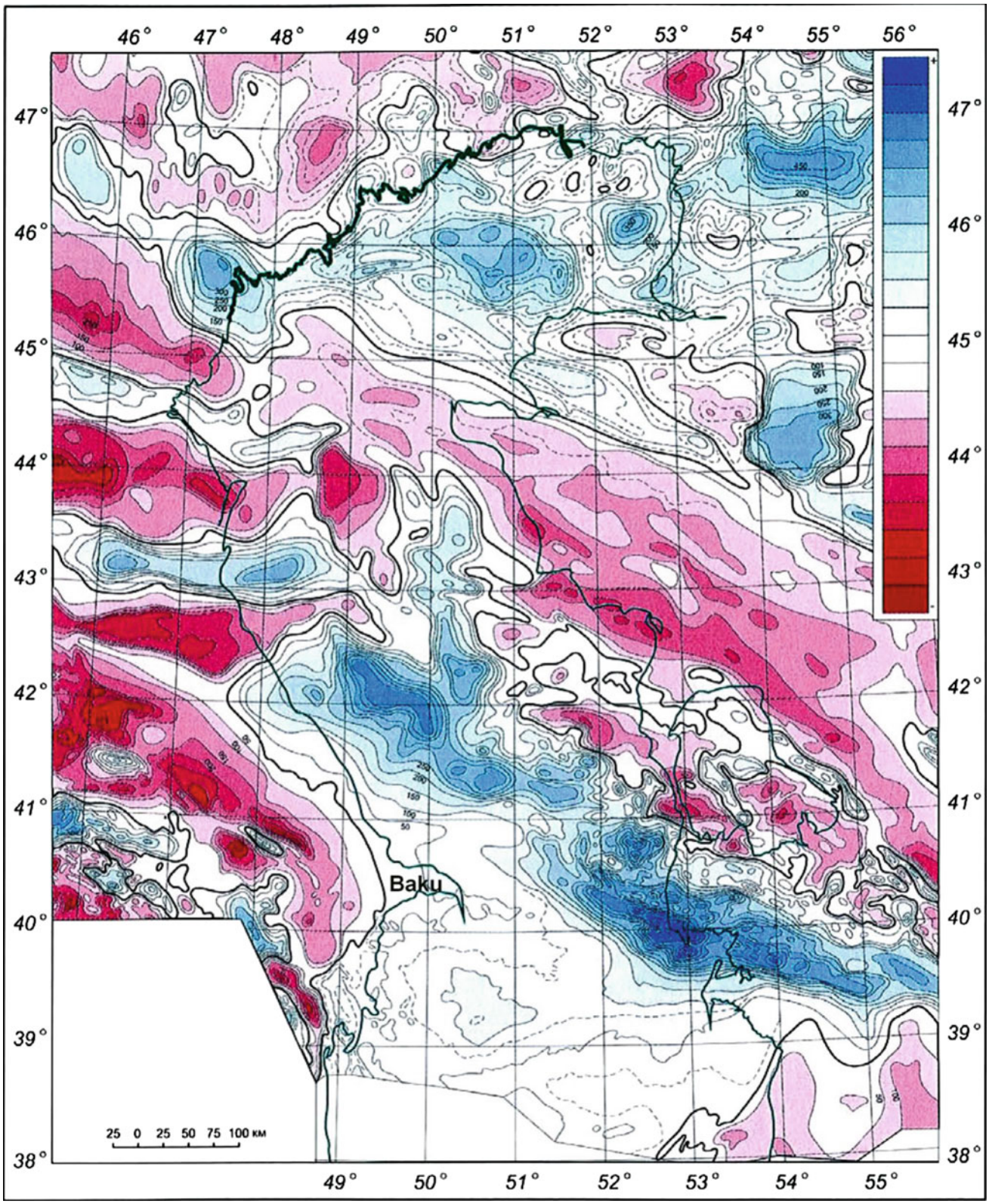

Fig. 5.44 Map of the anomalous magnetic field ΔT_a (after Glumov et al. 2004)

According to Dzabayev (1969) and Khesin et al. (1996), the depth to the upper surface of the anomalous body is 17–20 km, which coincides with the depth to the crystalline basement found by deep seismic sounding (e.g., Mamedov 2008; Abdullayev et al. 2015). Dzabayev (1969) connected this anomaly to the influence of magmatic rock complex of basic consistency occurring in the body of the basement. This point of view was confirmed by the behavior of the magnetic field continued upward to a level of 4 and 10 km: parameters of magnetic maximum change weakly with the level of upward continuation. At the same time, a careful analysis of this anomaly indicates that it is composed of several different anomalies. It was clearly detected from a combined interpretation of residual magnetic differential (0 $km_{earth's\ surface}$–10 $km_{upward\ anal.\ contin}$) anomalies and the regional magnetic field continued to the level of 10 km. It should be noted that the magnetic field maximum is localized in the northern area of a large gravity maximum corresponding to the western part of the SCB.

A similar interrelation of gravity and magnetic anomalies was studied in the Middle Kur Depression and was explained by the physical–geological model when younger (Mesozoic) magmatic rocks were introduced into a weakened zone on the peripheral part of the uplift of the pre-Alpine basement (Eppelbaum and Khesin 2012).

The Pliocene–Anthropogenic deposits in the SCB are the thickest. The paleomagnetic characteristics of these deposits on the eastern and western sides of the SCB are identical. This enables interpretation by applying the principles of directly magnetized deposits (Baku, a small interval of Absheron and the lower part of Akchagyl) and inversely magnetized deposits (Absheron, upper part of Akchagyl and productive red bed for western Turkmenistan) [Ismailzadeh (1983) and his unpublished reports (1972–1980)]. The average values of magnetic susceptibility usually range from 1000 to 2000 (up to 5000) × 10^{-6} SI in the Eastern Azerbaijan and 1000 × 10^{-6} SI in the western Turkmenistan.

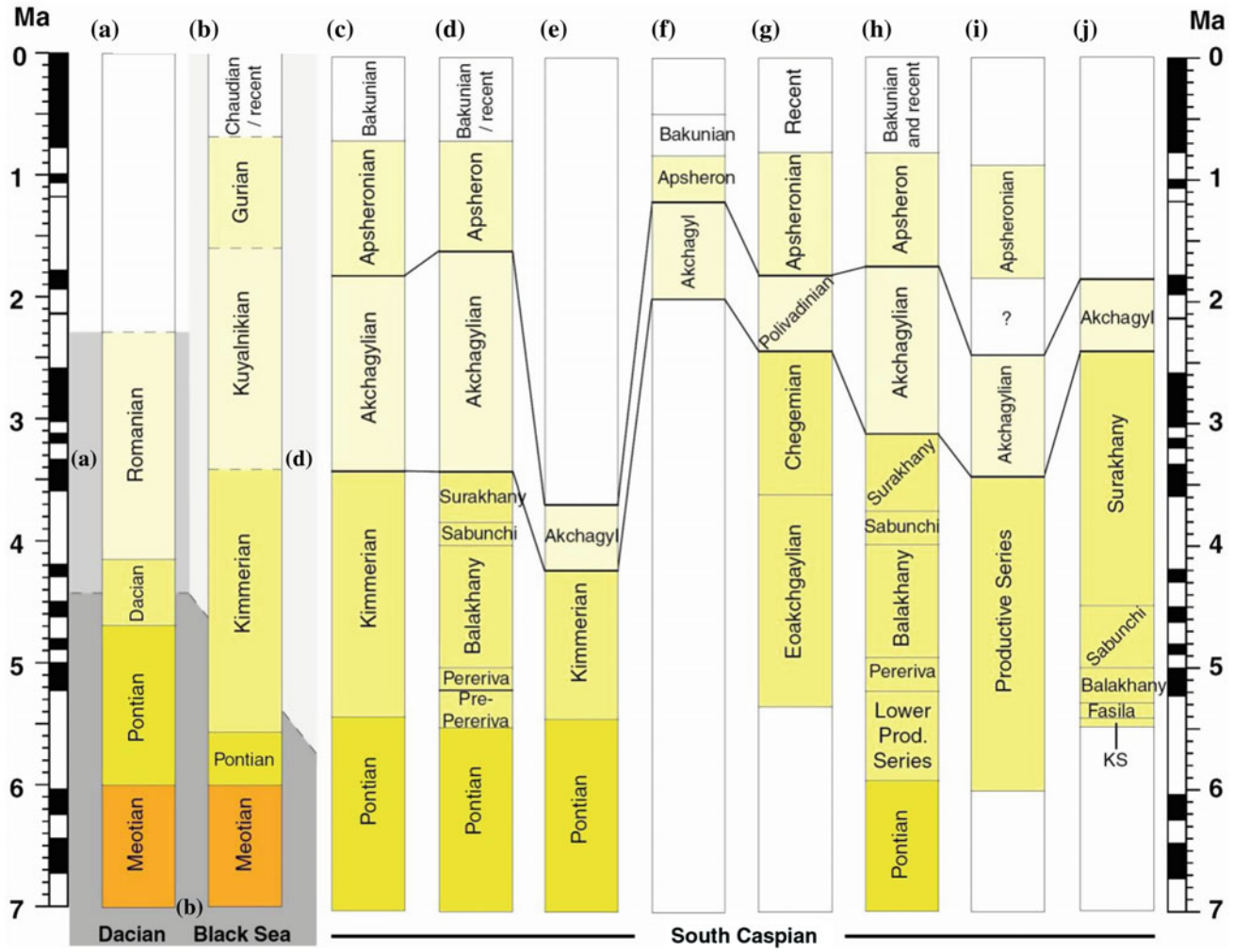

Fig. 5.45 Existing Caspian basin and Eastern Paratethys timescales (Van Baak et al. 2013). Lines connect the upper and lower boundaries of the Akchagylian regional stage. Authors of the works (*a*)–(*i*) are given in Van Baak et al. (2013)

Within the eastern part of the Caspian Sea and Gulf of Garabogaz-Gol is selected a central Caspian-Garabogaz-Gol zone of alternating mosaic field divided from the Mangyshlak zone of maximums by the Kendyrly zone of normal magnetic field.

Analysis of anomalous magnetic field of the folded zones extending to the South Caspian in the west (Caucasus) and in the east (Kopetdagh) does not show a continuation of these zones far out to the sea. Zone of magnetic minimums of the Greater Caucasus and located to the south Transcaucasian zone of intensive alternating mosaic field by extending to the sea coast sharply changes their orientation to the south, in direction to the Alborz folded construction (Glumov et al. 2004).

A magnetostratigraphic analysis of Plio–Pleistocene transgressions in the South Caspian basin combined with palaeoenvironmental reconstructions enables to develop the following conclusions (Van Baak et al. 2013). Rock magnetic analyses combined with thermal demagnetization data indicate that the magnetic signal is carried dominantly by the iron

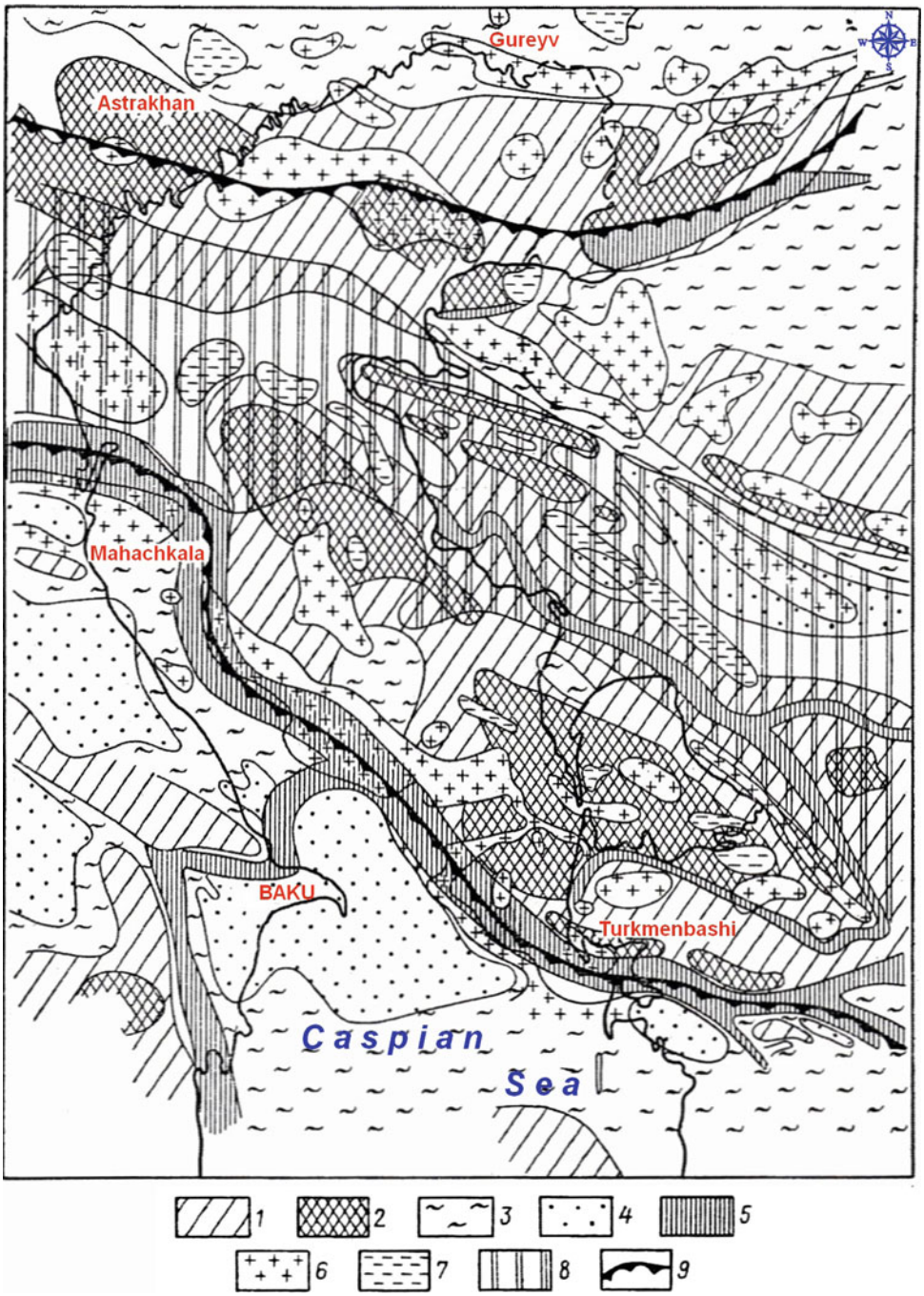

Fig. 5.46 Scheme of elements of geophysical fields of the Caspian Sea (after Malovitsky et al. 1977, with small modifications). Gravity anomalies: (*1*) relatively positive, (*2*) the same, most intensive, (*3*) relatively negative, (*4*) the same, most intensive, (*5*) gravity steps; and magnetic anomalies: (*6*) maximums, (*7*) minimums, (*8*) zone of regional strip depression, and (*9*) boundaries between the main different age tectonic elements

oxide magnetite in the Productive Series of the Lokbatan and Xocashen sections. The marine deposits Akchagylian and Apsheronian of Lokbatan are characterized by the iron sulphide greigite which appears to be of (near-) primary origin. The most logical correlation of the magnetic polarity patterns to the Geomagnetic Polarity Time Scale dates the Akchagylian transgression at ~3.2 Ma, a major transgression during the Apsheronian at ~2.0 Ma and the Bakunian transgression at 0.85–0.89 Ma (Fig. 5.45) (Van Baak et al. 2013).

All the conclusions are highly important for magnetic anomaly quantitative interpretation and 3D magnetic field modeling in this region.

An effective magnetic–gravity field generalization has been realized in Fig. 5.46 where the Caspian Sea and some adjacent areas were ranged by gravity–magnetic field intensities.

Apparently, development of combined seismic–gravity–magnetic profiles crossing the SCB will strongly help to unmask the deep structure of this region (similarly to unmasking the deep structure of the easternmost Mediterranean (Eppelbaum and Katz 2015).

5.3.4 Thermal Field Analysis

According to Mukhtarov (2004) calculations, the sedimentation rate in Jurassic in the SCB was 120–180 m/My, if the maximum thickness of the sedimentary covers for about 30 km. In Cretaceous and in Paleogene, it became lower, and in Pliocene, it reached avalanche values—1.8 km/My. Results of modeling of thermal evolution of the basin with account of non-stability of the heat field demonstrated that temperature in the base of the sedimentary layer changed 400–500 °C (Mukhtarov and Adigezalov 1997; Mukhtarov et al. 2003). Opinions have appeared lately on that the total thickness of the sedimentary cover in the SCB is up to 30 km. This may result that the rate of sedimentation at early stages of sedimentation will be more than it was calculated for the 20 km thickness of sediments. As a result, share of deep heat flow in the sedimentary thickness will be much lower.

Levin and Viskovski (2000) proposed that in Jurassic the rate of sedimentation in the SCB varied from 10–25 to 50 m/My. Temperatures in the base of the system were 150–200 °C. They increased in deeper blocks up to 300–450 °C. In Cretaceous, the rate of sedimentation was 2.5–10 m/My. Temperatures in the base were from 50–150 to 250–300 °C. In Oligocene–Miocene system, the rate of sedimentation was 0.025–0.4 km/My. Temperatures in the base of Miocene deposits were 50–100 °C and in some blocks only they were up to 200 °C. In Pliocene–Quaternary system, the rate of sedimentation changed from 0.75 to 1.75 m/My.

Table 5.2 Borehole maximum temperature data in SCB (after Mukhtarov 2004)

Structure	No of wells	Depth (m)	Temperature (°C)
Baku Archipelago			
Shakh deniz	4	6500	122
Bulla deniz	46	5730	115
Bulla deniz	38	6150	110
Bulla deniz	42	5850	110
Sangachal deniz	550	5770	113
Garasu	28	5650	112
Garasu	30	5683	106
Duvanny deniz	39	4450	111
Absheron and the Absheron Archipelago			
Absheron deniz	3	5000	110
Arzu	2	4708	105
Jenub	2	4710	102
Jenub	12	4127	100
Bakhar	19	5450	99
The South–West Caspian			
Gubkin uplift		3485	74.5
Barinov uplift		4420	91.5
Zhdanov uplift	24	3993	88
Lam uplift	1	4353	94

Temperatures were from 100–150 °C to 200–300 °C. It should take into account that in the SCB there a lot of wells were drilled. While considering temperature data from these wells one can be sure than the temperature regime of sedimentary layers uncovered by the wells is moderate enough (Table 5.2).

Sedimentation rate is one of the factors affecting the heat regime in sedimentary basins. With avalanche rates of sedimentation there occurs intensive decay of deep heat flow. For this reason, one can observe relatively low values of the heat flows density throughout the Caspian region. It should be noted that values of the heat flows determined by a well method (20–40 mW/m^2 in wells of the Baku archipelago and in the Absheron Sill) were lower than values of the heat flows determined by sea sounds (30–50 mW/m^2 and more). Without special investigations, one can hardly judge about the reason of this difference. To construct the map of heat flows in the water area of the Caspian Sea (Fig. 5.47), there were used results of the determination of the heat flow by marine thermal probes (Catalogue … 1973; Lyubimova et al. 1976; Tomara 1979; Aliyev et al. 1979; Lebedev and Tomara 1981). Moreover, there were used data obtained by the well method in the shelf zone and in the onshore territory (Catalogue … 1973; Kashkay and Aliyev 1974; Ashirov 1984, Aliyev 1988).

The main features of distribution of the heat flow in the water area of the Caspian Sea are very well correlated with tectonic peculiarities of its deep structure. For instance, increased values of the heat flow are conditioned by the impact of such tectonic structures such as faults and mud volcanoes. One of the stations in the west of the SCB recorded abnormally high value (480 mW/m^2) of the heat flow (Fig. 5.48). The available geophysical data do not explain this anomaly as impact of the intrusive body (Lebedev and Tomara 1981). That is due to the evacuation of fluids along the active dislocations (faults or vents of mud volcanoes).

It should be mentioned that measurement of the heat flow is of a point character and main geologic factors affecting the heat flow density are of a local character may reflect some local areal peculiarities. This causes necessity of performing special investigations in the zones covering local areas of

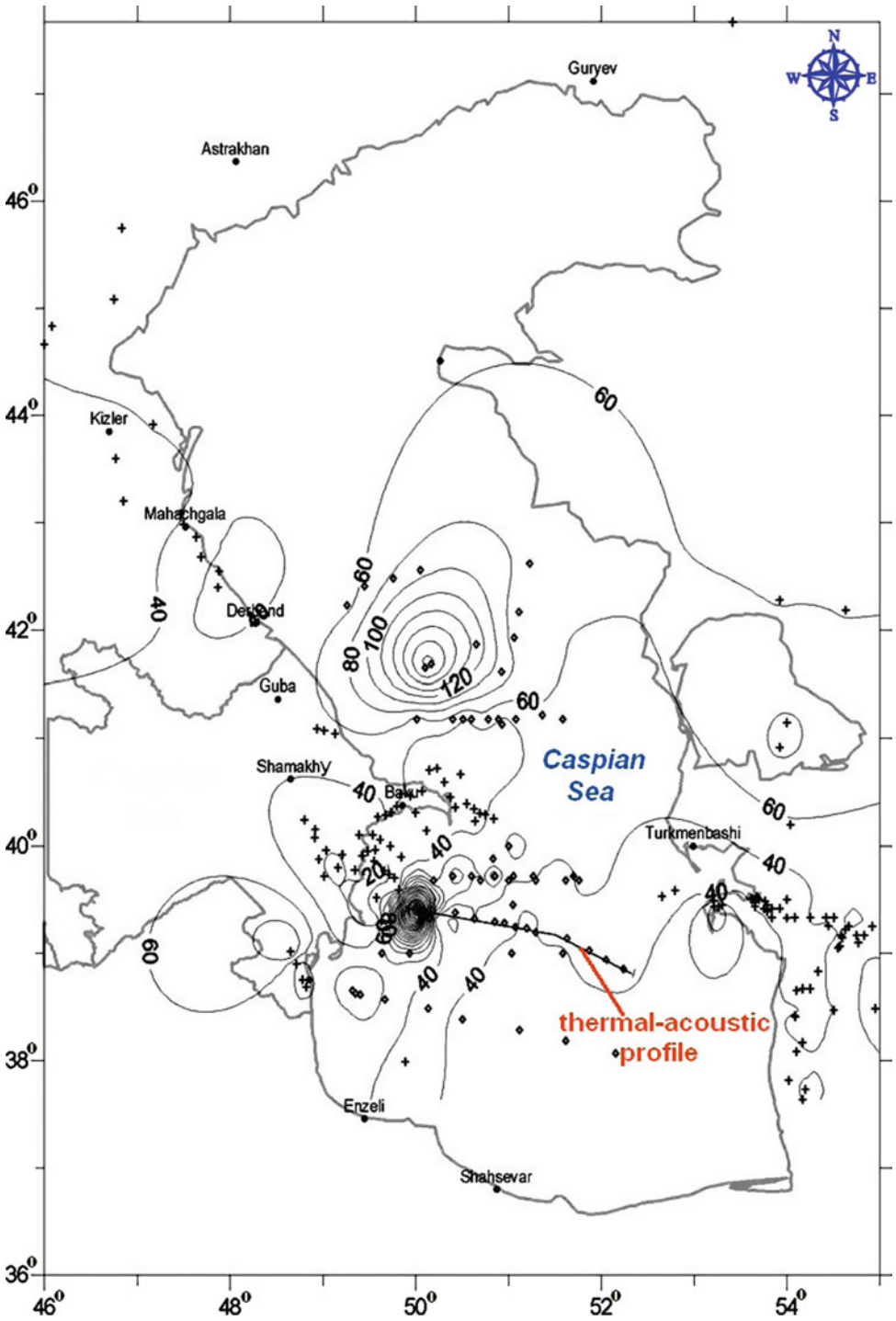

Fig. 5.47 Heat flow distribution map in the water area of the Caspian Sea. *Crosses* show the points of determination of density of the heat flow in wells, *rhombs* —points of determination of the heat flow density by sea thermal soundings (Mukhtarov 2004)

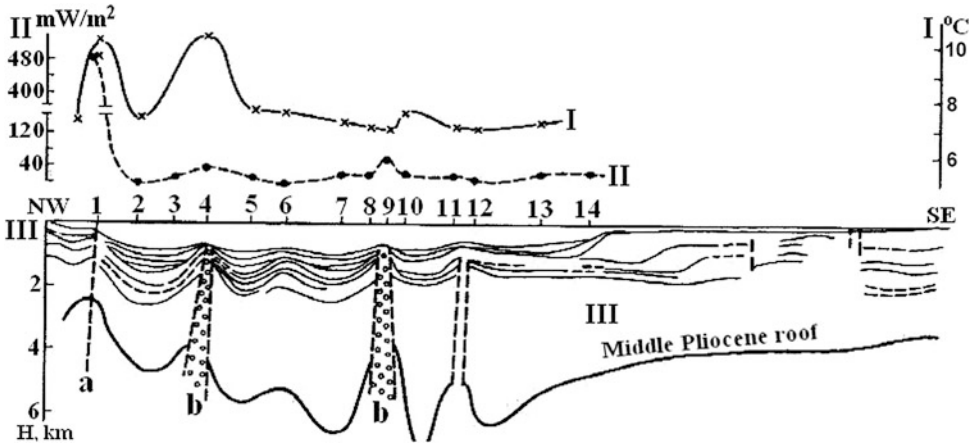

Fig. 5.48 Integrated geothermal–seismoacoustic profile through the SCB (position of the profile is shown in Fig. 2.4.46) (Lebedev and Tomara 1981; Mukhtarov 2004). *I*—temperature of the upper layer of see bottom sediments, °C; *II*—heat flow, mW/m^2; *III*—seismoacoustic profile of the sedimentary series as deep as the top of the Middle Pliocene; (*a*) zone of faults near the west coast; (*b*) mud volcano; 1–14 —numbers of stations

active faults and mud volcanoes and remote calm areas. Distribution of mud volcanoes and heat flows in the SCB proves the above mentioned. The mud volcanoes are mainly spread in the areas of contoured isolines of the heat flow 40 mW/m^2.

References

Abbasov A.B., 2002. Yevlakh-Agjabedi and South Kur troughs paleogeography based on seismostratigraphic studies. *Geophysics News in Azerbaijan*, Nos. 1-2, 11-15 (in Russian).

Abdullayev, N.R., Kadirov, F. and Guliyev, I.S., 2015. Subsidence history and basin-fill evolution in the South Caspian Basin from geophysical mapping, flexural backstripping, forward lithospheric modelling and gravity modelling. In: (Brunet, M.-F., McCann, T. and Sobel, E.R., Eds.), *Geological Evolution of Central Asian Basins and the Western Tien Shan Range*. *Geological Society*, London, *Special Publications*, **427**, 1-22.

Abers, G.A. and Roecker, S., 1991. Structure of an arc-continent collision: Earthquake relocation and inversion for upper mantle P and S wave velocities beneath Papua New Guinea. *Jour. of Geophys. Research*, **96**, No. B4, 6379-6401

Adamova, A.A. and Sabitova, T.M., 2004. 3D velocity model of Tyan-Shan earth's crust. *Izvestiya, Acad. Sci. Russ*., *Physics of the Earth*, No. 5, 58-67.

Aksenovich, G.I., Aronov, L.E., Gagelgants, A.A., Galperin, E.I., Kayonchkovskiy, M.A., Kosminskaya, I.P. and Krakshina, P.M., 1962. *Deep Seismic Sounding in the Central Part of the Caspian Sea*. Acad. Sci. USSR, Moscow (in Russian).

Alexeyev, V.V., Gadjiev, T.G., Karkoshkin, A.I., Khesin, B.E. and Ismailzadeh, T.A., 1988. *Gravity and Magnetic Anomalies in Azerbaijan and their Geological Interpretation*. Map Printing Factory, Leningrad (in Russian).

Aliyev, A.S., 1985. *Map of Heat Flows in the Depression Zones of Azerbaijan*. Scale 1: 500,000, (T.A. Ismailzadeh and T.G. Gadjiev, Eds.), Ministry of Geology of the USSR, Moscow.

Aliyev, G.A., Akhmedbeyli, F.S., Ismailzade, A.D., Kangarli, T.H. and Rustamov, M.I. (Khain, V.E. and Alizadeh, Ak.A., Eds.), 2005a. *Geology of Azerbaijan*, Vol. **IV**: Tectonics. Nafta-Press, Baku (in Russian).

Aliyev, S.A., 1988. Geothermal fields of depression zones in the SCB and their relation with oil-gas potential. *D.Sci. Thesis*, Inst. of Geology, Baku (in Russian).

Aliyev, S.A., Aliyev, C.S., Askerhanova, H.Q., Balakishibeyli, Sh.A., Qasanov, A.O., Qasanov, A.B., Zolotovichaya, T.A., Ismailzade A. D., Isayeva, M.I., Kadirov, F.A., Mukhtarov, A.Sh., Rzayev, A.Q., Cafarov, I.B. and Khalafly, A.A. (Ak.A. Alizadeh, Ed.), 2005b. *Geology of Azerbaijan*, Vol. **V**: *Physics of the Earth* (in Russian).

Aliyev, S.A., Ashirov, T. and Sudakov, N.P., 1979. New data on the heat flow through the Caspian Sea floor. *Izvestiya*, *Acad. Sci. Turkm. SSR*, Ser.: Phys-Tech. and Geol. Sci., No. 2, 124-126 (in Russian).

Alizadeh, Ak.A. (Ed.). 2012. *Modern Problems of Geology and Geophysics of the Caucasus*. Nafta-Press, Baku.

Alizadeh, Ak.A., V.E. Khain and A.D. Ismailzadeh (Eds.), 2000. *Saatly Superdeep Well. Studies of Deep Structure of the Kur Intermountain Depression Based on Materials of Drilling of Saatly Superdeep Well SG-1*. Nafta-Press, Baku (in Russian).

Ambraseys, N.N. and Melville, C.P., 1982. *A History of Persian Earthquakes*. Cambridge Univ. Press, N. Y.

Artyushkov, E.V., 1993. *Physical Tectonics*. Nauka, Moscow (in Russian).

Artyushkov, E.V., 2007. Formation of ultra-deep basin in the South Caspian as a result of phase transition in the continental crust. *Geology and Geophys*., **48** (12), 1289-1307 (in Russian).

Artyushkov, E.V., Mörner, N.-A. and Tarling, D.H., 2000. The cause of loss of lithospheric rigidity in areas far from plate tectonic activity. *Geophysical Journal International*, **143**, 752-766.

Azizbekov, Sh.A., Alizadeh, K.A., Shikalibeyli, E.Sh. and Gadjiev, T. G. (Eds.), 1972a. *Geology of the USSR*, *Azerbaijan*, Vol. **XLVII**, Nedra, Moscow (in Russian).

Azizbekov, Sh.A., Agabekov, M.G., Grigoryants, B.V., Shikalibeyli, E. Sh. and Mamedov, A.V., 1972b. The history of the geological evolution, In: (Sh.A. Azizbekov, K.A. Alizadeh, E.Sh. Shikalibeyli and T.G. Gadjiev, Eds.), *Geology of the USSR*, *Azerbaijan*, Vol. **XLVII**, Nedra, Moscow, 441-503 (in Russian).

Allen, M.B., Vincent, S.J., Alsop, G.I., Ismailzadeh, A. and Flecker, R., 2003. Late Cenozoic deformation in the South Caspian region: effects of a rigid basement block within a collision zone. *Tectonophysics*, **366**, 223-239.

Ashirov, T., 1984. *Geothermal Field of Turkmenia*. Nauka, Moscow (in Russian).

Babayev, D.Kh. and Gadjiyev, A.N., 2006. *Deep Structure and Prospects Oil-and-Gas Content Basin of Caspian Sea*. Geol. Inst., Azerb. Acad. Sci., Baku (in Russian).

Balakishibeyli, Sh.A., Salekhli, T.M., Gasanov, A.B. and Guliyev, R. D., 1996. Results of petrophysical research. In: *Geophysical Investigations in Azerbaijan*. Baku, Nafta-Press, 352-381 (in Russian).

Baranova, E.P., Kosminskaya, I.P. and Pavlenkova, N.I., 1991. A reinterpretation of south Caspian DSS data. *Geophysical Journal*, **10**, 666-677.

Barber, C.B., Dobkin, D.P. and Huhdanpaa, H.T., 1996. The Quickhull Algorithm for Convex Hulls. *ACM Trans. on Mathematical Software*, 22, No. 4, 469-483.

Barton, P.J., 1986. The relationship between seismic velocity and density in the continental crust – A useful constraint? *Geophys. Jour. Royal. Astr. Soc*., **87**, 195-208.

Brunet, M.-F., Korotayev, M.V., Ershov A.V. and Nikishin, A.M., 2003. The South Caspian Basin: a review of its evolution from subsidence modelling. *Sedimentary Geology*, **156**, 119-148.

Bulakh, E.G., 2000. Review of publication on minimization methods used in inverse gravimetry and magnetometry problems. *Geophysical Journal*, **19**, 709-733.

Bulakh, Y.G., Markova, M.N., Timoshenko, V.I. and Boiko, P.D., 1984. *Mathematical Support of Automated System of Gravity Anomaly Interpretation.* Naukova Dumka, Kiev (in Russian).

Catalogue of data on heat flow in the territory of the USSR, 1973. Nauka, Moscow (in Russian).

Dehghani, G.A. and Makris, J., 1983. The gravity field and crustal structure of Iran. *Geodynamic Project* (*Geotraverse*) *in Iran*. Final Report. 51. Geological Survey of Iran, 50-68.

Dzabayev, A.A., 1969. *Principles of the Searching and Study of Oil-and-Gas Bearing Structures by Aeromagnetic Method* (*South Caspian Basin*). Statistika, Ashkhabad (in Russian).

Egan, S.S., Mosar, J., Brunet, M.F. and Kangarli, T., 2009. Subsidence and uplift mechanisms within the South Caspian Basin: insights from the onshore and offshore Azerbaijan region. *Geol. Society, London*, *Special Publications*, **312**, 219-240.

Eppelbaum, L.V., 2014a. Estimating informational content in geophysical observations on example of searching economic minerals in Azerbaijan. *Izvestiya* (*Proceedings*), *Acad. Sci. Azerb. Rep., Ser.: Earth Sciences*, Nos. 3-4, 31-40.

Eppelbaum, L.V., 2014b. Four Color Theorem and Applied Geophysics. *Applied Mathematics*, **5**, 358-366.

Eppelbaum, L.V., 2015. Comparison of 3D integrated geophysical modeling in the south Caucasian and eastern Mediterranean Segments of the Alpine-Himalayan tectonic belt. *Izvestiya* (*Proceedings*), *Acad. Sci. Azerb*., Ser.: Earth Sciences, No. 3, 25-42.

Eppelbaum, L.V. and Katz, Yu.I., 2015. Eastern Mediterranean: Combined geological-geophysical zonation and paleogeodynamics of the Mesozoic and Cenozoic structural-sedimentation stages. *Marine and Petroleum Geology*, **65**, 198-216.

Eppelbaum, L.V. and Khesin, B.E. 2004. Advanced 3-D modelling of gravity field unmasks reserves of a pyrite-polymetallic deposit: A case study from the Greater Caucasus. *First Break*, **22**, No. 11, 53-56.

Eppelbaum, L. and Khesin, B., 2011. Development of 3-D gravity-magnetic models of Earth's crust of Azerbaijan and adjacent areas: A generalized review. *Positioning*, **2**, No. 2, 84-102.

Eppelbaum, L.V. and Khesin, B.E., 2012. *Geophysical Studies in the Caucasus*. Springer, Heidelberg – N.Y. – London.

Eppelbaum, L.V. and Pilchin, A.N., 2006. Methodology of Curie discontinuity map development for regions with low thermal characteristics: An example from Israel. *Earth and Planetary Sciences Letters*, **243**, Nos. 3-4, 536-551.

Eppelbaum, L.V., Kutasov, I.M. and Pilchin, A.N., 2014. *Applied Geothermics*. Springer, London - N.Y.

Firbas, P., 1987. Tomography from seismic profiles. In: (G. Nolet, Ed.), *Seismic Tomography, with Applications in Global Seismology and Exploration Geophysics,* Springer, Reidel, Dordrecht, 189- 202.

Forte, A.M., Cowgill, E., Murtuzayev, I., Kangarli, T. and Stoica, M., 2013. Structural geometries and magnitude of shortening in the eastern Kura fold-thrust belt, Azerbaijan: Implications for the development of the Greater Caucasus Mountains. *Tectonics*, **32**, 688-717.

Gadjiev, R.M., 1965. *Deep Geological Structure of Azerbaijan*. Azgosizdat, Baku (in Russian).

Gasanov, A.G., 2001. *Deep Structure and Seismicity of Azerbaijan in Relation to Hydrocarbons Prognosis*. Elm, Baku (in Russian).

Granath, J.W., Soofi, K.A., Baganz, O.W. and Bagirov, E., 2000. Gravity modelling and its implications to the tectonics of the south Caspian basin. *AAPG Inaugural Regional International Conf*., Extended Abstracts, 46-49.

Glumov, I.F., Malovitsky, Ya.P., Novikov, A.A. and Senin, B.V., 2004. *Regional Geology and Oil and Gas Bearing of the Caspian Sea*. Nedra, Moscow (in Russian).

Gravity map of the USSR, 1990. Scale 1:2,500,000, Ministry of Geology. Moscow.

Goldshmidt, V.I., Kuzmin, Yu.I. and Shabaldin, V.N., 1981. *An automated system of gravity data interpretation. In*: *Theory and Methods for Interpretation of Gravity and Magnetic Fields*. Naukova Dumka, Kiev, 58-70 (in Russian).

Green, T., Abdullayev, N., Hossack, J., Riley, G. and Roberts, A., 2009. Sedimentation and subsidence in the South Caspian Basin, Azerbaijan. In: (Brunet, M.-F., Wilmsen, M., Granath, J.W., Eds.), *South Caspian to Central Iran Basins*. The Geol. Society of London. Special Publ., **312**, 2241-2260.

Gugunava, G.E., 1988. Structure of Caucasus inferred from the analysis of some geophysical fields. *D. Sci. Thesis*. Inst. of Geophysics of the Georgian Acad. of Sci. – Inst. of Geology of the Azerb. Acad. of Sci. (in Russian).

Guliyev, I.S., Mamedov, P.Z., Feyzullayev, A.A., Huseynov, D.A., Kadirov, F.A., Aliyeva, E.H.-M., Tagiyev, M.F., 2003. (Ed. Guliyev, I.S.), *Hydrocarbon Systems of the South Caspian Basin*. Nafta-Press, Baku.

Guliyev, I. and Panachi, B., 2004. Geodynamics of the deep sedimentary basin the Caspian sea region: paragenetic correlation of the seismicity and mud volcanism. *Geo-Marine Letters*, **24**, No. 3, 169-176.

Ismailzadeh, A.D., Alizadeh, Ak.A., Guliyev, I.S., Babayev, D.Kh. and Hajiyev, A.H., 2004. On the possible mantle character of hydrocarbon fluids in the South Caspian Depression. *Izvestiya*, *Acad. Sci. Azerb*., Ser.: Earth Sciences, No. 3, 6-11 (in Russian).

Ismailzadeh, A.D., Mustafayev, G.V. and Rustamov, M.I. (Ak.A. Alizadeh, Ed.), 2005. *Geology of Azerbaijan*, Vol. **III**, *Magmatism*. Nafta-Press, Baku (in Russian).

Ismailzadeh, T.A., 1983. Paleomagnetic investigations of Meso-Cenozoic of Azerbaijan. *D.Sci. Thesis*, Inst. of the Physics of the Earth, Moscow (in Russian).

Jackson, J., Priestly, K., Allen, M. and Berberian, M., 2002. Active tectonics of the South Caspian Basin. *Geophys. Jour. Intern*., **148**, 214-245.

Jafarov, H.D., Kerimov, A.A. and Solomonov, B.I., 1967. Deep structure of the Ajinohur region by data of exploration geophysics. *Izvestiya VUZov*, No. 9, 11-14 (in Russian).

Kaban, M.K., 2002. A gravity model of the north Eurasia crust and upper mantle: 2. The Alpine-Mediterranean fold belt and adjacent structures of the southern former USSR. *Russian Jour. of Earth Sci*., **4**, No. 1, 19-33.

Kadirov, F.A., 2000a. Application of the Hartley transform for interpretation of gravity anomalies in the Shamakhy–Gobustan and Absheron oil- and gas-bearing regions, Azerbaijan. *Jour. of Applied Geophysics*, **45**, 49-61.

Kadirov, F.A., 2000b. *Gravity Field and Models of Deep Structure of Azerbaijan*. Nafta-Press, Baku (in Russian).

Kadirov, F.A., 2006. Nature of gravitational anomaly in the South Caspian Basin. *Trans. of the EAGE 68th Conference*, Vienna, P325, pp. 1-4.

Kadirov, F.A., Floyd, M., Reilinger, R., Alizadeh, Ak.A., Guliyev, I.S., Mammadov, S.G. and Safarov, R.T., 2015. Active geodynamics of the Caucasus Region: Implications For Earthquake Hazards in Azerbaijan. *Izvestiya* (*Proceedings*)*, Acad. Sci. Azerb*., Ser.: Earth Sciences, No. 3, 3-17.

Kadirov, F.A. and Gadirov, A.H., 2014. A gravity model of the deep structure of South Caspian Basin along submeridional profile Alborz–Absheron Sill. *Global and Planetary Change*, **114**, 66-74.

Kadirov, F.A., Mammadov, S.A., Reilinger, R. and McClusky, S., 2008. Some new data on modern tectonic deformation and active faulting in Azerbaijan (according to Global Positioning System Measurements). *Izvestiya* (*Proceedings*) *Acad. Sci. Azerb*., Ser.: Earth Sciences, No. 1, 82-88.

Kashkay, M.A. and Aliyev, S.A., 1974. Heat flow in the Kur Depression. In: *Deep Heat Flow in the European Part of the USSR*. Naukova Dumka, Kiev, 95-108 (in Russian).

Kazymova, S.E. and Kazymov, I.E., 2010. 1D velocity model of Kur Depression from the data of telemetric stations of Azerbaijan. In: *Science 21 Century, "Volgapromstroibezopasnost"*, Saratov, No. 2 (in Russian).

Kerimov, K.M., Pilchin, A.N., Gadzhiev, T.G. and Buachidze, G.Y., 1989. *Geothermal map of the Caucasus, Scale* 1:1,000,000 Baku, Cartographic Plant No. 11 (in Russian).

Khain, V.E., 1984. *Regional Geodynamics*. *Alpine Mediterranean Belt*. Nedra, Moscow (in Russian).

Khain, V.E., 2000. *Tectonics of Continents and Oceans*. Nauchnyi Mir, Moscow (in Russian).

Khain, V.E., 2005. The problem of origin and age of South Caspian Basin and its probable solutions. *Geotectonics*, No. 1, 40-44 (in Russian).

Khain, V.E., 2007. Mesozoic-Cenozoic accretionary complexes of the Greater Caucasus. *Doklady Earth Sciences*, **413A**, No. 3, 376-379.

Khalafly, A.A., 2006. *Paleomagnetism and Some Problems of Shear Deformations of the Lesser Caucasus*. Takhsil, Baku (in Russian).

Khalilov, E.N., Mekhtiyev, Sh.F. and Khain, V.E., 1987. On some geophysical data confirming the collision origin of the Greater Caucasus. *Geotectonics*, No. 2, 54-60 (in Russian).

Khesin, B.E., Alexeyev, V.V. and Eppelbaum, L.V., 1993. 3-D modelling of gravity and magnetic fields as a final stage of application of effective interpretation system of geophysical data under difficult geological conditions. *Geoinformatics*, **4**, No. 3, 177-188.

Khesin, B.E., Alexeyev, V.V. and Eppelbaum, L.V., 1996. *Interpretation of Geophysical Fields in Complicated Environments*. Kluwer Academic Publ. (Springer), Ser: *Modern Approaches in Geophysics*, Boston – Dordrecht – London.

Khesin, B.E. and Eppelbaum, L.V., 2007. Development of 3-D gravity/magnetic models of Earth's crust in complicated regions of Azerbaijan. *Proceed. of the 69th EAGE Conference*, P343, London, Great Britain, 1-5.

Knapp, C.C., Knapp, J.H. and Connor, J.A., 2004. Crustal-scale structure of the South Caspian Basin revealed by deep seismic reflection profiling. *Marine and Petroleum Geology*, **21**, 1073-1081.

Koronovsky, N.V., 2000. Seismic tomography. *Earth Sciences* (Soros' Russian Journal), **6**, No. 11, 63-68.

Koulakov, I., Zabelina, I., Amanatashvili, I. and Meshkina, V., 2012. Nature of orogenesis and volcanism in the Caucasus region based on results of regional tomography. *Solid Earth*, **3**, 327-337.

Krasnopevtseva, G.V., 1984. *Deep Structure of the Caucasian Seismoactive Region*. Nauka, Moscow (in Russian).

Krasnopevtseva, G.V., Matushkin, B.A., Shevchenko, V.I., 1970. Novel interpretation of the DSS data along the profile Stepnoe – Bakuriani in the Caucasus. *Soviet Geology*, No. 8, 113-120.

Lebedev, L.I. and Tomara, G.A., 1981. Some peculiarities of distribution of heat flow in the South Caspian. In: *Geothermometers and Paleotemperature Gradients*. Nauka, Moscow, 156-161 (in Russian).

Leonov, Yu.G. (Ed.), 2008. *The Greater Caucasus in the Alpine Epoch*. Geos, Moscow (in Russian).

Levin, L.E. and Viskovski, Yu.A., 2000. The SCB: evolution and thermal regime of oil gas systems. *Proceed. of the III Azerbaijan Intern. Geoph. Conf*. Baku, p.239.

Lyubimova, E.A., 1968. Thermal history of the Earth. *In*: *The Earth's Crust and Upper Mantle*, Amer. Geophys. Union, Geophys. Monogr. Ser., **13**, 63-77.

Lyubimova, E.A., Nikitina, V.N. and Tomara, G.A., 1976. *Thermal Fields of the Inner and Marginal Seas in the USSR*. Nauka, Moscow (in Russian).

Malovitsky, Ya.P., Kogan, L.I., Mistrukov, Yu.M. et al., 1977. *Marine Geophysical Investigations*. Nedra, Moscow (in Russian).

Mamedov, A.V., 1984. Tectonics of Quaternary deposits of Azerbaijan. In: *Essays of Geology of Azerbaijan*. Acad. Sci. Azerb., Baku, 256-270 (in Russian).

Mamedov, P.Z., 1991. Paleo-deltaic complexes in the north of the South Caspian depression. *Petroleum Geology*, **225**, Nos. 9-10.

Mamedov, P.Z., 1992. Seismostratigraphical investigations of geological structure of sedimentary cover of South Caspian superdepression and perspectives of oil–gas productivity. *D.Sci. Thesis*, National Academy of Sciences, Baku, Azerbaijan (in Russian).

Mamedov, P.Z., 2004. Genesis and seismic stratigraphic model of the South Caspian Megabasin architecture. In: (Alizadeh, Ak.A., Ed.), *South Caspian Basin: Geology, Geophysics, Oil and Gas Content*. Nafta-Press, Baku, 150-164.

Mamedov, P.Z., 2008. The subsidence evolution of the South Caspian Basin. *Abstract Book of Conference EAGE "Petroleum Geology & Hydrocarbon Potential of Caspian and Black Sea Regions"*, 6–8 October 2008, Baku, Azerbaijan.

Mamedov, P.Z., 2009. Sedimentation models in the SCMB and their seismostratigraphic characteristics. *Stratigraphy and Sedimentology of Oil-Gas Basins*, No. 3, 70-85.

Mamedov, P.Z., Guliyev, Q.Q., Kadirov, F.A., Shykhalyev, Y.A., Guliyev, I.S., Aliyeva, E.H., Feyzullayev, A.A., Dadashov, F.Q., Kheirov, M.B. and Tagiyev, M.F., 2008. (Ak.A. Alizadeh, Ed.), 2008. *Geology of Azerbaijan*, Vol. VII: *Oil and Gas*. Nafta-Press, Baku (in Russian).

Mangino, S. and Priestley, K., 1998. The crustal structure of the southern Caspian region. *Geophysical Jour. International*, **133**, 630-648.

Mederer, J., Moritz, R., Ulianov, A. and Chiaradia, M., 2013. Middle Jurassic to Cenozoic evolution of arc magmatism during Neotethys subduction and arc-continent collision in the Kapan Zone, southern Armenia. *Lithos*, **177**, 61-78.

Mosar, J., Kangarli, T., Bochud, M., Glasmacher, U.A., Rast, A., Brunet, M.-F. and Sosson, M., 2010. Cenozoic–Recent tectonics and uplift in the Greater Caucasus: A perspective from Azerbaijan. *Geological Society*, London, *Special Publications*, **340**, 261-280.

Mukhtarov, A.Sh., 2004. Heat flow distribution and some aspects of thermal field formation in the Caspian region. In: (Ed. Ak. A. Alizadeh), *South Caspian Basin: Geology, Geophysics, Oil and Gas Content*. Nafta-Press, Baku, 165-172.

Mukhtarov, A.Sh., 2011. Structure of thermal flow of sedimentary complex of the Southern Caspian Basin. *D.Sci Thesis*, Inst. of Geology, Baku (in Russian).

Mukhtarov, A.Sh. and Adigezalov, N.Z., 1997. Thermal regime of mud volcanos in the East Azerbaijan. *Proceed. of the Geol. Inst*., Acad. Sci. Azerb., **26**, Baku, 221-228 (in Russian).

Mukhtarov, A.Sh., Tagiyev, M.F. and Imamverdiyev, R.A., 2003. Models of oil-gas generation and prediction of the phase state of hydrocarbons in the Baku Archipelago. *Izvestiya, Acad. Sci. Azerb*., Ser.: Earth Sciences, No. 2, 17-25 (in Russian).

Pavlenkova, G.A., 2012. Structure of the Caucasus' earth crust along the deep seismic sounding profiles Stepnoe-Bakuriani and Volgograd-Nakhchivan (results of initial data re-interpretation). *Izvestiya*, *Physics of the Earth*, No. 5, 16-25.

Pilchin, A.N. and Eppelbaum, L.V., 1997. Determination of magnetized bodies lower edges by using geothermal data. *Geophysical Journal International*, **128**, No.1, 167-174.

Popov, V.S. and Kremenetsky, A.A., 1999. Deep and superdeep scientific drilling on continents. *Earth Sciences*, No. 11, 61-68 (in Russian).

Priestley, K., Baker, C. and Jackson, J., 1994. Implications of earthquake focal mechanism data for the active tectonics of the South Caspian Basin and surrounding regions. *Geophysical Jour. International*, **118**, 111-141.

Radjabov, M.M., 1974. Seismic models of the Earth's crust of Azerbaijan. *D. Sci. Thesis*. Inst. of the Physics of the Earth, Moscow (in Russian).

Radjabov, M.M., 1977. Compiling of velocity model of the Earth crust on example of the Kur Depression. *Izvestiya*, *Acad. Sci. Azerb*., Ser.: Earth Sci., No. 6, 13-17 (in Russian).

Rappel, C. and Mcnutt, M., 1990. Regional compensation of the Greater Caucasus mountains based on an analysis of Bouguer gravity data. *Earth and Planetary Science Letters*, **98**, 360-379.

Reilinger, R., McClusky, S., Vernant, P. Lawrence, S., Ergintav, S., Cakmak, R., Ozener, H., Kadirov, F., Guliyev, I., Stepanyan, R., Nadariya, M., Hahubia, G., Mahmoud, S., Sakr, K., ArRajehi, A., Paradissis, D., Al-Aydrus, A., Prilepin, M., Guseva, T., Evren, E., Dmitrotsa, A., Filikov, V., Gomez, F., Al-Ghazzi, R. and Karam, G., 2006. GPS constraints on continental deformation in the Africa-Arabia-Eurasia continental collision zone and implications for the dynamics of plate interactions. *Jour of Geophysical Research,* **111**, B05411, 1-26.

Rezanov, I.A. and Shevchenko, V.I., 1978. *Structure and Evolution of Earth's Crust of Geosynclines*. Nedra, Moscow (in Russian).

Richter, C.F., 1958. *Elementary Seismology*. W. H. Freeman & Co., San Francisco.

Ricketts, J.W., Takedatsu, R., Mellors, R.J., Sandwell, D., Gok, R. and Yetirmishli, G., 2008. Crustal Structure of the Caucasus and Caspian Region Using Gravity and Receiver Functions. *Proceed. of the American Geophysical Union Fall Meet*., abstract #T21A-1922.

Riordan, J., 2014. *An Introduction to Combinatorial Analysis*. Princeton Univ. Press.

Ruban, D.A., 2013. The Greater Caucasus – A Galatian or Hanseatic terrane? Comment on "The formation of Pangea" by G.M. Stampfli, C. Hochard, C. Vérard, C. Wilhem and J. von Raumer [*Tectonophysics*, **593** (2013), 1-19]. *Tectonophysics*, **608**, 1442-1444.

Saintot, A., Brunet, M.-F., Yakovlev, F., Sebrier, M., Stephenson, R., Ershov, A., Chalot-Prat, F. and McCann, T., 2006. The Mesozoic-Cenozoic tectonic evolution of the Greater Caucasus. *The Geological Society of London*, Memoirs, **32**, 277-289.

Salekhli, T.M., 1993. Facial alternation of Cenozoic deposits on the geotraverse Kyurdamir-Byandovan and its reflection on petrophysical characteristics. In: *Structural-Formational and Seismostratigraphic Investigation of Sedimentary Strata of South Caspian Mega-Depression*. AzVNIIGEOFIZIKA, 12-23.

Sarker, G. and Abers, G.A., 1998. Deep structures along the boundary of a collision belt: attenuation tomography of *P* and *S* waves in the Greater Caucasus. *Geophysical Jour. International*, **133**, 326-340.

Sharkov, E., Lebedev, V., Chugayev, A., Zabarinskaya, L., Rodnikov, A., Sergeyeva, N. and Safonova, I., 2015. The Caucasian-Arabian segment of the Alpine-Himalayan collisional belt: Geology, volcanism and neotectonics. *Geosciences Frontiers*, **6**, No. 4, 513-522.

Shekinsky, E., Radjabov, M., Timukyan, G., Levi, V. and Riger, R., 1967. Study of the Earth's crust structure in Azerbaijan using deep seismic sounding. *Izvestiya*, *Acad. Sci. Azerb.*, Ser.: Earth Sci., No. 5, 41-50 (in Russian).

Shikhalibeyli, E.Sh., 1972. Location of Azerbaijan in general structure of the Caucasus and surrounding folded region, In: (Azizbekov, Sh. A. Alizadeh, K.A., Shikalibeyli, E.Sh. and Gadjiev, T.G., Eds.), *Geology of the USSR, Azerbaijan*, Vol. XLVII. Nedra, Moscow, 286-290 (in Russian).

Shikhalibeyli, E.S. and Grigoriants, B.V., 1980. Principal features of the crustal structure of the South-Caspian Basin and the conditions of its formation. *Tectonophysics*, **69**, 113-121.

Shikhalibeyli, E.Sh., Askerhanova, N.G., Kadirov, F.A. and Gairov A. G., 1990. Gravity modeling along the GSZ No. 3, Poylu-Masalli profile. *Izvestiya*, *Acad. Sci. Azerb*., Ser.: Earth Sci., No. 2, 107-110 (in Russian).

Spichak, V.V., 1999. *Magnetotelluric Fields in Three-Dimensional Models of Geoelectrics*. Nauchnyi Mir, Moscow (in Russian).

Strakhov, V.N. 1976. *Main Ideas and Methods for Deriving Information from Gravitational and Magnetic Observations*. Nedra, Moscow (in Russian).

Tarakanov, R.Z., 2006. Velocity models and P-waves hodographs for the Far East region. *Herald of the Far East Branch of the Russ. Acad. Sci*., No. 1, 81-94 (in Russian).

Tikhonov, A.N. and Arsenin, V.Y., 1977. *Solutions of Ill-Posed Problems*. V. H. Winston and Sons (distributed by Wiley, N.Y.).

Tomara, G.A., 1979. Thermal stream of deepwater trough of Caspian Sea. In: *Experimental and Theoretical Study of Hot Streams*. Nauka, Moscow, 99-112 (in Russian).

Trofimov, I.L., 1995. Observations of telluric field variations in the seismic region of Azerbaijan. *Izvestiya*, *Acad. Sci. Russ*., *Physics of the Solid Earth*, 30, Nos. 7-8, 672-678.

Turcotte, D.L. and Schubert, G., 1982. *Geodynamics: Applications of Continuum Physics to Geological Problems*. John Wiley & Sons, NY.

Tzimelzon, I.O., 1965. Deep structure of the Earth's crust and tectonics of Azerbaijan on the geophysical data analysis. *Soviet Geology*, No. 4, 103-111 (in Russian).

Tzimelzon, I.O., 1970. Relation between the tectonics of sedimentary deposits of Azerbaijan and earth's deep structure. *Geotectonics*, No. 5, 69-81 (in Russian).

Ulomov, V.I., 2003. Voluminous model of dynamics of lithosphere, seismicity structure and variations of the level of Caspian Sea. *Izvestiya, Acad. Sci. Russ.*, *Phys. of the Earth*, No. 5, 5-17 (in Russian).

Usoltseva, O.A., 2004. *3D Velocity Models of the Tyan-Shan Earth's Crust on the Basis of Bi-Spline Parametrization and Delone Triangulation*. Nauka, Moscow (in Russian).

Usoltseva, O.A., Kazymova, S.E. and Kazymov, I.E., 2010. Seismotomographic investigation of crust of south-eastern Caucasus by the use of Delone triangulation by data of P-wave traveltime. In: *Dynamic Processes in Geospheres*, Russ. Acad. of Sci., Moscow, 140-147 (in Russian).

Van Baak, C.G.C., Vasiliev, I., Stoica, M., Kuiper, K.F., Forte, A.M., Aliyeva, E., and Krijgsman, W., 2013. A magnetostratigraphic time frame for Plio-Pleistocene transgressions in the South Caspian Basin, Azerbaijan. *Global and Planetary Change*, **103**, 119-134.

Yakubov, A.A., Alizade, A.A. and Zeynalov, M.M., 1971. *Mud Volcanoes of Azerbaijan Rep., Atlas*. Academy of Sciences of the Azerbaijan SSR. Acad. of Sci. of Azerbaijan, Baku (in Russian).

Yetirmishli, G.D. and Kazimova, S.E., 2013. Velocity model of crust of Azerbaijan from the data of digital seismic stations. *Geology and Geophysics of South of Russia*. No. 1, 59-74.

Yetirmishli, G.C., Kazimova, S.E. and Kazimov, I.E., 2011. One-dimensional velocity model of the Middle Kur Depression from the local earthquakes data of Azerbaijan. *Izvestiya*, *Russ. Acad. Sci., Physics of the Solid Earth*, **47**, No. 9, 847-856.

Yurov, Yu.G., 1963. Structure of Earth's crust in the Caucasus and isostasy. *Soviet Geology*, No 9, 42-47 (in Russian).

Zonenshain, L.P. and Le Pichon, X., 1986. Deep basins of the Black Sea and Caspian Sea as remnants of Mesozoic back-arc basins. *Tectonophysics*, **123**, 181-211.

Geodynamics and Seismology

6

6.1 Seismicity of Azerbaijan Territory

6.1.1 A Brief Background

Territory of Azerbaijan is located within the central part of the Mediterranean tectonic belt seismicity of which is caused by intensive geodynamic interaction of the Eurasian and Arabian lithospheric plates (Khain 2000).

Territory of Azerbaijan is characterized by high seismic activity where during historical period (registered), strong and catastrophic earthquakes with magnitude $M \geq 6$ were observed. Azerbaijan territory may be subdivided by the level of seismic activity and character of space distribution of strong and weak earthquakes into the following manner: (1) southern slope of the eastern part of the Greater Caucasus, (2) Kur Depression, (3) Talysh Mts., (4) Gusar-Devechi (now—Gusar-Shabran) depression, and (5) Caspian Sea (Aliyev et al. 2005).

The history of seismic studies in Azerbaijan can be divided into two main periods: (1) pre-instrumental (historical) including all the information from ancient times reflected in the historical Arab chronicles, manuscripts, travel notes of travelers, etc., and (2) instrumental (contemporary) period which includes information about earthquakes from the beginning of the twentieth century (when after strong Shamakhy earthquake in 1902, the first seismic station in Azerbaijan "Shamakhy" was founded) till the present time.

Among the strong (historical) earthquakes, we can note such events as Azerbaijan earthquake of 427, Goygel of 1139, Ganja of 1235, Eastern Caucasian of 1668, Mashtaga of 1842, numerous Shamakhy events (1192, 1667, 1669, 1828, 1859, 1868, 1872, 1902), Ardebil of 1924, Lenkaran of 1913, and Caspian earthquakes (957, 1812, 1842, 1852, 1911, 1935, 1961, 1963, 1986, 1989, 2000) triggered earth relief changing, building destructions, and numerous casualties.

A significant contribution to solving seismological problem in Azerbaijan was done by E.B. Agalarova, R.A. Agamirzoev, S.T. Agayeva, F.S. Akhmedbeyli, O.B. Babazade, G.R. Babayev, E.I. Byus, A.G. Gasanov, R.I. Gasanov, D.Kh. Jafarov, K.Sh. Islamov, F.A. Kadirov, I.K. Kerimov, V. P. Kouznetsov, F.T. Kuliyev, N.V. Malinovsky, T.Ya. Mammadli, B.M. Panakhi, Sh.S. Ragimov, Z.Z. Sultanova, G.D. Yetirmishli, and others.

Figure 6.1 shows the isoseist map of the Krasnovodsk (now—Turkmenbashi) (Caspian) earthquake (July 8, 1895). The earthquake had the following parameters (Kondorskaya and Shebalin 1977): coordinates of epicenter (long., 39.5; lat., 53.7); magnitude, 8.2; source depth, 60 km; and intensity of tremors in epicenter, 10.

One of the largest seismic events in Azerbaijan in twentieth century was a Shamakhy earthquake on February 13, 1902 (lat., 40.7 and long., 48.6; magnitude ≈ 7; depth of focus, 15 km (Fig. 6.2); intensity of motions in the center, VIII–IX) (Fig. 6.3). The number of victims in the city of Shamakhy is indicated in many sources erroneously repeating numbers reported by V.N. Weber for the surrounding villages only (86 killed and 60 wounded). The number of victims in Shamakhy was undoubtedly great.

6.1.2 Seismic Regioning of Azerbaijan

After a strong earthquake in the Caspian Sea on November 25, 2000 ($M = 6.3$, $\varphi = 40°$, $\lambda = 50°$, $h = 35$ km) with the aim to improve the monitoring of seismic activity in Azerbaijan, 14 modern telemetry stations of "Kinemetrics" (USA) with satellite communications system were mounted (Mellors et al. 2009; Yetirmishli and Kazimova 2013; Yetirmishli et al. 2013). Currently in Azerbaijan, a net of 31 telemetric seismic stations works (Fig. 6.4).

On the basis of using several Azerbaijanian, Caucasian, and Soviet earthquakes' reports and utilization of numerous

Fakhraddin Kadirov[1], Samir Mammadov[1], Michael Floyd[2], Robert Reilinger[2], Akif Alizadeh[1] and Lev Eppelbaum[3] [1]Geology and Geophysics Institute, National Academy of Sciences, Baku, Azerbaijan Republic; [2]Dept. of Earth, Atmospheric and Planetary Sciences, Massachusetts Institute of Technology, Cambridge, USA; [3]Dept. of Geosciences, Tel Aviv University, Tel Aviv, Israel

A.A. Alizadeh et al., *Geosciences of Azerbaijan*,
Regional Geology Reviews, DOI 10.1007/978-3-319-40493-6_6

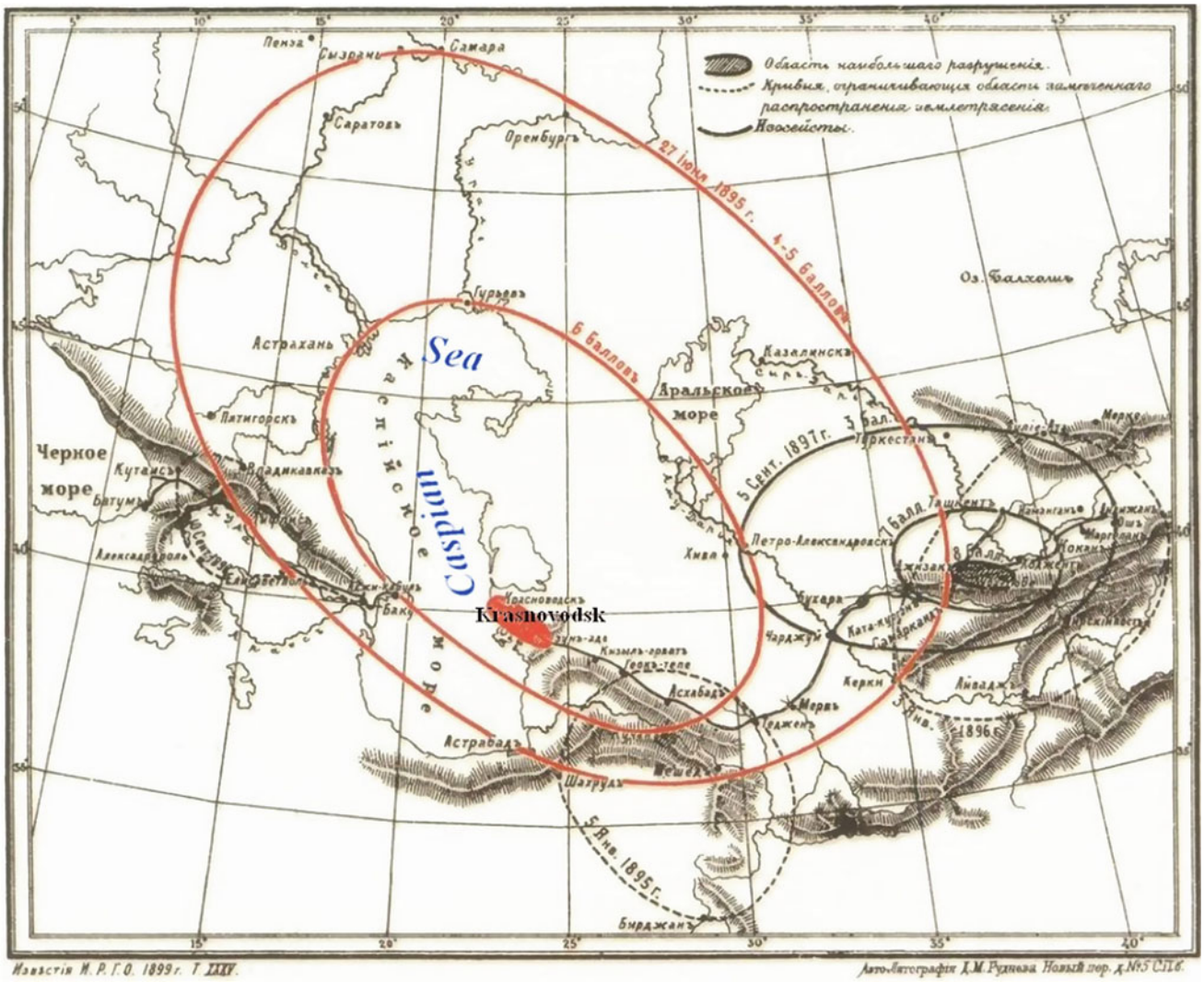

Fig. 6.1 Map of isoseist of the Krasnovodsk earthquake of July 08, 1895. (Author: I.V. Mushketov 1899)

international catalogs of earthquakes, a map of strong earthquake distribution in Azerbaijan was composed (Fig. 6.5).

Figure 6.5 displays strong earthquakes with ml ≥ 5.0 for the period of 427—03.30.2015 (n = 352 earthquakes). Distribution of earthquakes with ml ≥ 3.0 for the territory of Azerbaijan for the period 1963–2014 is shown in Fig. 6.6.

Distribution of earthquake focuses by depths is shown in Fig. 6.7. It is shown from this figure that the most part of the focuses are located within the interval of 5–20 km.

6.1.3 Repeatability of Earthquakes

A graph of repeatability of earthquakes indicates the energy component of earthquake distribution. For the estimation of the earthquake repeatability, usually log-linear equation of Gutenberg–Richter is applied (Gutenberg and Richter 1956). Assuming that the time of earthquake arising is random, their member decreases exponentially with magnitude increasing, and value of the magnitude is not limited.

On the basis of numerous statistical data, the relationship of $\log_{10}N$ from M is constructed, where N is the number of earthquakes with given magnitude M. Later, these data have been approximated by line of the kind:

$$\log_{10} N = a + bM \tag{6.1}$$

This equation presents the law of Gutenberg–Richter for the magnitude repeatability, where a and b are the empirical regional constants (Aki and Richards 1980). Seismic activity a and inclination b (or γ by using energetic class K) are the main parameters of seismic monitoring. In the selection of

Fig. 6.2 Oldest in Shamakhy Juma mosque (built in 809) after strong 1902 earthquake (photograph of that time)

the methodology of graph repeatability, construction preference usually is given to cumulative curve.

For the territory of Azerbaijan (for the period of 1963–2015), the number of seismic events N consists of 2810 and we have obtained the equation $Y = -0.95\ M + 6.65$.

The graph of repeatability function is shown in Fig. 6.8.

6.1.4 Map of Activity A_{10} and Maximal Possible Magnitude of Earthquakes

For the construction of a map of max possible number of earthquakes, a relationship between the seismic activity (A_{10}) and happened earthquakes with maximal amplitudes (M_{max} or energetic class K) is used (Riznichenko 1968, 1985; Kadirov et al. 2008a, b).

For the calculation of seismic activity (A), the region under study is divided into sectors with size 25 × 25 km, and for the central part of each sector, value (A) is computed by the use the following expression:

$$A = \frac{N_{\Sigma}(1 - 10^{-\gamma})1000}{10^{-\gamma}(K_{\min} - K_0)ST} \tag{6.2}$$

Here, S is the area of sector utilized for the calculation of concrete value A, N_{Σ} is the number of earthquakes happened in this area, γ is the angle of graph the earthquake repeatability (in our case $\gamma = 0.78$), $K_0 = 10$ and $K_{\min} = 12$ (where

Fig. 6.3 Map of isoseist of the Shamakhy earthquake of February 13, 1902. (Author: V. Weber 1899)

K is the energetic class of earthquakes), and T = 113 years (period for which we have data in seismic catalog). Between the energetic class K and magnitude M, a relationship $K = 4 + 1.8\ M$ was determined (Rautian 1964).

A map of seismic activity of Azerbaijan is shown in Fig. 6.9.

Analysis of the map of seismic activity A_{10} enables to delineate 4 separate zones with relatively high seismic activity (A_{10} = 2.4–2.8): (1) Belakan-Zagatala, (2) Shamakhy-Ismailly, (3) coastal plain of the Caspian Sea, and (4) Absheron Peninsula. The Talysh zone is distinguished with A_{10} = 1.8–2. Smaller values of seismic activity A_{10} = 1.2–1.4 were computed for comparatively small zones: Ganja, Sheki-Gabala, and Hachmaz. Other territories of Azerbaijan are reflected by nonsignificant seismic activity $A_{10} \leq 1.0$.

Map reflecting seismic activity in Azerbaijan and adjacent areas is shown in Fig. 6.10.

For construction of map of maximal possible earthquake' magnitudes (M_{max}), the well-known relationship between A and M_{max} (Riznichenko 1985) was used. The constructed map of the seismic activity for Azerbaijan and adjacent regions is shown in Fig. 6.11.

On the basis of seismic activity map A_{10} (for the period of 1902–2015), the map of maximal possible amplitudes was constructed (Fig. 6.12). As shown in Fig. 6.11, max amplitudes observed on the south of the Absheron Peninsula and in Shamakhy-Ismailly seismoactive zone. According to the computations in the Shamakhy-Ismailly area, earthquakes with magnitude M_{max} = 6.6 and in the south of Absheron Peninsula with M_{max} = 6.2 may happen. Other relative maximums are located in the area of Sheki town (M_{max} = 5.5), Lenkaran (M_{max} = 5.2), Jebrail town (M_{max} = 5.5), and Belakan town (M_{max} = 5.3). In the Greater Caucasus in the area of Racha (Georgia), a zone with max value of magnitude (M_{max} = 7.3) was revealed.

Fig. 6.4 The seismic network of Republican Seismic Survey Center of Azerbaijan National Academy of Sciences

6.1.5 Analysis of Stress State of the Earth's Crust in Azerbaijan and Surrounding Regions

The modern stress state of lithosphere of Azerbaijan and adjacent regions was studied on the basis of the World Stress Map (WSM), which includes different global and local databases about focus parameters from different catalogs (e.g., CMT of the Harvard University, USGS DB (Müller et al. 2005; Reinecker et al. 2005), and Azerbaijan Republic Center of Seismological Service). A map of the stress state of Azerbaijan lithosphere and adjacent regions was constructed (Fig. 6.12), with utilization of extended database for earthquake focuses for the Greater and Lesser Caucasus and by using the CASMO methodology (Müller et al. 2005; Reinecker et al. 2005; Babayev 2008, 2010).

Fig. 6.12 shows the Greater Caucasus dominant overthrust movements of N-NE direction that leads to Earth's crust compression.

A distribution of maximal horizontal stress of lithosphere for territory of the Caucasus was studied according to Sheorey (1994) methodology. Essence of this methodology consists of presentation of 1D layering spherical model of the Earth's crust with calculation of topography, acoustic properties, density, temperature, and some other parameters. Distribution of maximal horizontal stress for the Caucasian region at the depths of 10 and 20 km is shown in Fig. 6.13a and b, respectively.

6.2 Role of GPS Measurements in Seismological Studying in Azerbaijan

GPS observations play an important role in studying crustal deformation in the Africa–Arabia–Eurasia zone of plate interaction and use these observations to constrain broad-scale tectonic processes within the collision zone of the Arabian and Eurasian plates. Within this plate tectonics context, we examine deformation of the Caucasus system (Lesser and Greater Caucasus and intervening Caucasian Isthmus) and show that most crustal shortening in the collision zone is accommodated by the Greater Caucasus Fold-and-Thrust Belt (GCFTB) along the southern edge of the Greater Caucasus Mountains. The eastern GCFTB appears to bifurcate west of Baku, with one branch following the arcuate geometry of the Greater Caucasus, turning toward the south and traversing the Neftchala Peninsula. A second

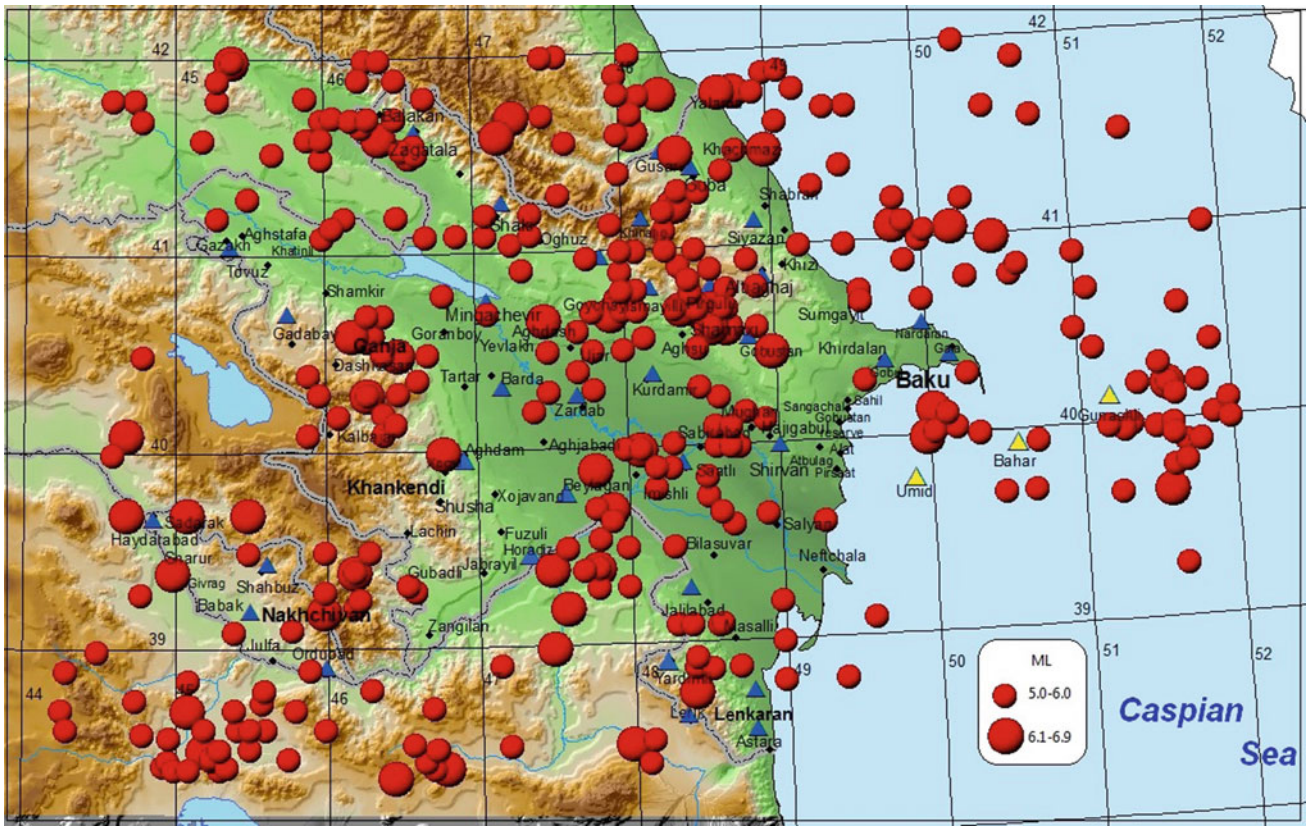

Fig. 6.5 Map of the epicenters of strong earthquakes was happened with ml ≥ 5.0 in Azerbaijan and adjacent areas in 427—03.30.2015 (edited by G. Yetirmishli)

branch (or branches) may extend directly to the Caspian Sea south of Baku, likely connecting to the Central Caspian Seismic Zone (CCSZ). We model deformation in terms of a locked thrust fault that coincides in general with the main surface trace of the GCFTB. We consider two end-member models, each of which tests the likelihood of one or other of the branches being the dominant cause of observed deformation. Our models indicate that strain is actively accumulating on the fault along the ~200 km segment of the fault west of Baku (approximately between longitudes 47–49°E). Parts of this segment of the fault broke in major earthquakes historically (1191, 1859, 1902), suggesting that significant future earthquakes ($M \sim 6$–7) are likely on the central and western segment of the fault. We observe a similar deformation pattern across the eastern end of the GCFTB along a profile crossing the Kur Depression and the Greater Caucasus Mountains in the vicinity of Baku. Along this eastern segment, a branch of the fault changes from a NW-SE-striking thrust to an ~N–S-oriented strike-slip fault (or in multiple splays). The similar deformation pattern along the eastern and central GCFTB segments raises the possibility that major earthquakes may also occur in the Eastern Azerbaijan. However, the eastern segment of the GCFTB has no record of large historical earthquakes and is characterized by thick, highly saturated, and overpressured sediments within the Kur Depression and adjacent Caspian Basin that may inhibit elastic strain accumulation in favor of fault creep, and/or distributed faulting and folding. Thus, while our analyses suggest that large earthquakes are likely in central and Western Azerbaijan, it is still uncertain whether significant earthquakes are also likely along the eastern segment and on which structure. Ongoing and future focused studies of active deformation promise to shed further light on the tectonics and earthquake hazards in this highly populated and developed part of Azerbaijan.

6.2.1 Combined Azerbaijan—US Investigations: A Short Background

The Geology and Geophysics Institute of the Azerbaijan National Academy of Sciences and the Department of Earth, Atmospheric, and Planetary Sciences at Massachusetts Institute of Technology have been using the Global Positioning System (GPS) to monitor crustal deformation in the territory of Azerbaijan since 1998 (Kadirov et al. 2008a, b, 2015a). These studies, coordinated and integrated with GPS studies in neighboring parts of the Arabia–Eurasia collision

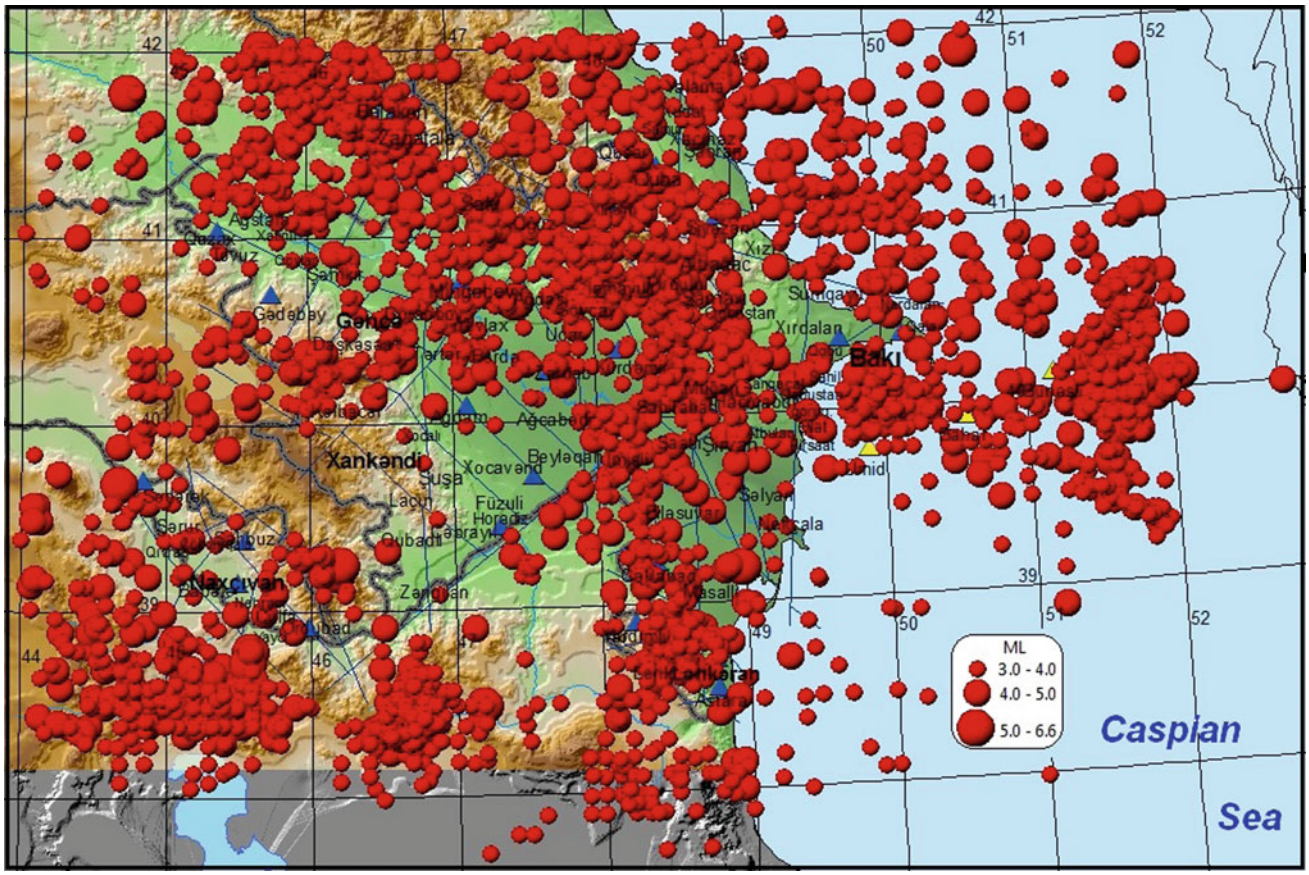

Fig. 6.6 Map of the epicenters of earthquakes was happened with ml ≥ 3.0 in Azerbaijan and adjacent areas in 1963—03.30.2015 (from materials of G. Yetirmishli)

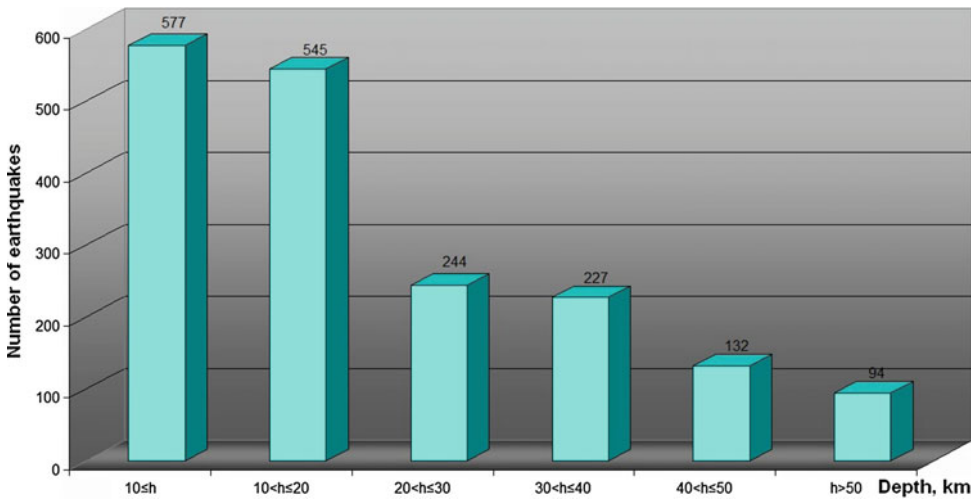

Fig. 6.7 The histogram of earthquake occurrences versus depth distribution was happened with ml ≥ 3 in Azerbaijan and adjacent areas in 1963—03.30.2015 (from materials of G. Yetirmishli)

zone, provide new constraints on the fundamental geodynamic processes that are actively deforming the collision zone (e.g., Reilinger et al. 2006; Kadirov et al. 2012, 2015a; Forte et al. 2012). These geodynamic processes produced and maintain the high elevation of the Turkish–Iranian Plateau (Fig. 6.14) and are the cause of the volcanic and earthquake activities that characterize this region.

The question of earthquake hazards has played a central role in our research because of the increasing vulnerability of the growing population and rapid infrastructure development

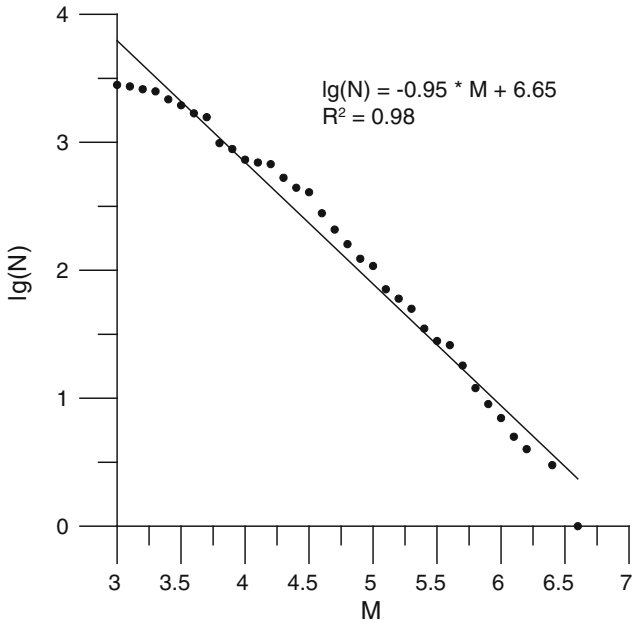

Fig. 6.8 Graph of earthquake repeatability on magnitudes

expected maximum magnitude, and their likelihood of occurrence. This information is necessary in order to take appropriate preparedness and mitigation measures to reduce the risk to the population and infrastructure, including the vulnerable facilities associated with the petroleum industry that are critical to the economy of Azerbaijan.

In this chapter, we use GPS observations to constrain Arabia–Eurasia relative plate motions and the character of interplate deformations in the Arabia–Eurasia collision zone. Within this broader context, we focus on earthquake hazards in the Azerbaijan Caucasus and SW Caspian Basin.

6.2.2 Tectonic Setting of the Caucasus Mountains

In the broadest context, the Lesser and Greater Caucasus Mountains lie within the zone of plate interaction where the African and Arabian plates are actively converging with the Eurasian Plate (Fig. 6.14). McKenzie et al.

Fig. 6.9 Map of seismic activity A_{10}

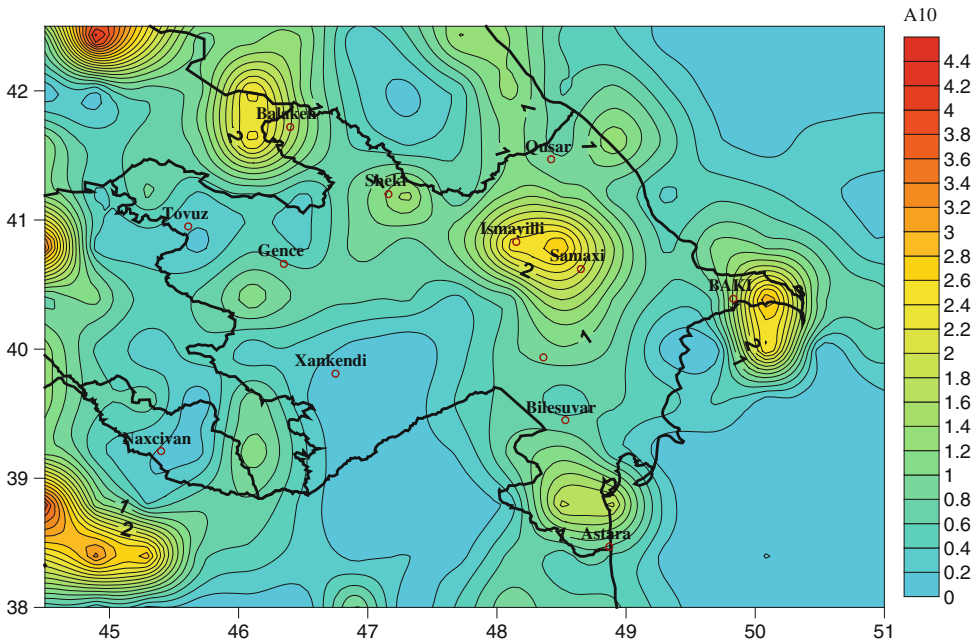

in Azerbaijan, particularly in the Baku-Absheron region. Azerbaijan has suffered earthquakes historically, including highly destructive earthquakes in 1191, 1859, and 1902 in the Shamakhy region. The 1191 and 1859 earthquakes devastated the then capital city of Shirvan, instigating a relocation of the capital to its present location in Baku (Mushketov and Orlov 1893; Kondorskaya and Shebalin 1982). Our GPS studies are part of the Geology and Geophysics Institute's mission that includes understanding the hazards associated with earthquakes: where they are most likely to occur, their

(1970), McKenzie (1970, 1972), and Jackson and McKenzie (1984, 1988) provided a plate tectonic description of the region, recognizing active continental collision in eastern Turkey, the Caucasus, and the Zagros; lateral transport of Anatolia (Turkey) toward the west; subduction of African oceanic lithosphere (i.e., Neotethys) along the Hellenic and Cyprus trenches; N-S extension in the Aegean and western Turkey; and ocean rifting along the Red Sea and Gulf of Aden. Convergence of Arabia and Africa with Eurasia has been occurring for >100 Ma

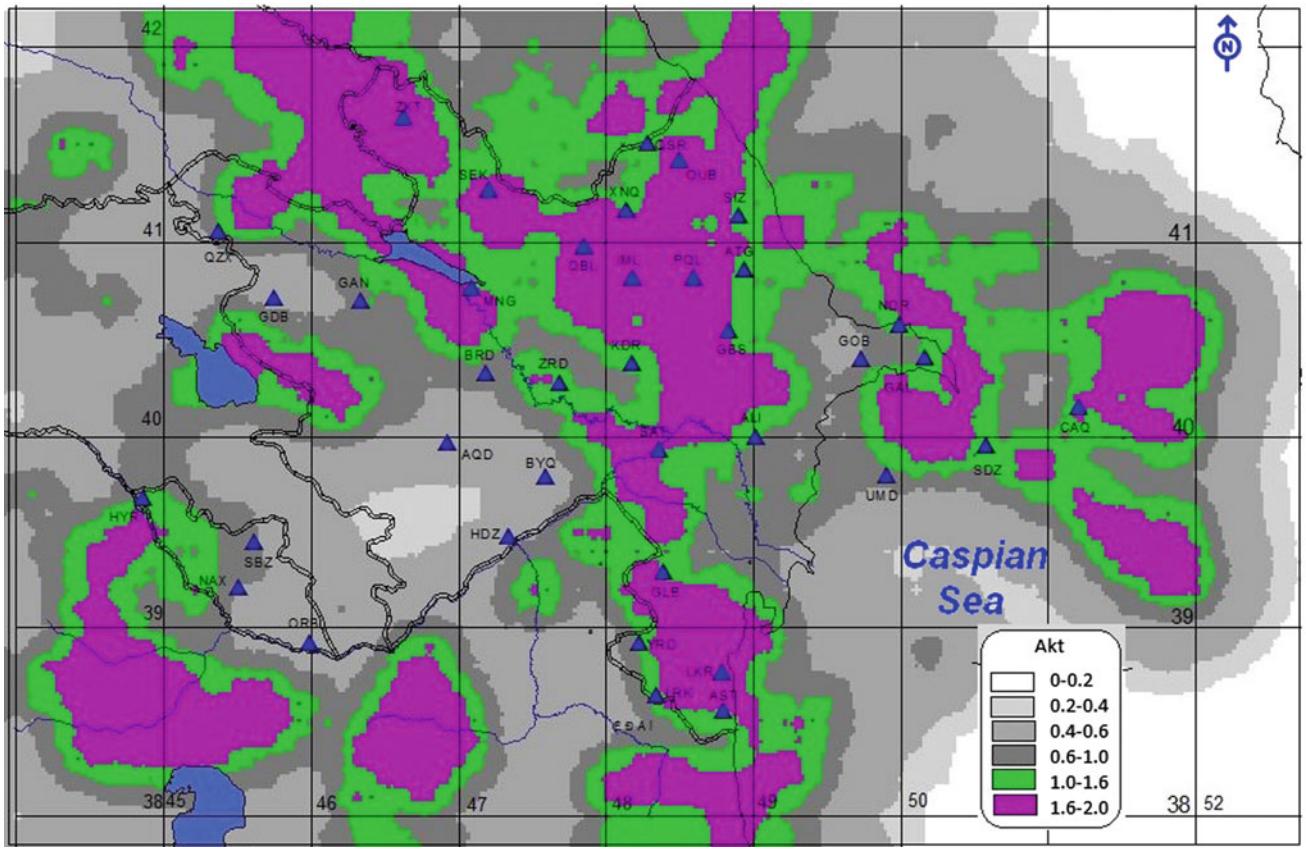

Fig. 6.10 Map of seismic activity in Azerbaijan and adjacent areas in 2000—03.30.2015

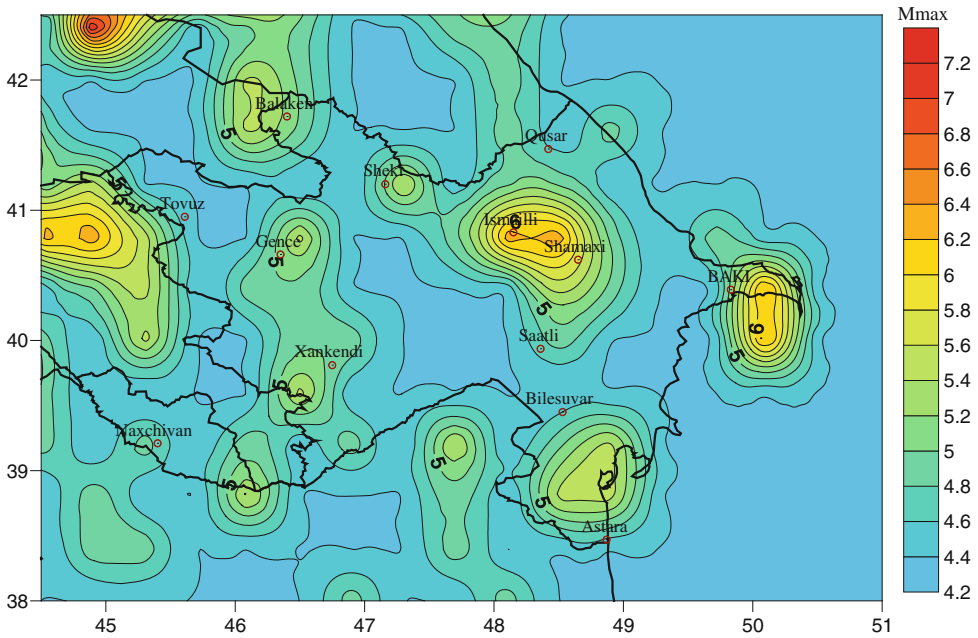

Fig. 6.11 Map of maximal possible magnitudes of earthquakes (M_{max}) (427—2015)

as the intervening Neotethys Ocean lithosphere has been subducting beneath Eurasia. While ocean subduction continues at present along the Hellenic and Cyprus trenches, complete ocean closure north of the Arabian Plate occurred ~27 Ma (e.g., McQuarrie and van Hinsbergen 2013).

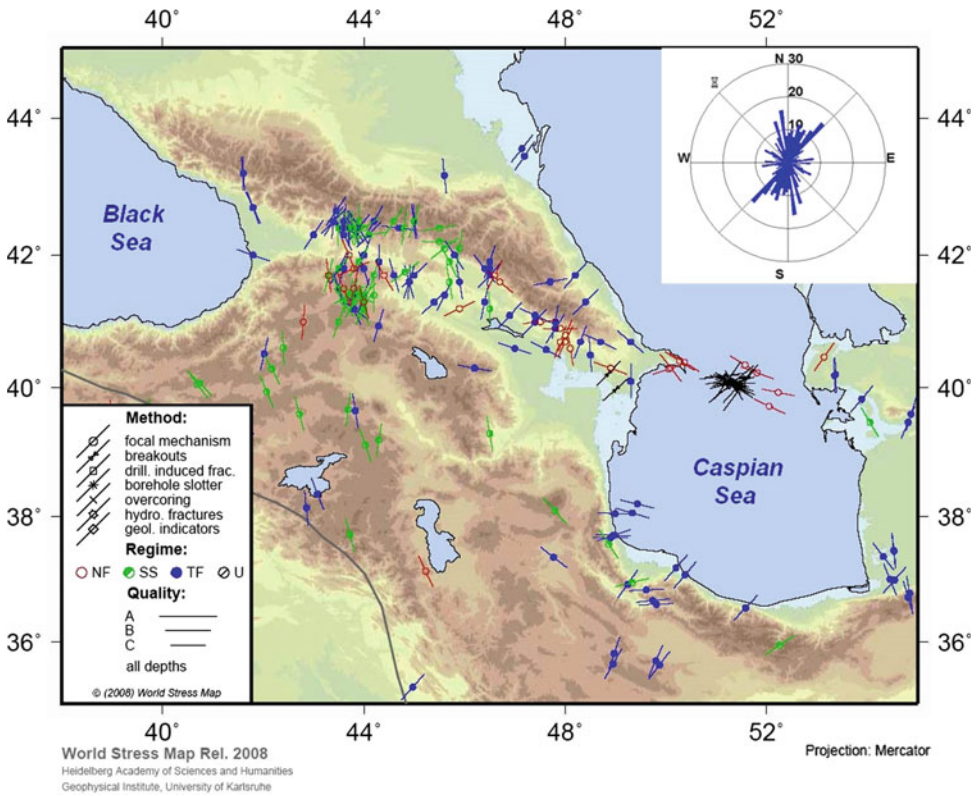

Fig. 6.12 Map of earthquake focus mechanisms for the Caucasus developed by the use of CASMO methodology (compiler: G.R. Babayev). *NF* Normal fault; *SS* Space strike; *TF* Thrust/fault

Subsequent seismological, geophysical, and geological studies added important refinements to this plate tectonic characterization, including the westward "extrusion" of Anatolia accommodated by the North and East Anatolian faults (Sengor et al. 1985), partitioning of crustal deformation in the eastern Turkey/Caucasus continental collision zone (Jackson 1992; Allen et al. 2004; Copley and Jackson 2006), the influence of slab detachment on uplift and volcanism of the Turkish–Iranian Plateau (e.g., Sengor et al. 2004; Barazangi et al. 2006), and early subduction of the South Caspian oceanic basin beneath the North Caspian Eurasian continental lithosphere along the CCSZ (e.g., Jackson et al. 2002).

The Greater Caucasus Mountains are thought to have formed by tectonic inversion of a former back-arc ocean that opened during north-dipping subduction of the Neotethys (e.g., Zonenshain and Le Pichon 1986; Forte et al. 2012), where the eastern Black Sea, Kur Depression in Azerbaijan, and southern Caspian Sea are the remaining remnants of the back-arc basin. Both the timing and spatial evolution of shortening and exhumation remain uncertain, with preferred estimates of the timing being Late Miocene to Early Pliocene (e.g., Kopp and Shcherba 1985; Philip et al. 1989; Vincent et al. 2007). Total shortening across the Greater Caucasus is also uncertain with estimates ranging from 150 to 400 km (e.g., McQuarrie and van Hindbergen 2013) and an increase in total shortening from west to east (e.g., Král and Gurbanov 1996; Avdeev and Niemi 2008; Forte et al. 2012).

6.2.3 Tectonics of the Africa–Arabia–Eurasia Plate System and GPS

During the past ~20 years, the active tectonics of the Africa–Arabia–Eurasia plate system has been measured directly by geodetic observations, most importantly the GPS (Hager et al. 1991; Dixon 1991). GPS consists of a system of 32 satellites 20,000 km above the earth's surface that complete 2 orbits of the earth each 24 h (http://tycho.usno.navy.mil/gpscurr.html). The satellites are operated by the US Department of Defense in cooperation with the Interagency GPS Executive Board. Other Global Navigation Satellite Systems (GNSS) have been developed by Russia (GLONASS), a European consortium (Galileo), Japan (QZSS), and China (Beidou), but these systems are not used in the results we report.

There are three components to use the GPS system for precise positioning: the satellite constellation, a global network of GPS tracking stations (Mueller and Beutler 1992), and data processing involving applying physical models and parameter estimation. Most importantly for this chapter, positions are determined with an accuracy of ~2 mm in

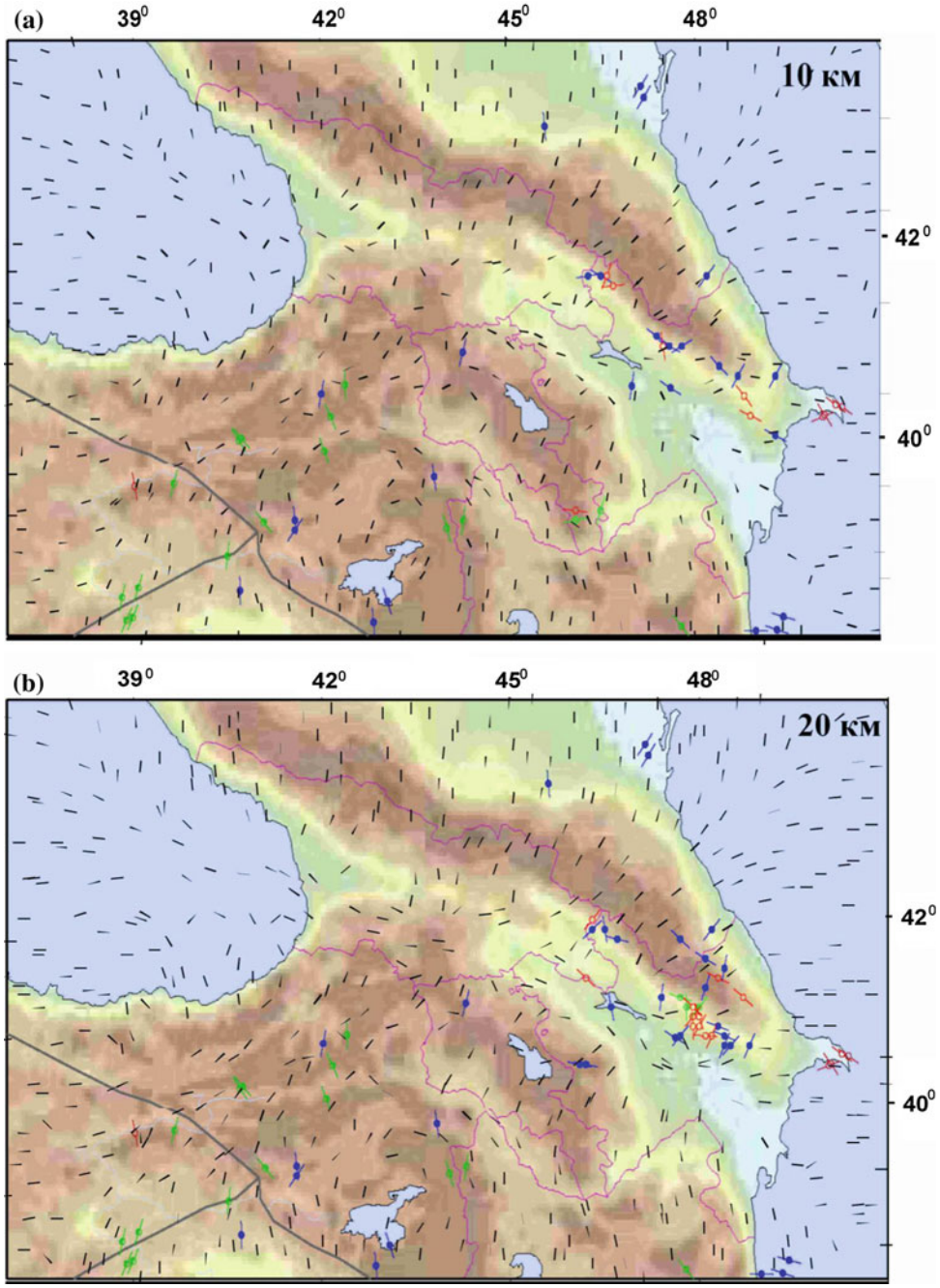

Fig. 6.13 Distribution of maximal horizontal stress at the depths of 10 (**a**) and 20 km (**b**) for the Caucasian region (compiler: G.R. Babayev)

horizontal coordinates and 3–10 mm in heights by recording data over a 24-h period. These precisions are possible because of highly accurate timing provided by atomic clocks on the GPS satellites, precise orbital positions for the satellites provided by the International GNSS Service (http://igs.org/) (determined from the global network of observing stations), and processing software that uses advanced mathematical models to account for the Earth's rotation, solid Earth and ocean tides, and the ionospheric and atmospheric delays of the GPS signal, among other factors that influence position estimates (e.g., Herring et al. 2010).

6.2.4 Estimating Surface Motions from GPS Observations

The GPS measurements presented in this chapter include both continuously recording stations (cGPS) that remain in

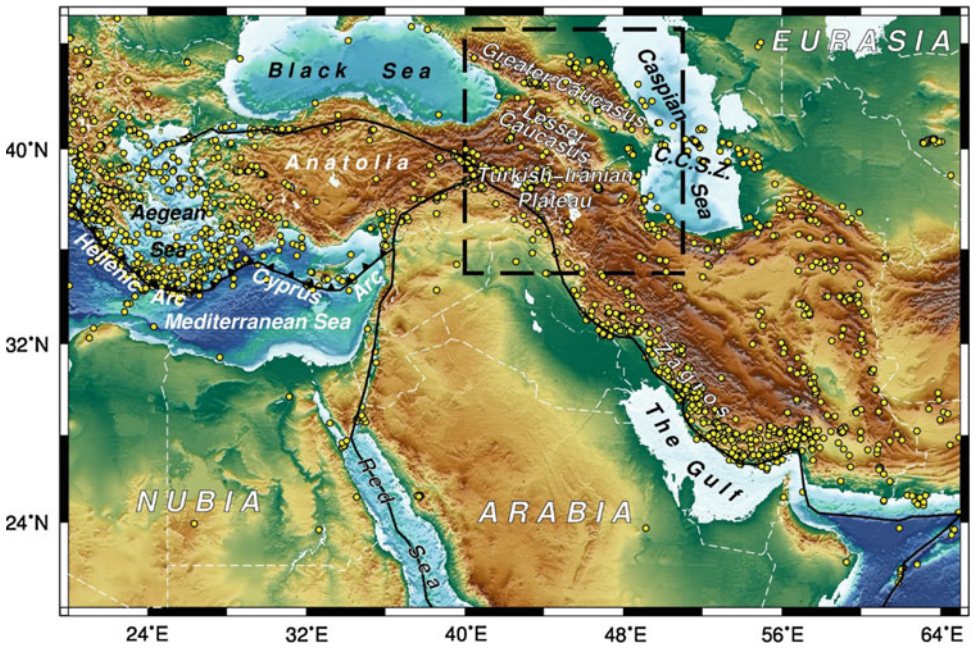

Fig. 6.14 Tectonic overview of the Arabia–Eurasia Collision Zone. *Yellow dots* are earthquakes from the EHB catalog (Engdahl et al. 1998) and updates thereof to 2008, plus ISC locations from 2009 onwards. Major plate boundaries are from Bird (2003)

place indefinitely (Fig. 6.15a) and survey-mode (sGPS) observations where the GPS antenna is positioned temporarily over a survey marker (Fig. 6.15b). By repeating the sGPS measurements episodically, we are able to estimate how the position has changed during the observation period. cGPS observations allow estimation of position on a daily basis or more frequently. However, reliable estimates of long-term, secular site velocities require a minimum of 2.5 years of observations even for cGPS because annual and semiannual systematic errors can bias estimates of steady-state motion (Blewitt and Lavellee 2002).

While the precision of our site velocities varies with observation period, the GPS horizontal velocities we determine using the GAMIT-GLOBK processing software (Herring et al. 2010) have 1-sigma uncertainties in the range of 0.2–0.9 mm/year, with most sites <0.5 mm/year. Because deformation rates across the Greater Caucasus Mountains vary from 2 to 14 mm/year from northwest to southeast, these precisions allow us to investigate details of the mountain building processes and associated earthquake hazards.

Velocity estimates are determined in a global reference frame, that is, with respect to the global network of tracking stations. The reference frame is determined and maintained (updated) by the International Terrestrial Reference Frame (ITRF) Service (Altamimi et al. 2012) using well-positioned stations, with a long history of well-behaved observations, located around the globe and accounting for motions of the Earth's tectonic plates. We determine site velocities from Altamimi et al. (2011), but we present them in a reference frame fixed to the Eurasian Plate. It is important to bear in mind that the relative motion between measurement sites (i.e., deformation or strain rate) is invariant to changes in reference frame.

6.2.5 Present-Day Arabia–Eurasia Continental Collision

Figure 6.16 shows the velocities of GPS sites in the zone of interaction of the African, Arabian, and Eurasian plates (Reilinger et al. 2006 and updates thereof for sites in Azerbaijan). Virtually all major active tectonic processes are well resolved and quantified by the GPS observations, including the northward motion and counterclockwise (CCW) rotation of the Arabian Plate and active opening of the Red Sea (e.g., ArRajehi et al. 2010), crustal shortening of the Zagros fold-and-thrust zone in Iran (e.g., Djamour et al. 2010), the CCW rotation of the Turkish region accommodated by the North Anatolian Fault (McClusky et al. 2000; Reilinger et al. 2006), northwest motion of the African Plate with respect to Eurasia (McClusky et al. 2003), and the change from NNW motion of Arabia to NNE motion of the Caucasus system (Reilinger et al. 2006; Vernant and Chery 2006).

Reilinger et al. (2006) used the GPS velocity field to estimate how AR-EU convergence is partitioned between lateral "extrusion" of crustal blocks and crustal shortening. They found that a large majority (~70 %) of the convergence is accommodated by lateral transport, and ~15 % by shortening along the GCFTB, with the remainder being accommodated by other structures or distributed strain. The only slightly thickened crust in the Lesser Caucasus—E Turkey Plateau (Gok et al. 2003; Barazangi et al. 2006), in spite of 150–400 km of continental convergence (McQuarrie and van Hindbergen 2013)—indicates that the geodetic results reflect long-term, tectonic deformation processes in the collision zone (i.e., if not for lateral transport, the crust would be expected to be much thicker). The utility of geodetic studies for constraining long-term

Fig. 6.15 **a** GPS continuously recording station located in Sheki, Azerbaijan. In the background, the project participants are shown (from *left* to *right*): Prof. R. Reilinger, Dr. S. Mammadov, and Prof. F. Kadirov **b**. GPS survey site in the Greater Caucasus. The antenna is precisely located above the mark that is cemented into the bedrock

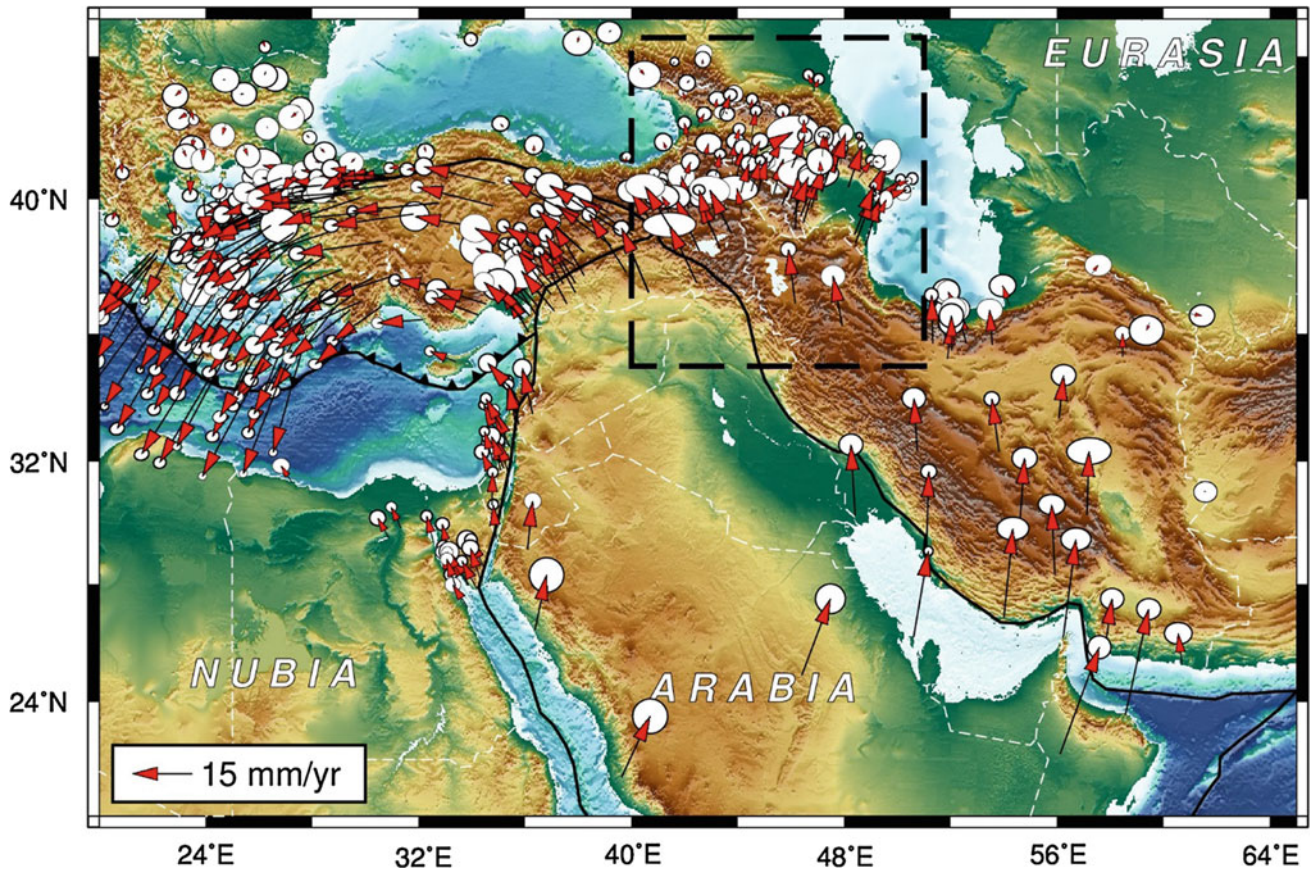

Fig. 6.16 GPS velocities and 95 % confidence ellipses with respect to Eurasia (according to Altamimi et al. 2012) within the Eastern Mediterranean from Reilinger et al. (2006), with updated velocities in Azerbaijan for the period of 1994.0-2013.5. Major plate boundaries are from Bird (2003), as in Fig. 6.14

geodynamic processes finds further support from comparison between present-day, geodetically derived Arabia–Eurasia convergence rates and longer-term plate convergence rates derived from plate tectonic reconstructions (e.g., McQuarrie et al. 2003) that indicate that these plate motions have been remarkably constant (±10–15 %) since the onset of continental collision in the Early Miocene (e.g., ArRajehi et al. 2010).

6.2.6 Deformation of the Greater and Lesser Caucasus

Figure 6.17 shows a close-up of the GPS velocity field around the Greater and Lesser Caucasus, providing a quantitative basis to estimate the locations and slip rates and directions on the major structures that accommodate deformation. As is clear from Fig. 6.17, the main shortening in the Arabia–Eurasia collision zone occurs along the southern boundary of the Greater Caucasus near the seismically active GCFTB. This is well illustrated in the series of velocity profiles in Fig. 6.18, which show the rate of motion versus distance along profiles parallel to (6.18a) and traversing (6.18b–e) the Caucasus system (profile locations on Fig. 6.17). Figure 6.18a shows the component of velocity perpendicular to the direction of the profile; Fig. 6.17b–e shows the component along the direction of the profile (i.e., shortening or lengthening). The plot shown in Fig. 6.4.18a for the profile aligned along strike of the Greater Caucasus demonstrates the progressive increase in convergence rate with Eurasia from west to east, from 1 to 2 mm/year near the eastern end of the Black Sea, to 13–14 mm/year south of Baku, Azerbaijan. The absence of any consistent change in rates in the direction of the profile traversing the Lesser Caucasus (i.e., Figure 6.18b, d, e) constrains active shortening in the Lesser Caucasus to <2 mm/year. These observations, and the low level of significant seismicity in the Lesser Caucasus (Fig. 6.14; the M6.8, 1988, Spitak, Armenia catastrophic earthquake being a notable exception), suggest that within the resolution of our GPS observations, the Lesser Caucasus behaves like a coherent block rotating in a counterclockwise sense with respect to Eurasia, around a pole near the eastern end of the Black Sea (e.g., Lawrence 2003; Reilinger et al. 2006; Copley and Jackson 2006). Rotation may be related to the closure of an intercontinental

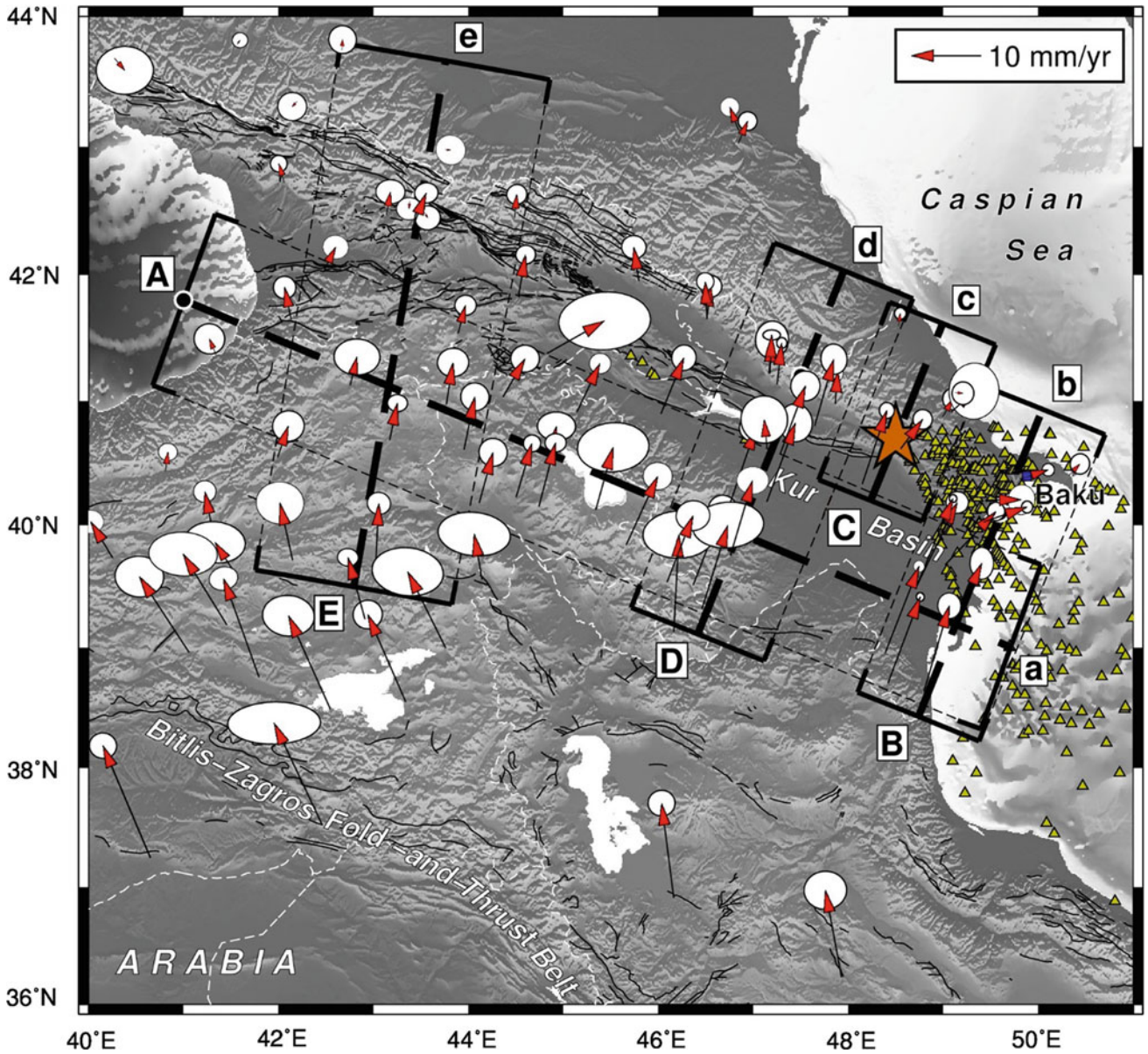

Fig. 6.17 GPS velocities and 95 % confidence ellipses w.r.t. (with respect to) Eurasia for the eastern AR-EU collision zone. *Orange* star shows 1902, M6.9 Shamakhy earthquake epicenter. *Yellow triangles* represent mud volcanoes". Velocity profiles **A**–**E** are shown in Fig. 6.18. Their origins are marked by *black dots* which, for profiles **B**–**E**, coincide approximately with the surface expression of the GCFTB

back-arc basin separating the Lesser and Greater Caucasus, with the Caucasian Isthmus (Kur Depression in Azerbaijan) being the last remnants currently undergoing the final stages of subduction/closure (e.g., Cowgill et al. 2012).

6.2.7 Geometry of the Eastern GCFTB

The nature of the eastern GCFTB remains an outstanding question in Caucasus tectonics with implications for earthquake hazards in the greater Baku region (Kadirov et al. 2012). Specifically, the physical connection (i.e., faults or zones of deformation) connecting the GCFTB and the CCSZ (CCSZ) (Fig. 6.14) remains uncertain. While both structures accommodate convergence with Eurasia, along the CCSZ it is manifest in moderately deep (~40 km) earthquakes with focal mechanisms indicative of deformation within the subducting plate rather than on the plate interface (Jackson et al. 2002), while the GCFTB has broken historically in shallow (~15–20 km) continental thrust events (e.g., Triep et al. 1995). It is possible that these differences may be due to differences in the nature of the crust and lithosphere (i.e.,

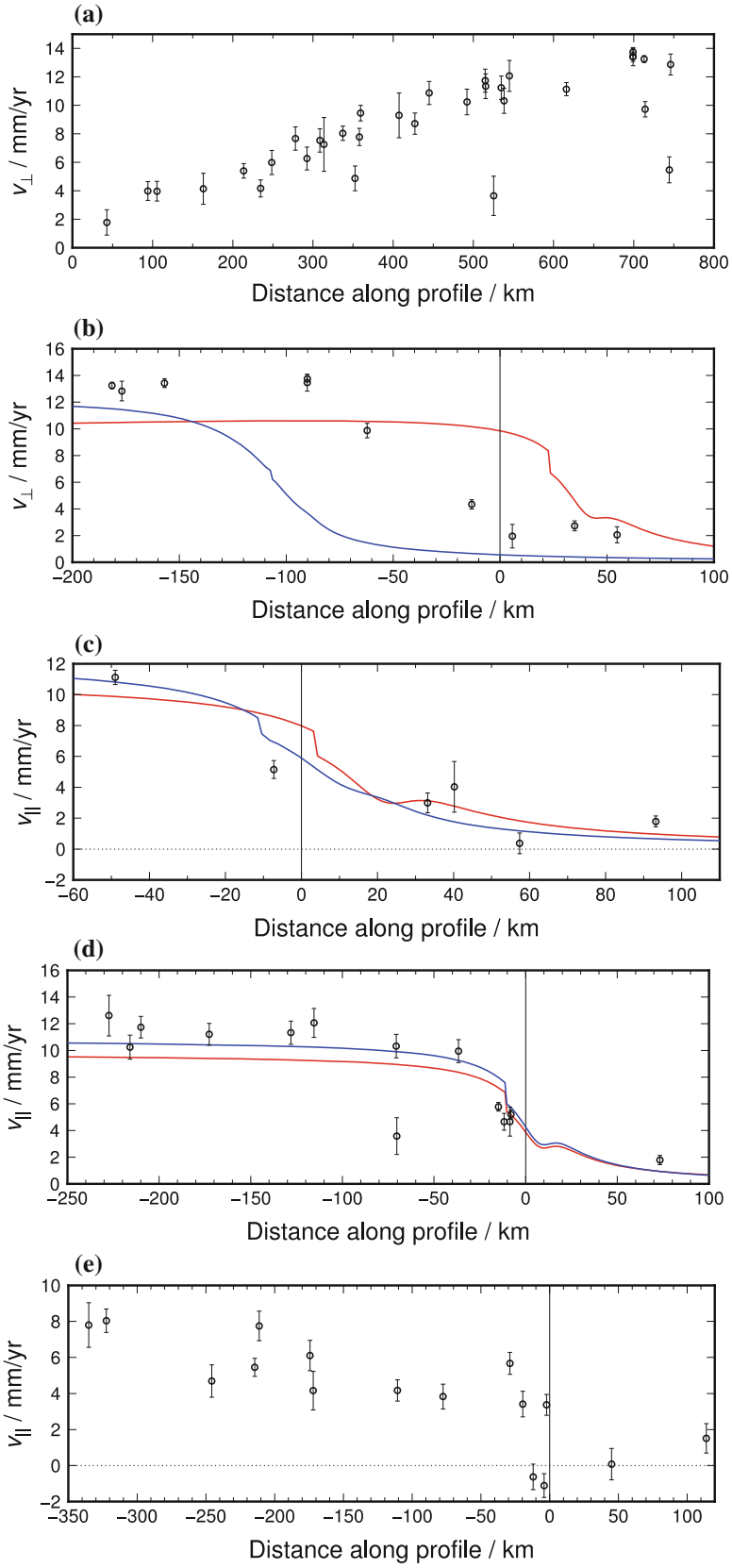

Fig. 6.18 Plots of transverse (**a**) and parallel (**b**–**e**) components of velocities versus distance along the profiles are shown in Fig. I.4.17. *Red curves* are velocity profiles from the model shown in Fig. 6.18a, and *blue curves* are velocity profiles from the model shown in Fig. 6.18b (see main text for descriptions). The approximate location of the surface trace of the GCFTB is shown by the vertical line at the origin (see *black dots* in Fig. 6.17). Note different scales

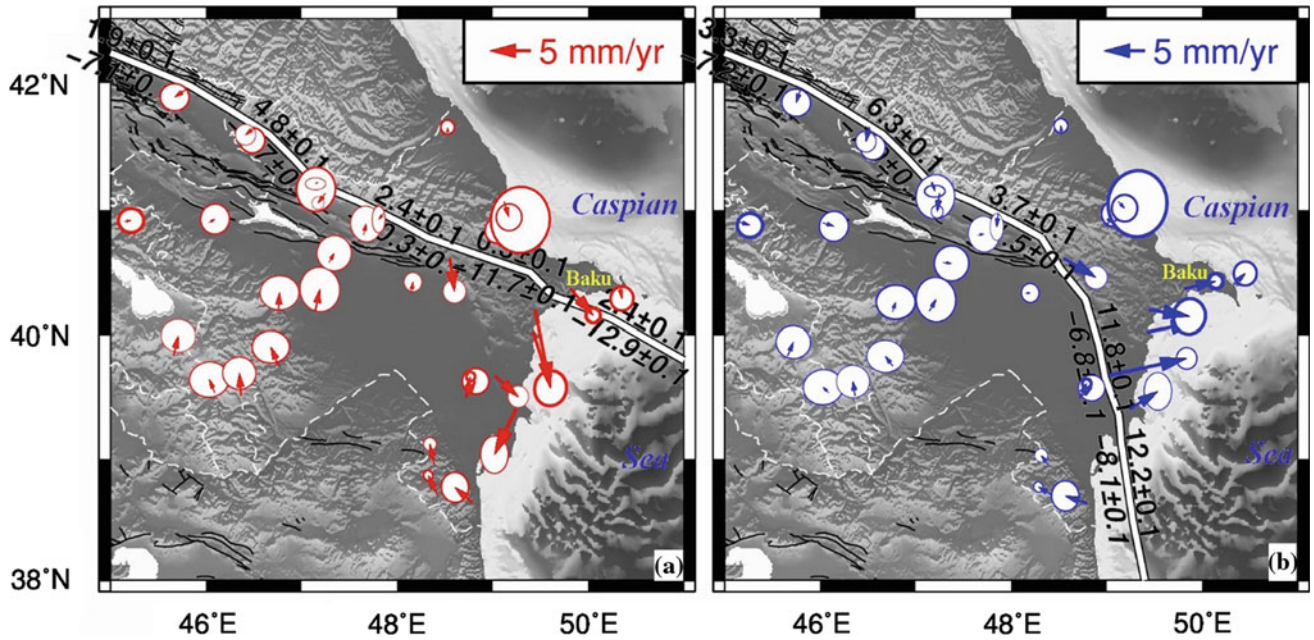

Fig. 6.19 Map showing GPS residual velocities for the two fault models: **a** with continuation of the GCFTB eastwards toward the CCSZ and **b** with change in strike of the GCFTB southward along the west coast of the Caspian Sea. The common fault (west of 49.5°E) is a thrust fault dipping north at 30°. In **a**, the continuation of the GCTFB is also modeled as a thrust fault dipping north at 30°; in **b,** the southward change in strike of the fault is accompanied by a gradual change in dip such that the fault is vertical along the Neftchala area. All segments of the faults are locked to 12 km depth. Model fault slip rates shown along the fault traces, where the upper number is the strike-slip rate (positive is right-lateral) and the lower number in *italics* is the dip-slip rate (positive is extension) in mm/year

rheology) at the junction of the GCFTB and CCSZ, continental for the Kur Depression and oceanic (with very thick and consolidated sediments) in the South Caspian Basin (Knapp et al. 2004; Kadirov and Gadirov 2014). It is also possible, perhaps likely, that the different modes of accommodating shortening at the plate interface reflect different dynamics, subduction in the CCSZ, and continental collision along the GCFTB (e.g., Reilinger et al. 2006; Vernant and Chery 2006; Copley and Jackson 2006).

New GPS observations on the Absheron and Neftchala peninsulas and on the southern edge of the Caspian Basin in Iran make it clear that a branch (or multiple branches) of the GCFTB follows the curved topographic break between the Kur Depression and Greater Caucasus/Absheron Peninsula, having a SSE orientation south of Baku (Figs. 6.17 and 6.19b). Structures accommodating deformation may merge offshore with the thick, folded sediments south of the Absheron Peninsula. This offshore geometry is supported by GPS velocities in the SW corner of the Caspian basin in Iran (Djamour et al. 2010) that indicate northerly motion with rates similar to those in the adjacent Lesser Caucasus to the west.

On the other hand, the set of velocity vectors from ~50 km SW of Baku (SHIK) to the eastern end of the Absheron Peninsula (GURK) indicates shortening at ~6 mm/year perpendicular to the easternmost Caucasus (Fig. 6.19a). We interpret these GPS observations to imply that crustal shortening accommodated by the GCFTB is partitioned between NE-SW shortening across the Absheron Peninsula and right-lateral, transpressive deformation S of Baku that joins the system of folded sediments in the SW Caspian Basin (Figs. 6.17 and 6.19a, b).

6.2.8 Implications for Earthquake Hazards in Azerbaijan

Earthquake hazard analysis includes estimating the most likely locations, magnitudes, and time of future earthquakes. We emphasize that it is not possible at present to determine these parameters precisely (e.g., Jordon 2014). However, with auxiliary information from geology (paleoseismology, geomorphology, e.g., Forte et al. 2012) and seismology (instrumental and historic, e.g., Ambraseys and Melville 1982; Philip et al. 2001; Jackson et al. 2002), it is possible to make estimates of location and, to a lesser extent, magnitude and time of anticipated events.

Our approach involves identifying zones of rapid, spatially systematic changes in site velocities that we observe occur almost exclusively across known faults (e.g., McClusky et al. 2000; Vernant et al. 2014). To the extent that the velocity changes across the faults are due to strain accumulation, the velocity field provides direct evidence for the likely locations

of future earthquakes. Some caution is needed since earthquakes are known to occur in areas of very low strain rates, including the 1988 Spitak, Armenia catastrophic earthquake. While it is difficult to quantify hazards in such cases, we expect very long repeat times for similar earthquakes (e.g., Westaway 1990), making their occurrence less likely than earthquakes on faults that are rapidly accumulating strain.

The magnitude of an earthquake is directly related to the total earthquake offset (coseismic fault slip) and the surface area of the fault break (Aki and Richards 1980; Wells and Coppersmith 1994). Some idea of the possible size of pending earthquakes can be garnered from the historic earthquake record and/or geological observations of surface faults (e.g., Weldon et al. 2004). With an estimate of the expected magnitude of an anticipated earthquake, we can use the time since the prior event, and the rate of offset accumulation across the fault to estimate the time until the next earthquake (i.e., when the offset accumulation equals the observed coseismic offset in prior earthquakes).

This simple approach assumes that (1) rate differences across the fault are due entirely to strain accumulation for the full time period since the prior earthquake and not permanent deformation or aseismic slip on the fault (i.e., the fault is fully coupled, or locked, and the crust adjacent to the fault is not deforming an elastically); (2) the GPS-determined rate of strain accumulation is constant throughout the period since the prior earthquake; and (3) the fault will fail in an earthquake of similar magnitude to the prior event(s) (i.e., "characteristic earthquake" model; Swartz and Coppersmith 1984).

Each of these assumptions requires consideration for each individual fault being analyzed (e.g., Working Group on California Earthquake Probabilities (WGCEP) 2008). Some faults are known to fail aseismically via fault creep up to the surface, either in steady-state or by episodic creep events. Sections of the San Andreas and North Anatolian strike-slip faults are well-studied examples (e.g., Lyons and Sandwell 2003; Cetin et al. 2014). The earth only accumulates elastic strain on faults in the outermost "elastic crust"—generally depths of less than ~25–30 km (we exclude discussion of deep earthquakes in the subducting lithosphere). However, we are not aware of evidence for shallow, aseismic slip on continental thrust faults such as those within the GCFTB (e.g., Bird and Kagan 2004). On the other hand, the easternmost segment of the GCFTB may curve to the south taking on a predominantly strike-slip geometry (Fig. 6.17b). To our knowledge, this segment, located south of Baku, has not experienced strike-slip earthquakes during the instrumental period (Jackson et al. 2002). However, whether this segment is creeping aseismically or accumulating strain without generating seismicity (the case for the southern San Andreas Fault; Bennett et al. 1996; Fialko 2006) remains conjectural.

GPS observations can help address the nature of fault coupling since the spatial pattern of deformation adjacent to a fault has a characteristic strain pattern for a locked fault (e.g., Okada 1985), and a step function offset for a freely slipping fault: directly identifiable "end-member" cases. Furthermore, the gradient of the velocity near the fault is directly related to the fault locking depth (i.e., below this depth, the fault creeps aseismically). Besides directly identifying locked fault segments (i.e., those capable of generating earthquakes), constraining the locking depth is important for estimating fault area and thus anticipated earthquake magnitude (e.g., Aki and Richards 1980).

Because the time between moderate and large earthquakes is long compared to the length of time, precise fault monitoring observations have been made (beginning in the 1970s with ground-based observations, e.g., Prescott and Savage 1976), it is not possible to directly determine the extent to which the rate and spatial geometry of strain accumulation remain constant through the period between earthquakes. While long-term slip rates estimated from offset features and topography agree well (±10 %) with present-day GPS slip rates (e.g., Reilinger et al. 2006), rates of strain accumulation on faults are known to vary between earthquakes. An important, well-observed case is the period of rapid surface deformation that occurs following earthquakes (postseismic period) (e.g., Nur and Mavko 1974). Postseismic deformation is thought to be due in part to slip on the fault below the seismogenic depth (at temperatures and pressures where the crust no longer behaves elastically) as it responds to the instantaneous stress transferred by the earthquake (e.g., Pollitz 1992). As the lower, aseismic part of the fault relaxes the coseismic-induced stress, it reloads the shallow, seismic segments. This mechanism can either drive after slip on the fault (in essence adding to the total coseismic slip, i.e., total earthquake slip prior to relocking) or reload the fault, thereby advancing the fault in time toward the next earthquake. Available evidence indicates that all fault types experience postseismic deformation of some kind that impacts the nature of strain accumulation on the earthquake fault.

For the few earthquakes studied in some detail, the postseismic period of rapid strain accumulation or release is short relative to the time between earthquakes (<5 %) (e.g., Lyzenga et al. 2000; Podgorski et al. 2007; Ergintav et al. 2009) and any increase in strain accumulation is to some extent offset by afterslip (i.e., afterslip releases strain and stress). Although insufficient case studies are available to determine the degree to which postseismic effects bias estimates of earthquake repeat times quantitatively, for the most part we assume this uncertainty is small compared to uncertainties due to deviations from the characteristic earthquake model.

The assumption that faults fail in "characteristic earthquakes" is the most critical and the most uncertain assumption necessary for any earthquake forecast (Working Group on California Earthquake Probabilities (WGCEP) 2008). Again, we are hampered by the long time between

earthquakes compared to the instrumental and historic records. Paleoseismic observations help fill this deficit, but the information on prior earthquakes becomes less precise with age. From the scant constraints we have, it is clear that even for faults that adhere to the characteristic earthquake model in a general way, appearing to behave quasiperiodically as evidenced by long historic records, variations in repeat times are high, introducing large uncertainties in timing and magnitude estimates (e.g., Weldon et al. 2004). In spite of this variability, repeating patterns have been reported when sufficiently long histories are available (e.g., Ambraseys 2000; Zoller et al. 2007; Meghraoui et al. 2012), and the notion that quasi-steady strain build-up (as evidenced by geodetic observations) will "periodically" overcome fault friction and lead to an earthquake is physically appealing.

Because of these outstanding uncertainties, rather than making estimates of future earthquake occurrences, we present general hypotheses that we hope will help focus on ongoing studies to constrain better active geodynamic processes, present-day fault behavior (locked vs. creeping), and paleoseismic and historic earthquake studies, all of which are needed to reduce forecast uncertainties. Furthermore, our identification of faults that are potentially accumulating strain in Azerbaijan contributes to the development of earthquake scenarios for estimating seismic ground motion and focusing on earthquake preparations and responses (e.g., Jones et al. 2008).

6.2.9 Deformation and Possible Strain Accumulation Along the Main Caucasus Thrust Fault

In Fig. 6.18b–d, we compare the results of simple, elastic models of strain accumulation for the wide profiles crossing eastern and west-central Azerbaijan (Fig. 6.17). We consider two models; the surface outcrops of both are shown in Fig. 6.19a and b, and the model parameters (fault locking depth and dip) are given in the caption of Fig. 6.19. Both models include thrusting along the segment of the GCFTB west of the Absheron Peninsula, where the fault dips northward at 30°. Model A has this same fault geometry extending to the east, south of Baku, and connecting with the CCSZ. Model B has the modeled fault following the topographic break of the GCFTB west of Baku, turning to the south and extending through the Neftchala Peninsula. In this latter model, the fault dip gradually increases with the change in strike to become vertical along the Neftchala area. The models show the deformation predicted by a fault that is locked to a certain depth and freely slipping below that depth following the formulation of Okada (1985). Figure 6.19 shows the residual (observed minus estimated) GPS velocities for each model.

Profile D crosses the GCFTB approximately 70 km WNW of the 1902, M6.9, Shamakhy earthquake epicenter. For perspective, a M6.9 thrust earthquake is expected to have a surface rupture length of ~40–70 km (Wells and Coppersmith 1994). The model results for the profile shown in Fig. 6.18d are almost identical for the 2 models considered; both models involve thrust faulting on a 30° dipping fault that is roughly coincided with the GCFTB in west-central Azerbaijan (Fig. 6.19). The width of the zone of shortening is consistent with a fault locked to a depth of at least 12 km (measured vertically from the surface) accumulating offset deficit at a rate of 10–12 mm/year (i.e., offset deficit is the missing slip on the fault that is expected to be released in an earthquake).

Figure 6.18c shows the shorter and sparser profile crossing the GCFTB at the location of the 1902 Shamakhy earthquake (Fig. 6.17). The Shamakhy region experienced earlier, devastating earthquakes in 1191 and 1859. As mentioned earlier, these events were so severe that they instigated the population to move the Azerbaijan capital from Shirvan to the present location of Baku. The total amplitude (~11 mm/year) and distribution of shortening (~70–100 km) along this short profile that crosses a segment of the fault system known to generate $M \sim 7$ earthquakes are very similar to that for profile D. In addition, the overall kinematics and morphology of the GCFTB is generally similar along this segment of the range. However, this is approximately the location at which the major GCFTB begins to bifurcate into several potentially active structures. The relatively sparse GPS data along profile C makes these end-member structures, as previously described and shown by the red and blue curves, in distinguishable. Nevertheless, these observations suggest that the entire GCFTB in Azerbaijan west of the Shamakhy earthquake region is likely to experience earthquakes in the future, possibly similar to the historic events near Shamakhy.

Profile B (Fig. 6.18b) crosses the Kur Depression, eastern Greater Caucasus, and Absheron Peninsula near Baku (Fig. 6.17). As described earlier, the new GPS observations presented here reveal that the trend and complexity of the easternmost GCFTB near Baku aid us in placing physical constraints on potentially active structures in an area that remains poorly understood. However, large misfits to both models confirm that there is likely to be deformation accommodated both on structures that continue east into the Central Caspian Sea and others that strike southward toward the Neftchala area. Figures 6.18b and 6.19 show that neither end-member model alone satisfactorily explain the observations. Neither model is significantly better than the other: The weighted root-mean-square (WRMS) residual to the model shown in Fig. 6.19a is 2.04 mm/year and the WRMS for the model shown in Fig. 6.19b is 1.96 mm/year, which is not a statistically significant difference. We do not consider complex models that include multiple branches of the GCFTB here since we have insufficient density of data and lack constraints on motion of the South Caspian Basin

southeast of the Absheron Peninsula. We emphasize that these are highly idealized models that do not include variations in elastic properties of the crust, or complexities in the geometry of the eastern GCFTB. More realistic models will require better geodetic constraints on the spatial distribution of motions around the eastern segment.

As indicated in Figs. 6.18 and 6.19, both these models do provide a good fit to the observed velocities in Western Azerbaijan, the Kur Depression, and near Baku and the Absheron region. This gives us confidence about the magnitude of convergent strain rate that must be accommodated by some active structure or structures as we move from Western Azerbaijan (convergence at ~8 mm/year) to east (convergence at ~12–13 mm/year). However, significant residual velocities in either one direction or the other exist in the area immediately southwest of the Absheron Peninsula along the coast of the Caspian Sea (Fig. 6.19a compared to Fig. 6.19b), indicating that the exact location and nature of these structures require further investigation. It is likely that a combination of the two modeled faults, possibly along with some other hybrid of intervening structures, is responsible for the observed deformation in this area.

In addition to its arcuate shape and the transition from a shallow dipping thrust fault in the west to a steeply dipping strike-slip fault south of Baku, the easternmost segment of the GCFTB is different in a number of ways from the central thrust segment. For example, the sedimentary section in the southern Caspian Sea south of the Absheron Peninsula reaches thicknesses of >15 km, roughly twice the thickness of that in the eastern Kur Basin. The Caspian Basin is underlain by ocean crust as opposed to the continental crust below the Lesser Caucasus and Kur Depression (e.g., Neprochnov 1968; Kadinsky-Cade et al. 1981; Jackson et al. 2002). Furthermore, the ubiquitous nature of mud volcanoes in the eastern Kur Depression (Aliyev et al. 2009) attests to the importance of hydrothermal processes in the crust not present along the GCFTB to the west. How these differences may affect seismogenic structures and earthquake activity is presently unknown.

In spite of these uncertainties, the pattern of deformation across the eastern branch of the GCFTB (Fig. 6.18b) is very similar to that across the central fault segment (Fig. 6.18c and d) that is known to generate significant earthquakes. In addition, the discrepancies between the model fits for our two end-member models (Figs. 6.18b and 6.19) appear to "bracket" the observations SW of Baku, suggesting that a hybrid model for strain accumulation is more representative of the actual fault configuration; in this sense, the GPS observations are at least consistent with active strain accumulation. On the other hand, the broad distribution of shortening (Fig. 6.18b) may be due to distributed, aseismic deformation associated with multiple, creeping fault branches, rather than strain accumulation on specific major faults. Aseismic deformation within the thick, water-saturated sediments of the eastern Kur Depression seems plausible. We caution, however, that the 2011, M9, Fukushima, Japan Earthquake unexpectedly ruptured through the thick, partially consolidated sediments offshore of Japan, producing a substantially larger earthquake than that was estimated for the fault and the accompanying destructive tsunami (e.g., Lay et al. 2011).

We can conclude that Azerbaijan has experienced large ($M \sim 7$) and highly destructive earthquakes in the past and almost certainly will suffer earthquakes in the future. The geodetic observations presented in this chapter demonstrate that strain is accumulating on the 200-km-long segment of the GCFTB from the Shamakhy region (~70 km west of Baku) to the Azerbaijan–Georgian border. Based on the historic earthquake record (destructive earthquakes in 1191, 1859, and 1902) and the geodetic evidence we present for active strain accumulation, M7 thrust earthquakes are likely along this entire segment.

Geodetic observations across the Kur Depression and Absheron Peninsula in the densely populated and highly developed easternmost part of Azerbaijan show a similar deformation pattern across the GCFTB as the observations crossing the central and eastern segments of the fault. While this may indicate active strain accumulation that could generate earthquakes, the absence of large historic earthquakes, the change in strike of the fault west of Baku, and the thick highly saturated sediments in the eastern Kur Depression and south Caspian Basin may preclude large events like those known to occur on the fault further east. However, given the rapid increase in the population and the extensive infrastructural development in this part of Azerbaijan, and the likelihood of gaining new insights from additional geodetic observations and complex fault models, it is essential that further studies be focused on the possibility and effects of damaging earthquakes along the eastern segment of the GCFTB. In particular, densifying GPS coverage along and across the Eastern Caucasus, Kur basin, and Greater Caucasus, constraining the subsurface geometry of the GCFTB and its extension into the Caspian Sea with seismic studies, and investigating the historic earthquake record and paleoseismic observations to extend the earthquake record will provide the constraints needed to clarify better earthquake hazards in Azerbaijan.

6.3 Analysis of Earth's Gravity Time Series in Sheki Gravity Station in Azerbaijan

6.3.1 Short Background

Earth's gravity field is mainly due to the tidal field resulting from the gravitational interaction between the Earth and

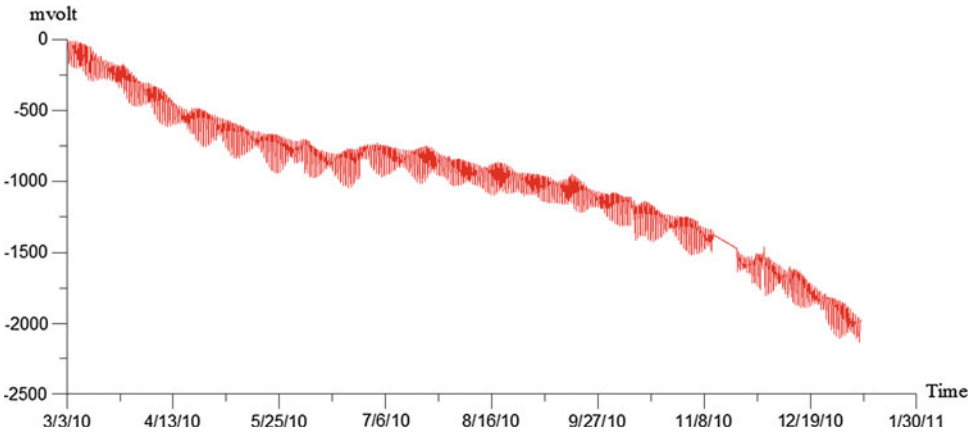

Fig. 6.20 Tidal observation at station SHEKI hourly values (calibration factor 1 mV = 12.88 nm/s^2)

other bodies of the solar system. The measurements of the Earth's gravity, i.e., the intensity of the Earth's gravity field, are perspective methods of geodynamic researches since they enable to define amplitude and phase–frequency characteristics of the various spheres of the Earth, giving information about their viscoelastic properties and tectonics (Melchior 1983; Torge 1989; Ducarme et al. 2002). Gravimetric methods also include measurements of the temporal changes of the Earth's gravity field. The value of gravity field at a point depends, among others, not only on the tidal forces and internal structure of the Earth, but also on other phenomena contributing to its variation. Seismic processes involve changes in the Earth's mass distribution with consequent modification of the gravity field. Therefore, gravity measurements are able to detect such changes providing some information useful for the understanding of the physical sources of such phenomena (Albano and Corrado 2013). In fact, several gravity anomalies are caused also by earthquakes, i.e., the Earth's crust vibrations generated by the propagation of seismic waves (Bogusz et al. 2013).

This situation changes nearby oceanic seaside where noticeable contribution is done by oceanic tides, which do not only create additional gravitation, but also deforms Earth's crust at the distances of many hundreds of kilometers (Kadirov et al. 2008a, b; Jentzsch 1997; Mammadov et al. 2011; Kadirov et al. 2013). Also, apparent gravity changes could originate from instrumental causes and human activities (Vidale et al. 1998; Young and Zürn 1979; Heaton 1982). As the observed gravity changes can be considered the sum of the effects of different sources active at any given time, it is crucial to separate the effects due to different sources. An installation of the gravimeter in a site which is not sensitive to oceanic effects could help in removing at least this very significant source of variation in gravimetric signals. With regard to this aspect, gravimetric observations performed in tectonically active regions such as the southern slope of the Greater Caucasus, which is far from the influences of oceanic and sea tides, are of great scientific interest (Kadirov et al. 2013; Telesca et al. 2013; Kadirov et al. 2008a, b; Kadirov 2000; Kadirov et al. 2012). The selection of the site Sheki (41.2220°N, 47.1710°E) in Azerbaijan was just based on its remoteness from the oceanic activity and effects of the Caspian and Black seas. Sheki station was installed by the Institute of Geology and Geophysics of the Azerbaijan National Academy of Sciences on the northwest of Azerbaijan and is surrounded by the seismogenic zones (Kadirov et al. 2013). It is located in the foothills of the Greater Caucasus at a height of 723 m and represents the main Earth tidal station in Azerbaijan.

6.3.2 Tidal Parameters: Results of Field Investigations and Data Processing

The gravity data were analyzed in our study span for 358 days from April 1, 2010 until April 8, 2011 (Mammadov et al. 2011).

As a result of the treatment, a time series of hourly values was obtained (Fig. 6.20). A linear drift superimposed by a seasonal period is clearly shown, in which the tidal amplitude is changing from about −100 nm/s^2 (10 μGal) to approx. −2000 nm/s^2 (−200 μGal). This drift rate is typical for spring gravimeters, even if they are specially constructed for the observation of Earth tides (Hegewald et al. 2011). Fortunately, there was only one bigger gap in the time series at the beginning of December 2010, due to power failure.

We have computed the amplitude and phase spectrum of the hourly time series (Fig. 6.21, amplitude in nm/s^2; Fig. 6.22, phase in degrees). The result shows clearly the diurnal and semidiurnal tidal wave groups (Fig. 6.21). The long and aperiodic drift behavior shown in Fig. 6.20 can be seen in the lower frequencies of the spectrum, where the values rise up to some hundreds nm/s^2.

The time series were analyzed using the tidal analysis program ETERNA3.4 (comp. Wenzel 1996), and 18 main tidal constituents are used. Unfortunately, the barometric

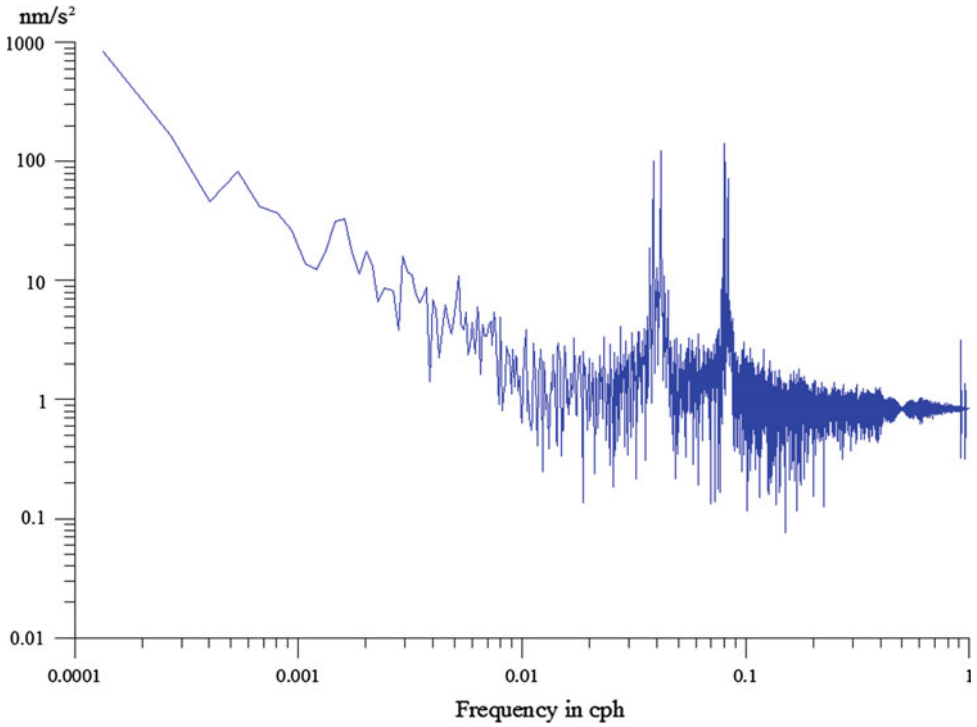

Fig. 6.21 Amplitude spectrum in nm/s^2

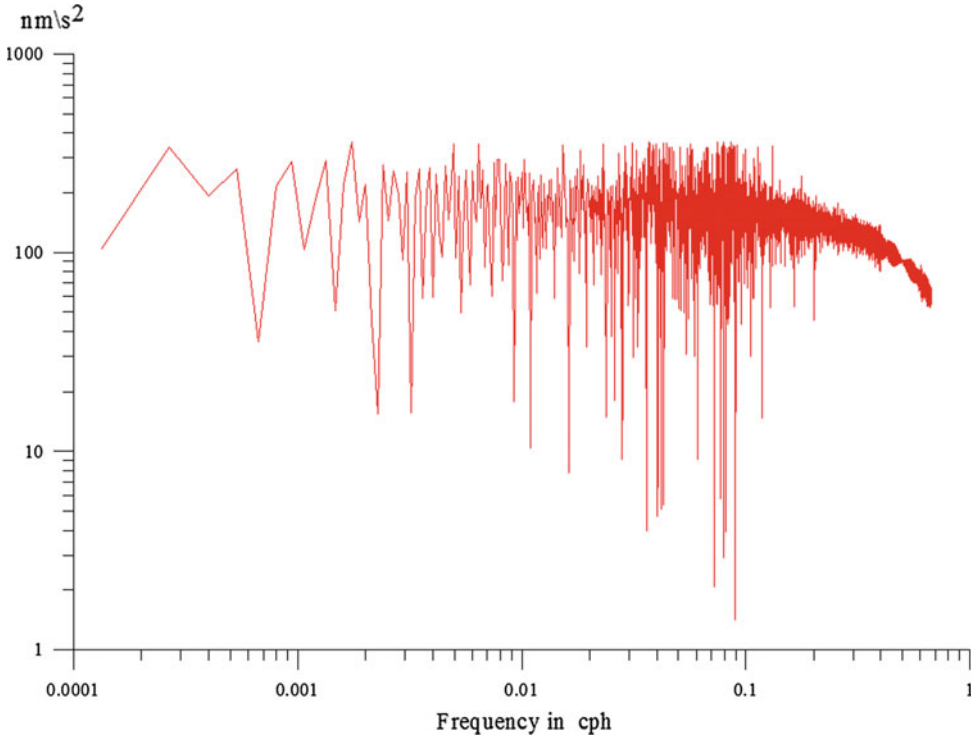

Fig. 6.22 Phase spectrum in degrees

pressure could not be taken into account, because no parallel recording could be provided. The results with a standard deviation of 2.3 nm/s^2 show the expected tidal parameters for an elastic Earth with a tidal factor of about 1.16 and phase differences close to zero for what concerns the main tidal constituents O1 and M2. The ocean tides' loading is certainly not very large. S2 is clearly affected by the atmospheric pressure effects. The amplitude factor of M3 is close to the theoretical value 1.07 for the ter-diurnal waves. Only the tidal waves with very small amplitudes such as J1, OO1, and also M4 show large errors or phase differences (Table 6.1). The good quality of the tidal analysis is also confirmed by the

Table 6.1 Adjusted tidal parameters estimated by the tidal analysis (ETERNA34)

From (cpd)	To (cpd)	Wave	Amplitude nm/s^2	Amplitude factor	Standard deviation	Phase lead (deg)	Standard deviation (deg)
0.501370	0.911390	Q1	68.2193	1.15701	0.01300	−1.1056	0.6430
0.911391	0.947991	O1	354.1556	1.15004	0.00247	0.0564	0.1227
0.947992	0.981854	M1	27.8636	1.15106	0.02475	−0.0024	1.2335
0.981855	0.998631	P1	168.0192	1.17278	0.00639	0.1383	0.3120
0.998632	1.001369	S1	9.9697	2.94461	0.40712	23.1128	7.9131
1.001370	1.004107	K1	487.6658	1.12644	0.00202	0.0386	0.1029
1.004108	1.006845	PSI1	9.2121	2.71957	0.27759	−63.8957	5.8598
1.006846	1.023622	PHI1	13.7586	2.23210	0.14630	−0.2523	3.7468
1.023623	1.057485	J1	25.0134	1.03295	0.03295	4.0132	1.8267
1.057486	1.470243	OO1	15.2876	1.15430	0.04641	4.2860	2.3005
1.470244	1.880264	2N2	15.7614	1.21233	0.07792	−0.4752	3.6800
1.880265	1.914128	N2	96.4778	1.18519	0.01470	−0.6918	0.7109
1.914129	1.950419	M2	496.8515	1.16864	0.00277	−0.3369	0.1357
1.950420	1.984282	L2	12.8293	1.06749	0.12653	0.2552	6.7904
1.984283	2.002736	S2	231.0796	1.16833	0.00600	−1.8217	0.2943
2.002737	2.451943	K2	63.9098	1.18932	0.02098	0.5638	1.0106
2.451944	3.381478	M3	6.5914	1.04852	0.0491	1.2240	2.6833
3.381379	4.347615	M4	0.1324	1.53400	2.34224	61.6109	87.4848

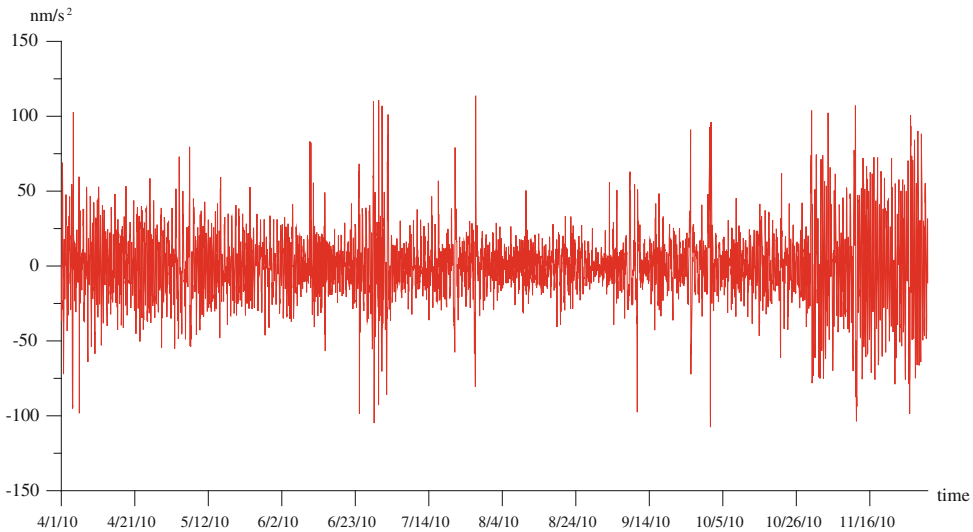

Fig. 6.23 Tidal residuals after tidal analysis (ETERNA3.4)

tidal residuals (Fig. 6.23). The residuals mainly consist of white noise; however, a seasonal variation can be seen. In the autumn and winter time, at the end and at the beginning of the time series higher residuals of up to ±10 nm/s^2 are observed, whereas in summer time (mid of time series), the amplitudes vary by about ±5 nm/s^2 only. This is probably caused by the effect of barometric pressure variations, which usually show higher amplitudes in winter than in summer time.

The tidal analysis also shows the well-known nearly diurnal free wobble (NDFW) of the Earth, which is caused by the forced oscillation of the Earth core (Zürn 1997). If the quality of the gravity time series is high enough, this geodynamic effect can be detected in the diurnal frequency band. The tidal parameters of small constituents of PHI1 and PS1 should be higher than 1.16 and for the main constituent K1 should be slightly reduced compared to O1.

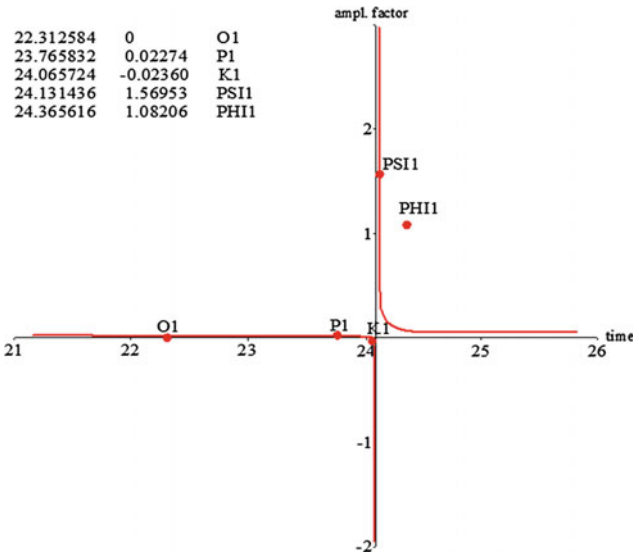

Fig. 6.24 Nearly diurnal free wobble caused by the Earth's core clearly indicated by the gravity observation in the SHEK station

Figure 6.24 shows these parameters over the time in hours, and it is obvious that the NDFW was significantly observed by the gravity record in the Sheki station.

The record was analyzed piecewise using moving windows of three months' length each, moved by one month. Thus, the results were allocated to the middle center month of the intervals. Figures 6.24 and 6.25 show obtained results for the amplitude factor and phase lead. Applying the errors obtained, in the semidiurnal tidal band the variations are not significant, whereas in the diurnal tidal band in some cases, the error bars do not overlap. In particular in the case of the phase, it seems to be strange that all the results show decreasing phases toward the end of the recording period. The fact the phase shift of M2 is nearly twice the phase shift of O1 points obviously to a timing error due to the drift of the clock.

6.3.3 Power Spectrum Analysis and Multifractal Detrended Fuctuation Analysis of the Earth's Gravity Time Series in Azerbaijan

We have been studied the gravity signal recorded in the Sheki gravity station using the multifractal detrended fluctuation analysis (MF-DFA) in order to characterize its time dynamics and identify the underlying mechanisms of generation of its temporal signal variability on a wide range of temporal scales (Telesca et al. 2015).

The gravity data analyzed in our study span for 358 days from 2011:11:28:08:48 to 2012:05:11:05:11:59. The data are acquired by the automated Burris Gravity Meter B-14 (Adams et al. 2004; Jentzsch 2008), provided by the company ZLS Corporation, Austin/Texas, USA. The data are stored on a PC memory card, used like a floppy disk to transfer data to a host computer equipped with a PC memory card interface. The sampling time was set at 3 min, and date and time were in UTC. GPS was used for automatic time correction. The accuracy of the singular measurement accounts for nearly 1 μGal (10 nm/s^2), which confirms the uniquely high precision of such equipment.

Multifractals are principally characterized by high signal variability on a wide range of temporal scales, thus being depicted as intermittent with sudden bursts of high-frequency fluctuations. The MF-DFA (Kantelhardt et al. 2002) is a multifractal method well known for its simplicity and effectiveness. It operates on the time series $x(i)$, with $i = 1, 2,\ldots, N$, and N is the length of the series. After subtracting the mean value of the series x_{ave}, we construct the "trajectory" or "profile" by integrating

$$y(i) = \sum_{k=1}^{i} [x(k) - x_{\text{ave}}]. \tag{6.3}$$

Next, the integrated series is divided into $N_S = \text{int}(N/s)$ nonoverlapping segments of equal length s. Since the length

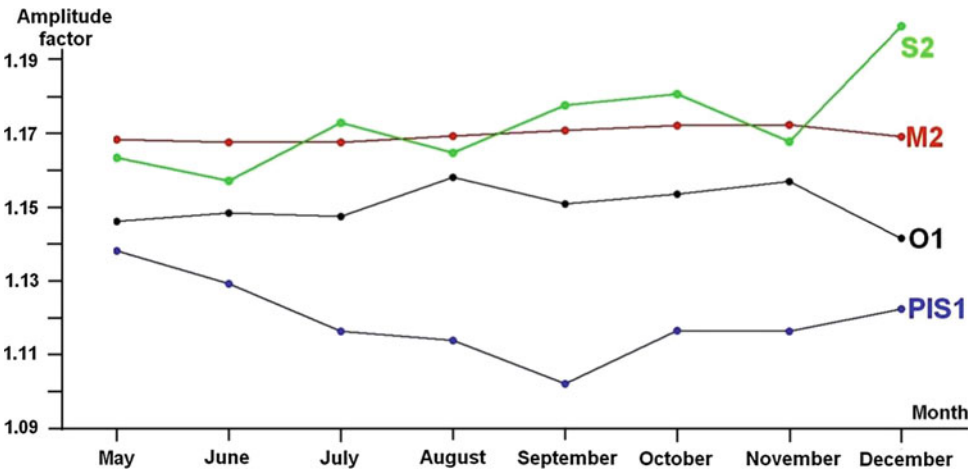

Fig. 6.25 Monthly main waves O1, P1S1, M2, and S2 estimated by the tidal analysis (ETERNA34)

N of the time series could not be a multiple of the time scale s, a short part of the profile $y(i)$ at the end may remain. Therefore, the same procedure is repeated starting from the opposite end. Thereby, $2N_S$ segments are obtained altogether. Then, we calculate the polynomial local trend for each of the $2N_S$ segments by a least square fit of the series. Then, the variance is calculated by the following formula:

$$F^2(s,v) = \frac{1}{s}\sum_{i=1}^{s}\{y[(v-1)s+i] - Y_v(i)\}^2. \tag{6.4}$$

for each segment ν, ν = 1, …, N_S and

$$F^2(s,v) = \frac{1}{s}\sum_{i=1}^{s}\{y[(v-N_S)s+i] - Y_v(i)\}^2, \tag{6.6}$$

where ν = N_{S+1}, ..., $2N_S$. Here, $y_v(i)$ is the fitting polynomial in segment v. Then, we average overall segments to obtain the qth order fluctuation function:

$$F_q(s) = \left\{\frac{1}{2N_s}\sum_{v=1}^{2N_s}\left[F^2(s,v)\right]^{\frac{q}{2}}\right\}^{\frac{1}{q}}, \tag{6.7}$$

where in general the index variable q can take any real value except zero. The parameter q enhances the small fluctuations if is negative; otherwise, if it is positive, it enhances the large fluctuations of the time series. Repeating the procedure described above, for several time scales s, $F_q(s)$ will increase with increasing s. Then, analyzing log–log plots $F_q(s)$ versus s for each value of q, we determine the scaling behavior of the fluctuation functions. If the series $x(i)$ is long-range increases for large values of s as a power law, we can write

$$F_q(s) \approx s^{h_q}. \tag{6.8}$$

The value h_0 corresponds to the limit h_q for $q \to 0$ and is obtained through the logarithmic averaging procedure:

$$F_0(s) \equiv \exp\left\{\frac{1}{4N_s}\sum_{v=1}^{2N_s}\ln\left[F^2(s,v)\right]\right\} \approx s^{h_0}. \tag{6.9}$$

In general, the exponent h_q will depend on q. For stationary series, h_2 is the Hurst exponent H (Feder 1988). Therefore, h_q is called the generalized Hurst exponent. Value of h_q independently from q characterizes monofractal series. If the scaling behavior of small fluctuations is different from that of the large ones, h_q depends on q and indicates that the series is multifractal.

Multifractality in a series can be also quantified by using the singularity spectrum, obtained applying the Legendre transform (Parisi and Frisch 1985). From the relationship

$$\tau(q) = qh_q - 1 \tag{6.10}$$

and

$$\alpha = \frac{d\tau}{dq} \tag{6.11}$$

we obtain

$$f(\alpha) = q\alpha - \tau(q), \tag{6.12}$$

where α is the Hölder exponent and $f(\alpha)$ indicates the dimension of the subset of the series that is characterized by α (Ashkenazy et al. 2003). The multifractal spectrum gives information about the relative importance of various fractal exponents present in the series. In particular, the width of the spectrum indicates the range of present exponents.

We analyzed the 3-min sampled data of the Earth's gravity field from November 28, 2011, until May 11, 2012. Figure 6.26 shows the investigated time series. The data demonstrate a clear decreasing gravity intensity behavior. We firstly removed such linear nonstationarity by linear fitting the data by a least square method. Then, we subtracted this linear approxmation from the observed data. The detrended data are shown in Fig. 6.27. We explored the spectral properties of the detrended data by using the periodogram method. The obtained results are shown in Fig. 6.28. The power spectrum is decreasing and decorated by two intense periodicities at 24 and 12 h. The amplitude of the 12-h cycle is higher than that of the 24-h cycle, and this indicates that the 12-h periodicity is not a higher harmonic of the 24-h one. We removed these two periodicities and obtained the residual data (standardized to null mean value and unitary standard deviation) (Fig. 6.29).

Figure 6.30 shows the power spectrum of the residual gravity data computed as the power spectrum of a power law of the frequency with a power law exponent of about 1.7.

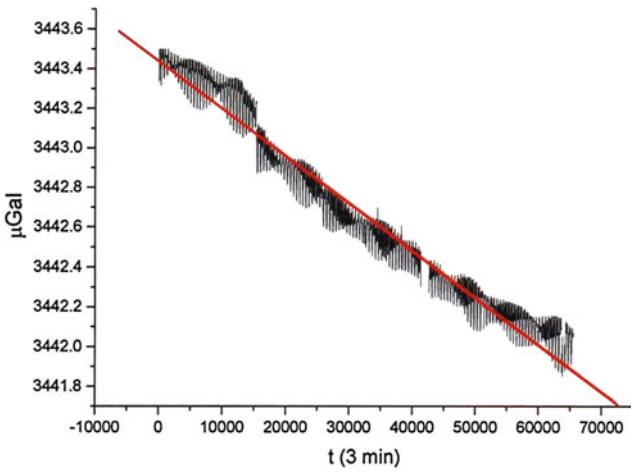

Fig. 6.26 Earth's gravity time series from 2011:11:28:08:48 to 2012:05:11:05:11:59. The sampling time is 3 min. The *red line* indicates the linear least square fitting of the data

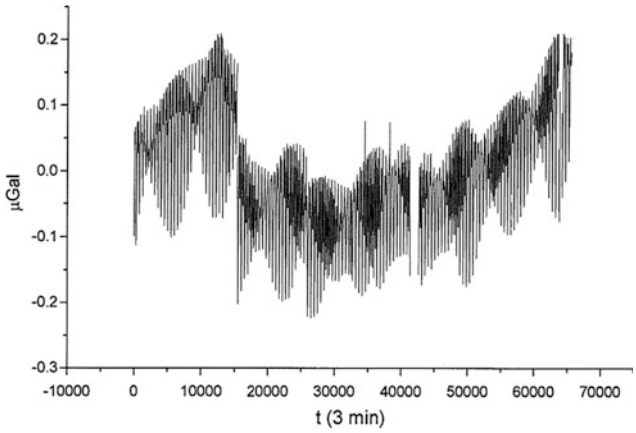

Fig. 6.27 Earth's gravity data detrended by the linear nonstationarity (the *red line* in Fig. II.4.26)

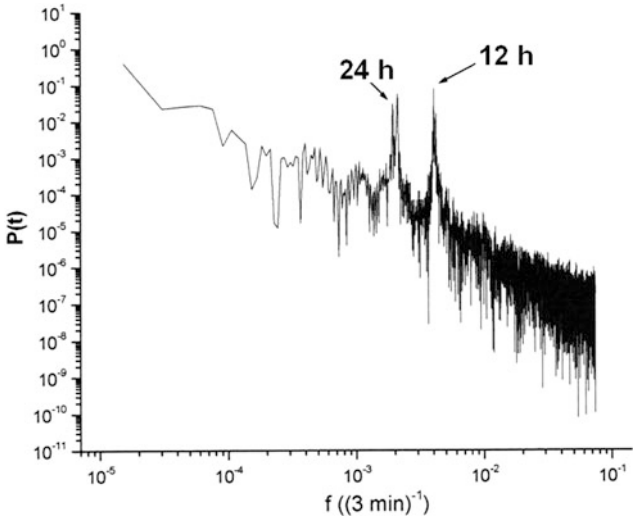

Fig. 6.28 Periodogram of the detrended gravity data shown in Fig. 6.27. The two oscillations at 24 and 12 h are clearly visible. The higher amplitude of the 12-h periodicity with respect to the 24-h cycle indicates that the 12-h periodicity is not a higher harmonic of the 24-h cycle

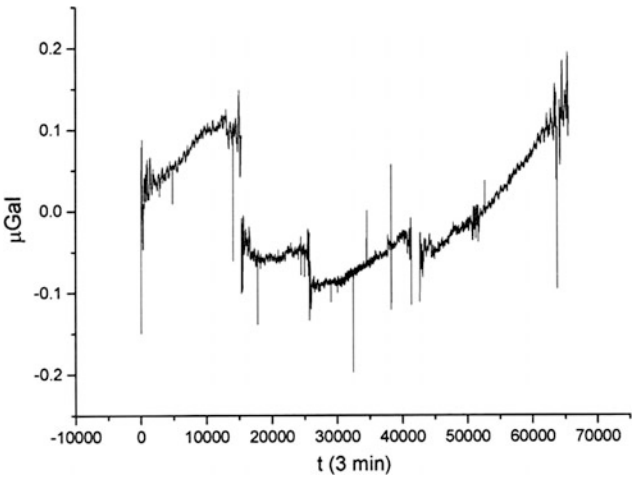

Fig. 6.29 Power spectrum of the residual data shown in Fig. 6.28. The spectrum does not show the two periodicities at 12 and 24 h. The spectrum of the residual data is a power law decreasing function of the frequency, with power law exponent of about 1.7

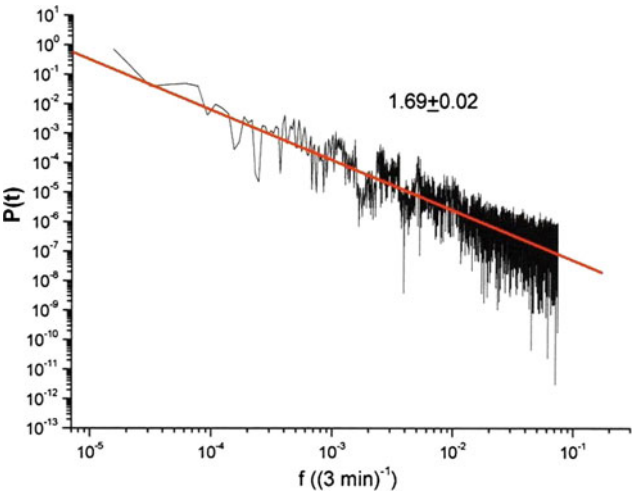

Fig. 6.30 Power spectrum of the residual data shown in Fig. 6.29. The spectrum does not show the two periodicities at 12 and 24 h. The spectrum of the residual data is a power law decreasing function of the frequency, with power law exponent of about 1.7

The non-stationary character of the residual Earth's gravity time series requires application of corresponding methods order to get into insight the time dynamics of the signal. The MF-DFA, developed by Kantelhardt et al. (2002) represents an efficient method to investigate the scaling properties of the time fluctuations of signals, even in the case these are affected by non-stationarities, whose origin is often not known. We firstly analyzed the behavior of the fluctuation functions $Fq(s)$ for $q = 2$. For this value of q, the MF-DFA coincides with the well-known detrended fluctuation analysis (DFA) (Peng et al. 1994). Figure 6.31 shows the fluctuation function $F_2(s)$ with degree $p = 1$ of the detrending polynomial. The fluctuation curve behaves as a linear function in log–log scales for approximately all the timescales s. The value of the scaling exponent $h_2 \sim 1.4$ that is in agreement with the value of the spectral exponent through the relationship $\alpha = 2h_2 - 1$, where α is the spectral exponent. In our case, for $\alpha \sim 1.7$ and $h_2 \sim 1.4$, the above relationship is held with a very good approximation. We varied the degree of the fitting polynomial up to $p = 5$. Figure 6.32 shows the fluctuation function F_2 for $p = 2$. The fluctuation function lays on a linear support with scaling exponent of about 1.4 that is in agreement with the previous value obtained with $p = 1$ and with the spectral exponent.

This indicates that the linear behavior (in log–log scales) of the fluctuation function F_2 does not depend on the order of the detrending polynomial p. For this reason, in order to

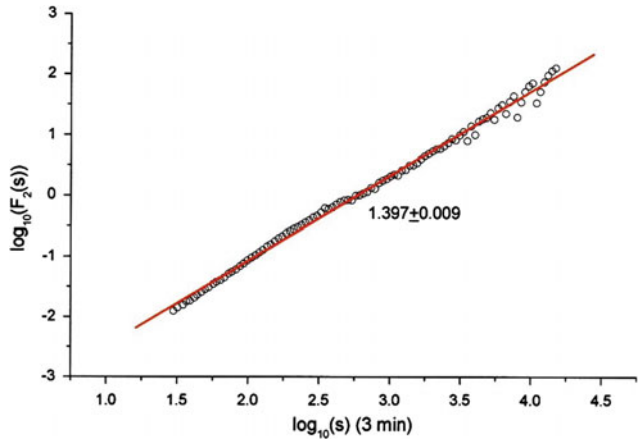

Fig. 6.31 $F_2(s)$ of the data shown in Fig. 6.29 with $p = 1$

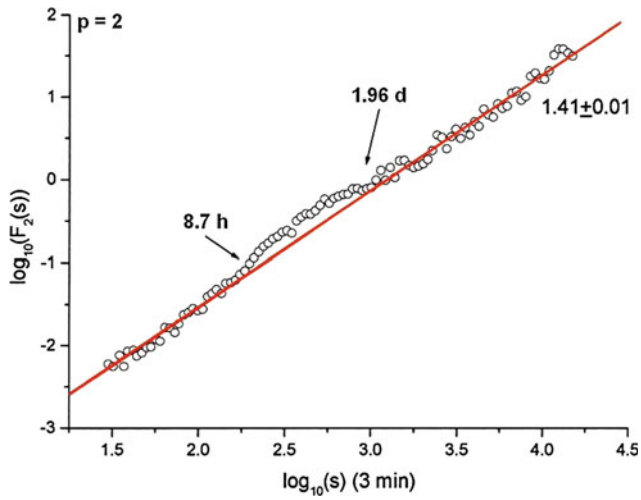

Fig. 6.32 F_2 (s) of the data shown in Fig. 6.29 with $p = 2$

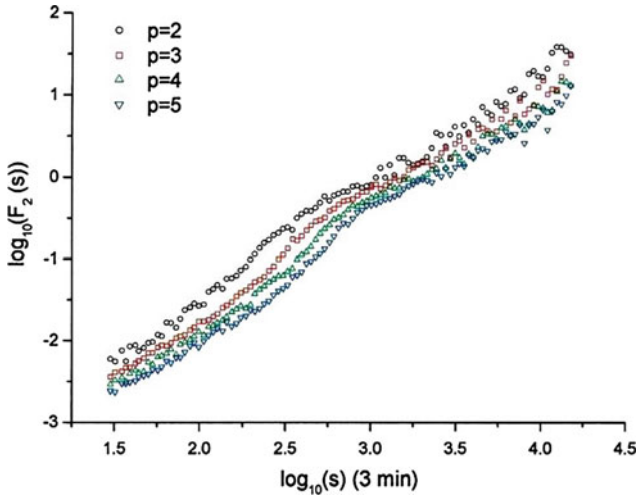

Fig. 6.33 Comparison of F_2 (s) of the data shown in Fig. 6.29 with $p = 2, 3, 4, 5$

not introduce possible disadvantages due to overfitting, it would be preferable to perform the multifractal analysis with $p = 1$.

However, what is interesting is that between the timescales of about 8.7 h and 1.96 days, the fluctuation function shows an excess of variation with respect to the linear behavior. Increasing the value of the degree of the fitting polynomial, we observe that this effect is still present and the band of timescales in which the fluctuation function show such excess of variation seems to shift up and becomes even more definite (Fig. 6.33).

This effect seems to be similar to what found by Hu et al. (2015); in this study, it was investigated the variation of the fluctuation function F_2 for several degrees of the fitting polynomial of a correlated signal (with exponent $0.5 < h_2 < 1$) corrupted by the superposition of a sinusoidal trend with a certain period. Hu et al. (2015) found a similar excess of variation in the fluctuation function with a crossover depending on the period of the sinusoidal trend. Even a shift of such crossover was observed with the increase of the degree of the fitting polynomial. We could probably attribute the effect found in the fluctuation curve of our gravity signal to a possible superposition of a periodical trend (which could be even a sum of sinusoids with different periods) on the gravity noise signal that was not removed just by applying the periodogram analysis. However, the results found by Hu et al. (2015) refer to the particular case of a signal with h_2 less than 1, while in our case, it is larger than 1. In future studies, we intend to better explore such effects and associate the studied effects with the crust deformation processes that are the main responsible source of variation of this signal in the Sheki site.

We performed the MF-DFA on the gravity residual time series. As an example of fluctuation functions varying with the parameter q, Fig. 6.34 shows the comparison between F_{-10} and F_{10}, obtained with degree of fitting polynomial $p = 1$. The two functions plotted in log–log scales have different slopes, suggesting the multifractal character of the gravity signal. Figure 6.35 shows the generalized Hurst exponents $hq \sim q$ that decrease monotonically from the highest value h_{-10} to the lowest h_{10}. The singularity spectrum obtained from the Legendre transform demonstrates that the singularity spectrum has the typical concave shape of multifractals. The width of the singularity spectrum can be used as a quantitative measure of the multifractality. In our case, the width, given by the difference between α_{max} and α_{min} (which are respectively the highest and the lowest α value in the spectrum), is about 0.9.

The singularity spectrum is visibly left-skewed, which indicates a dominance of low generalized Hurst exponents and, thus, a relative dominance of the large fluctuations in the gravity signal in the general multifractal character of the

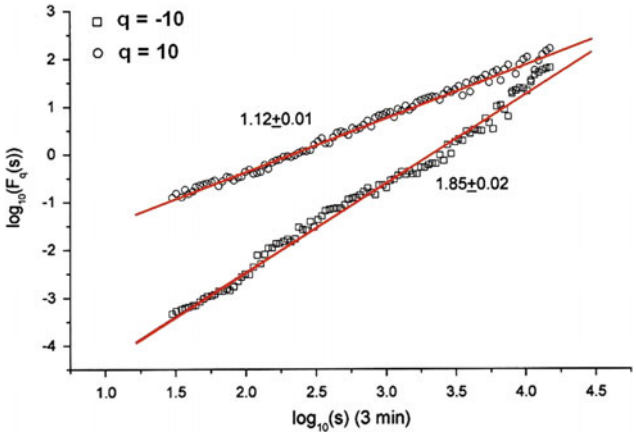

Fig. 6.34 Comparison of the fluctuation functions for $q = -10$ and $q = 10$

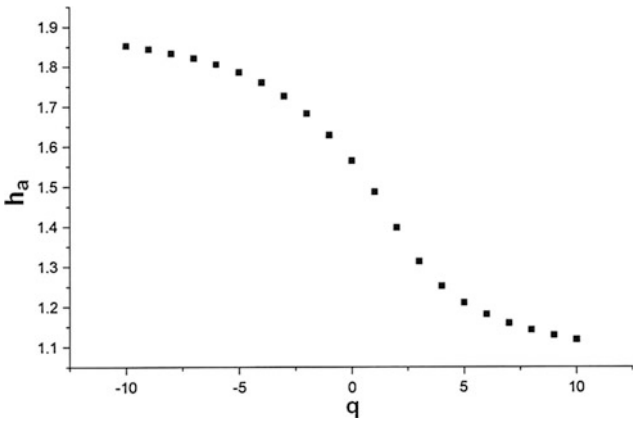

Fig. 6.35 Generalized Hurst exponents

series. In order to see whether such multifractality depends on the probability density function of the gravity signal or on the long-range correlations, we applied the MF-DFA to a randomly shuffled gravity series, which is obtained randomly shuffling the values of the series. This shuffling procedure does not change the probability density function of the series but destroys all the correlations. Therefore, if the multifractality is due to the presence of long-range correlations in the gravity data, the multifractal characteristics of the shuffled series should be different from those of the original series; this implies that the shuffled series should appear less multifractal than the original signal. If the multifractality is due to broad probability density function, then since the shuffling does not alter the probability density function of the original series, also the multifractal characteristics of the shuffled series would not be changed (Kantelhardt et al. 2002). Figure 6.36 shows the comparison between the singularity spectra of the original series and that of a shuffle. It is visibly clear that the singularity spectrum of the shuffle is much narrower than that of the original series;

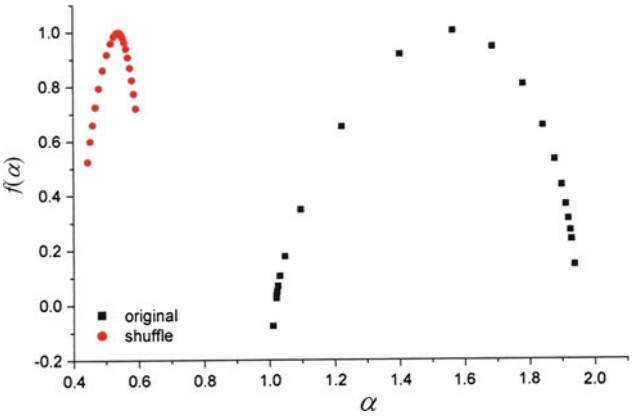

Fig. 6.36 Singularity spectrum of the original gravity signal (*black*) and its shuffle (*red*)

furthermore, its maximum is around 0.5 that is consistent with a random series. So, from this result, we can conclude that the multifractality of the gravity signal is due to the presence of long-range correlations.

6.3.4 Main Obtained Results

In this chapter, we investigated the dynamical properties of the gravity signal measured by Sheki station in Azerbaijan, a site that is affected mainly by crust deformation processes. Applying the power spectral density method and the MF-DFA, we found the following features characterizing the time dynamics of the gravity signal.

The gravity signal is mostly modulated by the 12- and 24-h periodicities. Earth tides are deformation of the solid Earth's body which occur under the influence of the Sun and Moon gravitational fields (Darwin 1962; Stacey 1969; Melchior 1983). The 12- and 24-h periodicities are those of tidal deformations of the Earth, induced by the Sun and Moon.

(i) After removing these two intense periodicities, the residual signal is not purely random but shows a dynamical structure indicated by the power law shape of the power spectrum with exponent around 1.7.
(ii) The analysis of the second-order fluctuation function reveals that the signal shows an excess (with respect to the simple linear behavior) of fluctuation variation between about 9 h and 2 days. It is still not very clear the nature of such excess of fluctuation at these timescales; maybe a correlation with the Earth's gravity field-triggered seismicity could be postulated (Chen et al. 2012).
(iii) The gravity signal appears multifractal, and its multifractality depends on the long-range correlations rather than the probability density function of its values.

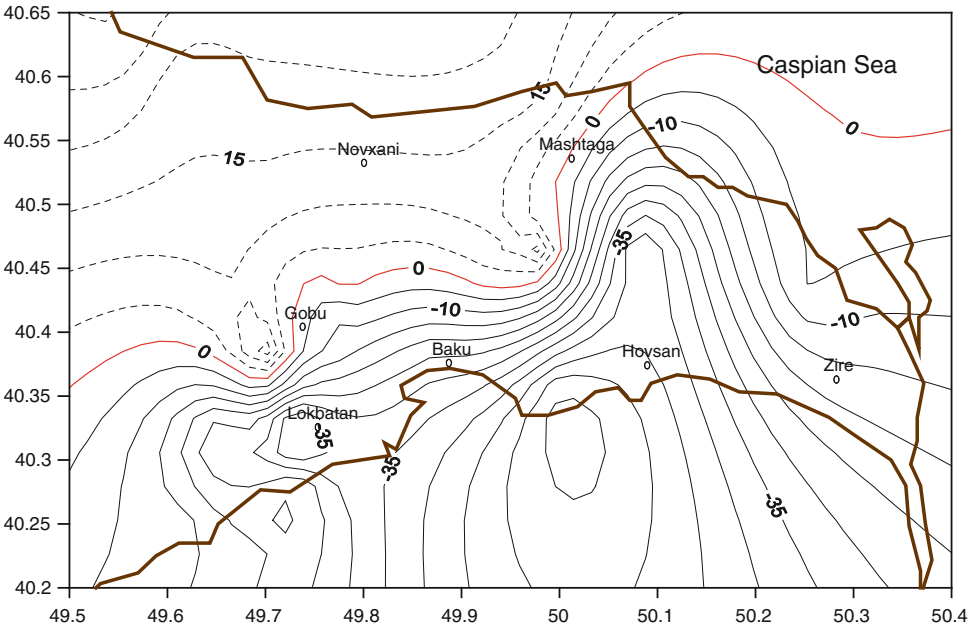

Fig. 6.37 Non-tidal variations in the Absheron Peninsula (isolines are given as μGal/year)

6.4 Investigations of Non-tidal Gravity Variations in the Absheron Geodynamic Polygon

Available geophysical, geological, geomorphological, and geodetic data indicate that the territory of Azerbaijan is now in tectonically stress condition that in turn is confirmed by results of high-precise repeated leveling. The disturbing influence of tectonic processes to the gravity field can be found by using repeated instrumental observations.

In Azerbaijan, such investigations have been conducting by the Laboratory of Gravimetry of the Institute of Geology and Geophysics of National Azerbaijan Academy of Sciences since 1976 (e.g., Gadjiev et al. 1984, 1988). For this aim, the following geodynamic polygons were used: (1) Precaspian (from Samur River to Astara city), (2) Kur Depression (Alyat town–Poilu town), and (3) Absheron.

In these polygons, special gravimetric stations (through each 6–10 km) were laid. The distance between the gravimetric stations was selected to minimize the influence of various kinds of noise. The gravity station is a reinforced concrete slab (with a length of 0.8 m, width of 0.8 m, and height of 0.4 m) established on the foundation over the geodetic datum.

The performed investigations showed that the observed gravity field variations are caused by different geological–geophysical processes including preparing dangerous geodynamic events at a depth (earthquakes).

In Azerbaijan part of the Caspian Sea, the non-tidal gravity variations were studied by Iskenderov (1978). He utilized in this investigation such objects as piers of various islands, marine buoys, and borehole foundations as references points.

Observation of gravity field difference between the neighboring stations has been carried out by the use of four gravimeters GNU-K2 and KNU-KV with application of simple "loop" scheme (A1 → B1 → A2). The control observations were done on finite stations by using helicopter.

Graduation of gravimeters scale was determined on the special reference equipment. Corrections for the temperature dependence, nonlinearity of the micrometer screw, and lunar–solar attractions were introduced by conventional ways (Veselov 1988).

Measurement results that do not fit in the normal distribution were rejected by the criterion of the maximum deviation with a probability of 0.95. The reliability of obtained differences was tested by the Fisher-Snedecor and Student criteria.

A map of the non-tidal gravity variations (NTGV) in the Absheron polygon is shown in Fig. 6.37. This figure suggests that in the southern part of polygon, a decreasing of the NTGV values occurs. A zone (band) of negative velocities of the NTGV continues from NE to SW and reaches values in the middle part of the band up to −58 microGal/year. In the northern part of Absheron polygon for the same period, positive NTGV values up to 20 microGal/year were observed.

With the aim to reveal the nature of observed gravity attraction anomalies, the gravity effects from the modern vertical movements of earth's crust (MVMEC), changing of underground water level (UWL), the Caspian Sea level, and atmospheric pressure, were calculated. Results of repeated

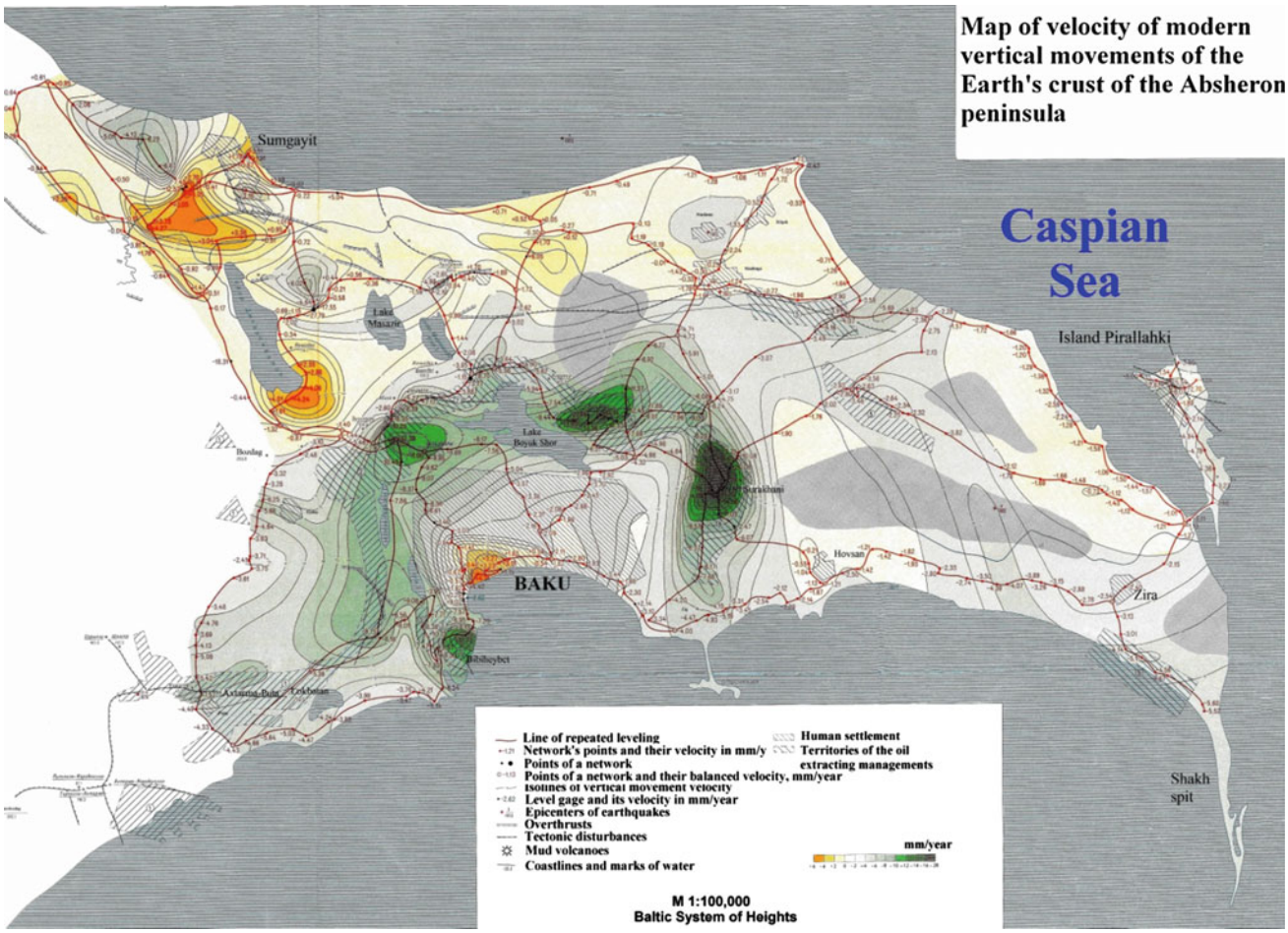

Fig. 6.38 Map of the modern vertical movements of Absheron Peninsula (on the basis of Yaschenko 1989)

levelling carried out in the Absheron Peninsula during 1977–1984 indicated that in the southern part, lowering-in with annual velocity—(0.21–5.6) mm/year (Yaschenko 1989) was observed. Maximal values of lowering-in were observed in the local areas of Syrakhany (−18 mm/year), Balajary (12 mm/year), Bibi-Heybat (12 mm/year), and in some other areas confining to arches of anticline structures (Fig. 6.38). At the same time in the northern part of Absheron, the significant vertical movements were not observed: Here, the annual values ranged from −1 to +2 mm/year.

Comparison of the map of no-tidal variations with the MVMEC map indicates that MVMEC changing both by direction and absolute values cannot explain observed gravity field variations. It should be noted that such regularity was observed also in other regions where significant non-tidal gravity field variations were observed. Analysis of changing of UWL showed that in the natural conditions, the UWL oscillates nonsignificantly, near the regional background typical for the peninsula. At the same time, it was revealed that for the period of 1978–1985 on the most area of Absheron Peninsula, the UWL increased due to various technogenic factors.

An average gravity effect caused by the UWL motion in the Absheron polygon changed from −5 to +2 microGal/year. During the period of 1978–1985, a level of the Caspian Sea (according to measurements in the Baku station) had risen on 1.06 m. The gravity effect of the Caspian Sea-level fluctuations can be calculated by the use of expression for parallelepiped with infinite strike:

$$\Delta g = G\sigma\left[L\ln\left(1+\frac{h^2}{L^2}\right)+2h\arctan\frac{L}{h}\right], \qquad (6.13)$$

where G is the universal gravity constant, σ is the density of marine water, h is the vertical thickness of prism (water level changing), and L is the width of the prism (averaged width of the Caspian Sea). Calculating vertical component of gravity attraction of infinite prism with vertical thickness h = 1 m and width L = 260 km on the upper side of this prism (i.e., on the sea shore), we find Δg = 24 microGal;

then, the average annual value is 4 microGal (Kadirov and Nabiyev 1991).

During the period of studying repeated gravity measurements in the Absheron polygon, the atmosphere pressure (P_{atm}) changes (from the meteorological stations Baku and Mashtagi town) were studied. Taking into account that the gravity measurements were carried out on the stations with distance between them ≈10 km radius of domain wrapping changing, P_{atm} was selected as 10 km. The calculated gravity effect caused by atmospheric pressure changing consisted of 1–2 microGal ($1–2 \cdot 10^{-8}$ m/s^2). Such an effect undoubtedly cannot significantly change the studied gravity field variations.

All the above-mentioned factors enable to conclude that the main part of gravity field decreasing observed in the southern part of Absheron polygon is probably associated with decompaction of sedimentary rocks under activation of different tectonic processes. It should be noted that the strengthening of endogenic processes (earthquakes, folding, etc.) may also increase an industrial impact to the geological medium. It is well-known that in the Absheron Peninsula, a lot of hydrocarbon deposits occur and exploration of these reserves with following water pumping in Pliocene deposits is a possible reason of the equilibrium disturbance of the peninsula geodynamics.

The Absheron Peninsula is located on the periclinal submersion of the southeastern continuation of the Greater Caucasus (see Chaps. 1–5 of Volume 1 "Geology of Azerbaijan"). From the stratigraphic and tectonic points of view, the regional uplift of the Absheron Peninsula as well numerous anticline and syncline structures is composed by rocks beginning from Upper Jurassic associations and ending Quaternary deposits. Assuming that the value of decompaction is equal in the depth ($\Delta\sigma$ = 0.001 g/cm^3 = 1 kg/m^3), it is possible to estimate the thickness of the fissuring zone. For estimation, we will apply known formula for plane-parallel layer (e.g., Veselov 1988):

$$\Delta g = 2\pi\gamma\Delta\sigma h,$$

where $\Delta\sigma$ is the contrast density and h is the vertical thickness of the layer.

Applying this formula, we obtain that non-tidal gravity field variations of −180 microGal may create a decompaction of the plane-parallel layer with a thickness of 3.7 km. Such a value corresponds to thickness of the Paleogene–Neogene complex. Positive gravity field variations observed in northern part of peninsula can be explained by compaction of sedimentary rocks.

Microtremor survey and spectral analyses of H/V (horizontal/vertical) ratio have been recently applied in Baku (Kadirov et al. 2015b). The ground response analysis was done on 255 different sites in Baku, and damage distribution (on the basis of local site effect) was estimated. As result, the maps showing the distribution of amplification and resonance frequency for the numerous types of Baku's grounds were developed. The maps indicating variability and heterogeneity of the city ground characteristics for the urban seismic hazard assessment examination.

6.5 Magnetic Field Analysis and Seismological Monitoring

Short- and long-term magnetic precursors are discussed abundantly in the geophysical literature (e.g., Pudovkin et al. 1973; Gokhberg et al. 1979; Eppelbaum and Finkelstein 1998; Alperovich and Zheludev 1999; Gaffet et al. 2003; Finkelstein et al. 2012).

Anomalous geomagnetic variations (AVG) have different characteristics, and their tectonomagnetic effects may only be seen after removing all the noise and incident factors (Fig. 6.39). As shown in this diagram, to reveal the tectonomagnetic effects (desired signal) from the total field of geomagnetic variations is not a simple problem.

The most important feature of these magnetic measurements is the amplitude of the dynamic band of the signal—more than 200 dB. Another peculiarity is the apparent error of magnetic measurements when a device with a reduced relative error of about 0.1 % is used for the measurements of values about 0.0001 % of its total scale. Thus, in such conditions, the selection of parameters characterizing measurement accuracy is crucial.

Figure 6.40 shows the negative tectonomagnetic effect of 1.5 days before the Salyan earthquake (M = 5–5.3) January 09, 1998. Such a clear magnetic effect could be recorded because of the proximity of the observation station to the earthquake epicenter. However, analysis of the differential magnetic function is preferable (Eppelbaum and Finkelstein 1998), but it is necessary to take into account that the most optimal distance between the magnetic observation stations is 30–50 km (Finkelstein et al. 2012).

An interesting approach to correlations between the regional magnetic field intensity and seismicity was applied by Riznichenko et al. (1983). It was assumed that the regional magnetic field reflected a sufficiently long history of the geological evolution of the region (including dangerous geodynamic events). Analysis of magnetic–seismological relations indicated that zones of high seismicity are not associated with the magnetic anomalies themselves but rather with zones of high gradients of magnetic field, which

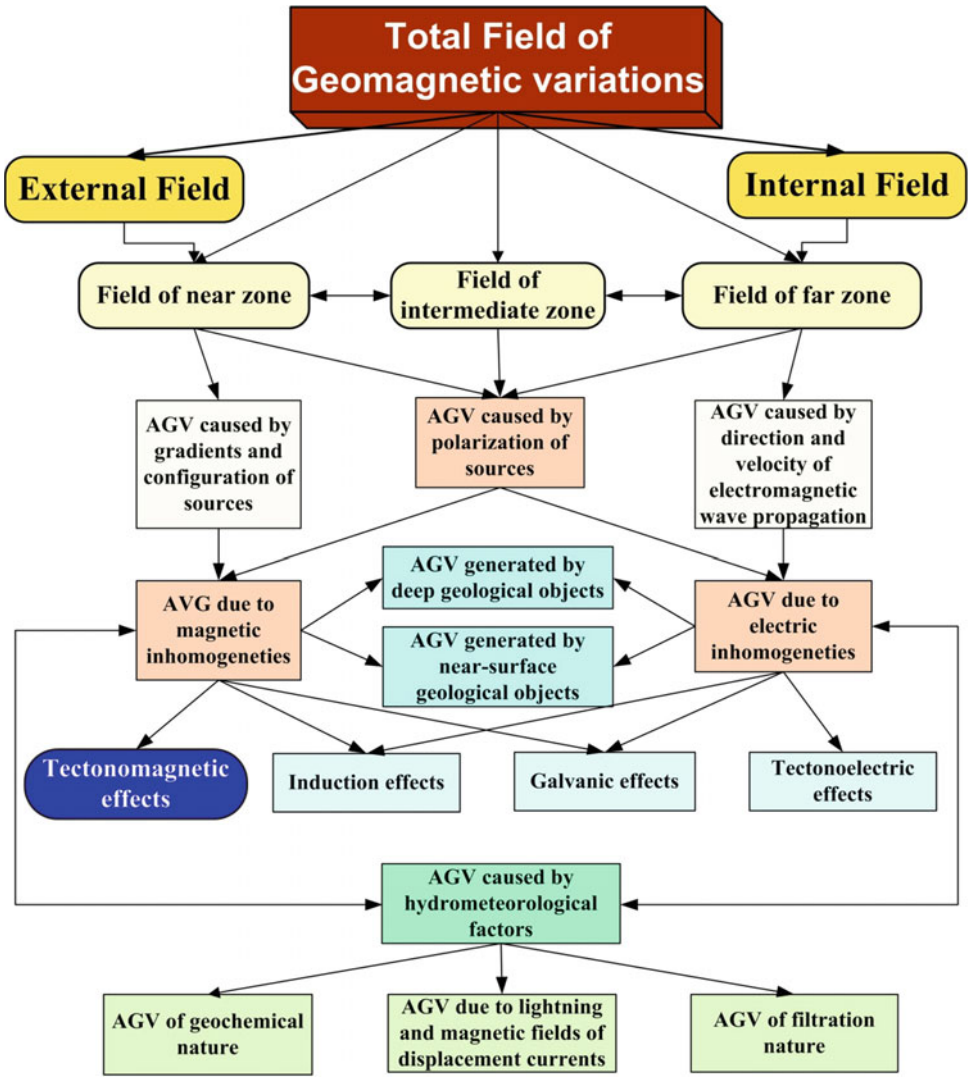

Fig. 6.39 Types of anomalous magnetic variations and their genesis (after Finkelstein et al. 2012, with small modifications)

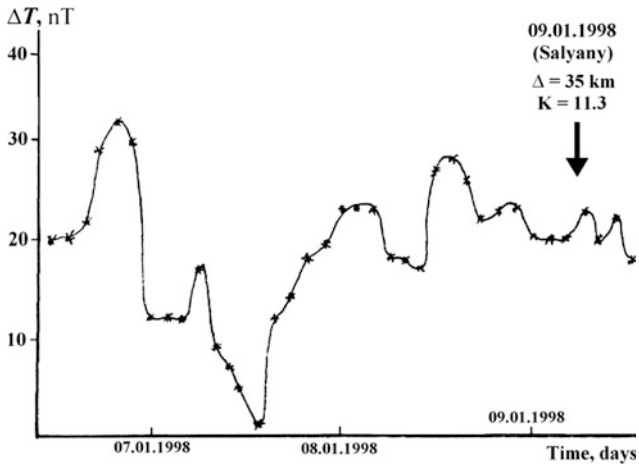

Fig. 6.40 Seismomagnetic effect before the Salyan earthquake January 09, 1998 (after Rzayev 2005, with small modification)

are indicative of the presence of large faults between blocks of the Earth's crust, and magnetic field behavior. Therefore, maps of seismic activity were compared with the maps of modules of horizontal gradients of magnetic field intensity. Magnetic field gradients were computed on a 5 × 5 km grid by the following formula:

$$\left|\frac{\Delta U}{\Delta l}\right| = \sqrt{\left(\frac{\Delta U_x}{\Delta x}\right)^2 + \left(\frac{\Delta U_y}{\Delta y}\right)^2}, \qquad (6.14)$$

where ΔU_x is the mean increment of U along the x-axis; ΔU_x is calculated on parallel sides of a cell with l dimensions in a sliding rectangular "apparent graticule"; ΔU_y is the corresponding increment along the y-axis; and $\frac{\Delta U}{\Delta l}$ is the mean value of the gradient modulus on the transformation cell (*grad U*). A comparison of these maps is shown in Fig. 6.41.

Zone I includes the high-seismicity areas of the Greater Caucasus, its SE submersion to the side of the Lower Kur Depression, and the Saatly-Kurdamir outcrop of the

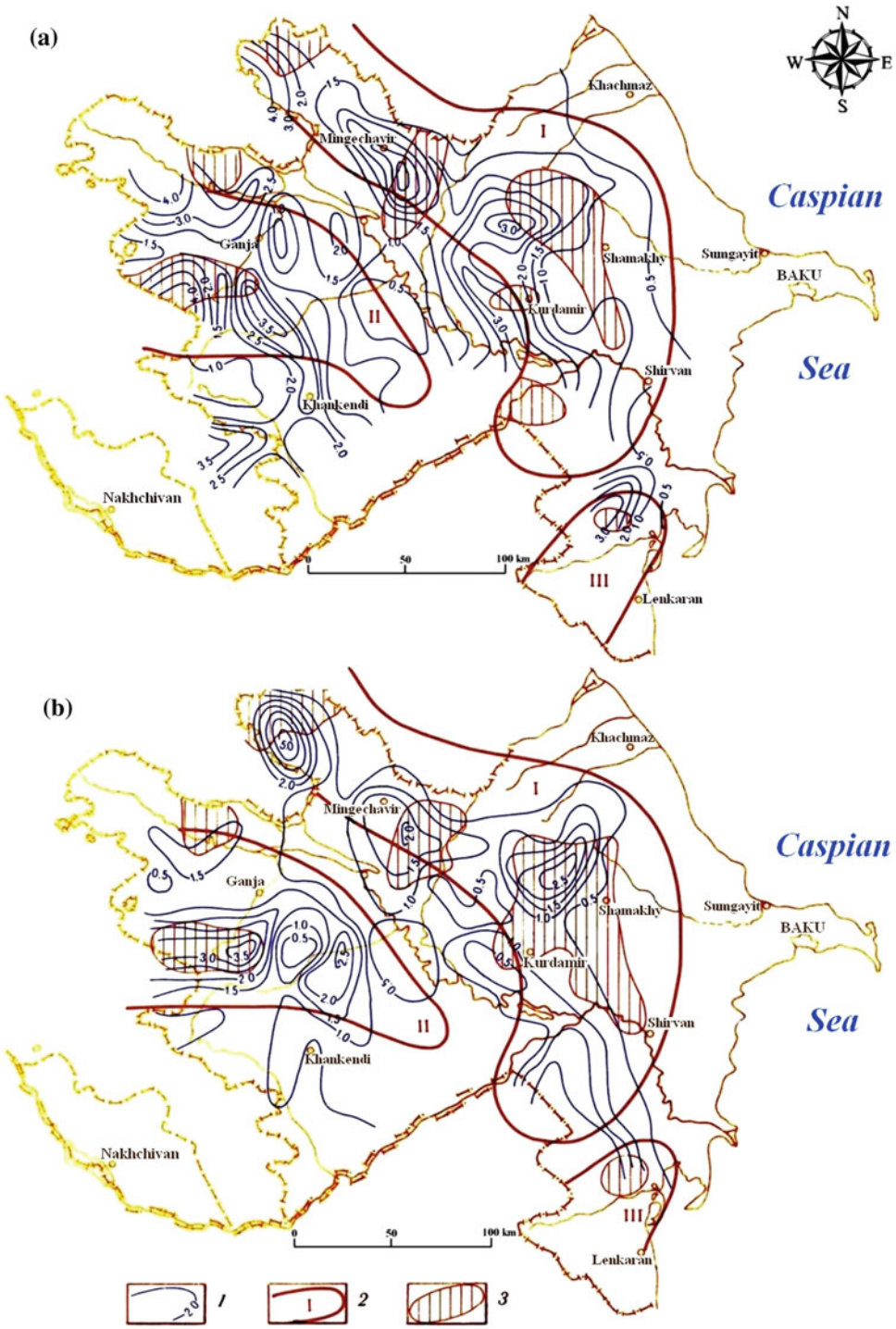

Fig. 6.41 Comparison of horizontal gradients of magnetic field maps with elements of seismic activity (after Riznichenko et al. (1983) and Eppelbaum and Khesin (2012), with modifications). **a** Constant level of detail and **b** constant accuracy. (*1*) Isolines of horizontal gradients in milliErsted/km, (*2*) contours and numbers of zones of heightened seismic activity, and (*3*) areas of heightened ($A > 0.2$) seismic activity

consolidated crust. Zone II is revealed in the Lesser Caucasus. Zone III represents the Talysh Mts. and their NE submersion. The correlation field (Fig. 6.42) contains concentrations of points representing zones I–III and values between the zones (0).

It is clear to see that the cluster of zone I also includes three points from zone III which located near the regression of A_T (seismic activity) on (grad u) for zone I. Several points from zone II are close to the same line. These points correspond to areas of the highest seismicity and the greatest magnetic gradients coinciding in the plane. Obviously, these points represent the general regularity between the values investigated in other areas masked by different kinds of noise.

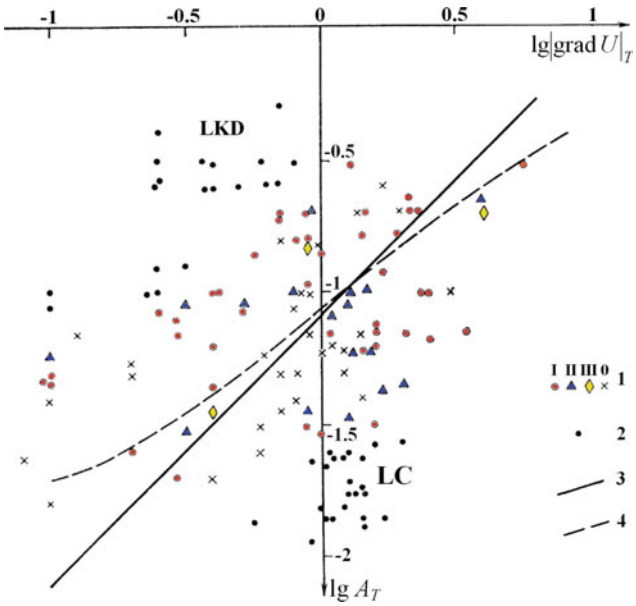

Fig. 6.42 Correlation of logarithms of seismic activity values and magnetic field gradients for Azerbaijan (after (after Riznichenko et al. (1983) and Eppelbaum and Khesin (2012), with modifications). (*1*) correlation points for zones I, II, and III, 0 displays values between the zones, (*2*) correlation points were not calculated by regression (*LC* Lesser Caucasus, *LKD* Lower Kur Depression), (*3*) regression, (*4*) projection in this logarithmic system of rectilinear regression A_T on $(\text{grad } u)_T$

6.6 VLF Field Investigation for Forecasting Dangerous Geodynamic Events at a Depth

Some authors have noted that VLF anomalies precede dangerous geodynamic events at certain depths (e.g., Meloni et al. 2004; Hayakawa 2007; Gokhberg and Shalimov 2008). The idea that electromagnetic precursors are generated before earthquakes is based on the assumption that the geodynamic event at the depth (earthquake) initiates in an alleged preparation zone where physical phenomena lead to the subsequent shock (e.g., Masci and Thomas 2015). At the same time as a whole, the physical mechanisms behind these processes remain enigmatic.

Figure 6.43 depicts the parcel-like negative VLF (H_φ is the total electromagnetic component of the registered VLF field according to peculiarities Soviet VLF equipment SDVR-4) anomalies recorded at two frequencies (11.9 kHz, Australia, and 15.1 kHz, Bordeaux, France) four days before an earthquake occurred in the Lesser Caucasus. It is obvious that such a simultaneous, sharp drop in VLF field intensity at two frequencies from the VLF-transmitters located in different regions of the world cannot be fortuitous.

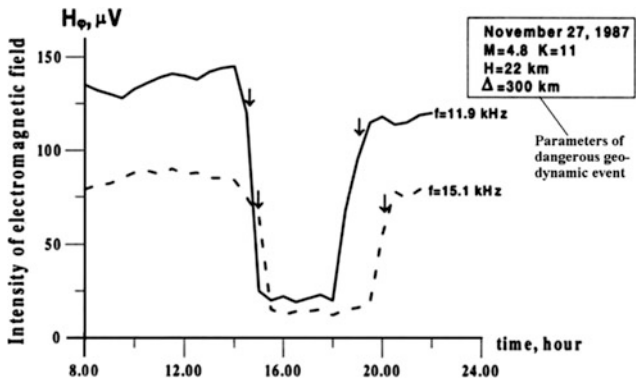

Fig. 6.43 Investigations of *VLF* variations as a possible earthquake precursor (results of observations at the Aghdara district (Western Azerbaijan), Lesser Caucasus, November 23, 1987) (Eppelbaum and Finkelstein 1998)

6.7 Temperature Precursors of Dangerous Geodynamic Effects

A relationship between the temperature anomalous variations in observed boreholes and danger geodynamic activity is known (e.g., Mogi et al. 1989; Singh and Dey 2003; Ouyang et al. 2009).

Temperature monitoring was carried out in the Biladzhik well (Sheki region of Azerbaijan, southern part of the Greater Caucasus) to correlate temperature variations with the earthquakes recorded in the region (Lyubimova et al. 1982). Monitoring was conducted at a depth of 110 and 335 m (Fig. 6.44). This figure shows that in general, the temperature graphs are synchronous at both depths, but in the two most striking cases, the distribution of the anomalous curves goes in opposite directions. Before the Kutkashen event, the temperature anomaly observed at a depth of 335 m exceeded the temperature anomaly at 110 m (which seems logical). However, before the Checheno-Ingushetiya event, the temperature anomaly observed at 110 m exceeded the 335 m anomaly tenfold. This phenomenon is difficult to explain from a physical–tectonic point of view. Undoubtedly, such investigations must be continued in various regions of Azerbaijan.

6.8 Earthquakes as a Strongly Nonlinear Event

There is growing recognition of the importance of nonlinear phenomena in many branches of geophysics. It was shown that phenomenon such as earthquakes (e.g., Keilis-Borok 1990; Voisin 2002) and their reflection in geophysical fields

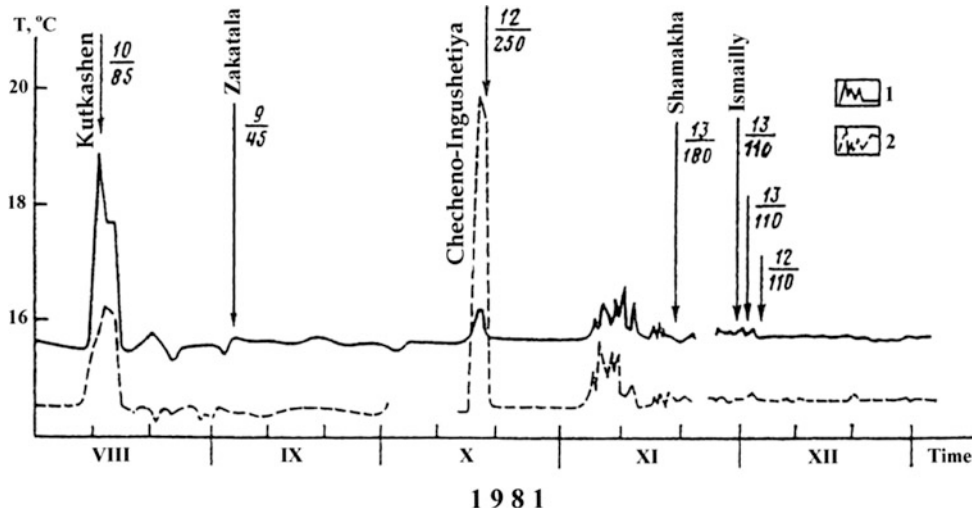

Fig. 6.44 Temperature variations in the Biladzhik well (Azerbaijan) and their comparison with the geodynamic events in the Caucasus. (*1*) and (*2*) are the temperatures observed at a depth of 335 and 110 m, respectively. The *arrows* indicate the time of the earthquake. The numbers in the numerator and denominator show the energy class of the earthquake and the epicentral distance in km between the earthquake and the well, respectively (Lyubimova et al. 1982)

as well as the propagation of geophysical fields in non-uniform geological media is a nonlinear process (e.g., Aleinikov et al. 2001). However, it is still common practice to solve complex geophysical problems by removing visible nonlinear effects and reducing the problem to a linear one. Such a linearization can eliminate useful effects and even radically change the notion of targets (Eppelbaum and Kardashov 1998). Therefore, many important geophysical problems cannot be solved without special nonlinear procedures. Analysis of such physical phenomena as thermal and gravity effects in the Earth shows that the nonlinear component may play a significant role in the process.

Azerbaijan occupies one of the first places in the world by a density of deep and intermediate borehole location where different physical parameters (firs of all, thermal) are observed.

By contrast, the problem of influence of *strongly* nonlinear sources on transitional dynamics has scarcely been investigated in geophysics (e.g., Kardashov et al. 2000; Eppelbaum and Kardashov 2001).

The process of thermal wave propagation in the Earth can be used as a possible geodynamic precursor. In general, the model of thermal wave propagation can be described by the following evolution equation:

$$\frac{\partial u}{\partial t} = \Delta u + f(u), \tag{6.16}$$

where $\Delta = \frac{\partial^2}{\partial x^2} + \frac{\partial^2}{\partial y^2} + \frac{\partial^2}{\partial z^2}$ is the Laplace operator and $f(u)$ is a nonlinear function of a thermal source. Let us assume the following form of the thermal source term:

$$f(u) = \alpha + \varepsilon g(u), \tag{6.17}$$

where α and ε are some parameters, and $g(u)$ is the nonlinear function which describes disturbances of the thermal field. Function $g(u)$ can be presented both as a conventional deterministic function and a random distribution function. If $\varepsilon = 0$, we obtain a linear equation corresponding to the conventional problem with a linear source term: $\frac{\partial u}{\partial t} = \Delta u + \alpha u$. The case of $\varepsilon \neq 0$ corresponds to a situation where the normal thermal field is disturbed by anomalous sources.

Under specific conditions, a nonlinear disturbance can cause the appearance of a shock wave even for extremely small values of the parameter ε (Eppelbaum and Kardashov 1998). This effect can be used to identify the target. On the other hand, Eq. (6.16) can take transient solutions under special conditions such as localized or switch (kink) waves. Note that the properties of both localized and shock waves are determined by the characteristics of the source function $f(u)$. Consequently, this makes it possible to estimate certain parameters of the medium. Here, this is limited to a nonlinearity of the type $g(u) = u^3$, but other types of nonlinearity have been analyzed as well. The temperature source term of the form $f(u) = \alpha u + \varepsilon u^3$ provides a solution to the traveling wave (Eppelbaum and Kardashov 2001):

$$u(t, x, y, z) = \psi\left(k_x x + k_y y + k_z z + vt\right), \tag{6.18}$$

where v is the wave propagation speed and $\mathbf{k} = \left(k_x, k_y, k_z\right)$ is the unit vector in the direction of wave propagation. Self-similar solutions of this kind were considered in detail

in Barenblatt (1996). Substitution of Eq. (6.18) in Eq. (6.16) yields:

$$v\psi'(s) = \psi''(s) + \alpha\psi(s) + \varepsilon\psi(s), \tag{6.19}$$

where $s = k_x x + k_y y + k_z z + vt$ since $k_x^2 + k_y^2 + k_z^2 = 1$. It was shown in Kardashov et al. (2000) that transitive waves (both switch and localized waves) corresponding to the source function of type (6.17) are the steady-state solutions ($v = 0$) of Eq. (6.18). Equation (6.16) may be generalized by including the effect of nonlinear diffusion. Such models are widely used, for instance, in descriptions of thermal propagation processes in media with nonlinear coefficients of thermal conductivity. Finally, we consider the following generalization of Eq. (6.16):

$$\left\{ \begin{array}{l} \dfrac{\partial u}{\partial t} = \displaystyle\sum_{i=1}^{3} \frac{\partial}{\partial x_i}\left[k_i\left(\frac{\partial u}{\partial x_i}\right)\frac{\partial u}{\partial x_i}\right] + f(u), \\ \dfrac{\partial u}{\partial t} = \displaystyle\sum_{i=1}^{3} \frac{\partial}{\partial x_i}\left[\bar{k}_i(u)\frac{\partial u}{\partial x_i}\right] + f(u). \end{array} \right\}. \tag{6.20}$$

This is a novel approach for the identification of nonequilibrium potential sources by using the corresponding transitional wave analysis. Transitional waves deterministically characterize the structural parameters of the nonlinear sources. Parameters of the transitional waves characterize the structure and the main characteristics of the geophysical (thermal) source function. Models with nonlinear diffusion and sources can be applied to the analysis of various geophysical events associated with nonlinear effects (first of all, earthquakes). The transitional waves obtained using these models serve to determine and estimate not only the parameters of the sources but also the nonlinear diffusion.

References

Adams, J., Burris, L., Jentzsch, G., Kopaev, A. and Valliant, H., 2004. The automated Burris gravity meter – a new instrument for surveying and continuous operation. *Proceed. of the 15th Int. Symp. Earth Tides*, Ottawa, August 2004.

Aki, K. and Richards, P.G., 1980. *Quantitative Seismology*, Vols. 1 & 2. W.H. Freeman and Co., San Francisco.

Albano, A. and Corrado, G., 2013. Five years of continuous gravity observations in the Neapolitan volcanic area. *Boll. Geofis. Teor. Appl.*, **54**, 1-21.

Aleinikov, A.L., Belikov, V.T. and Eppelbaum, L.V., 2001. *Some Physical Foundations of Geodynamics* (in Russian, contents and summary in English). Kedem Printing-House, Tel Aviv, Israel.

Allen, M., Jackson, J. and Walker, R., 2004. Late Cenozoic reorganization of the Arabia-Eurasia collision and the comparison of short-term and long-term deformation rates. *Tectonics,* **23**, TC2008, doi:10.1029/2003TC001530.

Aliyev, A.A., Guliyev, I.S. and Rahmanov, R.R., 2009. *Catalogue of Mud Volcanoes Eruptions of Azerbaijan* (1810 – 2007). Natfa-Press, Baku.

Aliyev, G.A., Akhmedbeyli, F.S., Ismailzade, A.D., Kangarli, T.H. and Rustamov, M.I. (V.E. Khain and Ak.A. Alizadeh, Eds.), 2005. *Geology of Azerbaijan*, Vol. **IV**: Tectonics. Nafta-Press, Baku (in Russian).

Alperovich, L.S. and Zheludev, V.A., 1999. Long-period geomagnetic precursors of the Loma-Prieta earthquake discovered by wavelet method. *In*: (Hayakawa, M., Ed.), *Atmospheric and Ionospheric Electromagnetic Phenomena Associated with Earthquakes*. Terra Scientific Publishing Company, Tokyo, 123-136.

Altamimi, Z., Meltivier, L. and Collilieux, X., 2011. ITRF2008: an improved solution of the international terrestrial reference frame. *Journal of Geodesy*, **85**, No. 8, 457-473.

Altamimi, Z., Meltivier, L. and Collilieux, X., 2012. ITRF2012 plate motion model. *Journal of Geophysical Research*, **112**, B07402, doi: 10.1029/2011JB008930, 1-14.

Ambraseys, N.N., 2002. The Seismic Activity of the Marmara Sea Region over the Last 2000 Years. *Seismo. Soc. Am. Bull.*, **92**, 1-18.

Ambraseys, N.N. and Melville, C., 1982. *A History of Persian Earthquakes*. Cambridge University Press, Cambridge.

ArRajehi, A., McClusky, S., Reilinger, R.E., Daoud, M., Alchalbi, A., Ergintav, S., Gomez, F., Sholan, J., Bou-Rabee, F., Ogubazghi, G., Haileab, B., Fisseha, S., Asfaw, L., Mahmoud, S., Rayan, A., Bendik, R. and Kogan, L., 2010. Geodetic constraints on present-day motion of the Arabian Plate: Implications for Red Sea and Gulf of Aden rifting. *Tectonics*, **29**, TC3011, doi:10.1029/2009TC002482.

Ashkenazy, Y., Baker, D.R., Gildor, H. and Havlin, S., 2003. Nonlinearity and multifractality of climate change in the past 420,000 years. *Geophys. Res. Lett.*, **30**, 2146-2149.

Avdeev, B. and Niemi, N.A., 2008. Constraints on the rates and timing of exhumation of the Greater Caucasus from low-temperature thermochronology. *Eos, Trans. Amer. Geophys. Union*, **89**, No. 53.

Babayev, G.R., 2008. Numerical modeling of topography-induced stress pattern of the Greater and Lesser Caucasus. *Trans. of the Azerbaijan National Academy of Sciences; Proceed. of Azerbaijan Association of Young Scientists*, No. 1, 44-56.

Babayev, G.R., 2010. About some aspects of probabilistic seismic hazard assessment of Absheron peninsula. *Trans. of the Republican Seismic Survey Center of the Azerbaijan National Academy of Sciences*. Catalogue of Seismoforecasting Research Carried Out in Azerbaijan Territory in 2009, "Tекнur", Baku, 59-64.

Barazangi, M., Sandvol, E. and Seber, D., 2006. Structure and tectonic evolution of the Anatolian plateau in eastern Turkey. *Geol. Soc. Amer. Special Paper* **409**.

Barenblatt, G.I., 1996. *Scaling, Self-Similarity, and Intermediate Asymptotics*. Cambridge Univ. Press.

Bennett, R.A., Rodi, W. and Reilinger, R., 1996. Global Positioning System constraints on fault slip rates in southern California and northern Baja, Mexico. *Jour. Geophys. Research*, **101**, 21,943-21,960.

Bird, P., 2003. An updated digital model of plate boundaries. *Geochemistry, Geophysics, Geosystems*, **4**, No. 3, doi: 10.1029/2001GC000252, 1-52.

Bird, P. and Kagan, Y.Y., 2004. Plate-tectonic analysis of shallow seismicity: Apparent boundary width, beta, corner magnitude, coupled lithosphere thickness, and coupling in seven tectonic settings. *Seismo. Soc. Amer. Bull.*, **94**, 2380-2399.

Blewitt, G. and Lavallee, D., 2002. Bias in geodetic site velocity due to annual signals. In "*Vistas for Geodesy in the New Millenium*", Int. Assoc. Geod. Symposia, **125**, 499-500.

Bogusz, J., Klos, A. and Kosek, W., 2013. Wavelet decomposition in the Earth's gravity field investigation. *Acta Geodyn. Geomater*., **10**, 47-59.

Cetin, E., Cakir, Z., Meghraoui, M., Ergintav, S. and Akoglu, A.M., 2014. Extent and distribution of aseismic slip on the Ismetpasa segment of the North Anatolian Fault (Turkey) from Persistent Scatterer InSAR. *Geochem. Geophys. Geosyst*., **15**, doi:10.1002/2014GC005307.

Chen, L., Chen, J.G. and Xu, Q.H., 2012. Correlations between solid tides and worldwide earthquakes M S ≥ 7.0 since 1900. *Nat. Hazards Earth Syst. Sci*., **12**, 587-590.

Copley, A. and Jackson, J., 2006. Active tectonics of the Turkish-Iranian Plateau. *Tectonics*, **25**, TC6006, doi:10.1029/2005TC001906.

Cowgill, E., Niemi, N.A., Forte, A.M., Elashvili, M., Javakishvili, Z. and Mumladze, T., 2012. Orogen-scale structural architecture and potential seismic sources resulting from Cenozoic closure of a relict Mesozoic ocean basin in the Greater Caucasus. *S43 J-07, 2012 Spring AGU Meeting*.

Darwin, G.H., 1962. *The Tides and Kindred Phenomena in the Solar System*. W. H. Freeman, San Francisco, CA.

Dixon, T., 1991. An introduction to the Global Positioning System and some geological applications. *Reviews of Geophys*., **29**, 249-276.

Djamour, Y., Vernant, P., Bayer, R., Nankali, H.R., Ritz, J.F., Hinderer, J., Hatam, Y., Luck, B., LeMoigne, N., Sedighi, M., Khorrami, F., 2010. GPS and gravity constraints on continental deformation in the Alborz mountain range, Iran. *Geophys. Jour. Int*., **183**, 1287-1301.

Ducarme, B., Sun, H.P. and Xu, J.Q., 2002. New investigation of tidal gravity results from GGP network. In: Proc. GGP Workshop, Jena, March 11-15, *Bull. Inf. Marées Terrestres*, **136**, 10761-10776.

Engdahl, E. R., van der Hilst, R. and Buland, R., 1998. Global teleseismic earthquake relocation with improved travel times and procedures for depth determination. *Bull. Seismol. Soc. Am*., **88**, 722-743.

Eppelbaum, L.V. and Finkelstein, M.I., 1998. Radon emanation, magnetic and VLF temporary variations: removing components not associated with dynamic processes. *Collection of Selected Papers of the XXVI General Assembly of the European Seismological Commission* (Tel Aviv, Israel), 122-126.

Eppelbaum, L.V. and Kardashov, V.R., 1998. Nonlinear geothermal processes in the Earth crust and transition waves. *Trans. of the International Conference* "*The Earth's Thermal Field and Related Research Methods*". Moscow, Russia, 82-85 (in Russian).

Eppelbaum, L.V. and Kardashov, V.R., 2001. Analysis of strongly nonlinear processes in geophysics. *In*: (Moresi, L. and Müller, D., Eds.) *Proceed. of the Chapman Conference on Exploration Geodynamics*. Dunsborough, Western Australia, 43-44.

Eppelbaum, L.V. and Khesin, B.E., 2012. *Geophysical Studies in the Caucasus*. Springer, Heidelberg – N.Y. – London.

Ergintav, S. McClusky, S., Hearn, E., Reilinger, R., Cakmak, R., Herring, T., Ozener, H., Lenk, O. and Tari, E., 2009. Seven years of postseismic deformation following the 1999, M = 7.4, and M = 7.2 Izmit-Duzce, Turkey earthquake sequence. *Jour. of Geophys. Res*., **114**, doi:10.1029/2008JB006021.

Feder, J., 1988. *Fractals*. Plenum Press, N.Y.

Fialko, Y., 2006. Interseismic strain accumulation and the earthquake potential on the southern San Andreas fault system. *Nature*, **441**, 968-971.

Finkelstein, M., Price, C. and Eppelbaum, L., 2012. Is the geodynamic process in preparation of strong earthquakes reflected in the geomagnetic field? *Jour. of Geophysics and Engineering*, **9**, 585-594.

Forte, A., Cowgill, E. Bernardin, T., Kreylos, O. and Hamann, B., 2012. Late Cenozoic deformation of the Kur fold-thrust belt, southern Greater Caucasus. *Geol. Society of Amer. Bull.*, **122**, Nos. 3-4, 465-486.

Gadjiev, R.M., Makarov, Y.M., Nabiyev, A.T. and Kadirov, F.A., 1984. Studying of not tidal variations of acceleration of gravity on the Absheron geodynamic polygon. In (Yu. D. Boulanger, Ed.), *Repeated Gravimetric Observations*. *Problems of the theory and results*. Academy of Sciences and the Soviet Geophysical Committee, Moscow, 55-59 (in Russian).

Gadjiev, R.M., Kadirov, F.A., Kadyrov, A.G. and Nabiyev, A.T., 1988. Repeated gravimetric survey on the Samur-Baku profile for 1978-1985. In: (Yu. D. Boulanger, Ed.), *Repeated gravimetric observations*. *Proceed. of the Meeting of the Commission for the Study of Non-Tidal Gravity Changes*. M., Academy of Sciences and the Soviet Geophysical Committee, Moscow, 151-154 (in Russian).

Gaffet, S., Guglielmi, Y., Virieux, J. Waysand, G., Chwala, A. Stolz, R., Emblanch, C., Auguste, M., Boyer, D. and Cavaillou, A., 2003. Simultaneous seismic and magnetic measurements in the Low-Noise Underground Laboratory (LSBB) of Rustrel, France, during the 2001 January 26 Indian earthquake. *Geophysical Jour. International*, **155**, 981-990.

Gok, R., Sandvol, E., Turkelli, N., Seber, D., and Barazangi, M., 2003. Sn attenuation in the Anatolian and Iranian plateau and surrounding regions. *Geophys. Res. Lett.*, **30**, No. 24, doi:10.1029/2003GL018020.

Gokhberg, M.B., Morgunov, A.V. and Aronov, E.L., 1979. On the high-frequency radiation by seismic activity. *Doklady AN USSR*, **248**, No. 5, 1077-1081.

Gokhberg, M.B. and Shalimov, S.L., 2008. *Influence of Earthquakes and Explosions to Ionosphere*. Nauka, Moscow (in Russian).

Gutenberg, B. and Richter, C.F., 1956. Magnitude and energy of earthquakes. *Annali di Geofisica*, **9**, 1-15.

Hager, B.H., King, R.W. and Murray, M. H., 1991. Measurements of crustal deformation using the Global Positioning System. *Ann. Rev. Earth Planet Sci*., **19**, 351-382.

Hayakawa, M., 2007. VLF/LF radio sounding of ionospheric perturbations associated with earthquakes. *Sensors*, **7**, 1141-1158.

Heaton, T.H., 1982. Tidal triggering of earthquakes. *Bull. Seismol. Soc. Amer*., **72**, 2181-2200.

Hegewald, A., Jentzsch, G. and Jahr, T., 2011. Influence of temperature variations on the noise level of the data of the LaCoste & Romberg Earth Tide gravity meter ET18. *Geochem. Geophys. Geosys*, **12**, No. 8, http://dx.doi.org/10.1029/2010GC003432.

Herring, T. A., King, R. W. and McClusky, S. M., 2010. Introduction to GAMIT/GLOBK Release 10.4. *Mass. Inst. of Technology*, 48 pp.

Hu, Kun, Ivanov, P.C., Chen, Z., Carpena, P. and Stanley, H.E., 2015. Effect of trends on detrended fluctuation analysis. *Phys. Rev. E*, **64**, 2001-434, doi:10.1016/j.physa.2015.02.034.

Iskenderov, I.M., 1978. Secular drift of gravity on the Baku archipelago. In: (Yu.D. Boulanger, Ed.), *Repeated Gravimetric Supervision*. The collection of works on research of not-tidal changes of gravity and accompanying development in the field of equipment and work methodology. Moscow, 65-69.

Jackson, J., 1992. Partitioning of strike-slip and convergent motion between Eurasia and Arabia in eastern Turkey. *Jour. of Geophys. Res*., **97**, 12471-12479.

Jackson, J. and McKenzie, D., 1984. Active tectonics of the Alpine-Himalayan belt between western Turkey and Pakistan. *Geophys. Jour. R. Astr. Soc*., **77**, 185-246.

Jackson, J. and McKenzie, D., 1988. The relationship between plate motions and seismic tremors, and the rates of active deformation in the Mediterranean and Middle East. *Geophys. Jour. R. Astr. Soc*., **93**, 45-73.

Jackson, J., Priestley, K., Allen, M. and Berberian, M., 2002. Active tectonics of the south Caspian Basin. *Geophys. Jour. Intern*., **148**, 214-245.

Jentzsch, G., 1997. Earth tides and ocean tidal loading. In: H. Wilhelm, W. Zürn and H.G. Wenzel (Eds.), *Tidal Phenomena*, In: Lecture Notes in Earth Sciences, Vol. **6**, Springer-Verlag, Heidelberg, 145-171.

Jentzsch, G., 2008. The automated Burris gravity meter – a new instrument using an old principle. In: Proc. Symposium on Terrestrial Gravimetry: Static and Mobile Measurements, St. Petersburg, Russia, 20-23 Aug. 2007, 21-28.

Jones, L., and 13 others, 2008. The Shake Out Scenario. U.S. Geological Survey Open File Report 2008-1150, California Geological Survey Preliminary Report 25, version 1.0.

Jordan, T. H., 2014. The prediction problems of earthquake system science. *Seismol. Res. Lett*., **85**, 767-769.

Kadinsky-Cade, K. Barazangi, M., Oliver, J. and Isacks, B., 1981. Lateral variations of high-frequency seismic wave propagation at regional distances across the Turkish and Iranian Plateaus. *Jour. of Geophysical Research*, **86**, doi:10.1029/JB080i010p09377.

Kadirov, F., 2000. *Gravity Field and Models of Deep Structure of Azerbaijan*. Nafta-Press, Baku, (in Russian).

Kadirov, F., Floyd, M., Alizadeh, A., Guliyev, I., Reilinger, R.E., Kuleli, S., King, R., Toksoz, M.N., 2012. Kinematics of the eastern Caucasus near Baku, Azerbaijan. *Natural Hazards*, **63**, No. 2, 997-1006.

Kadirov, F.A., Ahadov, B.G., Gadirov, A.H., Babayev, G.R., Mammadov, S.G. and Safarov, R.T., 2015b. Microtremor survey and spectral analyses of H/V ratio for Baku city (Azerbaijan). *Izvestiya* (*Proceedings*), *Acad. Sci. Azerb*., Ser.: Earth Sciences, No. 3, 18-24.

Kadirov, F.A., Floyd, M., Reilinger, R., Alizadeh, Ak.A., Guliyev, I.S., Mammadov, S.G. and Safarov, R.T., 2015a. Active geodynamics of the Caucasus Region: Implications for Earthquake Hazards in Azerbaijan. *Izvestiya* (*Proceedings*), *Acad. Sci. Azerb*., Ser.: Earth Sciences, No. 3, 3-17.

Kadirov, F.A. and Gadirov, A.H., 2014. A gravity model of the deep structure of South Caspian Basin along submeridional profile Alborz–Absheron Sill. *Global and Planetary Change*, **114**, 66-74.

Kadirov, F.A., Gadirov, A.G., Babayev, G.R., Agayeva, S.T., Mammadov, S.K. and Garagezova, N.R., 2013. Seismic zoning of the southern slope of the Greater Caucasus from the fractal parameters of the earthquakes, stress state, and GPS velocities. *Izvestiya*, *Phys. Solid Earth*, **49** (4), 554-562.

Kadirov, F., Mammadov, S., Reilinger, R.E. and McClusky, S., 2008a. Some new data on modern tectonic deformation and active faulting in Azerbaijan (according to Global Positioning System measurements). *Izvestiya* (*Proceedings*) *of the Azerb. Nat. Acad. of Sci., Section: Earth Sciences*, No. 1, 82-88.

Kadirov, F.A. and Nabiyev, A.T. 1991. To the nature of not tidal variations of the gravity on the Absheron Geodynamic polygon. *Izvestiya, Azerb. Nat. Acad. of Sci*., Section: Earth Sciences, № 5-6, 135-139.

Kadirov, F.A., Yetirmishli, G. and Kadyrov, A.G., 2008b. Estimation of the maximum magnitude and intensity earthquakes in the Azerbaijan territory. *Proceed. of the Geol. Institute of ANAS*, **36**, 81-87 (in Russian).

Kardashov, V.R., Eppelbaum, L.V. and Vasilyev, O.V., 2000. The role of nonlinear source terms in geophysics. *Geophysical Research Letters*, **27**, No. 14, 2069-2073.

Kantelhardt, J., Zschiegner, S., Koscielny-Bunde, E., Bunde, A., Havlin, S., Stanley, E., 2002. Multifractal detrended uctuation analysis of nonstationary timeseries. *Physica A*, **316**, 87-114.

Keilis-Borok, V.I., 1990. The lithosphere of the Earth as a nonlinear system with implications for earthquake prediction. *Reviews of Geophysics*, **28**, 19-34.

Khain, V.E., 2000. *Tectonics of Continents and Oceans*. Nauchyi Mir, Moscow (in Russian).

Knapp, C.C., Knapp, J.H. and Connor, J.A., 2004. Crustal-scale structure of the South Caspian Basin revealed by deep seismic reflection profiling. *Marine and Petroleum Geology*, **2**, 1073-1081.

Kondorskaya, N.V. and Shebalin, N.V., 1977. *A new Catalogue of Strong earthquakes in the Territory of the USSR from the Ancient Time to 1975*. Nauka, Moscow (in Russian).

Kondorskaya, N.V. and Shebalin N.V., 1982. (Eds.), New catalog of strong earthquakes in the USSR from ancient times through 1977, *World Data Centre A for Solid Earth Geophysics*, *Report SE-31*, English translation of Russian original, Boulder, Colorado, USA.

Kopp, M.L. and Shcherba, I.G., 1985. Late Alpine development of the Eastern Caucasus. *Geotectonics* (Geotektonika), **19** No. 6, 497-507 (in Russian).

Král, J. and Gurbanov, A.G., 1996. Apatite fission track data from the Greater Caucasus pre-Alpine basement. *Chemieder Erde*, **56**, 177-192.

Lawrence, S.A., 2003. Kinematically consistent, elastic block model of the Eastern Mediterranean constrained by GPS measurements. *M.S. Thesis*, Massachusetts Institute of Technology, Cambridge, MA.

Lay, T., Yamazaki, Y., Ammon, C.J., Cheung, K.F. and Kanamori, H., 2011. The 2011 Mw 9.0 off the Pacific coast of Tohoku Earthquake: Comparison of deep-water tsunami signals with finite-fault rupture model predictions. *Earth Planets Space*, **63**, 797-801.

Lyons, S. and Sandwell, D., 2003. Fault creep along the southern San Andreas from interferometric synthetic aperture radar, permanent scatterers, and stacking. *Jour. Geophys. Res*., **108**, B1, 2047, doi:10.1029/2002JB001831.

Lyubimova, E.A., Mukhtarov, A.Sh. and Ismailzadeh, T.A., 1982. Temperature variations in the "Biladzhik" drill hole (Azerbaijan) during regional seismic activity. *Izvestiya*, *Physics of the Earth*, **21**, No. 4, 319-322.

Lyzenga, G.A., Panero, W.R. and Donnellan, A., 2000. Influence of anelastic surface layers on postseismic thrust fault deformation. *Jour. Geophys. Res*., **105**, 3151-3157.

Mammadov, S., Jahr, T., Jentzsch, G., Kadirov, F., 2011. Primary results of new gravity station Sheki/Azerbaijan. *Marees Terrestres Bulletin D'informations*, International Center for Earth tides, BIM **147**, 11881-11890.

Masci, F. and Thomas, J.N., 2015. Are the new finding in the search for ULF magnetic precursors to earthquakes. *Jour. of Geophysical Research. Space Physics*, **120**, doi:10.1002/2015JA021336, 1-16.

Meghraoui, M., Aksoy, M.E., Akyuz, H.S., Ferry, M., Dikbas, A. and Altunel, E., 2012. Paleoseismology of the North Anatolian Fault at Guzelkoy (Ganos segment, Turkey): Size and recurrence time of earthquake ruptures west of the Sea of Marmara. *Geochem. Geophys. Geosys*, **13**, Q04005, doi:10.1029/2011GC003960.

Melchior, P.J., 1983. *The Tides of the Planet Earth*. Pergamon Press.

Mellors, R.J., Yetirmishli, G., Binter, C., Gok, R., Sandvol, E.A., Takedatsu, R., Godoladze, T., Turkelli N., 2009. Earthquake Hypocenters in the Kur Basin and Greater Caucasus. *Trans. of the American Geophysical Union*, Fall Meeting 2009, abstract #T53G-04.

Meloni, M., Di Mauro, D., Lepidi, S., Mele, G. and Palangio, P., 2004. Tectonomagnetic and VLF electromagnetic signals in Central Italy. *Annals of Geophysics*, **47**, No. 1, 29-37.

McClusky, S, Balassanian, S., Barka, A., Demir, C., Ergintav, S., Georgiev, I., Gurkan, O. Hamburger, M., Hurst, K., Kahle, H., Kastens, K., Kekelidze, G., King, R., Kotzev, V. Lenk, O.,

Mahmoud, S., Mishin, A., Nadariya, T.M., Ouzounis, A., Paradissis, D., Prilepin, M., Reilinger, R.E., Sanli, I., Seeger, H., Tealeb, A., Toksoz, M.N. and Veis, G., 2000. GPS constraints on plate kinematics and dynamics in the eastern Mediterranean and Caucasus. *Jour. of Geophys. Res.,* **105**, 5695-5719.

McClusky, S., Reilinger, R., Mahmoud, S., Ben Sari, D. and Tealeb, A., 2003. GPS constraints on Africa (Nubia) and Arabia plate motion. *Geophys. Jour. Intern*., **155**, 126-138.

McQuarrie, N., Stock, J.M., Verdel, C. and Wernicke, B.P., 2003. Cenozoic evolution of Neotethys and implications for the causes of plate motions. *Geophys. Res. Lett*., **30**, doi:10.1029/2003GL017992.

McQuarrie, N. and van Hinsbergen, D.J.J., 2013. Retro deforming the Arabia-Eurasia collision zone: Age of collision versus magnitude of continental subduction. *Geology*, **41**, 315-318.

McKenzie, D.P., 1970. Plate tectonics of the Mediterranean region. *Nature*, **226**, 239-243.

McKenzie, D.P., Davies, D. and Molnar, P., 1970. Plate tectonics of the Red Sea and East Africa. *Nature*, **226**, 243-248, 1970.

McKenzie, D.P., 1972. Active tectonics of the Mediterranean region. *Geophys. Jour. R. Astron. Soc*., **30**, 109-185.

Mogi, K., Mochizuki, H. and Kurokawa, Y., 1989. Temperature changes in an artesian spring at Usami in the Izu peninsula (Japan) and their relation to earthquakes. *Tectonophysics*, **159**, 95-108.

Mueller, I.I., and Beutler, G., 1992. The International GPS Service for Geodynamics - Development and Current Structure. *Proceed. of the 6th Symp. on Satellite Positioning*, Ohio State Univ., Columbus, Ohio.

Müller, B., Barth, A., Heidbach, O., Reinecker, J., Sperner, B., Tingay, M. and Wenzel, F. 2005. The World Stress Map – an essential and easy accessible tool for geohazard assessment. *Proceed. of the Int. Workshop Recent Geodynamics, Georisk and Sustainable Development in the Black Sea to Caspian Region*, Vol. **825**, Baku, AIP, 19-31.

Mushketov, I.V. and Orlov, A.P., 1893. Cataloque of earthquakes of the Russian Empire. *Notes of Russian Geographic Soc.,* St. Petersburg, **26**, 1-582 (in Russian).

Neprochnov, Y.U., 1968. Structure of the Earth's crust of epicontinental seas: Caspian, Black and Mediterranean. *Canad. Jour. Earth Sci*., **5**, 1037-1043.

Nur, A. and Mavko, G., 1974. Postseismic Viscoelastic Rebound. *Science*, **183**, 204-206.

Okada, Y., 1985. Surface deformation due to shear and tensile faults in a half-space. *Bull. Seismol. Soc. Am*., **75**, 1135-1154.

Ouyang, Z., Zhang, H., Fu, Z., Gou, B. and Jiang, W., 2009. Abnormal phenomena recorded by several earthquake precursor observation instruments before the M_s 8.0 Wenchuan, Sichuan earthquake. *Acta Geologica Sinica*, **83**, No. 4, 834-844.

Parisi, G. and Frisch, U., 1985. On the singularity structure of fully developed turbulence. In: (M. Ghil, R. Benzi and G. Parisi, Eds.), *Turbulence and Predictability in Geophysical Fluid Dynamics*, *Proceed. of the International School of Physics* "Enrico Fermi" (1983), North-Holland, 84-87.

Peng, C.K., Buldyrev, S.V., Havlin, S., Simons, S.M., Stanley, H.E. and Goldberger, A.L., 1994. Mosaic organization of DNA nucleotides. *Phys. Rev. E*, **49**, 1685-1689.

Philip, H., Cisternas, A., Gvishiani, A. and Gorshkov, A., 1989. The Caucasus: An actual example of the initial stages of continental collision. *Tectonophysics*, **161**, 1-21.

Philip, H., Avagyan, A., Karakhanian, A., Ritz, J.-F. and Rebai, S., 2001. Estimating slip rates and recurrence intervals for strong earthquakes along an intracontinental fault: Example of the Pambak-Sevan-Sunik fault (Armenia). *Tectonophysics*, **343**, 205-232.

Podgorski, J., Hearn, E., McClusky, S., Reilinger, R.E., Taymaz, T. and Tan, O., 2007. Postseismic deformation following the 1991 Racha, Georgia, earthquake. *Geophys. Res. Lett*., **34**, L04310, doi:10.1029/2006GL028477.

Pollitz, F.F., 1992. Postseismic relaxation theory on the spherical earth. *Bull. Seismol. Soc. Amer*., **82**, No. 1, 422-453.

Prescott, W.H. and Savage, J.C., 1976. Strain accumulation on the San Andreas Fault near Palmdale, California. *Jour. of Geophys. Res*., **81**, 4901-4908.

Pudovkin, I.M., Pogrebnikov, M.M., Pochtarov, V.I. and Bekzhanov, G.G., 1973. On the direct correlation between the geomagnetic variations and earthquakes. *Doklady AN USSR*, **208**, No. 5, 1074-1077.

Rautian, T.G., 1964. On the estimation of earthquake energy at distances up to 3,000 km. *Proceed. of the Inst. Phys. Earth*, No. 32, Nauka, Moscow, 88-93 (in Russian).

Reilinger, R.E., McClusky, S., Vernant, P., Lawrence, S., Ergintav, S., Cakmak, R., Ozener, H., Kadirov, F., Guliyev, I., Stepanyan, R., Nadariya, M., Hahubia, G., Mahmoud, S., Sakr, K., ArRajehi, A., Paradissis, D., Al-Aydrus, A., Prilepin, M., Guseva, T., Evren, E., Dmitrotsa, A. Filikov, S.V., Gomez, F., Al-Ghazzi, R. and Karam, G., 2006. GPS constraints on continental deformation in the Africa-Arabia-Eurasia continental collision zone and implications for the dynamics of plate interactions. *Jour. of Geophys. Res.,* BO5411, doi:10.1029/2005JB004051.

Reinecker, J., Heidbach, O. and Müller, B. 2005. The 2005 release of the World Stress Map, www.world-stress-map.org; last time was seen on 20.08.2015.

Riznichenko, Yu.V., 1968. Seismic activity and shockability. In: *Seismic regioning of the territory of the USSR*. Nauka, Moscow (in Russian).

Riznichenko, Yu.V., 1985. *Problems of Seismology*. Selected Publications. Nauka, Moscow (in Russian).

Riznichenko, Yu.V., Khesin, B.E. and Metaxa, Kh.P., 1983. Relation between seismicity and magnetic field according to observations in Azerbaijan. *Izvestiya, Ser. Physics of the Solid Earth*, No.1, 3-14 (in Russian).

Rzayev, A.G., 2005. Seismoprognostic investigations. *In*: (Ak.A. Alizadeh, Ed.), *Geology of Azerbaijan*, Nafta-Press, Vol. **5**, Physics of the Earth, 23-34 (in Russian).

Sengor, A.M.C., Gorur, N. and Saroglu, F., 1985. Strike-slip faulting and related basin formation in zones of tectonic escape: Turkey as a case study, In: (Biddle, K.T. and Christie-Blick, N., Eds.), *Strike-slip Faulting and Basin Formation*, *Society of Econ. Paleont. Min. Sec. Pub*, **37**, 227-264.

Sengor, A.M.C., Tuysuz, O., Imren, C., Sakinc, M., Eyidogan, H., Gorur, N., LePichon, X. and Rangin, C., 2004. The North Anatolian fault: A new look. *Ann. Rev. Earth Planet. Sci.,* **33**, 1-75.

Sheorey, P.R., 1994. A theory for in situ stresses in isotropic and transversely isotropic rock. *Intern. Jour. Rock. Mech. Min. Sci. & Geomech. Abstr*., **31**, No 1, 23-34.

Singh, R.P. and Dey, S., 2003. Surface latent heat flux as an earthquake precursor. *Natural Hazards and Earth System Sciences*, **3**, 749-755.

Stacey, F.D., 1969. *Physics of the Earth*. Wiley, N. Y.

Swartz, D.P. and Coppersmith, K.J., 1984. Fault behavior and characteristic earthquakes: Examples from the Wasatch and San Andreas Fault Zones. *Jour. of Geophys. Res*., **49**, 5681-5698.

Telesca, L., Lovallo, M., Babayev, G. and Kadirov, F., 2013. Spectral and informational analysis of seismicity: an application to the 1996–2012 seismicity of the Northern Caucasus–Azerbaijan part of the Greater Caucasus–Kopet Dagh region. *Physica A*, **392**, 6064-6078.

Telesca, L., Lovallo, M., Mammadov, S. Kadirov, F. and Babayev. G., 2015. Power spectrum analysis and multifractal detrended fluctuation analysis of earth's gravity time series. *Physica A*: *Statistical Mechanics and its Applications*, **428**, No. 4.

Torge, W., 1989. *Gravimetry*. De Gruyter. Berlin – N.Y.

Triep, E.G., Abers, G.A., Lerner-Lam, A.L., Mishatkin, V., Zakharchenko, N. and Starovoit, O., 1995. Active thrust front of the Greater Caucasus: The April 29, 1991 Racha earthquake sequence and its tectonic implications. *Jour. of Geophys. Res*., **100**, 4011-4033.

Vernant, P. and Chery, J., 2006. Low fault friction in Iran implies localized deformation for the Arabia–Eurasia collision zone. *Earth and Planetary Sci. Lett*., **246**, 197-206.

Vernant, P., Reilinger, R.E. and McClusky, S., 2014. Geodetic evidence for low coupling on the Hellenic subduction plate interface. *Earth, Planet. Sci*., **385**, 122-129.

Veselov, K.E., 1988. *Gravity Prospecting*. Nedra, Moscow (in Russian).

Vidale, J.E., Agnew, D.C., Johnston, M.J.S. and Oppenheimer, D.H., 1998. Absence of earthquake correlation with Earth tides: an indication of high preseismic fault stress rate. *Jour. of Geophys. Res*., *Solid Earth*, **103**, 24567-24572.

Vincent, S.J., Morton, A.C., Carter, A., Gibbs, S. and Teimuraz, G.B., 2007. Oligocene uplift of the Western Greater Caucasus: An effect of initial Arabia-Eurasia collision. *Terra Nova*, **19**, 160-166, doi:10.1111/j.1365-3121.2007.00731.x.

Voisin, S., 2002. Dynamic triggering of earthquakes: The nonlinear slip-dependent friction case. *Jour. of Geophysical Research*, **107**, B12, 2356, doi:10.1029/2001JB001121, 10_1-10_11.

Weldon II, R. J., Scharer, K., Fumal, T. and Biasi, G., 2004. Wrightwood and the earthquake cycle: what a long recurrence record tells us about how faults work. *GSA Today*, **14**(9), 4-10.

Wells, D.L. and Coppersmith, K.J., 1994. New empirical relationships among magnitude, rupture length, rupture width, rupture area, and surface displacement. *Bull. Seism. Soc. Am*., **84**, 974-1002.

Wenzel, H.-G., 1996. The nanogal software: Earth tide data processing package ETERNA 3.30. *Bulletin d'Informations Marees Terrestres*, Vol. **124**, 9425-9439.

Westaway, R., 1990. Seismicity and tectonic deformation rate in Soviet Armenia: Implications for local earthquake hazard and evolution of adjacent regions. *Tectonics*, **9**(3), 477-503, doi:10.1029/TC009i003p00477.

Working Group on California Earthquake Probabilities (WGCEP), 2008. The Uniform California Earthquake Rupture Forecast, Version 2 (UCERF 2). *U.S. Geological Survey Open-File Report 2007-1437 and California Geological Survey Special Report 203* [http://pubs.usgs.gov/of/2007/1091/].

Yaschenko, V.R., 1989. *Geodetic Investigation of Earth Crust Vertical Movements*. Nedra, Moscow (in Russian).

Yetirmishli, G.D. and Kazimova, S.E., 2013. Velocity model of crust of Azerbaijan from the data of digital seismic stations. *Geology and Geophysics of South of Russia*. No. 1, 59-74.

Yetirmishli, G.J., Mammadli, T.Y. and Kazimova, S.E., 2013. Features of seismicity of Azerbaijan part of the Greater Caucasus. *Jour. of Georgian Geoph. Society*, Iss. (A), Physics of Solid Earth, **16a**, 55-60.

Young, D. and Zürn, W., 1979. Tidal triggering of earthquakes in the Swabian Jura. *Jour. of Geophysics*, **45**, 171-182.

Zoller, G., Ben-Zion, Y., Holschneider, M. and Hainz, S., 2007. Estimating recurrence times and seismic hazard of large earthquakes on an individual fault. *Geophys. Jour. Int.*, **170**, 1300-1310.

Zonenshain, L.P., and Le Pichon, X., 1986. Deep basins of the Black Sea and Caspian Sea as remnants of Mesozoic back-arc basins. *Tectonophysics*, **123**, 181-211.

Zürn, W., 1997. The nearly diurnal free wobble-resonance. In: (H. Wilhelm, W. Zurn and H.-G. Wenzel, Eds.), *Tidal Phenomena*, Lecturer Notes in Earth Sciences, Vol. **66**, 95-109.

Oil and Gas Geophysics

7

It should be underlined that Azerbaijan is the most ancient hydrocarbon province of the world. For example, the world's first oil well was drilled in 1848 in the Absheron Peninsula. This event took place eleven years prior to the drilling of the first oil well in Pennsylvania. Geophysical methods for oil and gas searching (localization) began to apply in Azerbaijan since 20s of the XX century. However, it is not possible to present all obtained results in one chapter. Therefore, we confine ourselves here to a few typical examples.

7.1 The Kur Depression

It was initially believed that the Kur Depression was composed of thick sedimentary rocks deposited on the crystalline pre-Alpine basement and that these megastructures were separated by subvertical deep faults (Alizadeh et al. 1966). In 1965, the Saatly superdeep borehole (SD-1) was projected (drilling began in 1971 and stopped in 1991) to drill on the buried uplift of the basement of the Middle Kur Depression (Shikhalibeyli et al. 1988) (see also Chap. 6 of this volume). The SD-1 borehole (8324 m) was discovered Premolassic formations beginning Middle Jurassic which (as Upper Jurassic and Lower Cretaceous) composed by volcanites. In the SD-1 section, more than 5-km-thickness volcanites were found. Khain (2000) noted that these rocks have expressed island arc nature with prevalence of basalts and andesites (with the exception of a part of Upper Jurassic). Carbonaceous deposits of Upper Senonian and marls of Lower Paleogene overlie these volcanites. All these generations compose large gentle folds of northwest strike.

Numerous deep wells have been drilled in this area. They confirm this model of the deep structure of Kur Depression and the occurrence of hidden stocks of Mesozoic magmatic rocks (see Chap. 5 of this Volume). Inan et al. (1997) findings also mainly confirm this model.

Obviously, the oil and gas potential of the Kur Depression may be enormous (Kerimov 1996; Mamedov et al. 2008). The most recent investigations (e.g., Vincent et al. 2010) indicate that sandstones in the southern part of the Kur Depression have good and very good reservoir petrophysical properties.

7.1.1 Seismics

Seismic survey results in the Kur Depression are compiled mainly in Kerimov (1996), Aliyev et al. (2005), Mamedov et al. (2008), Mamedov (2009), Ak. Alizadeh (2012). Several examples of seismic profiles crossing the Kur Depression are presented in Chaps. 4 and 5 of this volume.

Deep seismic profile crossing the Kur Depression (NE–SW) is presented in Fig. 7.1. Sedimentation conditions of specific geological bodies' formation on an active margin (see Chap. 5 of this volume) in the divergent stage have been predetermined by the peculiarities of an island arch development. The seismic section gives information about the volcanic scarps and on the complex volcanogenic pattern of the island arch (Mamedov 2009).

Hoogendoorn et al. (2005) have investigated subsurface structure of the Kur delta by the use of combined analysis of surface geology, radiometric dating, well cores, and near-surface detailed seismics. On the basis of the afore-mentioned data examination, the Holocene of the Kur delta was reconstructed. One of the typical seismogeological sections is presented in Fig. 7.2.

Here, H1 and H2 are interpreted as prograding deposits, TS1 (out on this profile) and TS2—as prominent discontinuity surfaces on the sparker data. Furthermore, a drape of continuous reflectors is recognizable on all profiles and is considered to represent sedimentation of the modern Kur delta. Consequently, the base of this drape is interpreted as TS3. Four main features can be recognized within the profiles: (1) horizontal/subhorizontal reflectors (delta plain), (2) clinoform reflectors (delta front, prodelta), (3) concave-upward reflectors (distributary channels and possible incised channel), which are often associated with, and (4) hyperbolic reflectors (levees, barrier) (Hoogendoorn et al. 2005).

A.A. Alizadeh et al., *Geosciences of Azerbaijan*,
Regional Geology Reviews, DOI 10.1007/978-3-319-40493-6_7

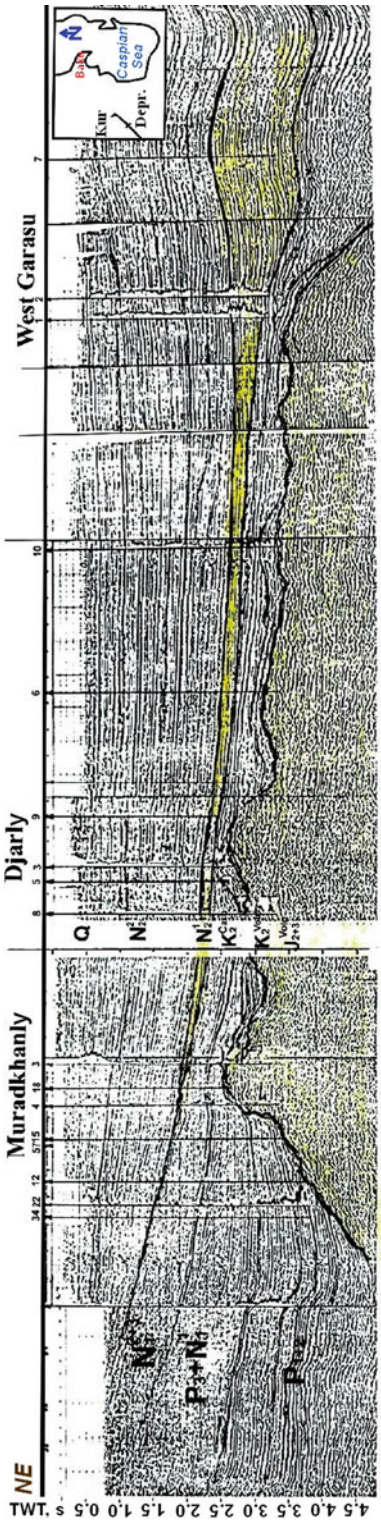

Fig. 7.1 Volcanogenic island arc reflection in time section (Mamedov 2009)

7.1.2 Gravity

One of the most effective gravity surveys in the Middle Kur Depression was carried out by Tzimelzon (1965). His gravity data analysis delineated the Muradkhanly anticline structure (Fig. 7.3) where later an oil deposit was discovered. More recently, Gadirov (2009) presented a more detailed physical–geological model of the Muradkhanly deposit on the basis of gravity (Δg_B) and magnetic (ΔZ) modeling. Amiraslanov (1990) identified several dozen local gravity maxima in the central part of the Middle Kur Depression joined to 20 anticline belts. According to this author, these gravity maxima correspond to uplifts and outcrops of Mesozoic (mainly Jurassic) rocks.

7.1.2.1 Gravity Field Transformations

Regional gravity field transformations (upward continuation and calculating difference anomalies for Azerbaijan and adjacent areas) are analyzed in Chap. 5 of this Volume.

Observed and analytically continued at different levels (1, 2.5, 4, 6, 8, and 20 km), the gravity field was employed as for direct analysis and then for computation of difference gravity anomalies (Δg_0–Δg_6, Δg_0–Δg_8, etc.) in the Middle Kur Depression (e.g., Nasruyev et al. 1975; Amiraslanov 1987). As a result, several previously unknown local gravity anomalies were detected and geologically interpreted.

Kadirov (2000) successfully applied the Hartley transform to separate the gravity field in the Shamakhy-Gobystan and Absheron regions. The author's analysis of the gravity field power spectrum indicates that the average depth of the targets ranged from 24.5 (crystalline basement surface) to 3.2 km (surface within the Cenozoic deposits). According to Kadirov (2000), most of the regional anomalies are caused by the topography of the pre-Mesozoic crystalline basement.

The regional gravity component was removed using correlation methods, and maps of local gravity anomalies were constructed for the northern Naftalan-Gedakboz (Middle Kur Depression) and Byandovan (Lower Kur Depression) areas (Gadirov 2009). These local gravity anomalies (0.1–0.2 mGal) in the SW part of the Byandovan area may reflect early unknown hydrocarbon deposits.

Gadirov and Gasanov (2013) present results of high-precision gravity exploration in the Kur-Talysh and Hajigabul areas of the Lower Kur Depression. The geological nature of the observed local gravity minimums has been analyzed, and their relationship with the Kur-Talysh structure of Productive Series is shown.

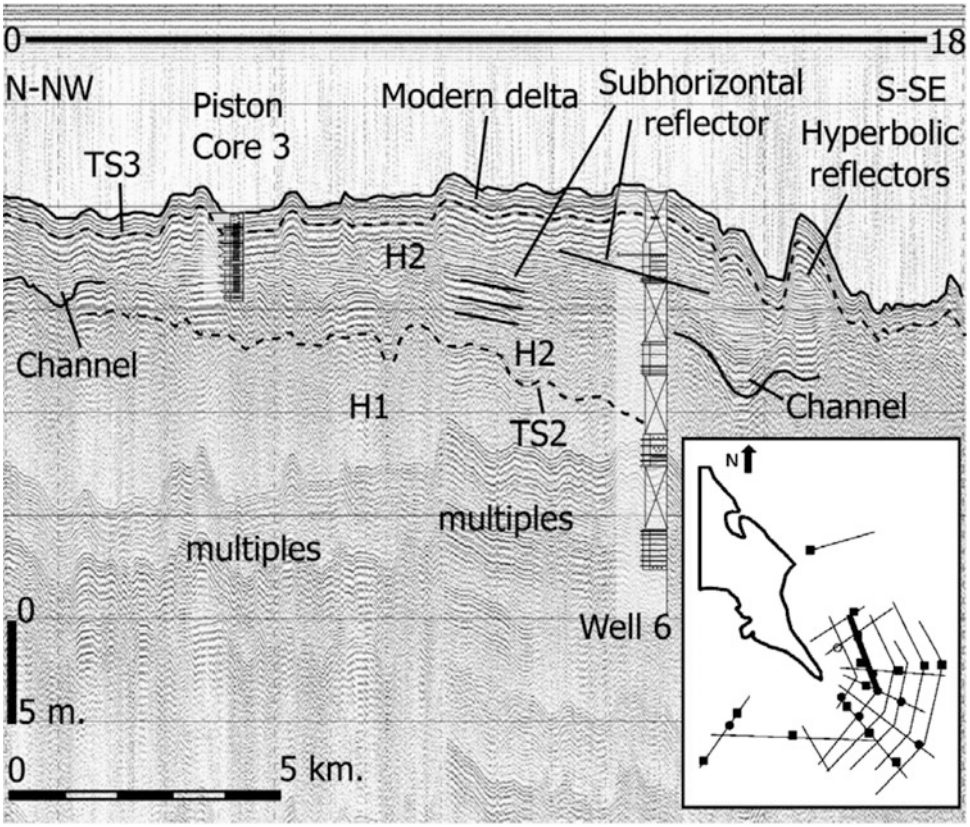

Fig. 7.2 Sparker profile 2 (0102) coast-parallel profile, illustrating the two channel types, the most S-SE channel (*right-hand side* of the figure) is horizontally filled with sediments and incised the underlying strata. The most N-NW channel (*left-hand side* of the figure) serves as an example for an aggradation channel since it is still visible in the surface topography (Hoogendoorn et al. 2005)

7.1.3 Magnetics

7.1.3.1 Magnetic Field Transformations

It is well known that hydrocarbon deposits typically manifest in a magnetic field in the form of low amplitudes where a weak negative field over a pool is bordered by ring of positive values (e.g., Donovan et al. 1979). This pattern is in line with the notion of a secondary generation of magnetic minerals caused by hydrocarbons migrating along subvertical zones (methane and hydrogen sulfide) confined to peripheral parts of the deposit, whereas in the central part, the hydrocarbon migration is less intensive.

This superimposition of the observed magnetic anomalies often makes it difficult to differentiate these circular (ring) structures from subsurface inhomogeneities. Therefore, in such situations, special methodologies are used (transformations, filtering, upward continuation, computing difference anomalies, etc.) to separate the useful signals from the noise background (e.g., Khesin et al. 1983, 1996; Eppelbaum 2007; Eppelbaum et al. 2011).

7.1.3.2 Magnetic Field Modeling

Magnetic surveys were used to classify a Mesozoic section in the Kur Depression into magmatic (magnetic) and carbonaceous (non-magnetic) complexes (e.g., Fig. 7.4) according to their composition. As a result, oil and gas traps of a previously unknown type were revealed in zones of carbonaceous rock pinch-outs near the stocks of igneous rocks and in eroded roofs of these stocks (Khesin and Eppelbaum 1997).

A respective scheme on the basis of Kh. Metaxas' data (Eppelbaum and Khesin 2012) is shown in Fig. 7.5.

7.1.4 Temperature

7.1.4.1 Analysis of Temperature in Wells

Temperature observation in wells is one of the most important tools of hydrocarbon geophysics (e.g., Kutasov and Eppelbaum 2015).

On the basis of analysis of numerous temperature data in boreholes of Azerbaijan the predicted deep tectonic signatures could be obtained by examining thermal data in wells at depths of 1–2 km. This would make it possible to localize hydrocarbon deposits at a depth of 3.5–4.5 km (and more) and estimate the occurrence of buried uplifts in the lowermost strata.

Values of the vertical geothermal gradient in the Middle Kur Depression (Azerbaijan) change at depth intervals

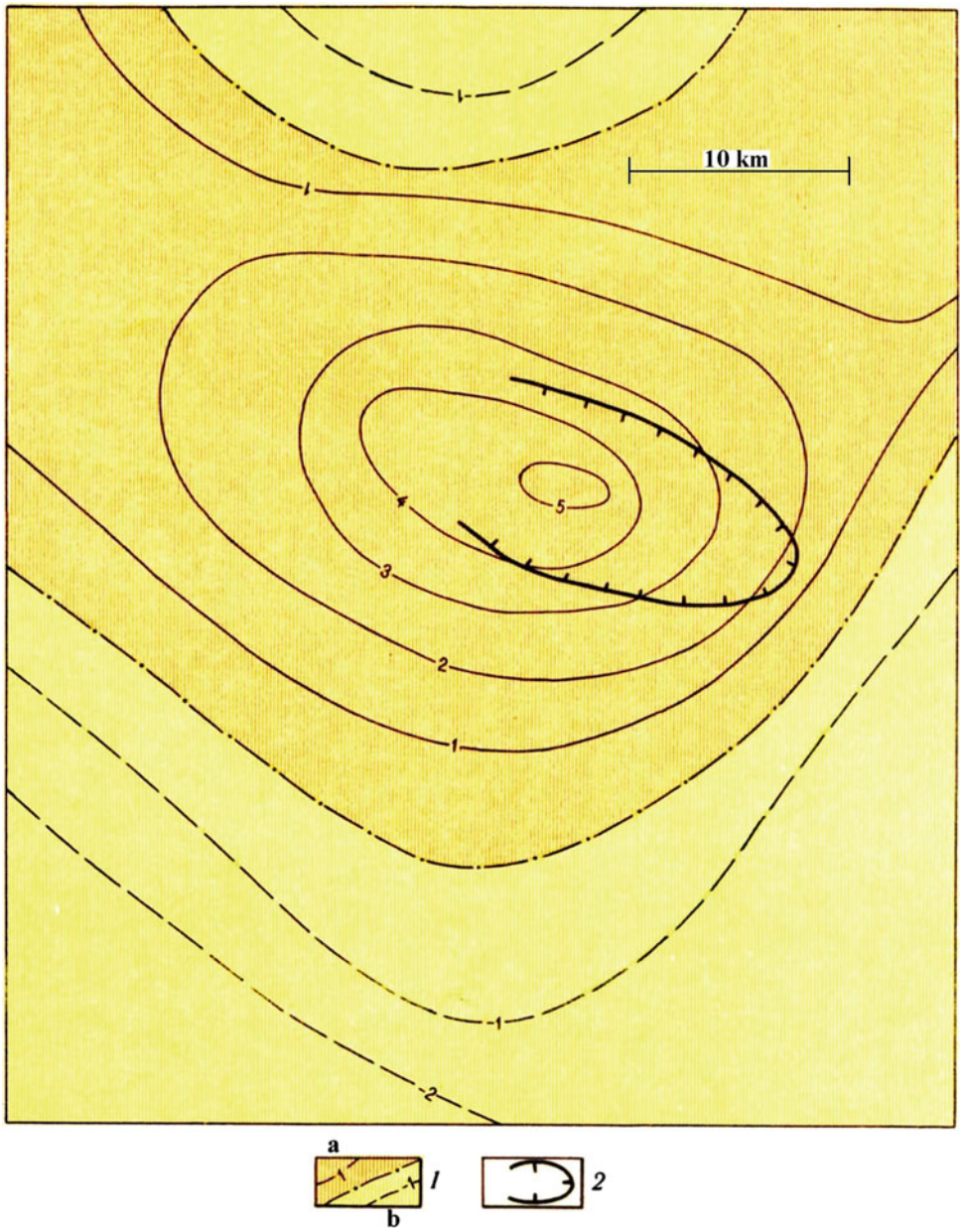

Fig. 7.3 Gravity method as a successful tool for delineation of the buried Muradkhanly structure (after Tzimelzon 1965). (*1*) Different gravity field Δg_{0-10}, mGal: (*a*) positive, (*b*) negative; (*2*) contour of Muradkhanly uplift according to seismic prospecting data and drilling

of 0–2000 m and 4000–6000 m from 25-43 °C/km to 20–30 °C/km (e.g., Kerimov et al. 1989). Using geothermal data for the Southern Caucasus, the depths of isotherm 200 °C (H_1), 400 °C (H_2) ,and the Curie temperature (H_c) for the Middle Kur Depression were determined.

Table 7.1 shows that depth H_1 for isotherm 200 °C increases from 5.5 km in the west to 7.5 km east of the Middle Kur Depression. Depth H_2 of isotherm 400 °C also increases from 13 to 14 km in the west to 21–22 km in the east of the Middle Kur Depression. Therefore, in the Middle Kur Depression, the most probable depth interval for the surface of wustite (iron suboxide) decomposition is the interval from 5.5 ÷ 7.5 km to 13 ÷ 22 km.

It can be seen from Table 7.1 that this interval is consistent with the depth of the magnetized bodies' lower edges calculated using magnetic data. It is obvious that this correlation is not accidental. Furthermore, the depth of the magnetized bodies' lower edges (H_m) only coincides with the depth of the Curie surface (H_c) in the area of three magnetic anomalies (Shamkir, Beilagan and Zardab). These anomalies are located in the zone of large faults, where conditions are favorable for the transformation of iron suboxide into iron

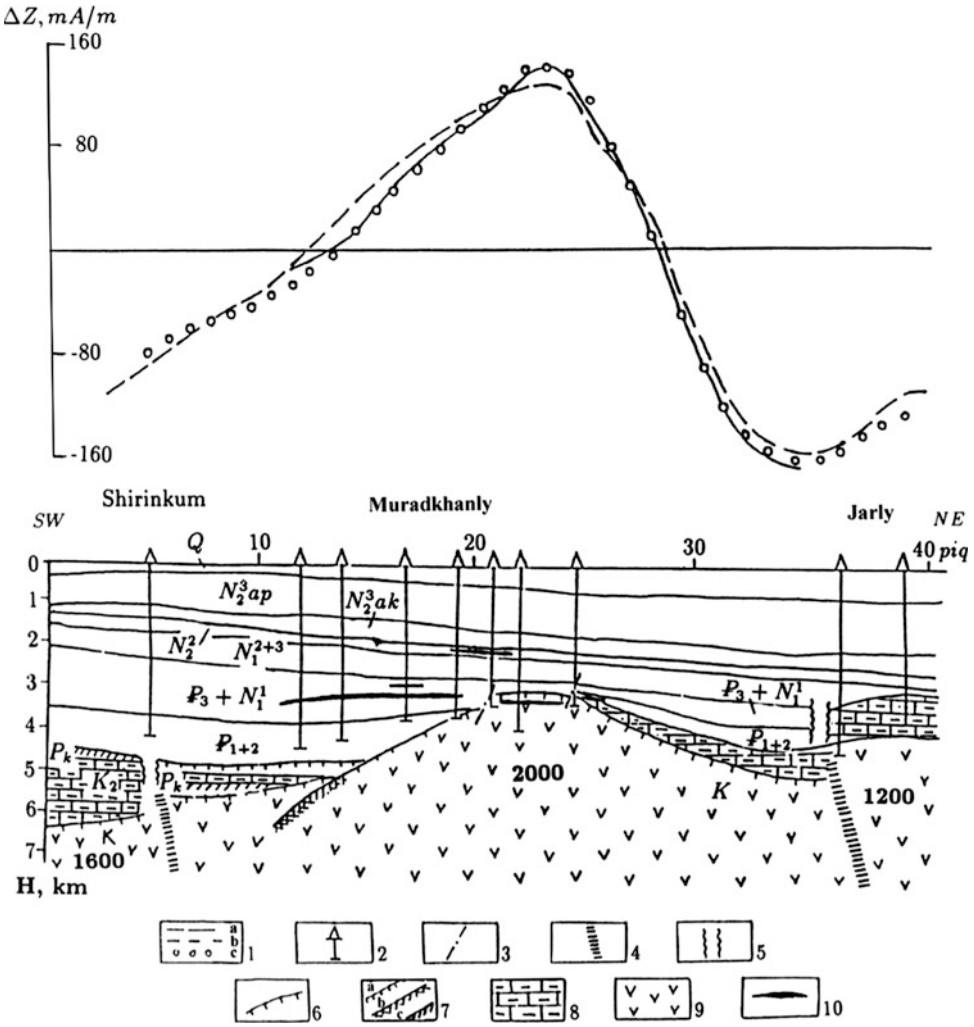

Fig. 7.4 Geological–geophysical section of a profile across the—Shirinkum Muradkhanly– Jarly areas (Middle Kur Depression) (Khesin and Eppelbaum, 1997). (*1*) ΔZ_a curves: (*a*) and (*b*) observed, (*c*) calculated; (*2*) deep boreholes; faults revealed by the data from: (*3*) drilling and seismic prospecting; (*4*) gravimetric and magnetic prospecting; (*5*) zones of complicated seismic recording; (*6*) location of magmatic rocks roof determined by modeling; (*7*) conventional seismic horizons: (*a*) *Mz* roof, (b) *Mz* volcanogenic rocks roof, (*c*) *Mz* carbonaceous rocks roof; (*8*) carbonaceous-terrigenous rocks; (*9*) magnetized magmatic rocks (in the figure the magnetization ***J*** is given in mA/m; (*10*) oil-bearing layers

oxide (Pilchin and Eppelbaum 2006). Oxidation conditions in such zones may be present at great depths. The depth of the magnetized bodies' lower edge for 14 other magnetic anomalies reflects the depth of the interval by the following eutectic reaction (Pilchin and Eppelbaum 1997):

$$4\mathrm{Feo} \overleftrightarrow{\longrightarrow} \mathrm{Fe} + \mathrm{Fe_3O_4}.$$

Heat flow and geothermal gradients for some areas of the Kur Depression and the South Caspian Depression are listed in Table 7.2.

Pilchin (1983) calculated values of geothermal gradient for the Middle Kur Depression as a function of depth. For instance, for the depth intervals 0–2000, 2000–4000, and 4000–6000 m these values consist of 25–43, 20–35, and 20–30 °C/km, respectively.

It is well known that analysis of changes in excess temperature ($T - T_0$) is an important parameter for searching hydrocarbon deposits (Eppelbaum et al. 2014). The values of temperature excess ($T - T_0$) at different depths for some areas of the Kur Depression are presented in Table 7.3.

7.1.4.2 Near-Surface Temperature Survey

This method was applied in the Muradkhanly oil deposit in Central Azerbaijan (Fig. 7.6), where the temperature was measured in 3 m deep wells, and the data thus obtained were smoothed by the use of a sliding interval average of three points. A fault was discovered by a field crew from the "YuzhVNIIGeofizika" (Baku) using gravity and magnetic methods, which was confirmed by drilling data. Thermal observations were also conducted by the "YuzhVNIIGeofizuka" (Sudzhadinov and Kosmodemyansky 1986). The position of the upper edge of the fault was calculated using the tangents and characteristic point method (Khesin and Eppelbaum 1994); its projection in plane coincided exactly with the fault position indicated by the independent geophysical and geological data.

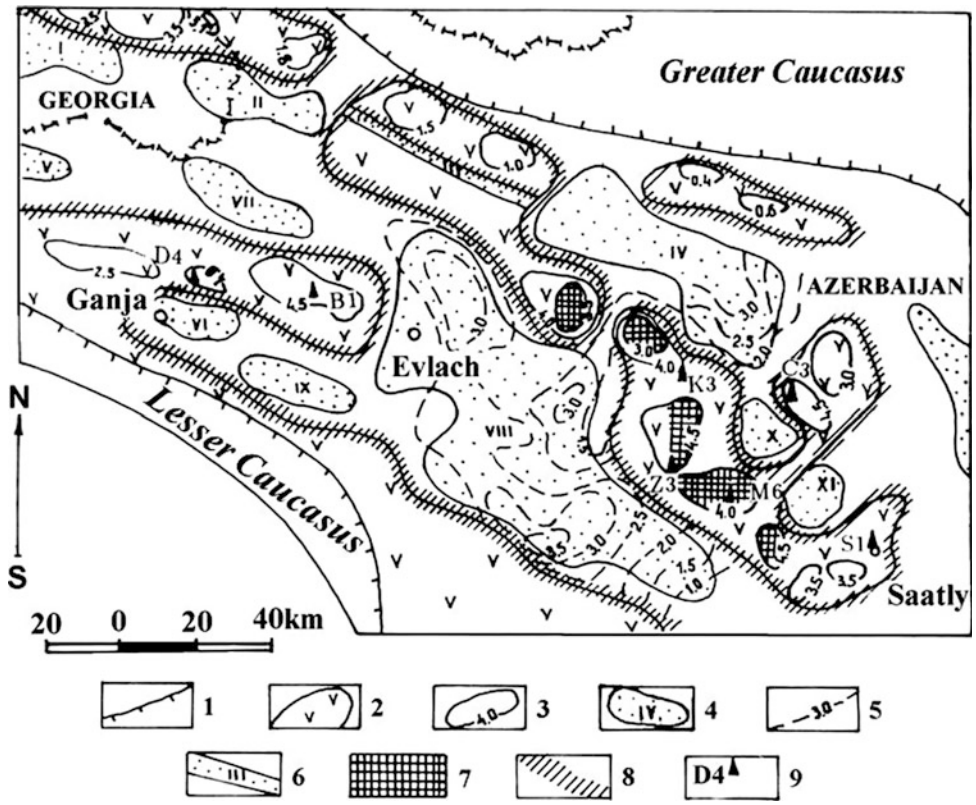

Fig. 7.5 Schematic chart of oil and gas prognosis for the Middle Kur Depression using the interpretation of magnetic and other geophysical data (Eppelbaum and Khesin 2012). (*1*) contour of mountain structures; (*2*) contour of Mesozoic magmatic associations of basic and intermediate composition according to magnetic prospecting data; (*3*) isodepths of magnetized (mainly, effusive) Mesozoic rocks according to magnetic prospecting data; (*4*) basins of normal sedimentary Meso-Cenozoic rocks according to a set of geological and geophysical data; (*5*) isopachs for an Upper Jurassic–Cretaceous complex of normal sedimentary deposits according to seismic and magnetic prospecting data; (*6*) part of the North-Kur fault zone with the most intensive movements (according to gravimetric and magnetic data); (*7*) most promising areas for detecting oil deposits in eroded magmatic rocks in arch structures; (*8*) most promising areas for detecting oil and gas deposits mainly in traps of a non-structural type (on the various pinched-out rock associations); (*9*) wells for deep drilling

7.1.5 Radiometric Survey

Hydrocarbon deposits within the Kur Depression and Absheron Peninsula are reflected in the gamma field by typical oval-shaped negative anomalies with a smooth drop of gamma radiation intensity (Ch. Aliyev and Zolotovitskaya 1996, 2005). In the Middle Kur Depression, several geological structures with the fluent fall of 1–1.5 μR/h were delineated after reducing the gamma background. Within the Muradkhanly structure, the gamma field consists of 4.5–7 μR/h. It was suggested that gamma surveys in geophysical integration increase the likelihood of detecting hydrocarbon deposits (Aliyev 1994).

Figure 7.7 shows a model of forming gamma field over the hydrocarbon deposits. As it can be seen from this figure, the fault zone serves as a channel for hydrocarbon fluid penetration to the upper part of geological section and leads to formation of surface radiometric anomalies.

7.1.6 Borehole Logging

Results of various geophysical method observations in boreholes in Azerbaijan are described in many publications (e.g., Kerimov et al. 1989; Akselrod et al. 1991; Kerimov 1996).

An interesting example of cooperative presentation of electric resistivity (blue) and self-potential (some authors call this methods as spontaneous polarization) (red) graphs observed in boreholes Mishovdagh 58 and Babazanan 43 (Kur Depression) is presented in Fig. 7.8.

As it is well known from the classical geophysical logging (e.g., Vaish 2005) and application of information and probabilistic methods in exploration geophysics (Eppelbaum 2014) such a combined analysis enables to increase the possibilities for detection of intervals' perspective for hydrocarbons accumulation.

Table 7.1 Depths of the Curie point isotherm (200 and 400 °C) and lower edges of magnetized bodies in the Middle Kur Depression, Azerbaijan (after Pilchin and Eppelbaum 1997)

Name of magnetic anomaly	H_1 (200 °C), km	H_2 (400 °C), km	H_C, km	H_m, km
Ismailly	5.5–6.5	14	25	14
Shamkir	5.0–6.0	12	18	20
Sarkyar	5.5	13	22	18
Borsunly	5.5–6.5	14	24	16
Lyaky	5.5–6.5	15	30	22
Karajaly	5.5–6.5	15	30	14
Sor–Sor	6.0–7.9	16	30	13
Ragimly	6.0–7.0	16	32	12
Imishly	7.5	20	44	11
Comushly	7.5	19	42	14
Saatly	7.5	18	40	9
Goyarch	5.5–6.6	14	24	16
Bashkarvand	5.5–6.5	15	26	10
Gindarch	5.5–6.5	15	25	15
Beilagan	6.5–7.0	15	25	26
Birmay	6.5–7.5	19	42	7

Table 7.2 Values of heat flow and geothermal gradient for some regions of Azerbaijan (after Pilchin 1983; Eppelbaum and Pilchin 2006)

Area	Heat flow, (mW/m^2)	Geothermal gradient, (°C/km)
Middle Kur Depression, Azerbaijan (western part)	45–104	30–43
Middle Kur Depression, Azerbaijan (eastern part)	33–50	20–30
Lower Kur Depression, Azerbaijan	17–42	10–25
South Caspian Depression, Azerbaijan	17–42	10–20

7.1.7 Remote Sensing

Figure 7.9 illustrates a relationship between the hydrocarbon accumulations and regional faults in the Lower Kur Basin. The tectonic pattern was obtained both from the known geology (Mamedov et al. 2008) and remote sensing data (Landsat-7). The map shows numerous faults with different orientations and styles of the movement (sublatitudinal, Caucasian, anti-Caucasian, submeridional, etc.), depth of occurrence (from pre-Mesozoic up to younger Cenozoic ages), and their associations with the hydrocarbon seeps and mud volcanoes. These interpretation results were used for estimating the fault sealing and hydrocarbon occurrence in the Lower Kur Basin (Zeynalov 2008).

Table 7.3 Changes in excess temperature ($T - T_0$) with depth (in K) for some oil and gas areas of the Kur Depression (Eppelbaum et al. 2014)

Area	Excess temperature ($T - T_0$) in K at depth, m				
	1000	2000	3000	4000	5000
Padar	5	8	20	27	31
Kyursangya	5	18	22	27	31
Kalmas	10	19	23	27	32
Mishowdag	5	12	13	22	28
Garabagly	2	8	13	20	28
Neftchala	5	8	19	35	42
Kyurovdagh	5	8	16.5	22	28
Borsunly	–	–	46	64	86
Zardab	–	–	25	41	48
Muradkhanly	–	21	38	45	73
Jarly—Sor–Sor	–	–	2.5	38	43
Beilagan	–	–	40.5	66	80
Terter	–	–	37	53	75
Garadzhally	–	–	36	55	75
Gazanbulagh	–	–	28	35	42

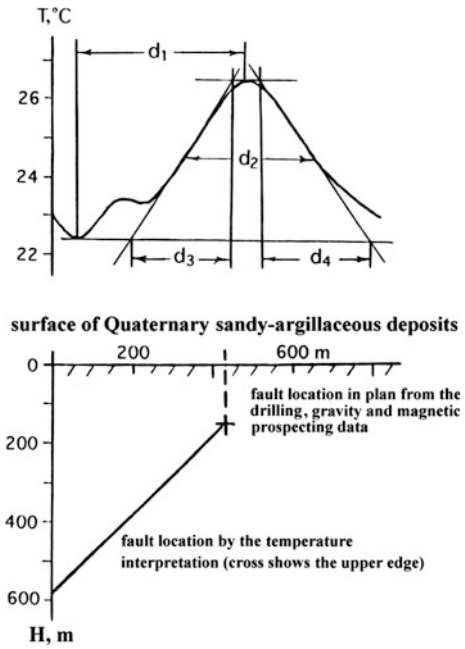

Fig. 7.6 Interpretation of the temperature anomaly in the district of the Muradkhanly oil field in the Middle Kur Depression (Khesin and Eppelbaum 1994)

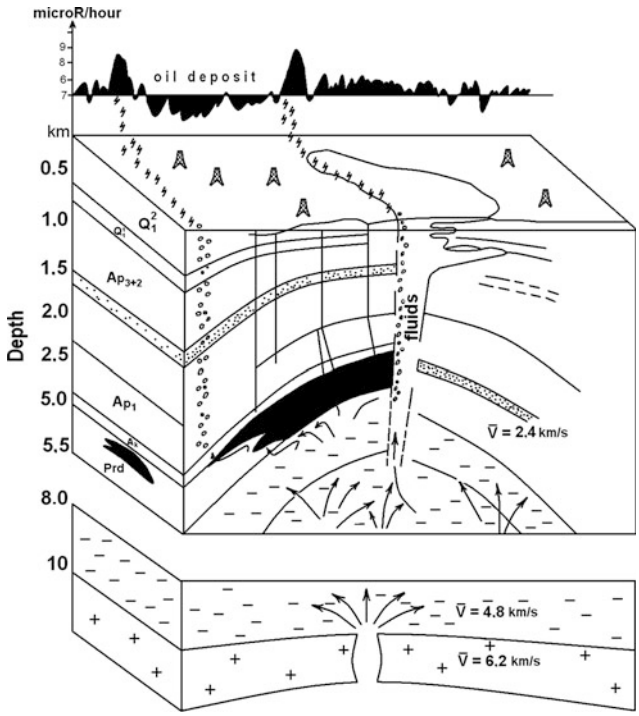

Fig. 7.7 Model of forming of the gamma-field's anomalies over the oil deposit (after Ch. Aliyev and Zolotovitskaya 2005)

7.1.8 Integrated Analysis

The connection of local low-amplitude gravity and magnetic anomalies with hydrocarbon deposits (HD) is well known (e.g., Nettleton 1976; Berezkin et al. 1978; Donovan et al. 1979; Saunders et al. 1999).

Development of modern generation of field gravimetric and magnetometric equipment enables to register promptly and digitally microGal (10^{-8} m/s^2) and picoTesla (10^{-12} T) anomalies that offer a new challenge in this direction. Advanced methods of detecting gravity–magnetic anomalies analysis and modern 3D modeling enable eliminating the most kinds of noise and unmasking very weak anomalies that previously were unrecognizing against the noise background.

Accomplished numerous petrophysical and geophysical materials in the Kur Depression (e.g., Gadirov 2009) testify that oil and gas deposits distinct by physical parameters from the host media (including water-bearing reservoirs). Within oil and gas deposit is observed a decrease on density on 100–250 kg/m^3, decrease on magnetization in 2-8 times, and temperature increase on 10–18 % (Berezkin et al. 1978; Gadirov 2009; Gadirov and Eppelbaum 2012, 2015).

It was suggested that main physical–geological precursors for the application of gravity and magnetic methods for HD prognosis are foremost decreasing of density and magnetization around the oil and gas deposit occurring (Gadirov and Eppelbaum 2012).

Practical analysis performed in the countries of the former USSR (Berezkin et al. 1978; Agulnik et al. 1982) indicates that density contrast within the HD occurring may consist –(70 ÷ 200) kg/m^3. This density contrast may provide appearing negative anomalies in the integral gravity field, value of which is estimated as 0.1–2.0 mGal, depending on the HD thickness and its consistency.

In a hydrocarbon deposit by magnetic properties, four elements characterized by different magnetization are selected: HD and host reservoir, reduction zone, zone of subvertical inhomogeneities, and oxidation zone (Elmore et al. 1987; Saunders et al. 1999). Distribution of main iron-containing minerals (magnetite, maghemite, hematite, etc.) in the HD sections founds a reflection in the observed magnetic field. It is known that the presence of secondary magnetite produces appearing saw-shape anomalies (e.g., Donovan et al. 1979; Elmore et al. 1987). Besides this, over HD relative magnetic minima with amplitude up to several tens of nanoTesla (nT) might be observed (Nikitsky and Glebovsky 1990).

Analysis of density characteristics in the Kur Depression displays decrease of rock density within HD up to 150–170 kg/m^3. Gravity field modeling indicates that gravity anomaly from the oil deposit may consist 0.15–0.25 mGal depending on its vertical thickness (mainly $\Delta h < 50$ m). Magnetization decreases in several times not only with HD, but in overlying deposits above HD. Gravity–magnetic surveys performed in the Kur Depression testify that over the known deposits (Muradkhanly, Jafarly, Tarsdallyar, Gaznbulag, Babazanan, Byandovan, etc.) gravity and magnetic minima of –(0.2 ÷ 0.8) mGal and –(20 ÷ 30) nT were observed. Therefore, integrating these methods increases an effectiveness of oil and gas deposit prognosis (theoretical basis of the integration preferences on example of Azerbaijan were given in Eppelbaum (2014)).

Quantitative estimation of changing of accomplished data of magnetization, density, and temperature was applied for development of detailed physical–geological model of Muradkhanly deposit (Fig. 7.10). Geometry, stratigraphy, lithology, and HD location in the model were taken from the drilled deep well cores (Alizadeh et al. 1966). Density contrast within the subvertical zone over HD was calculated by the use of developed approach (Gadirov and Eppelbaum 2012).

As it was shown in Fig. 7.10, physical parameters of the zone over the HD strongly differ from surrounding medium. With increase in depth, contrast parameters of magnetization (up to 200 × 10^{-5} SI) and temperature (up to 17 °C) are increased, and density contrast (up to 3.6 kg/m^3) in sedimentary deposits is decreased in the HD zone. Analysis of selected cores also shows essential decrease of magnetization in effusive associations in the structure arch in the vicinity of the HD occurring.

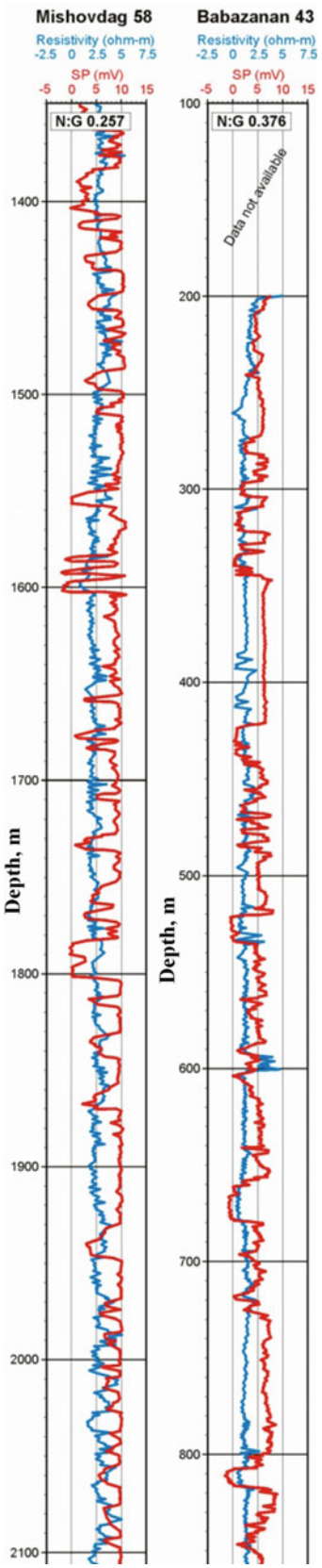

Fig. 7.8 Representative well log traces through two deposits in the Kur Basin, Azerbaijan (fragment of figure presented in Vincent et al. 2010)

Computed gravity and magnetic anomalies (curves 6 and 11 in Fig. 7.10) from subvertical zone (16) consist of ≈–0.35 mGal and ≈–35 nT. Comparison of theoretical curves of gravity and magnetic fields (graphs 1 and 9) with observed curves (graphs 2 and 10) indicates that they have a simular form. Both in observed and in theoretical graphs, relative decreasing of gravity and magnetic fields over the HD is shown. Retrieved maxima on gradient zone changing (4) clearly trace local gravity and magnetic minima.

It was proposed that just migration of hydrocarbon light fraction to overlying deposits (layers) influences to the physical properties of rocks occurring over HD. At the same time, it is necessary to note that secondary factors are studied insufficiently. Integrated effect of the aforementioned factors (both from HD pool and from zone overlying it) stipulates the anomalous changing of gravity and magnetic fields observed over HD. The observed precise gravity and magnetic data contain local anomalies reflecting the presence of HD in the geological section (Gadirov and Eppelbaum 2012).

Third derivatives of gravity potential W_{zzz} were computed along a few dozens of profiles crossing deep boreholes in the Muradkhanly area (Middle Kur Depression). It was detected that minima of W_{zzz} were registered both in intervals where oil and gas factors are known and in intervals where hydrocarbons were not detected. These data testify to the ambiguity of W_{zzz} data analysis. Results of gravity–magnetic field analysis carried out in different oil and gas areas of Azerbaijani land indicate that local gravity and magnetic anomalies over HD could be delineated by application of the developed approach. The main characteristic peculiarity of this approach is utilization of sharp potential field gradient changing and extracting local anomalies.

Figures 7.11 displays a segregation of local anomalies from the observed gravity–magnetic data along profiles (curves 1 and 2) on example of Jafarly area.

For this aim, regional trend (3) is constructed by such a manner that to connect to the anomalous curves from the side of the lowest values of the employed fields. Such an approach enables to delineate local maxima (4) caused by oil and gas structures. After this, by zones of changing gradients, local maxima (5) are re-established, and on their background, distinctive local maxima (6) caused by the presence of anomalous objects in the geological section are extracted.

Gadirov and Eppelbaum (2015) have analyzed in detail an influence of temperature regime over and outside hydrocarbon deposits (on example of the Muradkhanly deposit). It was concluded that the integrated density change (and corresponding gravity effects) can reach significant values exceeding the desired gravity anomalies from the studied hydrocarbon deposits. This leads to detailed cooperative studies of gravity effects and temperature regime over commercial oil and gas deposits.

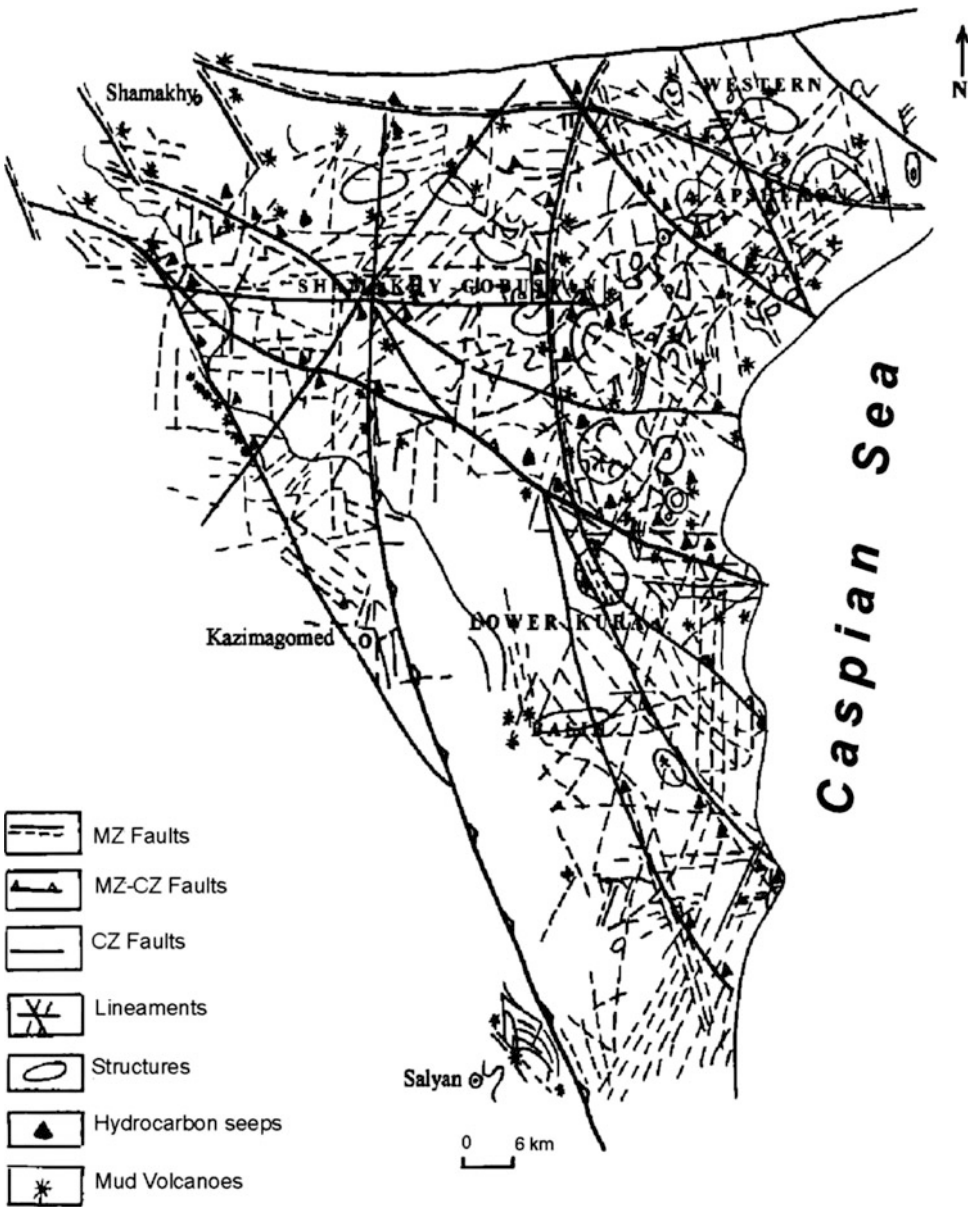

Fig. 7.9 Map showing tectonic elements, mud volcanoes, and hydrocarbon seeps in the Lower Kur Basin (Zeynalov 2008)

7.2 Gusar-Devechi Basin

7.2.1 Integrated Analysis

The Gusar-Devechi Basin is located in the Eastern Azerbaijan (see Chaps. 3 and 4 of the Volume 1 "Geology of Azerbaijan"). Integrated analyses of gravity, magnetic, VES, and seismic data are shown in Fig. 7.12 (the applied methodology is presented in detail in Eppelbaum (2014)). Note that integrated parameter ΣI clearly reflects the position of the predicted basement structure P_z.

7.3 South Caspian Basin

Investigating the South Caspian Basin to localize commercial oil and gas deposits is of great interest to geoscientists (e.g., Abrams and Narimanov 1997; Bagirov et al. 1997); Lerche et al. 1997; Abdullayev 2000; Katz et al. 2000; Buryakovsky et al. 2001; Diaconescu et al. 2001; Jackson et al. 2002; Allen et al. 2003; Brunet et al. 2003; Guliyev et al. 2003; Alizadeh 2004; Knapp et al. 2004; Manley et al. 2005; Artyushkov 2007; Golonka 2007; Granath et al. 2007; Mamedov et al. 2008; Egan et al. 2009; Green et al. 2009;

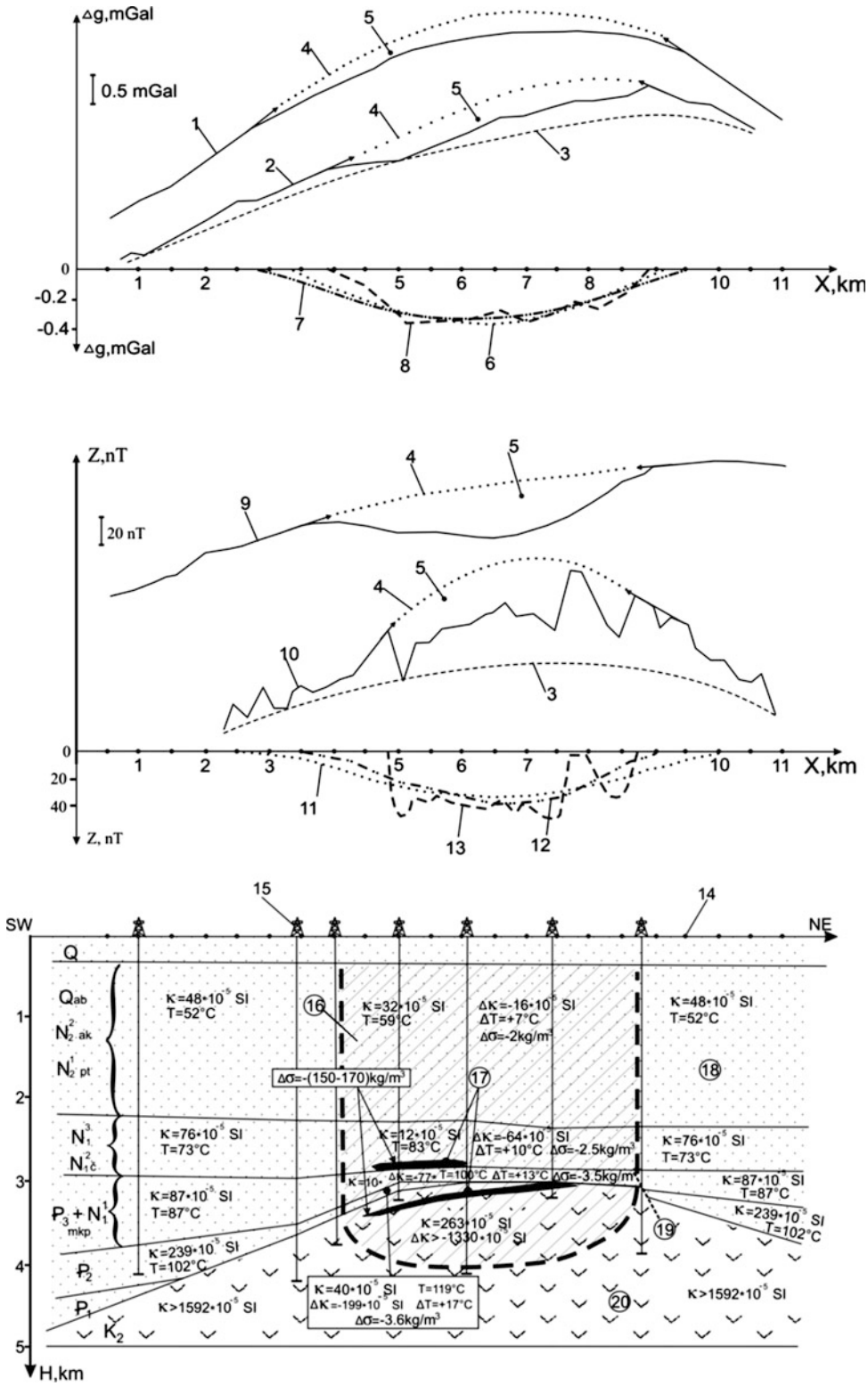

Fig. 7.10 Results of gravity–magnetic modeling in the Muradkhanly oil deposit (Gadirov and Eppelbaum 2012). (*1*) computed gravity effect from geological model; (*2*) observed field Δg_B; (*3*) regional trend; (*4*) restored maxima by changing of gradient zones; (*5*) local minima; (*6*) computed gravity effect from subvertical hydrocarbon zone; (*7*) and (*8*) local gravity anomalies extracted from graphs 1 and 2; (*9*) computed magnetic effect from geological model; (*10*) observed magnetic field; (*11*) computed magnetic effect from subvertical oil zone; (*12*) and (*13*) local magnetic anomalies extracted from graphs (*9*) and (*10*), respectively; (*14*) points where gravity–magnetic effects were computed; (*15*) deep boreholes; (*16*) subvertical hydrocarbon zone; (*17*) oil pool; (*18*) sedimentary deposits; (*19*) fault; (*20*) effusive associations

Mamedov 2009; Mukhtarov 2011; Richardson et al. 2011; Alizadeh 2012; Abdullayev et al. 2015).

In the Caspian Sea area, adjacent to Azerbaijan from the northeast and east, large areas of the Middle Caspian relating mainly to the epi-Hercynian platform and the South Caspian Basin (SCB) associated with the Alpine-Himalayan tectonic belt (Khain 1984) have been pinpointed. The SCB appears to behave like a relatively rigid aseismic block within the

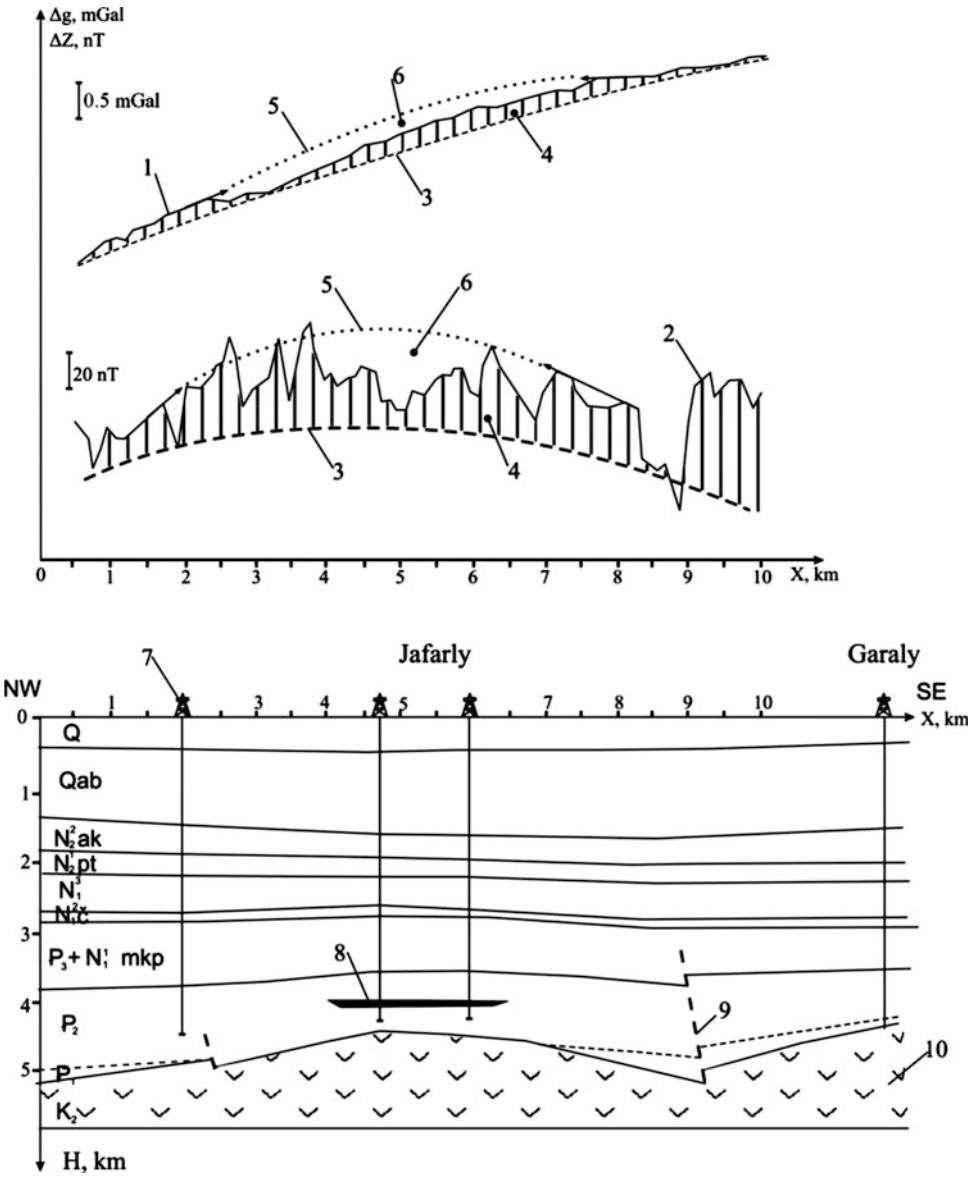

Fig. 7.11 Physical–geological model and extracting local gravity–magnetic anomalies produced by oil and gas indicators in the Jafarly area (Gadirov and Eppelbaum 2012). (*1*) observed field Δg_B, (*2*) observed field ΔZ; (*3*) regional trend; (*4*) local maxima; (*5*) maxima reestablished by changing of gradient zones; (*6*) local minima; (*7*) deep boreholes; (*8*) oil deposit; (*9*) faults; (*10*) effusive complexes

otherwise deforming Alpine-Himalayan tectonic belt. The comprehensive seismic data suggest that there is a fundamental compositional difference between the crust of the South Caspian Basin and that of the surrounding region (Mangino and Priestley 1998).

The central part of the Caspian Sea is characterized by a mosaic magnetic field; within the uplifted Kara-Bogaz-Middle Caspian block, a close association of negative and positive magnetic anomalies is found. This is typical in particular of the more elevated Kara-Bogaz arch where Permian-Triassic and Jurassic rocks are absent and terrigenous low-magnetic rocks occur directly on the pre-Permian basement.

The SCB is one of the deepest basins in the world with a depth to basement of over 20 km in places (Shikhalibeily and Grigoriants 1980; Brunet et al. 2003). Although it is widely accepted that the SCB was initiated by a Mesozoic back-arc extension related to the subduction of the Tethys Plate (e.g., Zonenshain and Le Pichon 1986), more than half of the 20 km subsidence presently observed occurred within the tectonic framework of the evolution of the Alpine-Himalayan tectonic belt (Egan et al. 2009).

Interestingly, up to now, the boundary between the epi-Hercynian platform and Alpine-Himalayan tectonic belt in the Caspian Sea has not been completely determined.

Submeridional zones in the SCB were identified by the combined geological, seismic, and potential geophysical field analysis. The western part of the SCB is fixed by clear meridional trends of geological structures; the eastern part of the SCB is divided into two zones: The western zone is characterized by comparatively smoothed tectonics, and the western part by more intensive tectonics.

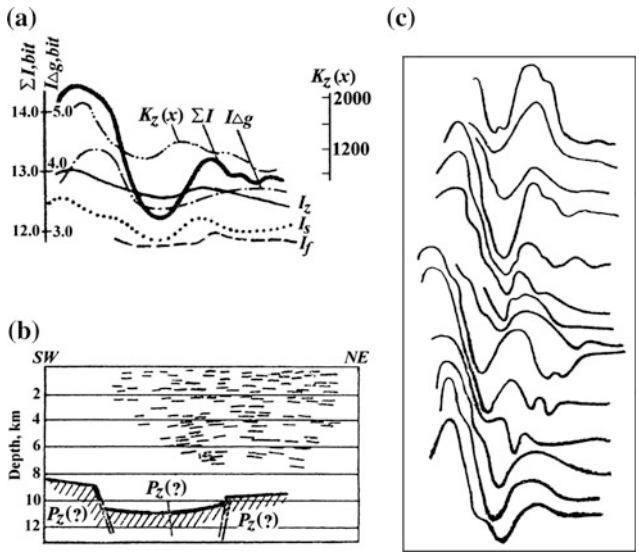

Fig. 7.12 Integrated interpretation of geophysical data using information units for the delineation of hidden fault zones under thick sedimentary cover in the Precaspian-Guba oil and gas area (Gusar-Devechi Basin) (after Eppelbaum and Khesin 2012). **a** Graphs of amount of specific information derived from the results of various geophysical methods and total information $\Sigma I = I_{\Delta g} + I_z + I_S + I_f$ (Δg is the gravity field, Z is the vertical component of the magnetic field, S is the series admittance according to VES data analysis, and f is the observed frequency of reflections (visible frequency of reflected waves) through comparison with the cross-correlation function $K_z(x)$), **b** distribution of reflected surfaces along seismic profile No. 85-10-03 and diagram of the proposed basement structure, **c** graphs of the total amount of information along 14 profiles including profile No. 85-10-03

7.3.1 Seismic Data Analysis

It is well known that seismic data analysis is considered as the main geophysical tool for the hydrocarbon deposits searching and detailed localization (especially in marine areas) (e.g., Avseth et al. 2005). Therefore, we will present here five different examples of seismic data analysis in the SCB.

Deltaic sedimentation was the main mechanism causing filling of the Late Cenozoic paleobasins in the SCB. The buried Pliocene deltaic systems of the Paleo Volga and Paleo Uzboy (Fig. 7.13a) can be clearly geologically and seismically distiguished within the studied basin. Combining the lithofacial composition and internal structure of the Paleo Volga exposed deltaic deposits with seismic reflection patterns a seismostratigraphic model of the sedimentation process for the Early Pliocene was constructed (Fig. 7.13b). It should be noted that the Pliocene time was very significant for the avalanche sedimentation and fast subsidence of the SCB crust. An amplitude of the subsidence only in Pontian (7.1–5.4 Ma) came to more than 1 km (Mamedov 2004). The big rivers (Paleo Volga, Paleo Kur and Paleo Uzboy) and dozens of small rivers have cut out the deep valleys and rushed toward the Pliocene lake carrying out an enormous quantity of clastic product (Fig. 7.13a). The relative large cuneate and lenticular elements, stream configurations, and external geomorphological features of these processes are displayed in the high-frequency dynamic sections (Fig. 7.13b) (Mamedov 2009).

The following example presents more detailed seismic data processing. Variations in pressure, fluid contacts, and fluid compositions within hydrocarbon reservoirs are commonly attributed to reservoir compartmentalization as a result of sealing faults or stratigraphic complexity. In this case, some non-conventional seismic methodologies may be applied. Figure 7.14 shows the sum of negative amplitude from a 48-ms window centered on the Pereriv B reservoir, derived from a fluid impedance seismic volume. The line of intersection between the best-fit oil–water contact and the Pereriv B top structure has been overlaid, together with the well data points which have been used to define this plane. The line corresponds to an abrupt change in seismic amplitude even in the eastern part of the Azeri field where the angle between structure and the contact is at its greatest. A range of different seismic attributes, window sizes, and seismic volumes shows a similar correspondence to the best-fit oil–water contact, providing important peculiarities about hydrodynamic model of the deposit (Tozer and Borthwick 2010).

3D seismic surveys were designed to overcome specific imaging problems at the Deep Water Gunashli (DWG) oil field (SCB) to reduce uncertainty during the predrill programs in these two areas. Figure 7.15 shows the DWG structure with the key horizons.

7.3.2 Gravity Field Analysis

3D gravity field modeling indicates that gravity field anomalies from hydrocarbon deposits in the SCB may reach (in the best case scenario) only 0.1 mGal (Bashirov et al. 1992). Such a gravity accuracy (shipborne, airborne, or satellite data retracked to the marine surface) at present and in the near future is unachievable one. Therefore, gravity field examination within the SCB is oriented mainly to deep study analysis that is considered in Chaps. 4 and 5 (Kadirov 2000, 2004, 2006; Kadirov and Gadirov 2014).

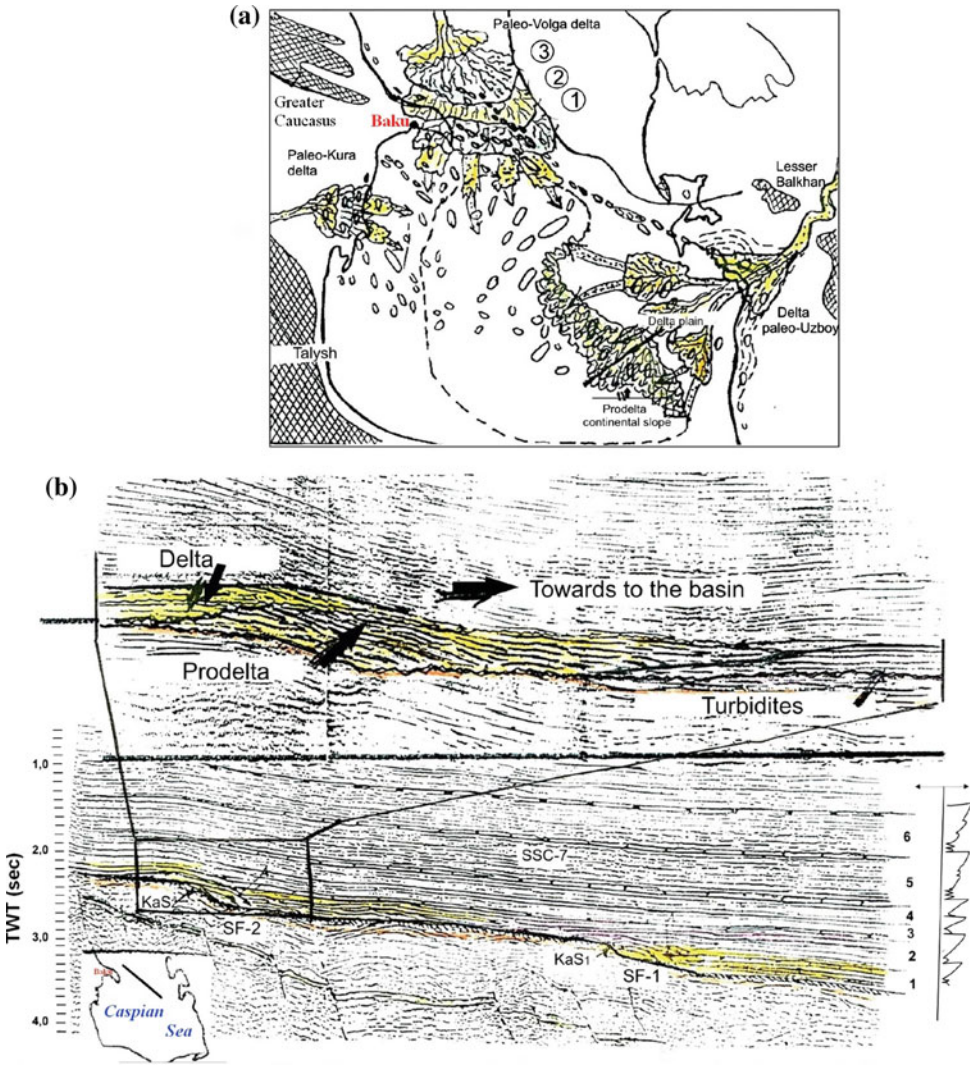

Fig. 7.13 The paleorivers deltas of the Early Pliocene (**a**) and deltaic deposit reflection in a time section (**b**) (Mamedov 2009)

7.3.3 Magnetic Field Analysis

Some peculiarities of regional magnetic field pattern in the SCB are presented in Chaps. 4 and 5. Analysis of low (or very low) magnetic anomalies over the hydrocarbon deposits obviously waits in the wings. A detailed magnetostratigraphic analysis of Plio-Pleistocene transgressions in SCB (Van Baak et al. 2013) is of special interest. Its extension to earlier geological epochs is highly desirable.

7.3.4 Temperature Field Analysis

7.3.4.1 Regional Thermal Analysis

As a rule, thermal data analysis plays important role in oil and gas geophysics (e.g., Mekhtiyev et al. 1960; Somerton 1992; Eppelbaum et al. 2014).

It is interesting to note that the Western Caspian Sea Basin and the Dead Sea Basin have several common geothermal and tectonic features (Eppelbaum and Pilchin 1998) that can lead to joint geological–geophysical data examination.

With the aim to unmask the contribution of lateral migration within the SCB, Katz et al. (2000) computed the considerable distance between the generative portion of the basin and portions of the known resource base (Fig. 7.16). This requires lateral migration in addition to the vertical component for hydrocarbon charging to have occurred. This conclusion suggests that the hydrocarbons should be present down-dip along the general hydrocarbon flow paths. The tracking of the hydrocarbons back to their effective generative prism appears to extend the system in a basinward direction (Katz et al. 2000).

Models of thermal evolution and hydrocarbon generation are of high importance in petroleum geology and

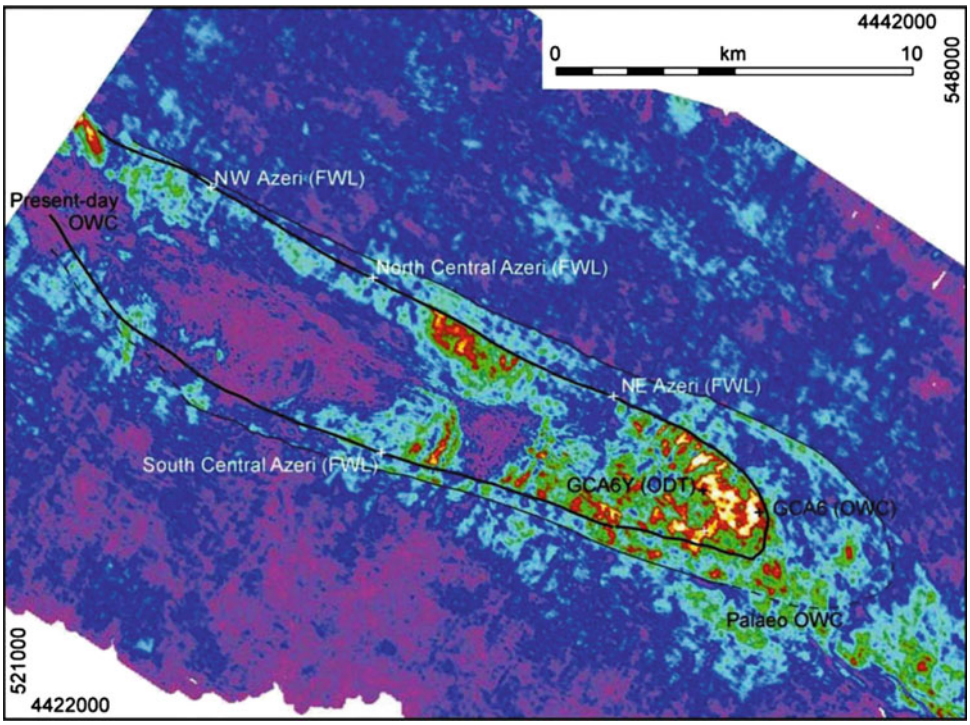

Fig. 7.14 Map showing the sum of negative amplitude (SNA) from a 48-ms window centered on the Pereriv B reservoir in Azeri oil deposit (SCB). The line of intersection between the present-day (hydrodynamic) oil–water contact and the Pereriv B top structure has been overlaid on this (*heavy black line*), together with the well data points. The line corresponds to an abrupt change in seismic amplitude even in the eastern part of the Azeri field. Below the present-day oil–water contact a possible paleo oil–water contact is also shown (*narrow black line*; *dashed* where uncertain) (Tozer and Borthwick 2010)

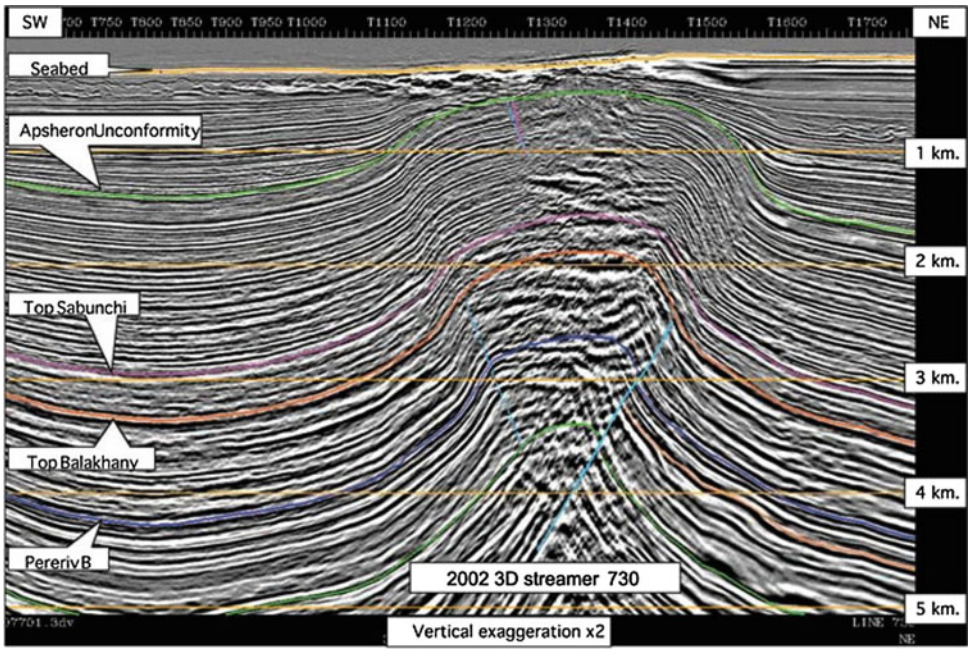

Fig. 7.15 3D streamer line 730 showing the main features of the Deep Water Gunashli structure (SCB). Note the noise contamination at the crest of the structure due to the gas cloud (Manley et al. 2005)

geophysics. Mukhtarov (2011) has computed such models for all large hydrocarbon deposits of Azerbaijan. We will present here three most significant models (Figs. 7.18, 7.19, and 7.20).

Figure 7.17 shows a set of thermograms for corresponding geological ages for the Bulla deniz area.

Figures 7.18 and 7.19 illustrate the models of fundamental petroleum problems: thermal evolution (a) and hydrocarbon generation (b) for the deposits of Pirsaat and Bakhar, respectively.

7.3.4.2 Near-bottom Temperature Survey

One example of quantitative examination of the near-bottom temperatures observed in the SCB over the oil Bakhar deposit (Fig. 7.20) is discussed below. The amplitude of the anticline structure where this deposit occurs is more than 600 m.

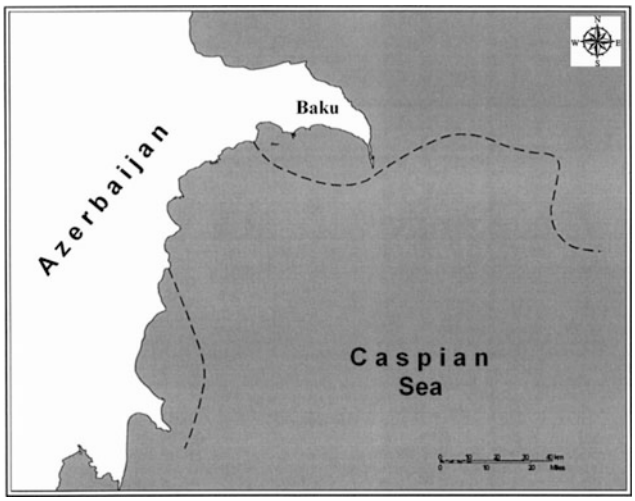

Fig. 7.16 Up-dip limit of the main stage of hydrocarbon generation on *top* of the Maykop suite using an average gradient of 15 °C/km (after Katz et al. 2000)

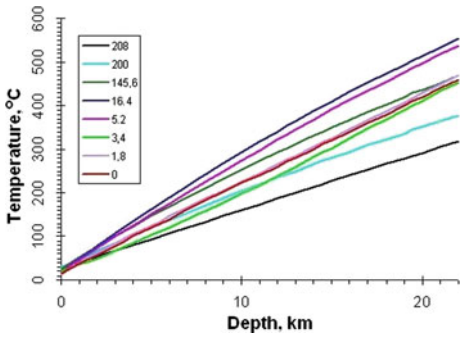

Fig. 7.17 Space-time temperature distribution in the Bulla Deniz area (SCB) computed by the use of MATURITY program. Digits in *right* part show geological time (m. y.) corresponding to each thermogram (after Mukhtarov 2011)

The accuracy of the near-bottom single temperature measurement was within 0.01 °C (Artemenko and Malovitsky 1977). As a result of quantitative interpretation (a model of a horizontal circular cylinder was used; Eppelbaum et al. 2014), the center of the anticline structure was identified. It is possible that the small negative temperature anomalies in the central part of the profile are caused by the influence of oil and gas deposits.

7.3.5 Integrated Analysis

Figure 7.21 presents one of the first examples of integrated geophysical (magnetotelluric sounding and seismics) analysis along the profile crossing the Caspian Sea. In this section, it is clearly seen a principal difference between the Turan Plate with the low sedimentary thickness and SCB

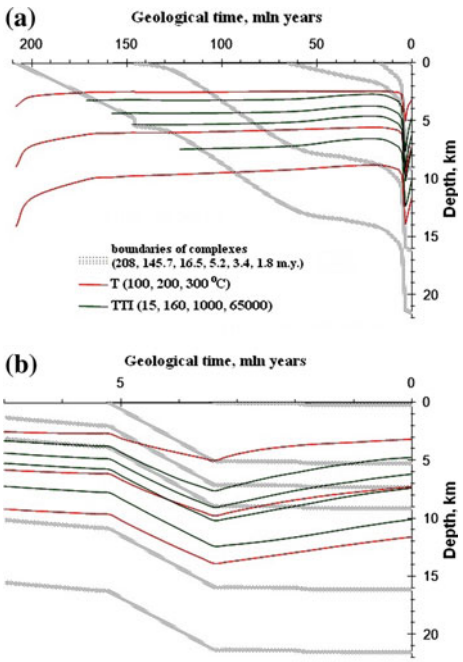

Fig. 7.18 Model of thermal evolution (**a**) and hydrocarbon generation (**b**) for the Pirsaat area (western flank of SCB) (after Mukhtarov (2011), with small modifications). TTI, temperature-time index (according to Lopatin 1971)

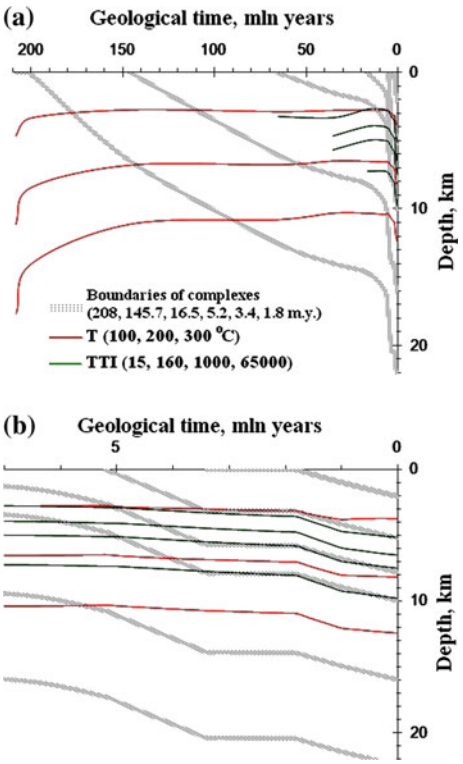

Fig. 7.19 Model of thermal evolution (**a**) and hydrocarbon generation (**b**) for the Bakhar area (SCB) (after Mukhtarov (2011), with small modifications). TTI, temperature-time index (according to Lopatin 1971)

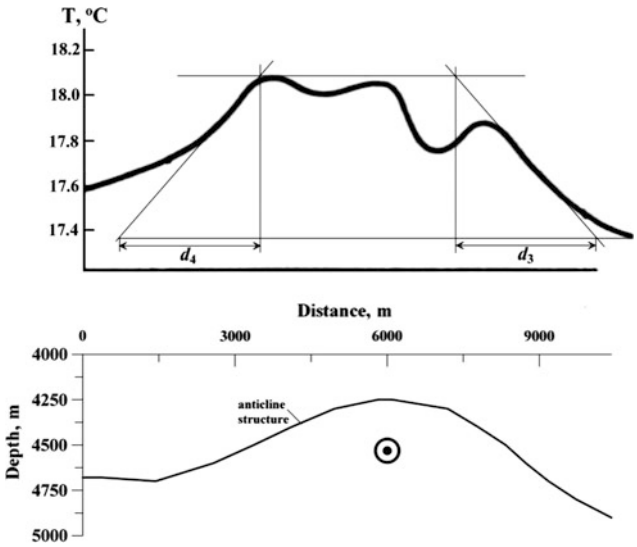

Fig. 7.20 Interpretation of the temperature anomaly observed in near-bottom sediments over the oil and gas Bakhar deposit (SCB) (initial data after Artemenko and Malovitsky 1977; analysis after Eppelbaum et al. 2014). The "⊙" symbol marks the position of the center of anticline structure

where the thickness of sedimentary strata reaches 17–20 km. In the SCB, sedimentary strata reveal upper and lower layers with relatively low resistivity. These layers are divided by a thick stratum of heightened resistivity. The upper layer relates to Paleogene–Neogene, middle later—to Mesozoic, and lower stratum, possibly, is composed of Paleozoic deposits (Malovitsky et al. 1977).

An interesting example of integrated seismic–gravity–magnetic analysis was carried out in the Zhdanov Shoal (Fig. 7.22) located in the southeastern part of the Caspian Sea. Besides conventional seismic and magnetic surveys, detailed bottom gravimetric investigations were performed (Malovitsky et al. 1977). Quantitative analysis of the bottom gravimetric data revealed a significant local gravity maximum against the regional gravity minimum. It was assumed that this maximum was caused by a gravitational effect of the Cheleken-Livanov high and other small local anomalies associated with the fault zones (Fig. 7.22). Later, in this area, the Jigalybek oil deposit was discovered.

At times, integrated geophysical field analysis is extremely useful even at the qualitative level. A Bulla deniz gas deposit located in the Bay of Baku is one of rich deep hydrocarbon accumulations occurring below 5000 m within the South Caspian Basin (Guliyev et al. 2011). To calculate the parameter I_{integr} (Eppelbaum 2014) in the area of Bulla deniz, three different fields were employed: local magnetic anomalies ΔT (marine survey data), the second horizontal derivative of the gravity potential W_{xz} (data from the bottom gravity survey were utilized), and $\Delta H/H$ (relative changes of the sea bottom topography) (Fig. 7.23). As can be seen from the graph of I_{integr}, both faults are reflected. The large

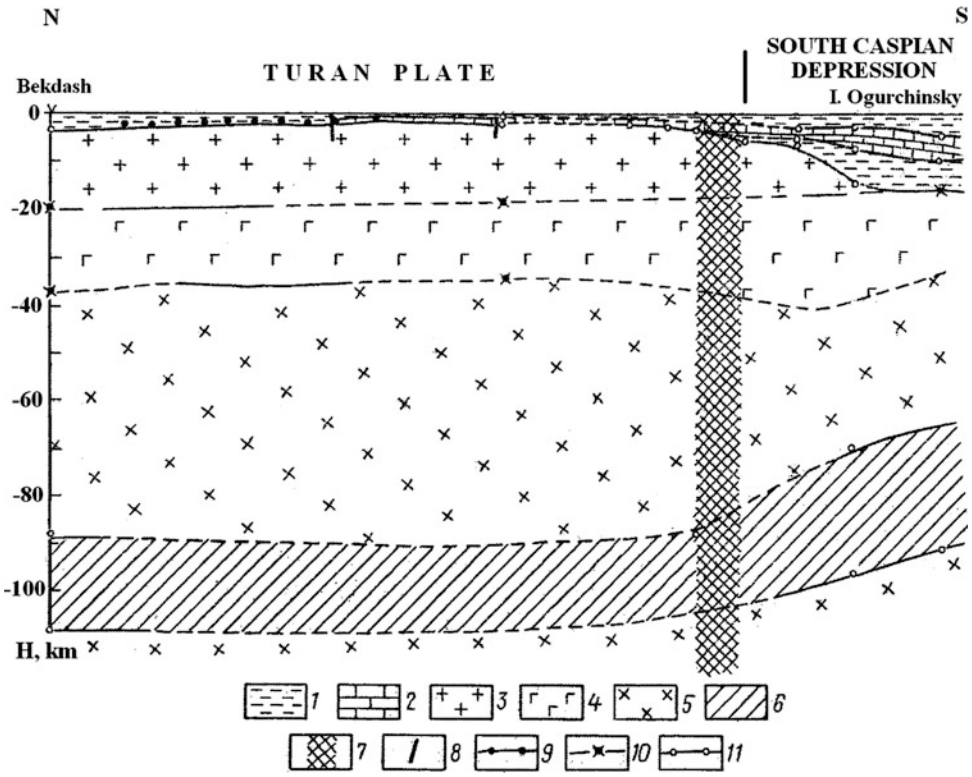

Fig. 7.21 Deep geological–geophysical section along the line village Bekdash—Ogurchinsky Island (Malovitsky et al. 1977). (*1*) low-conductive sedimentary deposits, (*2*) high-conductive sedimentary deposits, (*3*) "granitic" layer, (*4*) "basaltic" layer, (*5*) upper mantle, (*6*) intermediate conductive layer, (*7*) zone of deep fault at the boundary between the epi-Hercynian platform and SCB, (*8*) faults, delineated boundaries by: (*9*) NDOS, (*10*) deep seismic sounding, (*11*) magnetotelluric sounding

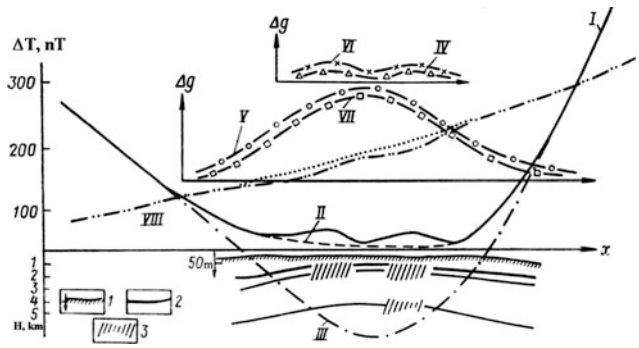

Fig. 7.22 Integrated geophysical–geological section across the Zhdanov Shoal (Malovitsky et al. 1977). (*1*) sea bottom (50 m only marks the position of the sea bottom), (*2*) reflective seismic horizons, (*3*) fault zones. **(I)** Δg_B, **(II)** graph of regional gravity background (parabolic interpolation with average radius of 3 km), **(III)** graph of regional gravity background (parabolic interpolation with average radius of 4.5 km), **(IV)** residual anomaly I–II, **(V)** residual anomaly **I–III**, **(VI)** computed gravity effect from fault zones, **(VII)** computed gravity effect from Cheleken-Livanov high, **(VIII)** graph ΔT

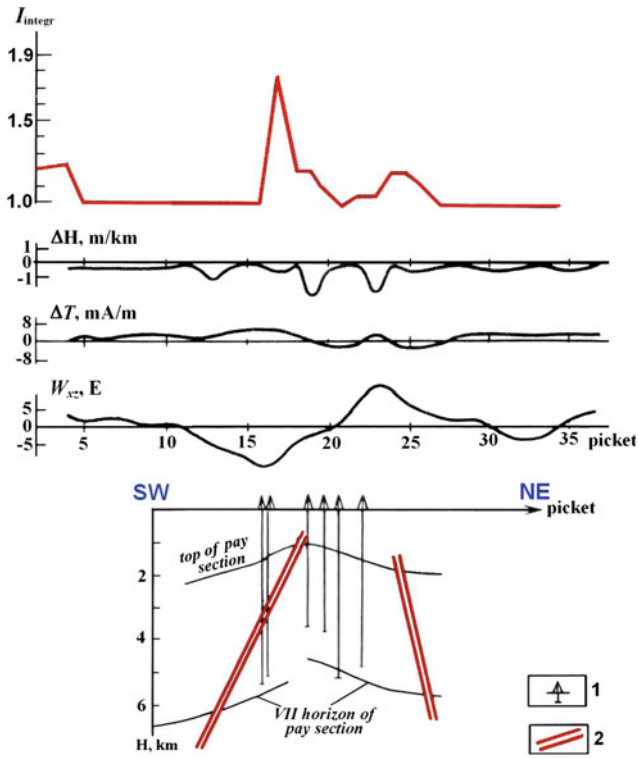

Fig. 7.23 Qualitative delineation of faults by computing parameter I_{integr} at the area of Bulla (Baku archipelago, Caspian Sea) (Eppelbaum 2014). (*1*) deep wells, (*2*) faults delineated by combined analysis of geological and geophysical data

amplitude of the SW anomaly of the I_{integr} parameter compared to NE may be explained by the proximity of the SW fault to the surface of the sea bottom.

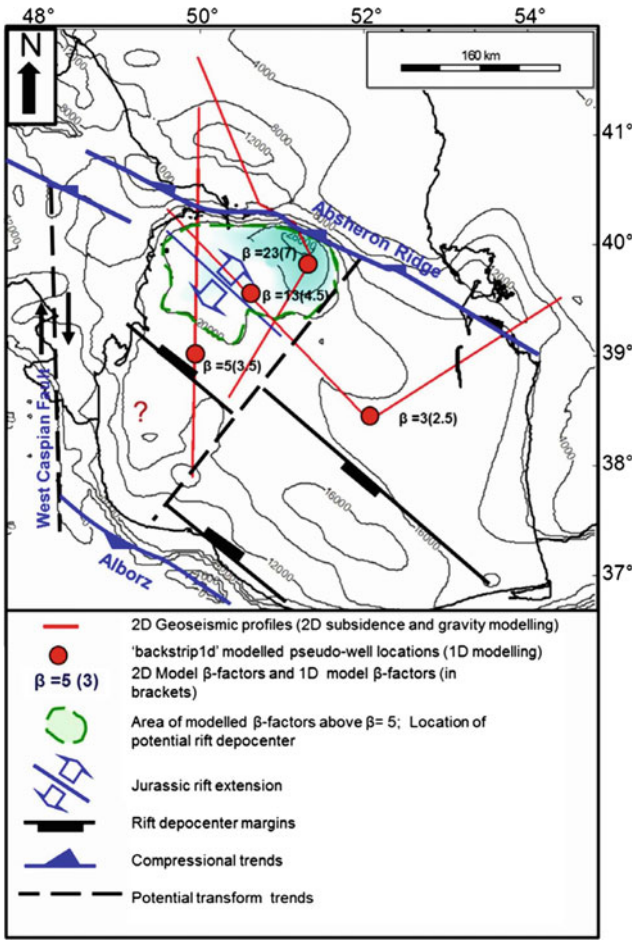

Fig. 7.24 Interpretation of the crustal structure shown over the depth to basement map of the SCB. This map shows a comparison of β-factors derived from the modeling of 2D lines and 1D strain-rate inversion (Abdullayev et al. 2015)

Abdullayev et al. (2015) have recently developed an effective combined model of the SCB crustal structure (e.g., Fig. 7.24) on the basis of: (a) utilization of 2D seismic profiles, (b) 2D gravity field modeling, (c) utilization of petrophysical data from wells, (d) flexural backstripping including simple assumptions for crustal stretching and thermal subsidence, and (e) one-dimensional subsidence modeling to constrain the values of 2D crustal stretching models using 1D backstripping and the strain-rate inversion method. The geophysical sections were backstripped with the thermal subsidence incorporated into the modeling using first an assumed stretch factor, (β), value of $\beta = 1$ implying no crustal deformation and then $\beta = 100$ to approximate the unlimited extension of 'oceanic type' crust. Constraints of the forward model were then used to vary the β-factor between these two extremes.

Combined modeling conducted in this study shows that the observed pattern of subsidence and sedimentation in the SCB can be explained by a process of thermal subsidence following Jurassic rifting and further enhanced subsidence that resulted from sediment-induced loading in the Late Tertiary, especially after a large-scale base-level fall after 6 Ma.

References

Abdullayev, N.R., 2000. Seismic stratigraphy of the Upper Pliocene and Quaternary deposits in the South Caspian Basin. *Jour. of Petroleum Science and Engineering*, **28**, 207-226.

Abdullayev, N.R., Kadirov, F. and Guliyev, I.S., 2015. Subsidence history and basin-fill evolution in the South Caspian Basin from geophysical mapping, flexural backstripping, forward lithospheric modelling and gravity modelling. In: (Brunet, M.-F., McCann, T. and Sobel, E.R., Eds.), *Geological Evolution of Central Asian Basins and the Western Tien Shan Range*. *Geological Society*, London, *Special Publications*, **427**, 1-22.

Abrams, M.A. and Narimanov, A.A., 1997. Geochemical evaluation of hydrocarbons and their potential sources in the western. South Caspian Depression, Republic of Azerbaijan. *Marine and Petroleum Geology*, **14**, No. 4, 451-468.

Agulnik, I.M., Zvyagin, E.M., Kolchin, S.A., Mikhalov, I.N. and Yakovenko, A.A., 1982. Experience and results of high-precise gravity prospecting application by direct searching of oil on example of Verkh-Tarskoe Maloichskoe deposit. In: Increasing Geological Effectiveness and Practical Methods of Gravity Surveys. VNIIGeofizika, Moscow, 58-65 (in Russian).

Akselrod, S.M., Danevich, V.I. and Sadykhov, D.M., 1991. *Nuclear-Magnetic Investigations of Borehole Sections in Azerbaijan*. Azerb. State Publ., Baku (in Russian).

Aliyev, Ch.S., 1994. *Radioactive fields of depression regions of Azerbaijan*. *D.Sci. Thesis*, Baku (in Russian).

Aliyev, Ch.S. and Zolotovitskaya, T.A., 1996. Results of radiometric investigations. *In*: (Kerimov, K.M., Ed.) *Geophysical Investigations in Azerbaijan*, Sharg-Garb, Baku, 386-389 (in Russian).

Aliyev, Ch.S. and Zolotovitskaya, T.A., 2005. Comparison of gamma-field with geological structure, geophysical fields, oil&gas bearing, and seismicity. *In*: (Alizade, Ak.A., Ed.), *Geology of Azerbaijan*, Vol. **V**, Physics of the Earth, Nafta-Press, 292-312 (in Russian).

Aliyev, S.A., Mukhtarov, A.Sh., Bagirly, P.J. et al., 2005. Geothermal investigations in Azerbaijan. In: (Ak.A. Alizadeh, Ed.), *Geology of Azerbaijan*, Vol. **V**, Physics of the Earth. Nafta-Press, Baku, 229-263 (in Russian).

Alizadeh, A.A., Akhmedov, G.A., Akhmedov, A.M., Aliyev, A.K., and Zeinalov, M.M., 1966. *Geology of Oil and Gas Deposits in Azerbaijan*. Nedra, Moscow (in Russian).

Alizadeh, Ak.A. (Ed.), 2004. *South Caspian Basin: Geology, Geophysics, Oil and Gas Content*. Nafta-Press, Baku (in Russian).

Alizadeh, Ak.A. (Ed.), 2012. *The Modern Problems of Geology and Geophysics of the Eastern Caucasus and South Caspian Depression*. Nafta-Press, Baku.

Allen, M.B., Vincent, S.J., Alsop J.I., Ismailzadeh, A. and Flecker, R., 2003. Late Cenozoic deformation in the South Caspian region: effects of a rigid basement block within a collision zone. *Tectonophysics*, **366**, 223-239.

Amiraslanov, T.C., 1987. Interpretation of gravitational and magnetic anomalies for complex constructed regions on the basis of geophysical field integrated analysis. *D. Sci. Thesis*, Baku (in Russian).

Amiraslanov, T.C., 1990. Geological interpretation of gravity and magnetic anomalies in the central part of the Middle Kur Depression. *Azerbaijan Oil Industry*, No. 7, 13-17 (in Russian).

Artemenko, V.I. and Malovitsky, Ya.P., 1977. Results of near-bottom temperature survey at oil&gas deposit Bahar. *Geology of Oil&Gas*, No.4, 50-54 (in Russian).

Artyushkov, E.V., 2007. Formation of the superdeep South Caspian basin: subsidence driven by phase change in continental crust. *Russian Geology and Geophysics*, **48**, 1002-1014.

Avseth, P., Mukerji, T. and Mavko, G., 2005. *Quantitative Seismic Interpretation*. Cambridge Univ. Press.

Bagirov, E. and Nadirov, R. and Lerche, I., 1997. Hydrocarbon evolution for a north-south section of the South Caspian Basin. *Marine and Petroleum Geology*, **14**, No. 7/8, 773-854.

Bashirov, A.E., Eppelbaum, L.V. and Mishne, L.R., 1992. Improving Eotvos corrections by wide-band noise Kalman filtering. *Geophysical Jour. International*, **108**, 193-197.

Berezkin, V.M., Kirichek, M.A. and Kunarev, A.A., 1978. *Application of Geophysical Methods for Direct Searching Oil and Gas Deposits*. Nedra, Moscow (in Russian).

Brunet, M.-F., Korotaev, M.V., Ershov, A.V. and Nikishin, A.M., 2003. The South Caspian Basin: A review of its evolution from subsidence modeling. *Sedimentary Geology*, **156**, 119-148.

Buryakovsky, L., Chilingar, G.V. and Aminzadeh, F., 2001. *Petroleum Geology of the South Caspian Basin*. Gulf Professional Publ., Wobum, USA.

Diaconescu, C.C., Kieckhefer, R.M. and Knapp, J.H., 2001. Geophysical evidence for gas hydrates in the deep water of the South Caspian Basin, Azerbaijan. *Marine and Petroleum Geology*, **18**, 209-221.

Donovan, D., Forgey, R.L. and Roberts, A.A., 1979. Aeromagnetic detection of diagenetic magnetite over oil fields. *AAPG Bulletin*, **63**, 245-248.

Dzabayev, A.A., 1969. *Principles of the Searching and Study of Oil-and-Gas Bearing Structures by Aeromagnetic Method* (*South Caspian Basin*). Statistika, Ashkhabad (in Russian).

Egan, S.S., Mosar, J., Brunet, M.-F. and Kangarli, T., 2009. Subsidence and uplift mechanisms within the South Caspian Basin: insights from the onshore and offshore Azerbaijan region. *Geol. Society, London, Spec. Publications*, **312**, 219-240.

Elmore, R.D., Engel, M.H., Crawford, K.N., Imbus, S. and Sofer, Z., 1987. Evidence for a relationship between hydrocarbon and authigenic magnetite. *Nature*, 325, 6103-6106.

Eppelbaum, L.V., 2007. Localization of Ring Structures in Earth's Environments. *Jour. of the Archaeological Soc. of the Slovakian Acad. of Sci., Spec. Issue: Arch. Prosp.*, XLI, 145-148.

Eppelbaum, L.V., 2014. Estimating informational content in geophysical observations on example of searching economic minerals in Azerbaijan. *Izvestiya* (*Proceedings*), *Acad. Sci. Azerb. Rep., Ser.: Earth Sciences*, Nos. 3-4, 31-40.

Eppelbaum, L.V., Alperovich, L., Zheludev, V. and Pechersky, A., 2011a. Application of informational and wavelet approaches for integrated processing of geophysical data in complex environments. *Proceed. of the 2011 SAGEEP Conference*, Charleston, South Carolina, USA, **24**, 24-60.

Eppelbaum, L. and Katz, Y., 2011. Tectonic-geophysical mapping of Israel and eastern Mediterranean: Implication for hydrocarbon prospecting. *Positioning*, Vol. **2,** No. 1, 36-54.

Eppelbaum, L.V. and Khesin, B.E., 2012. *Geophysical Studies in the Caucasus*. Springer, Heidelberg – N.Y. – London.

Eppelbaum, L.V., Kutasov, I.S. and Pilchin, A.N., 2014. *Applied Geothermics*. Springer, Heidelberg – N.Y. – London.

Eppelbaum, L.V. and Pilchin, A.N., 1998. Western Caspian Sea Basin and Dead Sea Basin: comparison of some physical-geological

characteristics. *Trans. of the III Intern. Conf. on the Eastern Mediterranean*, Cyprus, Aug. 1998, p.20.

Eppelbaum, L.V. and Pilchin, A.N., 2006. Methodology of Curie discontinuity map development for regions with low thermal characteristics: An example from Israel. *Earth and Planetary Sciences Letters*, **243**, No. 3-4, 536-551.

Gadirov, V.G., 2009. Results of application of gravity-magnetic surveys for prognosis oil&gas deposits in the Kur Depression of Azerbaijan. Geophysics (Geofizika), No. 2, 51-56 (in Russian).

Gadirov, V.G. and Eppelbaum, L.V., 2012. Detailed gravity, magnetics successful in exploring Azerbaijan onshore areas. *Oil and Gas Journal,* **110,** No. 11, 60-73.

Gadirov V. and Eppelbaum, L.V., 2015. Density-thermal dependence of sedimentary associations calls to reinterpreting detailed gravity surveys. *Annales Geophysicae*, **58**, No. 1, 1-6.

Gadirov, V.G. and Gasanov, V.S., 2013. Results of gravity survey in the perspective hydrocarbon areas Kur-Talysh and Hajigabul. *Proceed*. "*Geology, Geophysics and Prospecting of Oil and Gas Deposits*", No.4, 33-36.

Golonka, J., 2007. Geodynamic evolution of the South Caspian Basin. In: (P. O. Yilmaz and G. H. Isaksen, Eds.), *Oil and Gas of the Greater Caspian Area*: AAPG Studies in Geology **55**, 17-41.

Granath, J.W., Soofi, K.A., Baganz, O.W. and Bagirov, E. 2007. Gravity modeling and its implications to the tectonics of the South Caspian Basin. *In*: (Yilmaz, P.O. and Isaksen, G.H., Eds.) *Oil and Gas of the Greater Caspian Area. AAPG Studies in Geology*, **55**, 43-46.

Green, T., Abullayev, N., Hossack, J., Riley, G. and Roberts, A.M., 2009. Sedimentation and subsidence in the South Caspian Basin, Azerbaijan. *In*: (Brunet, M.-F., Wilmsen, M. and Granath, J.W., Eds.) *South Caspian to Central Iran Basins*. The Geological Society, London, Special Publications, **312**, 241-260.

Guliyev, I.S., Mamedov, P.Z., Feyzullayev, A.A., Huseynov, D.A., Kadirov, F.A., Aliyeva, E.H.-M., Tagiyev, M.F., 2003. (Ed. Guliyev, I.S.), *Hydrocarbon Systems of the South Caspian Basin*. Nafta-Press, Baku.

Guliyev, I., Aliyeva, E., Huseynov, D., Feyzullayev, A. and Mamedov, P., 2011. Hydrocarbon potential of ultra-deep deposits in the South Caspian Basin. Adapted from oral presentation at the *AAPG European Region Annual Conference*, Kiev, Ukraine, October 17-19, 2010. Search and Discovery Article #10312.

Hoogendoorn, R.M., Boels, J.F., Kroonenberg, S.B., Simmons, M.D., Aliyeva, E., Babazadeh, A.D. and Huseynov, D., 2005. Development of the Kur delta, Azerbaijan; A record of Holocene Caspian sea-level changes. *Marine Geology*, **222-223**, 359-380.

Inan, S., Yalcin, M.N., Guliyev, I.S., Kuliev, K. and Feizullayev, A.A., 1997. Deep petroleum occurrences in the Lower Kur Depression, South Caspian Basin, Azerbaijan: an organic geochemical and basin modeling study. *Marine and Petroleum Geology*, **14**, No. 7/8, 73l-762.

Ismailzadeh, T.A., 1983. Paleomagnetic investigations of Meso-Cenozoic of Azerbaijan. *D.Sci. Thesis*, Inst. of the Physics of the Earth, Moscow (in Russian).

Jackson, J., Priestley, K., Allen, M. and Berberian, M., 2002. Active tectonics of the South Caspian Basin. *Geophysical Jour. International*, **148**, 214-245.

Kadirov, F.A., 2000. *Gravity Field and Models of Deep Structure of Azerbaijan*. Nafta-Press, Baku (in Russian).

Kadirov, F.A., 2004. Gravity models of lithosphere in the Caucasus – Caspian region. In: (Alizadeh, Ak.A., Ed.), *South Caspian Basin: Geology, Geophysics, Oil and Gas Content.* Nafta-Press, *Baku*, 107-122.

Kadirov, F.A., 2006. Nature of gravitational anomaly in the South Caspian Basin. *Trans. of the EAGE 68th Conference*, Vienna, P325, 1-4.

Kadirov, F.A. and Gadirov, A.H., 2014. A gravity model of the deep structure of South Caspian Basin along submeridional profile Alborz–Absheron Sill. *Global and Planetary Change*, **114**, 66-74.

Katz, B., Richards, D., Long, D. and Lawrence, W., 2000. A new look at the components of the petroleum system of the South Caspian Basin. Jour. of Petroleum Science and Engineering, **28**, 161-182.

Kerimov, K.M. (Ed.), 1996. *Geophysical Investigations in Azerbaijan*. Sharg-Garb, Baku (in Russian).

Kerimov, K.M., Pilchin, A.N., Gadjiev, T.G. and Buachidze, G.Y., 1989. *Geothermal map of the Caucasus, Scale* 1:1,000,000 Baku, Cartographic Plant No. 11 (in Russian).

Khain, V.E., 1984. *Regional Geotectonics*. *The Alpine Mediterranean Belt*. Nedra, Moscow (in Russian).

Khain, V.E., 2000. *Tectonics of Continents and Oceans*. Nauchyi Mir, Moscow (in Russian).

Khesin, B.E., Alexeyev, V.V. and Eppelbaum, L.V., 1996. *Interpretation of Geophysical Fields in Complicated Environments*. Kluwer Academic Publishers, *Ser.: Modern Approaches in Geophysics*, Dordrecht - Boston - London.

Khesin, B.E., Alexeyev, V.V. and Metaxa, Kh.P., 1983. *Interpretation of Magnetic Anomalies in the Conditions of Oblique Magnetization and Rugged Topography*. Nedra, Moscow (in Russian).

Khesin, B.E. and Eppelbaum, L.V., 1994. Near-surface thermal prospecting: Review of processing and interpretation. *Geophysics*, **59**, No.5, 744-752.

Khesin, B.E. and Eppelbaum, L.V., 1997. The number of geophysical methods required for target classification: quantitative estimation. *Geoinformatics*, **8**, No.1, 31-39.

Knapp, C.C., Knapp, J.H. and Connor, J.A., 2004. Crustal-scale structure of the South Caspian Basin revealed by deep seismic reflection profiling. *Marine and Petroleum Geology*, **21**, 1073-1081.

Kutasov, I.M. and Eppelbaum, L.V., 2015. *Pressure and Temperature Well Testing*. CRC Press (Taylor & Francis Group). London - N.Y.

Lerche, A., Bagirov, E., Nadirov, R., Tagiyev, M. and Guliyev, I., 1997. (I. Lerche and A. Alizadeh, Eds.). *Evolution of the South Caspian Basin: Geological Risks and Probable Hazards*. Nafta-Press, Baku.

Logachev, A.A. and Zakharov, V.P., 1979. *Magnetic Prospecting*. Nedra, Leningrad (in Russian).

Lopatin, N.V., 1971. Temperature and geological time as a factor of coalization. *Izvestiya*, *Acad. Sci. USSR*, Ser.: Earth Sciences, No. 3, 95-106.

Malovitsky, Ya.P., Kogan, L.I., Mistrukov, Yu.M. et al., 1977. *Marine Geophysical Investigations*. Nedra, Moscow (in Russian).

Mamedov, P.Z., 2004. Genesis and seismic stratigraphic model of the South Caspian Megabasin architecture. In: (Ak.A. Alizadeh, Ed.), *South Caspian Basin*: *Geology, Geophysics, Oil and Gas Content*. Nafta-Press, Baku, 150-184.

Mamedov, P.Z., 2009. Sedimentation models in the SCMB and their seismostratigraphic characteristics. *Stratigraphy and Sedimentology of Oil-Gas Basins*, No. 3, 70-85.

Mamedov, P.Z., Guliyev, Q.Q., Kadirov, F.A., Shikhalyev, Y.A., Guliyev, I.S., Aliyeva, E.H., Feyzullayev, A.A., Dadashov, F.Q., Kheirov, M.B. and Tagiyev, M.F., 2008. (Ak.A. Alizadeh, Ed.), 2008. *Geology of Azerbaijan*, Vol. VII: *Oil and Gas*. Nafta-Press, Baku (in Russian).

Mangino, S. and Priestley, K., 1998. The crustal structure of the southern Caspian region. *Geophysical Jour. International*, **133**, 630-648.

Manley, D.M., Mohammed, S.F., Robinson, N.D. and Thomas, R.W., 2005. Structural interpretation of the deepwater Gunashli Field, facilitated by 4-C OBS seismic data. *The Leading Edge*, No. 9, 922-926.

Mekhtiyev, Sh. F., Mirzajanzadeh, A. Kh., Aliyev, S. A., Bagbanly, E. A. and Motyakov, V.I., 1960. *Geothermal Regime of Oil and Gas Deposis*. Azerneftneshr, Baku (in Russian).

Mukhtarov, A.Sh., 2011. Structure of thermal flow of sedimentary complex of the Southern Caspian Basin. *D.Sci Thesis*, Inst. of Geology, Baku (in Russian).

Nasruyev, N.P., Andreyev, L.I. and Eleseyenko, N.A., 1975. *In*: (Eds. Akhmedov, G.A. et al.) *Geophysical Investigations in Azerbaijan*, Vol. **III**, 87-91 (in Russian).

Nettleton, L.L., 1976. Gravity and Magnetics in Oil Prospecting. McGraw-Hill.

Nikitsky, V.E. and Glebovsky Yu.S. (Eds.), 1990. *Magnetic Prospecting. Reference Book*. Nedra, Moscow (in Russian).

Pilchin, A.N., 1983. Geothermal regime of the earth crust of the Kur Depression and its influence on the pressure distribution. *Ph. D. Thesis*, Geophysical Institute of Georgian Academy of Science (in Russian).

Pilchin, A.N. and Eppelbaum, L.V., 1997. Determination of magnetized bodies lower edges by using geothermal data. *Geophysical Jour. International*, **128**, No.1, 167-174.

Pilchin, A.N. and Eppelbaum, L.V., 2006. *Iron and Its Unique Role in the Earth Evolution*. Monogr., Mexican Geoph. Soc., 1-67.

Pilchin, A.N. and Eppelbaum, L.V., 2007. Stabilities of the iron oxides in the Earth and their role in the formation of rock magnetism. *Acta Geofisica*, **55**, No.2, 133-153.

Richardson, S.E.J., Davies, R.J., Allen, M.B. and Grant, S.F., 2011. Structure and evolution of mass transport deposits in the South Caspian Basin, Azerbaijan. *Basin Research*, **23**, 702-719.

Sandwell, D.T., Garcia, E., Soofi, K., Wessel, P. and Smith, W.H.F., 2013. Towards 1 mGal Global Marine Gravity from CryoSat-2, Envisat, and Jason-1. *The Leading Edge*, **32**, No. 8, 892899, 892-899.

Sandwell, D.T. and Smith, W.H.F., 2009. Global marine gravity from retracked Geosat and ERS-1 altimetry: Ridge Segmentation versus spreading rate. *Journal of Geophysical Research*, **114**, B01411, 1-18.

Saunders, D.F., Burson, K.R. and Thompson, C.K., 1999. Model for hydrocarbon microseepage and related near-surface alterations. *AAPG Bulletin*, **83**, No. 1, 170-185.

Shikhalibeyli, E.S., Abdullayev, R.N. and Alizade, A., 1988. Geological results of the super-deep well of Saatly. *Soviet Geology*, No. 11, 61-66 (in Russian).

Shikhalibeily, E.S. and Grigoriants, B.V., 1980. Principal features of the crustal structure of the South-Caspian Basin and the conditions of its formation. *Tectonophysics*, **69**, 113-121.

Somerton, W.H., 1992. *Thermal Properties and Temperature Related Behavior of Rock/Fluid Systems*. Developments in Petroleum Science, **37**. Elsevier, Amsterdam.

Sudzhadinov, R.A. and Kosmodemyansky, V.V., 1986. Mapping for oil and gas structures at large depth, In (T.A. Ismailzadeh, Ed.)*: Combined Interpretation of Geological-Geophysical Materials for Investigating the Structure and Prospecting for Oil and Gas at Large Depths*, ``YuzhVNIIGeofizika'', 94-103 (in Russian).

Tozer, R. S. J. and Borthwick, A. M., 2010. Variation in fluid contacts in the Azeri field, Azerbaijan: sealing faults or hydrodynamic aquifer? In: (Jolley, S. J., Fisher, Q. J., Ainsworth, R. B., Vrolijk, P. J. and Delisle, S., Eds.), *Reservoir Compartmentalization*. Geological Society, London, Special Publ., **347**, 103-112.

Tzimelzon, I.O., 1965. Earth's crust deep structure and tectonics of Azerbaijan by geophysical data. *Soviet Geology*, No. 4, 103-111 (in Russian).

Vaish, J.P., 2005. *Geophysical Well Logging – Principles and Practices*. Asian Books Private Ltd.

Van Baak, C.G.C., Vasiliev, I., Stoica, M., Kuiper, K.F., Forte, A.M., Aliyeva, E., and Krijgsman, W., 2013. A magnetostratigraphic time frame for Plio-Pleistocene transgressions in the South Caspian Basin, Azerbaijan. *Global and Planetary Change*, **103**, 119-134.

Vincent, S.J., Davies, C.E., Richards, K. and Aliyeva, E., 2010. Contrasting Pliocene fluvial depositional systems within the rapidly subsiding South Caspian Basin; a case study of the palaeo-Volga and palaeo-Kur river systems in the Surakhany Suite, Upper Productive Series, onshore Azerbaijan. *Marine and Petroleum Geology*, **27**, 2079-2106.

Zeynalov, G.A., 2008. Fluid flow and sealing properties associated with active faults - Kur Basin, Azerbaijan. *Trans. of the EAGE Conf. "Petroleum Geology & Hydrocarbon Potential of Caspian and Black Sea Regions*" 6–8 October 2008, Baku, Azerbaijan, P03, 1-6.

Zonenshain, L.P. and Le Pichon, X., 1986. Deep basins of the Black Sea and Caspian Sea as remnants of Mesozoic back-arc basins. *Tectonophysics*, **123**, 181-211.

Mining Geophysics

8

The specific nature of mining geophysics, models of media, and the details and the sequence of the interpretation process, including petrophysical studies, have been amply covered in the books (Ismailzadeh et al., 1983a, b; Khesin et al. 1983, 1996; Gadjiev et al., 1984; Karayev and Rabinovich, 2000; Eppelbaum and Khesin 2012) and numerous articles. A separate chapter (Khesin et al. 1988) in (Borisovich and Eppelbaum 1988) deals with the optimization of mining geophysical method interpretation for detailed prospecting under mountainous conditions. These works form the basis for the Azerbaijanian mining geophysics presented in this chapter.

The most specific conditions for geophysical mining studies are described below. In these regions, solid heterogeneous associations usually outcrop at the Earth's surface. These associations are multiply folded, with intensive rupture tectonics (including thrust tectonics). Rocks of various origins and compositions with a broad range of physical properties rapidly change along both the vertical and the lateral directions. This predetermines the complexity of the images of geophysical fields. Due to the curvature of the earth-to-air interface and the rugged observation surface, the relief exerts a pronounced effect on observations. The dissected relief, complex geology, difficulties in transporting, and observation are all factors that affect the investigation procedure. They restrict efficiency because they require more intricate and cumbersome equipment and survey systems.

At the same time, it would be a mistake to view mountainous conditions solely as an obstacle. Deep erosional truncation and a lack or low thickness of loose deposits encourages visual geological methods. These make it possible to obtain extensive geological evidence on the nature of anomaly sources and to correlate them with geophysical data, as well as to study physical properties of rocks and ores in natural and artificial exposures. Rugged relief can be used to calculate the real physical parameters of a section exposed to erosion based on measurements of the corresponding fields on an uneven surface. It also facilitates geological application of topography data. Outcroppings of mountainous regions promote the integrated application of conventional geophysical methods along not only with visual and geological methods, but also with geophysical, geochemical, petrophysical, and physical–chemical investigations (including areal study), which can dramatically lessen the ambiguity of geophysical interpretation.

According to Solovov (1985), open areas where ore-bearing rocks outcrop onto the surface or are covered with eluvial and deluvial products of their weathering can be divided into two groups. The first which has a severe topography is considered unfavorable for geophysical prospecting. This opinion as regards typical orogens (mountainous folded areas) of the open (one stage) type can be easily explained since complex geophysical equipment is difficult to transport and use in highly inaccessible mountainous regions, and anomalies caused by the relief are pronounced and difficult to take into account.

However, mountainous regions objectively call for a systematic application of geophysical methods of investigation. Moreover, only these methods can ensure a sequential, deep, and sufficiently rapid study of the endogenic mineralization distribution and its relations to geological structure. Prospecting for large hidden deposits is conducted with these issues in mind. Many valuable deposits of different types are located in mountainous regions above 2000 m, which make up about 12 % of the total continental area, and in areas over 1000 m, which account for as much as 30 % of the total land. A large portion of this area consists of mountainous structures formed or rejuvenated during the Alpine epoch (Khain 1984).

The requirements for geophysical techniques in mountainous conditions are less stringent in both regional and detailed prospecting. In regional prospecting, airborne surveys may be tied in with comparatively stable elements of the relief. In ground surveys, observations are linked to routes or riverbeds when making geophysical measurements with cumbersome equipment. In this way, key features are intersected and are then used as references for large-scale surveys of the area.

Let us first of all shortly consider the borehole logging.

A.A. Alizadeh et al., *Geosciences of Azerbaijan*,
Regional Geology Reviews, DOI 10.1007/978-3-319-40493-6_8

8.1 Borehole Logging in Mining Wells

Borehole logging in ore deposits can reveal enough physical characteristics to develop physical–geological models (PGMs) enabling electric, electromagnetic, and radiometric application methods. The results of borehole logging are found mainly in industrial geophysical reports.

Khesin and Sattarov (1967) successfully applied a gamma ray log in the Dashkesan and Filizchay ore fields. In the Dashkesan ore field, gamma ray analysis reliably detected intervals with tuffs and limestone; in the Filizchay boreholes, new prospective ore intervals were detected. Muradkhanov (1971) carried out comprehensive statistical processing of geophysical data from boreholes drilled in the Filizchay deposit. Radio-frequency cross-hole investigations (RFCI) on frequencies f = 21, 32, 128, and 512 kHz were employed in several deposits in the southern slope of the Greater Caucasus. Figure 8.1 shows the results of RFCI in the Filizchay deposit in boreholes 670 and 675 (these boreholes were located 550 m apart) (Borisovich et al., 1988).

To conduct the RFCI, well 670 was drilled deeper than was projected by 100 m. In the interwell space, two anomalous areas were detected. The first (located at a depth of 600 m) was caused by a small orebody and totally contoured. This ore target pinched out at a distance of about 100 m from well 675. The second anomalous area caused by the main orebody began at a depth of 709 m in well 670 and continued uninterruptedly to the boundary of the RFCI domain (in a line to well 675) for 260 m.

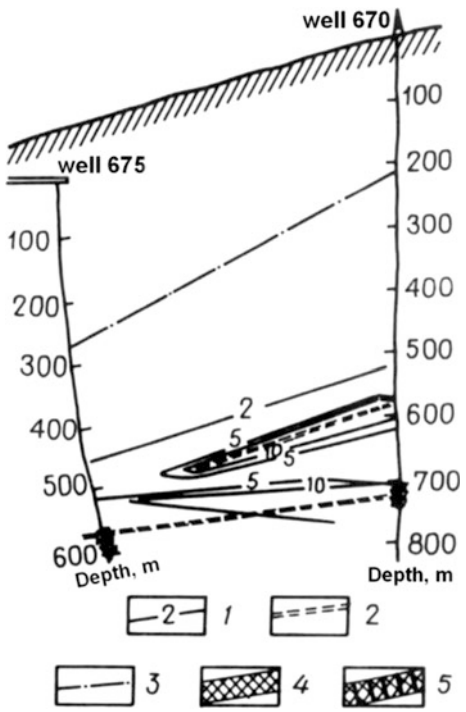

Fig. 8.1 Results of radio-frequency cross-hole investigation (RFCI) between wells 675 and 670 (f = 21 kHz) in the Filizchay deposit (southern slope of the Greater Caucasus) (Borisovich et al. 1988). (*1*) isolines of shielding coefficients, (*2*) axis of shield, (*3*) boundary of the RFCI, (*4*) massive ore, (*5*) streaky ore

The Karadagh copper-porphyry field is the most highly studied area of the Azerbaijan part of the Somkhet-Garabagh Zone (Kerimov 1996). Ore-bearing sites are located within hydrothermally altered rocks that were accurately detected by data showing a decrease in magnetic field and resistivity from an integrated geophysical survey on a 1:10,000 scale. The deposit area (400–900 × 2200 m) is outlined by a polarizability isoline of 7.5 %. Within the contour, local η_a maxima (up to 10–18 %) are related to the increase in the concentration of disseminated pyrite and certain other sulfides. These maxima coincide with the self-potential (spontaneous polarization) minima (down—60 mV). Method of partial extraction of metals (Ryss 1983) applied to the sites of the local anomalies showed 30 μg of the copper, 5 μg of the lead, and 500 μg of the iron on a background of 5, 2, and 200 μg, respectively. Nuclear geophysical methods were used here for drill core and well studies. They showed copper concentrations of 0.2–0.8 %; concentrations of 1.1–1.4 % were detected in several borehole intervals at thicknesses of up to 1.5 m. Induced polarization (IP) anomalies in the wells correlated closely with the ore cuttings (Fig. 8.2).

Besides the self-potential method, the electric method of sliding contacts, and the method of electrode potentials were succesfully applied. Abdullayev and Bagirov (1996), and Muradkhanov and Magerramov (1996) give a brief review of these mine-borehole and borehole logging methods applied to Caucasian ore deposits.

8.2 Azerbaijanian Part of the Greater Caucasus

Azerbaijanian part of the Greater Caucasus contains a lot of commercial ore deposits (see Chap. 2 of the present Volume). Geophysical–geological analysis of ore deposits usually began from the development of their Physical-Geological Models (***PGMs***).

8.2.1 Physical–Geological Models of Ore Deposits

PGMs are the easiest to grasp because they are usually displayed both in graphic and in table form. ***PGMs*** make it possible to resolve the dual problem of interpretation: (1) enhancing the informativity and reliability of geophysical data interpretation, (2) substantiating the selection of a set for further geophysical investigations and plan a strategy.

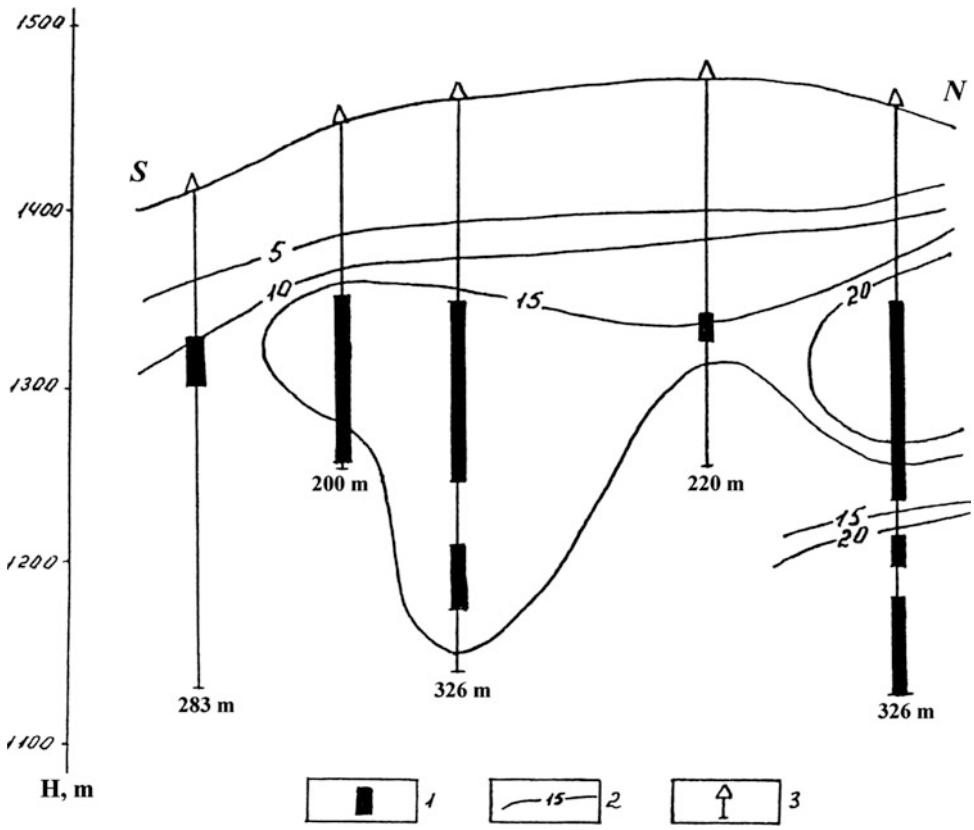

Fig. 8.2 Results of borehole η_a measurements in the Karadagh copper–porphyry deposit (Bagirov et al. 1996). (*1*) intervals of commercial concentrations of copper in the drill core; (*2*) η_a isolines (in %); and (*3*) borehole

A formalized Ostrovsky (1980) method as well as various informational methodologies (Khesin et al. 1996) was used to develop 3D models of ore deposits on the basis of surface and underground geophysical measurements (Eppelbaum and Khesin 2012).

8.2.2 Physical–Geological Models of a Pyrite–Polymetallic Deposit of the Filizchay Type

This subsection discusses a ***PGM*** of pyrite–polymetallic deposit of the Filizchay type (this deposit is one of the largest polymetallic deposits in the world). This ***PGM*** represents a large group of pyrite–polymetallic deposits concentrated in the pyrite-bearing provinces with a predominance of carbonaceous-terrigenous sediments (Borodaevskaya et al. 1977). Characteristic pyrite–polymetallic deposits of the Filizchay type are Sullivan (British Columbia, Canada), Coeur d'Alène (Idaho, USA), Mount-Isa (Australia), Rammelsberg (Germany), Ozernoye and Kholodninskoye (Baikal region, Russia), Filizchay, and other deposits (Katsdagh, Katekh, Jikhih, etc.) on the southern slope of the Greater Caucasus (Gorzhevsky et al. 1987; Tvalchrelidze 1978). These deposits on the southern slope of the Greater Caucasus are situated in a severely rugged relief and occur in sandy-shale rock masses of the Jurassic. The ***PGM*** for this type of deposit can be represented in the form of steeply dipping massive sulfide sheet-like deposits, which differ from the host medium on a number of contrasting properties such as excess density (1.3 ÷ 1.8 g/cm^3), higher (by a factor of 10^2–10^3) conductivity, thermal conductivity (2- to 3-fold) and polarization (up to 10-fold), and in some cases magnetization (10- to 50-fold) (Muradkhanov 1971).

The development of numerous disjunctive dislocations impeding geophysical data interpretation is typical of these deposits.

Gravity and magnetic fields predicted by a typical ***PGM*** of the Filizchay type deposits (Fig. 8.3), were computed using the GSFC program for different depths of occurrence of the upper orebody edge h (Table 8.1). For SP, VLF, IP, and thermal prospecting methods, the determination of these effects was carried out taking into account the results of physical and mathematical modeling and field investigations.

The resulting PGM substantiated the interpretation criteria and optimal geophysical sets for prospecting and estimation. For deposits of the Filizchay type, this set comprised of gravimetric and magnetic prospecting and the SP method. The IP method can be also a significant tool (see, for instance, Figs. 8.6 and 8.7). If ore objects differ only slightly in terms of their magnetic properties from the host sandy-shale deposits,

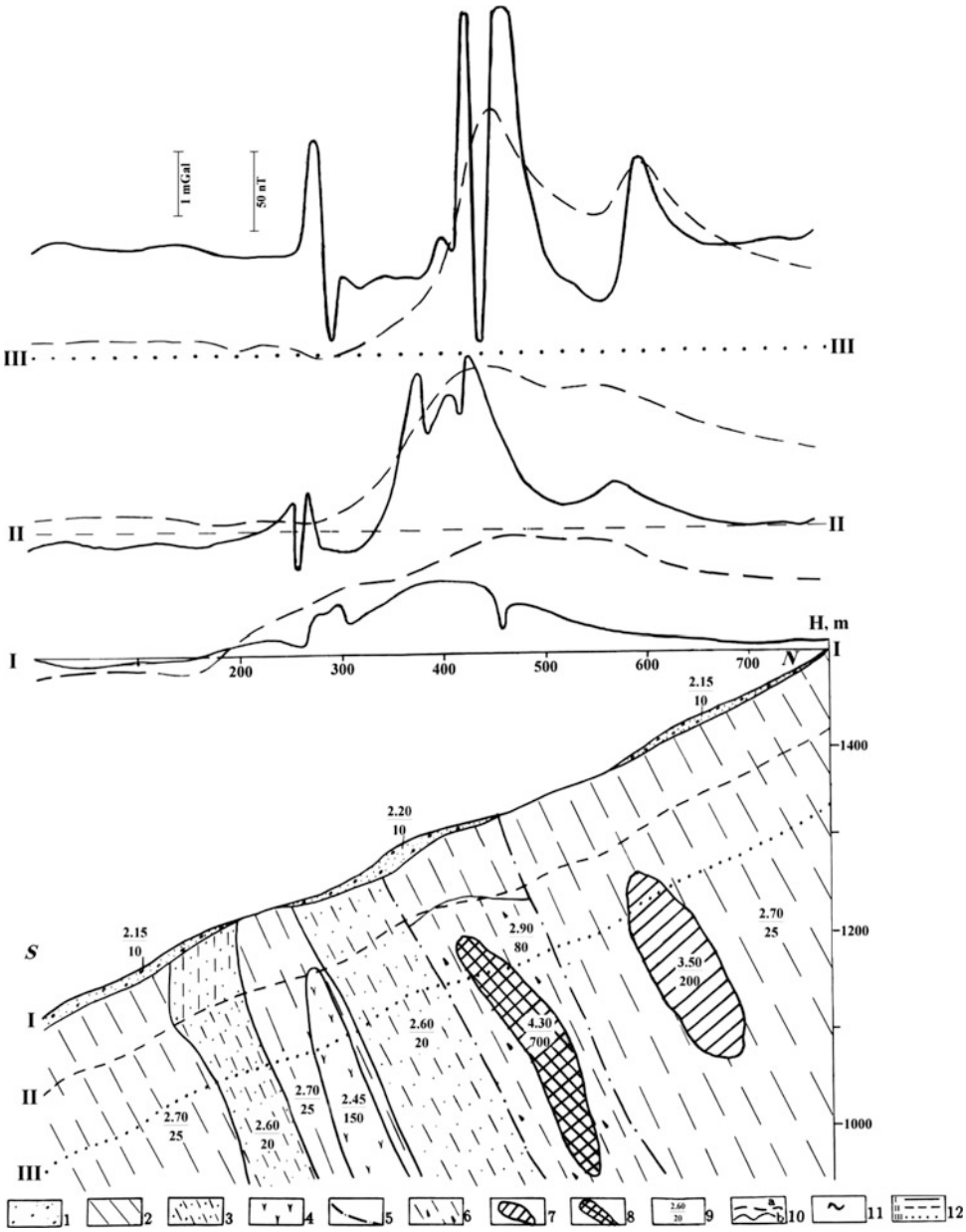

Fig. 8.3 A generalized physical–geological model of the pyrite-polymetallic deposit of the Filizchay type (after Eppelbaum 1989). (*1*) loose deposits; (*2*) clay shales; (*3*) clay shales with sandstone bands; (*4*) liparite–dacites; (*5*) disjunctive dislocations; (*6*) ore zone; pyrite-polymetallic ores: (*7*) impregnated-veined, (*8*) massive; (*9*) physical properties: numerator = density, g/cm^3, denominator = magnetization, mA/m; (*10*) computed values: (*a*) Δg, (*b*) ΔT; (*11*) boundary line for the anomaly plot overstepping the limits of the drawing; (*12*) levels of the erosional truncation: (*I*)—earth's surface, (*II*) and (*III*) depths of 80 m and 160 m from the earth's surface, respectively

Table 8.1 Geophysical effects for a ***PGM*** of the Filizchay type

h value (m)	Anomaly					
	Gravity (mGal)	Magnetic (nT)	*SP* (mV)	*VLF* (%)	*IP* (%)	Temperature (°C)
20	1.0 ÷ 2.2	150 ÷ 200	−(120 ÷ 300)	25 ÷ 50	7 ÷ 15	0.7 ÷ 2.0
60	0.6 ÷ 1.2	50 ÷ 70	−(60 ÷ 100)	10 ÷ 15	5 ÷ 9	0.2 ÷ 0.7
100	0.2 ÷ 0.6	25 ÷ 30	−(20 ÷ 40)	2 ÷ 4	2 ÷ 7	0.05 ÷ 0.10

it is worth using the VLF technique in the set instead of magnetic prospecting. Near-surface thermal prospecting can be also employed (Eppelbaum and Khesin 1988).

When comparing the two forms of ***PGM*** presentation, it should be noted that graphic ***PGM*** models (which are primarily quantitative) are easier to grasp. However, whereas the development of quantitative graphical ***PGM*** using computer-aided gravity and magnetic field computations presents no technical problems, quantitative computation of the temperature and self-potential fields using the same

PGM, as well as fields due to distant *VLF* transmitters, leads to many mathematical and computational difficulties. This is why the combined application of these two approaches supplementing each other seems more promising (Eppelbaum and Khesin 1988).

8.2.3 Gravity

The gravity method can be illustrated by a comprehensive gravity field examination in the Katekh deposit.

The Katekh pyrite–polymetallic deposit is situated in the southern slope of the Greater Caucasus (Northern Azerbaijan) under conditions of severe rugged topography. According to the data of the "Azerbaijangeologiya" Association, the geological section of the area is composed mainly of interstratifications of sandy-clay associations of the Upper Aalenian. Two subparallel stratified sheet-like bodies make up the Katekh deposit; tectonic faults control the space dislocation of all known economic orebodies.

The orebodies in this deposit are primarily characterized morphologically as lenticular. However, a combination of latitudinal and longitudinal faults complicates this type and they acquire the form of steam-chest beds. The Katekh deposit was investigated by mining and drilling up to a depth of 500 m. However, some experts note that due to the extremely complicated tectonics these operations failed to delineate the orebodies completely.

The following types of texture ores were identified in the Katekh deposit: (1) massive, (2) veiny-clastic, and (3) spotty-disseminated. The main ore minerals of the Katekh deposit are pyrite, sphalerite, chalcopyrite, and galena. The secondary ore minerals are represented by hepatic pyrite, wurtzite, arsenopyrite, and melnikovite; rare minerals are silver and gold (Mekhtiyev et al. 1976; Zaitseva et al. 1988).

A 3D combined modeling of the field $\Delta g_{\text{Bouguer}}$ (gravity field in the Bouguer reduction) and the magnetic field ΔZ (vertical component of the total magnetic field) was performed using the following procedure. A detailed PGM of the Katekh deposit with a length of 800 m and depth of 400 m was constructed from the Mekhtiyev et al. (1976) and Zaitseva et al. (1988) generalized data. Then, all the available data for this area on density (Gadjiev et al. 1984) and magnetic susceptibility (Ismailzadeh et al. 1983a, b) were utilized. For enhanced calculation of the surrounding terrain topography, a digital terrain relief model was created. The expressed SW–NE regional topography trend in the area of the Katekh deposit led to the selection of a rectangular digital terrain relief model (DTRM) with a length of 20 km and a width of 600 m (the physical–geological profile with a length of 800 m was located in the geometric center of the DTRM) (Fig. 8.4). On the whole, 1000 characteristic points describing the DTRM (with these points located close to the center of the DTRM and more rarely on these margins) were utilized.

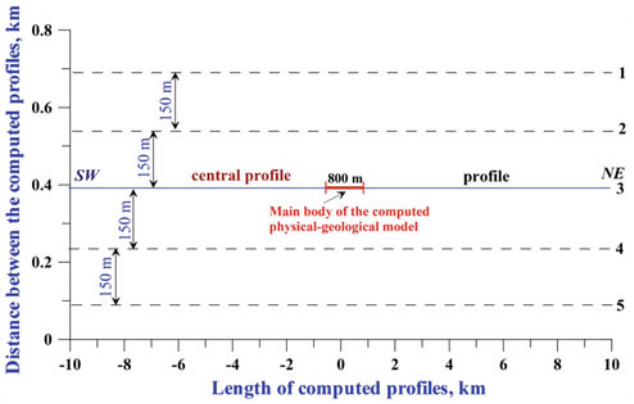

Fig. 8.4 Location of computed physical–geological model and profiles used for calculation of the surrounding terrain relief influence (after Eppelbaum and Khesin (2004), with small modifications)

The results of the first iteration of the gravity and magnetic fields modeling are presented in Fig. 8.5a. As indicated in this figure, the plots of ΔZ and ΔU_{SP} (self-potential anomalies) oscillate around zero and cannot provide useful information about the buried targets. This is due to the peculiarities of the mineralogical composition of ores in the Katekh deposit (only small SP anomaly was observed at 570-580 m of the profile). The almost total absence of magnetic mineral pyrrhotite causes the virtually non-magnetic nature of the ores. On other hand, the fairly large lead content impedes the normal course of oxidation–reduction reactions needed to trigger of intense SP anomalies. Thus, essential geophysical information can only be derived from the $\Delta g_{\text{Bouguer}}$ curve.

The analysis of the observed and computed gravity fields (Fig. 8.5a) shows that the initial PGM has a certain deficit of anomalous masses. 3D modeling of gravity field was carried out using about 25 sequential iterations. It yielded following results (Fig. 8.5b). Two orebodies of massive composition (not reflected in the previous geological constructions) were identified in the southwestern and northeastern segments of the deposit (Eppelbaum and Khesin 2004). It should be noted that the conclusion as to the presence of a hidden ore object in the southwestern portion of the profile is consistent with the results of independent investigations, namely underground geothermal observations and a ground geochemical survey. A temperature anomaly of 0.5–0.8 °C was recorded in adit 8 during the underground geothermal investigations at 250–300 m; the surface zone containing a large amount of lead and zinc was revealed at 150–200 m (according to Ginzburg et al. (1981) and data from the "Azerbaijangeologiya" Association). Finally, the small recognized SP effect at 570–580 m is an additional confirmation of ore body occurring below this anomaly.

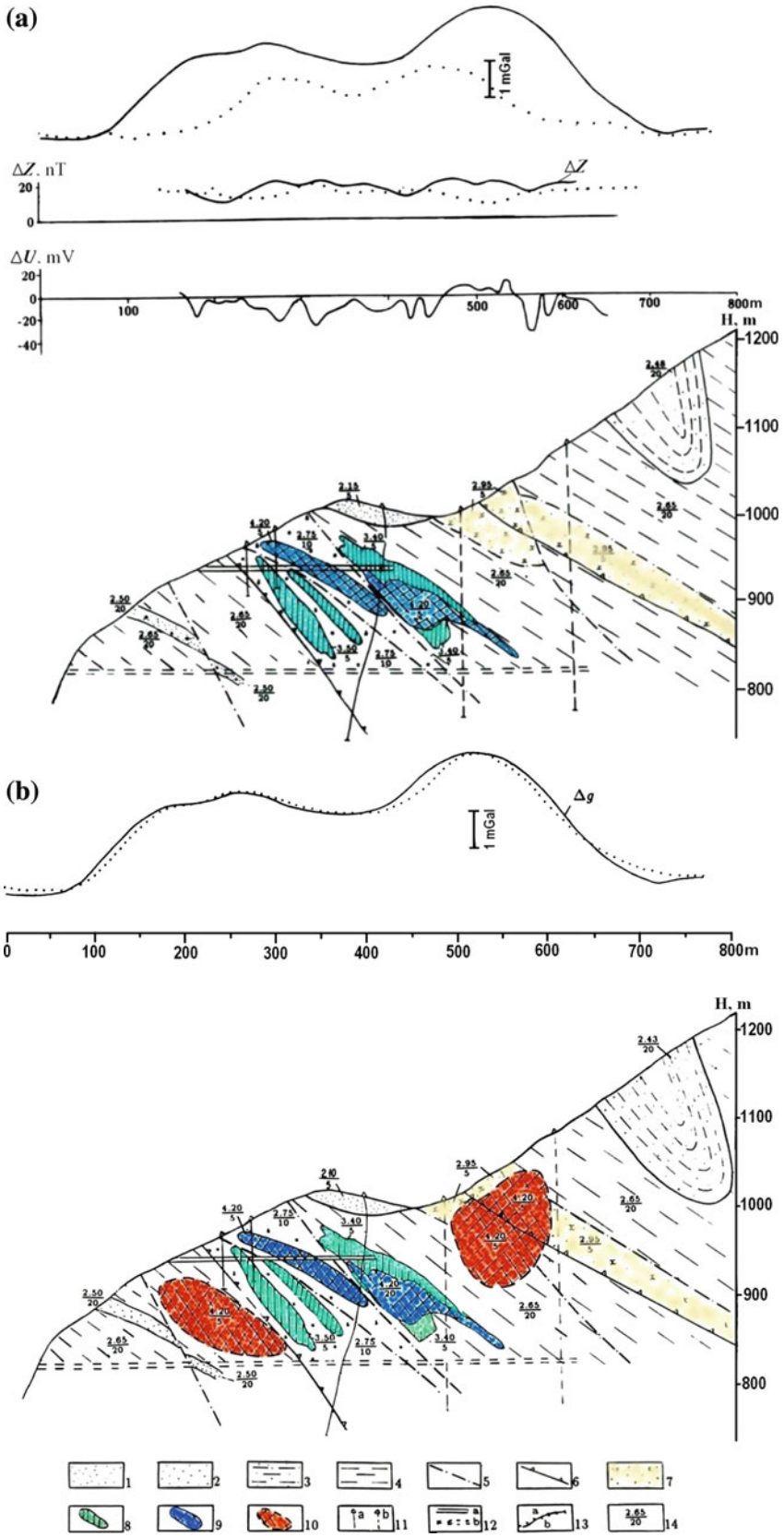

Fig. 8.5 **a** Computation of a geophysical effect based on a known geological section in the Katekh pyrite-polymetallic deposit (southern slope of the Greater Caucasus) (Eppelbaum and Khesin 2004). **b** Revised geological section model after a gravity field analysis (Eppelbaum and Khesin 2004) (*1*) Quaternary loose deposits; (2–4) Middle Jurassic deposits: (*2*) massive fine- and meso-grained sandstones, (*3*) interstratification of clay shales and sandstones, (*4*) rhythmical alternation of aleurolites and clay shales; (*5*) disjunctive dislocations; (*6*) upthrust-overthrust; (*7–9*) pyrite-polymetallic ores: (*7*) spotty, (*8*) stockwork-veiny, (*9*) massive; (*10*) contour of orebodies introduced during selection; (*11*) prospecting boreholes: (*a*) on the profile, (*b*) projected on the profile; (*12*) adits: (*a*) in the plane of the geological section, (*b*) projected onto the plane of the geological section; (*13*) curves of gravitational and magnetic fields: (*a*) observed, (*b*) selected; (*14*) physical properties: numerator = density, g/cm^3, denominator = magnetization, mA/m (*1–9* and *11–12* according to mining and drilling data)

8.2.4 Induced Polarization

The quantitative interpretation of electric (electromagnetic) survey data is very complicated without reference to gently sloping discontinuities. However, qualitative techniques in the IP method often provide valuable information about the geological section in question. For instance, visual analysis of η_a sections combined with η_a sections are often used while studying sulfide deposits in Canada and France. Such an approach is appropriate for the assessment of poorly accessible regions, where rapid interpretation results are necessary for planning further surveys.

The VES-IP method (vertical electric sounding with Schlumberger array) is widely used at various stages of prospecting in the almost inaccessible regions of the Greater and Lesser Caucasus (Khesin et al. 1997). Reference submeridional traverses of VES-IP (AB spacing up to 2–4 km, observation step 0.5–1.0 km) were performed from the foothills to the main watershed of the Greater Caucasus Ridge (Fig. 8.6).

In Fig. 8.6, the values of apparent polarizability η_a are shown under each sounding point at a depth of half the AB spacing. The pseudosection η_a thus obtained reflects the approximate change in the polarizability with depth.

This area is located on the southern slope of the Greater Caucasus, in the NW of Azerbaijan near its borders with Georgia and Dagestan. Its relief is highly complicated. This area is composed of intensely dislocated sandy-shale deposits which were earlier believed to be commercially worthless. However, combined electric and magnetic prospecting, as well as geochemical methods (spectrometallometry), led to the discovery of the Filizchay polymetallic deposit, the largest in the Caucasus. The main metals in this and several smaller ore deposits found in the same area (Katsdag, Katekh, Jikhikh, Katzmala, etc.) are copper, zinc, lead, and among others (Khesin et al. 1996). All these deposits formed a new ore province, confirmed by VES-IP reference crossings. In Fig. 2.6.6 and in other traverses, extended zones (I, II, III and IV) of high polarizability (tens of %) are evident. These zones include several copper and polymetallic deposits discovered later. The essential polarizability of the host rocks is caused by their pyritization and graphitization.

Figure 8.7 presents the interpretation results for the observed anomaly η_a obtained using a gradient array. The polymetallic body of complex composition occurs in a sand-shale stratum of the Upper Aalenian. The shape of the observed anomaly makes it possible to apply both inclined thin bed and horizontal circular cylinder interpretation models. The upper edge depth values for this body, computed by the methods of characteristic points and tangents for a thin bed model virtually, coincide. The HCC centers determined by the same techniques (assuming that a horizontal circular cylinder may be inscribed into the upper portion of the orebody) are slightly shifted with respect to each other. From the analysis of the geological section

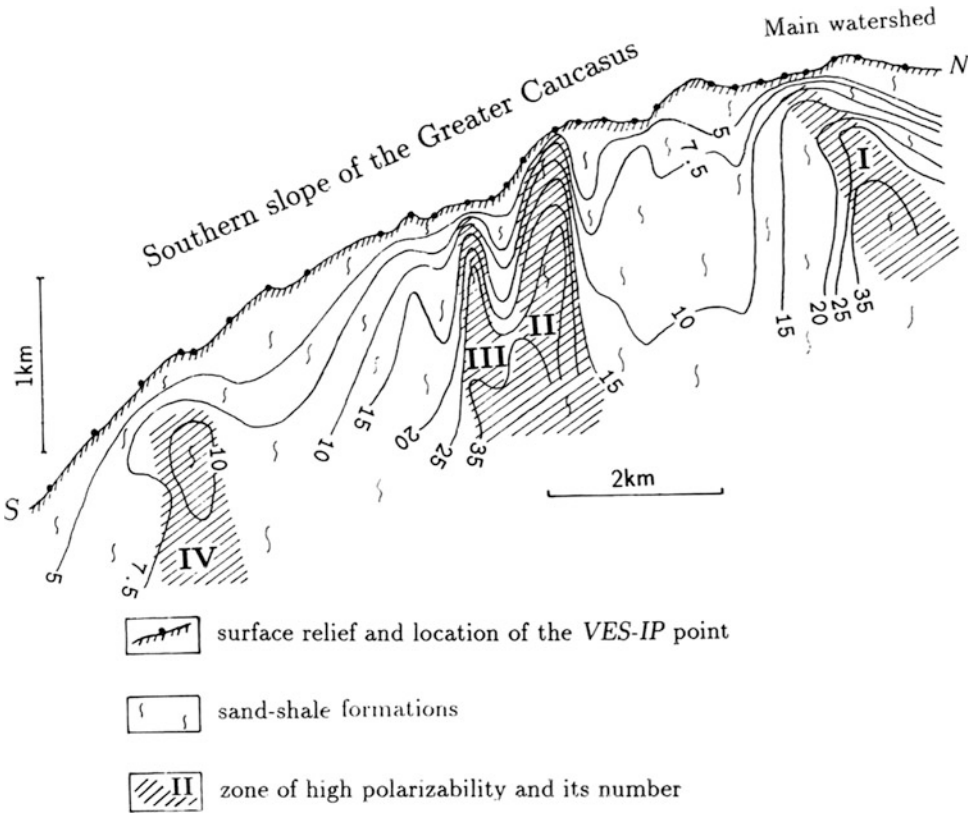

Fig. 8.6 Pseudosection of η_a (southern slope of the Greater Caucasus). Isolines are shown in % as a function of AB/2. The points of VES-IP are denoted by *black dots* (electrode spacing is oriented across the profile strike). The zones of high apparent polarizability in the Jurassic formations are shaded (Khesin et al. 1997)

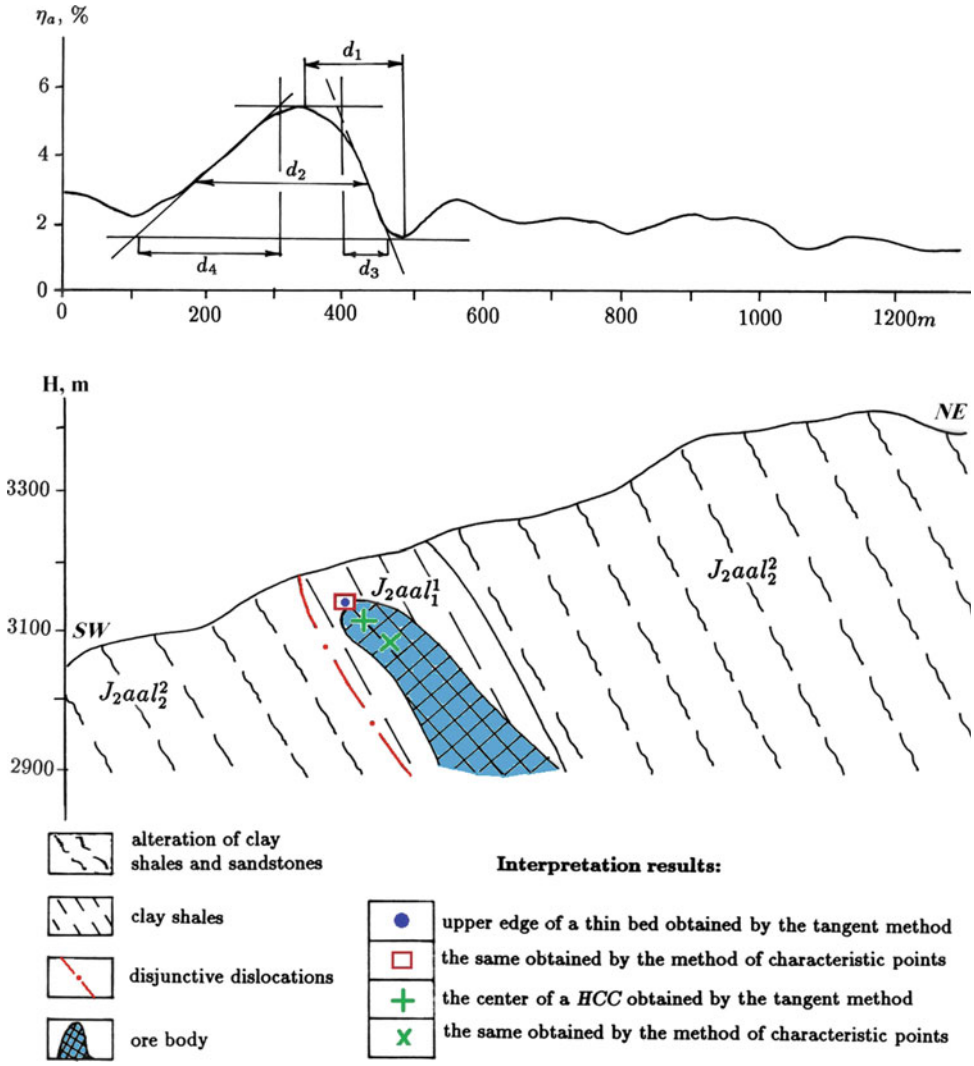

Fig. 8.7 Interpretation of the η_a anomaly (*gradient array*) in the Bazardyuzyu ore area (southern slope of the Greater Caucasus) by the developed techniques (after Khesin et al. (1997), with minor modifications)

(see Fig. 8.7) and both the thin bed and the HCC models (Eppelbaum and Khesin 2012), it was shown that both models are applicable. Thus, such results provide higher reliability for the location of an orebody. As shown in Fig. 8.7, the inclination of relief and polarization vector causes a displacement of the anomaly maximum relative to the projection of the upper edge of the body onto the earth's surface. As a result, without the quantitative interpretation, a testing well drilled on the maximum of η_a curve can miss the target.

8.2.5 VLF

Figure 8.7 illustrates the correlation between the topographic relief and the total horizontal component of the VLF magnetic field in the area of the Katsdagh pyrite–polymetallic deposit. The relief slope is about 40° and the orebodies occur in Middle Jurassic deposits. The frequency was 19.6 kHz with the transmitting station located near London and the profile azimuth was 80°. The different geological units had the following resistivity: pyrite–polymetallic orebodies (occurring in the bottom portion of the geological section)—several Ωm; mineralized zone (outcropping in the upper portion of the section)—10–30 Ω: sandstones—1200–1500 Ω; clay shales—700–1000 Ω; and liparite–dacites—400–700 Ω. These values indicate a relatively uniform background medium as far as resistivity is concerned. However, a distorting topographic effect tends to impair visual detection of an anomaly from a concealed orebody having the shape of a tilted plate. The correlation coefficient r was 0.97 (the broad anomaly from a mineralized zone was neglected, as shown in Fig. 8.8a).

When the topographic effect is removed, a weak anomaly due to the orebody and a strong field from the thick mineralized zone appear more clearly on the $H_{\varphi corr}$ plot (Fig. 8.8a).

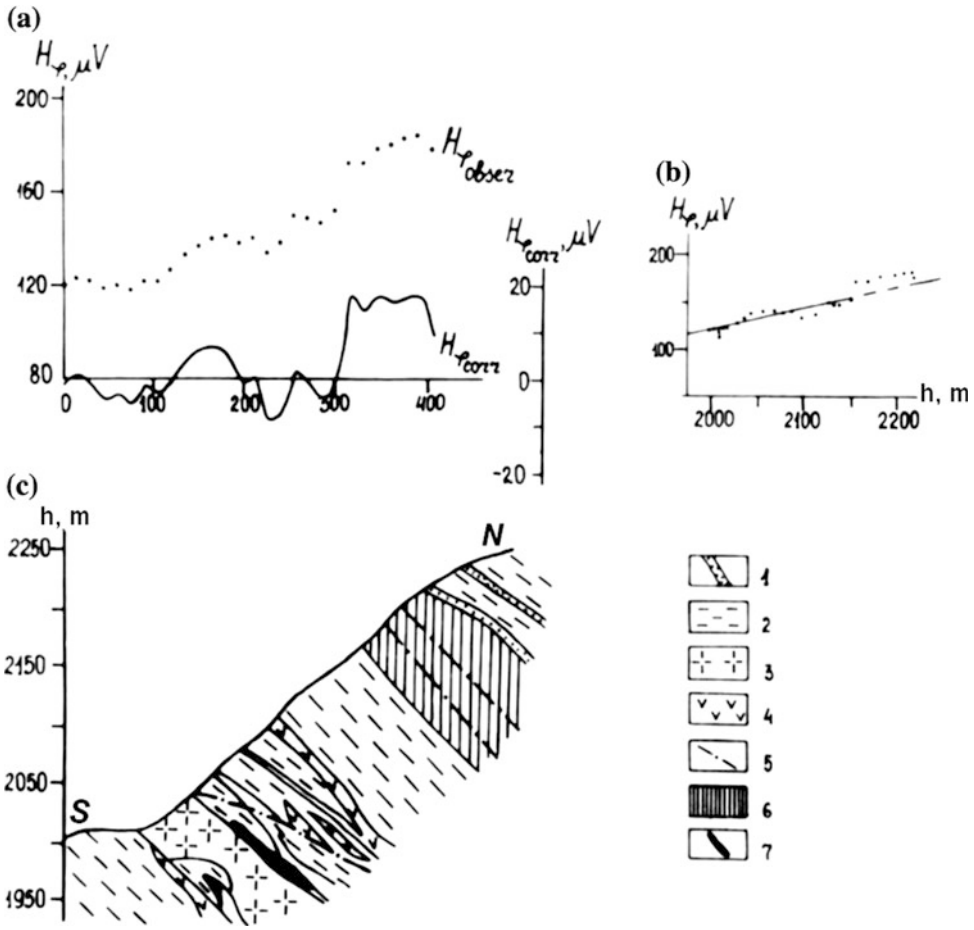

Fig. 8.8 Correlation technique for reducing the terrain relief effect on a portion of the Katsdagh pyrite-polymetallic deposit (southern slope of the Greater Caucasus, Azerbaijan). **a** Plots of observed and corrected H_{φ} values, **b** correlation, **c** geological section (after Eppelbaum 1991). (*1*) bands of sandstone, (*2*) clay shales, (*3*) liparite dacites, (*4*) dioritic porphyrites, (*5*) dislocations with breaks in continuity, (*6*) zone of intense ore mineralization, (*7*) massive ore

The next and geologically more complicated example illustrates the application of the correlation technique using the VLF method on a portion of the Katekh pyrite–polymetallic deposit (Fig. 8.9) in the same region. A frequency of 16.0 kHz was used in the investigation (the transmitter was in Rugby, Great Britain), and the profile azimuth was 60°. The ribbon-like band of the pyrite–polymetallic ore was located at a depth of about 60–80 m in the sandy-argillaceous series of the Upper Aalenian.

The average resistivity of the nearly uniform surrounding medium was in the range of 700–900 Ω; the resistivity of the massive orebody was a fraction of 1 Ω. The skin depth in the surrounding medium was about 110 m. Since a topographic anomaly was superimposed on a small signal from a relatively deep-seated anomalous object, it was difficult to detect the latter. Two different correlations were calculated for the southwestern and the northeastern slope, yielding correlation coefficients (between the relief heights and VLF intensity) of $r_1 = 0.988$ and $r_2 = 0.85$. The results for the southwestern slope were

$$H_{\varphi\text{appr}} = 84 + (0.6 \pm 0.09)h,$$

and the northeastern slope

$$H_{\varphi\text{appr}} = 105 + (0.6 \pm 0.09)h.$$

After removing the relief effect, a positive anomaly could clearly be seen on the northeastern slope in the $H_{\varphi\text{corr}}$ plot. This anomaly may have been due to the edge effect of a deep orebody, whereas the minimum on the southwestern slope could correspond to the opposite edge of the subhorizontal tabular orebody, since the anomaly was not very large in this case (Eppelbaum 1991).

8.2.6 Near-Surface Temperature Survey

Near-surface temperature survey has a great potential in ore geophysics (Khesin and Eppelbaum 1994).

Figure 8.10 presents the results of the interpretation of a temperature anomaly (applying the techniques described in Eppelbaum (1999)). In the figure, the results are given for a district with the steeply inclined relief of the Katekh deposit (southern slope of the Greater Caucasus). The temperature

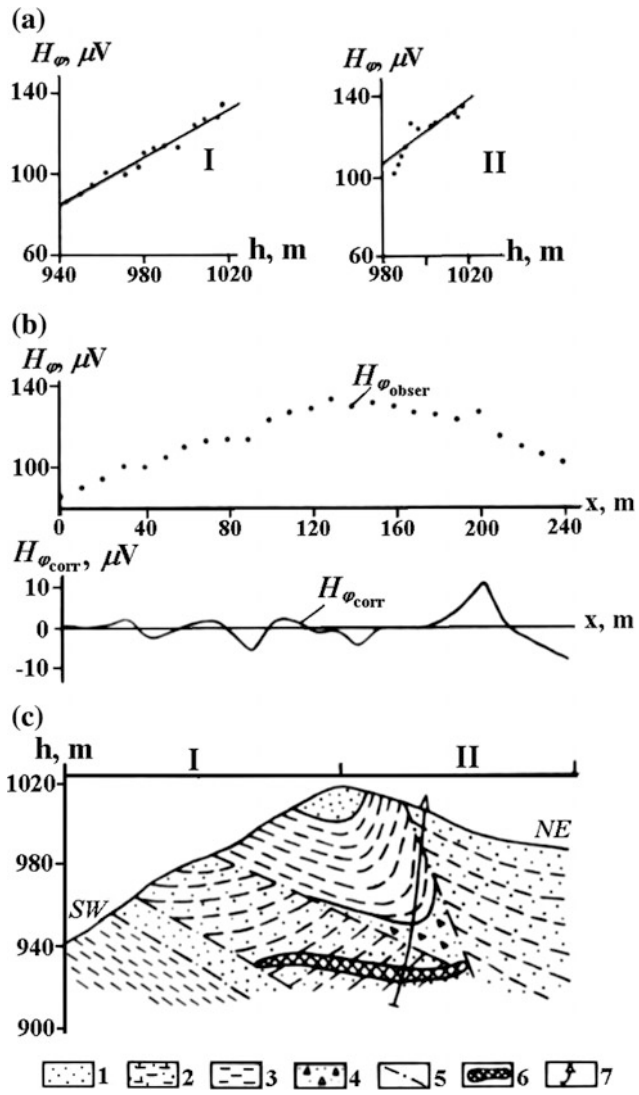

Fig. 8.9 Correlation technique for reducing the terrain relief effect on a portion of the Katekh pyrite-polymetallic deposit. **a** Correlation, **b** graphs of observed and corrected H_φ values, **c** geological section (Eppelbaum 1991). (*1*) fine- to medium-grained sandstones, (*2*) alternating sandstone and clay shale strata, (*3*) clay shales, (*4*) brecciated zone, (*5*) fractures, (*6*) orebody, and (*7*) borehole

was measured in 1.0–m-deep blastholes. The temperature plot shows two anomalies, one of which is due to the sub-horizontal ore deposit and is less pronounced. The thermal conductivities for the host rock and thick pyrite–polymetallic ore were 1.45 ± 0.35 and 3.87 ± 0.57 W/m °C, respectively (Zverev et al. 1982); i.e., their ratio exceeded 2.5. The upper part of orebody was completely oxidized and did not differ in thermal conductivity from the host medium. The results made it possible to localize the upper edge of the subvertical orebody within an acceptable error.

8.2.7 Self-potential Survey

Self-potential surveys were frequently applied on the pyrite–polymetallic deposits of the southern slope of the Greater Caucasus (e.g., Alexeyev 1971; Eppelbaum and Khesin 2002).

Four cases of *SP* interpretation are presented in Fig. 8.11a, b. A very intensive SP anomaly (about 600 mV) was observed in the Filizchay copper-polymetallic field (Fig. 8.11a). Use of the approach described in Eppelbaum et al. (2004) determined the position of upper edge of the orebody in conditions of sharply inclined relief. Three SP anomalies were successfully interpreted in the Katsdag copper–polymetallic deposit (Fig. 8.11b).

8.2.8 Magnetic Survey

Two examples of vertical components of magnetic field Z_a examination in the Filizchay ore field are shown in Fig. 8.12. Figure 8.12a illustrates the application of Logachev's method (Logachev and Zakharov 1979). As shown in Fig. 8.12a, reducing Z_a by the use of Logachev's method and interpretation of the obtained graphs Z_a and X_a by vector methodology defined the upper edge of orebody above the Earth's surface. Thus, this method is unacceptable in complex geological conditions (oblique magnetization, inclined rugged relief, and an unknown level of the normal magnetic field).

Application of the methodology as described in Eppelbaum and Khesin (2012) determined the position of the buried orebody with high accuracy (Fig. 8.12b).

It should be noted that magnetic field temporary variations cannot be assumed as 'noise' only. Careful differential analysis of magnetic variations behaviour over the sudied targets and in the 'normal field' area will allow, for instance, to distinguish 'ore' and 'non-ore' anomalies (Finkelstein and Eppelbaum, 2015).

8.2.9 Electromagnetic Methods

Among the electromagnetic methods used in mining geophysics, the most important are methods of partial extraction of metals (PEM), the transient electromagnetic method (TEM), and the contact method of polarization curves (CMPC).

The CMPC is based on the consecutive excitation of electrochemical reactions at the boundary of electron conductive minerals with moist rocks, and the recording of

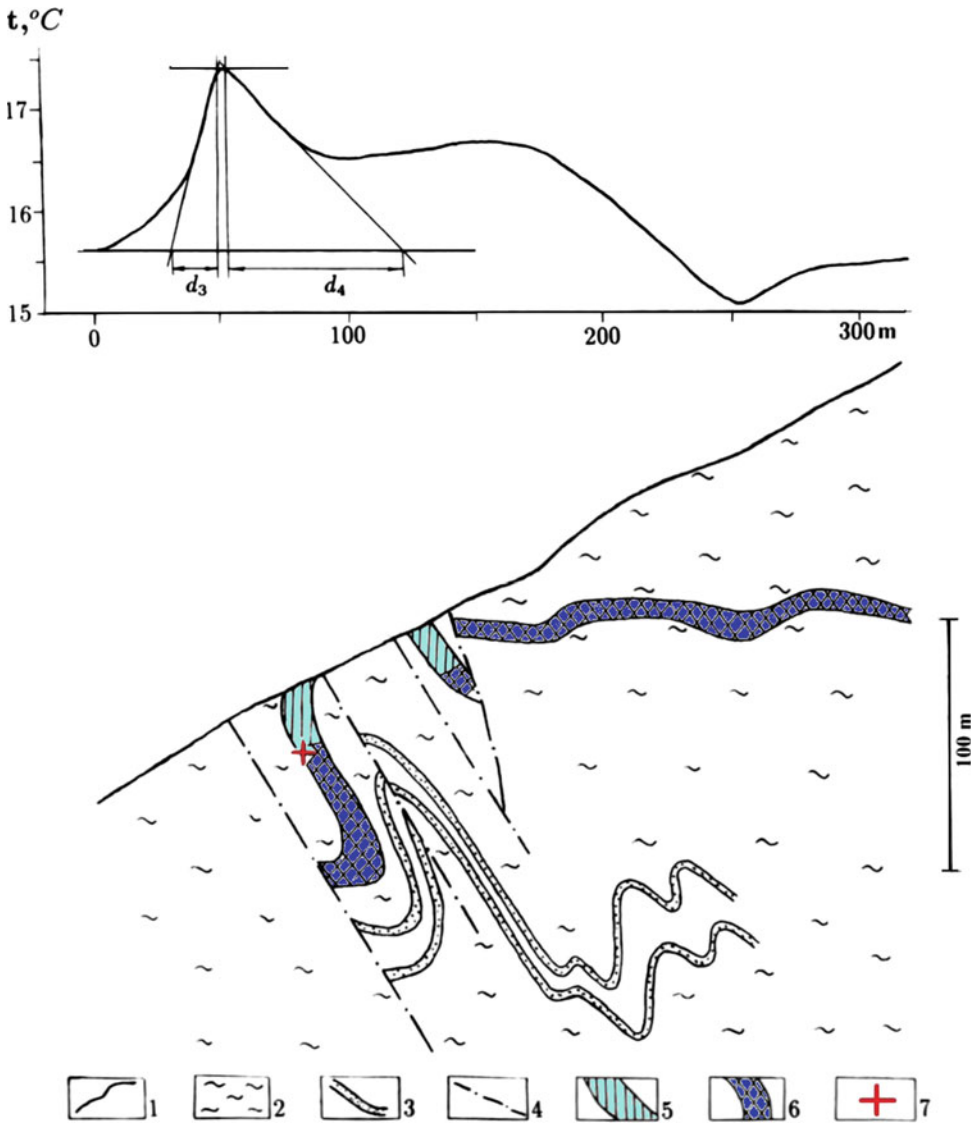

Fig. 8.10 Quantitative interpretation of the temperature anomaly at the Katekh pyrite-polymetallic deposit (southern slope of the Greater Caucasus, Azerbaijan). The observed temperature and geological sections are taken from (Zverev et al. 1982) and an unpublished report of the "Azerbaijangeologiya" Association. (*1*) observed temperature graph, (*2*) sandy-argillaceous sediments, (*3*) band of sandstone, (*4*) fault, (*5*) oxidized pyrite-polymetallic ore, (*6*) massive pyrite-polymetallic (sphalerite, chalcopyrite, etc.) ore, (*7*) position of the upper edge of ore body from the quantitative analysis of temperature anomaly (after Eppelbaum 1989)

electrochemical processes such as polarization curves. The CMPC was initially thought to be capable of solving the main problems of mining geophysics including quantitative calculation of metal components in each orebody. Field testing of this method in the southern slope of the Greater Caucasus unfortunately failed to confirm its effectiveness.

The PEM method (some scientists believe that this method is more geochemical than geophysical) was applied in the southern Caucasus to assess copper, zinc, lead, and gold content. In general, this method correlates well with other geophysical, geochemical, and geological methods.

Two variants of the TEM method have been applied: the one loop method and the frame-loop method; the size of the loops was 400 × 400, 200 × 200, and 100 × 100 m. This method covers large depths of investigation. It was proved to successfully calculate rugged terrain relief influence by the use of correlation methodology (Eppelbaum and Khesin 2012).

8.2.10 Integrated Analysis

The geophysical discovery of the Filizchay ore deposit by the integration of SP and magnetic fields is shown in Fig. 8.13.

The inverse probability method (IPM) was used on the Filizchay pyrite–polymetallic deposit revealed by geophysical methods. Application of IPM with the purpose of singling out weak magnetic anomalies showed that the ore deposit could be detected using this method (Fig. 8.13) even in that part of the area where it was not located in the observed field.

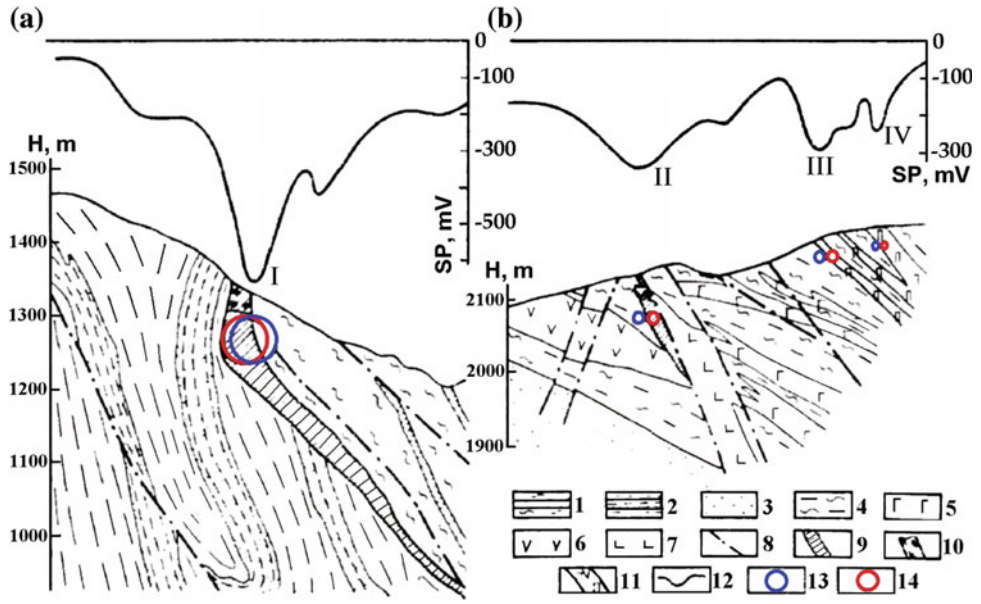

Fig. 8.11 Quantitative interpretation of *SP* anomalies at the Filizchay (**a**) and Katsdagh (**b**) copper–polymetallic deposits on the southern slope of the Greater Caucasus (Azerbaijan) (after Eppelbaum and Khesin (2012), with minor modifications) *I–IV*: numbers of interpreted SP anomalies (*1*) interbedding of sands and clay schists, (*2*) clay schists with the flysh packages, (*3*) clay sandstone; (*4*) sandy-clay schists; (*5*) diabases, gabbro-diabases and diabasic porphyrites; (*6*) andesites and andesite-porphyrites; (*7*) dacitic porphyrites; (*8*) faults; (*9*) massive ore of pyrite-polymetallic composition; (*10*) oxidized ore; (*11*) zones of brecciation, crush, and boudinage with lean pyrite-polymetallic ore; (*12*) *SP* curves; location of anomalous source (*13*) without calculation of inclined relief influence, (*14*) after introducing correction for relief

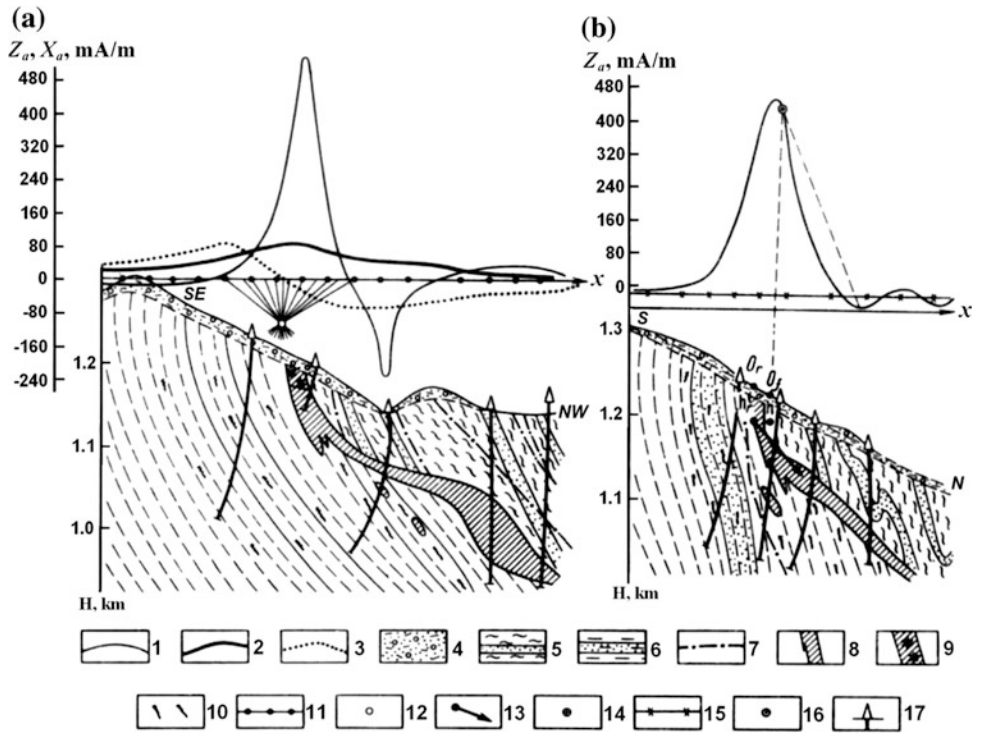

Fig. 8.12 Quantitative analysis of anomaly Z_a observed on an inclined relief. **a** By the use of preliminary reduction to the horizontal plane with Logachev's method (Logachev and Zakharov 1979), **b** using the methods presented in (Khesin et al. 1983) and Eppelbaum and Khesin (2012) Graphs (*1–4*): (*1*) Z_a (x, z), (*2*) Z_a (x, 0), (*3*) X_a (x, 0), (*4*) Quaternary deposits; (*5*) interbedding of sandstone, siltstone, and shales; (*6*) shales with flysch; (*7*) faults; (*8*) pyrite-polymetallic ore; (*9*) oxidized ore, (*10*) veiny ore, (*11*) horizontal level of magnetic anomaly reduction, (*12*) location of the middle of the upper edge of the orebody by interpretation of Z_a (x, 0) and X_a (x,0) on the level of reduction, results of interpretation of observed curve (*13–14*): (*13*) middle of the upper edge and direction of dipping of real body, (*14*) middle of the upper edge of fictitious body, (*15*) corrected line of the normal background of curve Z_a (x, z), (*16*) Reford's point (Reford and Samner 1964), (*17*) boreholes. 0_f and 0_r are the calculated origins of the coordinates for fictitious and real bodies, respectively

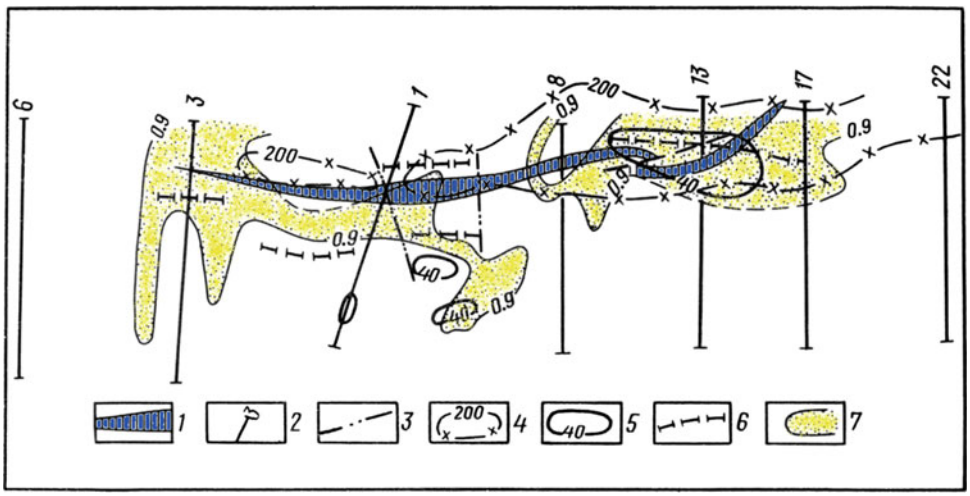

Fig. 8.13 Inverse probability and cross-correlation method testing on the Filizchay polymetallic deposit (southern slope of the Greater Caucasus) (geophysical surveys were carried out in the mid-1960s; Khesin et al. 1996). (*1*) upper edge projection of the deposit on the earth's surface by geological data; (*2*) profiles; (*3*) disjunctive dislocations; (*4*) isopotential lines of *SP* (mV); (*5*) isolines ΔZ (nT); (*6*) ΔZ anomaly axes obtained by cross-correlation; and (*7*) areas the probability of detecting the targets exceeded 0.9 after applying the inverse probability method

8.3 Azerbaijanian Part of the Lesser Caucasus

8.3.1 Self-potential Survey

In the 1930s, a self-potential survey was successfully carried out to study Chiragidzor pyrite stocks. A new Toganaly pyrite deposit was discovered on the contour of a SP anomaly in 1938 (Eppelbaum and Khesin 2012). SP observations were used together with other methods in the Gyzylbulagh gold–pyrite deposit for geological–geophysical mapping (Mekhmana ore district of the Daghliq (Mountainous) Garabagh, Western Azerbaijan). Altogether, SP investigations were applied at a few dozens of ore targets.

8.3.2 Physical–Geological Model of the Copper–Pyrite Deposit of the Lesser Caucasian Type

The ***PGM*** of the Lesser Caucasian type represents copper–pyrite deposits occurring in pyrite-bearing provinces with a predominance of volcanogenic rocks (Borodayevskaya et al. 1977). As reported in (Tvalchrelidze 1978), the following provinces are classified as the Phanerozoic pyrite provinces of the Lesser Caucasian type: the Caledonian (Tuva, Salair, Western Sayan), the Hercynian (Central Kazakhstan, Altai Mountains), the Cimmerian (Canadian Cordillera, Sierra-Nevada, Lesser Caucasus), and the Alpine (Eastern Serbia, Bulgarian Middle Upland, Anatolian Pont, Lesser Caucasus, Northern Iran, Japan, Taiwan, Philippines) geological structures. The pyrite deposits of this type, which are also termed South Uralian or Kuroko, are probed in detail in the Lesser Caucasus.

Copper–pyrite deposits of the Lesser Caucasian type in the Lok-Garabagh zone (e.g., Gedabey and Gyzylbulagh) are located at middle-height relief and localized in volcanogenic and volcanogenic-sedimentary associations of the Jurassic and Cretaceous. Constructing a PGM of the Lesser Caucasian type deposits is complicated by the enormous variability of rocks and ores and distinct tectonics. A ***PGM*** can be schematically represented as a set of small flat-dipping bodies of lens-like form, which differ from the host medium by certain contrasting properties. These include excess density (from 0.4 to 0.9 g/cm^3), higher conductivity (by a factor of 5×10 to 5×10^2), polarizability (several-fold), and thermal conductivity (1.5- to 2.5-fold) and lower magnetization (by a factor of 5×10 to 2×10^2).

The fields predicted by the typical ***PGM*** of deposits of the Lesser Caucasian type (Fig. 8.14) are compiled in Table 8.2.

A combination of gravity and magnetic prospecting, the VLF method, and near-surface thermal prospecting has proved to be efficient for determining deposits of the Lesser Caucasian type (Eppelbaum and Khesin 1988).

For SP, VLF, IP, and thermal prospecting methods, the determinations of expected effects take into account the results of physical and mathematical modeling and also the results of field investigations.

These PGMs substantiate the interpretation criteria and optimal geophysical sets for prospecting and estimation

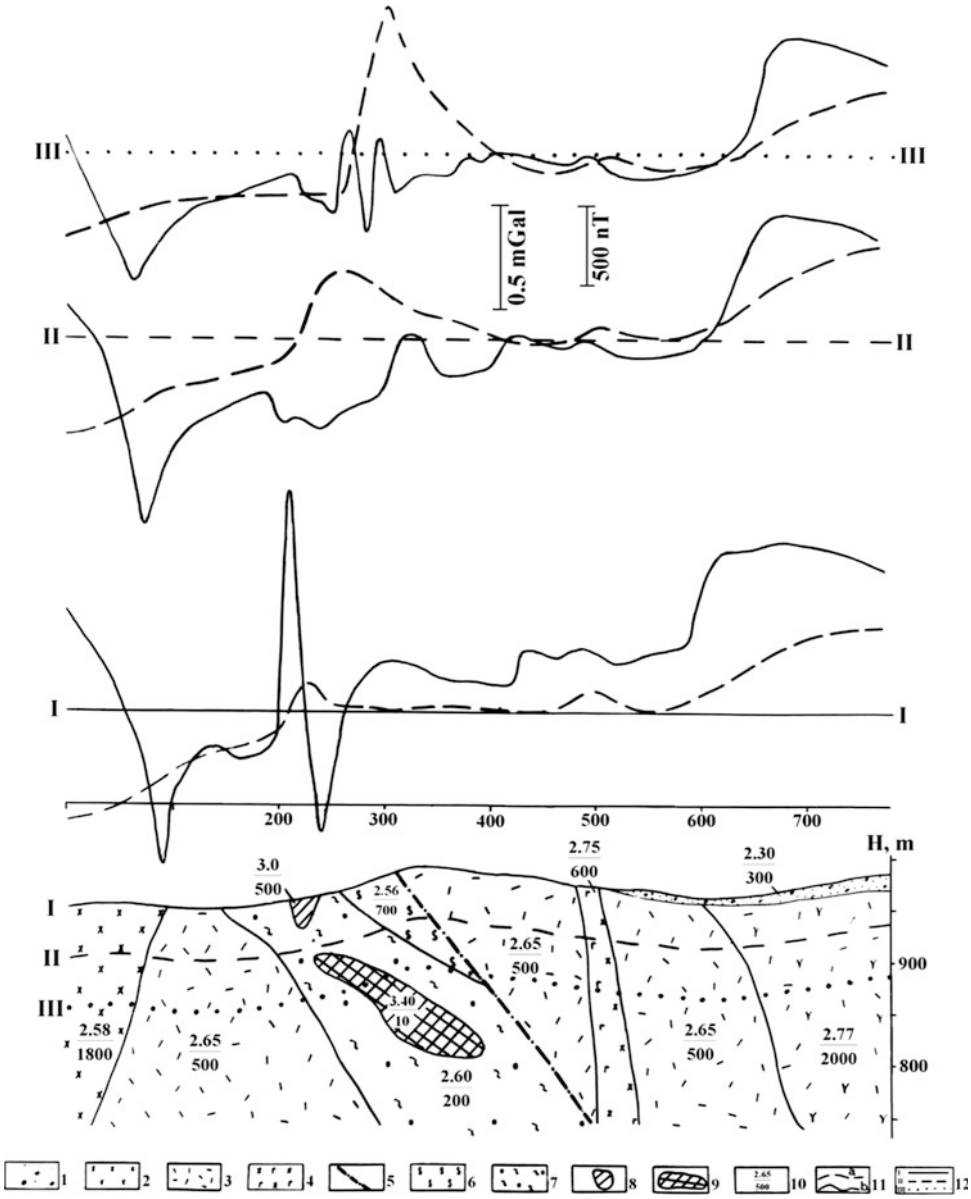

Fig. 8.14 A generalized physical–geological model of copper-pyrite deposit of the Lesser Caucasian type (Eppelbaum and Khesin, 1988). (*1*) deluvial deposits; (*2*) andesitic porphyrites; (*3*) tuffs of liparite dacites; (*4*) lavas of dacitic porphyrites; (*5*) dike of andesite basalts; (*6*) disjunctive dislocations; (*7*) zone of brecciation and crush with weak traces of pyritization; (*8*) zone of brecciation, crush, and boudinage, with lean ore; (*9*) oxidized orebody; (*10*) massive pyrite–chalcopyrite ore; (*11*) physical properties (numerator = density, g/cm^3, denominator = magnetization, mA/m); (*12*) computed geophysical fields: (*a*) Δg, (*b*) ΔT; (*13*) levels of the erosional truncation: (*I*) earth's surface; (*II*) and (*III*) depths of 50 and 100 meters from the earth's surface, respectively

Table 8.2 Geophysical effects for the ***PGM*** of the Lesser Caucasian type

h value (m)	Anomaly					
	Gravity (mGal)	Magnetic (nT)	*SP* (mV)	*VLF* (%)	*IP* (%)	Temperature (°C)
20	0.3 ÷ 0.5	−(70 ÷ 100)	−(20 ÷ 50)	15 ÷ 30	4 ÷ 12	0.5 ÷ 1.2
60	0.08 ÷ 0.15	−(20 ÷ 30)	−(15 ÷ 30)	5 ÷ 10	3 ÷ 6	0.1 ÷ 0.3
100	0.05 ÷ 0.08	−(5 ÷ 10)	−(5 ÷ 10)	1 ÷ 3	1 ÷ 4	0.03 ÷ 0.05

work. A combination of gravity and magnetic prospecting and VLF methods has proved to be efficient for deposits of the Lesser Caucasian type. IP, SP and near-surface thermal prospecting can be employed as subsidiary methods (Eppelbaum 1989; Khesin et al. 1996).

8.3.3 Gravity

The Chovdar barite deposit is located in the Lok-Garabagh zone of the NE slope of the Lesser Caucasus. Barite veins occurring at a depth up to 20 m have a density of

3.7–4.5 g/cm^3 and density of the host media (volcanogenic-sedimentary deposits of the Middle Jurassic)—2.50–2.87 g/cm^3. Gravity observations were carried out at a step of 2–5 m, and the amplitudes of the Bouguer gravity anomalies varied from +0.2 to +0.7 mGal (Khalilov 1996).

Iron-ore deposits of the Dashkesan ore region (Lesser Caucasus) are good targets for gravity surveys. High-density skarn–magnetite bodies of tabular or lenticular form occur in the limestone host media of the Upper Oxford and Lower Kimeridgian. The iron-ore bed in the SE Dashkesan skarn–magnetite deposit was traced by a local Bouguer gravity anomaly of 1.6 mGal (Malakhova 1996).

The Gyzylbulagh gold–pyrite deposit situated in Mekhmana ore district of Daghliq (Mountainous) Garabagh, Azerbaijan (Lesser Caucasus), has been investigated in detail by mining and drilling operations and can thus be used as a reference for testing geophysical method results. More than 2500 observation points were set up in the deposit over a network of 10 × 25 m, and the density and magnetization of 620 samples from the surface and drill cores were studied (Eppelbaum 1989; Khesin et al. 1993). The accuracy of measurement was +0.03 mGal. The heights of the observation points and their horizontal projections were determined by an accuracy of ±0.08 m and ±0.8 m, respectively.

Small ore objects and their low excess densities are expected to produce gravity anomalies of 0.2–0.3 mGal. The errors due to neglecting the effect of very rugged topography are, therefore, equivalent to the expected anomalies. Hence, the gravity results were processed by two methods: a conventional technique (Berezkin 1967; Nemtsov 1967; Veselov 1986) and by using a special processing scheme.

When faced with several problems, it seems worthwhile to consider eliminating the topographic effect step in 3D modeling of the whole medium. By excluding a separate procedure for terrain correction, calculation of the total error of processing and interpretation can take much less time. An example of such an approach was obtained in an area of the Gyzylbulagh gold–pyrite deposit (Khesin et al. 1993).

An isoline chart of $\Delta g_{B(0–50)}$, i.e., Bouguer anomalies including the total correction within a zone of 0–50 km (the heights of the surrounding relief elements varied from 0 to 4 km within a radius of 50 km) was compiled using the conventional method of terrain correction (Table 8.3).

Variations over the whole area ranged from 4.2 to 7.4 mGal, with maxima in the brook and crests and minima on the slopes. The Δg_B chart incorporating these corrections is characterized by a standard deviation amounting to ±0.11 mGal and is inconsistent with the geological evidence obtained by mining and drilling (Fig. 8.15).

Therefore, a special scheme for obtaining the Bouguer gravity anomalies was developed. It is based on determining the difference between free-air anomalies $\Delta g_{f.a}$ and the gravitational field computed by a 3D digital model of the homogeneous medium with $\sigma = 2.67$ g/cm^3 and real topography.

In the new method, the terrain relief effect was calculated during the interpretation. The terrain relief was simulated using six selected profiles 2c–7c in the central portion of the Gyzylbulagh area, crossing the deposit of the same name (800 m in length) (Fig. 8.14). Experimental calculations were carried out using the *GSFC* program to investigate the relief digital description range. These computations were made along profile 6c for both the 2D and the 3D models of the medium. For the 2D model, relief description intervals of 0.8 and 10 km were used, and for a 3D model, that of 0.8, 10, and 80 km were applied.

For the 3D model, the relief was described for all design profiles and, additionally, for four other profiles, two of which were to the left of profile 2c and the other two located to the right of profile 7c. The border profiles were selected so that they coincided with those observed in the Gyzylbulagh area. In this case, the Δg values were computed along profiles 2c–7c with a unified digital description of the terrain relief. The analysis showed that the difference in the results of 2D and 3D modeling was appreciable (up to ±1.5 mGal). At the same time, the curves obtained from the 3D model with a relief description interval of 10 and 80 km were practically identical (Khesin et al. 1993). This suggested that the description interval of 10 km was sufficient for 3D modeling. When the terrain relief receded from the selected points, it could be described more schematically, by singling out solely its major forms.

Table 8.3 Terrain correction zones in conventional gravity prospecting techniques

Zone	Radius of zone, km		Author of the methodology, SD (mGal)	Scale of topographic materials	Step of digital relief model (km)
	Inner	Outer			
Central	0.0	0.1	Berezkin (1967), ±0.06	1: 2000	–
Near	0.1	2.0	Lomtadze (1982), ±0.05	1: 25,000	0.1
Middle	2.0	10.0	Lomtadze (1982), ±0.05	1: 50,000	0.3
Distant	10.0	50.0	Lukavchenko (1951), ±0.05	1: 200,000	–

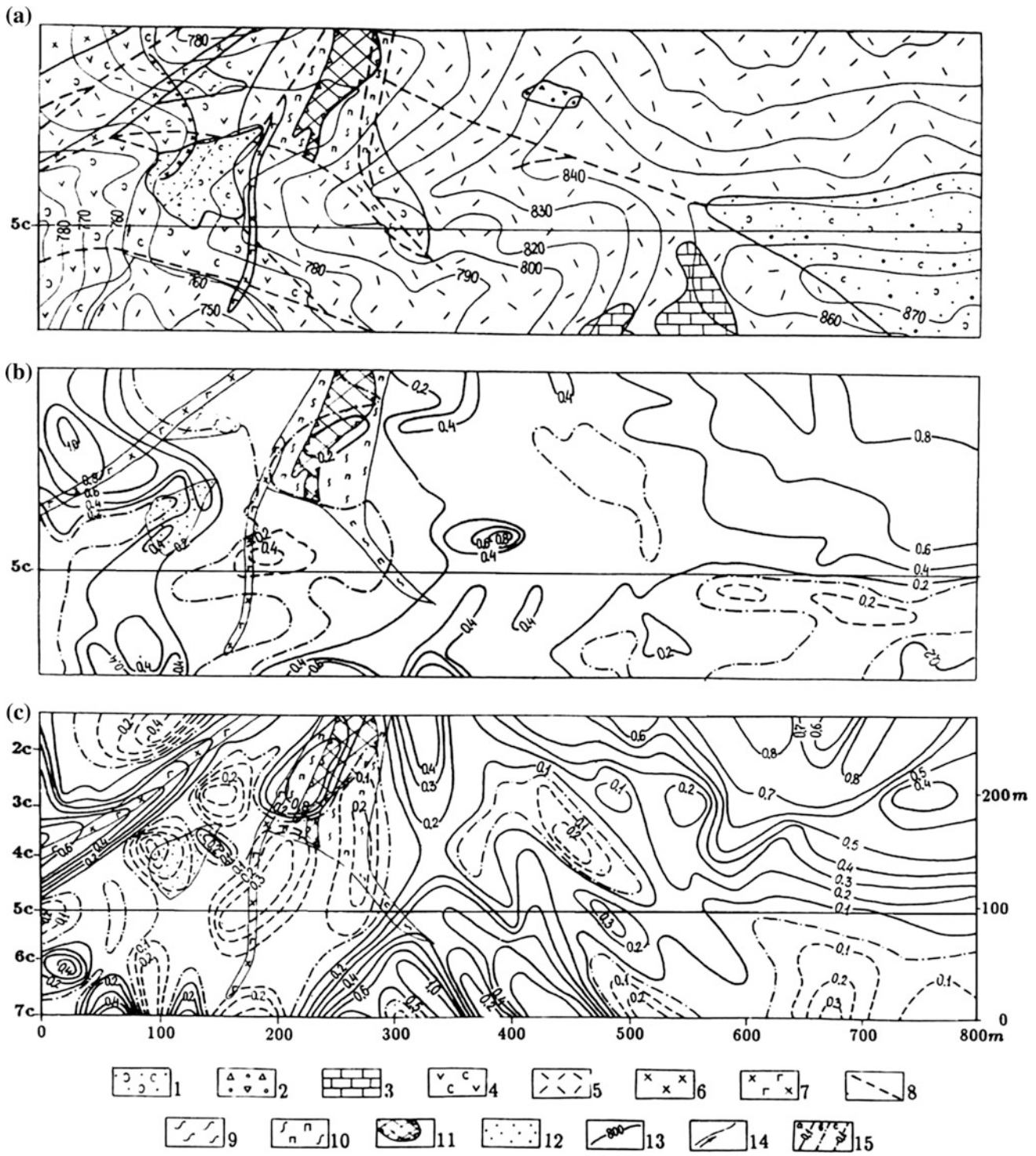

Fig. 8.15 Detailed gravimetric prospecting: A new method for $\Delta g_{\text{Bouguer}}$ computing (Eppelbaum 1989). (**a**) geological map of the central part of the Gyzylbulagh gold–pyrite deposit; (**b**) and (**c**) fragments of Δg field charts obtained by conventional and special techniques, respectively. (*1*) Quaternary deluvial deposits, (*2*) lens of tuffaceous conglomerate from the Upper Jurassic; (*3*) lenses of bone chert; (*4*) tuffs and lavas of andesitic porphyrites; (*5*) tuffs of liparite dacite porphyrites from the Upper Bajocian; (*6*) subvolcanic body of andesitic porphyrites; (*7*) dykes of andesite basalts from the Upper Jurassic; (*8*) disjunctive dislocations; (*9*) zones of brecciation and crush with weak pyrite–chalcopyrite mineralization; (*10*) zones of brecciation lean to pyrite–chalcopyrite ore content; (*11*) outcrop of orebody represented by oxidized pyrite–chalcopyrite ore; (*12*) dead rock and ore component pile; (*13*) terrain relief isolines; (*14*) brook bed; (*15*) isoanomals, mGal: (*a*) positive, (*b*) zero, (*c*) negative

After this experiment, subsequent processing of material from the Gyzylbulagh area involved the following steps. A 3D terrain relief model with a description interval of 10 km, in the points of profiles 2c–7c with a step of 8.46 m (95 points per each profile), was employed to compute the gravitational effect of the medium with $\sigma = 2.67$ g/cm^3 using the *GSFC* program. This effect was equal to an incomplete topographic correction (Δg_{ITC}) of the opposite sign. These corrections were subtracted from (i.e., added with their own sign) the values of $\Delta g_{\mathrm{f.a}}$ and Δg_{Bm} (subscript "m" stands for "model"). The latter were used to construct an isoanomaly map.

The accuracy of this Δg_{ITC} was considerably higher than that of the terrain correction by conventional techniques within a zone of 0–50 km. The standard deviation of Δg_{Bm} amounted to ±0.06 mGal.

The chart of Δg_{Bm} isoanomals (Fig. 8.15c) is much more differentiated than the Δg_{B} chart generated by conventional techniques (Fig. 8.15b) and is in better agreement with the available geological data (Fig. 8.15a).

8.3.4 Magnetic Survey

The Dashkesan iron-ore area of the Lesser Caucasus contains a group of magnetite–cobalt deposits. These massive magnetite ores contain of 79–90 % magnetite and 30–10 % non-ore minerals. Skarn–magnetite ores contain cobalt mineralization (Azizbekov et al. 1972). Obviously, one of the first magnetic surveys in Azerbaijan was carried out in the Dashkesan deposit in 1923–1924 by D. Ortenberg (Eppelbaum and Khesin 2012).

On the basis of a magnetic helicopter survey (conducted in the mid-1960s at a scale of 1:25,000), an illustrative magnetic map of this area was constructed (Fig. 8.16). Simple visual analysis of this map shows the effectiveness of magnetic prospecting for prospecting and localizing these magnetite-containing ores.

A comparison of this map and the map of a surface magnetic survey with the results of large-scale geological mapping indicated that within the anomalous zones bordering the Dashkesan intrusive from north and south, together with iron-ore deposits, gabbroids of various compositions were outcropped. The presence of maghemite testifies to the shallowness (up to 2 km) of the intrusive generation (Nagatha 1961). Magnetic anomalies from magnetite bodies are weakly present in the observed field (both ΔZ and ΔT) due to their deep occurrence and the subhorizontal location of the orebodies (Khesin et al. 1996). Therefore, to determine the sharp contacts of gabbroids (with which may be associated with orebodies) and localize the effects from a strongly magnetized lens, a map of the horizontal gradients of ΔT was constructed (Khesin et al. 1996). It showed that the maximal ΔT gradients coincided with the contours of the predicted ore reserves. Thus, the map of ΔT gradients could be used to discover new magnetite bodies in this area. A scheme of magnetic mass distribution at a depth was constructed by analyzing surface and airborne magnetic surveys, and the map of ΔT gradients incorporating several geological sections where quantitative computations were carried out. It showed that all the known iron-ore deposits were in the zones where gabbroids occur at comparatively low depths. This factor was an important search criterion.

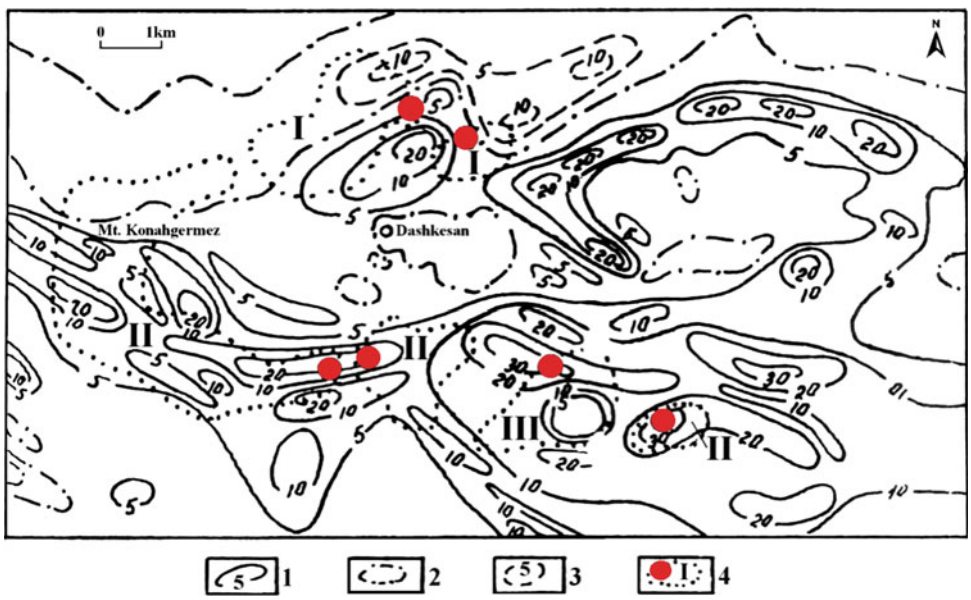

Fig. 8.16 Map of ΔZ isolines (in milliOersted) in the area of the Dashkesan group of iron-ore deposits ΔZ isolines: (*1*) positive, (*2*) zero, (*3*) negative; (*4*) contours of skarn–magnetite deposits: *I*—Dashkesan, *II*—south Dashkesan and its eastern portion, *III*—Damir

To reduce the influence of surface inhomogeneities and better identify the orebodies, the relief disturbing effect was calculated differently to include a correlation method (Khesin et al. 1996).

By applying the method of revealing buried structure crossing (Khesin and Eppelbaum 1997), a few nodes of hidden structure crossing were revealed (Fig. 8.17). This parameter does not guarantee absolute effectiveness, but the relation of the displayed nodes to the known ore mineralization was confirmed.

8.3.5 Induced Polarization

The IP method was one of the most frequently used geophysical methods for searching and prospecting ore deposits in the Lesser Caucasus.

Semi-quantitative interpretation of the VES-IP curves can serve to localize subhorizontal bodies with a high polarizability. This method was applied to localize a skarn–magnetite deposit in the Dashkesan ore field in the Lesser Caucasus (Eppelbaum and Khesin 2012). The results of borehole IP measurements in the Karadagh copper–porphyry deposit are shown earlier in Fig. 8.2.

An IP survey in the Lesser Caucasus revealed a smoother relief and not very complex tectonics. However, there were a wide range of magmatic and other rocks. This caused significant variability in the physical properties, both lateral and vertical, which made it difficult to interpret the geophysical data. The application of an approximate IP interpretation method successfully determined the depth of the upper edge of the magnetite body. It was characterized by an abrupt rise in the η_a value in the VES curve (Fig. 8.18).

8.3.6 VLF

Figure 8.19 illustrates the interpretation results for the H_φ curve along the profile across the Gyzylbulagh gold–pyrite deposit in the Mekhmana ore district (Garabagh, Azerbaijan). The anomaly over the ore object exposed by prospecting boreholes is shown in the central portion of the profile. In the southwestern portion, the anomaly over an anticipated object is marked.

In both cases, the approximation model was represented by an inclined thin bed. As shown in Eppelbaum and Khesin (1992), the magnetic field ΔZ was an analogue of H_x and H_φ components in the VLF method for the case of an inclined thin bed. A model magnetic field ΔZ_m due to the host medium and a near-surface orebody was computed for the central part of the profile. For modeling purposes, the following parameters were used: magnetization value: 300 mA/m for the host medium, and 1000 mA/m for the anomalous (ore) body; the vector of magnetization was assumed to be vertical for the host medium and along the dipping for the orebody. The azimuth of the selected profile was assumed to be 70°, which corresponds to the angle between the incoming *VLF* field and the real azimuth of the

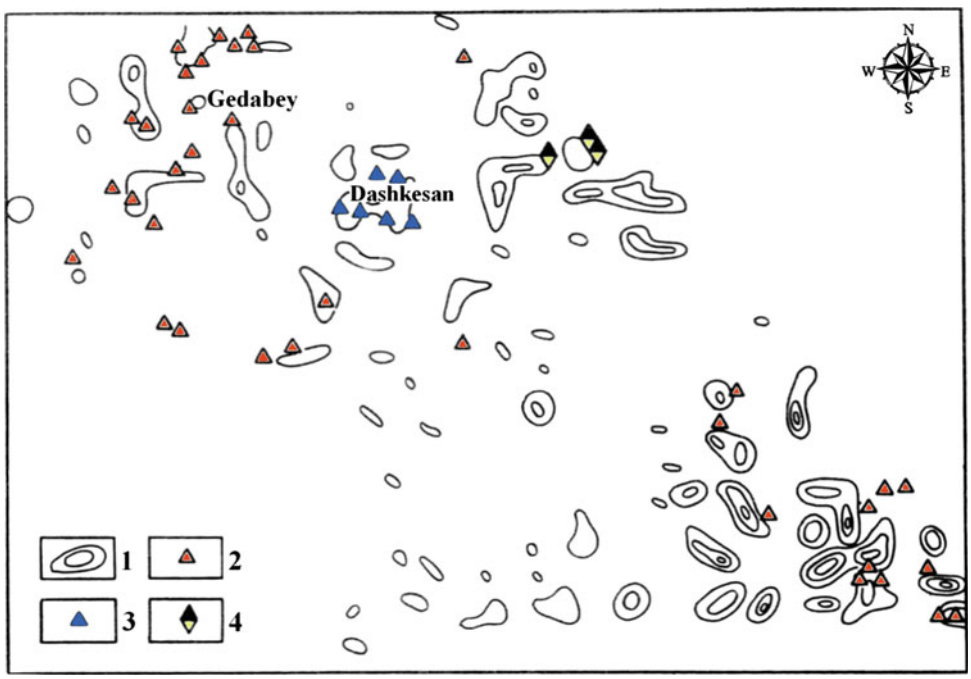

Fig. 8.17 Comparison of the nodes of hidden crossings of structures delineated by magnetic data with the distribution of ore mineralization in the northeast slope of the Lesser Caucasus (after Khesin et al. 1983, with modifications). (*1*) isolines of parameters, ore deposits, and manifestations: (*2*) copper–pyrite, (*3*) skarn–magnetite, (*4*) iron–manganese

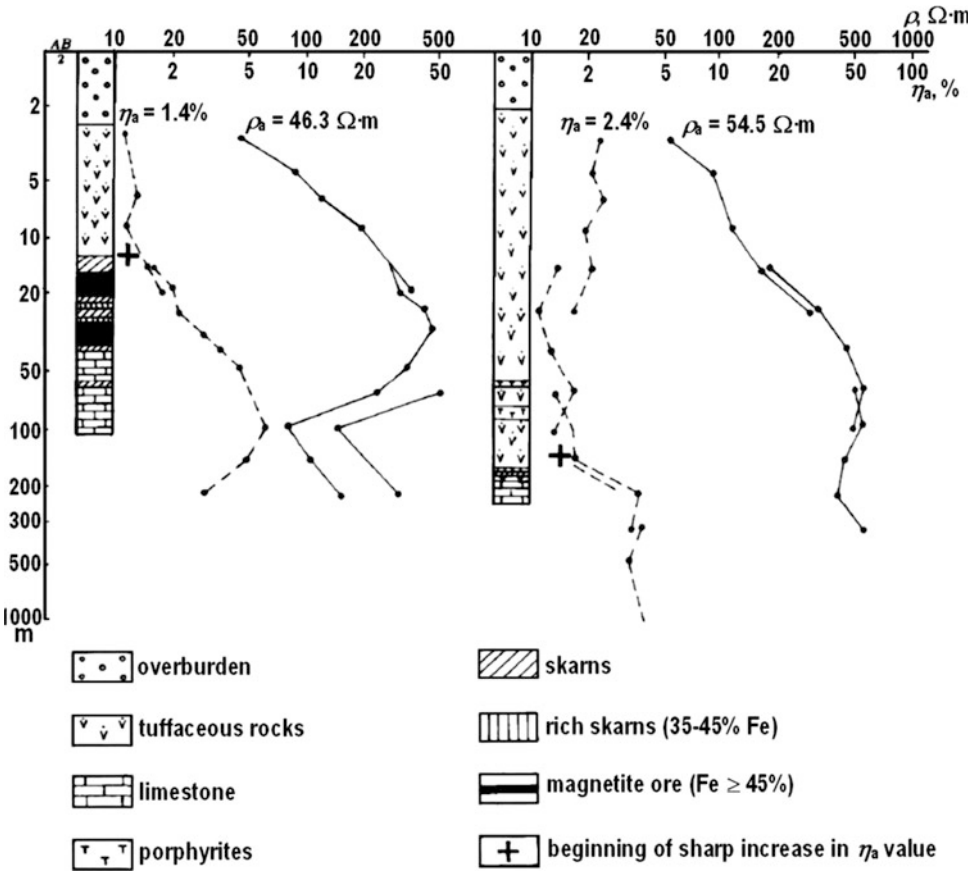

Fig. 8.18 Semi-quantitative interpretation of η_a curves in the Dashkesan iron deposit (Lesser Caucasus) (Khesin et al. 1997)

profile. It is clear from the figure that the H_φ and ΔZ_m curves are in good agreement. This provided additional proof of the similar nature of these fields.

8.3.7 Near-Surface Temperature Survey

Figure 8.20 illustrates the application of the correlation technique for eliminating the topographic effect in the district of the Gyzylbulagh gold–pyrite deposit. The equation for the terrain relief correction takes the form $T_{appr} = 15.6 - 0.07H$, where the correlation coefficient between the temperature$T$ and the height H is −0.8. Once the inclined relief effect has been eliminated, the anomalies from disturbing objects (massive ore in the southwestern part of the profile, and a vast zone of disseminated ore in the northeastern part) are more pronounced.

8.3.8 Electric and Electromagnetic Methods

Petrovsky and Skaryatin (1929) successfully applied a radio wave method to the translucent Chiragidzor pyrite stocks in Somkhet-Garabagh Zone (Azerbaijan). Balavadze (1944) delineated cobalt-bearing veins in the Dashkesan deposit using electric resistivity profiling. The identification of cobalt-bearing fragmentation zones by combined resistivity profiling and an emanation survey in the Chardakhly kaolinit deposit (Lesser Caucasus) is shown in Fig. 8.21.

The same electromagnetic methods (mentioned in subsection 8.2), namely PEM, TEM, and CMPC, were applied to ore deposit localization in the Lesser Caucasus. However, the effectiveness of these methods in this region (due to greater differentiation of electric and electromagnetic properties and the smaller size of the ore targets) was lower compared to the Greater Caucasus deposits.

8.3.9 Conventional Integrated Analysis

Visual analysis of the field is often enough to fulfill the geological objective, especially when a set of geophysical methods is employed. The mapping of intrusive rocks on the basis of data obtained by magnetic and emanation surveys in the Azerbaijanian part of the Lesser Caucasus revealed an intrusive body which intruded the limestone with sufficient precision, and even made it possible to classify its composition (Fig. 8.22).

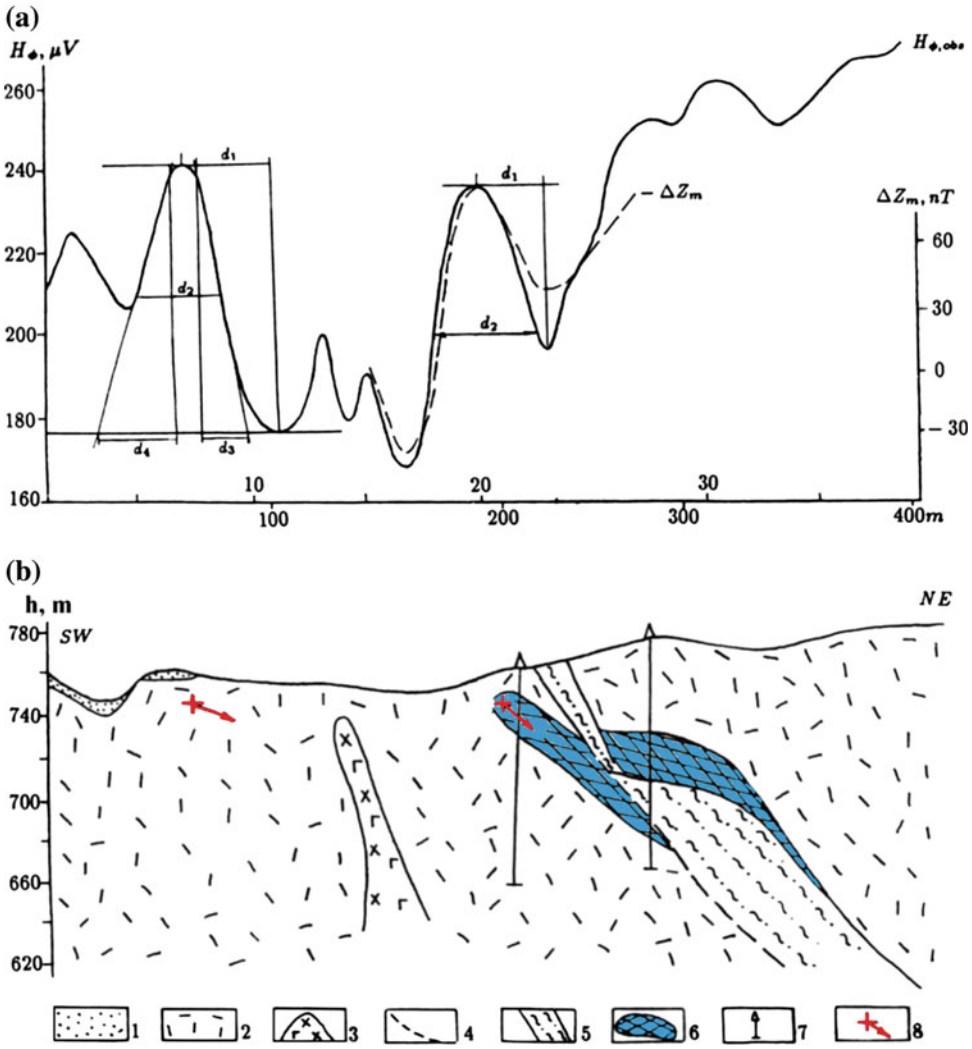

Fig. 8.19 Quantitative interpretation of the H_φ field in the area of the Gyzylbulagh gold–pyrite deposit (Lesser Caucasus): (**a**) the plots of H_φ and model magnetic field ΔZ_m, (**b**) geological section (Eppelbaum 1989). (*1*) loose deposits; (*2*) tuffs of liparite–dacitic porphyrites; (*3*) dike of andesite basalts; (*4*) disjunctive dislocation; (*5*) orebody; (*6*) zone of boudinage; (*7*) prospecting wells; (*8*) location of the conductive bodies' upper edge and direction of their dip by quantitative interpretation results

Figure 8.23 shows that seismic prospecting by the reflection and refraction methods clearly outlines the intrusive at a depth, whereas the local fault was detected by the diffraction method. Gravity and magnetic maxima additionally confirmed the presence of dense and magnetic basic intrusive rocks at a depth.

8.3.10 Integrated Analysis of the Basis of PGM

The techniques of processing and interpretation (presented in Khesin et al. (1996) and Eppelbaum and Khesin (2012) form a continuous sequence of procedures aimed at a final geological product—a map, a section, etc., in other words, a plot representing the final physical–geological model (***PGM***) of the medium.

For example, by summing up the amounts of information contained in the Δg and ΔT fields, and in the vertical component of VLF magnetic field H_z, we get the anomaly of the parameter $\frac{1}{3}\sum_{i=1}^{3} J_i$, which is more marked and reveals a gently sloping ore object on profile 5c through the Gyzylbulagh gold–pyrite deposit in the Lesser Caucasus (Fig. 8.24a).

The applied information technology was described in Eppelbaum (2014). It should be noted that the values of ΔT were calculated with an inverse sign (since pyrite deposits are characterized by lower magnetization against to strongly magnetized volcanogenic host rocks).

The rapid interpretation of Δg, ΔT, H_z, and H_φ plots (Fig. 8.24b) confirmed the available geological predictions and formed an initial approximation of the model of the medium which was further refined by interactive physical–geological modeling of the Δg and ΔT fields (Fig. 8.24c).

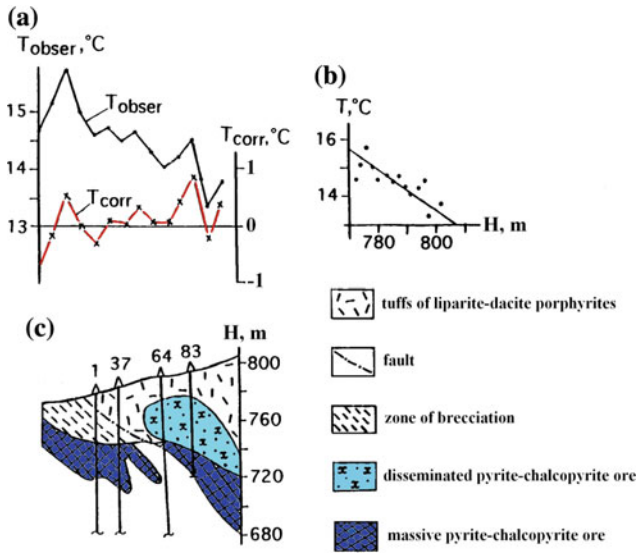

Fig. 8.20 Correlation technique for reducing the terrain relief effect in near-surface thermal prospecting in a district of the Gyzylbulagh gold–pyrite deposit (the Lesser Caucasus, Daghliq (Mountainous) Garabagh, Azerbaijan): (**a**) plots of observed and corrected temperature values, (**b**) correlation, and (**c**) geological section. Drill-holes 1, 37, and 64 continue below the section. Drill-hole 83 terminates as shown (Eppelbaum et al. 2014)

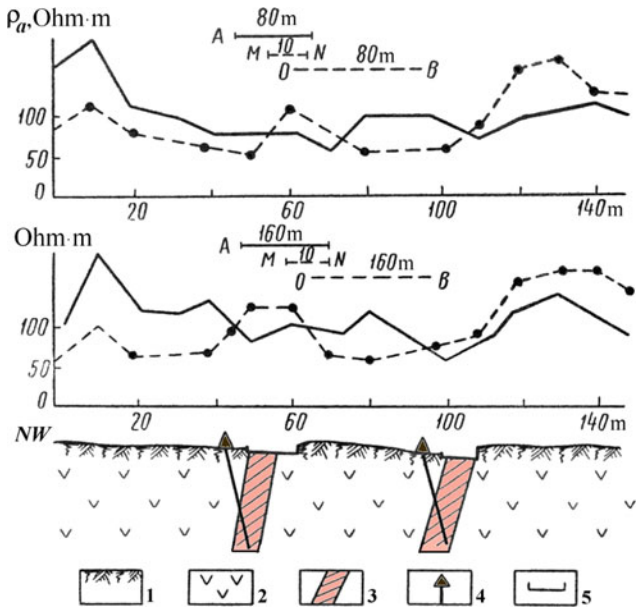

Fig. 8.21 1:5,000 combined profiling implemented for the detection of kaolinite clays, in the Chardakhly deposit (Gedabey ore area, Lesser Caucasus) (after Eppelbaum and Khesin 2012). (*1*) loose deposits, (*2*) secondary quartzite, (*3*) kaolinite and refractory clays, (*4*) borehole, and (*5*) trench

8.4 Underground Geophysics

Underground geophysics plays an important role in the investigation of ore deposits occurring in mountainous conditions. Below the geophysical methods that are best suited for underground geophysics are discussed.

8.4.1 Gravity

The methodology of underground gravity surveys is determined by the nature of the problem, as well as the physical–geological and environmental mine-technical conditions.

The following conditions are favorable for searching orebodies: (a) presence of contrast density and a sufficient volume of ore target causing a gravity effect of no less than 0.05–0.08 mGal, (b) comparatively small distance between the adit and ore target and its asymmetric position with respect to the adit (especially by dipping close to vertical), (c) comparatively uniform host medium (or the presence of data about density inhomogeneities), (d) desirably dense net of operational mines at different horizons. An underground gravity survey was successfully carried out, for instance, in the mining openings of the Katsdag pyrite–polymetallic deposit on the southern slope of the Greater Caucasus (Poltoratsky and Ginzburg 1989).

8.4.2 VLF

VLF method was successfully applied in mines at several polymetallic deposits on the southern slope of the Greater Caucasus (e.g., Ginzburg 1982; Brodovoi et al. 1989; Eppelbaum 1989; Eppelbaum and Khesin 2012).

8.4.3 Temperature Survey

A temperature survey in adits was performed by the use of following simple methodology. First of all, for this survey non-working adits without any industrial activity (primarily, without air supply) were selected. As a rule, positive temperature anomalies (or thermal flow) and heightened values of geothermal gradients are measured over orebodies. Hence, inside the target of heightened thermal conductivity, the geothermal gradient will be below the normal value. The width of the anomalous temperature interval gives definite information about the size of anomalous object, and the

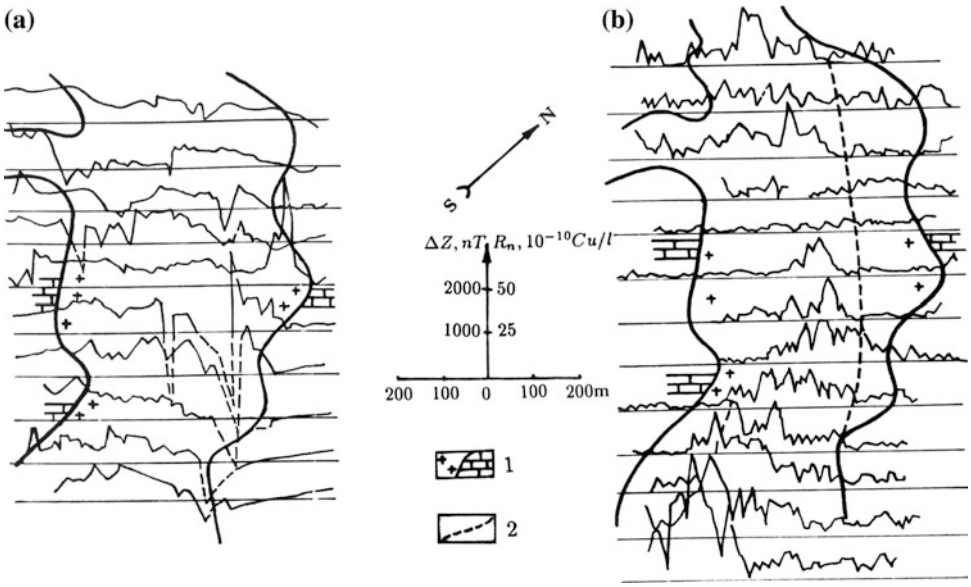

Fig. 8.22 Magnetic (**a**) and emanation (**b**) survey data employed for intrusive rock mapping (*dashed line* shows negative values of magnetic field graphs) (Lesser Caucasus) (Eppelbaum and Khesin 2012). (*1*) intrusion/limestone contact; (*2*) interface of alkaline rocks and gabbro-diabases by the emanation survey data

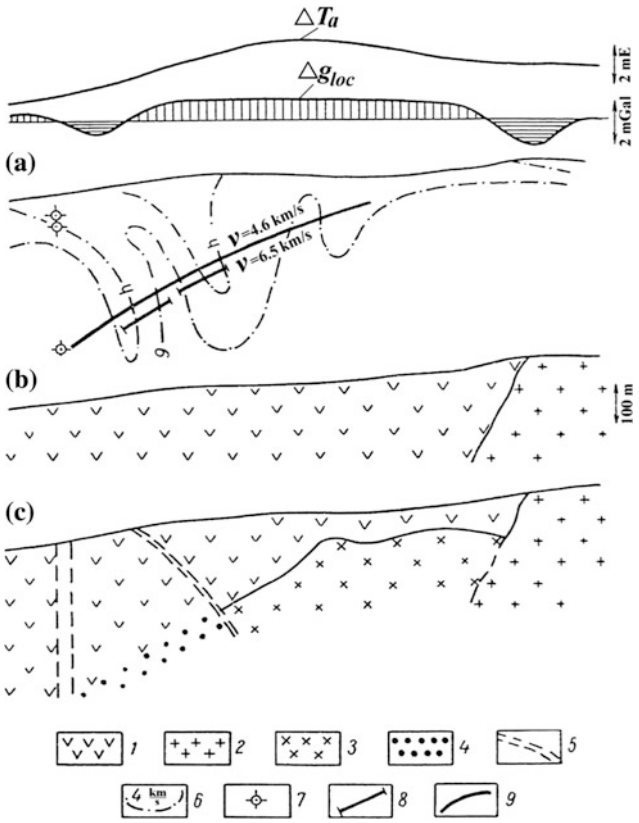

Fig. 8.23 Integration of seismic prospecting with other geophysical methods for the study of a hidden intrusive body to the NW of the Gedabey intrusive (on the basis of materials of A. Sh. Mamedzadeh, Yu. G. Shopin and S. A. Mirizadeh): (**a**) aeromagnetic and gravity anomalies over velocity section, (**b**) geological section, (**c**) result of interpretation of geophysical data. (*1*) porphyrites and tuffs of the Lower Bajocian; (*2*) intermediate intrusive rocks; (*3*) basic intrusive rocks; (*4*) zone of intense contact metamorphism; (*5*) disjunctive dislocation; (*6*) isolines of refraction wave velocities (km/s); (*7*) diffraction point; (*8*) reflection piece; and (*9*) refractor

temperature gradient is indicative of the distance to the observation line. The distribution of the temperature graph can in many cases be used to draw conclusions about the location of the anomalous target.

Temperature measurements in adit 10 of the Katsdagh deposit were made in glasses filled with water at an observation step of 10 m (Fig. 8.25). Analysis of the temperature field indicated that the temperature anomaly observed in the right portion of this geological section in general corresponded to the anomalous body. At the same time, the temperature anomaly observed in the left portion of this section testified to the presence of some additional orebodies not detected by geological means (Fig. 8.25).

An example of the influence of rugged terrain relief on adit temperature measurements is presented in Fig. 8.26. As is known, surface relief influences the temperature field at a distance of 4–5 amplitudes of the relief's maximal amplitude (e.g., Cheremensky 1972). A temperature survey was performed in blastholes of 1.5 m in the adit walls. The search targets in this case, namely massive pyrite–polymetallic orebodies, occurred in the sandy-argillaceous medium that provided a high thermophysical contrast. The observed temperature curve (Fig. 8.26b) was strongly distorted by the rugged relief influence. After application of the correlation approach (coefficients of linear regression were obtained by the least squares method), the corrected temperature graph was constructed (Fig. 8.26a). Quantitative analysis of the graph led to calculation of the position of the center of the anomalous target (the quantitative interpretation methods are presented firstly in Eppelbaum (1989)).

In the Katsdagh pyrite–polymetallic deposit, an areal temperature survey was performed (Fig. 8.27a). The temperature map for the normal field (which incorporates the

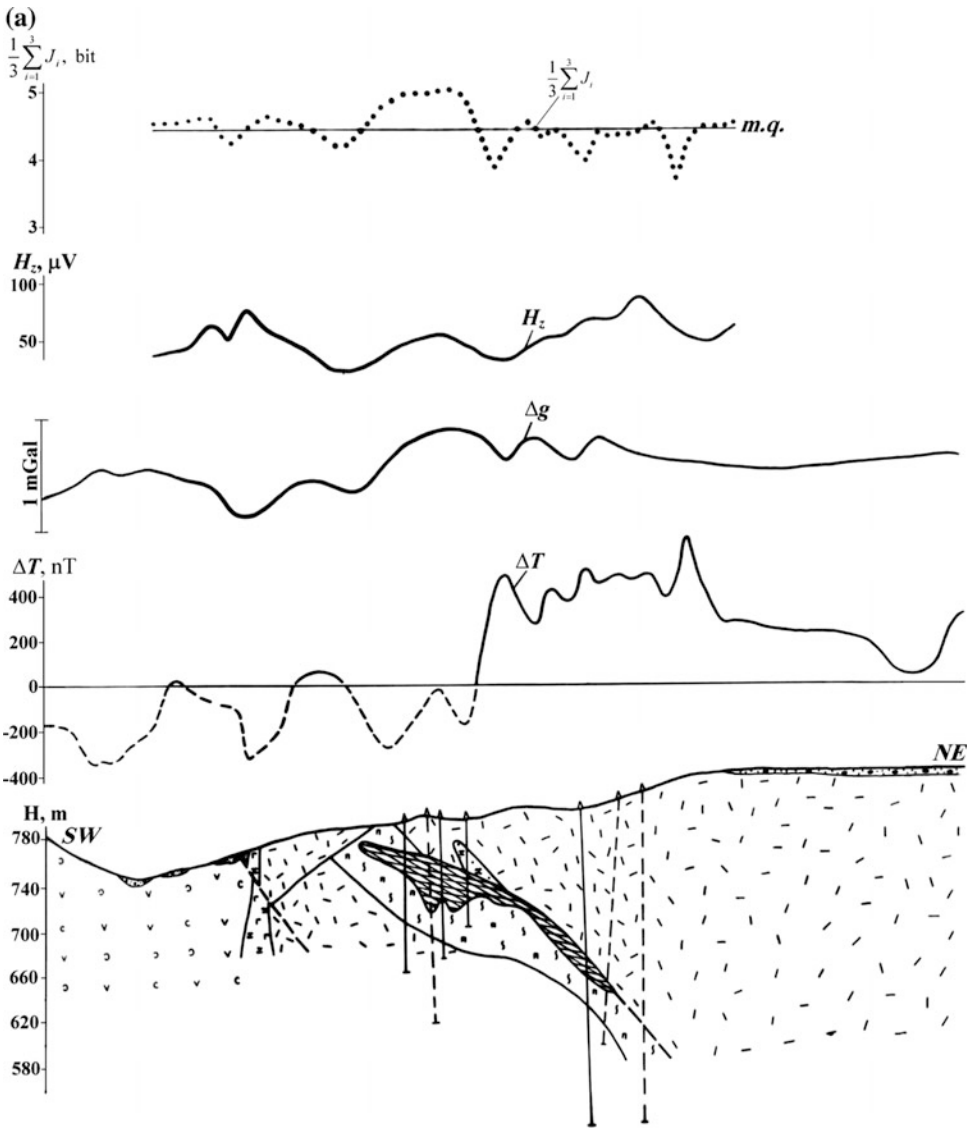

Fig. 8.24 Stages in geophysical data interpretation at the Gyzylbulagh gold–pyrite deposit (Lesser Caucasus) (Eppelbaum 1989; Khesin et al. 1993). **a** Identifying the target object (ore deposit) by summing up the information obtained by different geophysical methods. **b** Quantitative rapid interpretation of ΔT, Δg, H_z, and H_φ fields. **c** Selection of a geological section on the basis of gravity and magnetic data. (*1*) Quaternary deluvial deposits; (*2–8*) Middle and Upper Jurassic rocks: (*2*) silicificated limestone lens, (*3*) tuffs and lavas of andesitic porphyrites, (*4*) tuffs of liparite–dacitic porphyrites, (*5*) deconsolidated tuffs of liparite dacite porphyrites, (*6*) lavas of dacitic porphyrites, (*7*) consolidated lavas of dacite porphyrites, (*8*) dikes of andesite basalts; (*9*) disjunctive dislocations; (*10*) zone of brecciation and crush; (*11*) zones of brecciation, crush, and boudinage with lean pyrite–chalcopyrite ore; (*12*) zone of brecciation, crush, and boudinage with rich impregnating mineralization; (*13*) massive pyrite–chalcopyrite ore; (*14*) drilled wells: (*a*) on the profile, (*b*) projected on the profile; (*15*) terrain relief in the profile (in Fig. 8.24b only); results of rapid interpretation; (*16*) location of the center of HCC from the interpretation of Δg and ΔT plots; (*17*) location of the *HCC* center from the interpretation of the H_z (*a*) and H_φ (*b*) plots; (*18*) location of the upper edge of the thin bed from the interpretation of H_z and ΔT (*a*) and H_φ (*b*) plots; (*19*) physical properties (numerator = density, g/cm^3; denominator = magnetization, mA/m; (*20*) gravitational and magnetic fields: (*a*) observed, (*b*) selected; and (*21*) body contours assumed in the process of 3D modeling

Fig. 8.24 (continued)

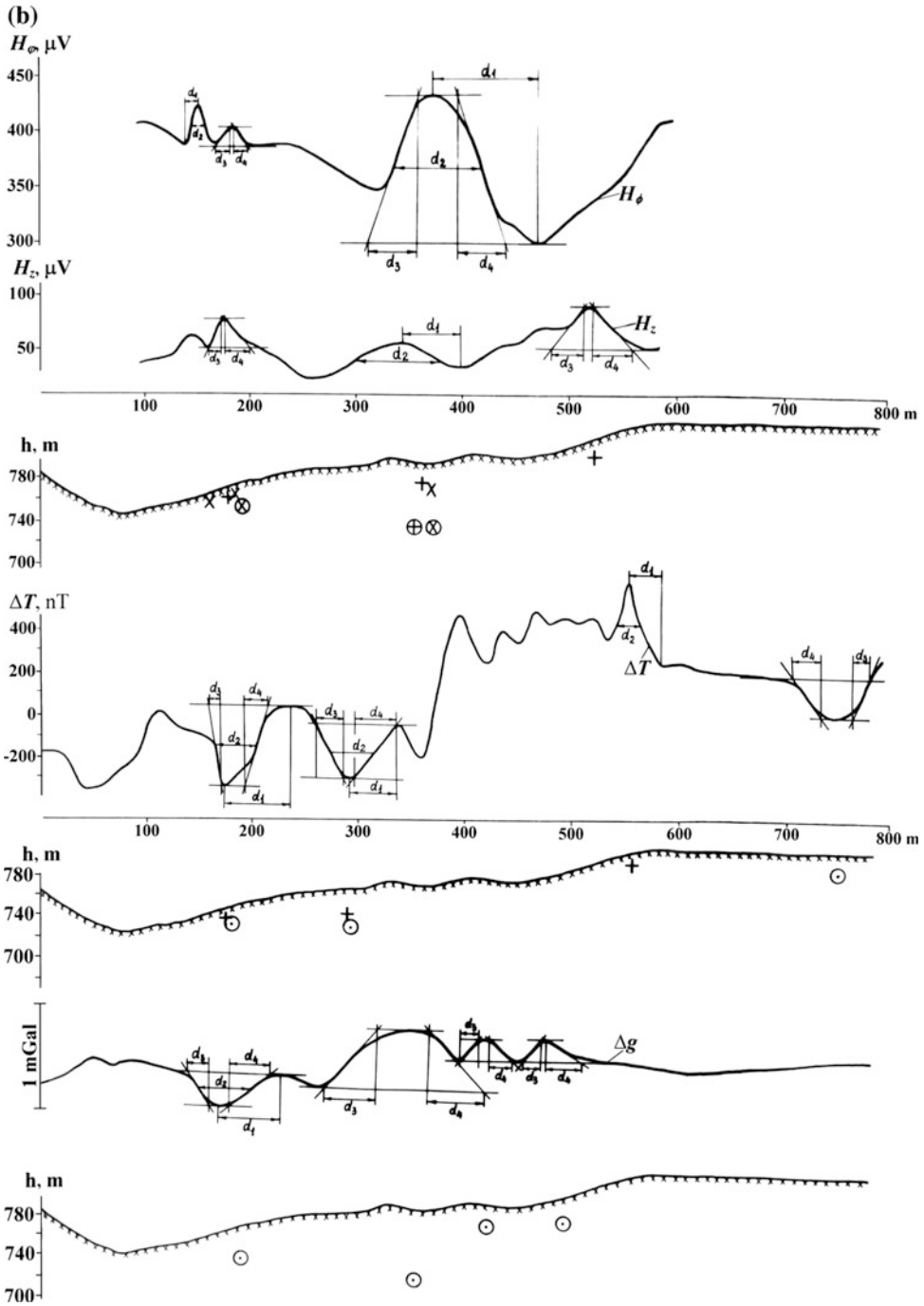

Fig. 8.24 (continued)

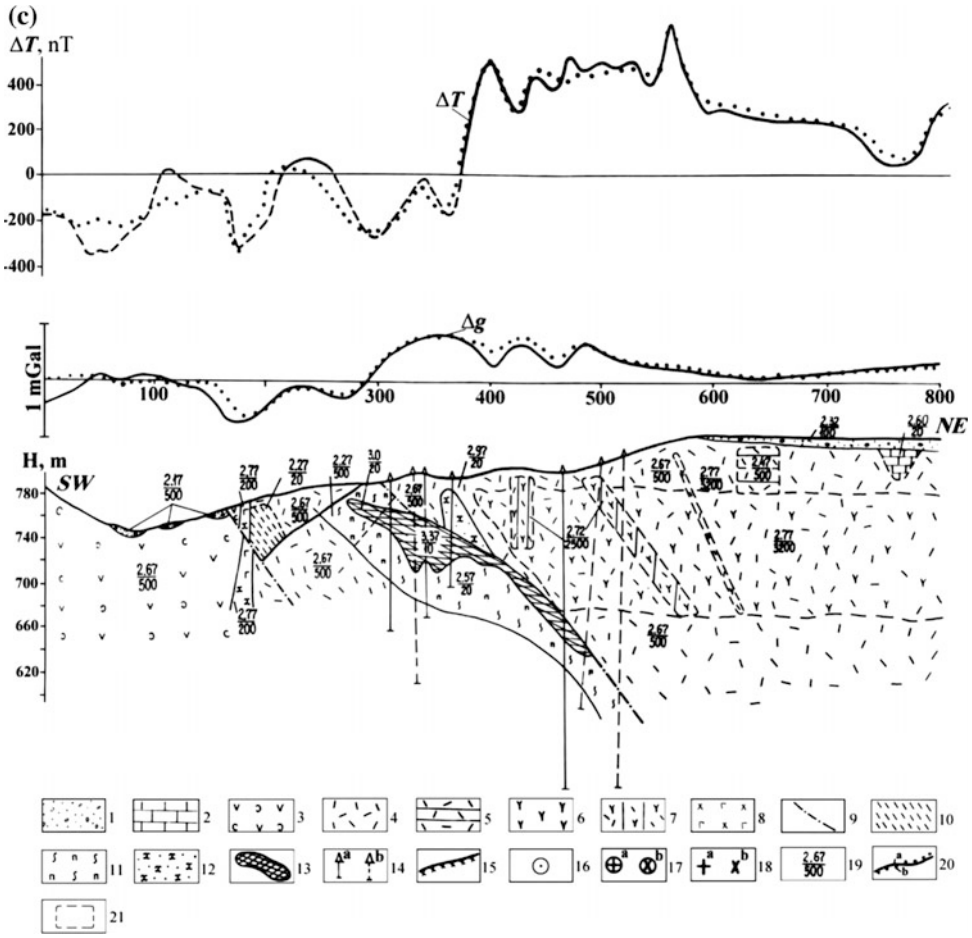

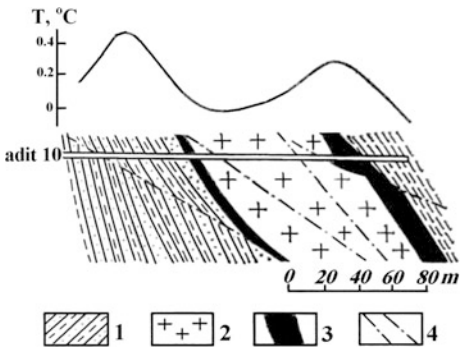

Fig. 8.25 Graph of the anomalous temperature distribution along the main opening of adit 10 in the Katsdagh polymetallic deposit, southern slope of the Greater Caucasus (Ginzburg et al. 1981; Eppelbaum et al. 2014). (*1*) sandstone, (*2*) liparite dacites, (*3*) massive copper–pyrite ore, and (*4*) faults

influence of the surface rugged relief, the depth of attenuation of annual temperature variations propagating from the earth's surface and other factors) is shown in Fig. 8.27b.

A residual anomalous temperature map is depicted in Fig. 8.27c. Clearly, the final anomalous map (Fig. 8.27c) differs considerably from the initial observations (Fig. 8.27a).

8.4.4 Self-potential Survey

An example of SP field changing at the various stages of underground mining in the Chiragidzor sulfur deposit (Lesser Caucasus) is shown in Eppelbaum and Khesin (2012).

8.4.5 Examples of Integrated Underground Observations

An impressive integration of gravity, temperature, and VLF observations in the Katsdagh deposit (Greater Caucasus) is presented in Fig. 8.28. Analysis of geophysical graphs in the

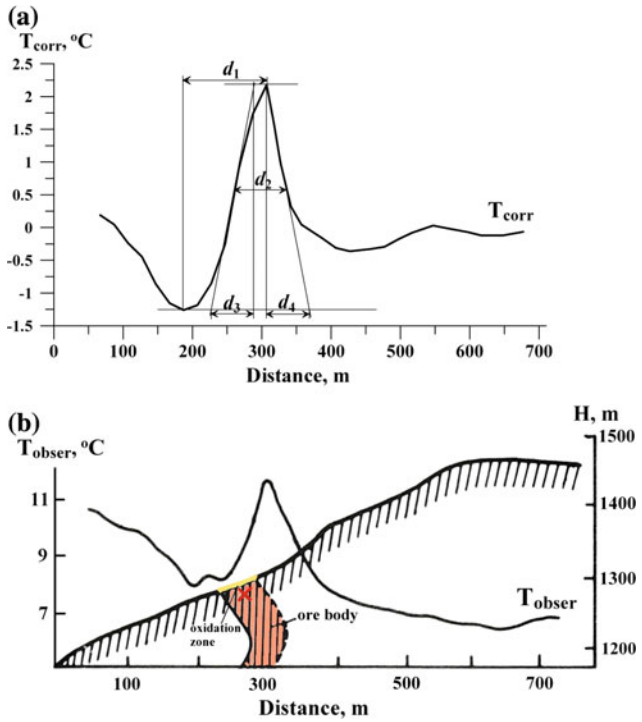

Fig. 8.26 Quantitative analysis of near-surface thermal investigations carried out in an adit of the Filizchay pyrite–polymetallic deposit (southern slope of the Greater Caucasus). Observed temperature field and geological section are adapted from (Borisovich et al. 1988). **a** Quantitative analysis of corrected temperature graph, **b** observed temperature field and geological section. The "×" symbol designates the position of the middle of the upper edge of the anomalous body

lower part of this figure and comparison of these data with the geological section provide rich data for integrated analysis and prospection. Certain geophysical graph distributions testify to the presence of previously unknown orebodies.

8.4.6 Seismic Methods

The seismic "central ray method" employed in the Filizchay deposit (southern slope of the Greater Caucasus) did not yield sufficiently reliable results since the area of high gradients of seismic velocities covered only the uppermost part of the geological section and information on the deeper horizons was extremely distorted (Karayev and Rabinovich 2000). Obviously, the recently developed seismic multifocusing technology for complex media (e.g., Gurevich et al. 2002; Berkovitch and Eppelbaum 2009) might be effectively applied in such areas. Undoubtedly, ore seismics must be integrated with other geophysical methods.

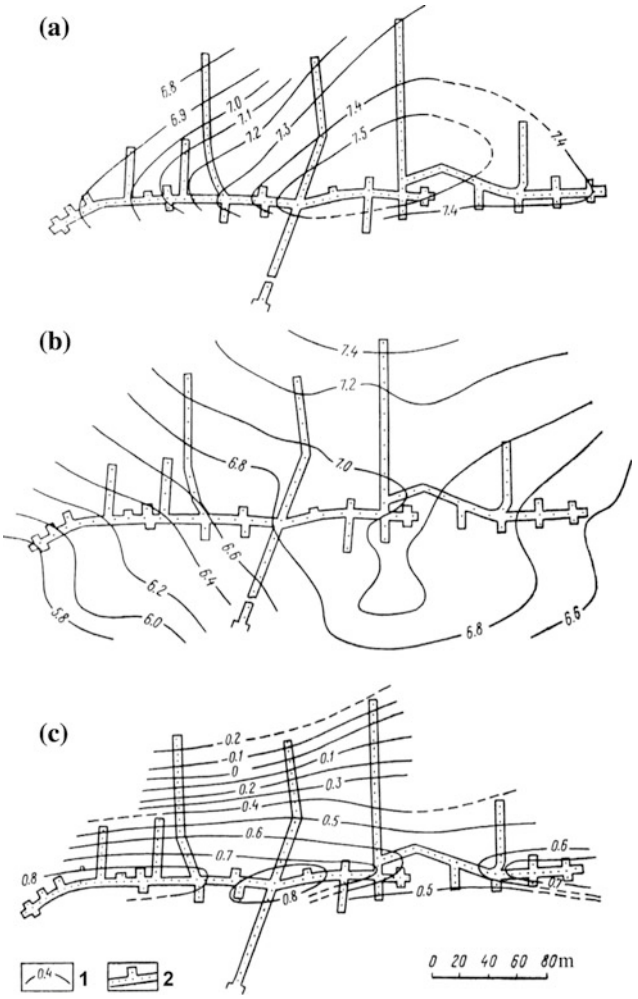

Fig. 8.27 Results of mine thermal prospecting in the Katsdagh pyrite–polymetallic deposit (southern slope of the Greater Caucasus) (after Ginzburg and Maslennikov, with minor modifications). Temperature maps: (**a**) observed values, (**b**) normal field, and (**c**) anomalous values. (*1*) temperature isolines and (*2*) underground shifts

8.5 Further Perspectives of Mining Geophysics in Azerbaijan

8.5.1 Development of Azerbaijan Mining Geophysics Database

The first priority in mining geophysics is the development of a comprehensive computer database covering all types of geophysical surveys (e.g., Eppelbaum and Khesin 2012), the observed data and the findings (Khesin et al. 1996).

The interpretation sequence and the interpretation procedures (stages) are listed in Table 8.4. As mentioned above,

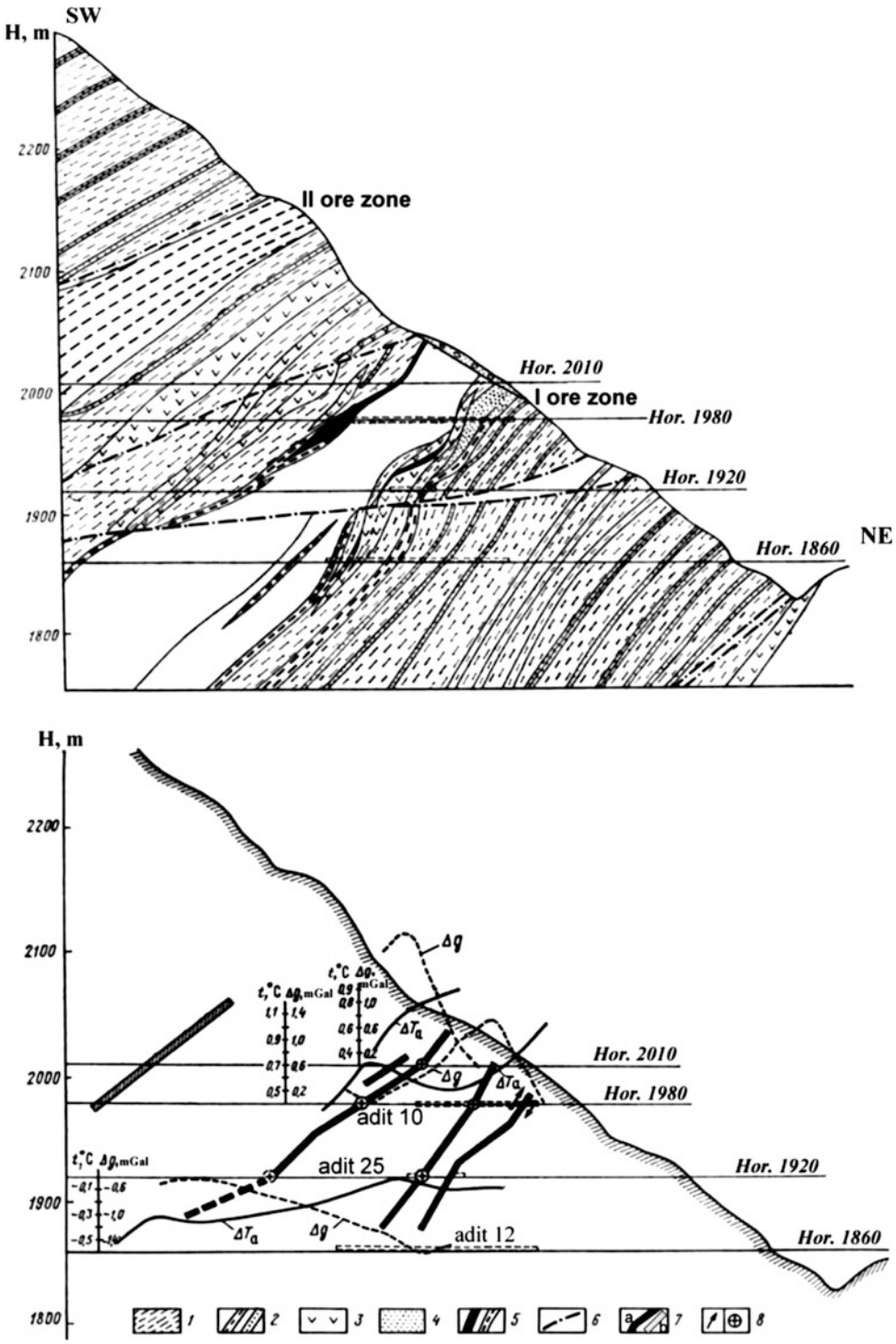

Fig. 8.28 Integrated geophysical investigations in mines of the Katsdagh deposit (southern slope of the Greater Caucasus, Azerbaijan) (Poltoratsky and Ginzburg 1989). (*1*) shales, (*2*) interbedding of shales, sandstones, and siltstones, (*3*) dioritic porphyry, (*4*) oxidizing zone, (*5*) polymetallic ores of I and II zones, (*6*) faults, (*7*) apparent beds of redundant: density (*a*) and thermal conductivity (*b*), and (*8*) current axes revealed by the VLF method

not all stages are equally susceptible to formalization and, as a consequence, to computer-assisted processing. However, mining geophysics databases make it possible to store the input and output data of all interpretation stages. Quite often in this case the output data of one stage are the input data for subsequent stages.

This interpretation technology is reviewed below.

1. Formulation of the initial model of the ore target

This stage basically employs the non-formal methods of prior information synthesis (Khesin et al. 1996). This yields a description of the geological space of the investigated area represented by a set of geological bodies (including ore objects) belonging to a particular association. These bodies

Table 8.4 Construction of mining geophysics databases: Main principles (after Eppelbaum and Khesin 2012)

No.	Interpretation procedures (stages)	Operations
1	Forming an initial ***PGM*** of ore target (on the basis of geological, drilling, and mining data as well as preliminary geophysical data examination including satellite imaging) aircraft, and ROV observations	Geological, geophysical and satellite data preparation and generalization, primary loading, and DB modification
2	Forming an indicator space of ore deposits according to the observation results	Computation of direct effects due to the relief forms and other known bodies. Excluding the computed effects from the observed fields
2.1	Eliminating disturbing factors due to the terrain relief effect and other known factors	Conversion of the upper half-space to different levels, averaging with different radii, computing gradients, calculating ruggedness measures, etc.
2.2	Computing secondary indicators by the initial field(s)	
3	Revealing and localizing; identifying the targets	Classification (taxonomy) of the investigation area by a specified (variable) set of indicators, including ruggedness. Correlation of linear zones and identifying ring zones. Determination of axes and contours of objects
4	Determination of the quantitative parameters of anomalous bodies	Parameter determination by application of quantitative analysis. Non-formalized simulation (modeling). Formalized simulation (optimization)
5	Integrated interpretation and physical–geological modeling; construction of a composite picture of the of ore deposit	Computing appropriate measures (probabilities, amount of information, etc.) by a set of fields of different kinds. Combined modeling of various fields
6	Graphic representation of the findings	Computer graphics operations (output of charts, schemes, plots, maps, 2D, and 3D physical–geological sections)

may be either diffused or localized and characterized by certain physical properties (for instance, density and magnetization). The coordinate representation of these objects is obtained according to description rules for each type of body. These data are loaded into the database together with the height information obtained over the area of investigation as a whole. In addition, gravity and magnetic fields as well as other measured fields are also loaded into the database.

2. Formulation of an indicator space

Drawing on the analysis of the observed fields and based on the objectives of the investigation, the interpreter makes decisions regarding the type of secondary indicators, ways to obtain them and the transformation parameters. If terrain corrections are called for, or correction of the fields due to large distant objects, appropriate data are loaded into the database as described above.

3. Revealing and localizing targets

Secondary indicators computed during the preceding stage are extracted from the database using special programs. The isoline maps are plotted for corresponding transforms. Their analysis and the display of the findings follow the rules given, for instance, in Khesin et al. (1996), Eppelbaum et al. (2011), and Eppelbaum and Khesin (2012). Data for initial modifications of the model of the geological target (ore manifestation, deposit or field) are obtained at this stage. They are introduced into the database.

4. Determination of quantitative parameters of anomalous body (inverse problem solution)

The substage involving choice of parameters for determination and preparation of the anomaly (numerical values or graphs) for computation precedes this stage (see Chap. 4 of this volume). At the end of this stage, additional data for model modification are obtained, and these data are introduced into the DB.

5. Integrated interpretation and physical–geological modeling

At the beginning of this stage, the interpreter has a sufficiently complete idea about the majority of sources of the anomaly field including deep-seated hidden sources. Therefore, the interpreter can distinguish objects (classes of objects) with expected properties. Physical–geological modeling on the basis of gravity, magnetic, resistivity, and

other fields is done with software in an interactive mode. At each modeling stage, the fields caused by the entire model are computed over a given profile (or a group of profiles). These fields are compared with the observed ones, and a decision is made regarding the necessary changes to the model and the nature of these changes. The modifications may be related to the physical properties of individual bodies or to the form of these bodies' surfaces (or both); certain bodies can be eliminated or, on the contrary, added. The changes are made on the basis of the analysis of both fields, which characterizes the integrated nature of physical–geological modeling. The modifications are loaded into the DB with the help of a special subroutine. Field computations, comparison of the computed fields with the observed ones, and modifications of the model are iterated until the fields fall within the defined limits of observation accuracy.

6. Developing a final model

Since modeling applies to geological objects rather than to physical sources, the final model has a geological content. The assignment of new bodies introduced during the selection to a certain classification is determined by analogy with bodies with close physical properties, proceeding from general geological notions in the forms of graphs, charts, maps, 3D ***PGM***, etc.

8.5.2 ROV Geophysical Surveys for the Delineation of New Ore Deposits

A long-term perspective in mining geophysics in the Caucasus, as in other regions of the world, involves the broad-scale application of geophysical measurements by the use of remote-operated vehicles (ROV) (e.g., Eppelbaum 2010; Eppelbaum and Mishne 2011). The main advantages of ROVs are the absence of an aircraft crew (GPS controlled unmanned surveys can be carried out even at very low altitudes and in risky conditions). In addition, most methods of geophysical field analysis require knowledge of the field distribution at different levels over the Earth's surface. The ROV facilitates the collection of these data without having to use transformation methods. Finally, unmanned air geophysical surveys are extremely cheap (many tens of times less than conventional aircraft surveys, and in many cases are less expensive than a land survey). These ROV geophysical surveys (first of all, magnetic and VLF) must be integrated with ground geophysical investigations and satellite imaging.

8.5.3 Geophysical–Geological Examination of Old Azerbaijanian Mine Spoils

Some geophysical methods (primarily, electric and electromagnetic) may be used to examine old Caucasian mine spoils (for instance, such "old" mines in today's terms are located in the Gedabey area of the Lesser Caucasus). The old spoils, according to Samykina et al. (2005) and Surkov et al. (2008), may contain large amounts of economically valuable minerals exceeding the volume of minerals mined throughout the entire history of humanity.

References

Abdullayev, D.I. and Bagirov, A.A., 1996. Mine-borehole geophysics. *In*: (Kerimov, K.M., Ed.) *Geophysical Investigations in Azerbaijan*, Sharg-Garb, Baku, 272-274 (in Russian).

Alexeyev, V.V., 1971. Application of the self-potential method under mountainous terrain relief. *Prospecting and Protection of Entrails* (*Razvedka i Okhrana Nedr*), No. 9, 38-43 (in Russian).

Azizbekov, Sh.A., Alizadeh, K.A., Shikalibeyli, E.Sh. and Gadjiev, T. G. (Eds.), 1972. *Geology of the USSR*, *Azerbaijan*, Vol. **XLVII**, Nedra, Moscow (in Russian).

Bagirov, A.A., Bektashi, A.P. and Malakhova, V.A., 1996. Copper-porphyry deposits. *In*: (Ed. K.M. Kerimov), *Geophysical Investigations in Azerbaijan*. Sharg-Garb, Baku, 286-288 (in Russian).

Balavadze, B.K., 1944. The results of electrometric investigations of Dashkesan cobalt deposits. *Bull. of the Georgian Acad. of Sci.* (Tbilisi), **5**, No. 10, 365-374 (in Russian).

Berezkin, V.M., 1967. *Calculation of Terrain Relief and Intermediate Layer Effects in Gravity Prospecting*. Nedra, Moscow (in Russian).

Berkovitch, A.L. and Eppelbaum, L.V., 2009. From seismic inversion to applied optics: A novel approach to design of complex systems. *Scientific Israel*, No 2, 12-26.

Borisovich, V.T. and Eppelbaum, V.M. (Eds.), 1988. *Optimization of Ore Exploration in Mountainous Regions*. Nedra, Moscow (in Russian).

Borisovich, V.T., Eppelbaum, V.M. and Ginzburg, S.N., 1988. Optimization of geophysical investigations in mountainous regions on the basis of integration of geophysical and mining-drilling works. *In*: (Borisovich, V.T. and Eppelbaum, V.M., Eds.). *Optimization of Ore Exploration in Mountainous Regions*, Nedra, Moscow, 123-133 (in Russian).

Borodaevskaya, M.B., Krivtsov, A.T. and Shirai, E.P., 1977. *Types of pyrite-bearing provinces and methods for predicting pyrite mineralization*. Review of VIEMS, Ser. Geology and Methods for Searching Useful Minerals, Moscow (in Russian).

Brodovoi, V.V., Ginzburg, S.N. and Haldeyev, O.D., 1989. Searching and prospecting of lead and zinc. *In*: (Brodovoi, V.V., Ed.), *Borehole and Mining Ore Geophysics*, Vol. **II**, Nedra, Moscow, 297-310 (in Russian).

Cheremensky, G.A., 1972. *Geothermics*. Nedra, Leningrad (in Russian).

Eppelbaum, L.V., 1989. The development of methods for processing and interpretation of natural geophysical fields in prospecting for pyrite ores under mountainous conditions. *Ph.D Thesis*, Institute of Geophysics (Georgian Acad. of Sciences), Tbilisi, 1989 (in Russian).

Eppelbaum, L.V., 1991. Examples of terrain corrections in the VLF-method in the Caucasian region, USSR. *Geoexploration*, **28**, 67-75.

Eppelbaum, L.V., 1999. Near-surface thermal prospecting in petroleum geology. *In: Applied Geothermics for Petroleum Engineers*, Elsevier, 274-301.

Eppelbaum, L.V., 2010. An advanced methodology for Remote Operation Vehicle magnetic survey to delineate buried targets. *Trans. of the 20th General Meeting of the Intern. Mineralogical Association*, ***CH30G: Archaeometry (general session): Composition, technology and provenance of archaeological artifacts***, Budapest, Hungary, p. 103.

Eppelbaum, L.V., 2014. Estimating informational content in geophysical observations on example of searching economic minerals in Azerbaijan. *Izvestiya* (*Proceedings*), *Acad. Sci. Azerb. Rep., Ser.: Earth Sciences*, Nos. 3-4, 31-40.

Eppelbaum, L.V., Alperovich, L., Zheludev, V. and Pechersky, A., 2011. Application of informational and wavelet approaches for integrated processing of geophysical data in complex environments. *Proceed. of the 2011 SAGEEP Conference*, Charleston, South Carolina, USA, **24**, 24-60.

Eppelbaum, L.V. and Khesin, B.E., 1988. Physical-geological models for pyrite deposits of the Filizchay and Lesser-Caucasian type (in Russian). *Proceed. of the All-Union Meeting "Multifactor Ore Deposit Models as the Basis for Development of the Effective Methods for Search, Evaluation and Prospecting"*. Tskhaltubo (Georgia), USSR, 126-127.

Eppelbaum, L.V. and Khesin, B.E., 1992. *VLF*-method: elimination of noise and quantitative interpretation. *Transactions of Regional Symposium on Electromagnetic Compatibility* "1992 - From a Unified Region to a Unified World", Section "LF to ULF Electromagnetics and the Earth", 5.2.1, Tel Aviv, (1992), 1-6.

Eppelbaum, L.V. and Khesin, B.E., 2002. Some common aspects of magnetic, induced polarization and self-potential anomalies interpretation: implication for ore target localization. *Collection of Selected Papers of the **IV** Intern. Symp. on Problems of Eastern Mediterranean Geology*, 279-293.

Eppelbaum, L.V. and Khesin, B.E., 2004. Advanced 3-D modelling of gravity field unmasks reserves of a pyrite-polymetallic deposit: A case study from the Greater Caucasus. *First Break*, **22**, No. 11, 53-56.

Eppelbaum, L.V. and Khesin, B.E., 2012. Geophysical Studies in the Caucasus. *Springer*, 411 p.

Eppelbaum, L.V., Kutasov, I.M. and Pilchin, A.N., 2014. Applied Geothermics. *Springer*, 751 p.

Eppelbaum, L.V. and Mishne, A.R., 2011. Unmanned Airborne Magnetic and VLF investigations: Effective Geophysical Methodology of the Near Future. *Positioning*, **2**, No. 3, 112-133.

Finkelstein, M. and Eppelbaum, L.V., 2015. Classification of Archaeological Targets by the Use of Temporary Magnetic Variations Examination. Trans. of the 11th EUG Meet., Geophysical Research Abstracts, **17**, EGU2015-6504, Vienna, Austria, 1-2.

Gadjiev, T.G., Karkoshkin, A.I., Khesin, B.E., Alexeyev, V.V., Potapova, E.I. and Salekhli, T.M., 1984. *Petrodensity Characteristics of Geological Associations in Azerbaijan*. Azerneshr, Baku (in Russian).

Ginzburg, S.N., 1982. VLF-method for searching and prospecting of pyrite-polymetallic deposits. *Prospecting and Protection of Entrails* (*Razvedka i Okhrana Nedr*), No.9, 39-44 In Russian).

Ginzburg, S. et al., 1981. *Underground geophysical investigations in ore deposits of Belokan-Zakatala ore field*. Unpublished Report of *TzNIGRI* (*Central Scient. Inst. of Non-Ferrous and Precious Metals*), Moscow (in Russian).

Gorzhevsky, D.I., Kurbanov, N.K., Filatov, E.I. et al., 1987. *Methodological Principles of Prediction and Prospecting for Lead and Zinc Deposits*. Nedra, Moscow, 1987 (in Russian).

Gurevich, B., Keydar, S. and Landa, E., 2002. Multifocusing imaging over an irregular topography. *Geophysics*, **67**, No. 2, 639-643.

Ismailzadeh, T.A., Gadjiev, T.G., Khesin, B.E., Karkoshkin, A.I., Alexeyev, V.V. and Metaxa, Kh.P., 1983a. *Petromagnetic Map of the Azerbaijan SSR*, *Scale 1:500,000*, Printing Map Factory, Leningrad.

Ismailzadeh, T.A., Gadjiev, T.G., Khesin, B.E., Karkoshkin, A.I., Alexeyev, V.V. and Potapova, E.I., 1983b. *Petromagnetic Characteristics of Azerbaijan*. Elm, Baku (in Russian).

Karayev, N.A. and Rabinovich, G.Ya., 2000. *Ore Seismic Prospecting*. Geoinformmark, Moscow (in Russian).

Kerimov, K.M. (Ed.), 1996. *Geophysical Investigations in Azerbaijan*. Sharg-Garb, Baku (in Russian).

Khain, V.E., 1984. *Regional Geotectonics*. *The Alpine Mediterranean Belt*. Nedra, Moscow (in Russian).

Khalilov, A.A., 1996. Chovdar barite deposit. *In*: (Kerimov, K.M., Ed.) *Geophysical Investigations in Azerbaijan*, Sharg-Garb, Baku, 292-293 (in Russian).

Khesin, B.E., Alexeyev, V.V., and Eppelbaum, L.V., 1988. Optimization of geophysical investigations in mountainous regions by increasing the effectiveness of interpretation. *In:* (Borisovich, V.T. and Eppelbaum, V.M., Eds.), *Optimization of Ore Exploration in Mountainous Regions*. Nedra, Moscow, 79-122 (in Russian).

Khesin, B.E., Alexeyev, V.V. and Eppelbaum, L.V., 1993. Investigation of geophysical fields in pyrite deposits under mountainous conditions. *Jour. of Applied Geophysics*, **30**, 187-204.

Khesin, B.E., Alexeyev, V.V. and Eppelbaum, L.V., 1996. Interpretation of Geophysical Fields in Complicated Environments. *Kluwer Academic Publishers* (*Springer*), *Ser.: Modern Approaches in Geophysics*, 368 p.

Khesin, B.E., Alexeyev, V.V. and Eppelbaum, L.V., 1997. Rapid methods for interpretation of induced polarization anomalies. *Jour. of Applied Geophysics*, **37**, No.2, 117-130.

Khesin, B.E., Alexeyev, V.V. and Metaxa, Kh.P., 1983. *Interpretation of Magnetic Anomalies in the Conditions of Oblique Magnetization and Rugged Topography*. Nedra, Moscow (in Russian).

Khesin, B.E. and Eppelbaum, L.V., 1994. Near-surface thermal prospecting: Review of processing and interpretation. *Geophysics*, **59**, No.5, 744-752.

Khesin, B.E. and Eppelbaum, L.V., 1997. The number of geophysical methods required for target classification: quantitative estimation. *Geoinformatics*, **8**, No.1, 31-39.

Khesin, B.E. and Sattarov, I., 1967. Efficiency of gamma-ray log in Dashkesan and Filizchay ore fields. *Izvestiya*, *Acad. Nauk Azerb. SSR, Ser. Nauki o Zemle*, No. 6, 43-46 (in Russian).

Logachev, A.A. and Zakharov, V.P., 1979. *Magnetic Prospecting*. Nedra, Leningrad (in Russian).

Lomtadze, V.V., 1982. *Software for Geophysical Data Processing*. Nedra, Leningrad (in Russian).

Lukavchenko, P.I., 1951. *Tables and Nomographs for Calculating Terrain Gravity Corrections in Survey with Gravimeters*. Gostoptekhizdat, Moscow (in Russian).

Malakhova, V.A., 1996. Iron-ore deposits of Dashkesan district. *In*: (Kerimov, K.M., Ed.) *Geophysical Investigations in Azerbaijan*, Sharg-Garb, Balu, 292-293 (in Russian).

Mekhtiyev, Sh.F., Gadjiev, T.G., Kashkay, M.A. and Akhmedov, A. M., 1976. *Geology of the USSR*. Vol. **XLVII**, Azerbaijan Republic. Economic Deposits. Nedra, Moscow (in Russian).

Muradkhanov, S.A., 1971. *Interpretation of geophysical data from the wells of Filizchay deposit using statistical methods*. Express-information of VIEMS, Ser. Region., Applied and Borehole Geoph., Moscow, No.88 (in Russian).

Muradkhanov, S.A. and Magerramov, M.R., 1996. Borehole logging. *In*: (Ed. K.M. Kerimov) *Geophysical Investigations in Azerbaijan*, Sharg-Garb, Baku, 275 (in Russian).

Nagatha, T., 1961. *Rock Magnetism*. Maruzen Co., Tokyo.

Nemtsov, L.D., 1967. *High-Precise Gravity Prospecting*. Nedra, Moscow (in Russian).

Ostrovsky, E.Ya., 1980. Comparative analysis of results of geo-observations. *Soviet Geology*, No. 10, 105-114 (in Russian).

Petrovsky, A.A. and Skaryatin, R.I., 1929. Ondometrical works of Institute of Applied Geophysics. *Proc. of the IAG*, No. 5 (in Russian).

Poltoratsky, V.V. and Ginzburg, S.N., 1989. Gravity prospecting. *In*: (Brodovoi, V.V., Ed.), *Borehole and Mining Geophysics*, Vol. **II**, Nedra, Moscow, 190-209 (in Russian).

Reford, M.S. and Sumner, I.S., 1964. Aeromagnetics. *Geophysics*, **29**, No.4, 482-516.

Ryss, Yu.S., 1983. *Geoelectrochemical Prospecting Methods*. Nedra, Leningrad (in Russian).

Samykina, E., Surkov, A., Eppelbaum, L. and Semenov, S., 2005. Do old spoils contain large amounts of economic minerals? *Minerals Engineering*, **18**, No. 6, 643-645.

Solovov, A.P., 1985. *Geochemical Methods for Searching Useful Minerals*. Nedra, Moscow (in Russian).

Surkov, A., Samykina, E., Eppelbaum, L. and Semenov, S., 2008. The main reason for mineral loss in gravity dressing. *The Open Mineral Processing Journal*, No.1, 37-44.

Tvalchrelidze, G.A., 1978. On types of pyrite deposits and provinces. *Izvestiya, USSR Acad. of Sci., Ser. Geolog*., No.10, 5-16 (in Russian).

Veselov, K.E., 1986. *Gravimetric Survey*. Nedra, Moscow (in Russian).

Zaitseva, I.V., Nagiyev, V.I., Kurbanov, N.K. et al., 1988. Detailed prospecting of Katekh pyrite-polymetallic deposit. Vols. 1 & 2, "*Azerbaijangeologiya*" *Association* (in Russian).

Zverev, V.P., Dolnikov, V.A., Khutorsky, M.D. and Fotogdinov, R.A., 1982. Thermal effect and sulphide oxidation rate in the Katekh deposit (as applied to the southern slope of the Greater Caucasus). *Doklady USSR Acad. of Sci.*, **265**, No.4, 960-962.

Engineering, Environmental, and Archaeological Geophysics

9

9.1 Engineering Geophysics

9.1.1 Monitoring of Oil and Gas Pipelines

Geophysical monitoring of oil and gas pipelines (primarily in Baku–Tbilisi–Ceyhan (BTC) and South Caucasus Pipelines (SCP)) (Balat 2006) is one of the most important problems in Caucasus engineering geophysics (Rabinowitz et al. 2004; Babazade et al. 2008; Tanircan et al. 2011; Bayramov et al. 2016) (Fig. 9.1). It is obvious that for this purpose, ground (e.g., Modin 2010) and satellite (e.g., Kostianoy et al. 2008) observations as well as underground geophysical monitoring can be used. An integrated wavelet approach (Eppelbaum et al. 2011) that associates different geophysical methods including satellite imaging as well topography data has proved to be the most successful.

Bayramov et al. (2016) carried out a comprehensive examination of ground cover restoration and soil erosion risks along petroleum and gas pipelines in Azerbaijan territory using GIS and remote sensing. Figure 9.2 shows important relationships between elevation and precipitation (a), elevation and evapotransportation (b), elevation and annual air temperature (c), and elevation and land surface temperature (d). Such an integration approach to these important targets is of high perspective, and the following stage of environmental analysis must include, apparently, employment of multifactor (or similar methodology) analysis.

9.1.2 Investigation and Monitoring of Dams

A comparative large number of studies have been devoted to seismic zonation and monitoring of the Caucasus dams. For instance, Agamirzoev et al. (1986) carried out a seismic micro-zonation of the vicinity of the Enikend dam located in Central Azerbaijan at the junction of the Lesser Caucasus and the Kur Depression.

9.1.3 Investigation of Rockslide

Investigation of rockslide by the method of vertical electric sounding (VES) was applied in Baku, Absheron, and various areas of Azerbaijan (e.g., Aliyev et al. 2008; Salamov et al. 2014, 2015).

An effective example of VES application in the Bailov area of Baku is given in Fig. 9.3. As a result of comprehensive VES data analysis, the dangerous sliding planes were delineated.

9.2 Environmental Geophysics

9.2.1 Radioactive Monitoring

Different authors paid attention to radioactive monitoring in Azerbaijan (e.g., Aliyev and Zolotovitskaya 1996, 2000, 2005; Aliyev et al. 2001; Feyzullayev et al. 2005b).

The developed map of radon volumetric activity indicates of Absheron peninsula indicates that on the most part of the peninsula, values of radon concentration range from 25 to 95 Bq/m^3 (Fig. 9.4).

A gamma survey at the Absheron peninsula (Azerbaijan) revealed a few spots of heightened radioactivity and a few districts with extremely high radioactivity up to 3000 μR/h that obviously constitutes a danger for people working at these sites (Aliyev and Zolotovitskaya 1996). These districts are located near old oil- fields and around iodine factories. Unfortunately, contamination of some new (previously "clean") areas increases very quickly. For instance, gamma radiation on Gum isle (Caspian Sea) rose from 4–5 to 600–700 μR/h in 5 years (Zolotovitskaya 2003).

It is established, for instance, that Oligocene clays of the Greater Caucasus and Talysh substantially differ in terms of quantitative and qualitative parameters of organic matter, its maturity, integral radioactivity, and composition of radioactive elements (Feyzullayev et al. 2005b). The most

A.A. Alizadeh et al., *Geosciences of Azerbaijan*,
Regional Geology Reviews, DOI 10.1007/978-3-319-40493-6_9

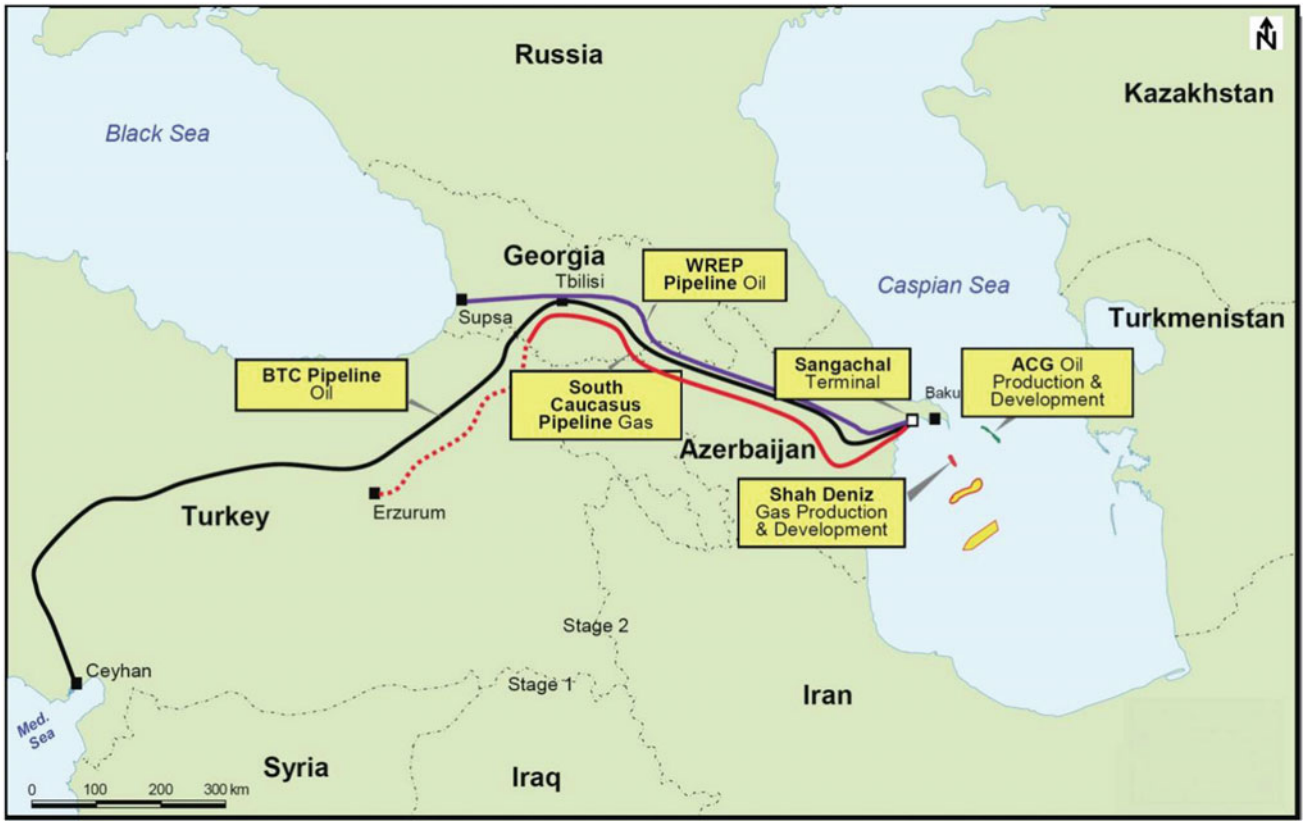

Fig. 9.1 Map showing recent major projects in the South Caspian (after Riley et al. 2011, with small modifications)

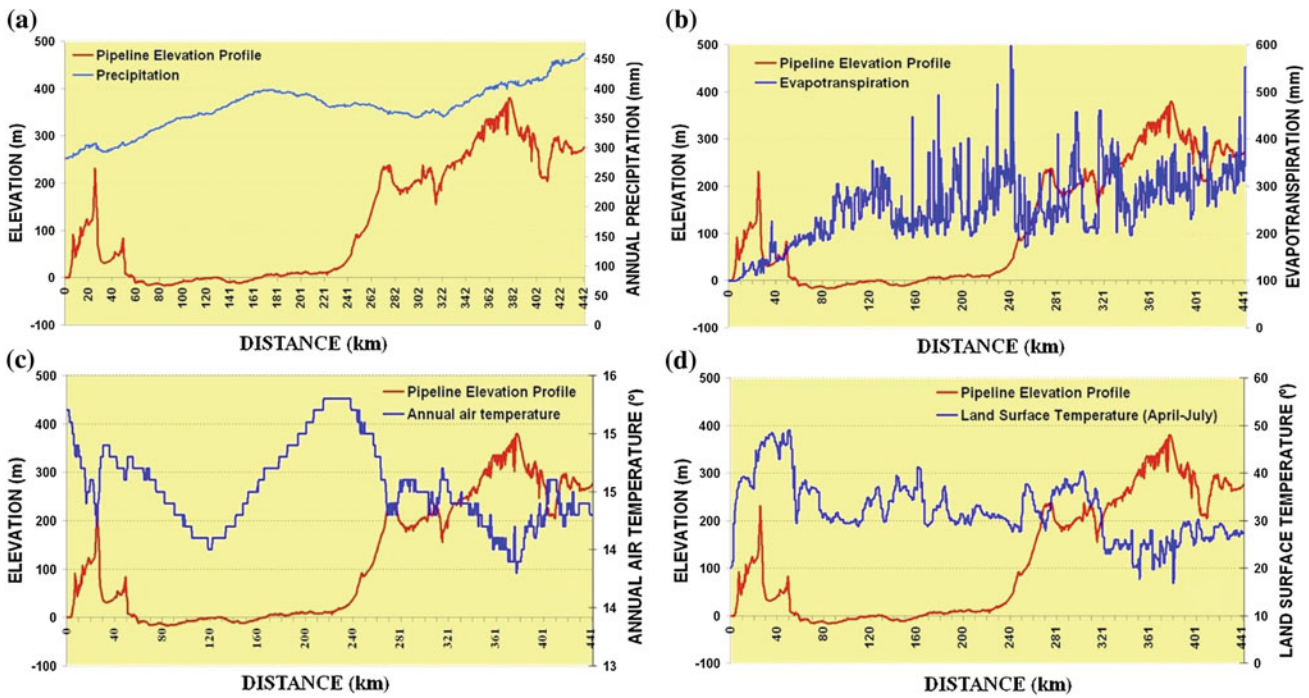

Fig. 9.2 **a** Elevation and precipitation along BTC and SCP pipelines; **b** elevation and evapotranspiration along BTC and SCP pipelines; **c** elevation and land surface temperature along the corridor of BTC and SCP pipelines; **d** elevation and annual air temperature along BTC and SCP pipelines (after Bayramov et al. 2016)

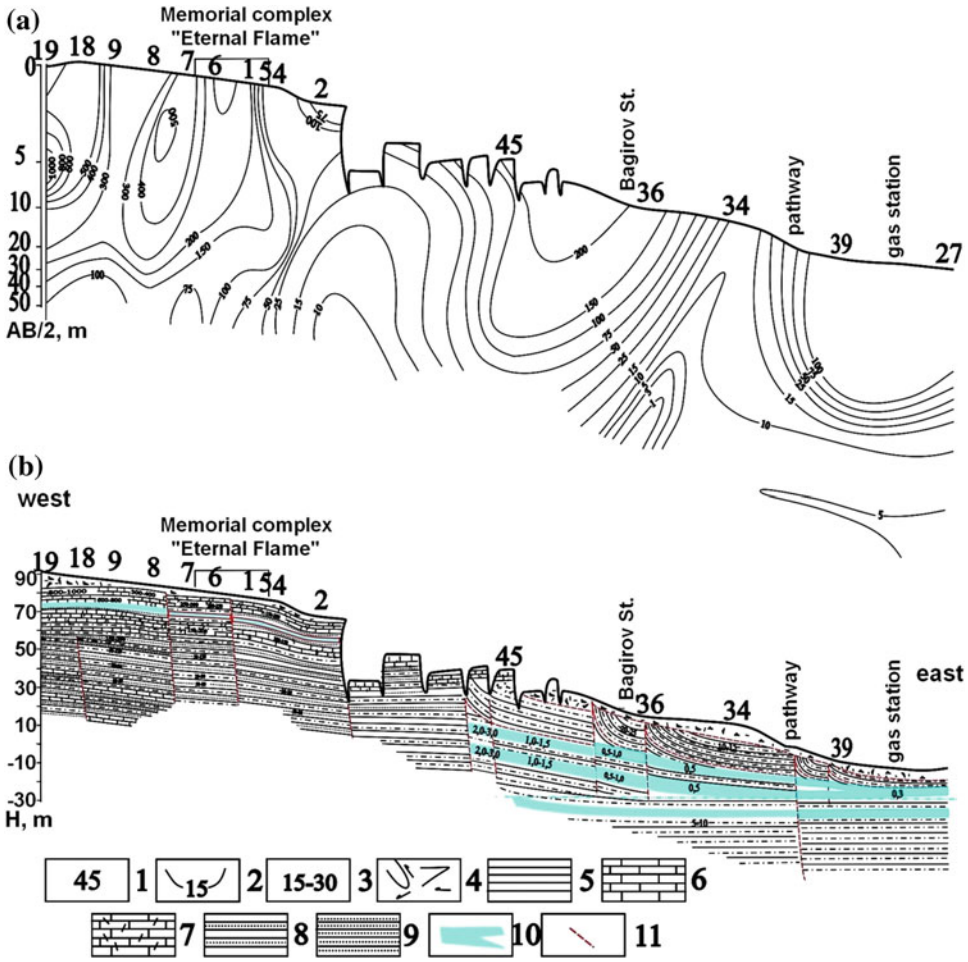

Fig. 9.3 Application of VES in the rockslide area of the Bailov district, Baku. **a** geoelectric section, **b** physical–geological model (from unpublished materials of A.M. Salamov). (*1*) VES number, (*2*) isolines of apparent electric resistivity, (*3*) specific electric resistivity, Ohm m, (*4*) technical soil, (*5*) clays, (*6*) limestone, (*7*) fissured limestone, (*8*) sandy clays, (*9*) clay sands, (*10*) revealed sliding plane, and (*11*) revealed explosive violation

significant quantitative variations in clays are typical of uranium (Greater Caucasus) and Thorium (Talysh) (Table 9.1).

It is well known that radon gas distribution in subsurface and surface is of great danger for people (e.g., Mishel 1987; Blue et al. 1989). It should be pointed out that radon measurements in the subsurface are influenced by a number of factors (Eppelbaum and Finkelstein 1998; Finkelstein et al. 2006):

$$F_{\text{sum}} = F_1 + F_2 + F_3 + F_4 + F_5 + F_6 + F_7 + F_8, \qquad (9.1)$$

where F_1 is the function of Rn emanation from the soil (including the influence of the external temperature); F_2 is the daily variation in Rn due to vertical warm convection arising shortly after sunrise; F_3 is the variation in Rn due to rain and Rn dissolved in underground water; F_4 is the variation in Rn due to fluctuations in atmospheric pressure; F_5 is the variation in Rn due to air movement (direction and speed of wind or ventilation); F_6 is the variation in Rn related to deep geodynamics, especially near earthquake epicenters; F_7 is the variation in Rn due to strong geomagnetic storms in periods of solar chromo spherical bursts; F_8 is the variation in Rn caused by the settling of aerosols following dust storms, which can transfer a number of radioactive elements and may lead to a sharp increase in radon.

The best ways of eliminating different kinds of noise, including shallow noise occurring down several meters in caves and more deeply in underground tunnels, are described in Finkelstein et al. (2006).

9.2.2 Geophysical Investigation of Mud Volcanoes

9.2.2.1 Gravity

Brief geological characteristics of mud volcanoes are presented in the Chap. 7 of Volume I. Here, we discuss some geophysical indicators of mud volcanoes and their eruptions.

Kadirov and Mukhtarov (2004) overlaid the position of mud volcanoes in Azerbaijan on the gravity map in the Bouguer reduction (Fig. 9.5).

Edifices over 200 m high exist in Azerbaijan, with large eruptions in some cases producing flames of a similar scale.

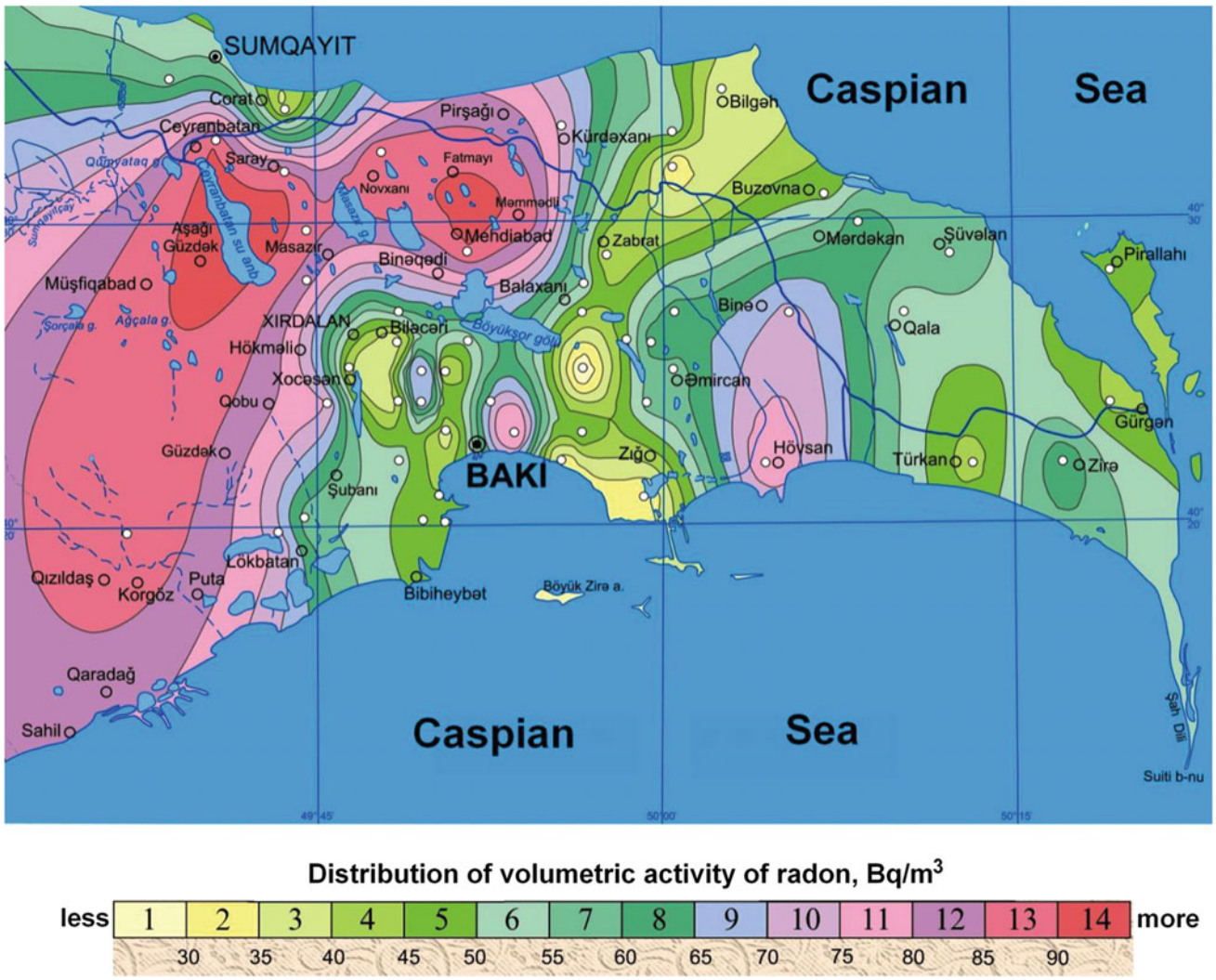

Fig. 9.4 Distribution of radon volumetric activity in the Absheron peninsula

In Azerbaijan, eruptions are driven from a deep mud reservoir which is connected to the surface even during dormant periods, when seeping water still comes from the depths. Seeps have temperatures up to 2–3 °C above the ambient temperature (Planke et al. 2003). The comparison of heat flow, gravity field and terrain relief over some mud volcanoes are shown in Fig. 9.6.

Seismic wave propagation in mud volcanoes zones is very complicated. In most cases, seismic prospecting has only provided some general data on the roots of mud volcanoes that are usually associated with crustal zones of deep-seated Mesozoic or Paleogene-Miocene highs (uplifts), where feeder channels originate from depths as low as 10 km (Rakhmanov 1987).

Results of physical–geological modeling by the use of gravity field along the profile Lokbatan–Akhtarma-Puta–Gushkhana are presented in Fig. 9.7. The density of intermediate layer was selected as 2.3 g/cm^3. As a result, the local negative Bouguer gravity anomalies of −5, −3, and −2 mGal were obtained in the areas of the Lokbatan, Akhtarma-Puta, and Gushkhana mud volcanoes, respectively. The initial geological–geophysical model this profile is represented by seven contact boundaries: (1) Akchagyl base (N_2^2; density contrast is +0.01 g/cm^3); (2) tentative seismic horizon in the productive sequence (N_2^1; density contrast is +0.04 g/cm^3); (3) top of the Kirmakinsk arenaceous formation (N_2^1; density contrast is +0.08 g/cm^3); (4) base of the Kirmakinsk formation (N_2^1; density contrast is −0.2 g/cm^3); (5) boundary between Middle Pliocene—Lower Pliocene and Lower Miocene—Oligocene sequences ($P_3 - N_1^1$; density contrast is −0.25 g/cm^3); (6) boundary between the Oligocene (P_3) and the Eocene ($P_1 + P_2$;

Table 9.1 Contents of radioactive elements and level of integral radioactivity in Oligocene clays of the Greater Caucasus and Talysh (Feyzullayev et al. 2005b)

Section	Number of examined samples	Uranium (ppm)	Thorium (ppm)	Potassium (%)	Integral radioactivity (μR/h)
Greater Caucasus					
Sumgayitchay	5	3.1 – 17.3 / 8.8	0 / 0	2.1 – 3.1 / 2.61	29 – 32 / 31.4
Perekeshkyul	4	0.2 – 2.8 / 2.0	0 – 4.6 / 1.25	1.2 – 2.0 / 1.61	–
Average	9	0.2 – 17.3 / 5.8	0 – 4.6 / 0.6	1.2 – 3.1 / 2.2	29 – 32 / 31.4
Talysh					
Perembel	1	0.8 / 0.8	5.8 / 5.8	2.2 / 2.2	30 / 30
Yardymly	4	1.0 – 3.2 / 2.2	2.3 – 16.3 / 6.6	1.9 – 5.1 / 3.0	27 – 32 / 29.3
Dashkend	3	1.4 – 8.3 / 4.2	1.4 – 11.7 / 5.7	3.0 – 5.6 / 3.9	30 / 30
Surrug	2	3.8 – 7.3 / 5.6	0 – 4.3 / 2.1	1.7 – 3.7 / 2.7	30 / 30
Arus	1	3.9 / 3.9	0 / 0	2.8 / 2.8	30 / 30
Vileshchay	10	0.7 – 5.0 / 2.6	0 – 9.3 / 3.2	2.2 – 3.3 / 2.7	23 – 30 / 27
Average	21	0.7 – 8.3 / 3.0	0 – 16.3 / 4.1	1.7 – 5.6 / 2.9	23 – 32 / 28.5

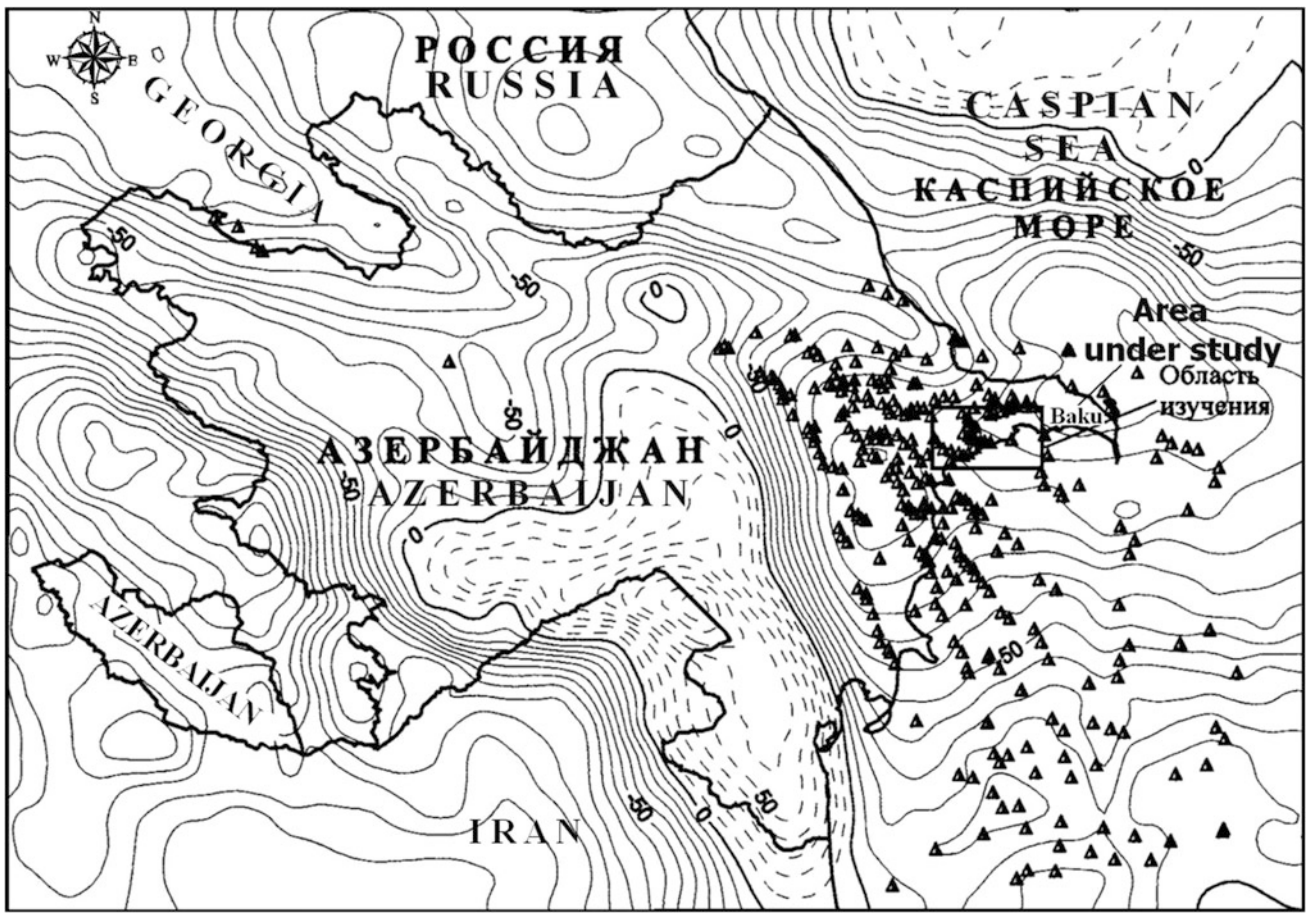

Fig. 9.5 Distribution of mud volcanoes (*black triangles*) in Azerbaijan and Bouguer gravity data (Kadirov and Mukhtarov 2004). Isoanomals (in milligals): *solid lines* denote negative values, and *dashed lines* denote positive values

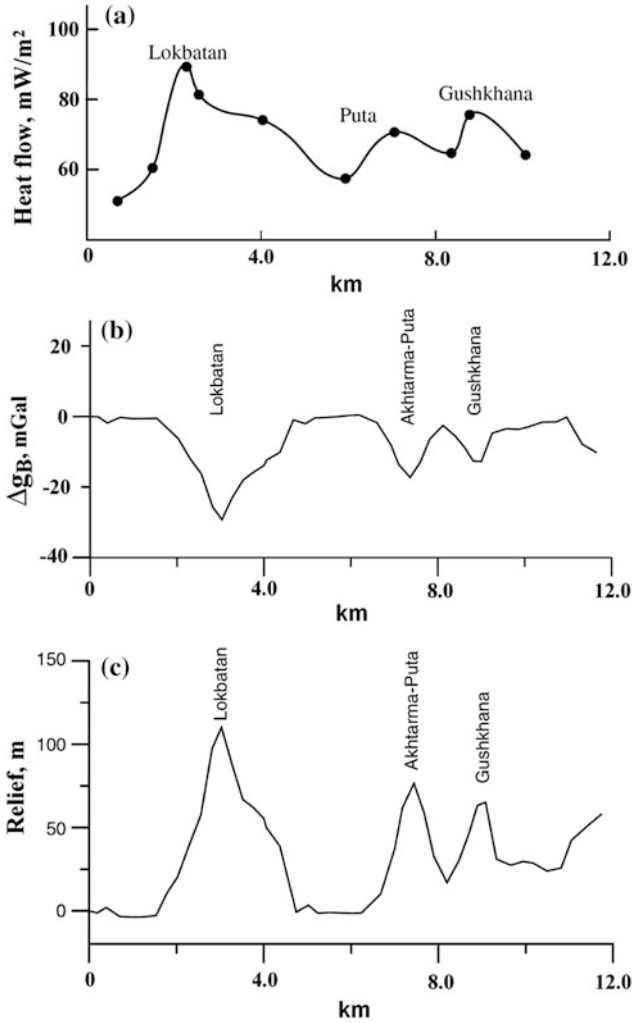

Fig. 9.6 Changes in heat flow (**a**), Bouguer gravity (**b**), and topography (**c**) along the profile crossing the Lokbatan–Akhtarma-Puta–Gushkhana mud volcanoes (compiled from Kadirov and Mukhtarov 2004; Kadirov et al. 2005, with modifications)

density contrast is +0.15 g/cm^3); and (7) Mesozoic surface (*Mz*; density contrast is +0.3 g/cm^3) (Kadirov et al. 2005). The gravity field calculated in terms of the model has shown some disagreements with the observed field. Therefore, the initial model of the section was compensated in the parts under the mud volcanoes by introduction of decompaction zones and additional contact boundaries with a density contrast of −0.15 g/cm^3 at the depths of 3 km and less (Fig. 9.7).

9.2.2.2 Resistivity

Resistivity measurements can be also effectively applied for studying the subsurface section of mud volcanoes structure. Marine electric prospecting was successfully used for resistivity mapping of mud (chaotic) breccia on the bottom of the Caspian Sea near the Makarov Bank (e.g., Shatsov 1969). Scholte et al. (2003) proved the potential of resistivity mapping of the Lokbatan and Bozdagh onshore mud volcanoes near Baku, where liquid mud chambers and feeder channels were identified by low resistivity. It is important that in the upper 2.5 m of Lokbatan volcano, exactly at the loci of surface combustion, the dry parts of the feeder channel could be detected by their increased resistivity due to the high temperature of gas seepage combustion. A 3D subsurface plot of a part of Lokbatan mud volcano is given in Fig. 9.8 with varying electric resistivity values from 1 to 41 Ωm^{-1} (Scholte et al. 2003).

Review of Guliyev and Feizullayev (1997) indicates that the Lokbatan mud volcano subsurface consists of a clay-type material. A lookup table is created to identify dry (red) and wet (blue) parts of the subsurface. Preliminary 3D data show, when looking from different angles, an irregular network of mud migration pathways.

9.2.2.3 Magnetics

The largest volume of magnetic data on mud volcanoes was obtained in the South Caspian Basin and the adjacent territory, where Dzabayev (1969) performed 1:200,000 aeromagnetic surveys by fluxgate magnetometer. The increased magnetic susceptibility (up to a few hundred 10^{-5} SI units) of several Neogene terrigenic strata within a thick sedimentary cover (Ismailzadeh et al. 1983) facilitated successful magnetic prospecting. Ferromagnetic minerals are partly altered or chaotically oriented in fault zones. The latter are, therefore, detected by zones of decreased ΔT field down to several tens of nanotesla. Isometric minima of higher amplitude indicate mud volcanoes (Fig. 9.9).

In general, mud volcanoes can be identified by magnetic maxima as well. Logachev and Zakharov (1979) described the magnetic survey results on the productive series of the Absheron peninsula where were found magnetite–siderite associations in oil-bearing and mud volcano rocks unlike other rocks. This magnetic association was formed from the reduction in finely dispersed iron oxides and hydroxides under the influence of hydrocarbons. The reduction in magnetite and its substitution by pyrite are also possible. The near-surface burning of mud volcano deposits can cause their increased magnetization. Therefore, magnetic anomalies over mud volcanoes can have different patterns.

9.2.2.4 Radioactivity

Offshore mud breccia is characterized by an increase in integral gamma radioactivity of several microRoentgen/hour (Shatsov 1969). Similar excesses were observed for onshore volcanoes (Aliyev et al. 2001). The minimal level of mud breccia radioactivity depends on the area, presumably

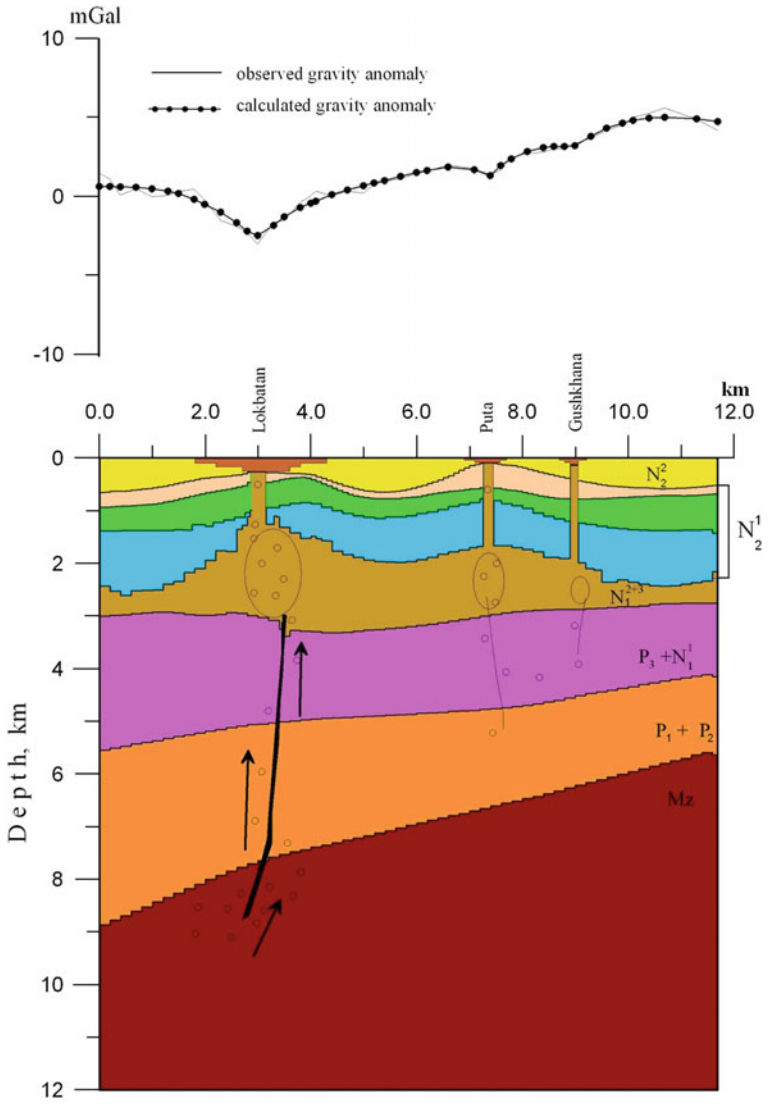

Fig. 9.7 Physical–geological model along profile Lokbatan–Akhtarma-Puta–Gushkhana (after Kadirov et al. 2005)

reflecting the radioactivity level in the mud volcano roots; for example, the increased radioactivity of Maykop clays. In marine volcanoes (Duvanny, Bulla, Garasu and Khara-Zire), radioactivity readings start from 10 to 10.5 μR/h; in volcanoes in the Near-Kur area (Bakhar, Ayranteken, Byandovan, Hamamdagh, and Agzibir), this ranges from 11 to 12.5 μR/h, and in the Absheron volcanoes (Keyreki, Bozdag-Gobi, Sarynja, Lokbatan and Otman-Bozdag), the values are from 13.5 to 18 μR/h. Relatively high radioactivity is usually typical of the central part of the volcano, near the crater (Fig. 9.10).

A total γ-ray intensity was also measured with a probe on the surface across the Lokbatan mud volcano on profile about 5 km long. The Lokbatan mud volcano is located at the center of the profile (shown by the dashed vertical line at 3 km in Fig. 9.11). Two days after the explosion on October 25, 2001, the γ-ray intensity in the crater was as high as 28 μR/h before returning in a few days to around 10–15 μR/h. Apart from the isolated high intensity point at the 1.5-km marker in Fig. 9.11 (likely to be due to either the radioactive waste being deposited in an old well or an open fault bringing up radioactive material from depth; it is not known which), noteworthy is the large increase in total intensity in the neighborhood of the Lokbatan volcano, associated with the ejected mud, which was transported from depth (Feyzullayev et al. 2005).

9.2.2.5 Seismics

High-resolution seismic survey is one of the most reliable tools of mud volcano delineation. Four examples of seismic images of mud volcanoes are presented in the Chap. 7 of Volume I (Figs. 7.15–7.18).

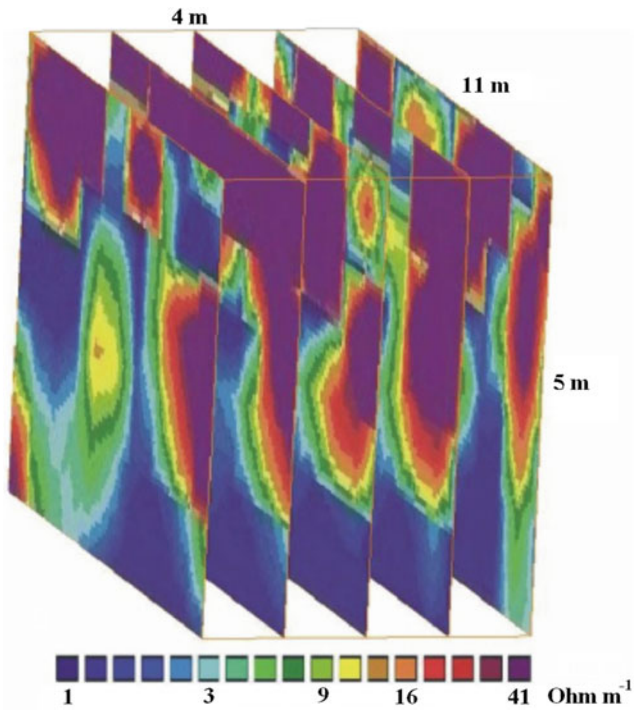

Fig. 9.8 Lokbatan mud volcano shallow subsurface derived from resistivity observations (after Scholte et al. 2003)

Numerous breccia bodies and buried mud volcanic structures are quite accurately identified on seismic-temporal cross sections of Azerbaijan sea area, which permits to conduct paleoreconstruction of mud volcanic process development in the Southern Caspian Basin. According to seismic materials, mud volcanic activity in the Southern Caspian Basin manifested itself in the offshore area's western part starting from the Lower Pliocene at the least (the Bakhar, Shakh deniz, Umid, D-3 structures) (Huseynov and Guliyev 2004; Fowler et al. 2000; Yusifov and Rabinowitz 2004). During the Upper Pliocene–Absheron stages, the mud volcanic activity areas expanded predominantly southward, and during the Pleistocene, in the northeastern, eastern, and southeastern directions.

Kieckhefer et al. (2003) successively applied advanced 3D seismic data analysis integrated with free-air gravity data modeling for delineating a submarine mud volcanic flow in complex physical–geological conditions of the Absheron block (offshore Azerbaijan).

Figure 9.12 displays the seismic section northwest to southeast along the crest of the Shah Deniz (dip-closed structure in the South Caspian), Azerbaijan. This section shows the majority of the main mud volcanoes that occur within the Shah Deniz area (Fowler et al. 2000). As shown in Fig. 9.12, here are only active mud volcanoes.

9.2.2.6 Thermal Field

It was noted by many authors (e.g., Pilchin 1985; Kadirov et al. 2005; Mukhtarov 2011; Eppelbaum et al. 2014) that mud volcanic activity is usually clearly reflected in thermal field. One of such examples is presented earlier in Fig. 9.6.

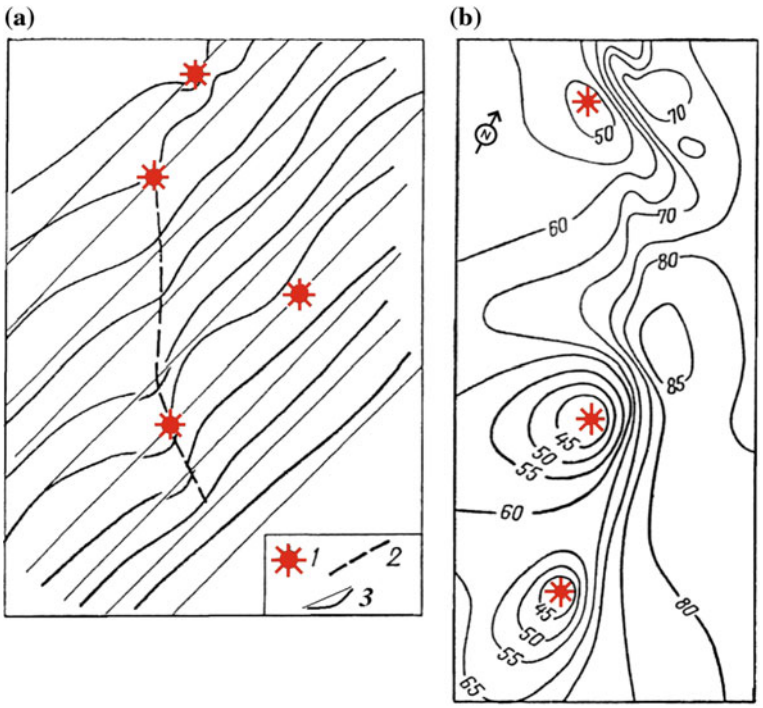

Fig. 9.9 Sites of ΔT map (compiled from Dzabayev, 1969): **a** graphs, and **b** isodynams (in nanotesla). (*1*) mud volcano, (*2*) fault zone, and (*3*) ΔT graph

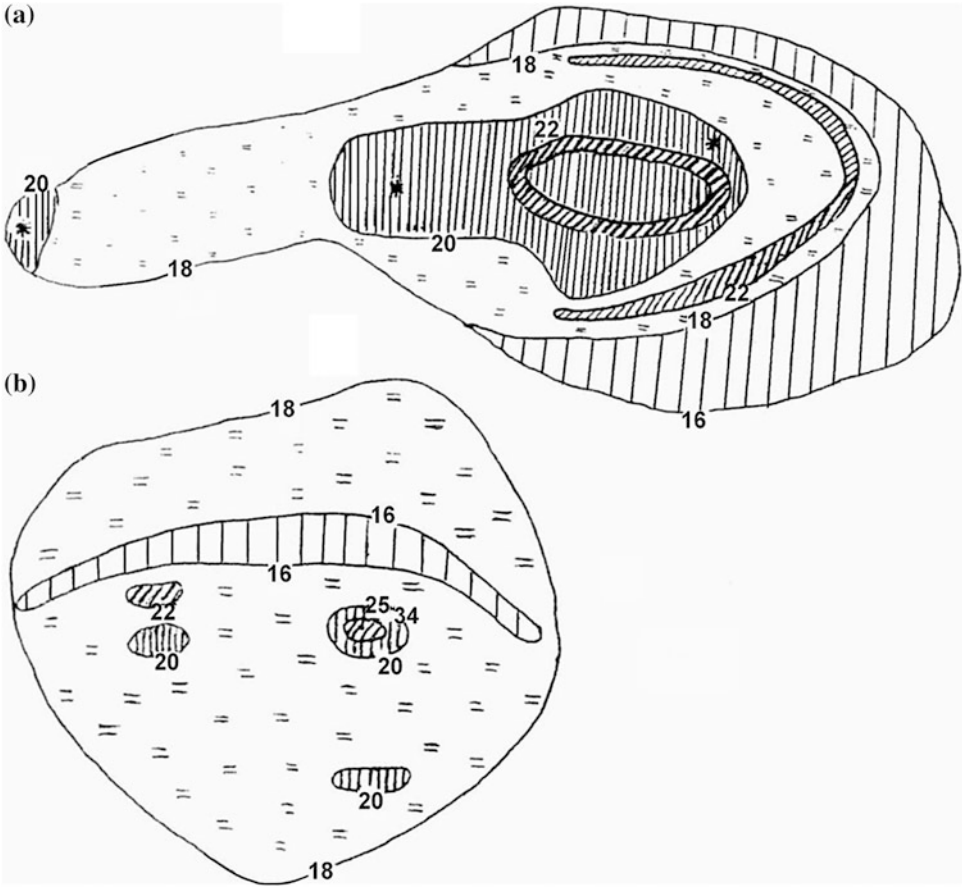

Fig. 9.10 Natural radioactivity fields over mud volcanoes; **a** Lokbatan, **b** Bozdag-Gobi (after Aliyev et al. 2001, with technical modifications). *Digits* in the figure show values of radioactivity, μR/h

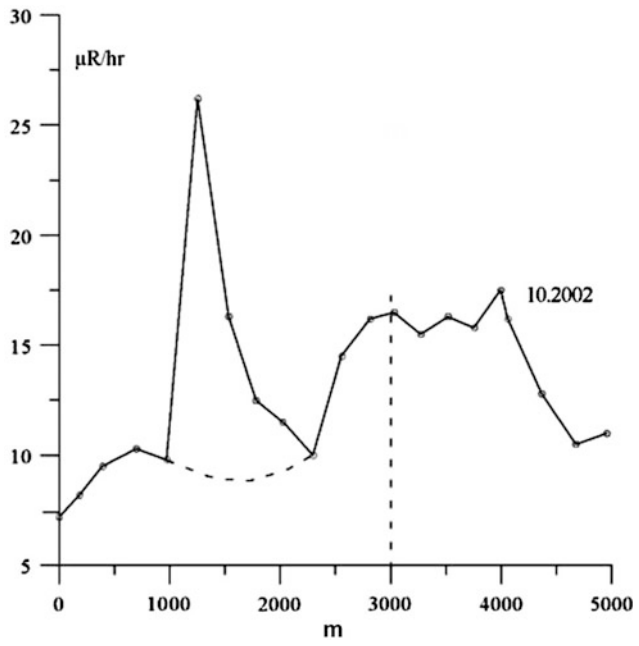

Fig. 9.11 Change in the total γ-ray count along a profile crossing the Lokbatan mud volcano (Feyzullayev et al. 2005a)

Characteristics of thermal mass transfer through channels of active mud volcanoes are presented in Table 9.2.

It should be noted that temperature field propagation in areas occupied by mud volcanoes apparently has nonlinear and even strongly nonlinear character for which special methodologies have been developed (Eppelbaum and Kardashov 1998; Kardashov et al. 2000).

9.2.2.7 Remote Sensing: GPS, DInSAR and Landsat

GPS measurements indicate a decrease in the velocity and a significant accumulation of elastic energy in the southern Absheron Peninsula. This phenomenon may be responsible for the activation of seismic events and mud volcanoes in this region, because ten mud volcanoes erupted during the 1998–2002 period in the Absheron and Shamakhy–Gobustan areas. The strong earthquake (approximate magnitude 6–6.3 on the Richter scale) in the Caspian Sea at the end of 2000, and its aftershocks, probably represent a response to the deformational processes and the related stress accumulation, ongoing at the foothills of the Greater Caucasus, the Absheron peninsula, and the middle Caspian Sea region. However, the tendency to have horizontal motions in the Azerbaijan territory suggests an activation of geologic

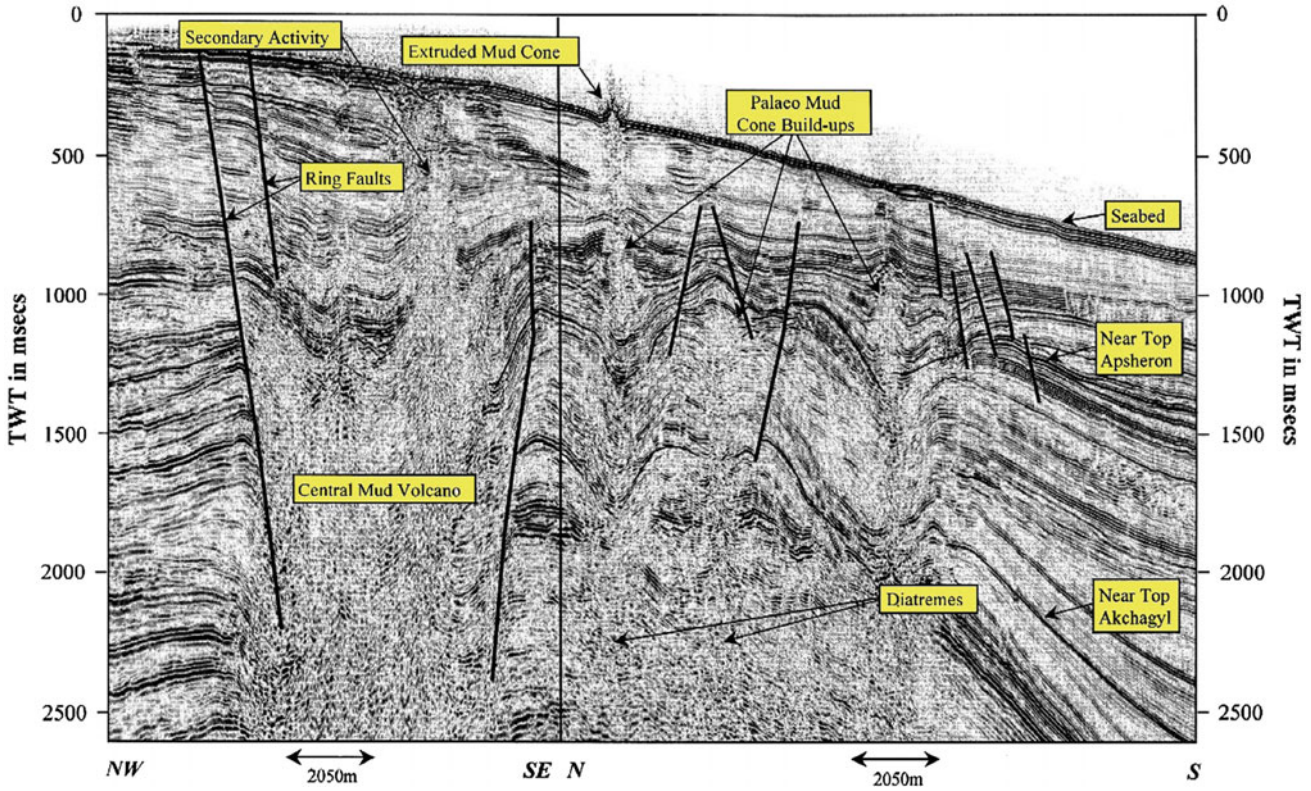

Fig. 9.12 3D seismic section of Shah Deniz mud volcano north to south along the crest of the structure showing the location and development of the major mud volcanoes. The collapsed caldera and later phase of activity can be clearly observed over the central mud volcano. The mud cone currently being extruded at the seabed over a palaeomud volcano can be seen to the south of the central mud volcano and is clearly a later, smaller scale phase of activity (after Fowler et al. (2000), with minor modifications)

Table 9.2 Characteristics of thermal mass transfer through channels of active mud volcanoes (Mukhtarov 2011)

Mud volcano	Temperature gradient				Density of thermal flow (average) (mW/m^2)
	Values in K/m (°C/m)		No.	Depth interval (m)	
	Minimum/maximum	Average			
Melikchobanly		4.65	1	0.4–0.8	62.78×10^2
Bakhar[a]	16.66/19.94	17.25 9.85 (out-side crater)	3 1	0.5–1.0 0.5–0.7	23.29×10^3 13.3×10^3
Dashgil	1.58/3.58	2.55	3	0.5–1.0	34.42×10^2
Airantekan	1.82/5.84	3.31	6	0.5–1.0	44.68×10^2
Cheildag	0.18/2.12	1.24	5	0.5–1.0	16.74×10^2
Agzybir	0.08/1.04	0.58	10	0.5–1.5	78.3×10^1
Zenbil Island[a]	10.5/21.25	15.62	4	0.5–1.5	21.09×10^3
Hara-Zire Island	0.07/2.42	0.87	7	0.5–15.0	11.75×10^2
Hamamdagh	−2.76/0.09	–	14	0.5–12.0	–
Otman-Bozdagh	2.35/6.67	3.51	6	0.6–1.5	47.38×10^2
Shorbulag	1.64/2.10	1.87	2	0.5–1.0	25.24×10^2
Gyrlykh (Shirvan)	3.30	3.30	1	0.6–1.0	44.55×10^2
Babazanan	3.54/4.10	3.82	2	0.5–1.0	51.57×10^2

[a]*Note* Temperature observations in the mud volcano Bakhar were done after 13 days, and in the mud volcano of Zenbil Island—after two months after eruption

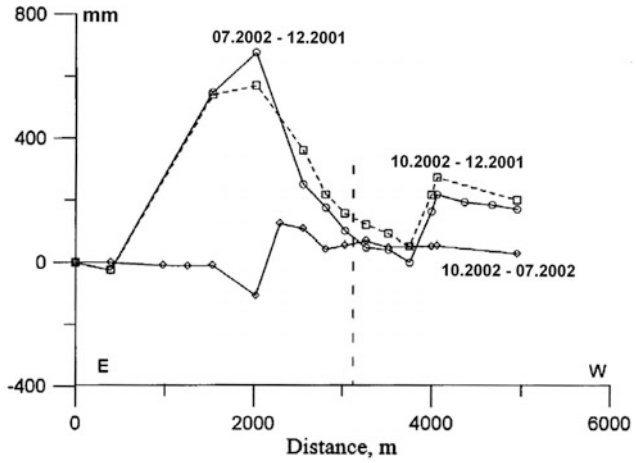

Fig. 9.13 Vertical movement along a profile crossing the Lokbatan mud volcano

processes (seismic activity, activation of mud volcanoes and, in adjacent zones, accumulation of elastic stress). The repeated geodetic leveling on the Lokbatan volcano shows that there are currently active geodynamic processes occurring there. During the period from November 2001 to November 2002, on the NE part of volcano (about 2 km in length), the contact boundary was as shallow as 60 cm (Kadirov and Mukhtarov 2004) (Fig. 9.13).

DInSAR satellite measurements were carried out in June in the Ayaz–Akhtarma mud volcano area (Antonielli et al. 2014). The Ayaz–Akhtarma mud volcano is a large edifice with elliptical base (major axis about 2700 m) characterized by a wide flat top surface that might be a filled caldera (Fig. 9.14a, b). Current fluid expulsion occurs at several gryphons and cones clustering in a circular area (about 430 m in diameter) at the center of the crater (Fig. 9.14a, b). The major eruptions in the last 20 years occurred in 2001, 2005, 2006, and 2007, even though the precise date of these eruptive events is unknown (Aliyev et al. 2009, 2015).

The performed analysis allowed the identification of a main fault/fracture 600-m long and in a direction trending about N42°E (Fig. 9.14a–g). The northeastern part of this brittle element is characterized by a normal vertical throw varying between 25 cm and 1 m (Fig. 9.14e, f). The

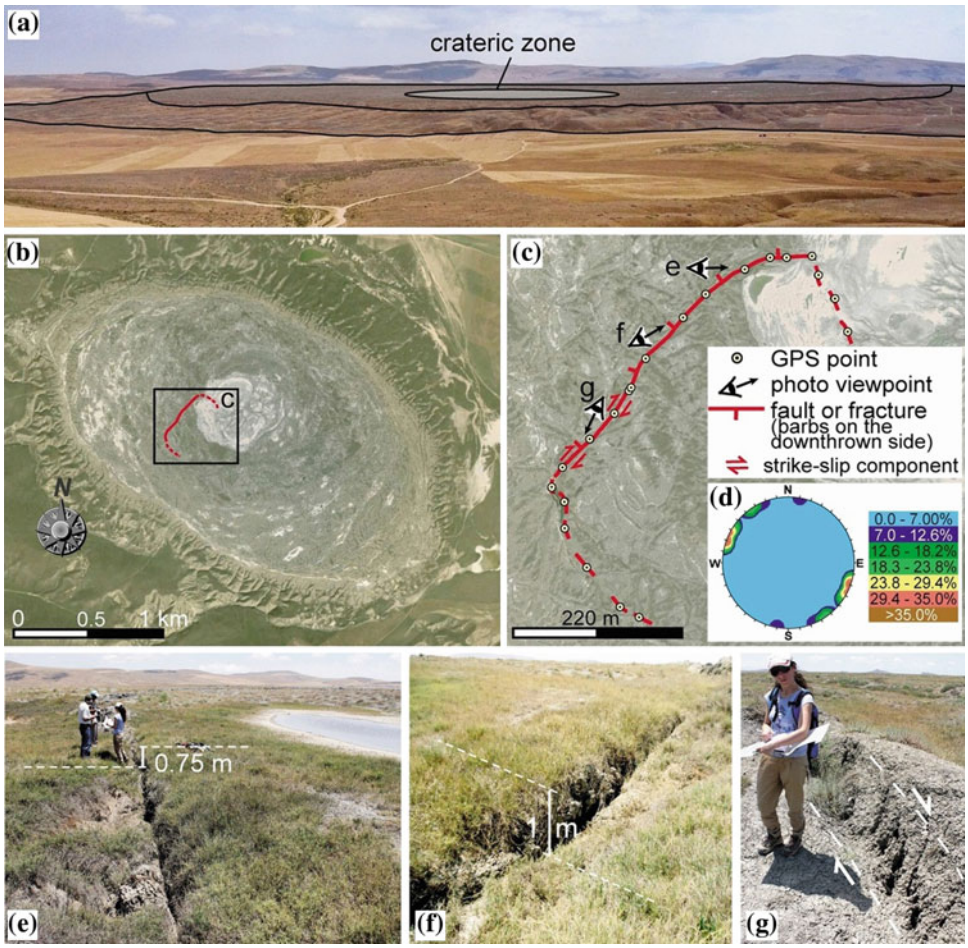

Fig. 9.14 Satellite-structural analysis performed in the Ayaz–Akhtarma mud volcano. **a** Panoramic view looking south. **b** Google Earth image (March 2004). **c** Fracture observed during the field survey carried out in June 2013. **d** Contour plot (Fisher distribution; equal area, lower hemisphere) of poles to fracture and fault segments. **e–f** Fault segments showing dominant vertical displacement (maximum vertical throw ~1 m). **g** Enechelon fractures pointing to some dextral strike–slip component of displacement. Images in (**b**) and (**c**) are extracted from Google Earth (Antonielli et al. 2014)

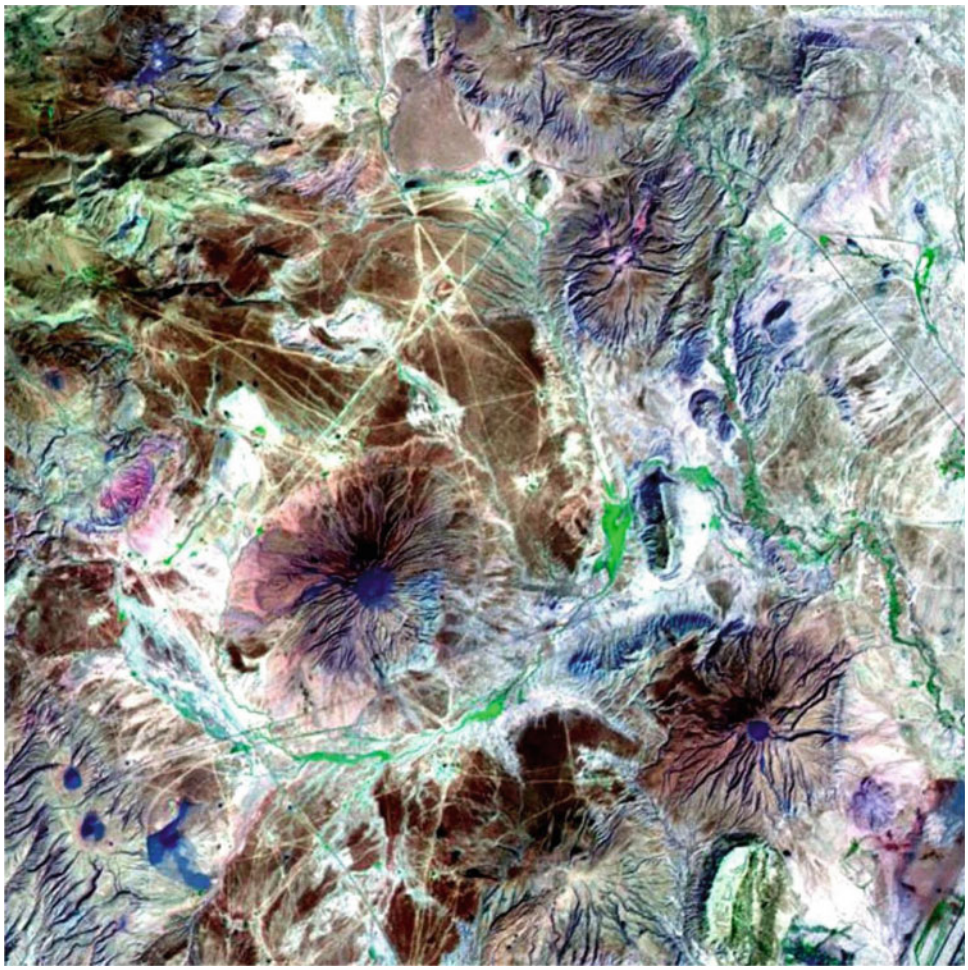

Fig. 9.15 Satellite Image Landsat-7 (Bands 7, 4, 2). Fragment of the distribution of mud volcanoes in the Kur basin (Zeynalov 2008)

remaining southwestern tract consists of enechelon fractures, which suggest a right strike-slip component of displacement (Fig. 9.14g). GPS reference points were collected and used to locate the fault/fracture on the geocoded radar digital data and on Google Earth images.

Such powerful toll as stereoscopic data obtained from the Landsat and SPOT imagery may be effectively applied for localization of mud volcanoes (Fig. 9.15). These images can provide exact pattern of faults' structural–geological elements and geomorphology of mud volcanoes.

9.2.2.8 Association of Mud Volcanism with Geodynamic and Extraterrestrial Factors

Irregular degassing of the Earth is a fundamental feature of its evolution reflecting in tectonic and sedimentation cycles, sea-level fluctuations, accumulation of mineral resources, and other phenomena. This peculiarity of global-scale Earth degassing is related to cosmic and endogenic rhythms or cycles. The conventional cycles may consist from hundreds and tens of thousands to millions years [cyclicity of tectonic and endogenic processes is analyzed in detail in Aleinikov et al. (2001)]. However, shorter geological cycles were also registered. One of a such short periodicity is the rhythmic hydrocarbon gassing (Guliyev 2005). The rhythms of hydrocarbon degassing are most obviously manifested in the periodicity of eruptions and activity of mud volcanoes which are accompanied by the release of hundreds of millions of cubic meters of methane, oil, and groundwater. The periodicity in eruptions established for a sufficiently long-time interval indicates a stable correlation between the mud volcanism from one side and solar activity, Caspian Sea level

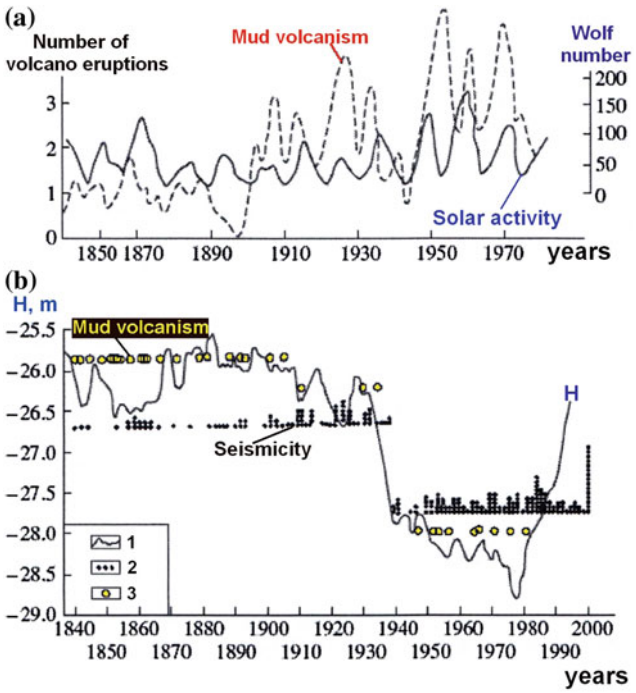

Fig. 9.16 Relationships between the mud volcanism and some periodical natural processes in the South Caspian Basin (after Guliyev (2005), with modifications). **a** Comparison of mud volcanism and solar activity (Wolf number), **b** comparison of mud volcanism with the Caspian Sea level fluctuations and seismicity. (*1*) Caspian Sea level fluctuations (in **b**), (*2*) seismicity, (*3*) mud volcanism (in **b**)

fluctuations and seismicity from second side (Guliyev 2005) (Fig. 9.16).

It should be noted that the Moon–Sun gravity/magnetic influence to many environmental processes in the Earth are more significant than it was earlier considered (Eppelbaum and Isakov 2015).

9.2.3 Effects of Magnetic and Electromagnetic Field Variations and Human Health

Studies have confirmed the relationship between geomagnetic activity and human health (e.g., Chizhevsky 1930, 1963; Rapoport et al. 2006). Babayev and Allahverdiyeva (2007) described the effect of variations in geomagnetic activity (GMA) on human health. Their experiments, as well as statistical and biomedical analyses, confirmed the influence of changes in GMA on the brain and on human emotions.

Experimental data from medical clinics and in some Caucasus resorts should prompt researchers to further explore the relationship between the pathogenic effects of magnetic storms, geoecological problems, and magneto-variational monitoring (Lyubimov et al. 1993).

Studies of the influence of geomagnetic storms of various intensities on electric power supply systems in Azerbaijan

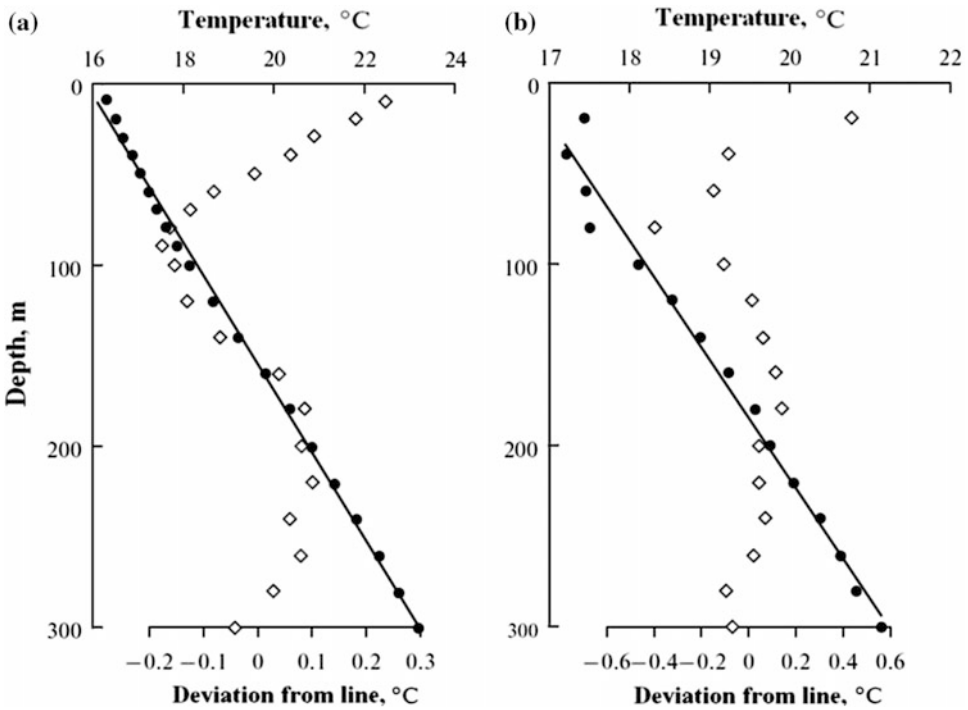

Fig. 9.17 Termograms of wells of Garadja-16 (**a**) and Gemigaya-14 (**b**) (Kur Depression, Azerbaijan) (Mukhtarov et al. 2010). *Circles* designate values of temperature observed in wells, *direct line* shows their general trend, and *rhombs* indicate deviation of temperature from the linear trend

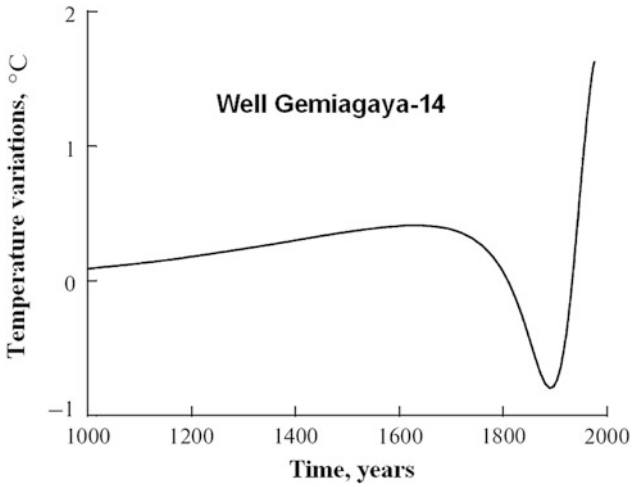

Fig. 9.18 Inversion of temperature by the use of data observed in well Gemigaya-14 (Mukhtarov et al. 2010)

are discussed in (Babayev et al. 2006). It was concluded that large geomagnetic storms could seriously damage the electric power systems, and geophysicists studying magnetic events should work closely with experts in power engineering.

The Sun is the main source of electromagnetic radiation on the human body. Many villages in Azerbaijan are located at heights of more than 2000 m, where the influence of solar radiation is especially strong. However, the same these villages hold longevity records (42 % of the all individuals living to be 100 and over reside in the Caucasus). As frequently happens, there is doubtless a combined set of influences which need to be untangled for correct interpretation.

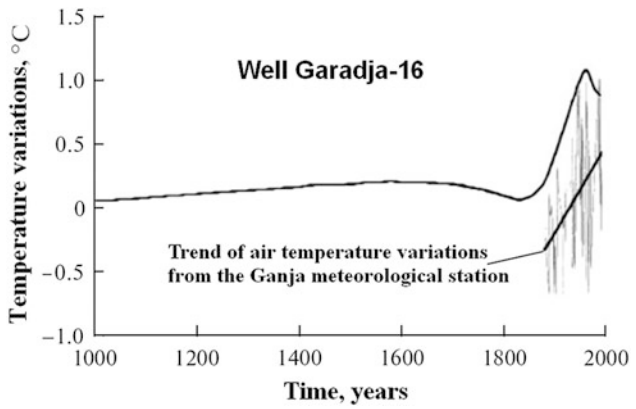

Fig. 9.19 Inversion of temperature by the use of data observed in well Gemigaya-14 and air temperature variations observed in Ganja station (Mukhtarov et al. 2010)

9.3 Unmasking Climate of the Past by the Use of Borehole Temperature Data Analysis

Analysis of the climate of the past has attracted the attention of many experts working in the field of borehole temperature measurements who use this information to reconstruct ancient temperatures (e.g., Huang et al. 2000; Bodri and Cermak 2005; Eppelbaum et al. 2006). In Azerbaijan, these investigations were employed in two boreholes—Garadzha-16 and Gemigaya-14 located in the Kur Depression (Mukhtarov et al. 2010) (Fig. 9.17). These boreholes were selected mainly because of the high accuracy (no less than 0.01 °C) and small steps (10–20 m) of temperature observations in the boreholes. The observed temperature data were processed by the methodology developed by Shen and Beck (1991). It was found that in the Kur Depression, in the seventeenth and eighteenth centuries, the temperature decreased for 1 °C, and in the second half of nineteenth century there was warming of 1–2 °C (Figs. 9.18 and 9.19). Undoubtedly, such geophysical investigations (having hot only meteorological and environmental, but also geological importance) should be carried out in other regions of Azerbaijan.

Besides this, unmasking climate of the past is important for: (1) tracing some important historical events, (2) obtaining averaged ancient estimation, (3) assessment of certain physical-chemical properties of ancient constructions (Eppelbaum and Kutasov 2014).

9.4 Examination of Areas of Dams and Lakes

The Mingechavir water reservoir is the largest artificial lake in the Caucasus region (15.7 km^3 of freshwater). Given the importance of this reservoir, the lake and surrounding areas were carefully studied tectonically and geophysically from a regional point of view (e.g., Gadjiev et al. 1989; Alexeyev et al. 1989; Kerimov 1996; Gasanov 2001; Aliyev et al. 2005a, b).

Detailed electric prospecting was carried out for the first time on the right shore of the Mingachevir reservoir by Salamov et al. (2010) to identify multidirectional fractures caused by tectonic movements. It was suggested (and later confirmed) that the recognized fractures are the edges of future landslides. Monitoring by electric observations indicated that the changes in the physical parameters of the ground are the harbingers of rockslide activation.

We propose that integrated remote-operated vehicles (ROV) geophysical surveys at low altitudes (e.g., Eppelbaum and Mishne 2011) are a valuable tool for tectonic–

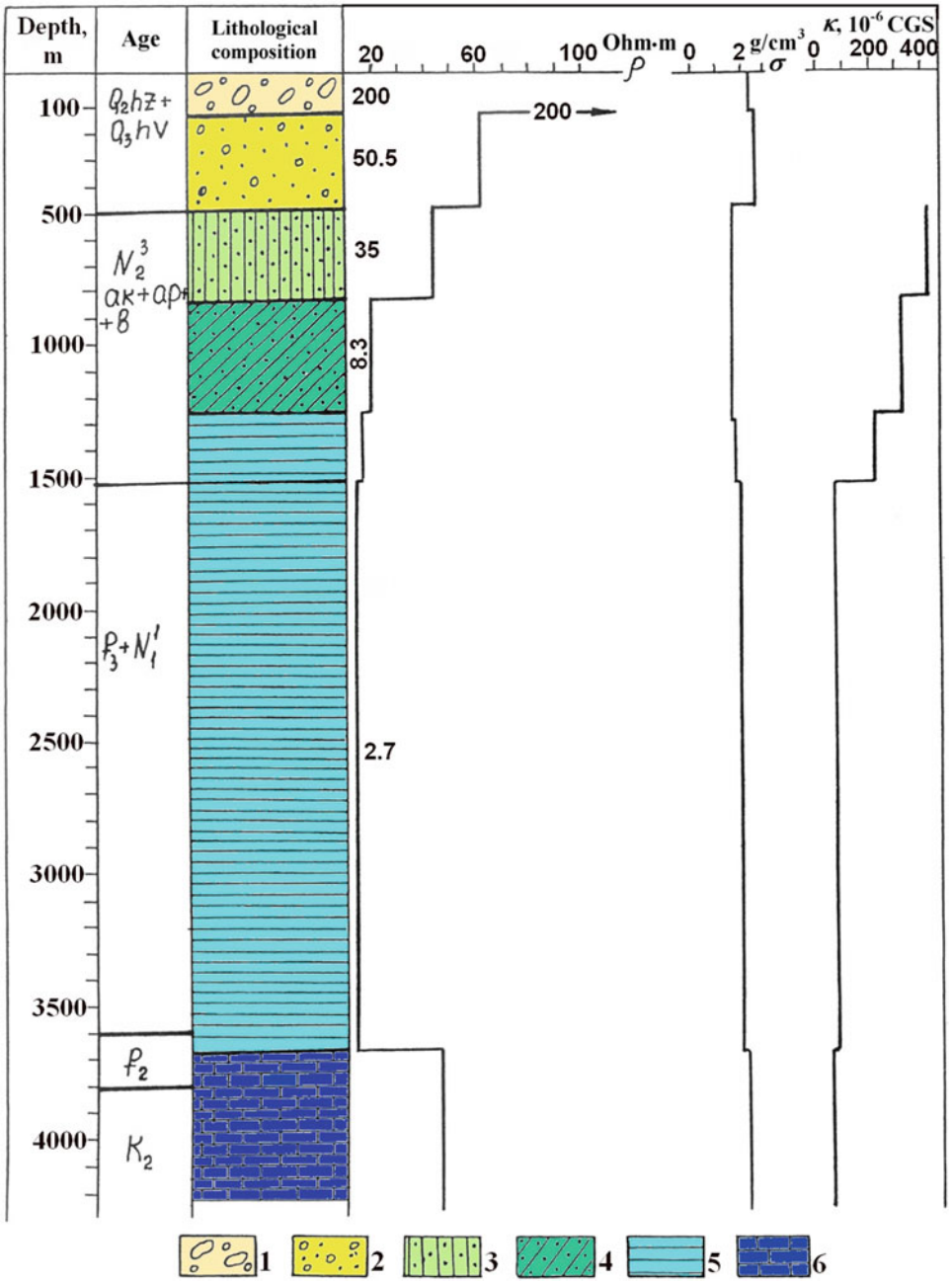

Fig. 9.20 Generalized petrophysical (electric resistivity ρ, density σ, and magnetic susceptibility κ) column of the Mesozoic–Cenozoic deposits in the northeastern immersion of the Lesser Caucasus (Ganja region) (after Eppelbaum and Khesin 2012). (*1*) boulder pebbles, (*2*) sand pebbles, (*3*) chiefly sand deposits, (*4*) clayey sand deposits, (*5*) sandy clay deposits, (*6*) mainly carbonate deposits

structural investigations and monitoring of dams, lakes, and their surroundings.

9.5 Application of Geophysical Methods in Hydrology

Hydrogeological reserves and their localization and monitoring are of great importance for Azerbaijan Republic (see Chap. 1 of this volume).

Hydrogeological studies require a large volume of drilling and other expensive operations, similar to petroleum exploration. Actually, revealing water flow ways, water collectors, and impermeable strata, as well as direct water detection, is similar to indirect and direct hydrocarbon prospecting. The use of geophysical methods cuts down drilling time, increases the uniformity of the medium, and reduces total expenses and environmental damage (Eppelbaum and Khesin 2012). Hydrogeophysics methodology is well developed for platform conditions with large structural

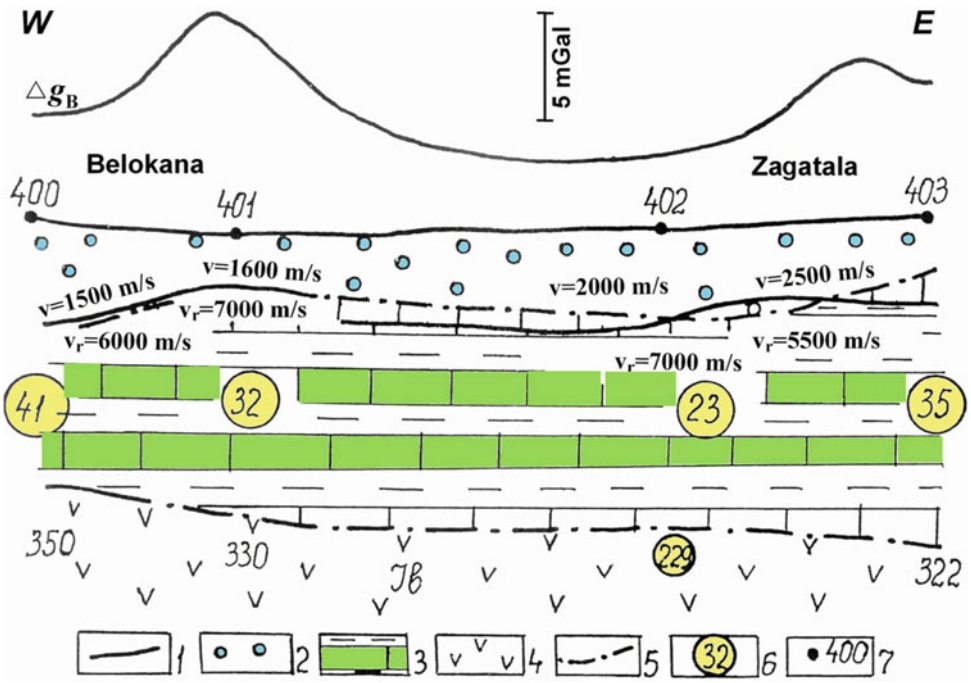

Fig. 9.21 Geological–geophysical section along the southern foothills of the Greater Caucasus. *Note* The vertical scale of the section is multiplied by 10 (Eppelbaum and Khesin 2012). (*1*) refracting boundary, (*2*) Quaternary boulder pebbles, (*3*) Cretaceous carbonate–clay deposits, (*4*) Jurassic volcanogenic rocks, (*5*) geoelectric layer boundary, (*6*) ρ, Ohm meters, (*7*) VES point and its number

forms, stable petrophysical sections, and favorable near-surface environments. The geological–geophysical characteristics of submountain and mountain regions including the Caucasus are more complicated, and the hydrogeophysics methodology is specific to it.

The development of new oil production and transportation techniques in the Caucasus prompted the need to provide reliable groundwater protection (e.g., Aliyev and Askerov 2002). For this different geophysical method, integrations may be used.

Underground fresh and/or low mineralization waters in mountain and submountain regions are mainly distributed within alluvial fans and artesian basins. The upper part of these multilayer systems is the most valuable (zone of active water exchange) and is studied to find solutions to water supply, land reclamation, and irrigation. The key features of these systems are heterogeneity and variability. Water-bearing deposits in the foothills are mainly represented by boulder pebbles with thin clay bands (upper molasses formation). As it moves off the mountain frame, the content of thin-grain matter (clay particles) in the water-bearing deposits increases. These lithological variations are reflected in the differentiation of petrophysical characteristics, and first of all, by rock resistivity (Fig. 9.20).

It is clear that boulder pebble deposits have the highest resistivity. Clayey deposits are characterized by low resistivity. In general, the electrical properties of rocks are the most sensitive to their lithological composition, water content, and its mineralization. The increase in mineralization decreases water-bearing collector resistivity, whereas their polarizability (chargeability) intensifies the IP effects over pyrite-rich disseminated ores. Self-potential anomalies indicate sites of water filtration. These features explain the widespread application of electric prospecting methods especially since similar applications of seismic prospecting are complicated by complex near-surface seismic–geological conditions and considerably higher cost. Quantitative interpretation of vertical electric sounding (VES) gives the thickness and true specific resistivity (ρ) of each geoelectric layer.

At the same time, other geophysical methods can supply important information on the deep structure that often controls the spatial distribution of aquifers and aquicludes (Fig. 9.21). In some cases, these methods facilitate the lithological separation of water-bearing sections. For example, boulder gravels and clays are differentiated by their low and high velocity of compression (longitudinal) waves, respectively (Fig. 9.21).

Water exploration can reach a depth of several hundred meters (usually up to 300 m); the extent of alluvial fans (foothills of the Greater and Lesser Caucasus) and artesian basins (Kur Depression) go down several kilometers or more. Thus, integrated geophysical studies based on VES are carried out at larger and more regional scales (usually,

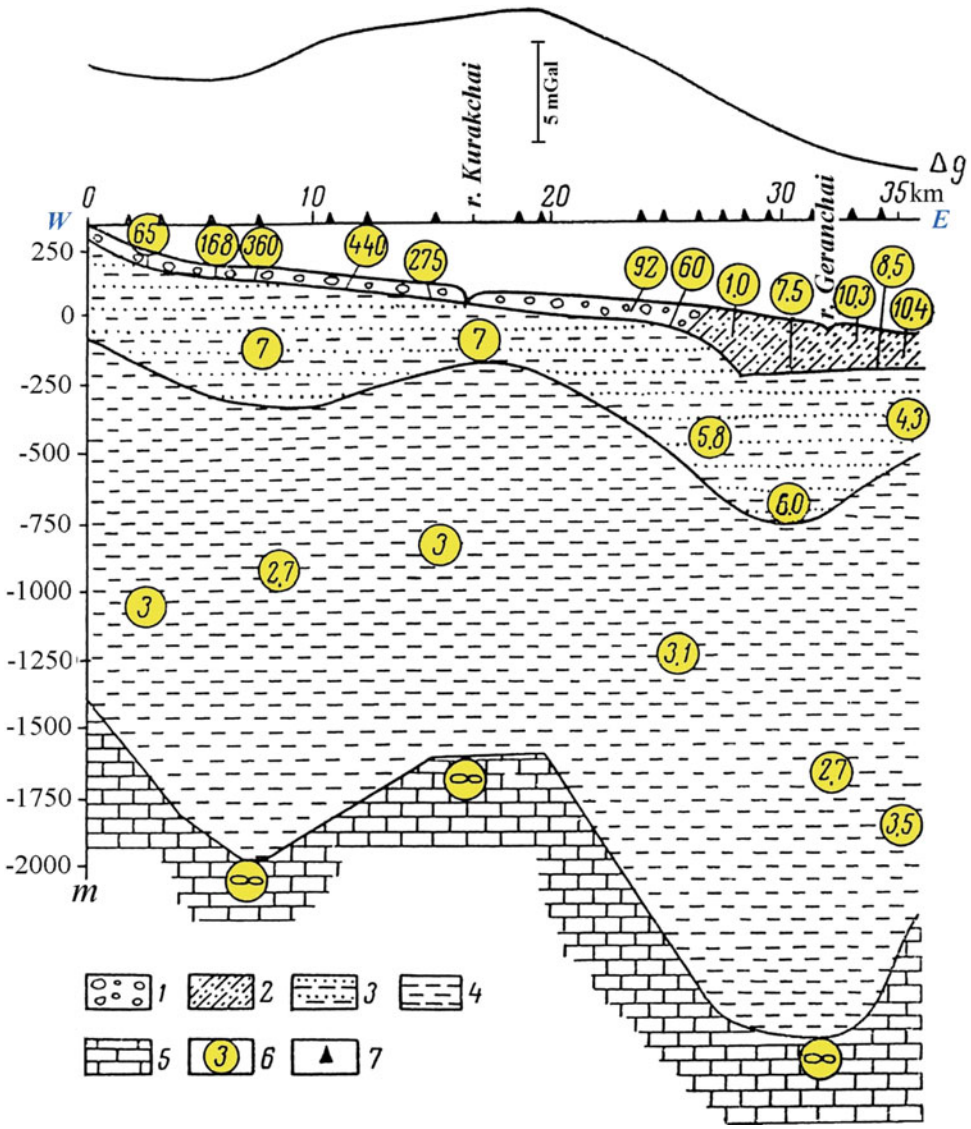

Fig. 9.22 Geoelectric section according to VES data in the Gazagh-Ganja Massif (Eppelbaum and Khesin 2012). (*1*) boulder pebble deposits, (*2*) clay sandy deposits of buried debris cone, (*3*) sandy clay deposits of Akchagyl and Absheron, (*4*) clay deposits of the Maykop series, (*5*) foraminiferal layer, (*6*) values of real electric resistivity, Ohm m, (*7*) VES points

1:100,000–1:200,000), and VES separations often attained 5–10 km. For the detection of water-bearing horizons of small thicknesses, additional conventional separations are added in the AB/2 interval of 500–1500 m. Sometimes, the VES are combined with electrical profiling and SP methods.

Discovering freshwater sources in the Kur Depression and in its vicinity is of great applied interest. The key characteristics of water-bearing Upper Pliocene recent deposits, their thickness, and lithofacial composition were obtained on the basis of a combination of VES, other geophysical methods, and drilling. During two field seasons, an area of 5400 km^2 was studied by 590 VES with AB arrays up to 10 km. Sandy-pebble collectors saturated by freshwater were identified on the maps of isoOhms and in the upper part of geoelectric sections on the basis of their high resistivity. Regularities in their distribution were revealed in comparison with dip structure features. A characteristic section is shown in Fig. 9.21 (Fig. 9.22).

Discovering freshwater sources in the Kur Depression and in its vicinity is of great applied interest. The key characteristics of water-bearing Upper Pliocene recent deposits, their thickness, and lithofacial composition were obtained on the basis of a combination of VES, other geophysical methods, and drilling. During two field seasons, an area of 5400 km^2 was studied by 590 VES with AB arrays up to 10 km. Sandy-pebble collectors saturated by freshwater were identified on the maps of isoOhms and in the upper part of geoelectric sections on the basis of their

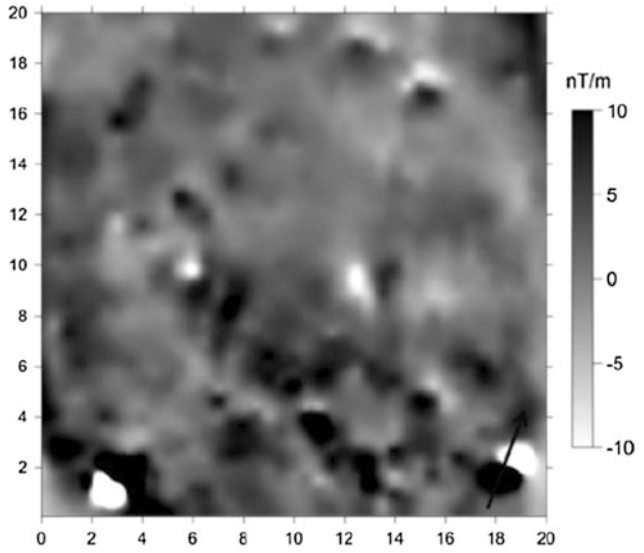

Fig. 9.23 Magnetic gradientometry results over the kurgan, showing a circular geometry outlining the topographic shape of the kurgan, and intricate anomalous effect inside the circle considering the likelihood of burials. A metal stake at (x = 3.5, y = 2) accounts for a strong dipolar anomaly (Sternberg et al. 2012)

high resistivity. Regularities in their distribution were revealed in comparison with dip structure features. A characteristic section is shown in Fig. 9.21 (Fig. 9.22).

9.6 Archaeological Geophysics

Geophysical methods are recognized now as a powerful tool for effective and prompt localization of buried ancient remains. Geophysical methods (according to our experience and personal communications) were comparatively widely applied in archaeological sites in Azerbaijan. However, the number of publications is unjustifiably small. Thus, the greater part of these archaeogeophysical investigations is still being held in archives as unpublished works (e.g., Barrett et al. 2004). Geophysicists of the Azerbaijanian Geological Association successfully employed a vertical electric sounding (VES) method to study the foundation of the famous Maiden Tower ("Gyz Galasy") in the center of Baku (about 1980). VES helped define the position of the foundation and even determine that it was reconstructed over the centuries. B.E. Khesin with collaborators (YuzVNII-GEOFIZIKA) in 1978–1980 have applied VES for searching old draw-wells in the "Old City" of Baku. Experimental dowsing [details of this procedure can be found, for instance, in van Leusen (1998)] by two geophysicists from the YuzhVNIIGeofizika on the tower also suggested there was a previously unknown underground cave under this town.

Burlatskaya and Chernykh (1989) studied the geomagnetic field intensity in Azerbaijan over the last 2200 years. Analysis of these data is of high importance for decoding complex magnetic field in multilayer ancient targets.

Magnetic gradientometry survey at Oglanqala, a first-millennium Iron Age fortress site (Nakhchivan, Azerbaijan), was successfully applied for revealing geometric anomalies, presumably due to architecture, in areas of the site not covered by intensive excavation. Magnetic gradientometric anomalies also delineated geological outcrops and scree, the circular outline of a kurgan and patterning within, and a modern component at the site (Sternberg et al. 2012). Figure 9.23 shows the magnetic gradient field observed over the kurgan. A general circular anomaly seems to outline the topography of the feature. A few strong dipole anomalies may represent the presence of modern metal targets. A rectangular outline located at (x = 13, y = 4) has an interesting shape, particularly considering that burials are expected within the kurgan (Sternberg et al. 2012).

The advanced geophysical field methodology for complex environments tested at archaeological sites in Israel (e.g., Eppelbaum et al. 2001, 2010; Eppelbaum 2011, 2015) can also be employed in Azerbaijanian archaeological sites.

Obviously, during next years, remote operated vehicles for land, air, underground, water and underwater archaeogeophysical observations will be widely applied (Eppelbaum 2016). Azerbaijan territory with its variety of archaeological targets occurring in different physicalgeological environments is an optimal testing area for these investigations.

The continuous increase in geophysical–archaeological data and their revision have necessitated the development of an Integrated Archaeological–Geophysical Data Base (IAGDB). Obviously, it must be multicomponental and dynamic in character (Eppelbaum et al. 2010). Besides spatial topographic coordinates (x, y, z) of archaeological sites, the IAGDB should include all values of geophysical field(s) observations over or under the earth's surface, results of repeated measurements of the geophysical field(s) over different periods of time as well as during archaeological excavations (Fig. 9.24). It is also necessary to digitize the geophysical survey results of previous years and their relation to other databases (e.g., geological, geochemical, paeleostructural, paleosedimentation, paleobotanical, and paleobiogeographical).

As a basis for the IAGDB development, one could use Access, obviously, with utilization of all necessary graphic archaeological–geological datasets. Development of such continuously expanding database will increase effectiveness of geophysical examination of archaeological targets by simplifying and hasten the planning, implementation and analysis of archaeological–geophysical investigations. From a regional point of view, the Azerbaijan IAGDB could be connected with similar databases from the neighboring countries.

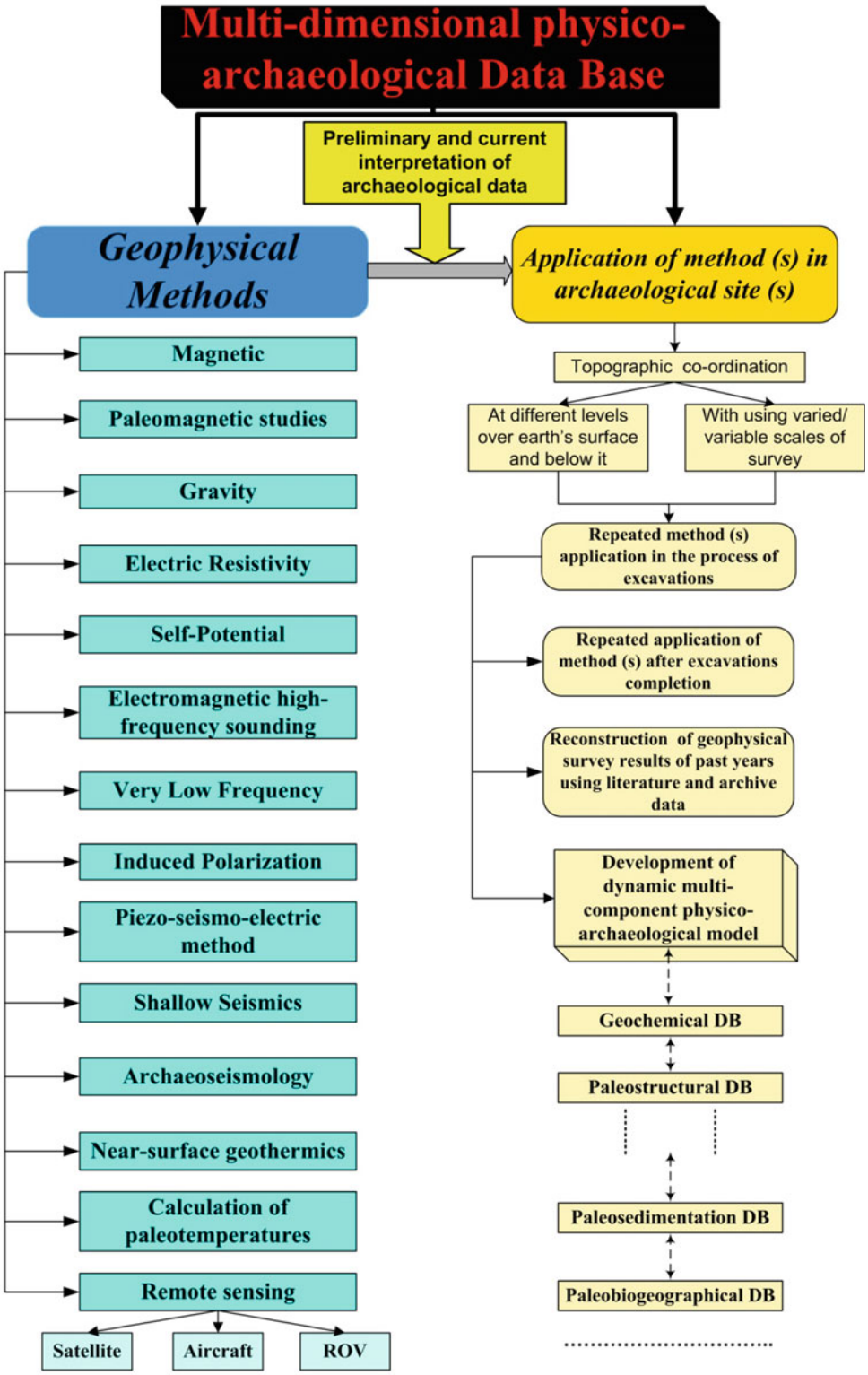

Fig. 9.24 Development of a multicomponent physical–archaeological database for Azerbaijan environments

References

Agamirzoev, R.A., Kuliev, F.T., Korobanov, V.V., Panakhi, B.M. and Aliyeva, C.T., 1986. Seismic micro-zonation of territory of the Enikend hydrosystem. *Izvestiya*, *Acad. Sci. Azerb.,* Ser.: Earth Sci., No.1, 79-83 (in Russian).

Aleinikov, A.L., Belikov, V.T. and Eppelbaum, L.V., 2001. *Some Physical Foundations of Geodynamics* (in Russian, contents and summary in English). Kedem Printing-House, Tel Aviv, Israel.

Alexeyev, V.V., Gadjiev, T.G., Karkoshkin, A.I. and Khesin, B.E. (T. A. Ismailzadeh and B.E. Khesin, Eds.), 1989. *Gravity and Magnetic Anomalies of Azerbaijan and Their Geological Interpretation*, Printing Map Factory, Leningrad (in Russian).

Aliyev, Ad.A., Guliyev, I.S. and Rakhmanov, R.R., 2009. *Catalogue of Mud Volcano Eruptions of Azerbaijan* (1810-2007). Nafta-Press (in Russian).

Aliyev, Ad.A., Guliyev, I.S., Dadashov, F.H. and Rakhmanov, R.R. (Ak.A. Alizadeh and A.D. Ismailzadeh, Eds.), 2015. *Atlas of the World Mud Volcanoes*. Nafta-Press, Baku.

Aliyev, Ch.S., Fezullaeyv, A.A., Zolotovitskaya, T.A., Aliyeva, E.A., Aliyeva, C.K. and Aliyev, K.A., 2001. Radioactive fields of mud volcanoes of Azerbaijan. *Geophysics News in Azerbaijan*, **3**, 25-32.

Aliyev, Ch.S. and Zolotovitskaya, T.A., 1996. Results of radiometric investigations. *In*: (Kerimov, K.M., Ed.) *Geophysical Investigations in Azerbaijan*. Sharg-Garb, Baku, 386-389 (in Russian).

Aliyev, Ch.S. and Zolotovitskaya, T.A., 2000. Radioactivity of Eocene rock complexes in the Central Talysh. *Izvestiya*, *Acad. Sci. Azerb*., Ser.: Earth Sci., No. 1, 67-72.

Aliyev, Ch.S. and Zolotovitskaya, T.A., 2005. Comparison of gamma-field with geological structure, geophysical fields, oil&gas bearing, and seismicity. *In*: (Ak.A. Alizadeh, Ed.), *Geology of Azerbaijan*, Vol. **V**, Physics of the Earth, Nafta-Press, 292-312 (in Russian).

Aliyev, F.Sh. and Askerov, F.S., 2002. Groundwater protection in the Republic of Azerbaijan related to the production and transportation of oil. *In*: (Israfilov, R.G. and Howard, K.W.F., Eds.), *Current Problems of Hydrogeology in Urban Areas, Urban Agglomerates and Industrial Centres*. Kluwer Acad. Publ., NATO Science Series: **IV**: Earth and Environmental Sciences, Volume **8**, 301-315.

Aliyev, F.Sh., Salamov, A.M., Alizadeh, Kh.A., Gyul, A.K. and Mammadov, Y.G., 2008. Geomorphological and technogenic preconditions of Bailov slope landslides (volume-graphic model). *Izvestiya*, *Acad. Sci. Azerb*., *Ser.: Earth Sciences*, No. 2, 63-73 (in Russian).

Aliyev, G.A., Akhmedbeyli, F.S., Ismailzade, A.D., Kangarli, T.H. and Rustamov, M.I. (V.E. Khain and Ak.A. Alizadeh, Eds.), 2005a. *Geology of Azerbaijan*, Vol. **IV**: Tectonics. Nafta-Press, Baku (in Russian).

Aliyev, S.A., Aliyev, C.S., Askerhanova, H.Q., Balakishibeyli, Sh.A., Gasanov, A.O., Qasanov, A.B., Zolotovichaya, T.A., Ismailzade A. D., Isayeva, M.I., Kadirov, F.A., Mukhtarov, A.Sh., Rzayev, A.Q., Cafarov, I.B. and Halafly, A.A. (Ak.A. Alizadeh, Ed.), 2005b. *Geology of Azerbaijan*, Vol. V: *Physics of the Earth* (in Russian).

Antonielli, B., Monserrat, O., Bonini, M., Righini, G., Sani, F., Luzi, G., Feyzullayev, A.A. and Aliyev, C.S., 2014. Pre-eruptive ground deformation of Azerbaijan mud volcanoes detected through satellite radar interferometry (DInSAR). *Tectonophysics*, **637**, 163-177.

Babayev, E.S. and Allahverdiyeva, A.A., 2007. Effects of geomagnetic activity variations on the physiological and psychological state of functionally healthy humans: Some results of Azerbaijanian studies. *Advances in Space Research*, **40**, 1941-1951.

Babayev, E.S., Hashimov, A.M., Yusifbeyli, N.A., Rasulov, Z.G. and Asgarov, A.B., 2006. Geomagnetic storm risks to electric power distribution and supply systems at mid-latitude locations and their vulnerability from space weather. *Proceed. of the 3rd Intern. TPE Conf*., Sect: Technical and Physical Problems in Power Engineering, Gazi University, Ankara, Turkey, 1097-1104.

Babazade, O.B., Babazade, N.O., Griesser, N. and Romanov, B., 2008. Dynamic prediction and earthquake monitoring – one of possible approaches to decrease the risk for oil and gas pipeline. *Trans. of the 14th World Conference on Earthquake Engineering*, Beijing, China, Paper 14_07-0078, 1-10.

Balat, M., 2006. The case of Baku-Tbilisi-Ceyhan oil pipeline system: A review. *Energy Sources,* Part B, 1, 117-126.

Barrett, L., Mathey, T. and Park, L., 2004. Teaching archaeogeophysical survey and mapping any time of the Year: An interdisciplinary course. *Jour. of Geoscience Education*, **52**, No. 3, 236-244.

Bayramov, E.R., Buchroithner, M.F. and Bayramov, R.V., 2016. Multi-temporal assessment of ground cover restoration and soil erosion risks along petroleum and gas pipelines in Azerbaijan using GIS and remote sensing. *Environmental Earth Sciences*, **75** (256), 1-22.

Blue, T.E., Holcomb, D.E. and Iarscmba, M.S., 1989. Steady-state absorption of radon on charcoal canisters in cavities in the soil. *Radiation Protection Dosimetry*, **29**, No.3, 199-202.

Bodri, L. and Cermak, V., 2005. Borehole temperatures, climate change and the pre-observational surface air temperature mean: Allowance for hydraulic conditions. *Global Planetary Change*, **45**, 265–276.

Burlatskaya, S.P. and Chernykh, I.Ye., 1989. Change in geomagnetic field strength in Azerbaijan during last 2200 years determined from archaeomagnetic data. *Izvestiya*, *Earth Physics*, USSR Acad. of Sci, **25**, No. 7, 594-597.

Chizhevsky, A.L., 1930. *Epidemic Catastrophes and Periodic Activity of the Sun*. Moscow (in Russian).

Chizhevsky, A.L., 1963. *The Sun and We*. Moscow (in Russian).

Dzabayev, A.A., 1969. *Principles of the Searching and Study of Oil-and-Gas Bearing Structures by Aeromagnetic Method* (*South Caspian Basin*). Statistika, Ashkhabad (in Russian).

Eppelbaum, L.V., 2011. Study of magnetic anomalies over archaeological targets in urban conditions. *Physics and Chemistry of the Earth*, **36**, No. 16, 1318-1330.

Eppelbaum, L.V., 2015. Quantitative interpretation of magnetic anomalies from thick bed, horizontal plate and intermediate models under complex physical-geological environments in archaeological prospection. *Archaeological Prospecting*, **23**, No. 2, 1-14, doi:10.1002/arp.1511.

Eppelbaum, L.V., 2016. Remote Operated Vehicles geophysical surveys in air, land (underground) and submarine archaeology: General peculiarities of processing and interpretation. *Trans. of the 12th EUG Meet*., Geophysical Research Abstracts, Vol. **18**, EGU2016-10055, Vienna, Austria, 1-7.

Eppelbaum, L.V., Alperovich, L., Zheludev, V. and Pechersky, A., 2011. Application of informational and wavelet approaches for integrated processing of geophysical data in complex environments. *Proceed. of the 2011 SAGEEP Conference*, Charleston, South Carolina, USA, **24**, 24-60.

Eppelbaum, L.V. and Finkelstein, M.I., 1998. Radon emanation, magnetic and VLF temporary variations: removing components not associated with dynamic processes. *Collection of Selected Papers of the XXVI General Assembly of the European Seismological Commission* (Tel Aviv, Israel), 122-126.

Eppelbaum, L. and Isakov, A., 2015. Implementation of the geo-correlation methodology for predictability of catastrophic weather events: long-term US tornado season and short-term hurricanes. *Environmental Earth Sciences*, **74**, 3371-3383.

Eppelbaum, L.V. and Kardashov, V.R., 1998. Nonlinear geothermal processes in the Earth crust and transition waves. *Proceed. of the International Conference "The Earth's Thermal Field and Related Research Methods"*. Moscow, Russia, 82-85.

Eppelbaum, L.V. and Khesin, B.E., 2012. *Geophysical Studies in the Caucasus*. Springer, Heidelbeg – N.Y. – London.

Eppelbaum, L.V., Khesin, B.E. and Itkis, S.E., 2001. Prompt magnetic investigations of archaeological remains in areas of infrastructure development: Israeli experience. *Archaeological Prospection*, **8**, No.3, 163-185.

Eppelbaum, L.V., Khesin, B.E. and Itkis, S.E., 2010. Archaeological geophysics in arid environments: Examples from Israel. *Jour. of Arid Environments*, **74**, No. 7, 849-860.

Eppelbaum, L.V. and Kutasov, I.M., 2014. Advanced analysis of thermal data observed in subsurface wells unmasks the ancient climate. *Trans. of the* 10*th EUG Meet*., Geophysical Research Abstracts, Vol. **16**, EGU2014-3261, Vienna, Austria, 1-3.

Eppelbaum, L.V., Kutasov, I.M. and Barak, G., 2006. Ground surface temperature histories inferred from 15 boreholes temperature profiles: Comparison of two approaches. *Earth Sciences Research Jour.*, **10**, No. 1, 25-34.

Eppelbaum, L.V., Kutasov, I.M. and Pilchin, A.N., 2014. Applied Geothermics. Springer, London – N.Y.

Eppelbaum, L.V. and Mishne, A.R., 2011. Unmanned Airborne Magnetic and VLF investigations: Effective Geophysical Methodology of the Near Future. *Positioning*, **2**, No. 3, 112-133.

Feyzullayev, A.A., Kadirov, F.A. and Aliyev, C.S., 2005a. Mud volcano model resulting from geophysical and geochemical research. In: (G. Martinelli and B. Panahi, Eds.), *Mud Volcanoes, Geodynamics and Seismicity*, Springer, 251-262.

Feyzullayev, A. A., Kheirov, M. B., Aliyev, Ch. S., Abbasova, S. B. and Aliyev, K. A., 2005b. Comparative Characteristics of Composition and Radioactivity of Oligocene Clays in the Greater Caucasus and Talysh. *Lithology and Mineral Resources,* **40**, No. 4, 376-385.

Finkelstein, M., Eppelbaum, L. and Price, C., 2006. Analysis of temperature influences on the amplitude-frequency of Rn gas concentration. *Jour. of Environmental Radioactivity*, **86**, No. 2, 251-270.

Fowler, S. R., Mildenhall, J., Zlova, S., Riley, G., Elsley, G., Desplanques, A. and Guliyev, F., 2000. Mud volcanoes and structural development on Shah Deniz. *Jour. of Petrol. Sci. and Engin*., **28**, 189-206.

Gadjiev, T.G., Nechayev, Yu.V., Potapova, E.I. and Sattarova, V.M., 1989. *The Map of Deep Structure of the Caucasus According to Cosmic Data*. Map Printing Factory of the Ministry of Geology of the USSR, Baku.

Gasanov, A.G., 2001. *Deep Structure and Seismicity of Azerbaijan in Relation to Oil-and-Gas Prognosis*. Elm, Baku (in Russian).

Guliyev, I.S., 2005. Mud volcanism in Azerbaijan. In: (A.T. Ismailzadeh, Ed.) *Recent Geodynamics, Georisk and Sustanaiable Development in the Black Sea to Caspian Sea Region*. Proceed. Of the Intern. Workshop, AIP Conf. Proceed., Vol. **825**, Baku, 11-18.

Guliyev, I.S. and Feizullayev, A.A., 1997. *All about Mud Volcanoes*. Nafta-Press, Baku (in Russian).

Huang, S., Pollack, H.N. and Sheen, P.Y., 2000. Temperature trends over past five centuries reconstructed from borehole temperatures. *Nature*,**403**, Feb. 17, 756-758.

Huseinov, D.A. and Guliyev, I.S., 2004. Mud volcanic natural phenomena in the South Caspian Basin: geology, fluid dynamics and environmental impact. *Environmental Geology*, **46**, 1012-1023.

Ismailzadeh, T.A., Gadjiev, T.G., Khesin, B.E., Karkoshkin, A.I., Alexeyev, V.V. and Potapova, E.I., 1983. *Petromagnetic Characteristics of Azerbaijan*. Elm, Baku (in Russian).

Kadirov, F.A., Lerche, I., Guliyev, I.S, Kadyrov, A.G., Fezullayev, A. A. and Mukhtarov, A.Sh., 2005. Deep structure model and dynamics of mud volcanoes, southwest Absheron Peninsula (Azerbaijan). *Energy Exploration & Exploitation*, **23**, No. 5, 307-332.

Kadirov, F.A. and Mukhtarov, A.Sh., 2004. Geophysical fields, deep structure, and dynamics of the Lokbatan Mud Volcano. *Izvestiya, Physics of the Solid Earth*, **40**, 327-333.

Kardashov, V.R., Eppelbaum, L.V. and Vasilyev, O.V., 2000. The role of nonlinear source terms in geophysics. *Geophysical Research Letters*, **27**, No. 14, 2069-2073.

Kerimov, K.M. (Ed.), 1996. *Geophysical Investigations in Azerbaijan*. Sharg-Garb, Baku (in Russian).

Kieckhefer, R. M., Herkenhoff, E. F., Wright, J. Q., Mollenkopf, R., Smith, N., Kuliyeva, R. and Connor, J. A., 2003. Sea-Floor properties from the inversion of 3D multichannel seismic data: A submarine mud-volcanic flow in the Absheron Block, offshore Azerbaijan. *IEEE Proceed*., Oceans, Vol. **5**, 2728-2734.

Kostianoy, A.G., Ermakov, P.N. and Soloviev, D.M., 2008. Complex satellite monitoring of the Nord Stream gas pipeline construction. *Trans. of the IEEE Conf*., No. 978-1-4244-2268, 1-5.

Logachev, A.A. and Zakharov, V.P., 1979. Magnetic Prospecting. Nedra, Leningrad (in Russian).

Lyubimov, V.V., Gurfinkel, Yu.I. and Oraevskii, V.N., 1993. Experience of application of diagnostic magnetometers in city and resort conditions. *IZMIRAN Publ*., No. 99 (1046), Moscow (in Russian).

Mishel, J., 1987. Sources. In: *Environmental Radon* (C.R. Cothern and J.E. Smith, Eds.). Plenum Press, N. Y. – London, **35**, 81-130.

Modin, I.N., 2010. Electric prospecting in technical and archaeological geophysics. *D.Sci. Thesis*, Moscow State Univ. (in Russian).

Mukhtarov, A.Sh., 2011. Structure of thermal field of sedimentary complex of the South Caspian Basin. *D.Sci. Thesis*, Inst. of Geology, National Acad. of Sci. of Azerbaijan, Baku (in Russian).

Mukhtarov, A.Sh., Kadirov, F.A. and Mamedov, V.A. 2010. Reconstruction of the surface temperature in the Kur depression (Azerbaijan) by the inversion of borehole data. *Izvestiya*, *Physics of the Solid Earth*, **46**, No. 6, 524-528.

Pilchin, A.N., 1985. On the genesis of mud volcanos. Soviet Geology, No. 10, 78-81 (in Russian).

Planke, S., Svensen, H., Hovland, M., Banks, D.A. and Jamtveit, B., 2003. Mud and fluid migration in active mud volcanoes in Azerbaijan. *Geo-Marine Letters*, **23**, 258-268.

Rabinowitz, P.D., Yusifov, M.Z, Arnoldi, J. and Hakim, E., 2004. Geology, oil and gas potential, pipelines, and geopolitics of the Caspian Sea region. *Ocean Development and International Law*, **35**, No. 1, 19-40.

Rakhmanov, R.R., 1987. *Mud Volcanoes and Their Implications for the Oil and Gas Content of Deep Formations*. Nedra, Moscow (in Russian).

Rapoport, C.I., Btreus, T.K. and Kleimenova, N.G., 2006. Geomagnetic pulsations and cardiac infarction. *Therapeutic archive*, No. 4, p. 56.

Riley, G., Javanshir, R., Abdullayev, N. and Duppenbecker, S., 2011. Exploration in an overpressured lacustrine petroleum system; the South Caspian Basin. *Trans. of the 73rd EAGE Conference & Exhibition incorporating SPE EUROPEC 2011*, Vienna, Austria, 1-4.

Salamov, A.M., Gabibov, F.G. and Bogomolova, O.A., 2010. Investigation of landslide on the right coast of the Mingachevir reservoir by electrical prospecting methods. *Bull. of the Volgograd State Architectural-Building Univ*., No. 20, 33-39 (in Russian).

Salamov, A.M., Kadyrov, A.G., Salamov, F.A. and Pashayev, T.R., 2015. Survey of the landslide in the Khyzy region of Azerbaijan by the method of vertical electric sounding. *EngGeo*, Nos. 5-6, 50-56 (in Russian).

Salamov, A.M., Kadyrov, A.G. and Zamanova, A.G., 2014. Integrated investigations of seismological and engineering conditions in a territory of projected construction in the south-eastern part of the Absheron peninsula. *EngGeo*, No. 3, 60-65 (in Russian).

Shatsov, A.N., 1969. *Marine Radiometry*. Nedra, Moscow (in Russian).

Shen, P.Y. and Beck, A.E., 1991. Least squares inversion of borehole temperature measurements in functional space. *Jour. of Geophys. Research*, **96**, 19.965-19.979.

Scholte, K.H., Hommels, A., Van der Meer, F.D., Slob, E.C., Kroonenberg, S.B., Aliyeva, E., Huseynov, D. and Guliyev, I., 2003. Subsurface resistivity in combination with hyperspectral field and satellite data for mud volcano dynamics, Azerbaijan. *IEEE Trans*., 0-7803-7929-2/03, 3395-3397.

Sternberg, R., Dee, S., Johnson, T., Ristvet, L. and Bakhshaliyev, V., 2012. Magnetic Gradiometry at Oglanqala, A 1st Millennium Iron Age Fortress Site, Nakhchivan, Azerbaijan. *Proceed. of the 39th Intern. Symp. for Archaeometry*, Leuven, 306-309.

Tanircan, G., Tsereteli, N., Garaveliev, E., Siyahi, B., Varazanashvili, O., Mammadli, T., Yetirmishli, Q., Chelidze, T., Akhundov, A. and Safak, E., 2011. Seismic Hazard Assessment for Southern Caucasus-Eastern Turkey Energy Corridor. *Proceed. of the EGU Conf.,* Vienna, *Geophysical Research Abstracts*, Vol. **13**, No. 1744.

van Leusen, M., 1998. Dowsing and archaeology. *Archaeological Prospection*, **5**, 123-138.

Yusifov, M. and Rabinowitz, P.D., 2004. Classification of mud volcanoes in the South Caspian Basin, offshore Azerbaijan. *Marine and Petroleum Geology*, **21**, 965-975.

Zeynalov, G.A., 2008. Fluid flow and sealing properties associated with active faults - Kur Basin, Azerbaijan. *Trans. of the EAGE Conf. "Petroleum Geology & Hydrocarbon Potential of Caspian and Black Sea Regions*" 6–8 October 2008, Baku, Azerbaijan, P03, 1-6.

Zolotovitskaya, T.A., 2003. Mechanisms of formation of radionuclide contamination at the oil fields of Azerbaijan. *In*: (Birsen, N. and Kadyrzhanov, K.K., Eds.), *Environmental Protection Against Radioactive Pollution*. Kluwer Acad. Publ., NATO Science Series, Earth & Environmental Sci., Vol. **33**, 74-77.

Index

A.A. Alizadeh et al., *Geosciences of Azerbaijan*,
Regional Geology Reviews, DOI 10.17/978-3-319-40493-6